ANNUAL REVIEW

INSTITUTE FOR MOLECULAR SCIENCE

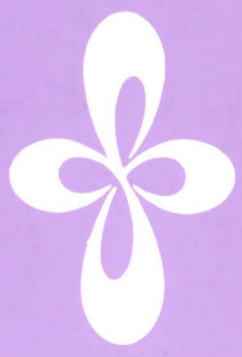

1997

ANNUAL REVIEW

INSTITUTE FOR MOLECULAR SCIENCE

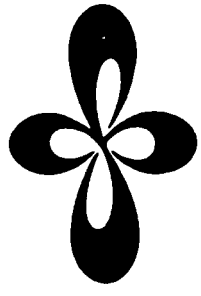

1997

Published by
Institute for Molecular Science
Okazaki National Research Institutes
Myodaiji, Okazaki 444-8585, Japan
Phone: 0564-55-7418 (Secretary Room)
Telex: 4537-475 KOKKEN J
FAX: 0564-54-2254
Home Page: http://www.ims.ac.jp/

Editorial Committee 1997

Chairperson	Koichiro MITSUKE	
Vice-Chairperson	Satoshi TAKEUCHI	Hirofumi SATO
	Jun-ichiro KISHINE	Hiroyuki OZEKI
	Keisuke TOMINAGA	Hironori OGATA
	Katsuya INOUE	Kiyoshi TSUGE
	Tetsunori MIZUKAWA	Toshiya TAKAMI
	Daisuke KUWAHARA	Kayoko SUGIYAMA
	Atzko SATO	

IMS 1997

This is the year of a turning point for IMS. Two research facilities have been established in April 1997. Their establishment is a realization of our future plan for the IMS extensively discussed for the last three years. It was based on the critical review of the research activity of IMS which was carried out by external reviewers in 1993. New research facilities are the Laser Research Center for Molecular Science and the Research Center for Molecular Materials.

The former consists of three research groups and the latter of four research groups, each of them being headed by an Associate Professor. The aim of these research centers is to carry out extensively research on specific subjects which are expected to produce a great impact in molecular science. A close collaboration between a new group and an existing group or groups on a subject of common interest will be greatly encouraged. We hope that a small but original idea born in IMS will be developed into a new large field or concept of molecular science through the newly added reserach centers.

As usual, there has been a high turnover of personnel during the last year. Professor K. Yoshihara and Professor I. Hanazaki in the Department of Electronic Structure, who have contributed a great deal in the development of IMS since the establishment of the institute, retired from IMS and were appointed to professorship positions at Japan Advanced Institute of Science and Technology and Hiroshima University, respectively. Their successors are Professor N. Nishi from Kyushu University and Professor M. Fujii from Waseda University. Associate Professor Y. Matsumoto of the same department has been promoted to professor of the Graduate University for Advanced Studies. Associate Professor K. Kanoda of the Department of Molecular Assemblies has been assigned an associate professorship of the Tokyo University. Both Professors Matsumoto and Kanoda continue their research activity at IMS for a while as adjunct professors. We have appointed Dr. M. Fujita of Chiba University as an associate professor of the Coordination Chemistry Laboratories. Professor N. Ueno and Associate Professor M. Sakurai took positions in the Department of Vacuum UV Photoscience by transfering from their positions at Chiba University and Kobe University, respectively. Professor R. D. Levine of Hebrew University of Jerusalem and Professor C. S. Parmenter of Indiana University were assigned as foreign Councillors to succeed Professor E. W. Schlag and Professor M. A. El-Sayed.

Finally, I would like to congratulate Professor H. Kobayashi and Professor N. Nishi for the Divisional Award of the Chemical Society of Japan in Physical Chemistry. The Chemical Society of Japan Award for Technical Achievement was awarded to Mr. K. Kato, technical section chief of Research Center for Molecular Science, to whom I would like to congratulate.

September, 1997

Mitsuo Ito

Mitsuo Ito
Director-General

CONTENTS

IMS 1997 ..... Mitsuo Ito iii
CONTENTS v
ORGANIZATION AND STAFF 1
COUNCIL 13
BUILDINGS AND CAMPUS 15
RESEARCH ACTIVITIES I
Department of Theoretical Studies
A. Development of New Theoretical and Numerical Techniques in the Study of Molecular Structures 17
1 Superposition of Nonorthogonal Slater-Determinants towards Electron Correlation Problems 17
2 Theoretical Studies of the Dipole Bound Anions of Molecular Clusters and the Photo-detachment Cross Section with Hybrid Basis Sets of Gaussian Functions and Plane Waves 17
3 Static Structure Factor and Electron Correlation Effects Studied by Inelastic X-ray Scattering Spectroscopy 17
4 Construction of Two Electron Reduced Density Matrix for Static Structure Factor Calculation 17
B. Hybrid Procedures of Ab Initio MO Calculations and Monte Carlo Samplings 18
1 Theoretical Prediction of Intracluster Reactions of $B^+(H_2O)_2$ and $B^+(H_2O)_3$ Clusters: Hybrid Calculations of Ab Initio MO and Monte Carlo Samplings 18
2 Ab Initio Monte-Carlo Simulation Using Multi-Canonical Algorithm: Application to Water Dimer 18
C. Structures and Reactions of Atomic and Molecular Clusters 19
1 Structures of Water Cluster Anions 19
2 Intracluster Reaction Dynamics of Argon Tetramer Ions 19
3 *Ab Initio* MO Studies of Si_4NO^+ 19
4 Ab Initio Study of Photochemical Reactions of Ammonia Dimer Systems 20
5 Theoretical Studies of Cyclic Radicals NO_x (x=2–6) 20
6 Six-Membered Rings N_xO_{6-x} (x=0–5): Theoretical Examination of the Stability 20
7 Ab Initio MO Studies of Neutral and Anionic SiC_n Clusters (n=2–5) 20
8 Geometric and Electronic Structures of Silicon-Sodium Binary Clusters: Ionization Energy of Si_nNa_m 20
9 Ab Initio Studies on the Structures, Vertical Electron Detachment Energies and Stabilities of C_nP^- Clusters 21
10 Theoretical Study of the Structure and internal motion of $(N_2)_2$ Cluster 21
D. Structures and Vibrational Frequencies of Infinite Polymer Chains 21
1 Density Functional Crystal Orbital Study on the Normal Vibrations of Poly-acetylene and Polymethineimine 21
2 Density Functional Crystal Orbital Study on the Normal Vibrations and Phonon Dispersion Curves of All-*Trans* Polyethylene 22
E. Accurate Studies of Low-Lying States of Diatomic and Triatomic Molecules 22
1 Portrait of Diatomic FeN. A Theoretical Study 22
2 A Theoretical Study of the Electronic Structure and Spectroscopic Properties of the Low-Lying Electronic States of the Molecule SiB 22
3 Ab Initio Calculations for Potential Surfaces of HNO 23
F. Application of Ab Initio Molecular Orbital and Density Functional Methods to Experimentally Relevant Systems 23
1 Comparative Ab Initio and Hybrid DFT Studies Relevant to An Experimental Investigation of Neutral and Cationic [Si,P,H_2] Isomers 23
2 Ab Initio Study of the Isomers: HNNSi, HSiNN, and HNSiN 23
3 The Ground and Low-Lying Excited States of the Phenyl Cation $C_6H_5^+$: Revisited 23
4 Ab Initio MO and Density Functional Studies on the Vibrational Spectra of 1,4-Benzoquinone, and Its Anion and Dianion 24
5 Ab initio Study of Internal Rotation of Methyl Groups in Toluene Derivatives 24
6 Local Hard-Soft Acid Base Principle: A Critical Study 24

7 An Ab Initio MO Study of Esa(1-*para*-methoxy-stylbene) and Its *para*-Alogen Substituents: A Model of Interdigitated Organization Within the Smectic Layer ---- 25
G. Prediction of Protein Tertiary Structures from the First Principles ---- 25
1 Monte Carlo Simulations in Generalized Ensemble: Multicanonical Algorithm versus Simulated Tempering ---- 25
2 Numerical Comparisons of Three Recently Proposed Algorithms in the Protein Folding Problem ---- 25
3 Calculation of Hydration Free Energy for a Solute with Many Atomic Sites Using the RISM Theory: Robust and Efficient Algorithm ---- 25
4 Solvation Structure and Stability of Peptides in Aqueous Solutions Analyzed by the Reference Interaction Site Model Theory ---- 25
5 A Simple Ansatz to Describe Thermodynamic Quantities of Peptides and Proteins at Low Temperatures ---- 26
6 Characteristic Temperatures of Folding of a Small Peptide ---- 26
7 Tertiary structure prediction of C-Peptide of ribonuclease A by multicanonical algorithm ---- 26
8 First-Principle Determination of Peptide Conformations in Solvents: Combination of Monte Carlo Simulated Annealing and RISM Theory ---- 26
9 Calculation of Solvation Free Energy for a Peptide in Salt Solution Using the RISM Theory ---- 27
10 Electrostatic Effects on the α-Helix and β-Strand Folding of BPTI(16-36) as Predicted by Monte Carlo Simulated Annealing ---- 27
11 Effective Parameters for Solvation Energy of Proteins Based on Solvent Accessible Surface Area ---- 27
12 Classification of Low-Energy Conformations of Met-Enkephalin with Hydrophobic Interactions Based on the Scaled Particle Theory Taken into Account ---- 27
H. Development of Simulation Algorithms for Complex Systems ---- 27
1 Generalized-Ensemble Monte Carlo Method for Systems with Rough Energy Landscape ---- 27
2 Simulated Annealing with Tsallis Weights — A Numerical Comparison ---- 28
3 An Effective Way for Determination of Multicanonical Weights ---- 28
4 A New Look at the 2d Ising Model from Exact Partion Function Zeros for Large Lattice Sizes ---- 28
5 Parallel Tempering Algorithm for Numerical Studies of Biological Macromolecules ---- 28
6 Molecular Dynamics, Langevin, and Hybrid Monte Carlo Simulations in Generalized Ensemble ---- 28
I. Theoretical Studies of Chemical Reaction Dynamics ---- 28
1 Quantum Dynamics of $O(^3P) + HCl \rightarrow OH + Cl$: Effects of Reagent Rotational Excitation ---- 28
2 Hyperspherical Elliptic Coordinates for the Theory of Light Atom Transfer Reactions ---- 29
3 Quantum Mechanical Elucidation of Reaction Mechanisms of Heavy-Light-Heavy Systems: Role of Potential Ridge ---- 29
4 Cumulative Reaction Probability without Absorbing Potentials ---- 29
J. Theory of Nonadiabatic Transitions ---- 29
1 Semiclassical Theory of Multi-Channel Curve Crossing Problems: Landau-Zener Case ---- 29
2 Usefulness of the Newly Completed Semiclassical Theory of Curve Crossing: Multi-Channel Resonant Scattering ---- 29
3 Semiclassical Theory of Multi-Channel Curve Crossing Problems: Nonadiabatic Tunneling Case ---- 30
4 Semiclassical Theory of Time-Dependent Curve Crossing Problems ---- 30
5 Exact Analytical Solution of the N-Level Landau-Zener Type Bow-Tie Model ---- 30
6 Semiclassical Theory of Nonadiabatic Transition in a Two-State Exponential Model ---- 30
7 Semiclassical Mechanics of Cubic Potentials ---- 30
K. Theoretical Studies of Characteristics and Dynamics of Superexcited States of Diatomic Molecules ---- 31
1 Characteristics and Dynamics of Superexcited States of Diatomic Molecules ---- 31
2 Two-Center of Coulomb Functions ---- 31
3 Gausian Expansions of the Two-Center Coulomb Functions ---- 31
L. New Molecular Switching Elements ---- 31
1 Molecular Switching in One-Dimensional Finite Periodic Nonadiabatic Tunneling Potential Systems ---- 31
M. Rydberg States in External Fields ---- 31

1 Rydberg Atom in Time-Periodic Fields: Intrashell Dressed States and Quasienergy Spectrum ---- 31
N. Some Basics of Scattering Theory ---- 32
1 Siegert Pseudo-States as a Universal Tool: Resonances, S-Matrix, Green Function ---- 32
2 Flux Formulations of Scattering Theory ---- 32
O. Fokker-Planck Equation Approach to Quantum Dynamics in Condensed Phases ---- 32
1 Gaussian-Markovian Quantum Fokker-Planck Approach to Nonlinear Spectroscopy of a Displaced Morse Potentials System: Dissociation, Predissociation and Optical Stark Effects ---- 32
2 Fifth-Order Two-Dimensional Vibrational Spectroscopy of a Morse Potential System in Condensed Phases ---- 32
P. Path integral Approach to Nonlinear Optical Spectroscopy of Molecules in the Condensed Phase ---- 33
1 Sensitivity of Two-Dimensional Fifth-Order Raman Response to the Mechanism of Vibrational Mode-Mode Coupling in Liquid Molecules ---- 33
2 Interplay of Inhomogeneity and Anharmonicity in 2D Raman Spectroscopy of Liquids ---- 33
3 Coherent Two-Dimensional Raman Scattering: Frequency-Domain Measurement of the Intra- and Intermolecular Vibrational Interactions ---- 33
4 Two-Time Correlation Functions of a Harmonic System Nonbilinearly Coupled to a Heat Bath: Spontaneous Raman Spectroscopy ---- 33
5 The Optimized Perturbation Theory to Femtosecond Vibrational Spectroscopy of a Diatomic Molecule System in Condensed Phases ---- 33
Q. Theoretical Studies of Molecular system coupled to nonGaussian-Markovian Environment ---- 34
1 Spectral Random Walks and Line Broadening of Impurity Molecules in an Ising Spin Glass Environment ---- 34
2 Effects of Colored Noise Bath on the Spectra of a Strongly Driven Two-Level System ---- 34
R. Electronic Structure of a Molecule in Solution ---- 34
1 *Ab initio* Study of Water: Self-consistent Determination of Electronic Structure and Liquid State Properties ---- 34
2 Molecular Theory of Solvent Effect on keto-enol Tautomers of Formamide in Aprotic Solvents: RISM-SCF Approach ---- 35
S. Solvation Thermodynamics of Protein and Related Molecules ---- 35
1 Analysis on Salt Effects on Solubility of Noble Gases in Water Using the Reference Interaction Site Model Theory ---- 35
2 Calculation of Hydration Free Energy for a Solute with Many Atomic Sites Using the RISM Theory: Robust and Efficient Algorithm ---- 36
3 Ion Hydration: Thermodynamic and Structural Analysis with an Integral Equation Theory of Liquids ---- 36
4 Solvation Structure and Stability of Peptides in Aqueous Solutions Analyzed by the Reference Interaction Site Model Theory ---- 36
5 Calculation of Solvation Free Energy for a Peptide in Salt Solution Using the RISM Theory ---- 37
6 First-Principle Determination of Peptide Conformations in Solvents: Combination of Monte Carlo Simulated Annealing and RISM Theory ---- 37
T. Spatial and Temporal Density Fluctuation in Molecular Liquids ---- 38
1 Shear-Induced Distortion of Intramolecular and Intermolecular Correlations in Liquids: Time-Dependent Density-Functional Theory ---- 38
2 Statistical Mechanics of Deformable Molecular Liquids: Thermal Expansion and Isomerization of Diatomic Molecules ---- 38
3 Nonlinear Electrical Potential Fluctuations of Solvent around Solutes: an Integral Equation Study ---- 38
4 Interaction-Site Representation for Collective Excitations in Diatomic Dipolar Liquid ---- 39
5 Theoretical Study for Water Structure at Highly Ordered Surface: Effect of Surface Structure ---- 39
U. Theoretical Studies of Low-Dimensional Correlated Electron Systems ---- 39
1 Various Transitions in Quasi-One-Dimensional Systems under High Pressure ---- 39
2 Phonon Effects on Superconducting Phase in Two-Chain Electron Systems ---- 40
3 Renormalization-Group Approach to the Metal-Insulator Transitions in $(DCNQI)_2M$ (DCNQI is *N,N'*-Dicyanoquinonediimine and *M*=Ag, Cu) ---- 40
4 Spin Gap of $S=1/2$ Heisenberg Ladder: Field Theoretical Study of Magnetic Susceptibility and NMR Relaxation Rate ---- 40

5 Nuclear Gaussian Spin Echo Decay in S=1/2 Heisenberg Ladder ---- 40
6 Spin Fluctuations in Magnetically Coupled Bilayer Cuprates ---- 40
7 Quantized Conductance of One-Dimensional Doped Mott Insulator ---- 41
8 The Effect of Electron Interaction on the Coherence Length of Polymer ---- 41
9 Electron Correlation and SDW in Polymer ---- 41
10 Off-Diagonal Interation, Bond Density Correlation, and Their Effects on the Excitons in Conjugated Polymers ---- 41
V. Theoretical Studies of Superconductors under Magnetic Field ---- 42
1 Quasi-Particle Band Structure and Gapless Superconductivity in the Vortex-Lattice State ---- 42

RESEARCH ACTIVITIES II

Department of Molecular Structure

A. Laboratory and Astronomical Spectroscopy of Transient Molecules ---- 43
1 The Microwave Spectrum of the NH_2 Radical: The Hyperfine Structure of the $^2B_1$ Ground State ---- 43
2 Submillimeter-Wave Spectrum of the NH_2 Radical: Line Frequencies for Astronomical Observations in the 900 GHz Region and their Assignment ---- 43
3 Far-Infrared Spectra of the NH_2 Radical Observed by a Laser Sideband Spectrometer ---- 44
4 The Microwave Spectrum of the NHD Radical in the Ground Electronic State, $^2A''$ ---- 44
5 Microwave Spectra of the AsH_2 and AsD_2 Radicals in the $^2B_1$ Ground Electronic State ---- 45
6 Microwave Spectrum of a New Phosphorus Containing Free Radical, $CH_2CP(X^2B_1)$ ---- 45
7 Microwave Spectrum of NF in the Second Electronically Excited State, $b^1\Sigma^+$ ---- 46
8 The Microwave Spectra of Copper Monoxide, CuO ($^2\Pi_i$) and Silver Monoxide, AgO ($^2\Pi_i$) ---- 46
9 Microwave Spectra of Molecular Ions: Monodeuterated $HCNH^+$ and SD_3^+ ---- 47
B. Development of a Mt. Fuji Submillimeter-Wave Telescope ---- 47
1 Development of a Wide-Band Acousto Optical Spectrometer(AOS) for the Mt. Fuji Telescope ---- 47
C. Laser Investigation of Antiproton-Helium Compounds ---- 48
1 Observation of Double-Resonant Laser-Induced Transitions in the v=n-l-1=2 Metastable Cascade of Antiprotonic ^{4}He Atoms ---- 48
2 Laser Resonance Studies of the Interactions of Metastable Antiprotonic Helium Atomcules $\bar{p}^4He^+$ with Surrounding H_2 Molecules ---- 48
3 Hydrogen-Assisted Laser-Induced Resonant Transitions between Metastable States of Antiprotonic Helium Atoms ---- 48
4 High-Precision Structural Studies of the Antiprotonic Helium Atom $\bar{p}^4He^+$ by Observing Laser Resonances with $\Delta\nu = \Delta(n\text{-}l\text{-}1)=2$ ---- 49
D. Laser Cooling and Trapping of Neutral Atoms ---- 49
1 Branching Ratio of Penning and Associative Ionization Processes due to Ultracold Collision between Laser-Trapped He* Atoms ---- 49
2 Theoretical Investigation on the He* + He* Ultracold Collision in a Laser Trap ---- 50
E. Spectroscopy of Ions and Atoms in Liquid Helium ---- 50
1 Laser Spectroscopy of Ba Ions in Liquid Helium ---- 50
2 Laser Spectroscopy of Mg Atoms in Liquid Helium ---- 51
F. Biomolecular Science ---- 51
1 Purification of Bovine Soluble Guanylate Cyclase and ADP-Ribosylation on Its Small Subunit by Bacterial Toxins ---- 51
2 Tyrosine Phosphorylation-Induced Changes in Absorption and UV Resonance Raman Spectra of Src-Peptides ---- 52
3 Resonance Raman, Infrared and EPR Investigation on the Binuclear Site Structure of the Heme-Copper Ubiquinol Oxidases from *Acetobacter Aceti*: Effect of the Heme Peripheral Formyl Group Substitution ---- 52
4 Solvent Effects of 1,4-Benzoquinone and Its Anion Radicals Probed by Resonance Raman and Absorption Spectra and Their Correlation with Redox Potentials ---- 52
5 UV Resonance Raman Studies of Quaternary Structures of Nitrosyl Hemoglobin ---- 52
6 A Third-Generation UV Resonance Raman Spectrophotometer Using a Solar-Blind ICCD and a Quasi-CW UV Light Source for Biological Applications ---- 53
G. Fast Dynamics of Photoproducts in Solution Phases ---- 53
1 Direct Observation of Cooling of Heme upon Photodissociation of Carbonmonoxy Myoglobin ---- 53
2 Developments of Widely Tunable Light Sources for Picosecond Time-Resolved Resonance Raman Spectroscopy ---- 53

3 Time-Resolved UV Resonance Raman Detection of a Transient Open Form of the Ligand Pathway in Tyr64(E7) Myoglobin ---- 54
4 Time-Redolved Resonance Raman Study of Intermediates Generated After Photodissociation of Wild-Type and Mutant CO-Myoglobins ---- 54
5 Picosecond Time-Resolved Stokes/Anti-Stokes Resonance Raman Study of Non-Planar Nickel-Octaethyltetraphenylporphyrin in Solution ---- 54
H. Molecular and Electronic Structures of Metallofullerenes and the Fullerene Radical Anions ---- 55
1 Theoretical Prediction on the Molecular Structure of C_{60}^- ---- 55
I. Site Selective Spectroscopy in Solid Crystals ---- 56
1 Nuclear Quadrupole Resonance of ^{139}La around Pr^{3+} Doped in LaF_3. Raman Heterodyne Detection Using Optical Transition of Pr^{3+} Ions ---- 56
J. State Correlated Raman Spectroscopy ---- 57
1 Ordering of Liquid Crystals Studied by Polarized Vibrational Raman Spectroscopy ---- 57
2 The Analysis of the Vibrational Raman Lines of the Pyridine-Water System Measured by a Tandem Type Spectrograph ---- 57
K. Double Resonance Spectroscopy Using Two Phase-Locked Lasers ---- 57
1 Development of a Phase-Locking System between Two Single Mode Lasers ---- 57
2 Optical-Optical Double Resonance Study on the D_2 Line of Rubidium Atom ---- 58

RESEARCH ACTIVITIES III
Department of Electronic Structure

A. Ultrafast Intermolecular Electron Transfer ---- 59
1 Substituent Effect and Deuterium Isotope Effect of Ultrafast Intermolecular Electron Transfer: Coumarin in Electron Donating Solvent ---- 59
2 Ultrafast Intermolecular Electron Transfer Dynamics in Coumarin-Hydrazine System ---- 59
3 Ultrafast Intermolecular Electron Transfer and Back Electron Transfer in Coumarin-Aniline System ---- 60
4 Oscillatory Fluorescence Decay of Electron-Donor-Acceptor Complex ---- 60
B. Liquid Dynamics Studied by Higher Order Nonlinear Spectroscopy ---- 61
1 Overtone Vibrational Dephasing in Chloroform and Deuterated Chloroform ---- 61
C. Studies on Ultrafast Solvent Dynamics by Optical Kerr Effect ---- 61
1 Ultrafast Optical Kerr Effect and Solvation Dynamics of Liquid Aniline ---- 61
2 Ultrafast Dynamics of Liquid Anilines Studied by the Optical Kerr Effect ---- 62
3 Deuterium Isotope Effect on Ultrafast Polarizability Anisotropy Relaxation in Methanol ---- 62
D. Ultrafast Dynamics of UV-Photoexcited Simple Molecules in Solution by Femtosecond Transient Absorption Spectroscopy ---- 62
1 The Polarization Response of I_2 Produced by Photoinduced Chemical Reaction in Neat CH_3I ---- 62
2 The I_2 Formation by UV Excitation in CH_3I/CH_3CN System ---- 63
3 Solute Concentration Dependence of Complex Formation I and CH_2I_2 by Photodissociation of CH_2I_2 in Solution ---- 63
4 Ultrafast Dynamics of Photoexcited *trans*- and *cis*-1,3,5-Hexatriene in Solution ---- 64
5 Formation of Benzene Dimer Cations in Neat Liquid Benzene ---- 65
E. Dynamical Behavior of Electronically Excited States ---- 65
1 Relaxation Processes from a Higher Excited State of a Dye Molecule in Solution Studied by Femtosecond UV Fluorescence Up-Conversion Method ---- 65
F. Photochemistry on Well-Defined Surfaces ---- 66
1 Comparative Study of Photochemistry of Methane on Pt(111) and Pd(111) Surfaces ---- 66
2 Photodesorption Dynamics of Methane on Pd(111) ---- 67
G. Reaction Dynamics on Well-Defined Surfaces ---- 67
1 Effective Carbonate Formation Induced by Thermal Dissociation of N_2O on Si(100) ---- 67
H. Multiphoton Photoelectron Spectroscopy of Electronic States at Metal Surfaces ---- 68
1 Angle-Resolved Multiphoton Photo-electron Spectroscopy of a Clean Pt(111) Surface ---- 68
2 Two-Photon Photoemission Study of CO adsorbed on Pt(111) ---- 68
I. Potentials for Large-Amplitude Vibrations of Molecules in van der Waals Complexes ---- 69
1 Electronic Spectra of the 2,2'-Bithiophene·Ar Complex ---- 69

J. Self-Organization in Chemical Reactions ---- 70
1 Photo-Induced Excitability in the *Tris*-(bipyridyl)ruthenium(II)-Catalyzed Minimal Bromate Oscillator ---- 70
2 Pulse-Light Induced Phase Shifts of Oscillations in the Minimal Bromate Oscillator ---- 70
K. Spectroscopy and Dynamics of Vibrationally Excited Molecules and Clusters ---- 71
1 Nonresonant Ionization Detected IR Spectroscopy for the Vibrational Study in a Supersonic Jet ---- 71
2 Overtone Spectroscopy of Phenol Studied by the Nonresonant Ionization Detected IR Spectroscopy ---- 71
L. Large Amplitude Motion in Molecular Cation Studied by Pulsed Field Ionization Zero Kinetic Energy Photoelectron Spectroscopy ---- 72
1 Internal Rotation of Methyl Group in *o*- and *m*-Toluidine Cations as Studied by Pulsed Field Ionization-Zero Kinetic Energy Spectroscopy ---- 72
M. Laser Investigation of Molecular Photodissociation Dynamics ---- 72
1 Quantal and Semiclassical Analysis of Vector Correlation in Molecular Photodissociation ---- 72
2 A Test of Semiclassical Analysis of Vector Correlation in Photofragment Imaging: 355 nm Photodissociation of NO_2 ---- 73
3 Non-Adiabatic Bending Dissociation of OCS ---- 73
4 C-Cl Bond Rupture in Ultraviolet Photo-dissociation of Vinyl Chloride ---- 73
5 C-Br Bond Rupture in 193 nm Photodissociation of Vinyl Bromide ---- 74
6 Detection of Metastable Triplet Acetylene Produced by Intersystem Crossing from the Excited $A(^1A_u)$ State ---- 74
7 Pump-Probe Measurements of the Predissociation Reaction Time of C_2H_2 from $\tilde{A}(^1A_u)$ State ---- 74
8 Dissociation of Metastable CH_3CO Radical Observed by Subpicosecond Time-Clocked Imaging ---- 74
9 2D Imaging of Dissociative Ionization of Molecules in Intense Laser Fields ---- 74
N. One Atom Cage Effect and a Search for Dynamical Resonance ---- 75
1 Detection of Ar-HI by (2+1) REMPI ---- 75
O. Laser Investigation of Bimolecular Reaction Dynamics ---- 75
1 Testing Crossed Beam Imaging Apparatus by Observing Inelastic Scattering of NO with Ar at E_{coll} = 70 meV ---- 75
P. Jet Spectroscopy of Free Radicals ---- 76
1 Jet Spectroscopy of the $D_1\ ^2B_1$ - $D_0\ ^2B_1$ Transition of the *p*-Cyanobenzyl Radical ---- 76
2 Laser Induced Fluorescence Spectroscopy of Jet Cooled Benzophenone Ketyl Radical ---- 76
Q. Photochemistry in Molecular Clusters ---- 77
1 Photochemical Reaction in the Neutral Molecular Clusters of Benzophenone with Hydrogen Donors Formed in a Supersonic Free Jet Expansion ---- 77
R. Photochemical Processes Studied by Time-Resolved ESR ---- 77
1 The First Observation of CIDEP Generated through the Interaction between an Excited Singlet Oxygen Molecule and a Free Radical ---- 77
S. Magnetic Behavior of Stable Radical Crystals with Delocalized Spin Structures and Electronic Excited States of Stable Radicals and Their Molecular Crystals ---- 78
1 Magnetic Properties of Stable N-[(Dichlorophenyl)thio]-2,4,6-tri-phenylphenyl-aminyl and N-[(Dichlorophenyl)thio]-2,4,6-tris(chloro-phenyl)phenylaminyl Radical Crystals ---- 78
2 Magnetic Properties of Stable Pyridyl-Thioaminyl Radical Crystals ---- 78
3 Electronic Excited States of Stable Radicals and Their Molecular Crystals ---- 78
T. Conformation, Photoisomerization and Solvent Effect of Merocyanine Dyes ---- 79
1 Conformational Analysis and Photoisomerization of Merocyanine Dyes Studied by Visible Absorption, Resonance Raman and IR Spectroscopies ---- 79
2 Intermolecular Interaction of Merocyanine Dyes Studied by Visible Absorption, Resonance Raman and Infrared Spectroscopies ---- 79

RESEARCH ACTIVITIES IV
Department of Molecular Assemblies

A. Solid State Properties of Phthalocyanine Salts and Related Compounds ---- 80
1 High-Pressure Study of One-Dimensional Phthalocyanine Conductor, $NiPc(AsF_6)_{0.5}$ ---- 80

2 New Conducting Composite Material Based on a Platinum Phthalocyanine (PtPc) Charge Transfer Salt and Poly-bisphenol-A-carbonate (PBC). Electrochemical, Optical, Magnetic, and Structural Properties ---- 80
3 Electrochemical and Spectroelectrochemical Properties of a New Stable Composite Film Electrode. Platinum Phthalocyanine — Poly-bisphenol-A-carbonate ---- 80
4 Magnetic Susceptibility of Oriented Single Crystals of $CoPc(AsF_6)_{0.5}$ ---- 81

B. Structure and Properties of Organic Conductors ---- 81
1 Peierls Transition of DMTSA-BF_4 Having a Half-Filled Quasi-One-Dimensional Band ---- 82
2 Electronic Structure of κ-ET_2X salts, Where "ET" is Bis(ethylenedithio) tetra-thiafulvalene (BEDT-TTF) Molecule ---- 82
3 Charge-Transfer Salts of $M(mnt)_2$ (M=Ni, Pd, Pt, Au) with BDNT: Ferromagnetic Interaction in Conductive $(BDNT)_2$-$[Ni(mnt)_2]$ ---- 82

C. Development of a Spiro-Conjugated Donor System: a New Type Donor able to form Charge-Transfer Salts with a 2-D or 3-D Electronic Conduction Band ---- 83
1 New Spiro Donor Molecules: Bis(tetra-thiafulvalenyldithio)-Methane and -Germane ---- 83

D. NMR Study of Organic Conductors ---- 83
1 ^{13}C NMR Study of Nesting Instability in α-$(BEDT\text{-}TTF)_2RbHg(SCN)_4$ ---- 83
2 Deuterated κ-$(BEDT\text{-}TTF)_2Cu[N(CN)_2]Br$: a System on the Border of the Superconductor/ Magnetic-Insulator Transition ---- 84
3 ^{13}C NMR Study on Deuterated κ-$(BEDT\text{-}TTF)_2Cu[N(CN)_2]Br$ ---- 84
4 Electron Correlation, Metal-Insulator Transition and Superconductivity in Quasi-2D Organic Systems, $(ET)_2X$ ---- 85
5 ^{13}C and ^1H NMR Study of Vortex Dynamics in a Layered Organic Superconductor at Selective Nuclear Sites ---- 85

E. Electron Transport and Magnetic Study of Anisotropic Superconductors ---- 86
1 Phase Diagram of Vortices in the Quasi-Two-Dimensional Organic Superconductor, α-$(BEDT\text{-}TTF)_2NH_4Hg(SCN)_4$; a System of Pancake Vortices with Out-of-Plane Coupling Dominated by the Electromagnetic Energy ---- 86

F. Thermodynamic Study of Organic Conductors ---- 87
1 Reply to the "Comment on 'Electronic Structure of Insulating Salts of the κ-$(BEDT\text{-}TTF)_2X$ Family Studied by Low-Temperature Specific Heat Measurements'" ---- 87
2 Low-Temperature Specific Heat of κ-$(BEDT\text{-}TTF)_2Cu[N(CN)_2]Br$ in the Superconducting State ---- 87
3 Thermodynamic Property of Organic Superconductor κ-$(BEDT\text{-}TTF)_2X$ ---- 88

G. Novel Electronic States of d-π System of $(DCNQI)_2M$ ---- 88
1 Wigner-Crystal Type of Charge Ordering in an Organic Conductor with a Quarter-Filled Band; $(DI\text{-}DCNQI)_2Ag$ ---- 88
2 ^{13}C-NMR Study of Metal-Insulator Transition in $(DMe\text{-}DCNQI)_2Cu$ with Partial Deuteration ---- 89

H. Electric and Magnetic Properties of a Series of λ-Type BETS Conductors and Related Organic Conducting Systems ---- 90
1 Low-Temperature Phase Diagram of λ-Type Organic Superconductor ---- 90
2 The First Organic Superconductor Exhibiting a Superconductor-to-Antiferromagnetic Insulator Transition, λ-$BETS_2(Fe_xGa_{1-x})Cl_4$ ---- 90
3 The Origin of the π-d Coupled Metal-Insulator Transition in Highly Correlated Organic Conductor with Magnetic Anions, λ-$BETS_2FeCl_4$ ---- 91
4 Three-Dimensional (T-P-H) Phase Diagram of λ-$BETS_2$ $FeCl_4$ ---- 91
5 Electrical and Structural Properties of κ-Type BETS Conductors ---- 92
6 Structural, Electric and Magnetic Properties of EDT-XYF_2Z (X,Y=S or Se; Z=PF_6, TaF_6, ClO_4, $GaCl_4$, $FeCl_4$,..) ---- 92

I. Electric and Magnetic Properties of $Ni(dmix)_2$ (x= t, se) Complexes ---- 93
1 Magnetic Properties of $Ni(dmit)_2$ Conductors with Stable Metallic States ---- 93
2 New Metallic $Ni(dmise)_2$ Complex ---- 93

J. X-Ray Studies at Low Temperature and High Pressure ---- 94
1 Low-Temperature X-Ray Diffraction Studies on Molecular Conductors ---- 94
2 High Pressure X-Ray Crystal Structure Analyses of Molecular Conductors ---- 95

K. Development of New Molecular Conductors ---- 95
1 Development of New Selenium Containing Metal Complex $M(ddds)_2$ ---- 95

2 Synthesis of Novel Extended Fulvalene-Metaldithiolene Complexes and Mixed Ligand Metal Complexes ---- 96
3 Synthesis, Structure and Properties of New Sulfur-Bridged TTF Dimer ---- 96
4 Synthesis, Structure and Physical Properties of Pentathio-Substituted TTF Derivative; Ethylenedithio(pentathio)tetra-thiafulvalene ---- 96
5 Crystal Structures and Electrical Conductivities of Cation-Radical Salts of a Tellurium-Containing Donor: 2,3-DMTTeA ---- 97
6 Development of Novel Organic Conductors Based on Tellurium Containig Electron Donors ---- 97
7 Development of New Donor Components with Magnetic Moiety ---- 98
L. Development of Pulsed Field Gradient NMR Spectroscopy ---- 98
1 High Speed Controller for Very Intense Magnetic Field Gradient Pulses in PGSE-NMR ---- 98
2 Personal Computer-Controlled 16 Channel Versatile Pulse Generator for Nuclear Magnetic Resonance ---- 99
M. Phase Transitions and Dynamical Ordering in Liquid Crystals ---- 99
1 General Theory for the NMR Spectra of Liquid Crystals ---- 100
2 Complete Assignment of the ^{13}C NMR Lines in Antiferroelectric MHPOBC ---- 100
3 Natural Abundance ^{2}H NMR Spectroscopy: Anomalous Deuteration Effect on the Chain Dynamics of a Doubly Reentrant Liquid Crystal ---- 100
4 Transient Oscillation of Magnetization in ^{13}C-^{1}H Dipole Coupled Spin Systems in Liquid Crystal ---- 101
5 Unusual Ordering of a Di(oxyethylene) Chain in a Dialkoxy Laterally Substituted Nematogen as Evidenced by ^{13}C NMR ---- 101
6 Low Melting Point Nematic Liquid Crystals with Oxyethylene Units: ^{13}C NMR Study of the Unusual Conformation ---- 102
7 Design and Construction of Hydrostatic Pressure NMR Probehead ---- 102
N. Hydrogen/Deuterium Dynamics in Organic Hydrogen-Bonded Solids ---- 103
1 Phase Transitions and Hydrogen/ Deuterium Ordering in 9-Hydroxyphenalenone Derivatives in the Solid State ---- 103
2 Structures and Hydrogen Dynamics in 9-Hydroxyphenalenone Derivatives with Additional Hydrogen-Bonding Site at the 5-Position ---- 104
O. Electronic Properties of Alkali-Hydrogen-Carbon Systems ---- 105
1 Theoretical Study on Electronic States of Sodium-Hydrogen-Graphite Ternary Intercalation Compounds ---- 105
2 ^{13}C NMR Study in Na_4HC_{60} Superconductor ---- 105
P. Search for Novel Charge Transfer Complexes Based on BEDT-TTF Type Organic Donors ---- 106
1 Synthesis and Properties of CT Complexes of BMDT-TTF Involving Double-Chain Donor Arrangements ---- 106
2 Electronic States and Anti-Ferromagnetic Order in Mixed-Stack Charge Transfer Compound (BEDT-TTF)(F_2TCNQ) ---- 106
Q. Photoelectron Spectroscopy of Organic Solids in Vacuum Ultraviolet Region ---- 106
1 Ultraviolet Photoemission Spectra of Perchlorate-Doped *cis*- and *trans*-Polyacetylene ---- 106
R. Electrical Conduction and its Related Properties of Organic Solids ---- 107
1 Crystal Structure and Thermodynamic Behavior of Tetrabenzo[*de*,*hi*,*op*,*st*]pentacene Endoperoxide ---- 107
2 Calorimetric Studies of Tetrakis(alkyl-thio)tetrathiafulvalene, TTC_n-TTF (n=3,8) ---- 107
3 Superconductivity in Sodium-Hydrogen-C_{60} Ternary Compound ---- 108
4 Rietveld Analysis of the Super-conducting $Na_xH_yC_{60}$ ---- 108
5 Recovery and Enhancement of Superconductivity in the Sodium-Hydrogen-C_{60} Ternary System ---- 108
6 Phase Transition and Isotope Effect in $Na_xH_yC_{60}$ Superconductor ---- 108
7 Electronic Structure Calculations of $Na_xH_yC_{60}$ ---- 108
S. NMR Study of Functional Interactions in Molecular Based Solids: Magnetic, Electronic, and Dynamic Interactions ---- 109
1 Solid State ^{1}H-MAS-NMR and Spin Densities on Protons of the Organic Ferro-magnetic Tempo Derivatives ---- 109
2 Thermochromism and Dynamics of Organometallic Conjugated System: Zirconocene Complex of 1,4-Diphenyl-1,3-butadiene ---- 109
3 Synthesis and Gas-Occlusion Property of Dinuclear Molybdenum (II) Dicarboxylates ---- 110

4 Determination of the Electron Spin Density Distribution and Magnetic interaction Path in 4-(Hydroxyimino)-TEMPO Crystal by Solid State High Speed Magic Angle Spinning D-NMR ---- 110
5 Proton Dynamics in Interacting Hydrogen Bonds in Crystals: Proton Tunneling in the NHO Hydrogen Bonds of N,N'-Di(2-hydroxy-1-naphthylidene)-*p*-phenylenediamine ---- 111
6 Solid State High Resolution 2H-NMR Study of Spin Density Distribution in Hydrogen-Bonded Organic Ferromagnet HQNN ---- 111

T. Electronic Structures and Physical Properties of Quasi-One-Dimensional Halogen-Bridged Mixed-Valence Metal Complexes ---- 111
1 Electronic Structure of the Quasi-One-Dimensional Halogen-Bridged Ni Complexes ---- 111
2 Dynamics of Photoinduced Gap States and Self-Trapped Excitons in the MX Chain Compounds with Degenerate and Non-Degenerate CDW Ground States ---- 112
3 Determination of the Electronic Structure in the Strongly Correlate 1-D Electron Systems: X-Ray Photoelectron and Auger Spectroscopy of Halogen-Bridged Nickel Complexes ---- 112
4 The Metallic State in a MMX-Chain Complexes, Pt2(dta)4I ---- 112
5 Competition between Electron-Correlation in Ni(III) and Electron-Lattice Interaction in Pd(II)-Pd(IV) in Mixed-Metal MX-Chain, $Ni_{1-x}Pd_x(chxn)_2Br_3$ ---- 112
6 Dynamics of Solitons and Polarons in the Quasi-One-Dimensional MX Chain Compound $[Pt(en)_2][Pt(en)_2I_2](ClO_4)_4$ ---- 113

U. Low-Dimensional Magnetic Systems ---- 113
1 S=1 New Haldane Gap Systems and Spin Glass Behaviors: Syntheses, Structures and Magnetic Properties of Linear-Chain Ni(II) Complexes ---- 113
2 Inducing a Magnetic Ordering in the Haldane Material $Ni(C_5H_{14}N_2)_2N_3(ClO_4)$ by Magnetic Field ---- 113

V. Organic-Inorganic Hybrid-Type Charge Transfer Complexes ---- 113
1 Physical Properties of Quasi-One-Dimensional Charge-Transfer Metal Complexes; $[M(HBQD)_2]TCNQ$ (M=Ni, Pd; H_2BQD=1, 2-Benzoquinoedioxime) ---- 113

RESEARCH ACTIVITIES V
Department of Applied Molecular Science

A. Molecular Mechanisms of Oxygen Activation by Heme Enzymes ---- 115
1 Effects of Concerted Hydrogen Bonding of Distal Histidine on Active Site Structures of Horseradish Peroxidase. Resonance Raman Studies with Asn70 Mutants ---- 115
2 Conversion of Myoglobin into a Highly Stereospecific Peroxygenase by L29H/H64L Mutation ---- 115
3 Catalytic Intermediates of Polyethylene Glycolated Horseradish Peroxidase in Benzene ---- 115

B. Molecular Mechanism of Substrate Metabolisms by Heme Enzymes ---- 116
1 Mechanistic Studies of *N*-Demethylation of Dimethylaniline Derivatives by $O=Fe^{IV}$ Por-phyrin π-Cation Radicals of Peroxidases and Their Synthetic Models ---- 116
2 Mechanistic Studies of a Suicidal *meso*-Oxidation of Novel Iron Porphyrin Complexes as a Model of the Formation of α-*meso*-Hydroxyheme by Heme Oxygenase ---- 116

C. Model Reactions of Non-Heme Proteins ---- 117
1 A Model for Lipoxygenases: Synthesis, Structures, and Reactivity of (Hydroxo) Iron(III) Complexes with a Tetradentate Tripodal Ligand ---- 117

D. Aqueous Organometallic Chemistry ---- 117
1 A New, Aqueous ^1H NMR Shift Reagent Based on Host-Guest Molecular Recognition Principles for Organic Compound Structural Analysis: Non-Covalent π-π and Hydrophobic Interactions Using a Supramolecular Host, $[Cp^*Rh(2'\text{-deoxyadenosine})]_3(OTf)_3$ ---- 117

E. New High-Dimensionality Molecule-Based Magnets ---- 118
1 Spontaneous Magnetization in a 2 : 3 Complex Formed by 3,4',5-Tris(N-oxy-*tert*-butylamino)biphenyl and Manganese(II) bis(hexafluoro-acetylacetonate) ---- 118
2 High-Spin Polynitroxide Radicals as Versatile Bridging Ligands for Transition Metal Complexes with High Ferri/Ferromagnetic T_C ---- 119
3 Magnetic Characterization of One-Dimensional Molecule-Based Metamagnet made of Mn(II)$(hfac)_2$ and 1,3-Bis(*N*-oxy-*tert*-butylamino)-benzene ---- 119

4 Ferrimagnets Made By Assembling High-Spin Organic Polyradicals By Mean of Complexation With Magnetic Metal Ions. VII. One-Dimensional Chains Made by an Alternating Array of Mn(II)(hfac)$_2$ and 1,3-Bis-(N-oxy-tert-butylamino)benzenes ---- 120
F. Magnetism in Quantum Spin Systems ---- 120
1 Construction of spin-1/2 Heisenberg Chains with Ferromagnetic and Antiferromagnetic Interactions ---- 120
2 Magnetic Properties of spin-1/2 Heisenberg Honeycomb Lattice with Ferro-magnetic and Antiferromagnetic Interactions ---- 120
3 Spin-1/2 Heisenberg Model with Ferromagnetic and Antiferromagnetic Interactions on a Honeycomb Lattice ---- 121
G. Pressure Effect on Molecular Magnetism ---- 121
1 Magnetic Properties of Pure Galvinoxyl under Pressure—Suppression of the Structural Change and Observation of the Magnetic Ordering ---- 121
H. New Charge-Transfer Complexes Exhibiting Novel Magnetic Properties ---- 121
1 1:2 TCNQ/TCNQ$^-$ Mixed Salts Exhibiting Ferromagnetic Behavior at Room Temperature ---- 122
2 Temperature Dependence of Crystal Structures, and Electrical Conducting and Magnetic Properties in Plate Crystals of 1:2 Tetrafluorotetracyanoquinodimethane /Tetra-fluorotetracyano-quinodimethanide Mixed Tetramethyl-ammonium and -Phosphonium Salts ---- 122
3 Synthesis, and Electrical Conducting and Magnetic Properties of a Neutral Bis-(dimethylthiotetrathiafulvalenyldithiolate)-copper Complex ---- 123
4 Highly-Conducting Neutral Copper Complexes Substituted with Two Tetrathiafulvalenyldithiolato Groups ---- 123
5 New Spiro Donor Molecules: Bis(tetra-thiafulvalenyldithio)-methane and -germane ---- 123
6 A Novel Tetrathiafulvalenoquinodimethane Derivatives Exhibiting Strong Electronic Absorption in a Near-Infrared Region ---- 124
I. Syntheses, Crystal Structures, and Solid State Properties of Halogen-Bridged Metal Complexes with Linear Chain Structures ---- 124
1 Intramolecular Twisting Motion and Phase Transition of Halogen-Bridged One-Dimensional Compound, $Pt_2(dta)_4I$ ---- 124
J. Spectroscopic Studies on Charge Delocalization and Charge Transfer in Molecular Clusters and in Pure Liquids ---- 125
1 Infrared Photodissociation Spectroscopy of Benzene Trimer Ions. Switching of the Dimer Ion Core in Vibrationally Excited States ---- 125
2 Charge Delocalization in Benzene-Naphthalene Hetero-Dimer Cation ---- 126
3 Electronic Structures and Photo-evaporation Dynamics of Benzene Cluster Ions ---- 126
4 Pump-Probe Photodepletion Spectroscopy of $(C_6H_6)_2^+$. Identification of Spectrum in the Charge Resonance Band Region ---- 127
5 Formation of Benzene Dimer Cations in Neat Liquid Benzene Studied by Femtosecond Transient Absorption Spectroscopy ---- 127
6 Nanosecond Time-Resolved Study on the Electronic Spectra of Jet-Cooled Anthracene Dimer ---- 128
K. Molecular Clusters Formed in Aqueous Solutions ---- 128
1 Low Frequency Raman Spectroscopy of Ethanol-Water Mixtures: Evidence for Self-Association of Solute and Solvent Molecules ---- 128
2 Cohesion of Alcohols in Propanol-Water Mixtures ---- 129
L. Structures and Dynamics of Negatively-Charged Molecular Clusters ---- 130
1 Photoelectron Spectroscopy of $(CO_2)_n^-$: Core Switching in the $2 \leqq n \leqq 16$ Range ---- 130
2 Photoelectron Spectroscopy of $(CS_2)_n^-$: Coexistence of Electronic Isomers ---- 131
3 Electronic Structures of $(SO_2)_n^-$ as Studied by Photoelectron Spectroscopy ---- 131
4 Nucleophilic Reactivity of Gas-Phase Cluster Anions ---- 132
5 Photoabsorption and Photo-fragmentation Studies of Acetyloxy Iodide Anion $CH_3CO_2I^-$ ---- 132
6 Photoabsorption and Photo-fragmentation Studies of Nitric Oxide Cluster Anions $(NO)_n^-$ ---- 132
7 *Ab Initio* MO Calculations on Acetyloxy Iodide Anion $CH_3CO_2I^-$ ---- 133

RESEARCH ACTIVITIES VI
Department of Vacuum UV Photoscience
A. Electronic Structure and Decay Mechanism of Inner-Shell Excited Molecules ---- 134
1 Angular Distribution of the Fragment Ions Following the S 1*s* Photoexcitations of OCS ---- 134

2 Angular Distribution of the Fragment Ions following the S 1*s* Photoexcitations of CS_2 ---134
3 Vibronic Couplings in the C 1*s* → *ns* σ_g Rydberg Excited States of CO_2 ---135
4 Fixed-Molecule $1s\sigma_{g,u}$ Photoelectron Angular Distributions as a Probe of σ_g* and σ_u* Shape Resonances of CO_2 ---135
5 Soft X-ray Absorption and X-ray Photoelectron Spectroscopic Study of Tautomerism in Intramolecular Hydrogen Bonds of *N*-Salicylideneaniline Derivatives ---135

B. Soft X-ray Photoelectron-Photoabsorption Spectroscopy and Electronic Structure of Transition Metal Compounds ---135
1 Polarization Dependence of Ni 2*p* Photoabsorption of $K_2Ni(CN)_4 \cdot H_2O$ ---136
2 Polarization Dependence of Ni 2*p* Photoabsorption of Ni Dimethyl-glyoxime ---136
3 Resonant Behavior in Ni 3d, 3p and 3s Photoelectron Spectra at the Ni 2p Excitation of Planar Molecular Complex $Ni(Hdmg)_2$ ---136

C. Studies on Primary Photochemical/physical Processes using Femtosecond Time-Resolved Electronic Spectroscopy ---137
1 Observation of Dimer Excited-State Dynamics in the Double Proton Transfer Reaction of 7-Azaindole by Femtosecond Fluorescence Up-Conversion ---137
2 Construction of a Femtosecond UV-VIS-NIR Transient Absorption Spectrometer ---138
3 Construction of a Flow System of Supercritical Fluids for Ultrafast Spectroscopy ---138
4 Femtosecond Time-Resolved Fluorescence Measurements of Coumarin153 in Supercritical Fluids ---139

D. Studies on Photochemical Reactions using Picosecond Time-Resolved Vibrational Spectroscopy ---139
1 Construction of a Picosecond Time-Resolved Raman Spectrometer ---139
2 Observation of the Picosecond Dynamics of Photoexcited *all-trans* Retinal by Time-Resolved Spontaneous Raman Spectroscopy ---140

E. Development of Time-Resolved Spectroscopy using Synchrotron Radiation ---141
1 Construction of a Setup for Subnanosecond Time-Resolved Far-Infrared Measurement using Synchrotron Radiation ---141

F. Synchrotron Radiation Stimulated Surface Reactions ---141
1 Potential of Site Specific Photo-chemical Processing Using Synchrotron Radiation ---141
2 Structural Changes of Silicon Dioxide Films Caused by Synchrotron Irradiation ---142
3 Extremely High Quantum Yield of Thin Film Deposition Reaction by Core Electron Excitations ---142
4 Growth Mechanisms in the Synchrotron Radiation-Assisted Silicon Gas Source Molecular Beam Epitaxy Using Disilane ---142
5 Infrared Reflection Absorption Spectrum of Silicon Deuterides on Si(100) Surface ---143
6 Chemisorption of Deuterium on Ultrathin Ge Film Deposited over Si(100)-2x1: Existence of Dideuteride Phase ---143
7 Design and Performance of a Multilayered Mirror Monochromator in the Low Energy Region of Vacuum Ultra Violet ---143
8 Double MultiLayered Mirror Monochromator Beamline BL-4A1 for Synchrotron Radiation Stimulated Processing Study ---144

G. Ion Desorption Induced by Core-Electron Transitions Studied by Electron-Ion Coincidence Spectroscopy Combined with Synchrotron Radiation ---145
1 Study of Ion Desorption Induced by a Resonant Core-Electron Transition of Condensed H_2O by Using Auger Electron Photo-Ion Coincidence (AEPICO) Spectroscopy Combined with Synchrotron Radiation ---145
2 Study of Ion Desorption Induced by a Resonant Core-Electron Transition of Condensed NH_3 Using Auger Electron Photo-Ion Coincidence (AEPICO) Spectroscopy Combined with Synchrotron Radiation ---145
3 Photon Stimulated Ion Desorption of Condensed Acetonitrile Induced by Carbon Core Excitation ---146

H. Photoionization Dynamics Studied by Electron Spectroscopy Combined with a Continuous Synchrotron Radiation Source ---147
1 Two-Dimensional Photoelectron Spectroscopy of Acetylene: Rydberg-Valence Interaction between the $(3\sigma_g)^{-1}(3p\sigma_u)^1$ and $(3\sigma_g)^{-1}(3\sigma_u)^1$ States ---147
2 Superexcited States of OCS Probed by Using Photoelectron Spectroscopy for Autoionizing Atomic Sulfur ---147
3 Branching Ratios from a Rydberg State Converging to $OCS^+(B^2\Sigma^+)$ to Probable Decay Pathways ---147

I. Vacuum UV Spectroscopy Making Use of the Combination of Synchrotron Radiation and a Mode-Locked UV Laser ---- 148
1 Development of a Tunable UV Laser System Synchronizing Precisely with Synchrotron Radiation Pulses from UVSOR ---- 148
2 Apparatus for Laser Induced Fluorescence Spectroscopy of Ions or Neutral Fragments Prepared by VUV Photoexcitation ---- 148
3 Laser Induced Fluorescence Excitation Spectroscopy of N_2^+ Produced by Photoionization of N_2 and N_2O with Synchrotron Radiation ---- 149
4 Time-Resolved Fluorescence Spectroscopy of the Products Resulting from VUV Excitation by Using a Streak Camera ---- 149
J. Rebuilding the Monochromator on Beamline BL2B2 in UVSOR ---- 150
1 Design of an 18 m Spherical Grating Monochromator at UVSOR ---- 150
K. Absolute Photoabsorption Cross Section and Radiative Dissociation of Polyatomic Molecule Excited at Valence Shell ---- 151
1 C_6F_5X (X = H, F, Cl, Br, and I) Radical Cation Formation in the 10-40 eV Region ---- 151
2 Photodissociation Spectroscopy of Some Small Nitriles in the Vacuum Ultraviolet Region ---- 151
3 Photoabsorption and Fluorescence Cross Sections of $SiCl_4$ in the Region of 6.2-31 eV ---- 151
4 Dissociative Excitation Cross Section of Formic Acid in the 105 - 155 nm Region ---- 152
L. Creation of High-Sensitive Photorefractive Glasses and Photoinduced Structural Changes ---- 152
1 Preparation of Bragg Gratings in Sputter-Deposited GeO_2-SiO_2 Glasses by Excimer-Laser Irradiation ---- 152
2 Defect Formation in SiO_2:GeO_2 Glasses Studied by Irradiation with Excimer Laser Light ---- 152
M. Creation of Amorphous Metallic Conducting Amorphous Oxides ---- 152
1 Working Hypothesis to Explore Novel Wide Band Gap Electrically Conducting Amorphous Oxides and Examples ---- 153
2 Novel Oxide Amorphous Semi-conductors: Transparent Conducting Amorphous Oxides ---- 153
N. Ultraviolet Photoelectron Spectroscopy of Organic and Inorganic Solids ---- 153
1 Angle-Resolved UPS of Ultrathin Films of Functional Organic Molecules with Synchrotron Radiation: Determination of Molecular Orientation by Quantitative Analysis of Photoelectron Angular Distribution ---- 153
2 Angle-Resolved Ultraviolet Photo-electron Spectroscopy of Thin Films of Bis(1,2,5 Thiadiazolo)-*p*-Quinobis (1,3-Dithiole) on the MoS_2 Surface3 Ultraviolet Photoelectron Spectroscopy of N-Type Conducting Polymers ---- 154
3 Ultraviolet Photoelectron Spectroscopy of N-Type Conducting Polymers ---- 154
4 Photoelectron Spectra of Metallo-fullerenes, GdC_{82} and La_2C_{80}: Electron Transfer from Metal to the Cage ---- 154
5 Structure and Catalysis of $Li_xNi_{2-x}O_2$ Oxide Systems for Oxidative Coupling of Methane ---- 155
6 Resonant Photoemission Study of Ladder Compound $Sr_{14}Cu_{24}O_{41}$ ---- 155
O. Desorption Induced by Electronic Transitions from Cryogenic Surfaces ---- 156
1 Excitonic Energy Transfer Process in Ne-Kr Alloy Studied by Photon Stimulated Desorption of Metastable Atoms ---- 156
2 Absolute Desorption Yield of Meta-stable Atoms from the Surface of Solid Rare Gases Induced by Exciton Creation ---- 156
3 Long Lifetime Emission of the Excited Species Ejected from the Surface of Solid Ne ---- 156
P. Structure and Vibrational Spectra of Molecules Physisorbed on Metal Surfaces ---- 156
1 Upgraded Infrared Beamline BL6A1 at UVSOR ---- 157
2 Development of the Cryogenic Sample Holder for Low Energy Electron Diffraction and Electron Energy Loss Spectroscopy ---- 157
3 Structure of the NO Molecule on the Pt(111) Surface at Low Temperature ---- 157
Q. Electronic Structures of Functional Organic Materials Studied by Spectroscopies Using Synchrotron Radiation ---- 157
1 Energy Level Alignment at Organic /Metal Interfaces Studied by UV Photoemission: Breakdown of Traditional Assumption of a Common Vacuum Level at the Interface ---- 157
2 Electronic Structures Of Polysilanes And Related Compounds ---- 158
3 Polarized VUV Absorption and Reflection Spectra of Oriented Films of Poly-(tetrafluoroethylene) $(CF_2)_n$ and its Model Compound ---- 158

4 Soft X-ray Absorption and X-ray Photoelectron Spectroscopic Study of Tautomerism in Intramolecular Hydrogen Bonds of N-Salicylideneaniline Derivatives---158
R. Growth and Characterization of InAs Nanometer-Scale Island on InP (001) Substrate---159
1 Formation of InAs Islands on InP (001) by Droplet Hetero-Epitaxy---159
2 InAs Dots Grown on InP (001) by Droplet Hetero-Epitaxy Using OMVPE---159

RESEARCH ACTIVITIES VII
Coordination Chemistry Laboratories

A. Surface Coordination Chemistry towards Molecular Protonic Devices---160
1 Synthesis of pH-Response Dinuclear Ru Complexes with an Internal Reference---160
2 pH-Sensitive Self-Assembled Mono-layer Based on Ru Complexes Containing 2,6-Bis(N-(1-mercaptooctyl)-benzimidazolyl)-pyridine on the Au Surface: Synthesis and Proton-Coupled Redox Properties---161
B. Synthesis and Characterization of Self-Assembled Organic Ligands and Metal Complexes on Surface Towards Solution-Phase Molecular Epitaxy---161
1 Preparation of Surfactant Ruthenium Complexes Containing (Benzimidazolyl)-pyridine Derivatives With Long Alkyl Chains---161
2 Ultraviolet Photoelectron Emission from Langmuir Monolayer of Ru Complex at the Air-Water Interface---162
3 Metal Coordination Incorporating with Amphiphilic Ru Complexes at the Air-Water Interface---162
C. Redox Chemistry of Inorganic Metal Complexes---163
1 Trinuclear Ruthenium Complex with Face Capping Benzene Ligand. Hapticity Change Induced by Two Electron Redox Reaction---163
2 Synthesis and Crystal Structure of A Cationic Trinuclear Ruthenium(II) Complex $[Ru_3(\mu_2\text{-}Cl)_3(\mu_3\text{-}Cl)_2\{1,2\text{-bis(diphenylphosphino)-benzene}\}_3]PF_6$---163
3 1,8-Diphenyl-octa-1,3,5,7-tetraene Complexes of Ruthenium(II): Crystal Structures of [μ-(s-*cis*-1,2,3,4-η:s-*cis*-5,6,7,8-η-PhCH =CHCH=CHCH=CHCH=CHPh)(RuClCp*)2] and [μ-(s-*trans*-1,2,3,4-η:s-*trans*-5,6,7,8-η-PhCH= CHCH=CHCH=CHCH=CHPh) -{Ru(acac)$_2$}$_2$]---164
4 Synthesis and Redox Properties of Ruthenium(II) Complexes with Tetradentate 6,6'-Bis(benzimidazolyl)-2,2'-bipyridine Ligand---164
5 Synthesis and Photoinduced Electron Transfer Processes in Ru(II)(bpy)$_2$/Os(III)(bpy)$_2$-Based Triad Complexes Containing Functionalized Diimide Ligands---165
6 Ruthenium(II) Complexes with Tetradentate 6,6'-Bis(oxazolinyl or benzimidazolyl)-2,2'-bipyridine Ligand: Synthesis, Electrochemical Properties, and Catalytic Reactivities---165
7 Spectroelectrochemical Analysis of Intervalence Band in Mixed-Valence Di- and Tetranuclear Ru Complexes by Flow-Through Method---166
D. Metal Ions in Biological Systems---167
1 Reduction and Oxidation Processes of Blue Copper Proteins, Azurin, Pseudoazurin, Umecyanin, Stellacyanin, Plantacyanin, And Plastocyanin Approached by Cyclic and Potential Step Voltammetries---167
2 Intracomplex Quenching by Copper(II) Ion of Exited Singlet and Triplet States of Zinc Myoglobin Modified with Diethylenetriaminepentaacetic Acid---167
3 Isolation and Characterization of Nitric Oxide Reductase from Paracoccus halodenitrificans---167
4 Spectral Properties of Cytochrome c_{553} and a Membrane-Bound Cytochrome *b* from Alcaligenes xylosoxidans GIFU 1051---167
5 Observation of Cu-N_3^- Streching and N_3^- Asymmetric Stretching Bands for Mono-Azide Adduct of Rhus vernicifera Laccase---168
6 Magnetic Studies of the Trinuclear Center in Laccase and Ascorbate Oxidase Approached by EPR Spectroscopy and Magnetic Susceptibility Measurements---168
7 Isolation and Characterization of Vanadium Bromoperoxidase from a Marine Macroalga, Ecklonia stolonifera---168
8 Damping Wave Packet Approach: a Calculation Method of Nonpertubative Nonlinear Optical Susceptibilities Including Effects of nNuclear Motion at Finite Temperatures---168
9 Calculation of Magnetization by Path Integral Method I---168
10 Calculation of Magnetization by Path Integral Method II---169
11 Path Integral Formation for Many-Electron System---169
12 Many-Electron-Wavepackets Method---169
13 Nonadiabatic Treatment of Molecular System by the Wavepackets Method---169
14 Path Integral Monte Carlo Method for ab Initio cCalculation---169

15 Many-Electron Hyperpolarizability Density Analysis: Application to Dissociation Process of One-Dimensional H_2 ---- 170
16 Theoretical Study on the Second Hyperpolarizability of H_3^+ System by Path Integral Method ---- 170
17 Theoretical studies for second hyperpolarizabilities of alternant and condensed-Ring cconjugated systems II ---- 170
18 Calculation of Magnetization by Path Integral Method ---- 170
19 Path Integral Method by Means of Generalized Coherent States and its Numerical Approach to Molecular Systems. I. Ensemble aAverage of Total Energy ---- 170
20 Theoretical Study of Second Hyperpolarizability by Path Integral Method: Effects of External Magnetic Field ---- 171
21 Possibilities of Charge- and/or Spin-Mediated Uperconductors and Photo Induced Superconductor in the Intermidiated Region of Metal-Insulator Transitions ---- 171
22 Finite Temperature ab Initio Calculation by Path Integral Monte Carlo Method ---- 171
23 A Theory of High Tc Superconductors via Electron Correlation: I. Superconductive Phase and Spin Gap ---- 171
24 A Theory of Symmetry and Model Hamiltonian for High Tc Superconductors ---- 172
25 Non-Adiabatic Molecular Theory and It's Application ---- 172
26 Non-Adiabatic Molecular Theory and It's Application. II Water Molecule ---- 172

E. Metal Assisted Control and Functionalization of Biomolecules ---- 172
1 Macrocyclic Zinc(II) Complexes for Selective Recognition of Nucleic Acid Bases in Single- and Double-Stranded Polynucleotides ---- 172
2 Denaturation of Double-Stranded Oligonucleotides Containing an AT-Rich TATA-Box Sequence by a Macrocyclic Zinc(II) Complex ---- 173
3 Novel Synthetic Receptors for AT Base Pairs ---- 173
4 Design and Synthesis of DNA Binding Metallopeptides ---- 174
5 Double-Stranded Artificial DNAs by Metal Complexation ---- 174
6 Artificial Peptides: Alignment of Functionalized Metal Complexes on Peptide Backbone ---- 174
7 Molecular Recognition of DNA by Metal Assisted Self-Assembly ---- 174
8 Alignment of Functionalized Metal Complexes on DNA by Non-Covalent Interactions ---- 175
9 A Model Study for DNA Polymerases using a Newly Designed Dinuclear Metal Complex ---- 175
10 A Novel Macrocyclic Terbium Complex Targeting Telomere DNA ---- 175
11 Structure and O_2–Uptake Properties of a Novel Nickel(II) Complex of Pyridyl–Pendant Dioxocyclam ---- 176
12 Metal Assisted Self-Replicating of Small Molecules and DNA ---- 176

F. Stereochemistry of Coordination Compounds and Adsorption Phenomena of Various Gases on Inorganic Solids ---- 176
1 Stereochemistry and Electrochemistry of Cobalt(II) and Cobalt(III) Complexes Containing Optically Active Tetradentate Schiff Base Ligands ---- 176
2 Interconversion between Polymeric Orange and Monomeric Green Forms of a Schiff Base-Oxovanadium(IV) Complex ---- 177
3 Chromatographic Resolusion Mechanism of a Tris(1,10-phenanthroline)-Silicon(IV) Complex ---- 177
4 Mononuclear and Mixed-Valence Trinuclear Manganese Complexes Containing Tripodal Tetradentate Ligands. Phenolato, Carboxylato, and Alkoxo Bridges ---- 177
5 Stabilization of Copper Metal Cluster in Mordenite Nanopores: Water Treatment of Evacuated Copper Ion-Exchanged Mordenite at 300 K ---- 178
6 Characterization of Active Sites on Copper Ion-Exchanged Mordenite for Dinitrogen Adsorption by Using CO as a Probe Molecule ---- 178
7 Specific Feature of Dielectric Behavior of Water Adsorbed on Ag_2O Surface ---- 178

G. Creation of Complexes Containing New Types of Bonds between a Transition Metal and a Phosphorus ---- 179
1 Reactivity of Cationic Phosphenium Complexes of Molybdenum: Migration of OR, SR, and NR_2 on a Tertiary Phosphorus Compound to a Phosphenium Ligand ---- 179
2 Formation of a Six Membered Metallacycle Consisting of Iron, Carbon, Phosphorus, Boron, and Two Oxygens: The First Example of Precedence of Migratory Insertion of CO into an M-C Bond over OR Abstraction from Coordinating Phosphite by BF_3 ---- 179
3 Reaction of Cationic Piano Stool Iron Complexes Containing Phosphorus Ligands with Phosphorus Ylide ---- 179
4 Comparison of the Reactivity of Cationic Phosphenium Complexes of Iron Containing a Group 14 Element Ligand ---- 180

5 A Novel Synthesis, X-ray Crystal Structures and Spectroscopic Properties of Metallated Hypervalent Phosphorus Complexes, $Cp(CO)LFe\{P(OC_6H_4Y)(OC_6H_4Z)\}$ (L = CO, $P(OPh)_3$, PMe_3; Y, Z = NH, NMe, O)---180
6 Migration Reaction of a Hypervalent Fragment: Base-Induced Migration of a Phosphorane Fragment from Iron to the Cyclopentadienyl Ring in $Cp(CO)_2Fe\{P\text{-}(OC_6H_4Y)(OC_6H_4Z)\}$---180

H. Activation of Carbon Dioxide on Metal Complexes---181
1 Seven-Coordinated 2,2':6'2"-Terpyridinemolybdenum(II) Complexes: Synthesis, Structure and Reactivity of $[Mo(CO)(C_7H_8)\text{-}(4,4',4''\text{-}R_3terpy)X]X'$ (R= H or ^{t}Bu)---181
2 *Cis*-μ-1,2-Peroxo Diiron Complex: Structure and Reversible Oxygenation---181
3 Crystal Structure of $[Ru(bpy)_2(CO)(\eta^1\text{-}C(O)OH)]^+$ as a Key Intermediate in CO_2/CO Conversion---182
4 Catalytic Generation of Oxalate through Activation of Two CO_2 Molecules on $[(IrCp^*)_2(Ir\text{-}\eta^4\text{-}Cp^*CH_2CN)(\mu_3\text{-}S)_2]$---182
5 Structural and Electrochemical Comparison of Copper(II) Complexes with Tripodal Ligands---183
6 Control of Coordination Mode of η^1- and η^2 -1,8-Naphthyridine Ligated to Ru(II)-bis(bipyridine) Complexes---183
7 Resonance Equilibrium between Ru^{III}-(catechol) and Ru^{II}(semiquinone) and Stable Electron Localized Form of RuII(quinone) in Ru-dioxolene-terpyridine Complex---183
8 Oxide Transfer Reaction from Carbonate to Metal-CO Complex, Affording Metal-η^1-CO_2 Complex and Carbon Dioxide---183
9 Determination of Basicity of μ_3-X and η^1-Y Ligands (X, Y = S, Se) of Reduced, Oxidized and Super-Oxidized Forms of $[Fe_4X_4\text{-}(YAd)_4]^{2-}$ (Ad = 1-Adamantane) in Aqueous Solutions---184

I. Supramolecular Self-Assembly through Coordination---184
1 On the Structure of Transition Metal-Linked Molecular Squares---184
2 Catenane Formation from Two Molecular Rings through Very Rapid Slippage. A Möbius Strip Mechanism---185
3 Made-to-Order Assembling of [2]-Catenanes from Palladium(II)-Linked Rectangular Molecular Boxes---185
4 A Nano-Sized Macrocycle Constructed From Four Organic Ligands Held Together by Six Metal Ions---185
5 Binding Property of a Coordination Nanocage Self-Assembling From Ten Components---185
6 Coordination Polymers Self-Assembl-ing From Cadmium(II) Ions and Flexible Pyridine-Based Bridging Ligands---186
7 Self-Assembled Molecular Ladders---186
8 A "Swellable" Two-Dimensional Coordination Network---186

J. Multidimensional Crystal Engineering of Supramolecular Metal Complexes---187
1 Double Hydrogen-Bonds and π-π Stacking Assembled Two-Dimensional Copper(I) Complex of 2-Hydroxy- quinoxaline---187
2 Assembly of a Mixed-Valence Cu(I/II) System Coupled by Multiple Hydrogen Bondings through Tetrahydroxybenzoquinone---187
3 S···S Contact Assembled Silver(I) Complexes of 4,5-Ethylenedithio-1,3-dithiole-2-thione Having Unique Supramolecular Networks---187
4 Syntheses, Structures and Properties of Linear Copper(I) Coordination Polymers with Tetrakis(ethylthio)tetrathiafulvalene and Tetrakis(propylthio)tetrathia-fulvalene---188
5 Two Types of New Polymeric Copper(I) Complexes of Pyrazinecarboxamide Having Channel and Helix Structures---188
6 A S···S Contact Assembled Tetranuclar Copper(I) Complex with Sulfur-Rich Ligand, 4,5-Ethylenedithio-1,3-dithiole-2-thione---188
7 Construction and Conductivity of W-Type Sandwich Silver(I) Polymers with Pyrene and Perylene---189
8 Synthesis and Structure of a Three-Dimensional Copper(II) Coordination Polymer with 1,2-Bis(imidazol-1'-yl)ethane---189
9 Crystal Engineering of Multidimensional Copper(I) and Silver(I) Coordination Supermolecules and Polymers with Functions---189
10 The Solid and Solution Structures of Ternary Gold(I) Complexes with Triphenylphosphine and N- Ligands---190

K. Interconversion between Monomeric and its Self-Assembled Oligomeric Metal Complexes---190

1 Proton-Dependent Monomer ↔ Oligomer Interconversion of Copper(II) Complexes with *N*-(2-Substituted-imidazol-4-ylmethylidene)-2-aminoethylpyridine (2-Substituent = Methyl and Phenyl) ---- 190
2 Steric-Hindrance Effect of a Substituent in the Self-Assembly Process of Copper(II) Complexes with Quadridentate Schiff-Base Ligands Involving a 2-Substituted-Imidazole Moiety ---- 192
3 Copper(II) Complexes of *N*, *N'*-Bis(2-substituted-imidazol-4-ylmethylene)-3, 3'-diaminodipropylamine (2-Substituent=H, Me): Δ and Λ Enantiomorphs of the Protonated Complex and Helical Structure of the Deprotonated Complex Formed by Hydrogen Bonds ---- 193

L. Synthesis and Reactivity of Complexes Containing Peculiar Bonds between Transition Elements and Main Group Elements of Group 14 ---- 194
1 Iridium-Catalyzed Redistribution of Hydrodisilanes *via* a Silyl(silylene)iridium(III) Complex: Synthesis of a Donor-Stabilized Silyl(silylene)iridium(III) Complex ---- 195
2 Reactivity of a Donor-Stabilized Bis(silylene)ruthenium Complex toward Nucleophiles ROH (R = Me, H) ---- 195
3 Reaction of Silyl(carbonyl)iron Complexes with $LiAlH_4$ Giving Methylsilanes: Reduction of a Carbonyl Ligand and Coupling with a Silyl Group ---- 196

RESEARCH ACTIVITIES VIII

Computer Center

A. Theoretical Studies of Highly Excited Vibrational States in Polyatomic Molecules ---- 197
1 Theoretical Study of the Photodissociation Dynamics of OCS ---- 197
2 Semiclassical Study of Avoided Crossing ---- 197
3 Theoretical Study of the Potential Energy Surfaces and Dynamics of CaNC/CaCN ---- 197
4 Theoretical Study of Elementary Reactions Relevant to Low-Temperature Silane Oxidation ---- 197
5 Theoretical Study of Reaction Rate Constant of Hydrofluorocarbon ---- 197

Laser Research Center for Molecular Science

B. Developments and Researches of New Laser Materials ---- 199
1 Nanosecond Pump-and-Probe Study of Wurtzite GaN ---- 199
2 14-mJ Ultraviolet Short Pulses from an All-Solid-State Ce:LiCaF Master Oscillator and Power Amplifier System ---- 199
3 High Average Power THz-Radiation from Femtosecond-Laser Irradiated InAs in a Magnetic Field and Its Elliptical Polarization Characteristics ---- 199

Research Center for Molecular Materials

C. Preparation and Properties of Novel Heterocyclic Compounds for Advanced Materials ---- 201
1 Unusual Cation Radical Salts of Non-Planar Bis(1,3-dithiole) Donors Incorporating Solvent Molecules ---- 201
2 Crystal Structure of Cation Radical Salts of Non-Planar Bis(1,3-dithiole) Donors ---- 201
3 Novel Bis(1,3-dithiole) Electron Donors by Oxidative Intramolecular Cyclization of 2,2'-Bis(1,4-dithiafulven-6-yl)-3,3'-bithienyls ---- 202
4 Preparation, Properties, and Oxidation of Novel Bis(1,3-dithiole) Compounds Containing a Di(2-thienyl)methane Unit ---- 202
5 Synthesis and Reactions of 3,3'-Dibromodihydrodipyrrins ---- 203
6 Synthesis and Properties of Benzobis(thiadiazole)s with Nonclassical π-Electron Ring Systems ---- 203
7 A Novel Building Unit for Single Molecular Wires Based on *N*-Silylated Diaminothiophene ---- 203

D. Studies of Nanoscale Carbons ---- 204
1 Apparatus for High Yield Production of Single Wall Carbon Nanotube using Pulsed Laser Vaporization Method ---- 204
2 Effect of Target Temperature for Yielding of Single Wall Carbon Nanotubes ---- 205
3 Diameter-Selective Raman Scattering from Vibrational Modes in Carbon Nanotubes ---- 205
4 Evidence for Charge Transfer in Doped Carbon Nanotube Bundles from Raman Scattering ---- 206
5 Purification of Single Wall Carbon Nanotubes by Microfiltration ---- 206
6 Magnetic Properties of Purified Multi- and Single-Wall Carbon Nanotubes ---- 206

E. The Applications of a Magic-Angle Turning Technique for Half-Integer Quadrupolar Nuclei ---- 207
1 Spinning-Sideband Suppression in DOR NMR Spectra Using a Magic-Angle-Turning Technique ---- 207

Equipment Development Center

F. Activities of Division of "IMS Machines" ---- 208
1 Ultra-Thin-Window Optical Cell ---- 208
2 High Precision Slit Driver for Ultra-High-Vacuum Monochromator ---- 208
G. Development of Experimental Devices ---- 209
1 New Apparatus for the Precise Temperature Control of ^{3}He Refrigerator ---- 209

Ultraviolet Synchrotron Orbital Radiation Facility

H. Development of the UVSOR Light Source ---- 210
1 Development of the Transverse Resonance Kicker ---- 210
I. Development of Beam Lines and Equipment for UVSOR ---- 210
1 Construction and Performance Test of SGM-TRAIN at UVSOR ---- 210
J. Researches by the USE of UVSOR ---- 210
1 Desorption of H Ions from Water Chemisorbed on Si(100) by O-1s Excitation - An Auger Electron-Photoion Coincidence Spectroscopy study ---- 210
2 Photoelectron Spectroscopic Study of Coadsorbed States of Cs and O on GaAs(100) ---- 210
3 Combined Systems of SR and Laser for Solid-State Researches ---- 211
4 Resonant Photoemission Studies of Thulium Monochalcogenides around the Tm 4*d* Threshold ---- 211
5 Resonant Photoemission Studies of Thulium Monochalcogenides around the Tm 3*d* Threshold ---- 211
6 Core Level Photoemission Spectroscopy and the Resonance Behavior of Mixed-Valence Tm Monochalcogenides ---- 212
7 Optical Study on Heavy Fermion and Mixed Valence in Yb_4As_3 ---- 213
8 Photoabsorption Spectrum of Ozone in the K-Edge Region ---- 213
9 Mixed Valence of Yb_3S_4 ---- 213

RESEARCH FACILITIES

Computer Center ---- 214
Laser Research Center for Molecular Science ---- 214
Research Center for Molecular Materials ---- 214
Equipment Development Center ---- 214
Division of IMS Machines ---- 214
Ultraviolet Synchrotron Orbital Radiation Facility ---- 214

SPECIAL RESEARCH PROJECTS

(1) Development of Microscopic Environments with Functionality and Quantum Steering for Reactions ---- 216
Structures, Reactions and Spectroscopies of Molecules and Molecular Clusters ---- 216
Prediction of Protein Tertiary Structures by Generalized-Ensemble Algorithms ---- 216
Quantum Mechanical and Semiclassical Studies of Chemical Dynamics ---- 216
Fifth-Order Two-Dimensional Vibrational Spectroscopy of a Morse Potential System in Condensed Phases ---- 217
Constructing Molecular Theory of Chemical Processes in Solution ---- 217
Development of High-Sensitivity Submilli-meter-Wave to Far Infrared Spectrometer Systems for the Study of Transient Molecules ---- 217
(1) Studies on Laser Cooling and Trapping of Neutral Atoms
(2) Laser Spectroscopic Studies of Ions in Liquid Helium ---- 218
Mechanism of Oxygen Activation by Heme-Copper Terminal Oxidase Superfamily ---- 218
Laser Raman Beat Detection of Magnetic Resonance ---- 218
Liquid Dynamics Studied by New Ultrafast Nonlinear Spectroscopy ---- 219
Studies of Laser-Induced Photochemistry on Solid Surfaces ---- 219
Higher Vibrational States of Molecules and Clusters as Studied by Nonresonant Ionization Detected IR Spectroscopy ---- 219
Laser Investigation of Elementary Reactions in the Gas Phase ---- 220
Light Induced Intermolecular Charge Trans-port in Organic Insulator Systems ---- 220
Photoabsorption and Photofragmentation of Triiodide Anion: Gas-Phase Analogue to I_3^- in Solution ---- 220
Time-Resolved Spectroscopic Studies on Chemical Reactions Using Ultrafast Laser and Synchrotron Radiation ---- 221
Development of UHV-STM System for Study of Surface Photochemical Reactions Induced by Synchrotron Radiation ---- 221
Pump-Probe Spectroscopy of Atoms and Molecules with the Combination of an Ultraviolet Laser and Synchrotron Radiation ---- 222
Vibrational Spectroscopy on Cryogenic Surfaces using Synchrotron Radiation ---- 222

Rotation Induced Vibrational Mixing in Highly Excited Vibrational States of Formaldehyde ---- 223
Developments and Researches of New Laser Materials ---- 223
Ultra-High-Vacuum Friction Test Apparatus ---- 223
Investigation of Electronic Structures of Solid/ Surface by Using Synchrotron Radiation ---- 223
Study for High Brilliant Radiation Using the UVSOR Electron Storage Ring ---- 224
Studies of Solid Surfaces by Photoelectron Spectroscopy ---- 224
(2) Study of Molecular Solid toward Molecular Electronics ---- 225
Theory of Electronic Phases in Molecular Conductors and Insulators: Electron Correlations in Quasi-One-Dimensional Systems ---- 225
Materials Science on Molecular Devices π-d Interaction in Molecular Metals ---- 225
Search for Negative-U Materials in Molecular Solid ---- 226
Toward Comprehensive Understanding of Various Electronic Phases in Molecular Conductors; Role of Long-Range Coulomb Repulsion ---- 226
Development of New Organic Metals and Superconductors ---- 227
High Pressure Structures of Molecular Conductors ---- 227
NMR Study of Liquid Crystals ---- 227
Solid State NMR Studies of Hydrogen-Bonded Dielectrics and C_{60}-Based Superconductors ---- 227
Pressure Effect on Molecule-Based Magnetic Materials ---- 227
Quantitative Analysis of Organic Thin Films Using Angle-Resolved UPS ---- 228
Construction of UV-Inverse Photoemission Spectrometer and Measurements of Conduction Band DOS of Transparent Conducting Oxides ---- 228
New Organic Materials Based on Novel Heterocyclic Compounds ---- 228
(3) Material Control in Multi-Reaction Centers ---- 229
Conversion of Myoglobin into a Peroxygenase: A Catalytic Intermediate of Sulfoxidation and Epoxidation by the F43H/H64L Mutant ---- 229
Molecular Assembly on Surface through Coordination Bonds Towards Solution-Phase Molecular Epitaxy ---- 229
Assembled Metal Centers in Enzymes ---- 229
Metal Assisted Control and Functionalization of Biomolecules ---- 230
Activation of Carbon Dioxide on Metal Complexes Directed Toward Carbon-Carbon Bond Formation ---- 230
Self-Assembling Molecular Systems ---- 230
OKAZAKI CONFERENCES ---- 232
JOINT STUDIES PROGRAMS
(1) Special Projects ---- 236
(2) Research Symposia ---- 239
(3) Cooperative Research ---- 239
(4) Use of Facilities ---- 240
(5) UVSOR ---- 240
FOREIGN SCHOLARS ---- 241
AWARDS ---- 245
LIST OF PUBLICATIONS ---- 247
REVIEW ARTICLES AND TEXTBOOKS ---- 263
AUTHOR INDEX TO RESEARCH ACTIVITIES AND SPECIAL RESEARCH PROJECTS ---- 265

ORGANIZATION AND STAFF

Organization

The Institute for Molecular Science comprises twenty three research laboratories —each staffed by a professor, an associate professor, two research associates and several technical associates—, two research laboratories with foreign visiting professors, and five research facilities. The laboratories are grouped into six departments and one facility for coordination chemistry:

Department of Theoretical Studies	Theoretical Studies I
	Theoretical Studies II
	Theoretical Studies III[1)]
	Theoretical Studies IV
Department of Molecular Structure	Molecular Structure I
	Molecular Structure II[1)]
	Molecular Dynamics
Department of Electronic Structure	Excited State Chemistry
	Excited State Dynamics
	Electronic Structure[1)]
	Molecular Energy Conversion[2)]
Department of Molecular Assemblies	Solid State Chemistry
	Molecular Assemblies Dynamics
	Molecular Assemblies[1)]
Department of Applied Molecular Science	Applied Molecular Science I
	Applied Molecular Science II[1)]
	Molecular Clusters[3)]
Department of Vacuum UV Photoscience	Photochemistry
	Chemical Dynamics
	Interface Molecular Science[3)]
	Synchrotron Radiation Research[2)]
Coordination Chemistry Laboratories	Synthetic Coordination Chemistry[3)]
	Complex Catalysis
	Functional Coordination Chemistry
	Coordination Bond[1)]
Research Facilities are:	Computer Center
	Chemical Materials Center (-March '97)
	Instrument Center (-March '97)
	Low-Temperature Center (-March '97)
	Laser Research Center for Molecular Science (April '97-)
	Research Center for Molecular Materials (April '97-)
	Equipment Development Center
	UVSOR (Ultraviolet Synchrotron Orbital Radiation) Facility

1) Professors and associate professors are visiting professors from other universities.
2) Research laboratories with foreign visiting professors.
3) Professors, associate professors, and research associates, along with their positions, are transferred from other universities.

Scientific Staff

Mitsuo ITO	**Professor, Director-General**

Emeritus Professors

Saburo NAGAKURA	President, The Kanagawa Academy of Science and Technology
Eizi HIROTA	President, The Graduate University for Advanced Studies
Katsumi KIMURA	Professor, Japan Advanced Institute of Science and Technology
Keiji MOROKUMA	Professor, Emory University, U.S.A.
Hiroo INOKUCHI	Distinguished Research Consultant, Institute for Molecular Science
Yusei MARUYAMA	Professor, Hosei University
Keitaro YOSHIHARA	Professor, Japan Advanced Institute of Science and Technology
Ichiro HANAZAKI	Professor, Hiroshima University
Hiizu IWAMURA	Professor, Kyushu University

Department of Theoretical Studies

Theoretical Studies I

Suehiro IWATA	Professor
Yuko OKAMOTO	Associate Professor
Tsutomu IKEGAMI	Research Associate
Ulrich HANSMANN	Research Associate
Takeshi TSURUSAWA	Technical Associate
Masato MASUYA	IMS Fellow
Toshiaki MATSUBARA	IMS Fellow (December '96- March '97)
Feiwu CHEN	IMS Fellow (June '97-)
Andreas FIEDLER	Visiting Scientist; JSPS Post-Doctoral Fellow
Katsuhiko SATOH	JSPS Post-Doctoral Fellow (April '97-)
Toshiaki FUJII	Graduate Student (-September '96)
Hidekazu WATANABE	Graduate Student (-March '97)[1]
Pradipta BANDYOPADHYAY	Graduate Student
Ayori MITSUTAKE	Graduate Student (from Nara Women's University)* (-March '97), Graduate Student (April '97-)
Tadayoshi SUZUKI	Graduate Student (from Waseda University)* (-March '97), Graduate Student (April '97-)
So HIRATA	Graduate Student (April '97-)
Hiroshi OHTSUKA	Graduate Student (April '97-)
Kazutoshi OKADA	Graduate Student (April '97-)
Yumin LI	Visiting Scientist; JSPS Post-Doctoral Fellow (June '95-May '97), Visiting Scientist (June '97-)
Jan HRUSAK	Visiting Scientist (from J. Heyrousky Institute of Physical Chemistry Academy of Sciences of the Czech Republic, Czech); MONBUSHO Invited Fellow (-December '96)[2]
Patrizio SEVERINO	Visiting Scientist; EC Fellow
Yehuda B. BAND	Visiting Scientist (from Ben-Gurion University, Israel); JSPS Invited Fellow (January-February '97)[3]
Sourav PAL	Visiting Professor (from National Chemical Laboratory, India) (March '97-)

Theoretical Studies II

Hiroki NAKAMURA	Professor
Yoshitaka TANIMURA	Associate Professor
Chaoyuan ZHU	Research Associate
Ko OKUMURA	Research Associate
Yoko SUZUKI	Technical Associate
Oleg Isaakovich TOLSTIKHIN	IMS Fellow
Gautam GANGOPADHYAY	Visiting Scientist; JSPS Post-Doctoral Fellow (March '97-)
Miyabi HIYAMA	Graduate Student (-September '96)[4]
Yutaka MARUYAMA	Graduate Student

Yutaka IMAMURA	Graduate Student
Yoshiaki TERANISHI	Graduate Student
Henrik SZICHMAN	Visiting Professor (from Soreq Nuclear Research Institute, Israel) (-September '96)[5]
Jiri HORACEK	Visiting Professor (from Charles University, Czech Republic) (October '96- January '97)[6]
Valentine N. OSTROVSKY	Visiting Professor (from the University of St.Petersburg, Russia) (October '96- July '97)[7]
Inna YOUROVA	Visiting Scientist (from the University of St. Petersburg, Russia) (October '96- July '97)[8]
Rob D. COALSON	Visiting Scientist (from University of Pittsburgh, USA); JSPS Invited Fellow (-December '96)[9]
Minhaeng CHO	Visiting Scientist (from Korea University, Korea); MONBUSHO Invited Fellow (July- August '97)[10]
Jose N. ONUCHIC	Visiting Scientist (from University of California, USA); MONBUSHO Invited Fellow (August '97-)

Theoretical Studies III

Shigeki MITAKU	Visiting Professor (from Tokyo University of Agriculture and Technology) (-March '97)[11]
Toyonori MUNAKATA	Visiting Professor (from Kyoto University) (April '97-)
Atsunari HIRAYA	Visiting Associate Professor (from Hiroshima University) (-March '97)[12]
Masao OGATA	Visiting Associate Professor (from the University of Tokyo) (April '97-)
Seiichiro TEN-NO	Research Associate
Katsuyuki NOBUSADA	Research Associate

Theoretical Studies IV

Fumio HIRATA	Professor
Kenji YONEMITSU	Associate Professor
Hirofumi SATO	Research Associate
Jun-ichiro KISHINE	Research Associate (September '96-)
Ryo AKIYAMA	IMS Fellow (October '96- March '97), JSPS Post-Doctoral Fellow (April '97-)
Michiyasu MORI	IMS Fellow (April '97-)
Takuhiro OGAWA	JSPS Post-Doctoral Fellow (April '97-)
Takashi IMAI	Graduate Student (April '97-)
Xin SUN	Visiting Professor (from Fudan University, China) (July '97-)

Department of Molecular Structure

Molecular Structure I

Shuji SAITO	Professor
Norio MORITA	Associate Professor
Yoshiki MORIWAKI	Research Associate
Hideo FUJIWARA	IMS Fellow (-November '96), Research Associate (December '96-)
Mitsutaka KUMAKURA	Technical Associate
Kaori KOBAYASHI	Technical Associate
Imtiaz K. AHMAD	Visiting Scientist; JSPS Post-Doctoral Fellow
Tsuyoshi HIRAO	Graduate Student (-March '97), Research Fellow (April-July '97)[13]
Kei-ichi NAMIKI	Graduate Student (-March '97), Research Fellow (April-September '97)[14]
Naomi INADA	Graduate Student (from Hiroshima University)* (-March '97)[15]
Mitsunori ARAKI	Graduate Student

Molecular Structure II

Isao MORISHIMA	Visiting Professor (from Kyoto University) (-March '97)
Mitsutoshi TANIMOTO	Visiting Professor (from Shizuoka University) (April '97-)
Hideto KANAMORI	Visiting Associate Professor (from Tokyo Institute of Technology)
Takashi OGURA	Research Associate

Hiroyuki OZEKI	Research Associate

Molecular Dynamics

Teizo KITAGAWA	Professor
Tatsuhisa KATO	Associate Professor
Michio MATSUSHITA	Research Associate
Yasuhisa MIZUTANI	Research Associate
Masahiro MUKAI	Research Associate (-March '97)[16]
Naoki HAYASHI	Technical Associate
Shigeki NAGATOMO	Technical Associate
Yong-Rok KIM	Visiting Scientist; MONBUSHO Invited Fellow (December '96- February '97)[17]
Jörg MATYSIK	Visiting Scientist; JSPS Post-Doctoral Fellow (-June '97)[18]
Xiaojie ZHAO	Visiting Scientist (-March '97)[19]
Kruglik SERGEI	Visiting Scientist (February '97-)
Tadashi IWASE	Graduate Student
Takeshi TOMITA	Graduate Student
Yuki UESUGI	Graduate Student
Michihiko AKI	Graduate Student
Koji YAMAMOTO	Graduate Student
Akiko MUTO	Graduate Student (from Kitazato University)* (October '96-)

Department of Electronic Structure

Excited State Chemistry

Keitaro YOSHIHARA	Professor (-March '97)[20]
Yoshiyasu MATSUMOTO	Associate Professor (-March '97), Professor (April '97-)[21]
Keisuke TOMINAGA	Research Associate
Kazuya WATANABE	Research Associate (April '97-)
Shigeichi KUMAZAKI	Technical Associate (-March '97)[22]
Kazuo WATANABE	Technical Associate
Toshihisa ANAZAWA	JSPS Post-Doctoral Fellow
Igor V. RUBTSOV	IMS Fellow (-March '97)[23]
Hiroyuki KATO	Graduate Student (-September '96), JSPS Post-Doctoral Fellow (October '96- March '97)[24]
Ken-ichi SAITOW	Graduate Student (-March '97)[25]
Hideaki SHIROTA	Graduate Student (-December '96)[26]
Kaoru OHTA	Graduate Student (from Kyoto University)*
Kentaro KOSUGI	Graduate Student (April '97-)
Ikuo KINOSHITA	Visiting Scientist (from Yokohama City University) (-March '97)
Narayanan GAYATHRI	Visiting Scientist (from Indian Institute of Science, India); JSPS Invited Fellow (-September '96)
Tai Jong KANG	Visiting Scientist (from Taegu University, Korea) (December '96- February '97)
Neil A. SMITH	Visiting Graduate Student (from University of East Anglia, UK) (January- March '97)
Stephen R. MEECH	Visiting Scientist (from University of East Anglia, UK) (March- April '97)

Excited State Dynamics

Ichiro HANAZAKI	Professor (-March '97)[27]
Masaaki FUJII	Professor (April '97-)
Toshinori SUZUKI	Associate Professor
Kenichi TONOKURA	Research Associate (-March '97)[28]
Suketu R. GANDHI	Research Associate (-March '97)
Hideki KATAYANAGI	Technical Associate
Akiko KAMINAGA	Technical Associate
Noriaki OKAZAKI	IMS Fellow (-March '97)[29]
Gyula RÁBAI	JSPS Fellow (-November '96)[30]
Hiroshi KOHGUCHI	Visiting Scientist (-October '96), IMS Fellow (October '96-)
Yuxiang MO	JSPS Post-Doctoral Fellow (April '97-)
Nobuhisa HASHIMOTO	Graduate Student (-September '96)[31]
Takeshi SHIBATA	Graduate Student
Shun-ichi ISHIUCHI	Graduate Student (from Waseda University)*

Kazunari SUZUKI	Graduate Student (from Waseda University)*
Ruriko YOSHINO	Graduate Student (from Waseda University)*
Yang SHI	Visiting Scientist (from Institute of Chemistry, Chinese Academy of Sciences, China); JSPS Invited Fellow (-November '96), Visiting Scientist (November '96- April '97)[32]
Christian GEBAUER	Visiting Scientist (January '97-)
Haiyang LI	Visiting Scientist (from Dalian Institute of Physics, China) (June '97-)
Electronic Structure	
Kinichi OBI	Visiting Professor (from Tokyo Institute of Technology)
Yoshio TEKI	Visiting Associate Professor (from Osaka City University) (-March '97)
Masao TAKAYANAGI	Visiting Associate Professor (from Tokyo University of Agriculture and Technology) (April '97-)
Yukito NAITOH	Research Associate (-June '97)[33]
Nobuaki TANAKA	Research Associate (-September '96)[34]
Molecular Energy Conversion	
Oleg VASYUTINSKII	Visiting Professor (from Russian Academy of Science) (July '97-)
Department of Molecular Assemblies	
Solid State Chemistry	
Kyuya YAKUSHI	Professor
Kazushi KANODA	Associate Professor[35]
Akito UGAWA	Research Associate
Yasuhiro NAKAZAWA	Research Associate
Ken-ichi IMAEDA	Technical Associate
Kazuya MIYAGAWA	Technical Associate
Mikio URUICHI	Technical Associate
Makoto INOKUCHI	JSPS Post-Doctoral Fellow (-October '96)[36]
Yukako YONEHARA	Graduate Student
Jianyong OUYANG	Graduate Student (October '96-)
Hiromi TANIGUCHI	Graduate Student (-March '97)[35]
Ko-ichi HIRAKI	Graduate Student (-March '97)[35]
Valery A. IVANOV	Visiting Scientist (from Kurnakov Institute of General and Inorganic Chemistry of Russian Academy of Science, Russia); MONBUSHO Invited Fellow (-November '96)[37]
Iakov KOGAN	Visiting Scientist (from Institute of Chemical Physics of Russian Academy of Sciences); MONBUSHO Invited Fellow (September '96-August '97)
Jian DONG	Visiting Scientist (-May '97)[38]
Tian FULI	Visiting Scientist (from Inner Mongolia University) (May-July '97)[39]
Chikako NAKANO	Visiting Scientist
Molecular Assemblies Dynamics	
Hayao KOBAYASHI	Professor
Seiichi MIYAJIMA	Associate Professor
Hironori OGATA	Research Associate
Hideki FUJIWARA	Research Associate
Osamu OISHI	Technical Associate
Hiroki AKUTSU	IMS Fellow
Takafumi ADACHI	IMS Fellow (April '97-)
Hiroki FUJIMORI	JSPS Post-Doctoral Fellow (-March '97)[40]
Akane SATO	Graduate Student
Emiko ARAI	Graduate Student (April '97-)
Molecular Assemblies	
Hidetoshi FUKUYAMA	Visiting Professor (from the University of Tokyo) (-March '97)[41]
Takashi NOGAMI	Visiting Professor (from The University of Electro-Communications) (April '97-)

Masahiro YAMASHITA	Visiting Associate Professor (from Nagoya University) (-March '97)[42]
Sadamu TAKEDA	Visiting Associate Professor (from Gunma University) (April '97-)
Shinji HASEGAWA	Research Associate
Tomoyuki MOCHIDA	Research Associate (-March '97)[43]

Department of Applied Molecular Science

Applied Molecular Science I

Yoshihito WATANABE	Professor
Katsuya INOUE	Associate Professor
Kwang-Hyun AHN	Visiting Associate Professor (from Kyung Hee University, Korea); MONBUSHO Invited Scientist (December '96-February '97)[44]
Sutter Jean PASCAL	Visiting Associate Professor (from CNRS (Toulouse), France); MONBUSHO Invited Scientist (December '96-March '97)[45]
Shin-ichi OZAKI	Research Associate
Yuko HOSOKOSHI	Research Associate
Ashot S. MARKOSYAN	Visiting Scientist (from Moscow State University, Russia); JSPS foreign researcher (March '97-)
Senji WADA	IMS Fellow (-April '97)[46]
Hitoshi KUMAGAI	IMS Fellow (April '97-)
Huijun YANG	Visiting Scientist (from Beijing Health School, China) (-March '97)[47]
Keiichi KATOH	Visiting Scientist (from Science University of Tokyo) (April '97-)
Toshitaka MATSUI	Graduate Student
Yoshio GOTO	Graduate Student
Minoru MITSUMI	Graduate Student (-March '97)[48]
Koichi TAMAKI	Graduate Student
Fumiyasu IWAHORI	Graduate Student (April '97-)
Takako KUGA	Graduate Student (April '97-)
Miki KANAZAWA	Graduate Student (April '97-)

Applied Molecular Science II

Toyonari SUGIMOTO	Visiting Professor (from Research Institute for advanced Science and Technology, Osaka Prefecture University)
Koshiro TORIUMI	Visiting Associate Professor (from Himeji Institute of Technology) (-March '97)[49]
Norio SAITOH	Visiting Associate Professor (Electrotechnical Laboratory) (April '97-)
Seiji OGO	Research Associate

Molecular Clusters

Nobuyuki NISHI	Professor
Takashi NAGATA	Associate Professor
Kazuhiko OHASHI	Research Associate
Lei ZHU	Research Associate
Yoshiya INOKUCHI	Graduate Student (from Kyushu University)*
Morihisa SAEKI	Graduate Student (from the University of Tokyo)*
Masaharu NISHIGUCHI	Graduate Student (from Kyushu University)* (April '97-)

Department of Vacuum UV Photoscience

Photochemistry

Nobuhiro KOSUGI	Professor
Tahei TAHARA	Associate Professor
Yasutaka TAKATA	Research Associate
Satoshi TAKEUCHI	Research Associate
Haruhiko OHASHI	Technical Associate (-October '96)[50]
Jun-ichi ADACHI	Technical Associate
Shigeki MATSUO	IMS Fellow (-March '97)[51]
Atsuhiko SHIMOJIMA	IMS Fellow
Misa KAYAMA	Graduate Student
Takaki HATSUI	Graduate Student

Sae Chae JEOUNG	Visiting Scientist (from KRISS, Korea) (July '97-)
Chemical Dynamics	
Tsuneo URISU	Professor
Koichiro MITSUKE	Associate Professor
Kazuhiko MASE	Research Associate
Hiroaki YOSHIDA	Research Associate (-June '97)[52]
Yoshiyuki TSUSAKA	Research Associate (-September '96)[53]
Hideo HATTORI	Technical Associate
Mitsuru NAGASONO	Technical Associate
Masakazu MIZUTANI	IMS Fellow (-May '97), Visiting Scientist (June '97-)
Gheyas Syed IRFAN	Visiting Scientist (-November '96), IMS Fellow (November '96- March '97), MONBUSHO Invited Fellow (July '97-)
Takayuki MIYAMAE	IMS Fellow (April '97-)
Yasumasa HIKOSAKA	Graduate Student (from Tokyo Institute of Technology) (-March '97), IMS Fellow (April '97-)
Yoshiaki IMAIZUMI	Graduate Student (-March '97)[54]
Shinya HIRANO	Graduate Student
Harutaka MEKARU	Graduate Student
Hiromichi NIIKURA	Graduate Student (April '97-)
Hideyuki NODA	Graduate Student (from Meijo University) (April '97-)
Noriaki HORIO	Graduate Student (from Meijo University) (April '97-)
Interface Molecular Science	
Toshio IBUKI	Professor (-March '97)[55]
Nobuo UENO	Professor (April '97-)
Hideo HOSONO	Associate Professor (-March '97)[56]
Makoto SAKURAI	Associate Professor (April '97-)
Naoyuki UEDA	Research Associate (-March '97)[57]
Hisao ISHII	Research Associate (-March '97)[58]
Masuaki MATSUMOTO	Research Associate (April '97-)
Youichi NONOGAKI	Research Associate (April '97-)
Kazumasa OKADA	IMS Fellow (-March '97)[59]
Mitsuhiko KONO	JSPS Post-Doctoral Fellow (School of Chemistry, University of Bristol) (-March '97)[60]
Kazushige UEDA	Graduate Student (from Tokyo Institute of Technology) (-March '97)[61]
Masafumi MIZUGUCHI	Graduate Student (from Tokyo Institute of Technology) (-March '97)[62]
Hiroshi YANAGI	Graduate Student (from Tokyo Institute of Technology) (-March '97)
Masaru AOKI	Visiting Scientist (April '97-)
Eisuke ITO	Visiting Scientist (April '97-)
Yasushi AZUMA	Graduate Student (April '97-)
Daisuke YOSHIMURA	Graduate Student (April '97-)
Synchrotron Radiation Research	
Enrique J. SZICHMAN	Visiting Professor (from Soreq Nuclear Research Institute, Israel) (-September '96)[63]
Jiri HORACEK	Visiting Professor (from Charls University, Czecho) (October- December '96)[64]
Jean-Pierre BAYLE	Visiting Professor (from University of Paris-Sud, France) (January- May '97)[65]
Xin SUN	Visiting Professor (from Fudan University, China) (July '97-)
Michail A. TEREKHIN	Visiting Professor (from Kurchatov Institute, Russia) (October '96-)
Coordination Chemistry Laboratories	
Koji TANAKA	Director
Synthetic Coordination Chemistry	
Masa-aki HAGA	Professor
Takeshi SAKURAI	Associate Professor
Hideaki MONJUSHIRO	Research Associate

Hidemi NAGAO	Research Associate
Yasushi KAWATA	IMS Fellow (April '97-)
Kazumasa HARADA	IMS Fellow (-January '97)[66]
Ke-zhi WANG	JSPS Post-Doctoral fellow (April '97-)
Hun-gi HONG	Visiting Scientist (from Sejong University, Korea) (June-August '97)[67]
Nobuhiko SAKURAI	Graduate Student (from Kanazawa University)*
Hong-wei HUANG	Graduate Student (from Kanazawa University)*
Isao HARA	Graduate Student (from Kanazawa University)*
Hiroki MATSUMOTO	Graduate Student (from Nagoya University)*
Hideyuki KUMITA	Graduate Student (from Nagoya Institute of Technology)*
Itsuko MURATA	Graduate Student (from Mie University)* (-March '97)
Delower Md. HOSSAIN	Graduate Student (from Mie University)*

Complex Catalysis

Mitsuhiko SHIONOYA	Professor
Yuzo YOSHIKAWA	Visiting Professor (from Okayama University)
Hiroshi NAKAZAWA	Visiting Associate Professor (from Hiroshima University)
Luigi Gaetano MARZILLI	Visiting Scientist (from Emory University, U.S.A.) (February- August '97)[68]
Patricia Ann MARZILLI	Visiting Scientist (from Emory University, U.S.A.) (June-August '97)[69]
Jik CHIN	Visiting Scientist (from McGill University, Canada) (June-August '97)[70]
Kentaro TANAKA	Research Associate
Akio OJIDA	IMS Fellow (-March '97)[71]
Michito SHIOTSUKA	IMS Fellow (-March '97)[72]
Motoyuki TASAKA	Graduate Student
Hiromasa MORISHITA	Graduate Student (April '97-)
Kazuki SHIGEMORI	Graduate Student (April '97-)
Akihiko HATANO	Graduate Student (April '97-)

Functional Coordination Chemistry

Koji TANAKA	Professor
Makoto FUJITA	Associate Professor
Kiyoshi TSUGE	Research Associate
Takahiro KUSUKAWA	Research Associate (July '97-)
Tetsunori MIZUKAWA	Technical Associate
Hideki SUGIMOTO	IMS Fellow (April '97-)
Shu-yan YU	Visiting Scientist (July-August '97)
Masaru AOYAGI	Graduate Student (April '97-)
Fumiaki IBUKURO	Graduate Student (April '97-)
Md. Meser ALI	Graduate Student (from Mie University)

Coordination Bond

Megumu MUNAKATA	Visiting Professor (from Kinki University) (-March '97)
Naohide MATSUMOTO	Visiting Professor (from Kyushu University) (-March '97)[73]
Ginya ADACHI	Visiting Professor (from Osaka University) (April '97-)
Hiromi TOBITA	Visiting Associate Professor (from Tohoku University) (April '97-)

Research Facilities

Computer Center

Suehiro IWATA	Director
Mutsumi AOYAGI	Associate Professor
Shinkoh NANBU	Research Associate
Toshiya TAKAMI	Research Associate
Satoshi MINAMINO	Technical Associate
Kouichi MOGI	IMS Fellow (-March '97)
Masakatsu ITO	IMS Fellow (April '97-)
Takeshi NISHIKAWA	Graduate Student (from Keio University)
Albert F. WAGNER	Visiting Scientist (from Argonne National Laboratory, U.S.A.) (January- April '97)[74]

Laser Research Center for Molecular Science

Shuji SAITO	Director
Nobuhiko SARUKURA	Associate Professor
Hideyuki OHTAKE	Research Associate
Takashi AZUHATA	IMS Fellow (April '97-)
Shinji IZUMIDA	Graduate Student
Zhenlin LIU	Graduate Student

Research Center for Molecular Materials

Hayao KOBAYASHI	Director
Yoshiro YAMASHITA	Associate Professor
Shoji TANAKA	Research Associate
Shunji BANDOW	Research Associate
Daisuke KUWAHARA	Research Associate
Masaaki TOMURA	Technical Associate
Chitoshi KITAMURA	JSPS Post-Doctoral Fellow (-March '97)[75]
Akira OHTA	JSPS Post-Doctoral Fellow (-March '97)[76]
Kazuharu SUZUKI	Graduate Student

Equipment Development Center

Teizo KITAGAWA	Director
Michio WATANABE	Associate Professor
Shuji ASAKA	Research Associate

Ultraviolet Synchrotron Orbital Radiation Facility

Nobuhiro KOSUGI	Director
Masao KAMADA	Associate Professor
Toyohiko KINOSHITA	Associate Professor
Hiroyuki HAMA	Associate Professor
Kazutoshi FUKUI	Visiting Associate Professor (from Fukui Univ.) (-March '97)
Hitoshi TANAKA	Visiting Associate Professor (from SPring-8) (April '97-)
Aleksandr LUSHCHICK	Visiting Associate Professor (from Estonian Academy) (- September '96)[77]
Michael TEREKHIN	Visiting Associate Professor (from Kurchatov Institute, Russia) (October '96-)
Shin-ichiro TANAKA	Research Associate
Shin-ichi KIMURA	Research Associate
Masahito HOSAKA	Research Associate
Tatsuo GEJO	Research Associate
Sayumi HIROSE	JSPS Post-Doctoral Fellow (-October '96)[78]
Yuichi HARUYAMA	IMS Fellow (April '97-)
Masamitsu WATANABE	IMS Fellow (-September '96)[79]
Naoshi TAKAHASHI	Graduate Student (-March '97)[80]
Kazuhiko KIMURA	Graduate Student (-March '97)
Krishna G. NATH	Graduate Student
Masatake ICHIKAWA	Graduate Student (-March '97)[81]
Shigeki FUJIWARA	Graduate Student (October '96-)
Junichi MURAKAMI	Graduate Student (April '97-)

* Carries out graduate research of IMS on Cooperative Education Program of IMS with other graduate schools.

Technical Staff

Kusuo SAKAI	Technical Division Head
Osamu MATSUDO	Technical Section Chief
Kiyonori KATO	Technical Section Chief
Fumio NISHIMOTO	Technical Section Chief
Fumitsuna TESHIMA	Computer Center
Fumiyasu MIZUTANI	Computer Center
Shigeki NAITO	Computer Center
Takaya YAMANAKA	Laser Research Center for Molecular Science (Unit Chief)
Noboru KODABASHI	Laser Research Center for Molecular Science
Masaaki NAGATA	Research Center for Molecular Materials (Unit Chief)
Hisashi YOSHIDA	Research Center for Molecular Materials (Unit Chief)
Sachiyo NOMURA	Research Center for Molecular Materials
Masahiro SAKAI	Research Center for Molecular Materials
Takashi TAKAYAMA	Research Center for Molecular Materials
Hideo SHIBAYAMA	Research Center for Molecular Materials
Toshio KINOSHITA	Electronic Structure (Unit Chief)
Toshio HORIGOME	Equipment Development Center (Unit Chief)
Tatsuharu TORII	Equipment Development Center
Nobuo MIZUTANI	Equipment Development Center
Kouichi UCHIYAMA	Equipment Development Center
Tomonori TOYODA	Equipment Development Center
Takayuki YANO	Equipment Development Center
Takuhiko KONDOU	Equipment Development Center
Masami HASUMOTO	UVSOR Facility (Unit Chief)
Jun-ichiro YAMAZAKI	UVSOR Facility
Eiken NAKAMURA	UVSOR Facility (-May '97)[82]
Kenji HAYASHI	UVSOR Facility (June '97-)
Naonori KONDO	UVSOR Facility (April 97-)

List of Present Addresses

1) The Institute of Physical and Chemical Research (RIKEN), Wako, Saitama 351-01
2) J. Heyrousky Institute of Physical Chemistry Academy of Sciences of the Czech Republic, Dolejskova 3, CZ-18223 Parque 8, Czech Republic
3) Department of Chemistry, Ben - Gurion University, Beer Sheva, 84105 Israel
4) Department of Pure and Applied Sciences, Graduate School of Arts and Sciences, The University of Tokyo, 3-8-1, Komaba, Meguro-ku, Tokyo 153
5) Soreq Nuclear Research Institute, Yavne, 81800, Israel
6) Department of Theoretical Physics, Faculty of Mathematics and Physics, Charles University, V. Holesovickach 2, 18000 Prague 2, Czech Republic
7) Institute of Physics, The University of St. Petersburg, 198904, St. Petersburg, Russia
8) Institute of Physics, The University of St. Petersburg, 198904, St. Petersburg, Russia
9) Department of Chemistry, University of Pittsburgh, PA 15260, U.S.A.
10) Department of Chemistry, Korea University, 1, Anam-dog, Songbuk-ku, Seoul 136-701, Korea
11) Department of Biotechnology, Faculty of Technology, Tokyo University of Agriculture and Technology, 2-24-16 Nakamachi, Koganei 184
12) Department of Materials Science, Faculty of Science, Hiroshima University, 1-3-1 Kagamiyama, Higashi-Hiroshima 739
13) Department of Chemistry, University of Waterloo, Waterloo Ontario, N2L 3G1 Canada
14) Department of Chemistry, Arizona State University, Tempe AZ 85287-1604, U.S.A.
15) Department of Chemistry, Faculty of Science, Hiroshima University, 1-3-1 Kagamiyama, Higashi-Hiroshima 739
16) Biophysical Chemistry Laboratory, The Institute of Physical and Chemical Research (RIKEN), Wako, Saitama 351-01
17) Department of Chemistry, Yonsei University, 134, Seodaemoon-Gu Shinchon-Dong Seoul, 120-749, Korea
18) Gorlaeus Laboratories POB 9502, 2300 RA Leiden, The Netherlands
19) Department of Chemistry, Princeton University, Princeton, NJ 08544, U.S.A.
20) School of Materials Science, Japan Advanced Institute of Science and Technology, Tatsunokuchi, Ishikawa 923-12
21) Permanent Address: The Graduate University for Advanced Studies, Hayama, Kanagawa 240-01

22) School of Materials Science, Japan Advanced Institute of Science and Technology, Tatsunokuchi, Ishikawa 923-12
23) School of Materials Science, Japan Advanced Institute of Science and Technology, Tatsunokuchi, Ishikawa 923-12
24) Surface Chemistry Laboratory, The Institute of Physical and Chemical Research (RIKEN), Wako, Saitama 351-01
25) Advanced Research Center, Kansai Research Establishment, Japan Atomic Energy Research Institute, 25-1 Mii-Minami-Machi, Neyagawa, Osaka 572
26) Department of Chemistry and Biotechnology, Graduate School of Engineering, The University of Tokyo, 7-3-1 Hongo, Bunkyo-ku, Tokyo 113
27) Department of Chemistry, Faculty of Science, Hiroshima University, Kagamiyama, Higashi-Hiroshima 739
28) Department of Chemical System Engineering, School of Engineering, The University of Tokyo, 7-3-1 Hongo, Bunkyo-ku, Tokyo 113
29) Department of Chemistry, Faculty of Science, Hiroshima University, Kagamiyama, Higashi-Hiroshima 739
30) Institute of Physical Chemistry, Kossuth Lajos University, H-4010 Debrecen, Hungary
31) National Research Institute of Metals, 3-13 Sakura, Tsukuba, Ibaraki 305
32) Department of Chemistry, University of Nevada, Reno, Nevada 89557-0020, U.S.A.
33) Inoue Photochirogenesis Project, ERATO, Japan Science and Technology Corporation (JST), 4-6-3 Kamishinden, Toyonaka 565
34) Department of Chemistry and Materials Engineering, Shinshu University, 500 Wakasato, Nagano 380
35) Department of Applied Physics, The University of Tokyo, Bunkyo-ku, Tokyo 113
36) Department of Materials Science and Engineering, Science University of Tokyo in Yamaguchi, Onoda, Yamaguchi 756
37) N. S. Kurnakov Institute General & Inorganic Chemistry of the Russian Academy of Sciences, 31, Leninskii prospekt, GSP-1, Moscow 117907, Russia
38) Department of Chemistry, State University of New York at Binghamton, Binghamton, NY 13902-6016, U.S.A.
39) Chemistry Department, Inner Mongolia University, Hohhot 010021, China
40) Department of Chemistry, Nihon University, Sakurajosui, Setagaya-ku, Tokyo 156
41) Department of Physics, Faculty of Science, The University of Tokyo, Bunkyo-ku, Tokyo 113
42) Department of Natural Science Informatics, Nagoya University, Furo-cho, Chikusa-ku, Nagoya 464-01
43) Department of Chemistry, Toho University, Funabashi 274
44) Department of Chemistry, Kyung Hee University, Seochun, Kihung-Eup, Yongin-Kun, Kyung Ki-Do, South Korea
45) Institute for Chemistry and Material Science of Bordeaux, Avenue du Docteur A. Schweizer, 33608 Pessac, Cedex, France
46) Asahi Denka, Arakawa-ku, Tokyo 116
47) Department of Chemistry, Beijing Health School, Beijing 100053, P.R.China
48) Faculty of Science, Himeji Institute of Technology, Harima Science Garden City, Kamigori-cho, Hyogo 678-12
49) Faculty of Science, Himeji Institute of Technology, Harima Science Garden City, Kamigori-cho, Hyogo 678-12
50) Japan Synchrotron Radiation Research Institute, Kamigouri, Ako-gun, Hyogo 678-12
51) Department of Mechanical Engineering, Faculty of Engineering, The University of Tokushima, 2-1, Minami Josanjima-cho, Tokushima 770
52) Faculty of Science, Hiroshima University, Kagamiyama 1-3-1, Higashi-Hiroshima 739
53) Faculty of Science, Himeji Institute of Technology, Kanaji 1479-1, Kamigouri, Ako 678-12
54) Institute of Materials Research, Tohoku University, Katahira 2-1-1, Aoba-ku, Sendai 980
55) Faculty of Science, Kyoto University of Education, Fushimi-ku, Kyoto 612
56) Tokyo Institute of Technology, Midori-ku, Yokohama 226
57) Tokyo Institute of Technology, Midori-ku, Yokohama 226
58) Department of Chemistry, Nagoya University, Chikusa-ku, Nagoya 464-01
59) Department of Chemistry, Hiroshima University, Kagamiyama 1-3-1, Higashi-Hiroshima 739
60) Graduate School of Arts and Sciences, The University of Tokyo, 3-8-1, Komaba, Meguro-ku, Tokyo 153
61) Tokyo Institute of Technology, Midori-ku, Yokohama 226
62) Tokyo Institute of Technology, Midori-ku, Yokohama 226
63) Department of Physics and Applied Mathematics, Soreq Nuclear Research Center, Yavne 70600, Israel
64) Department of Theoretical Physics, Charles University Prague, V Holesovickach 2, 180 00 Praha 8, Czech Republic
65) Laboratoire de Chimie Structurale Organique, Bat. 410. Université Paris XI, 91405, ORSAY Cedex, France
66) Mac Science Co. Ltd., 1-5-1 Shinyokohama, Kohoku-ku Yokohama, Kanagawa 222
67) Department of Chemistry, College of Natural Sciences, Sejong University, KoonHadong 98, KwangJinKoo Seoul, 143-747, Korea
68) Department of Chemistry, Emory University, Atlanta, Georgia 30322, U.S.A.
69) Department of Chemistry, Emory University, Atlanta, Georgia 30322, U.S.A.

70) Department of Chemistry, McGill University, 801 Sherbrooke Street West, Montreal, PQ, Canada H3A2K6
71) Takeda Healthcare Company, 4-1-1 Dosho-machi, Chuo-ku, Osaka 541
72) Nagoya Institute of Technology, Gokiso-cho, Showa-ku, Nagoya 466
73) Department of Chemistry, Faculty of Science, Kumamoto University, Kurokami 2-39-1, Kumamoto 860
74) Argonne National Laboratory, Argonne IL 60439, U.S.A.
75) Faculty of Science, Himeji Institute of Technology, Kanaji 1479-1, Kamigohri, Akoh 678-12
76) Department of Chemistry and Materials Engineering, Shinshu University, 500 Wakasato, Nagano 380
77) Institute of Physics, Estonian Academy of Science, Riia 142, EE2400 Tartu, Estonia
78) Sumitomo Heavy Industry Ltd., Kusatsu 525
79) National Research Institute for High Energy Physics, Oho 1-1, Tsukuba 305
80) Düsseldorf Univ., Germany
81) Aisin AW Ltd., Kariya 448
82) Japan Advanced Institute of Science and Technology (JAIST), Asahidai, Tatsunokuchi-machi, Ishikawa 923-12

COUNCIL

Mitsuo ITO **Director-General**

Councillors

Chairperson	Yukio HORI	Vice President, Kanazawa Institute of Technology (-May '97)
Chairperson	Mitsuo TASUMI	Professor, Saitama University (June '97-; Vice-Chairperson, -May '97)
Vice-Chairperson	Haruo HOSOYA	Professor, Ochanomizu University (June '97-)
	Schunichi AKIMOTO	Professor Emeritus, The University of Tokyo (-May '97)
	Keishi GOTO	President, Toyohashi University of Technology (June '97-)
	Kenichi HONDA	President, Tokyo Institute of Polytechnics; Professor Emeritus, The University of Tokyo (June '97-)
	Yoshikazu ITO	Chairman of the Board, Toray Industries, Inc. (-May '97).
	Hiizu IWAMURA	Professor, Kyushu University (-May '97)
	Nobuo KATO	President, Nagoya University
	Haruo KURODA	Professor, Science University of Tokyo
	Yoshimasa KYOGOKU	Director-General, Institute for Protein Research, Osaka University (June '97-)
	Kazuhiro MARUYAMA	President, Kyoto Institute of Technology
	Noboru MATAGA	Division Head, Institute for Laser Technology; Professor Emeritus, Osaka University
	Yoshio MATSUNAGA	Professor, Kanagawa University (-May '97)
	Hidetake MORIMOTO	Adviser, Toyota Centeral Research & Development Laboratories, Inc. (-May '97)
	Toru MORIYA	Professor, Science University of Tokyo (-May '97)
	Atsuo NAKANISHI	Executive Director, Chemical Society of Japan (June '97-)
	Hitoshi OHTAKI	Professor, Ritsumeikan University
	Eiko OHTSUKA	Professor, Hokkaido University (June '97-)
	Shinichi SASAKI	President, Toyohashi University of Technology (-May '97)
	Ryoichi SHIMIZU	Director-General, The Institute of Statistical Mathematics
	Hiroshi SHIONO	Professor, Seikei University
	Riichi TAKAHASHI	Executive Vice President, Toyota Central Research & Development Laboratories, Inc. (June '97-)
	Hisashi TANAKA	Professor Emeritus, Kyoto University (-May '97)
	Soji TSUCHIYA	Professor, Japan Women's University
	Toshimitsu YAMAZAKI	Inspector, Japan Society for the Promotion of Science; Professor Emeritus, The University of Tokyo (June'97-)
	Hiroshi YASUOKA	Director-General, Institute for Solid State Physics, The University of Tokyo (June '97-)
	Edward William SCHLAG *	Director, Institute for Physical Chemistry, Technical University of Munchen (-May '97)
	Mostafa A. EL-SAYED *	Professor, Georgia Institute of Technology (-May '97)
	Raphael D. LEVINE *	Professor, The Hebrew University of Jerusalem (June '97-)
	Charles S. PARMENTER *	Professor, Indiana University (June '97-)

The Council is the advisory board for the Director-General.
* Two of the councillors are selected among distinguished foreign scientists.

Distinguished Research Consultants

Hiroaki BABA	Professor Emeritus, Hokkaido University
Kenichi FUKUI *(deceased)*	President, Institute for Fundamental Chemistry (-Jan. '98)
Hiroo INOKUCHI	Professor Emeritus, Institute for Molecular Science
Saburo NAGAKURA	President, The Kanagawa Academy of Science and Technology
Ikuzo TANAKA	President, National Institute for Academic Degrees

Administration Bureau

Mikio HASHIMOTO	Director-General, Administration Bureau (-March '97)
Kouichiro OSAKA	Director-General, Administration Bureau (April '97-)
Akihiro SHIBASAKI	Director, General Affairs Department
Kenji KANDA	Director, Finance and Facilities Department (-March '97)
Chikashi SAISHO	Director, Finance and Facilities Department (April '97-)
Masaki YOKOYAMA	Head, General Affairs Division
Youji IWAI	Head, Personnel Division
Yousuke HASHIMOTO	Head, Research Cooperation Division
Kouji TAKAHARA	Head, International Affairs Division
Norimichi IMAZU	Head, Budget Division
Kenzo KOZEKI	Head, Accounts Division
Takeshi KITATANI	Head, Construction Division
Yoshitaka MOCHIZUKI	Head, Equipment Division

BUILDINGS AND CAMPUS

The IMS campus covering 62,343 m^2 is located on a low hill in the middle of Okazaki city. The inequality in the surface of the hill and growing trees are preserved as much as possible, and low-storied buildings are adopted for conservation of the environment. The buildings of IMS are separated according to their functions as shown in the map. The Research Office Building and all Research Facilities except for the Computer Center are linked organically to the Main Laboratory Buildings by corridors. Computer Center, Library and Administration Buildings are situated between IMS and neighboring National Institute for Basic Biology and National Institute for Physiological Sciences, because the latter two facilities are common to these three institutes.

The lodging facility of IMS called Yamate Lodge, located within ten minutes' walk, has sleeping accommodations for 15 guests and two families. Mishima Lodge, located within four minutes' walk east of IMS can accommodate 74 guests and 20 families. Scientists who visit IMS as well as the two other institutes can make use of these facilities. Foreign visiting scientists can also live at these lodgings with their families during their stays. The Okazaki Conference Hall was built in April, 1997 in Mishima area, which has four conference rooms capable of between 50 and 250 attendance.

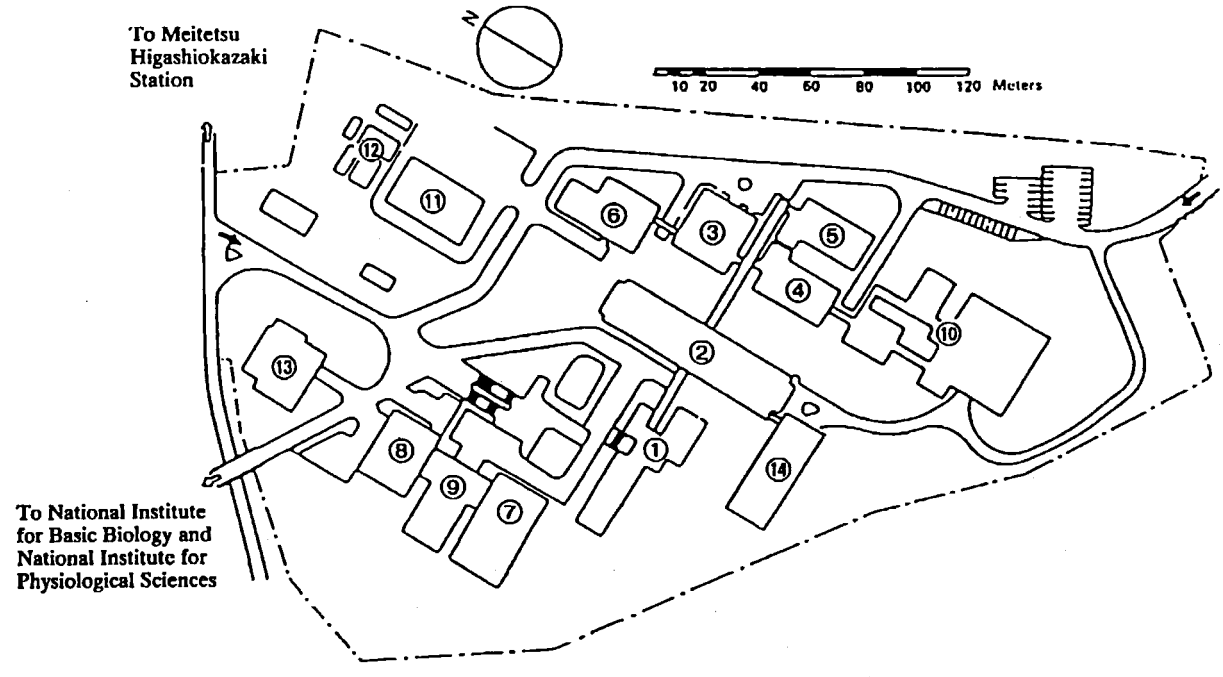

1. Research Office Building
2 Main Laboratory Building
3. Equipment Development Center
4. Laser Research Center for Molecular Science
5. Research Center for Molecular Materials
6. Low-Temperature Facilities Building
7. Computer Center
8. Library
9. Central Administration
10. UVSOR Facility
11. Power Station
12. Waste-Water Disposition Facilities
13. Faculty Club
14. South Laboratory Building

Okazaki (population 320,000) is 260 km west of Tokyo, and can be reached by train in about 3 hours from Tokyo via New Tokaido Line (Shinkansen) and Meitetsu Line.
The nearest large city is Nagoya, about 40 km northwest of Okazaki.

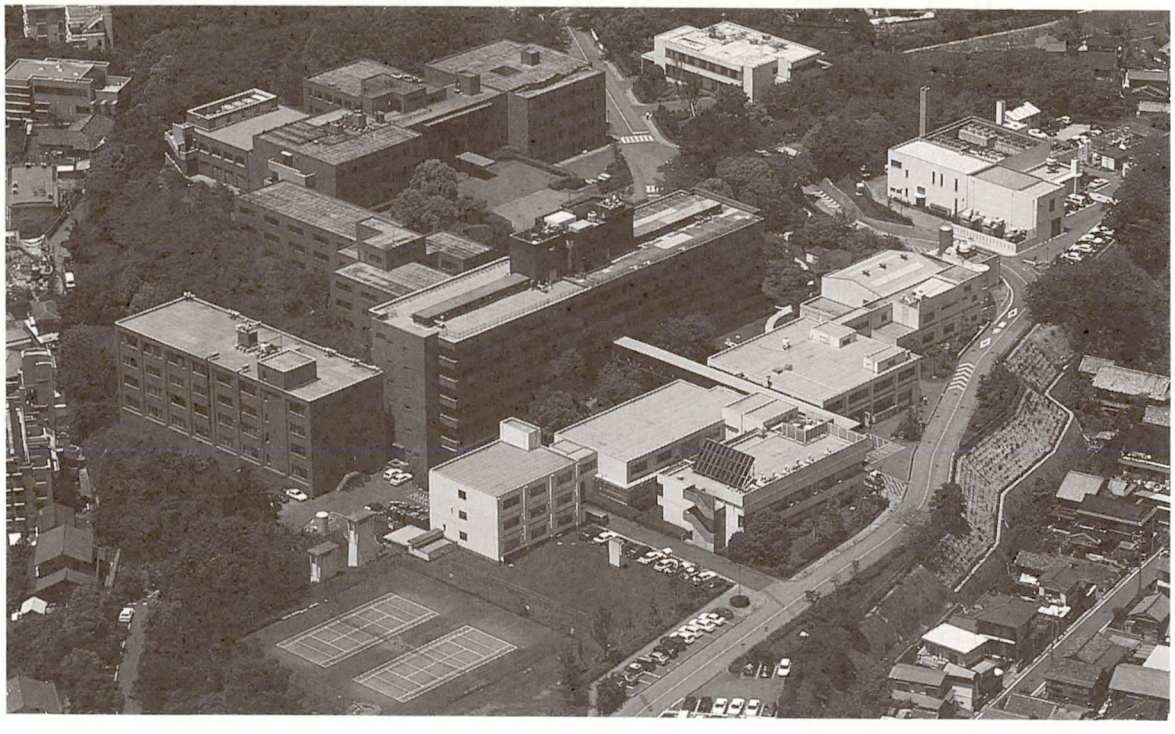

RESEARCH ACTIVITIES I
Department of Theoretical Studies

I-A Development of New Theoretical and Numerical Techniques in the Study of Molecular Structures

Theories of the electronic structure of molecules have been extensively developed for last four decades. The theories seem to be at a matured stage. But, it is not true. There are challenging and practically important problems to be solved.

I-A-1 Superposition of Nonorthogonal Slater-Determinants towards Electron Correlation Problems

Seiichiro TEN-NO

[*Theor. Chem. Acc.* in press (1997)]

We propose variational and nonvariational methods based on superposition of nonorthogonal Slater-determinants. Properties of the reference functions are discussed. In the nonorthogonal configuration interaction method, all the excited configurations of multiple determinants are integrated into a variational space. An efficient way to manipulate matrix elements over determinants of distinct vacuums is presented by introducing similarity transformed operator and bracket transformations. The method enables us to map a matrix multiplication in the nonorthogonal problem to an orthogonal one, and thus maintains a fundamental scaling property along with the amount of data processed in the corresponding orthogonal configuration interaction method. Furthermore, we discuss a coupled-cluster theory employing a vacuum dependent wave-operator, which is entirely size-consistent as well as core-extensive. These methods are applied to H_2O + nHe (n=0–2) and a single-bond dissociation of the HF molecule, compared with conventional methods including full and multireference configuration interaction methods.

I-A-2 Theoretical Studies of the Dipole Bound Anions of Molecular Clusters and the Photodetachment Cross Section with Hybrid Basis Sets of Gaussian Functions and Plane Waves

Feiwu CHEN, Takeshi TSURUSAWA and Suehiro IWATA

We develop the method for calculating of the photodetachment cross section using L^2 basis set and conventional ab initio MO CI wave functions. To augment the gaussian type functions, we introduce a set of plane wave functions to describe the excess electron as well as the ejected electron. We code a new integral calculation package, in which the molecular integrals for the mixed basis set of the gaussian and plane wave functions are evaluated. To reduce the number of integrals to be evaluated, only the coulomb (gg'lkk') and exchange (gklg'k') types of two-electron integrals are calculated, where g and g' stand for the gaussian functions, and k and k' for plane waves. Under this limitation of the integrals, we introduce a series of the approximations for many-electron wave functions of the initial and final states. Since the role of the electron correlation in the wave functions of the anion (initial state) and of the neutral (final state after an electron ejection) is different, special cares should be taken in developing the approximations. Because we use the discrete k values for plane waves (wave functions of a particle in a box), the hybrid basis set is still a L^2 basis set. To evaluate the photodetachment cross section, we use the Stieltjes Imaging (Lanczos Recursive) method.

I-A-3 Static Structure Factor and Electron Correlation Effects Studied by Inelastic X-ray Scattering Spectroscopy

Noboru WATANABE *(Tohoku Univ.)*, **Hisashi HAYASHI** *(Tohoku Univ.)*, **Yasuo UDAGAWA** *(Tohoku Univ.)*, **Seiichiro TEN-NO and Suehiro IWATA**

[*J. Chem. Phys.* submitted]

Inelastic X-ray scattering spectra of methanol, acetonitrile, benzene and cyclohexane have been measured with 2 eV resolution for momentum transfer q between 0.69 and 2.77 a.u. using synchrotron radiation from the PF storage ring. By utilizing the Bethe sum rule, the spectra were brought onto an absolute scale, so that the static structure factor S(q) has been obtained. S(q) of these molecules has also been calculated at the single reference configuration interaction (CI) with several types of basis sets. A new formula is proposed to carry out spherical averaging accurately. It is concluded that the CI singles and doubles (CISD) treatment is necessary to predict correct S(q), and that an inclusion of polarization function influences S(q) significantly at this level. An addition of f functions also improves the agreement with the experiments. S(q)'s based on CISD wave functions are in good agreement with the experimental ones, in particular at large q.

I-A-4 Construction of Two Electron Reduced Density Matrix for Static Structure Factor Calculation

Sourav PAL *(Nat. Chem. Lab., India and IMS)*, **Seiichiro TEN-NO and Suehiro IWATA**

The static structure factor has been known to be a very sensitive probe to the correlation effects. This is obtained from the inelastic X-ray scattering spectroscopy. This S(q) depends on the two electron re-

duced density matrix, which is sensitive to the electron correlation and can be theoretically computed. A high level of correlated wave function is required in many cases to obtain accurate two electron reduced density matrix and subsequently the S(q). We have developed a code to calculate this two electron reduced density matrix using a coupled-cluster (CC) wave function at the singles and doubles level. The CC wave function is known to take into account high degree of excitations in the wave function and evaluates the energies and properties in a size-extensive manner. The formulae for two electron reduced density matrix in terms of the CC amplitudes is, in principle, an infinite series. We have retained in this code most important terms up to the cubic power of the cluster amplitudes. We propose to use this code to study the static structure factors for molecules where electron correlation plays an important role.

I-B Hybrid Procedures of Ab Initio MO Calculations and Monte Carlo Samplings

Monte Carlo (MC) method was combined with the ab initio MO calculations. The procedure is applied for the molecular clusters. Besides, multi-canonical algorithm was used to study the temperature dependency of the properties of water dimer. A new more efficient code for the hybrid procedure is being in progress.

I-B-1 Theoretical Prediction of Intracluster Reactions of $B^+(H_2O)_2$ and $B^+(H_2O)_3$ Clusters: Hybrid Calculations of Ab Initio MO and Monte Carlo Samplings

Hidekazu WATANABE *(Grad. Univ. for Advanced Studies and IMS)*, **Toshio ASADA and Suehiro IWATA**

[*Bull. Chem. Soc. Jpn.* in press (1997)]

A recently developed hybrid procedure of ab initio molecular orbital (MO) calculations and Monte Calro (MC) samplings is applied to investigate the intracluster reactions of $B^+(H_2O)_n$ (n=2 and 3). In this procedure we do not assume the potential energy functions during MC samplings. At every step the ab initio MO method is directly used to evaluate the electronic energy. The procedure makes it possible to deal with the intra-cluster reaction involving any rearrangement of atoms such as isomerization and dissociation. The many-body effects on the energy are taken into account within the approximation used in the MO calculation. During the MC samplings at room temperature, the $B^+(H_2O)_2$ cluster undergoes a series of isomerization reactions, and eventually forms the most stable isomer, sp^2 type of trans $HBOH^+$ (H_2O). For $B^+(H_2O)_3$, the reactions turn out to be more complicated, and a few times simulations suggest that there are several reaction products as well as intermediates in the reactions. The MO-MC procedure is proved to be a powerful tool to search for many isomers, reaction intermediates, and the products as well as the transition state structures between them although it is still very time-consuming.

I-B-2 Ab Initio Monte-Carlo Simulation Using Multi-Canonical Algorithm: Application to Water Dimer

Pradipta BANDYOPADHYAY *(Grad. Univ. for Advanced Studies and IMS)*, **Seiichiro TEN-NO and Suehiro IWATA**

Recent upsurge of simulation of molecular systems using realistic potentials has been triggered by the seminal work of Car–Parrinello in 1985. However use of plane-wave expansion hinders the realistic simulation to a considerable extent. Recently we have applied the conventional ab initio MO method for Monte-Carlo samplings to study the structures and isomerizations to molecular clusters. We may call the procedure Molecular-Orbital-Monte-Carlo (MO-MC) method. In the present study, we extend the method to study the temperature dependence of the cluster structure, combining it with multi-canonical algorithm. The basic problems in the simulation of realistic molecular systems are two-fold. Due to complicated nature of potential surface, only a part of the surface is usually explored by conventional simulation algorithms. Enormous computational cost for evaluating the potential energy at every step is the other bottle-neck. Multi-canonical Algorithm was invented to overcome the former difficulty and was proved to be highly efficient to study multiple-minima problems. This algorithm, which explores any parts of the potential surface with equal ease, allows us to evaluate properties at any temperature from a single multi-canonical run. The latter property makes it possible to study temperature dependent properties. Because only a single run is required in this algorithm, we can substantially reduce the total computation time to evaluate various temperature dependent properties. Thus, we can use the ab initio MO (or density functional method) with gaussian basis sets in calculate the potential energy at every step. To demonstrate the applicability of the method, we examine water-dimer in the present study. The potential energies are calculated at each step of the simulation using RHF/6-31G* method. The ground state of water dimer has a C_s structure. Eight equivalent structures are connected through C_i and C_{2h} transition states. By examining the temperature dependence of the radial (and other geometric) distributions and of the correlation between two parameters, we can see the structural change of the dimer and even its dynamics. The distribution of the inter-molecular O-H distance clearly indicates that some structural and dynamical changes take place between 170 and 300 K.

I-C Structures and Reactions of Atomic and Molecular Clusters

The research on the atomic and molecular clusters has been one of the best research field where theory and experiment have worked hand in hand for last decades. We may say that the following reports are some of the representatives. Professors Nagata and Kanamori report the abstracts of our collaborative works in this Annual Review.

I-C-1 Structures of Water Cluster Anions

Takeshi TSURUSAWA and Suehiro IWATA

In recent experiments various gas phase water cluster anions $(H_2O)_n^-$ were observed but for the small cluster, n<10, only n=2,6 and 7 were identified. The vertical detachment energies (VDE) of these water cluster anions are about 34 meV, 0.5 eV and 0.5 eV, respectively. There are also several theoretical treatments about the water cluster anions which includes ab initio MO calculations, and quantum simulation with model potential. In using the ab initio MO method to describe water cluster anions, it is important to employ the basis set which contains very diffuse functions, especially to obtain the positive VDE for the dimer cluster anion. The importance of the diffuse function not only for the dimer cluster anion but also for larger cluster anions is also concluded in the quantum simulation with model potential. In this study we investigate the small water cluster anions for n=2–6 by using the ab initio MO method with the basis sets augmented by several diffuse functions. We first performed the geometry optimization at UHF, MP2 and B3LYP levels of methods with standard 6-311++G** basis set. The optimized geometries are very similar to each other, independent of the levels of the approximation. But the O-O distance between hydrogen-bonded waters become shorter when the electron correlation is taken account. The structures of the isomers of anion clusters are classified to 'internal' and 'surface' with respect to the location of the excess electron. For all isomers, the excess electron is bound by the H-atoms which are not taking part in making hydrogen-bonding between the neighboring waters. From this preliminary calculations it is found that the surface state structures of dimer and trimer cluster anions act as building blocks to construct larger size water cluster anions. In the next step, the 6-311++G** basis set augmented by two s-type functions on each atoms is used in the optimization. A large change is found for the internal isomers; the distribution of the excess electron becomes very diffuse and thus water molecules are apart from each other (more than 10Å). On the other hand, the structures of surface isomers are not affected so much by adding diffuse functions. This means, as also mentioned by the quantum simulation with model potential, that for small size clusters only the surface states are favored. The following pictures show the SOMO of the (a) surface state of dimer (b) internal state of dimer (c) surface state of trimer when the augmented basis set are used.

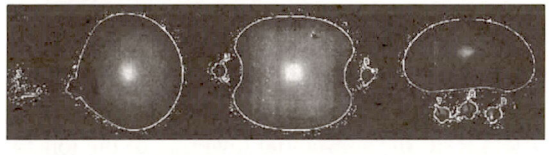

I-C-2 Intracluster Reaction Dynamics of Argon Tetramer Ions

Tsutomu IKEGAMI and Suehiro IWATA

[*Transition State Theory* Ed. by Fueno (1997)]

The potential energy surface of the argon tetramer ion was closely surveyed to study the reaction dynamics on the electronic ground state. The tetramer ion consists of a neutral argon atom and a trimer ion core. Because of strongly anisotropic interaction between the atom and the ion core, some isomers do exist for the tetramer ion, and isomerization reactions are possible among them. Besides the isomerization reactions, the core switching reaction, in which one of the atoms in the ion core is substituted for the neutral atom, is possible. The latter reaction is much important, since it is accompanied with the break and the formation of chemical bonds. The potential energy surface was calculated by using diatomics-in-molecules method. The gradient and the hessian are obtained analytically, and are used to locate stationary points on the surface. The gradient extremal path is used as the reaction paths connecting these stationary points. Two isomers and three transition states are found below the dissociation limit. The most stable isomer has a distorted T-shape (T), and two equivalent T isomers are separated by an potential barrier of 3.2 meV. Another isomer is a linear one (L), and 3.2 meV higher in energy than the T isomer. The isomers T and L are connected through the transition state, which is 22 meV higher in energy than the T isomer. The last transition state is the one for the core-switching reaction, which connects two equivalent L isomers. The barrier height for the reaction is found to be 3.5 meV.

I-C-3 *Ab Initio* MO Studies of Si_4NO^+

Wen-Ning WANG *(Fudan Univ. and IMS)*, **Knag-Nian FAN** *(Fudan Univ.)* **and Suehiro IWATA**

[*Chem. Phys. Letters* **273**, 337 (1997)]

The isomers of Si_4NO^+ cluster have been examined with ab initio MO calculations. The structures were determined at the MP2/6-31G* level of approximation, and their stability was verified by evaluating the harmonic frequencies. The most stable isomer of Si_4NO^+ is a complex of a Si_3N^+ ring and SiO, the structure of which is indicative of the eventual dissociation products, $Si_3N^+ + SiO$. This is consistent with the experimental result of the $Si_n^+ + NO$ reaction leading to $Si_{n-1}N^+ + SiO$ fragments. A set of NO weakly adsorbed

isomers was also located and verified to be easily yielded from Si_4^+ + NO reaction.

I-C-4 Ab Initio Study of Photochemical Reactions of Ammonia Dimer Systems

Jong K. PARK *(Pusan Univ. and IMS)* **and Suehiro IWATA**

[*J. Phys. Chem.* A **101**, 5103 (1997)]

Potential energy surfaces of ammonia dimer systems corresponding to the proton (hydrogen) transfer reaction from the reactant (NH_3 + NH_3) to the product (NH_4 + NH_2) have been calculated with ab initio HF, MP2, and SECI methods using a TZP basis set including diffuse Rydberg basis functions. The reaction path surfaces of the neutral, excited, and cationic states have each one local minimum corresponding to complexes such as (NH_3 ... NH_3) for a neutral one, (H_3N^*-H ... NH_2) for an excited one, and (H_3N^+-H ...NH_2) for a cation, respectively. Dimer complexes such as (H_3N-HÖNH_2) and (H_3NÖ.H-N^+H_2) do not exist. The photoionization and -dissociation reactions take place along the potential energy surfaces of the neutral, excited, and cationic states. The binding energies of the complexes relative to the asymptote are small. Particularly, the binding energies of H_3N^*-HÖNH_2(^{1}A") and (H_3NÖNH_3) are only 0.24 and 0.16 eV, respectively. And the head-to-head type [(H_3NÖNH_3)$^+$] with a binding energy of 1.52 eV does not exist on the proton transfer reaction surfaces.

I-C-5 Theoretical Studies of Cyclic Radicals NO_x (x=2–6)

Yumin LI and Suehiro IWATA

[*Chem. Phys.* **219**, 209 (1997)]

Ab initio MO calculations at the UHF and MP2 levels with 6-31G* basis set are carried out to examine the stability and the structure of a series of NO_x (x=2–6) radicals. We have located a series of exotic but stable radicals with a ring comprised of one nitrogen atom and two to six oxygen atoms. The stability is confirmed by evaluating the harmonic frequencies at both levels. The bonds in the cyclic radicals are discussed by comparing with both lengths and bond stretching vibrational frequencies of the related known molecules. The reaction energy for

$$NO_x \rightarrow NO_2 + (x-2)/2\ O_2$$

is evaluated with the MP4SDTQ approximation, and it is shown that the cyclic NO_x is a new type of energy-rich molecules. Besides, all the ring radicals of being stable not only on UHF/6-31G* but also on MP2/6-31G* are further investigated by density functional theory with nonlocal corrections (Becke3LYP). Most of them become unstable, except for three-membered NO_2 ring and four-membered NO_3 ring. The different stability for some NO_x ring radicals on MP2 and DFT levels are illustrated.

I-C-6 Six-Membered Rings N_xO_{6-x} (x=0–5): Theoretical Examination of the Stability

Yumin LI and Suehiro IWATA

Various levels of many-electron wave functions in ab initio MO and density functional theories are used to study six-membered ring isomers of N_xO_{6-x} (x=0-5). The methods examined are HF(UHF), MP2, and QCISD, and density functional of B3LYP. The basis set used in all four levels of approximation is Dunning's cc-pVDZ. For x=4 and 5, all four levels of calculations results in the similar geometric structures, harmonic frequencies and relative energy of boat and twist isomers. For x=0 and 1, three MO calculations leads to a stable chair isomer, but DFT does not give any stable isomer. For x=2 and 3, we have failed to locate any stable isomer with all of four levels of approximations.

I-C-7 Ab Initio MO Studies of Neutral and Anionic SiC_n Clusters (n=2–5)

Motoki GOMEI *(Keio Univ.)*, **Reiko KISHI** *(Keio Univ.)*, **Atsushi NAKAJIMA** *(RIKEN and Keio Univ.)*, **Suehiro IWATA and Koji KAYA** *(RIKEN and Keio Univ.)*

[*J. Chem. Phys.* in press (1997)]

The geometries and energies of SiC_n and SiC_n^- (n=2–5) were investigated with ab initio calculations including electron correlation effects with MP2/6-31G* method, followed by MP4 and CCSD(T) single point calculations to determine the most stable isomers. The adiabatic electron affinities (AEA) were evaluated with the DMP4 method. Because of the complexity of the electronic structure of SiC_2, its AEA was calculated at the CCSD(T)/aug cc-pVTZ // CCSD(T)/aug cc-pVDZ level of approximation. When the triplet state is the ground state in the SiC_n clusters, the isomer has a large electron affinity, whereas the singlet ground state isomer has a small electron affinity. This is attributed to the bonding character between Si and C atoms in the orbital occupied by the extra electron. The calculated electron affinity was used to assigning the photoelectron spectra of SiC_n^- reported previously. Furthermore, the effects of Renner–Teller splitting for the linear isomers of anions are discussed.

I-C-8 Geometric and Electronic Structures of Silicon-Sodium Binary Clusters: Ionization Energy of Si_nNa_m

Reiko KISHI *(Keio Univ.)*, **Suehiro IWATA, Atsushi NAKAJIMA** *(Keio Univ. and RIKEN)* **and Koji KAYA** *(Keio Univ. and RIKEN)*

[*J. Chem. Phys.* in press (1997)]

Sodium doped silicon clusters (Si_nNa_m; $1 \le n \le 14$, $1 \le m \le 5$) produced by two types of laser vaporization were studied. The adsorption of Na atoms on the Si_n clusters leads the substantial lowering of the ionization

energy E_i of Si_nNa_m clusters. Their reactivity toward NO molecules was measured with a fast flow reactor, and the anti-correlation between the E_i's and the reactivity was clearly observed; species having low E_i exhibit high reactivity and vice versa. Moreover, the clear parallelism between the E_i's of Si_nNa and the electron affinities of Si_n is found. This is consistent with the facts that the structure of Si_nNa clusters keeps the frame of the corresponding Si_n cluster unchanged and that the electronic structure of Si_nNa is similar to that of the corresponding Si_n^-. In addition to the experimental studies, the geometries, adsorption energies, and vertical ionization energies of Si_nNa (n=1–7) were investigated with ab initio MO calculations including electron correlation; The Mˉller–Plesset perturbation theory was used and the configuration interaction calculation was carried out for diatomic molecule, SiNa.

I-C-9 Ab Initio Studies on the Structures, Vertical Electron Detachment Energies and Stabilities of C_nP^- Clusters

Chang-Guo ZHAN *(Central China Normal Univ. and IMS)* **and Suehiro IWATA**

[*J. Phys. Chem.* in press]

In this work, the structures, vertical electron detachment energies and fragmentation energies of C_nP^- clusters (n=1 to 7) have been investigated by carrying out the geometry optimizations with MP2 method using 6-31G(d) augmented with a set of diffuse sp functions followed by the energy calculations at higher levels. It can be concluded from our calculated results that for the ground states the linear structures are stable only for C_2P^- and C_3P^-. Other C_nP^- (n=4 to 7) clusters are slightly bent, and the bent C_nP^- with odd n is very floppy for bending motion. The contributions of the bending of the structures of C_nP^- with odd n to the stability can be ignored, and therefore these clusters could appear pseudo linear in experiment. The calculated vertical electron detachment and fragmentation energies of C_nP^- (n=1 to 7) in their ground states reveal that the C_nP^- clusters with odd n are more stable than those with even n, which is consistent with the observed odd-even alternation in the TOF signal intensities. It has been also found that the odd-even alternation in fragmentation energies of C_nP^- is weaker than that of C_nN^-. Therefore, the stability difference for C_nP^- between the odd n and even n is smaller than that for C_nN^-. This conclusion is also coincident with the experimental observation.

I-C-10 Theoretical Study of the Structure and internal motion of $(N_2)_2$ Cluster

Akira WADA *(Tokyo Inst. Tech)*, **Hideto KANAMORI** *(Tokyo Inst. Tech. and IMS)* **and Suehiro IWATA**

N_2 dimer is a typical weak bounded Van der Waals complex, consisting of two identical molecules with no permanent dipole moment. The direct experimental information on the molecular structure are very limited[1] Theoretical studies using ab-initio calculation have been reported by several groups[2)3)]. However, those results were not adequate to predict reliable transition frequencies and intensities, which are useful for a spectroscopic experiment.

We calculated an internal potential energy surface of this complex by using CCSD(T)/cc-pVQZ in Gaussian 94 package. This is a state-of-art of calculations at the present day. The inter-nuclear distance of the monomer is fixed to the optimized value of N_2 and four other coordinates to represent the inter-molecular motion were running to optimize the local minimum structure. The basis set superposition error was corrected at each geometric configuration. The parallel structure (D_2) with 45 degree is found to be the lowest, and the T-shape structure (C_{2v}) becomes a transition state. In the previous calculations[3], however, the opposite results were reported. The out-of-plane motion changing from D_2 to a cross shape (D_{2d}) lies on a higher valley than the in-plane motion. From the binding energy of 80 cm^{-1}, the fundamental frequency of the Van der Waals stretching mode is roughly estimated as 20 cm^{-1}. The only 5 cm^{-1} energy difference between the D_2 and C_{2v} structures suggests that two N_2 should move coherently like a gear rotation within the plane. Thus, rotational energy states would be extremely modulated by this internal motion, and a very complex spectrum pattern is expected.

References

1) A. R. W. McKellar, *J. Chem. Phys.* 88, 4190 (1988).
2) V. Magnasco, C. Costa and G. Figari, *CPL.* 160, 469 (1989).
3) F. Uhlik, Z. Slanina, and A. Hinchliffe, *J. Mol. Struc. (Theochem)* 282, 271 (1993).

I-D Structures and Vibrational Frequencies of Infinite Polymer Chains

A new code of density functional crystal orbital method was developed for the infinite polymer chains with the analytical energy gradient evaluation. The force constants were evaluated numerically, and the calculated harmonic frequencies are systematically compared with the observed ones.

I-D-1 Density Functional Crystal Orbital Study on the Normal Vibrations of Poly-acetylene and Polymethineimine

So HIRATA *(Grad. Univ. for Advanced Studies and IMS)* **and Suehiro IWATA**

[*J. Chem. Phys.* in press]

Optimized molecular structures and k=0 (Brillouin zone center) vibrational frequencies were obtained for *trans*-transoid and *cis*-transoid polyacetylenes and for *anti*-transoid and *syn*-transoid polymethineimines by the density functional crystal orbital method with the Becke3–Lee–Yang–Parr (B3LYP) functional. The analytical energy gradient scheme was implemented in the density functional crystal orbital method, and the force constants of the infinite polymers were evaluated by numerical differentiation of the analytical energy gradients. For the *trans*-transoid and *cis*-transoid isomers of polyacetylenes, the vibrational frequencies calculated and then uniformly scaled by a single scale factor were in reasonable agreement with the observed frequencies. For polymethineimines, it was found that the calculated frequencies of the *anti*-transoid isomer completely disagreed with the observed frequencies In contrast, the calculated frequencies of *syn*-transoid polymethineimine were in agreement with the observed ones for three observed frequencies available. The total energy of *syn*-transoid polymethineimine was found to be lower than that of the *anti*-transoid isomer by 15.6 kJ mol^{-1}.

I-D-2 Density Functional Crystal Orbital Study on the Normal Vibrations and Phonon Dispersion Curves of All-*Trans* Polyethylene

So HIRATA *(Grad. Univ. for Advanced Studies and IMS)* **and Suehiro IWATA**

Optimized molecular structures and frequencies of the infrared and Raman active vibrations were obtained for all-*trans* polyethylene by using the analytical energy gradients of the density functional crystal orbital method. The Slater–Vosko–Wilk–Nusair (SVWN), the Becke–Lee–Yang–Parr (BLYP), and the Becke3–Lee–Yang–Parr (B3LYP) functionals were used with the 3-21G and 6-31G* basis sets. The frequencies calculated with the 6-31G* basis set were found to be in better agreement with the observed frequencies than those calculated with the 3-21G basis set regardless of the exchange-correlation functionals used. The root mean square deviations between the calculated and observed frequencies were 21, 20, and 14 cm^{-1} for the SVWN/6-31G*, the BLYP/6-31G*, and the B3LYP/6-31G* calculations, respectively (only the frequencies calculated at the B3LYP/6-31G* were scaled uniformly). Phonon dispersion curves were calculated in the 700–1500-cm^{-1} region at the SVWN/6-31G* level by taking a C_7H_{14} unit as an elementary unit cell. The calculated phonon dispersion curves were in fair agreement with the curves experimentally determined by the frequencies of n-alkane molecules except for the ν_4 branch. Inelastic neutron scattering spectrum calculated with the force field derived at the SVWN/6-31G* level reproduced the overall profile of the recently observed high-quality spectrum.

I-E Accurate Studies of Low-Lying States of Diatomic and Triatomic Molecules

I-E-1 Portrait of Diatomic FeN. A Theoretical Study

Andreas FIEDLER and Suehiro IWATA

[*Chem. Phys. Letters* **271**, 143 (1997)]

The ground and low-lying excited states of the diatomic molecule FeN were systematically studied. For this purpose a density functional/Hartree–Fock hybrid method and the internally contracted averaged quadratic coupled cluster approach with large basis sets were used. In agreement with previous reports the calculations revealed the $^2\Delta$ state to be the lowest in energy and only 3 kcal/mol higher lies the $^4\Pi$ state. In addition, we found another very low-lying $^4\Phi$ state and an even less energy demanding state of $^6\Sigma^+$ symmetry. The computations showed excitation energies of 5 and 0.5 kcal/mol, respectively. If the uncertainties of the methods are considered, all four states are good candidates for the real ground state.

I-E-2 A Theoretical Study of the Electronic Structure and Spectroscopic Properties of the Low-Lying Electronic States of the Molecule SiB

Fernando R. ORNELLAS *(Sao Paulo Univ. and IMS)* **and Suehiro IWATA**

[*J. Phys. Chem.* in press (1997)]

Twenty two lowest-lying electronic states of the species SiB are described theoretically using the internally contracted multi-reference configuration interaction approach and natural orbitals generated from a state-averaged density matrix. Correlated consistent valence quadruple-zeta (cc-PVQZ) atomic functions are used in the expansion of the one-electron basis. Potential energy curves are presented for all the states as well as a description of the electronic structure characterizing the most relevant ones. Dissociation and excitation energies, and dipole moment functions complete the electronic structure description. Solution of the radial nuclear equation allowed the determination of vibrational energies, and vibrational and rotational constants. For the ground state ($X\,^4\Sigma^-$), R_e = 1.918 ˜ and D_e = 3.27 eV. The first excited quartet ($A\,^4\Pi$) is located 2.60 eV (T_e) higher in energy and has a slightly shorter equilibrium distance (1.811 ˜) and a smaller D_e, 1.00 eV; the transitions $X\,^4\Sigma - A\,^4\Pi$ are expected to fall in the visible (green-yellow) region. Higher lying $^4\Pi$ states show very noticeable changes in the potential function due to avoided crossings. Within about 1.5 eV from the ground state there are located five doublet states; the lowest one a $^2\Pi$, with T_e = 0.73 eV, R_e = 1.845 ˜, and D_e = 2.54 eV. For selected states, transition dipole moments, transition probabilities and radiative lifetimes are also presented. Crossings of various states

and the energetic closeness of others are expected to play non-negligible perturbative effects in the spectra. The global picture of the electronic states presented will certainy be an important aid to experimentalists in the spectroscopic investigation of this species

I-E-3 Ab Initio Calculations for Potential Surfaces of HNO

Pradipta BANDYOPADHYAY *(Grad. Univ. for Advanced Studies and IMS)*, **Seiichiro TEN-NO and Suehiro IWATA**

For more than three decades HNO molecule has been remained as one of the most extensively studied molecule both theoretically and experimentally. Several reactions important in combustion and atmospheric chemistry occur in the HNO–HON surfaces. In the present work more than one states in each of the symmetries ^{1}A', ^{3}A", ^{1}A", ^{3}A' are studied. Using Dunning correlation consistent double-zeta natural orbital basis set (aug-cc-VDZ), the state averaged CASSCF/internally contracted multi-reference configuration interaction calculations are carried out. The active space for CASSCF calculations as well as in MRCI are full-valence (12 electrons in the 9 orbitals) of the molecule. It was found that 1^1A', 1^3A', 1^3A", 1^1A" states correlate to H+NO ($^2\Pi$) at the dissociation limit. The 2^3A' and 2^3A" states correlate to H+NO ($^4\Pi$), and the 2^1A' and 2^1A" states correlate to H+NO ($^2\Pi$) (excited state of NO) at the dissociation limit. The optically allowed 2^1A', which was not well-studied before, is expected to be predissociative by coupling with the repulsive 1^3A' state. Variation of potential energy surface with H-N-O angle shows that at the linear geometry $^2?^-$ is the lowest energy state and that for the 2^1A' state the lowest energy structure is linear, which makes this state a good candidate for further study, in particular, related with the UV photodissociation process.

I-F Application of Ab Initio Molecular Orbital and Density Functional Methods to Experimentally Relevant Systems

I-F-1 Comparative Ab Initio and Hybrid DFT Studies Relevant to An Experimental Investigation of Neutral and Cationic [Si,P,H_2] Isomers

Jan HRUSAK *(J. Heyrovsky Inst. Phys. Chem. and IMS)*, **Detlef SCHRÖDER** *(Tech. Univ. Berlin)*, **Helmut SCHWARZ** *(Tech. Univ. Berlin)* **and Suehiro IWATA**

[*Bull. Chem. Soc. Jpn.* **70**, 777 (1997)]

The neutral and the lowest cationic (singlet and triplet) potential-energy surfaces (PES) of [Si,P,H_2] have been explored by means of ab initio MO calculations at the G2 level of theory as well as the hybrid DFT (B3LYP/6-311G**) method. Contrary to the neutral and triplet surfaces, where the $H_2SiP^{+/0}$ isomers represent the global minima, for the singlet cation a doubly bridged $P(H)_2Si^+$ structure has been identified as the most stable isomer with the non-bridged H_2SiP^+ species being significantly less stable (ΔE = 31.7 kcal/mol at G2). As far as the comparison of the two quantum-chemical methods (i.e. G2 and B3LYP) is concerned, the calculated relative energies ΔE are quite close to each other with deviations smaller than 4 kcal/mol. However, while the non-bridged $SiPH_2^+$ (^{1}A') represents a minimum at the G2 level, it could not be located using the hybrid DFT method. The computationally predicted singlet and triplet $[Si,P,H_2]^+$ potential-energy surfaces provide insight into the course of the ion/molecule reactions of $Si^{+\bullet}$ with phosphine and P^+ with silane, respectively, which were examined experimentally. Thus, the reaction of the doublet species $Si^{+\bullet}$ with phosphine allows access to the non-classical, bridged $P(H)_2Si^+$ structure, while in the reaction of the P^+ triplet cation with silane, no evidence for Si-P bond formation is obtained.

I-F-2 Ab Initio Study of the Isomers: HNNSi, HSiNN, and HNSiN

Fernando R. ORNELLAS *(Sao Paulo Univ. and IMS)* **and Suehiro IWATA**

[*Bull. Chem. Soc. Jpn.* **70**, 2057 (1997)]

This work reports new structural, energetics, and vibrational frequency data for three isomers on the potential energy surface [H,Si,N,N] calculated at the UHF, MP2, and CCSD(T) /6-311G(2d) levels of theory. Similarly to SiNN, conventional methods fail to predict a thermodynamic stability for the isomer HSiNN. However, at the CCSD(T) level, the species HSiNN was found to lie 13.63 kcal/mol lower in energy than HNNSi; the isomer HNSiN was located 47.62 kcal/mol above the global minimum. Inclusion of zero-point energies causes the isomer HSiNN and its dissociation products HSi and N_2 to be about isoenergetic, what makes its detection plausible only at low temperatures.

I-F-3 The Ground and Low-Lying Excited States of the Phenyl Cation $C_6H_5^+$: Revisited

Jan HRUSAK *(J. Heyrovsky Inst. Phys. Chem. and IMS)*, **Detlef SCHRÖDER** *(Tech. Univ. Berlin)* **and Suehiro IWATA**

[*J. Chem. Phys.* **106**, 7541 (1997)]

The ionization of the phenyl radical $C_6H_5^\bullet$ ($^2A_1$) is examined by high level theoretical means. On the basis of a comparison of MCSCF, B3LYP, and CCSD(T) results, the ground state of the phenyl cation is definitely identified as $C_6H_5^+$ ($^1A_1$) with a conservative estimate of 8.1 ± 0.1 eV for the associated adiabatic ionization energy for the transition $C_6H_5^\bullet$ ($^2A_1$) → $C_6H_5^+$ ($^1A_1$).

The lowest lying triplet state $C_6H_5^+$ ($^3B_1$) is ca. 0.8 eV higher in energy, but yet the theoretical results suggest that formation of triplet cation is favored in photoionization experiments because the Franck-Condon factors are much favorable for the transition $C_6H_5^\bullet$ ($^2A_1$) → $C_6H_5^+$ ($^3B_1$) as compared to generation of the singlet ground state $C_6H_5^+$ ($^1A_1$). These features are revealed in the calculated photoionization spectra of [D_0]- and [D_5]-phenyl radical to yield either singlet or triplet cations.

I-F-4 Ab Initio MO and Density Functional Studies on the Vibrational Spectra of 1,4-Benzoquinone, and Its Anion and Dianion

Chang-Guo ZHAN *(Central China Normal Univ. and IMS)* **and Suehiro IWATA**

[*J. Phys. Chem.* submitted]

Ab initio MO and density functional calculations have been carried out for evaluating fundamental vibrational frequencies of 1,4-benzoquinone (BQ), BQ^-, BQ^{2-} and their various isotopomers. The vibrational frequencies calculated with the Hartree–Fock (HF), second-order M¨ller-Plesset (MP2) and density functional theory (DFT) with two functionals are qualitatively consistent with each other, though the HF frequencies are significantly larger as they always are. The MP2 frequencies are substantially improved from those of HF levels both for frequencies and their isotope shifts of BQ. Two DFT calculations (BPW91 and B3LYP) further improve the agreement with the experimental ones. The vibrational frequencies of BQ, BQ^-, BQ^{2-} and their various isotopomers calculated with BPW91 have been employed to further discuss the assignments of the recently reported resonance Raman (RR) bands of the BQ^- and BQ^{2-}. The previous assignments of the most vibrational bands are well confirmed. However, the assumption of the effective C_s symmetry of the BQ^- used for the previous assignments of the five polarized bands at 1046, 780, 748, 638 and 525 cm^{-1} is not appropriate. Based on the calculated results, it is more reasonable to re-assign the three bands at 1046, 748 and 638 cm^{-1} in the spectra of the BQ^- existing in CH_3CN to the fourth b_{2u}, the b_{1g} and the fourth b_{3g} fundamental modes, respectively. It seems also reasonable to assign the weaker band at 864 cm^{-1} appeared in the spectra of BQ^{2-} in the aqueous solution to the first b_{2g} fundamental mode, in place of an unknown overtone or combination mode suggested previously. But, we cannot completely exclude the possibility of the first a_u fundamental mode before the RR spectra of the $^{16}O_2/^{18}O_2$-substituted BQ^{2-} isotopomer in the region below 800 cm^{-1} are obtained.

I-F-5 Ab Initio Study of Internal Rotation of Methyl Groups in Toluene Derivatives

Tadayoshi SUZUKI *(Grad. Univ. for Advanced Studies and IMS)*, **Masaaki FUJII and Suehiro IWATA**

Potential energy curves and surfaces of internal rotation of methyl group(s) in o- and m-isomers of xylene, toluidine, cresol and tolunitrile in their ground (S_0), first excited (S_1), and cation ground (D_0) states, were calculated with ab initio molecular orbital methods. The approximation methods for many-electron wave functions are Hartree–Fock (HF) for closed-shell, S_0 states of neutral molecules, singly excited configuration interaction (SCI) for single electron excited states (S_1), and unrestricted Hartree–Fock (UHF) for open-shell (doublet) cation in the ground electronic states. The basis set used is 6-31G**. The state- and substituent-dependencies of the barrier height were compared with the experimental results. The interaction between methyl group and the other substituent group in the molecule was examined. Both dependencies are in good agreement with the experimental findings. In order to evaluate the theoretical internal rotation levels from the calculated potential surface, these potential surfaces are expressed by triangular functions, and Schr^dinger equation was build for the coupled internal rotation. The program is developed to solve this equation.

I-F-6 Local Hard-Soft Acid Base Principle: A Critical Study

Sailaja KRISHNAMURTYA *(Nat. Chem. Lab., India)*, **Ram Kinkar ROY** *(Nat. Chem. Lab., India)*, **Rajappan VETRIVEL** *(Nat. Chem. Lab., India)*, **Suehiro IWATA and Sourav PAL** *(Nat. Chem. Lab., India and IMS)*

[*J. Phys. Chem.* in press (1997)]

The recently proposed local Hard-Soft Acid-Base (HSAB) principle characterizes the reactive centers of two systems on the basis of equal Fukui functions or local softnesses. The Fukui functions are defined as the derivative of density at a point with respect to the number of particles. This can be also shown as the first order change of chemical potential with respect to the local external potential at a point. Thus Fukui functions are known to be the reactivity indices. The local softness is related to the Fukui function through a factor of global softness. In general, it has been shown that for any individual molecule the most reactive site is located at the atom with the largest value of local softness or Fukui function. However, recently Gazquez and Mendez have shown that the interaction between two molecules will occur not necessarily through their softest atoms, but through those atoms, the Fukui functions of which are same. Assuming the global softnesses of the molecules to be similar, the local HSAB principle states that the local softnesses of the interacting atoms are same. It is interesting to investigate cases where global softnesses of the two systems are not same. We make a critical study of the above principles of reactivity using the interaction of molecules such as CO, NH_3, and H_2O with the faujasite X type zeolite represented by a dimer cluster model $(OH)_3Si\text{-}OH\text{-}Al(OH)_3$. We have used the Hartree–Fock and nonlocal density functional theory (DFT) using B3LYP functional for this study. The global softnesses of the interacting systems

are not same in this case. We find from our study similar conclusions using both principles as Gazquez and Mendez did, and they agree with the known modes of interaction. However, for the study of the local HSAB principle, we find that there are some minor differences in the quality of matching of local softness and Fukui functions. The results are still not convincing to show which of the two parameters, local softnesses or Fukui functions, should be used in implementing local HSAB principle in cases like this, where global softnesses of the interacting systems are quite different.

I-F-7 An Ab Initio MO Study of Esa(1-*para*-methoxy-stylbene) and Its *para*-Alogen Substituents: A Model of Interdigitated Organization Within the Smectic Layer

Patrizio SEVERINO

The conductivity value and interdigitated organization within the smectic layer for clusters of esa(1-para-methoxy-phenyl,2-trans-para-alogen-phenyl, ethylene) were calculated by using GAUSSIAN92 and GAUSSIAN94 programs with STO-3G basis set. Even though the above basis set is minimal, the electronic and structural analysis should give a first reasonable indication for the correspondent properties of poly(1-para-N-nonanoxy-phenyl, 2-trans-para-alogen-phenyl, ethylene) ethylene because in both compounds there are the same methoxy-alogen-stilbene monomeric units: the superposition of the aromatic rings to form stacks of p-interacting systems would match the topological requirements for efficient doping process (*e.g.* via formation of charge transfer complexes) and optimal electron transport efficiency.

I-G Prediction of Protein Tertiary Structures from the First Principles

Prediction of the three-dimensional structures of protein molecules by computer simulations is a very challenging problem in theoretical molecular science. The difficulty of the problem lies in two facts: (1) the inclusion of accurate solvent effects is non-trivial and time-consuming (2) there exist huge number of local minima in the energy function, forcing conventional simulations to get trapped in states of energy local minima. We have been exploring the strategies that allow us to overcome these difficulties.

I-G-1 Monte Carlo Simulations in Generalized Ensemble: Multicanonical Algorithm versus Simulated Tempering

Ulrich H. E. HANSMANN and Yuko OKAMOTO

[*Phys. Rev. E* **54**, 5863 (1996)]

It is shown that two Monte Carlo methods in generalized ensemble, multicanonical algorithm and simulated tempering, are closely related. The equivalence and effectiveness of the two methods are illustrated by taking an energy function for the protein folding problem as an example.

I-G-2 Numerical Comparisons of Three Recently Proposed Algorithms in the Protein Folding Problem

Ulrich H.E. HANSMANN and Yuko OKAMOTO

[*J. Comp. Chem.* **18**, 920 (1997)]

We compare numerically the effectiveness of three recently proposed algorithms, multicanonical simulations, simulations in a 1/k-ensemble, and simulated tempering, for the protein folding problem. For this we perform simulations with high statistics for one of the simplest peptides, Met-enkephalin. While the performances of all three approaches is much better than traditional methods, we find that the differences among the three are only marginal.

I-G-3 Calculation of Hydration Free Energy for a Solute with Many Atomic Sites Using the RISM Theory: Robust and Efficient Algorithm

Masahiro KINOSHITA *(Kyoto Univ.)*, **Yuko OKAMOTO and Fumio HIRATA**

[*J. Comp. Chem.* **18**, 1320 (1997)]

We have developed an algorithm for solving the reference interaction site model (RISM) equations for water near a solute molecule with many atomic sites (interaction sites). It is a hybrid of the Newton-Raphson and Picard methods and is judiciously constructed. Various considerations are given so that the computer time can be saved as much as possible. The robustness and high efficiency of the algorithm has been demonstrated for calculating hydration free energies of Met-enkephalin (a peptide with 75 sites) with different conformations. The Jacobian matrix is treated as part of the input data, and it has been found that the same matrix can be used for a considerably large set of different conformations of the solute molecule.

I-G-4 Solvation Structure and Stability of Peptides in Aqueous Solutions Analyzed by the Reference Interaction Site Model Theory

Masahiro KINOSHITA *(Kyoto Univ.)*, **Yuko OKAMOTO and Fumio HIRATA**

[*J. Chem. Phys.* **107**, 1586 (1997)]

We report results of numerical analyses on solvation structure and conformational stability of a dipeptide and Met-enkephalin in the extended simple point charge (SPC/E) model water. The reference interaction site model (RISM) theory is fully solved using our robust, highly efficient algorithm. It is shown that water structure near the peptides and the hydration free en-

ergy are greatly dependent on the peptide conformations. Stability of Met-enkephalin is examined in terms of the total energy defined as the sum of the conformational energy and the hydration free energy of the peptide. We test several different conformations including that with the minimum energy in gas phase, which takes rather compact form due to an intramolecular hydrogen bond. It is shown that a fully extended conformation has the highest stability in water. Our results are in qualitative accord with the recent nuclear magnetic resonance (NMR) experiments which suggest fully extended conformations with large fluctuations for the solution structure of the peptide. A conformation which is similar to that obtained from the NMR experiments in miceller solutions, is much less stable when it is put in water. Thus, the peptide conformations are greatly sensitive to microscopic solvent environment, and any native treatment of the solvent such as the continuum model will end in failure.

I-G-5 A Simple Ansatz to Describe Thermodynamic Quantities of Peptides and Proteins at Low Temperatures

Ulrich H. E. HANSMANN and Philippe de FORCRAND *(ETH)*

[*Int. J. Mod. Phys.* C in press]

We describe a simple ansatz to approximate the low temperature behavior of proteins and peptides by a mean-field-like model which is analytically solvable. For a small peptide some thermodynamic quantities are calculated and compared with numerical results of an all-atoms simulation. Our approach can be used to determine the weights for a multicanonical simulation of the molecule under consideration.

I-G-6 Characteristic Temperatures of Folding of a Small Peptide

Ulrich H. E. HANSMANN, Masato MASUYA and Yuko OKAMOTO

[*Proc. Natl. Acad. Sci. USA* **94**, 10652 (1997)]

We perform a generalized-ensemble simulation of a small peptide taking the interactions among all atoms into account. From this simulation we obtain thermodynamic quantities over a wide range of temperatures. In particular, we show that the folding of a small peptide is a multi-stage process with two characteristic temperatures, the collapse temperature T_θ and the folding temperature T_f. Our results give supporting evidence for the energy landscape picture and funnel concept. These ideas were previously developed in the context of studies of simplified protein models, and here checked in an all-atom Monte Carlo simulation.

I-G-7 Tertiary structure prediction of C-Peptide of ribonuclease A by multicanonical algorithm

Ulrich H. E. HANSMANN and Yuko OKAMOTO

[submitted for publication]

We have performed multicanonical Monte Carlo simulations of C-peptide of ribonuclease A. It is known by CD and NMR experiments that this peptide has high α-helix content in aqueous solution and that the side-chain charges of residues Glu-2$^-$ and His-12$^+$ play an important role in the stability of the a -helix. In order to confirm these experimental implications, we have used two analogues of the peptide with charged and neutral side chains of Glu-2 and His-12. Two dielectric functions, distance-dependent and constant, are considered to study the effects of solvent contributions. All the simulations were started from random initial conformations. Various thermodynamic quantities such as average helicity as a function of residue number and average distance between two side chains as a function of temperature are calculated. The results are found to be in accord with the implications of CD and NMR experiments. The lowest-energy conformation obtained has an a -helix from Ala-4 to Gln-11 in complete agreement with the corresponding structure deduced from an X-ray crystallography experiment of ribonuclease A. It is shown that the salt bridge between the side chains of Glu-2$^-$ and Arg-10$^+$, which is known to exist from both NMR and X-ray experiments, is formed only when the side chains are properly charged. Its formation is greatly enhanced when the distance-dependent dielectric function is used.

I-G-8 First-Principle Determination of Peptide Conformations in Solvents: Combination of Monte Carlo Simulated Annealing and RISM Theory

Masahiro KINOSHITA *(Kyoto Univ.)*, **Yuko OKAMOTO and Fumio HIRATA**

[submitted for publication]

This paper contributes to development of a microscopic approach to predicting stable conformations of proteins in solvent. We report results of the first attempt to combine Monte Carlo simulated annealing, a powerful conformational sampling technique, and the reference interaction site model (RISM) theory, a statistical-mechanical treatment for molecular fluids. In solvent the key function is the total energy defined as the sum of the conformational energy and the solvation free energy, and the RISM theory is employed to calculate the latter. Starting from an initial conformation given, our computer program samples many conformations, and then finds the conformation with the minimum total energy. Met-enkephalin in the two different solvents, a model water and a simple, repulsive-potential system, are considered. In water the solvation free energy varies greatly from conformation to conformation, while in the simple solvent it remains almost unchanged against conformational changes. In water most of the conformations with larger solvation free energies are strongly rejected ant the number of probable conformations is drastically reduced, which is suggestive that Met-enkephalin is forced to take conformations favored by water far more rapidly than in gas phase and in the simple solvent. The set of stable conformations

obtained in water are quite different from those in gas phase and the simple solvent: they are characterized by almost fully extended conformations with large fluctuations in side-chain structure, which are in excellent agreement with those determined by the recent nuclear magnetic resonance (NMR) experiments.

I-G-9 Calculation of Solvation Free Energy for a Peptide in Salt Solution Using the RISM Theory

Masahiro KINOSHITA *(Kyoto Univ.)*, **Yuko OKAMOTO and Fumio HIRATA**

[submitted for publication]

We have developed an algorithm for solving the full reference interaction site model (RISM) equations for salt solutions near a solute molecule with many atomic sites. It is obtained as an extension of our previously reported algorithm for pure water near the solute molecule. The robustness and high efficiency of the algorithm has been demonstrated for a dipeptide with 23 atomic sites in a 1M-NaCl solution. The extended simple point charge (SPC/E) model is employed for water molecules. Two different conformations of the dipeptide are considered. It is assumed for each conformation that the dipeptide is present either as an unionized form or as a zwitterion. The structure of the salt solution near the dipeptide and salt effects on the solvation free energy have also been analyzed.

I-G-10 Electrostatic Effects on the α-Helix and β-Strand Folding of BPTI(16-36) as Predicted by Monte Carlo Simulated Annealing

Takashi NAKAZAWA *(Nara Women's Univ.)* **and Yuko OKAMOTO**

[submitted for publication]

The electrostatic effects on the tertiary structure of a peptide with residues 16-36 of bovine pancreatic trypsin inhibitor, BPTI(16-36), are studied using Monte Carlo simulated annealing. For this purpose, three dielectric functions $\varepsilon(r)$ of distance r are considered: constant dielectric function (ε=2) and sigmoidal functions with e(8)=47 and e(8)=78. Simulations with ε=2 suggest that the peptide exhibits a significant propensity for β-strand without allowing the possibility for α-helix, as the relevant segment folds into a β-sheet structure in native BPTI. Roughly equal probability for the formation of α-helix and β-stand is found in the simulation with e(8)=47, leading to no conspicuous conformational propensity. The calculation with e(8)=78 shows a strong tendency of the peptide to form α-helices but not β-strands, thereby many lower-energy conformations have extended α-helices. These results demonstrate that the peptide with the same amino-acid sequence can form both α-helix and β-strand structures depending on the strengths of the electrostatic interactions.

I-G-11 Effective Parameters for Solvation Energy of Proteins Based on Solvent Accessible Surface Area

Masato MASUYA and Yuko OKAMOTO

We compare five sets of parameters for solvation energy of proteins based on solvent accessible surface area. The criteria for effectiveness that we adoped are (1) the total energy, sum of structural energy of protein and solvation free energy, is lower for compact structures than for extended structures and (2) among compact structures the native structure has the lowest solvation free energy. We have found that two out of the five parameters are unsatisfactory and the remaining three are satisfactory.

I-G-12 Classification of Low-Energy Conformations of Met-Enkephalin with Hydrophobic Interactions Based on the Scaled Particle Theory Taken into Account

Ayori MITSUTAKE *(Graduate Univ. for Advanced Studies)*, **Masayuki IRISA** *(Kyushu Inst. Tech.)*, **Fumio HIRATA and Yuko OKAMOTO**

The low-energy conformations of Met-enkephalin that are obtained by Monte Carlo simulated annealing are analyzed and classified. The total energy is given by the sum of the structural energy and solvation free energy. The latter term is approximated by the hydrophobic contributions based on the scaled particle theory. Twenty conformations obtained are classified into groups of similar structures. Various implications for the effects of the hydrophobic contributions of solvent on the peptide structures are presented.

I-H Development of Simulation Algorithms for Complex Systems

Developing a powerful simulation algorithm that can alleviate the multiple-minima problem is important in many complex systems such as protein systems and spinglass systems. We have been advocating the use of simulated annealing and the so-called generalized-ensemble algorithms. We try to develop a new method and test its effectiveness.

I-H-1 Generalized-Ensemble Monte Carlo Method for Systems with Rough Energy Landscape

Ulrich H. E. HANSMANN and Yuko OKAMOTO

[*Phys. Rev. E* **56**, 2228 (1997)]

We present a novel Monte Carlo algorithm which enhances equilibrization of low-temperature simulations and allows sampling of configurations over a

large range of energies. The method is based on a non-Boltzmann probability weight factor and is another version of the so-called generalized-ensemble techniques. The effectiveness of the new approach is demonstrated for the system of a small peptide, an example of a frustrated system with a rugged energy landscape.

I-H-2 Simulated Annealing with Tsallis Weights — A Numerical Comparison

Ulrich H. E. HANSMANN

[*Physica A* **242**, 250 (1997)]

We discuss the use of Tsallis generalized mechanics in simulated annealing algorithms. For a small peptide it is shown that older implementations are not more effective than regular simulated annealing in finding ground state configurations. We propose a new implementation which leads to an improvement over regular simulated annealing.

I-H-3 An Effective Way for Determination of Multicanonical Weights

Ulrich H. E. HANSMANN

[*Phys. Rev. E* in press]

We discuss the use of Tsallis generalized mechanics in simulated annealing algorithms. For a small peptide it is shown that older implementations are not more effective than regular simulated annealing in finding ground state configurations. We propose a new implementation which leads to an improvement over regular simulated annealing.

I-H-4 A New Look at the 2d Ising Model from Exact Partion Function Zeros for Large Lattice Sizes

Nelson A. ALVES *(Univ. Sao Paulo)*, **J. R. Drugowich de FELICIO** *(Univ. Sao Paulo)* **and Ulrich H. E. HANSMANN**

[*Int. J. Mod. Phys* in press]

A general numerical method is presented to locate the partition function zeros in the complex b plane for large lattice sizes. We apply this method to the 2D Ising model and results are reported for square lattice sizes up to L=64. We also propose an alternative method to evaluate corrections to scaling which relies only on the leading zeros. This method is illustrated with our data.

I-H-5 Parallel Tempering Algorithm for Numerical Studies of Biological Macromolecules

Ulrich H. E. HANSMANN

[*Chem. Phys. Lett.* submitted]

We discuss the use of Tsallis generalized mechanics in simulated annealing algorithms. For a small peptide it is shown that older implementations are not more effective than regular simulated annealing in finding ground state configurations. We propose a new implementation which leads to an improvement over regular simulated annealing.

I-H-6 Molecular Dynamics, Langevin, and Hybrid Monte Carlo Simulations in Generalized Ensemble

Ulrich H. E. HANSMANN and Yuko OKAMOTO

We demonstrate that the newly developed generalized-ensemble algorithm (U. H. E. Hansmann and Y. Okamoto, *Phys. Rev. E* **56**, 2228 (1997)) is not restricted to Monte Carlo methods, but can also be applied to simulation techniques such as molecular dynamics, Langevin, and hybrid Monte Carlo algorithms. The effectiveness of the methods are tested with an energy function for the protein folding problem. Simulations in the generalized ensemble by the three methods are performed for a penta peptide, Met-enkephalin. For each algorithm, it is shown that from only one simulation run one can not only find the global-minimum-energy conformation but also obtain probability distributions in canonical ensemble at any temperature, which allows the calculation of any thermodynamic quantity as a function of temperature.

I-I Theoretical Studies of Chemical Reaction Dynamics

I-I-1 Quantum Dynamics of O(^{3}P) + HCl → OH + Cl: Effects of Reagent Rotational Excitation

Katsuyuki NOBUSADA, Kengo MORIBAYASHI *(NIFS, Nagoya)* **and Hiroki NAKAMURA**

[*J. Chem. Soc. Faraday Transactons* **93**, 721 (1997)]

Accurate quantum dynamics of the chemical reaction O (^{3}P) + HCl (j_i, v_i=0) → OH (j_f,v_f=0) + Cl is studied using the hyperspherical coordinate approach and the Koizumi-Schatz-Gordon (KSG) potential-energy surface. The effects of reagent rotational excitation on the dynamics are investigated. The study considers total energies up to 0.7 eV and reagent rotational states, j_i=0-10. The total reaction cross-section shows a strong dependence on j_i. This overall trend is enhanced on increasing the total energy. The final rotational state (j_f) distributions are also investigated. Interestingly, the distribution shows a peak at high j_f ($\approx$ 10) irrespective of j_i and the total energy. The qualitative features are quite similar to the experimental results. Finally, the state-resolved rate constant and the thermal rate constant are evaluated. Because of the enhancement of the reaction by the reagent rotational excitation, the state resolved rate constants for $8 \lesssim j_i \leqq 10$ are two or three orders of magnitude larger than those for j_i=5. The thermal rate constant obtained is thus much larger than

the experimental data implying that the barrier height of the KSG surface may be too low.

I-I-2 Hyperspherical Elliptic Coordinates for the Theory of Light Atom Transfer Reactions

Oleg I. TOLSTIKHIN *(Lebedev Inst., Russia and IMS)* **and Hiroki NAKAMURA**

The newly developed hyperspherical elliptic coordinates system is applied to heavy-light-heavy reactions. The whole reactive scattering process is formulated. This coordinate system combined with the Slow/Smooth Variable Discretization method proves to be very effective not only in numerical calculations but also in elucidating reaction mechanisms. Noadiabatic couplings between the two angle variables and also between the hyperradius and the 2D angle variables can be nicely treated. Adiabatic separation between the two angle variables also holds well.

I-I-3 Quantum Mechanical Elucidation of Reaction Mechanisms of Heavy-Light-Heavy Systems: Role of Potential Ridge

Katsuyuki NOBUSADA, Oleg I. TOLSTIKHIN *(Lebedev Inst., Russia and IMS)* **and Hiroki NAKAMURA**

A new idea to elucidate quantum reaction dynamics of heavy-light-heavy (HLH) systems is proposed on the basis of a hyperspherical elliptic coordinates approach. This coordinate system has a big advantage of nicely expressing good vibrational adiabaticity in the HLH systems. Taking this advantage, the concept of potential ridge is introduced, for the first time, in three-dimensional reactions. The potential ridge is proved to be very useful to extract some important avoided crossings which dominate the reaction dynamics. In fact, qualitative features of the reaction dynamics can be interpreted in terms of non-adiabatic transitions at those important avoided crossings near the potential ridge. Examples are: (i) onset of reactions for specified initial rotational states, and (ii) major reactive transition for a specified initial rotational state. Avoided crossings away from the ridge are also useful to interpret certain aspects of reactions accompanying vibrational transitions. The new idea mentioned above is applied to a typical HLH reaction $O\ (^3P) + HCl \rightarrow OH + Cl$ with the use of two types of potential energy surfaces.

I-I-4 Cumulative Reaction Probability without Absorbing Potentials

Oleg I. TOLSTIKHIN *(Lebedev Inst., Russia and IMS)*, **Valentine N. OSTROVSKY** *(Univ. St. Petersburg, Russia and IMS)* **and Hiroki NAKAMURA**

Cumulative reaction probability, introduced in the collision theory by W. H. Miller, characterizes a net efficiency of a rearrangement process as a function of the collision energy. We derive a formula that expresses this quantity in terms of the outgoing wave Green function. Our formula is free from the ambiguities of previous formulations; in particular, no absorbing potentials are required for its implementation. The formula has a potentially wide range of applications in atomic collision physics as well as in chemical reaction dynamics. As an illustration, we consider the rearrangement collisions in the dtμ system for the energies up to the n=6 threshold.

I-J Theory of Nonadiabatic Transitions

I-J-1 Semiclassical Theory of Multi-Channel Curve Crossing Problems: Landau-Zener Case

Chaoyuan ZHU and Hiroki NAKAMURA

[*J. Chem. Phys.* **106**, 2599 (1997)]

A two-by-two diabatic propagation method is developed to deal with general one-dimensional multi-channel curve crossing problems. Each crossing is treated within the newly completed two-state semiclassical theory in the diabatic representation and is represented by a nonadiabatic transition matrix (I-matrix). A product of all the I- matrices yields the reduced scattering matrix for the entire system. This theory can handle the multi-channel curve crossing problems as simply as a two-state problem. An analysis of the complex crossing points in the momentum space can provide a comprehensive illustrative criterion of this method. A detailed severe numerical test is made by taking a seven-state system with six and twelve nonzero diabatic couplings. It is demonstrated that dominant processes among the state-to-state transitions are well reproduced by the present semiclassical theory.

I-J-2 Usefulness of the Newly Completed Semiclassical Theory of Curve Crossing: Multi-Channel Resonant Scattering

Chaoyuan ZHU and Hiroki NAKAMURA

[*Chem. Phys. Lett.* **274**, 205 (1997)]

A resonant multi-channel curve crossing problem is investigated by using the two-state semiclassical theory recently completed by the authors. The complex phase integral in the nonadiabatic tunneling type curve crossing is accurately replaced by the phase integral on the real axis. Thanks to this, the transition matrix propagation method based on the two-state theory can be easily applied to multi-state curve crossing problems without any restriction on the number of crossings and states. The present theory can nicely handle even the case that the collision energy is lower than the highest avoided crossing. Numerical comparisons with the exact quantum results for a three-state problem clearly demonstrate excellence of the theory. Even detailed feature of dense resonances is very accurately reproduced. It should be emphasized that the theory does not

require any complex calculus, any diabatization procedure, and any information on the couplings.

I-J-3 Semiclassical Theory of Multi-Channel Curve Crossing Problems: Nonadiabatic Tunneling Case

Chaoyuan ZHU and Hiroki NAKAMURA

[*J. Chem. Phys.* in press]

Based on the new two-state theory of curve crossing recently completed by the authors, a compact and powerful theory is formulated for a general resonant multi-channel scattering with nonadiabatic tunneling (NT) type curve crossings. This theory is demonstrated to work remarkably well by comparing with the numerical solutions of close-coupling equations. Even detailed structures of overlapping resonances are nicely reproduced by the theory. Furthermore, this theory is very simple, not requiring any non-unique diabatization procedure, any complex calculus and any information on the couplings, neither diabatic nor nonadiabatic. The theory is based only on the adiabatic potentials on the real axis. Together with the previously proposed theory for the Landau-Zener (LZ) type curve crossings, the present semiclassical theory provides a complete picture of and a very powerful tool for multi-channel curve crossing problems.

I-J-4 Semiclassical Theory of Time-Dependent Curve Crossing Problems

Yoshiaki TERANISHI *(Grad. Univ. for Advanced Studies)* **and Hiroki NAKAMURA**

[*J. Chem. Phys.* **107**, 1904 (1997)]

It is shown that the newly completed accurate semiclassical theory for time-independent curve crossing problems can be usefully utilized to study various time-dependent curve crossing problems. Quadratic time-dependent problems can be solved exactly with use of the theory developed for the time-independent linear potential model. Furthermore, accurate and compact semiclassical theory can be formulated for general curved potentials. Even diabatically avoided crossing cases can be nicely treated. Multi-level problems can also be handled without difficulty with use of a new method to evaluate the necessary basic parameters directly from adiabatic potentials on the real axis in the fully diagonalized adibatic representation. This method does not require a search for complex crossing points in the multi-level system, which is practically very difficult especially when the number of levels exceeds three.

I-J-5 Exact Analytical Solution of the N-Level Landau-Zener Type Bow-Tie Model

Valentine N. OSTROVSKY *(Univ. St. Petersburg, Russia and IMS)* **and Hiroki NAKAMURA**

[*J. Phys. A.* **30**, 6939 (1997)]

The non-stationary Schrödinger equation in finite basis of states is considered for the Hamiltonian matrix linearly depending on time. Exact analytical solutions of asymptotic transition probabilities are obtained for a bow-tie model, in which an arbitrary number of linear time-dependent diabatic potential curves cross at one point and only a particular horizontal curve has interactions with the others. Based on the contour integral method used, some mathematical aspects such as a possible generalization of the Whittaker functions are also briefly discussed.

I-J-6 Semiclassical Theory of Nonadiabatic Transition in a Two-State Exponential Model

Vladimir I. OSHEROV *(Inst. Chem. Phys., Russia and IMS)*, **Vladimir G. USHAKOV** *(Inst. Chem. Phys., Russia)* **and Hiroki NAKAMURA**

A general two-state exponential potential model is solved with use of the Bessel transformation and the WKB (Wentzel-Kramers-Brillouin) type semiclassical approximation. Accurate expressions are obtained for the nonadiabatic transition probability for one passage of the transition point and for the two dynamical phases. Functionalities of these quantities in terms of two basic parameters are the same as those obtained before by Nikitin. The two basic parameters are, however, expressed in more general and accurate forms. Accuracies of these expressions are numerically confirmed. The three quantities, the nonadiabatic transition probability and the two dynamical phases, constitute the nonadiabatic transition matrix and can be used to describe various (spectroscopic as well as scattering) processes not only for a two-state but also for a multi-channel system. A possible generalization of the present theory is also briefly discussed to formulate a unified theory which can cover both Landau-Zener-Stueckelberg and Rosen-Zener-Demkov cases within the adiabatic state representation.

I-J-7 Semiclassical Mechanics of Cubic Potentials

Yoshiaki TERANISHI *(Grad. Univ. for Advanced Studies)* **and Hiroki NAKAMURA**

It is well known that linear and quadratic potential problems can be solved exactly by the Airy and Weber functions. Recently, Zhu and Nakamura derived analytical solutions of the Stokes constants for general cubic potential problems. However, the solutions are given in the forms of infinite series and are not very convenient for applications. Here, we have derived simple and accurate fitting formulas of the Stokes constants, which enable us to deal with quantum mechanical problems of cubic potentials easily. This solution can also be applied to such higher order potential problems in which three turning points are close together and separated from the others.

I-K Theoretical Studies of Characteristics and Dynamics of Superexcited States of Diatomic Molecules

I-K-1 Characteristics and Dynamics of Superexcited States of Diatomic Molecules

Miyabi HIYAMA *(Grad. Univ. for Advanced Studies)* **and Hiroki NAKAMURA**

Characteristics and dynamics of superexcited states (SES) of diatomic molecules are discussed mainly from the theoretical view-point. A recently developed general theoretical procedure to reveal the characteristics and dynamics is briefly reviewed. The method is based on the multi-channel quantum defect theory (MQDT), but effectively utilizes quantum chemical calculations of electronic states and spectroscopic experiments. This would break the bottleneck of the theoretical studies and is expected to be useful to reveal SESs of diatomic molecules. The framework of MQDT is briefly explained to help understanding the procedure. Theoretical studies of the SESs of H_2, NO, and CO made so far are also shortly summarized.

I-K-2 Two-Center of Coulomb Functions

Miyabi HIYAMA *(Grad. Univ. for Advanced Studies)* **and Hiroki NAKAMURA**

[*Comp. Phys. Comm.* **103**, 209 (1997)]

Two-center Coulomb functions are crucial to describe the ionization continua of diatomic molecules, since the latter cannot be well represented by linear combinations of one-center Coulomb functions. A code to numerically evaluate the two-center angular as well as radial regular Coulomb functions is presented here.

I-K-3 Gausian Expansions of the Two-Center Coulomb Functions

Miyabi HIYAMA *(Grad. Univ. for Advanced Studies)* **and Hiroki NAKAMURA**

[*Comp. Phys. Comm.* **103**, 197 (1997)]

Short range portions of two-center Coulomb functions at positive energies are decisive to evaluate the various transition matrix elements between ionization continua and bound states. A method to represent them in terms of Gaussian functions is developed here. This enables us to effectively utilize a conventional quantum chemical CI code to evaluate the electronic transition matrix elements to describe the ionization processes of diatomic molecules.

I-L New Molecular Switching Elements

I-L-1 Molecular Switching in One-Dimensional Finite Periodic Nonadiabatic Tunneling Potential Systems

Shinkoh NANBU, Hiroki NAKAMURA and Frank O. GOODMAN *(Univ. Waterloo, Canada and IMS)*

[*J. Chem. Phys.* **107**, 5445 (1997)]

A new idea of molecular switching is presented. The idea is based on the intriguing phenomenon of complete reflection which occurs in a two-state potential curve crossing of the nonadiabatic tunneling type. Complete switching of transmission is theoretically possible in one-dimensional systems by introducing impurities in the system. The basic semiclassical theory is presented, and the phenomenon of complete reflection is clearly interpreted and numerically demonstrated. An idea of an energy filter is also introduced to facilitate the switching efficiently. The possibility of bound states in the continuum is also clarified. This new molecular switching is numerically realized by the wave packet propagation.

I-M Rydberg States in External Fields

I-M-1 Rydberg Atom in Time-Periodic Fields: Intrashell Dressed States and Quasienergy Spectrum

Andrey K. KAZANSKY *(Univ. St. Petersburg, Russia and IMS)*, **Valentine N. OSTROVSKY** *(Univ. St. Petersburg, Russia and IMS)* **and Hiroki Nakamura**

[*Laser Phys.* **7**, 1 (1997)]

Time evolution of a hydrogen Rydberg atom placed in homogeneous electric and magnetic fields with an arbitrary time dependence is considered. Within the manifold of electronic states with the same principal quantum number n, the problem is effectively reduced to solution of two independent two-state problems. Thus, the "dressed states" are constructed which account exactly for all intrashell transitions. For the time-periodic fields, the general structure of the quasienergy spectrum is recovered as two equidistant overlaying patterns. The Rydberg atom placed in the monochromatic elliptically polarized electric fields with a possible presence of its static component and of the static magnetic field is considered in more detail as a generic case. We show that by varying the fields parameters the whole quasienergy spectrum could be shrinked to zero. The possible applications of this effect are discussed. The revivals of Rydberg wave packets and the possibility of complete population transfer (or quantum control) are also analyzed.

I-N Some Basics of Scattering Theory

I-N-1 Siegert Pseudo-States as a Universal Tool: Resonances, S-Matrix, Green Function

Oleg I. TOLSTIKHIN *(Lebedev Inst., Russia and IMS)*, **Valentine N. OSTROVSKY** *(Univ. St. Petersburg, Russia and IMS)* **and Hiroki NAKAMURA**

[*Phys. Rev. Lett.* **79**, 2026 (1997)]

The Siegert states have been long recognized as a potentially powerful tool in the formal scattering theory. Here we propose an efficient method to implement this power in practice. Our method yields bound states, complex-energy resonances, and scattering wave functions, i. e. a complete solution of the Schrödinger equation. We also obtain a representation of the Green function suitable for a variety of applications. The method is demonstrated by realistic examples of the eep and dtμ three-body Coulomb systems.

I-N-2 Flux Formulations of Scattering Theory

Oleg I. TOLSTIKHIN *(Lebedev Inst., Russia and IMS)*, **Valentine N. OSTROVSKY** *(Univ. St. Petersburg, Russia and IMS)* **and Hiroki NAKAMURA**

Scattering theory is reformulated in terms of the flux in a fully systematic way. Scattering matrix is expressed in terms of flux and Green function. By choosing the integration surfaces on which the fluxes are evaluated to be close to the interaction domain, we can derive a new general formula for the cumulative reaction probability for rearrangement collisions.

I-O Fokker-Planck Equation Approach to Quantum Dynamics in Condensed Phases

We have discussed quantum dynamics of molecular system in condensed phases using the multi-state quantum Fokker-Planck equation for a colored Gaussian-Markovian noise bath, which was derived by Tanimura and Wolynes. Effects of dissipation on various quantum processes are discussed.

I-O-1 Gaussian-Markovian Quantum Fokker-Planck Approach to Nonlinear Spectroscopy of a Displaced Morse Potentials System: Dissociation, Predissociation and Optical Stark Effects

Yoshitaka TANIMURA and Yutaka MARUYAMA

[*J. Chem. Phys.* **107**, 1779 (1997)]

Quantum coherence and its dephasing by coupling to a dissipative environment play an important role in time-resolved nonlinear optical response as well as nonadiabatic transitions in the condensed phase. We have discussed nonlinear optical processes on a multi-state one- dimensional system with Morse potential surfaces in a dissipative environment. This was based on a numerical study using the multi-state quantum Fokker-Planck equation for a colored Gaussian-Markovian noise bath, which was expressed as a hierarchy of kinetic equations. This equation can treat strong system-bath interactions at a low temperature heat bath, where quantum effects play a major role. The approach applies to linear absorption measurements as well as four- wave mixing including pump-probe spectroscopy. Laser induced photodissociation and predissociation have been studied for the potential surfaces of Cs_2. We have calculated nuclear wave packets in Wigner representation and their monitoring by femtosecond pump-probe for various displacements of potentials and heat-bath parameters. Numerical calculations of probe absorption spectra for strong pump pulse are also presented and discussed. The results show dynamical Stark splitting, but, in contrast to the Bloch equations which contain an infinite-temperature dephasing, we find that at finite temperature their peaks have different heights even when the pump pulse is on resonance.

I-O-2 Fifth-Order Two-Dimensional Vibrational Spectroscopy of a Morse Potential System in Condensed Phases

Yoshitaka TANIMURA

[*Chem. Phys.* in press]

The nonlinear optical response of a molecular system in the condensed phase subjected to a series of five off-resonant femtosecond laser pulses has been studied using a quantum Gaussian-white Fokker-Planck equation. This equation can treat a molecular system with any shape of potential coupled to a Gaussian-white noise-bath. We have presented the procedure to calculate third- and fifth-order response functions, which are equivalent to the second- and third order correlation functions of molecular coordinate, based on the equation of motion approach.

Assuming the potential surface of Cesium dimer [Cs_2], which is described by the Morse potential, and the linear and nonlinear coordinate dependence of polarizability, we calculated third- and fifth-order response functions for various temperature and heat-bath coupling. By plotting two time-evolution period involved in the fifth-order spectroscopy, we obtained the two-dimensional profiles of signal. These 2D profiles are sensitive for a shape of potential and poralizability, even for a strong damping case, and depend on the temperature. This indicates that fifth-order two- dimensional spectroscopy carried out for different temperature allows us to access information of potential surfaces and polarizability.

I-P Path integral Approach to Nonlinear Optical Spectroscopy of Molecules in the Condensed Phase

The nonlinear optical response of molecules in condensed phases subjected to femtosecond laser pulses is studied using path integral techniques.

I-P-1 Sensitivity of Two-Dimensional Fifth-Order Raman Response to the Mechanism of Vibrational Mode-Mode Coupling in Liquid Molecules

Ko OKUMURA and Yoshitaka TANIMURA

[*Chem. Phys. Lett.* in press]

We study coupling mechanism of inter- and intramolecular modes of liquids by using a multi-mode Brownian oscillators model. The coupling between modes comes into play through polarizability and/or potential expanded with respect to vibrational coordinates. We take into account these two causes of coupling and present analytical expressions for the Fourier transform of the time-domain fifth-order Raman signal. We demonstrate a notable sensitivity of the Fourier-transformed quantity to the coupling mechanism through numerical calculations for chloroform.

I-P-2 Interplay of Inhomogeneity and Anharmonicity in 2D Raman Spectroscopy of Liquids

Ko OKUMURA and Yoshitaka TANIMURA

[*Chem. Phys. Lett.* **277**, 159 (1997)]

Molecular vibrational modes of liquids are studied using the multi-mode Brownian motion model. We examine the effects of inhomogeneity on anharmonic contribution to the 2D Raman spectroscopy. We consider three types of inhomogeneous distribution of local oscillators and present analytical expressions for the 2D signal where the lowest-order anharmonicity is taken into account. Numerical estimations of them in the case of a simple single-mode system clarify the effects of the inhomogeneity. A multi-mode system with anharmonicity and nonlinear polarizability is also studied and numerically compared with a recent experiment on CS2, which suggests a minor role of the inhomogeneity in this substance.

I-P-3 Coherent Two-Dimensional Raman Scattering: Frequency-Domain Measurement of the Intra- and Intermolecular Vibrational Interactions

Minhaeng CHO *(Korea University and IMS)*, **Ko OKUMURA and Yoshitaka TANIMURA**

[*J. Chem. Phys.* in press]

A new experiment of frequency-domain coherent two-dimensional Raman scattering is theoretically proposed. By using three fields whose wavevectors and frequencies are independently controlled, one can measure the nonlinear Raman responses in either gas or condensed phases. The connection ~o the time-domain femtosecond two-dimensional Raman spectroscopy is completely established. By considering several limiting cases in detail, it is found that from the coherent 2D Raman scattering spectrum one can obtain quantitative information on the anharmonicity, anharmonic mode coupling, and polarizability coupling.

I-P-4 Two-Time Correlation Functions of a Harmonic System Nonbilinearly Coupled to a Heat Bath: Spontaneous Raman Spectroscopy

Ko OKUMURA and Yoshitaka TANIMURA

[*Phys. Rev. E* **56**, 2747 (1997)]

A harmonic system coupled to a heat bath comprised of harmonic oscillators through a non-bilinear system-bath interaction q2 qj is considered, where q and qj are the system and bath coordinates, respectively. The two-time correlation functions for the model are analytically obtained through a diagrammatic expansion. Numerical calculations of the analytical results are presented for the spontaneous (frequency-domain) Raman spectroscopy. Comparison with numerical results from the conventional linear-coupling model (the Brownian oscillator model) are made, which indicates experimentally distinguishable temperature dependencies.

I-P-5 The Optimized Perturbation Theory to Femtosecond Vibrational Spectroscopy of a Diatomic Molecule System in Condensed Phases

Yoko SUZUKI and Yoshitaka TANIMURA

We apply the optimized perturbation theory (OPT) to a dimer molecule system in condensed phases described by a Morse potential system coupled to a heat-bath. The OPT combines the techniques based on the variational principle and the perturbative method. It can give non-perturbative results and the first order approximation of the OPT agrees with the Feynman's variational theory developed for the polaron problem. The Morse potential system is anharmonic and a molecule described by this potential shows dissociation at high temperatures. The OPT allows us to include anharmonicity of potential non-perturbatively. Using the OPT in path integral formalism, we calculate the absorption spectrum of the molecule system which relates to a two-time correlation function of a nuclear coordinate.

I-Q Theoretical Studies of Molecular system coupled to nonGaussian-Markovian Environment

We study dynamics of two-level molecular system driven by a nonGaussian-Markovian noise, such as fractal noise. We calculate various physical observable corresponding to optical measurements and explore the novel feature of nonGaussian-Markovian noise as a subject of femtosedond spectroscopy.

I-Q-1 Spectral Random Walks and Line Broadening of Impurity Molecules in an Ising Spin Glass Environment

Yoshitaka TANIMURA, Hiroshi TAKANO *(Keio Univ.)* **and Joseph KLAFTER** *(Tel-Aviv Univ.)*

[*J. Chem. Phys.* in press]

Transition energy fluctuations in impurity molecules, embedded in an inhomogeneous environment, are investigated within an Ising spin model of the environment. The spatially distributed impurity molecules are assumed to interact with the Ising spin glass through dipole- dipole type of interaction. We calculate the fluctuations in the transition energies of each molecule, for different temperatures and various Ising parameters, and find that the spectral distribution of the fluctuations follows approximately 1/f power law. The fluorescence spectra of the impurity molecules yield microscopic information about domain structures in the Ising environment. In the case of large disorder, the distribution of transition energies shows profiles similar to those observed in single molecule spectroscopy.

I-Q-2 Effects of Colored Noise Bath on the Spectra of a Strongly Driven Two-Level System

Gautam GANGOPADHYAY, Sharmisthia GHOSALL and Yoshitaka TANIMURA

[*J. Phys. Soc. Jpn.* submitted]

We have constructed a system-heat bath theory for a two-level system coupled to the colored bath in the Born approximation at finite temperature. It is shown that depending on the bandwidth and temperature of the bath, a coherent dynamics may set in the reduced system, when the reduced system is already driven by a strong field. In absence of the driving field, the reduced system assumes the Boltzmann distribution in the steady state. We have shown the effect of colored bath on the strong field induced resonance fluorescence spectra. When the driven system is probed by a weak field the absorption and dispersion profiles show up some dramatic effect due to finite temperature of the colored bath.

I-R Electronic Structure of a Molecule in Solution

Chemical reaction is undoubtedly the most important issue in the theoretical chemistry, and the electronic structure is a key to solve the problem. As long as molecules in the gas phase are concerned, the theory for the electronic structure has been enjoying its great success. However, when it comes to molecules in solution, the stage of theory is still an infant. We have recently proposed a new method refered to as RISM-SCF based on the integral equation theory of molecular liquids (RISM) and the ab initio electronic structure theory (SCF).[1] The integral equation approach replaces the reaction field in the continuum models by a microscopic expression in terms of the site-site radial distribution functions between solute and solvent.

$$V_\lambda = \rho \sum_j \int_0^\infty \frac{q_j}{r} g_{\lambda j}(r) 4\pi r^2 \mathrm{d}r$$

where j and λ specify solvent and solute sites, respectively, and r denotes the solvent density. The site-site radial distribution functions $g_{\lambda j}(r)$ can be calculated from the extended RISM equation. Using V_λ the solvated Fock operator is defined as, where b_λ is a population operator of solute atoms. The statistical solvent distribution around solute is determined by the electronic structure or the partial charges of solute, while the electronic structure of solute is influenced by the solvent distribution. Therefore, the Hartree-Fock equation and the RISM equation should be solved in a self-consistent manner. It is this self-consistent determination of the solute electronic structure and the solvent distribution around the solute that features the RISM-SCF procedure.

The method has been further generalized to the multi configurational self - consistent field (MCSCF) method which enables us calculation of the excited state as well as optimized molecular geometry in solution.[2]

The latest development along this line are reported below.

References

1) S. Ten-no, F. Hirata and S. Kato, *Chem. Phys. Lett.* 214, 391 (1993); *J. Chem. Phys.* 100, 7443 (1994).
2) H. Sato, F. Hirata and S. Kato, *J. Chem. Phys.* 105, 1546, (1996).

I-R-1 *Ab initio* Study of Water: Self-consistent Determination of Electronic Structure and Liquid State Properties

Sarah MAW *(Univ. Manchester)*, **Hirofumi SATO, Seiichiro TEN-NO and Fumio HIRATA**

[*Chem. Phys. Lett.* **276**, 20 (1997)]

We proposed a theoretical study of liquid water based on the coupled ab initio electronic structure theory and the integral equation method of liquids. The effective atomic charges of a water molecule determined from the ab initio method in liquid were greater by about twenty percent than the corresponding empirical parameters for the SPC and TIP3P models due essentially to the use of insufficient basis sets. The effective charge monotonically decreased with increasing temperature. The behavior was attributed to the decreased anisotropy of the electrostatic field due to the increased molecular rotation. The free energy was decreased monotonically with temperature. The behavior is in qualitative accord with experiments.

I-R-2 Molecular Theory of Solvent Effect on keto-enol Tautomers of Formamide in Aprotic Solvents: RISM-SCF Approach

Tateki ISHIDA *(Kyoto Univ.)*, **Fumio HIRATA, Hirofumi SATO and Shigeki KATO** *(Kyoto Univ.)*

[*J. Phys. Chem.* submitted]

By using RISM-SCF method, the optimized geometries and solvation free energies of the keto and enol tautomers of formamide were calculated in six organic aprotic solvents (CS_2, CCl_4, DME, THF, acetonitrile, and DMSO). From the analysis of the solvation free energies, it was shown that the solute-solvent hydrogen bonding largely contributed to them and that the ability of the solvent to form hydrogen bondings is very important. It was also shown that Taft's β parameters are well-correlated to the calculated well-depth of hydrogen bonding. The results that the solvation free energies for both the tautomers showed the irregularity in acetonitrile solution are in qualitative accord with the empirically determined solvent parameters. The empirical measure of solvent ability to form hydrogen-bonding with solute is explained at a molecular level.

The solvent effects on the energy difference between the keto-enol tautomers were examined. It was found that the keto tautomer was stabilized largely compared to enol form. These tendencies are consistent with the experimental and previous theoretical results. In both tautomers, the dipole moments of solutes were enhanced in polar solvents and the geometric structures were changed, so as to increase the solute dipole moment. It was found that the tendency of solute dipole moments was correlated to Taft's parameters with respect to solvent polarity.

I-S Solvation Thermodynamics of Protein and Related Molecules

Concerning biomolecules such as protein, it is a final goal for the biochemistry and biophysics to explore the relation between conformations and biological functions. The first important step toward the goal would be to explain the conformational stability of biomolecules in terms of the microscopic structure of the molecules in solvent. It is an extremely difficult problem by any means due to the overwhelmingly large degrees of freedom to be handled, including protein and solvent. As long as the small and/or short-time fluctuations of protein around the native structure is concerned, a variety of molecular simulation techniques is a quite powerful tool to explore the microscopic structure of protein and solvent. However, the techniques are not so effective to characterize stability of the macromolecules, to which the thermodynamic limit is concerned. The semi-microscopic approach based on the Poisson-Boltzmann equation and the scaled particle theory deserves to draw attention from such a view point.[1] In spite of the oversimplification employed for the model of solvent, the method could have succeeded to reproduce fundamental characteristics of the solvation thermodynamics of a protein, including the cold denaturation. An well-addressed weakness of the treatment is the less sophisticated representation of the microscopic structure of solvent water. The extended RISM theory has potential capability of overcoming the problem at least in the level of microscopic description based on the pair correlation functions. Obvious technical difficulties which one may face in applying the theory to such a large system are not only the computation time but also the stability of the numerical solution.[2]

Here, we present our recent effort to tackle the problem based on the two theoretical tools: extended RISM and the scaled particle theory (SPT). The studies for the solvation thermodynamics of small molecules such as ions are also included because it is regarded as elementary processes for the solvation of biomolecules, and because it is prerequisite for studying the more complicated molecules.

References

1) M. Irisa, K. Nagayama and F. Hirata, *Chem. Phys. Lett.* 207, 430 (1993); M. Irisa, T. Takahashi, K. Nagayama and F. Hirata, *Mol. Phys.* 85, 1227 (1995).
2) A. Kitao, F. Hirata and N. Go, *J. Phys. Chem.* 97, 10231 (1993).

I-S-1 Analysis on Salt Effects on Solubility of Noble Gases in Water Using the Reference Interaction Site Model Theory

Masahiro KINOSHITA *(Kyoto Univ.)* **and Fumio HIRATA**

[*J. Chem. Phys.* **106**, 5202 (1997)]

We have developed robust and very efficient algorithms for solving the reference interaction site model (RISM) equations for salt solutions in the bulk and near a solute atom of noble gases. The theory of dielectric consistency recently developed for solutions at finite

salt concentrations is employed in the formalism. The change in water structure in the bulk caused by addition of salts have been examined for model 1-1 salt solutions (LiCl, NaCl, KCl, KF, KBr, KI and CsI). The density and orientational structures of each salt solution near a solute atom have been analyzed. Ions characterized by positive hydration (F^-, Li^+ and Na^+) are strongly hydrated in the bulk and stay sufficiently far from the atom. Those of negative hydration (Cl^- and Br^-) or hydrophobic hydration (Cs^+ and I^-) are excluded from the bulk to the atom. Due to a specific orientational order of water molecules adjacent to the solute atom, there is a trend that cations stay less closer to the atom than anions. The relation between these structures and the salting coefficient is discussed in detail. The agreement between the calculated and experimental values for the salting coefficient is excellent for He. However, the discrepancy becomes larger as the number of electrons of the solute atom increases (the calculated value is always larger), which implies that the ion-induced dipole interaction neglected has significantly large effects.

I-S-2 Calculation of Hydration Free Energy for a Solute with Many Atomic Sites Using the RISM Theory: Robust and Efficient Algorithm

Masahiro KINOSHITA *(Kyoto Univ.)*, **Yuko OKAMOTO and Fumio HIRATA**

[*J. Comp. Chem.* **18**, 1320 (1997)]

We have developed a rebust and very efficient algorithm for solving the reference interaction site model (RISM) equations for water near a solute molecule with many atomic sites (interaction sites). It is a hybrid of the Newton-Raphson and Picard methods. Various considerations are given so that the computer time can be saved as greatly as possible. It has been demonstrated for calculating hydration free energies of metenkephalin (a peptide with 73 sites) with different conformations. Its stability is quite insensitive to the initial guess. The Jacobian matrix is treated as part of the input data, and even the same matrix can be used for another conformation unless the conformation is considerably different from the last one.

I-S-3 Ion Hydration: Thermodynamic and Structural Analysis with an Integral Equation Theory of Liquids

Song-Ho CHONG *(Kyoto Univ.)* **and Fumio HIRATA**

[*J. Phys. Chem. B* **101**, 3209 (1997)]

We present a theoretical study for the ion hydration based on an integral equation method referred to as the extended reference interaction site method (ex-RISM). We analyze the thermodynamic functions of solvation, especially the partial molar volumes of individual ions at infinite dilution. A special attention is paid to information contained in the partial molar volumes, and to the problem if the partial molar volumes of individual ions reflect the true nature of ion-water interactions. Our results suggest, on the contrary to the previous work given by Kusalik and Patey, that the partial molar volumes do reflect the nature of ion-water interactions. Concerning the microscopic description of the ion hydration, the earlier model proposed by Samoilov is revisited based on ex-RISM. Characterization due to the integral equation method is found to be in an accord with that proposed by Samoilov. We also discuss the structural changes of water due to the presence of an ion utilizing the density derivatives of the solvent distribution functions. Qualitative difference of the density derivatives between the so-called 'positively hydrated' and 'negatively hydrated' ions was observed and found to be consistent with the analysis of the potential of mean force.

I-S-4 Solvation Structure and Stability of Peptides in Aqueous Solutions Analyzed by the Reference Interaction Site Model Theory

Masahiro KINOSHITA *(Kyoto Univ.)*, **Yuko OKAMOTO and Fumio HIRATA**

[*J. Chem. Phys.* **107**, 1586 (1997)]

The full RISM equations have been solved for a dipeptide and Met-enkephalin in the SPC/E water using our robust, highly efficient algorithm. Some different conformations of these peptides have been considered. The site - site pair distribution functions and hydration free energies calculated as major output data have been analyzed in detail. It has been shown that solvent plays essential roles in determining the conformation of the peptide and that the RISM theory is a promising tool for taking account of the solvent effects.

The most stable conformation of the peptide in water is the one that has the lowest total energy. The total energy is determined not only from the conformational energy but from the interactions with water molecules which are greatly dependent on the peptide conformations. The conformations of Met-enkephalin determined in NMR experiments are quite different from the lowest-energy conformation in gas phase. We have tested four different conformations including the lowest-energy conformation (conformation 1) and a conformation which is similar to the experimentally determined conformations (conformation 4). It has been shown that conformation 4 is the most stable in water with the lowest total energy in both of the unionized and zwitterion cases. (Actually, we have tested more conformations that we described in the present article, and still conformation 4 is the most stable.) It is interesting that a conformation which is similar to that obtained from the NMR experiments in miceller solutions, is the least stable when it is put in water. Although the effects due to 0.05*M* CH_3COONa in the solution used in the NMR experiments are unknown and need to be investigated in further studies, our results are quite encouraging. When the SPC/E water is replaced by a simple, repulsive potential system, the lowest-energy conformation in gas phase is still the most stable among the four conformations, because the solvation free energy is much less dependent on the conformations than in the water case. Water is clearly distinguished from the simple solvent even when all the site-charges of the peptide are set to zero.

The site-site pair distribution function $g_{AB}(r)$ for atom A (B is a water hydrogen or oxygen) and the conformation from this atom to the hydration free energy is greatly dependent on the neighboring atoms. An atom with a large (negative or positive) site - charge is covalently bonded with oppositely charged atoms with certain core diameters in most cases. Consequently, the first-peak values of $g_{AB}(r)$ for carbonyl carbons, oxygens, and nitrogens are much lower than those for the isolated atoms (imaginary spherical particles). Compared with the hydration free energies of the isolated atoms, the contributions from these atoms of the peptide to the hydration free energy are considerably shifted in more hydrophobic directions. The superposition approximation, in which the entire free energy of a peptide is expressed as the sum of the potential of mean forces between pairs of isolated atoms, is a poor approximation.

The carbonyl oxygen is covalently bonded only with one atom (carbonyl carbon), and it often forms very strong bonding with water-hydrogens. In general, oxygens and nitrogens often have relatively large, negative contributions to the hydration free energy due to the formation of hydrogen bonding. This is particularly true for the two oxygens at the C-terminus of zwitterions. When more than two carbonyl oxygens are close together, well exposed to water, and at least one of them is sufficiently far apart from a hydrophobic portion, strong hydrogen bonding is formed between the carbonyl oxygen and water-hydrogens.

The hydration free energy for a portion of the peptide is also greatly dependent on the neighboring portions. For example, the value for CONH of the unionized dipeptide is in the range from 1-3 kcal/mol, while that of Met-enkephalin (unionized) is more variable, ranging from 2-10 kcal/mol. The value for COOH of the dipeptide (1-5 kcal/mol) is smaller than that of Met-enkephalin (4-10 kcal/mol). (We repeat that we have tested more conformations than we describe in the present article.) This is because Met-enkephalin has larger hydrophobic portions (*e.g.* the phenyl group) and they are often close to CONH or COOH.

In the course of the present study, we have noticed the following. When a hydrophobic atom gets very close to a hydrophilic atom, the hydration free energy for the former decreases while that for the latter increases. However, the sum of the two hydration free energies tends to increase (i.e. shift in a more hydrophobic direction). Though this could be an artifact of the RISM theory and needs to be investigated further, we are inclined to think that for a larger peptide the contribution from the hydrophobic interaction with water becomes larger. In fact, the values of $(\Delta\mu_{SB}-\Delta\mu_{SA})/\Delta\mu_{SB}$ are around 0.9 for the dipeptide while they are -0.35 for Met-enkephalin.

We are now combining the solution of the full RISM equations with powerful conformational sampling methods to find the lowest-energy conformation of a peptide in water. This can be done with moderate computational effort on a workstation because the algorithm used for solving the RISM equations is robust and extremely fast.

I-S-5 Calculation of Solvation Free Energy for a Peptide in Salt Solution Using the RISM Theory

Masahiro KINOSHITA *(Kyoto Univ.)*, **Yuko OKAMOTO and Fumio HIRATA**

[*J. Comp. Chem.* submitted]

We have developed an algorithm for solving the RISM equations for salt solutions near a peptide. It is obtained as an extension of our previously reported algorithm for pure water by solving nontrivial problems posed by the inclusion of salts. The robustness and high efficiency of the algorithm has been demonstrated for a dipeptide with 23 atomic sites in a 1M-NaCl solution. Two different conformations of the dipeptide are considered. It is assumed that the dipeptide is present either as an unionized form or as a zwitterion. The structure of the salt solution near the dipeptide and salt effects on the solvation free energy are briefly discussed.

I-S-6 First-Principle Determination of Peptide Conformations in Solvents: Combination of Monte Carlo Simulated Annealing and RISM Theory

Masahiro KINOSHITA *(Kyoto Univ.)*, **Yuko OKAMOTO and Fumio HIRATA**

[*J. Am. Chem. Soc.* submitted]

We have developed a computer program combining the Monte Carlo simulated annealing and RISM methods. After sampling many conformations of peptides in accordance with the simulated annealing technique, the program finds the conformation with the minimum total energy. The total energy is the sum of the conformational energy and the solvation free energy, and the latter is calculated by the full RISM theory. The usefulness of the program has been demonstrated for Met-enkephalin in water and in a simple repulsive potential system. We have found that only one Jacobian matrix calculated for a conformation can be used throughout the conformational sampling in all the runs tested, leading to considerable saving of computation time. The RISM equations must be solved a number of times, but this can be performed with moderate computational effort because our algorithm for solving the equations is extremely fast. The algorithm has never failed to give convergence.

Since in simple fluids the solvation free energy remains roughly constant against conformational changes, the conformational energy is more important. The most stable conformation in gas phase is still considerably stable in the simple fluids, In water, on the other hand, the relative values of the solvation free energy among different conformations are considerably large. Most of the conformations are strongly rejected by water and the number of probable conformations is drastically reduced, which is suggestive that Met-enkephalin is forced to take conformations favored by water quite rapidly. This result is important in the following two respects: water plays essential roles in stabilizing particular conformations of peptides; and the number of conformations to be sampled is drastically

reduced in water, which could remove computational bottlenecks expected for much larger polypeptides or proteins. It has been shown that in water there are a set of different conformations of Met-enkephalin having almost the same total energies, nearly the lowest values. These conformations exhibit characteristics of almost fully extended ones with large fluctuations, which are in very good agreement with the observations in the recent NMR experiments (these conformations are quite different from the most stable conformation in gas phase).

I-T Spatial and Temporal Density Fluctuation in Molecular Liquids

The latest development in the experimental techniques including the high resolution NMR and a variety of techniques in the time-resolved laser-spectroscopies have revealed the molecular nature of the solvent dynamics around solute or the solvation dynamics, which refuse any naive interpretation based on the continuum models. A microscopic or statistical-mechanical description for the solvation dynamics requires the formulation of the temporal as well as spatial fluctuations of solvent density around solute. A general recipe to such a problem is to use the generalized Langenvin equation (GLE). The GLE in principle gives the dynamics of a system in any resolution in space and time depending on the level of projection. However, its actual usefulness for a problem is largely determined by a choice of dynamic variables onto which other degrees of freedom are projected. It is the pair correlation functions which researves the microscopic nature of the system and yet tractable within the current development in the statistical-mechanical theory of liquids. A natural choices of the dynamic variables which lead to the density-density pair correlation function as an important ingredient in the dynamical equations is a set of the collective density field and its conjugate momentum density field. Such a choice leads to a Smoluchowsky-Vlasov type diffusion equation in the overdamped limit. As to the model for molecular diffusion in polar liquids, there are two quite different point of view. One is the traditional rot-translational model[1] and the other the interaction-site description which sees the diffusion of a molecule as a correlated motion of each atoms (sites).[2][3] The interaction-site description employes the site-site Ornstein-Zernike (SSOZ) equation (or RISM equation) in order to represent the site-site direct correlation functions, which proves to be successful in a variety of application to molecular liquid including water.[3]

In what follows, the latest progress which we have made in the theory of the structure and dynamics of molecular liquids is reviewed. We also report our effort to formulate the non-equilibrium free energy profile along a solvent coordinate based on the extended RISM theory, which has played an essential role in the Marcus theory of the electron transfer reaction.

References

1) D. F. Calef and P. G. Wolynes, *J. Chem. Phys.* 78, 4145 (1983).
2) F. O. Raineri, Y. Zhou, H. L. Friedman and G. Stell, *Chem. Phys.* 152, 202 (1991).
3) F. Hirata, *J. Chem. Phys.* 96, 4619 (1992).

I-T-1 Shear-Induced Distortion of Intramolecular and Intermolecular Correlations in Liquids: Time-Dependent Density-Functional Theory

Shuhei YOSHIDA *(Kyoto Univ.)*, **Fumio HIRATA, and Toyonori MUNAKATA** *(Kyoto Univ.)*

[*Phys. Rev. E* **54**, 1763 (1996)]

Shear viscosity of molecular liquids is formulated and calculated with use of a time-dependent density functional theory. Allowing for nonrigidity of each molecule, we obtain shear-induced distortion of both intramolecular and intermolecular correlations self-consistently, witch makes it possible to calculated the shear viscosity. As a by-product we derive and solve a hypernetted-chain closure for equilibrium correlation in deformable molecular liquids.

I-T-2 Statistical Mechanics of Deformable Molecular Liquids: Thermal Expansion and Isomerization of Diatomic Molecules

Toyonori MUNAKATA *(Kyoto Univ.)*, **Shuhei YOSHIDA** *(Kyoto Univ.)* **and Fumio HIRATA**

[*Phys. Rev. E* **54**, 3687 (1996)]

Equilibrium two-body correlations in liquids composed of deformable molecules are formulated with use of the density functional theory and the interaction site formalism. As applications, we study two model systems, liquid nitrogen and simplified liquid n butane, in which each molecule has two stable bond lengths. The latter may be considered as a toy model to study conformational equilibrium.

I-T-3 Nonlinear Electrical Potential Fluctuations of Solvent around Solutes: an Integral Equation Study

Song-Ho CHONG *(Kyoto Univ.)* **and Fumio HIRATA**

[*J. Chem. Phys.* **106**, 5225 (1997)]

We present s theoretical formulation for the solvent force constant and the asymmetry parameter which characterize the free energy profile governing the electrical potential fluctuations of the solvent molecules around solutes. This formulation allows us the calculation of these parameters via the extended reference interaction site method (ex-RISM), an inte-

gral equation theory developed for molecular liquids and solutions. Since ex-RISM is inherently a nonlinear theory, we can shed some light on the possible nonlinear effects in the electrical potential fluctuations. The nonlinear effects in the solvent force constants and the validity of the linear approximation will be examined by a series of calculations for monatomic and diatomic solutes immersed in various solvents. The origin of the solute-dependent solvent force constants is briefly discussed.

I-T-4 Interaction-Site Representation for Collective Excitations in Diatomic Dipolar Liquid

Song-Ho CHONG *(Kyoto Univ.)* **and Fumio HIRATA**

[*J. Mol. Liq.* submitted]

We described a molecular theory for solvent dynamics which provides a method for calculating the dynamical correlation functions of molecular fluids. The theory is based on the generalized Langevin equation and on the interaction-site model of molecular liquids, and is capable of treating the general class of molecular fluids. As an application of the theory, we calculated the longitudinal current spectra of diatomic dipolar liquid, and discussed the collective excitations in this solvent.

The theory presented here can be applied to the description of time-dependent phenomena in polar fluids: solvation dynamics and dynamical solvent effect on charge transfer reactions will be among the most interesting applications.

In order to refine our theory further, several extensions are conceivable by developing approximation schemes for memory functions. The most promising extension will be adopting the mode-coupling approximation, in view of the success of the mode-coupling theory in describing the time-correlation functions of simple liquids.

I-T-5 Theoretical Study for Water Structure at Highly Ordered Surface: Effect of Surface Structure

Ryo AKIYAMA and Fumio HIRATA

[*J. Chem. Phys.* submitted]

Liquid structures of water at electrode-solution interface were investigated by RISM integral equation, putting special stress on the effect of surface structure. Two types of surface geometry were examined: Au(111)-like geometries which is characterized by the threefold hollow sites in which a water molecule can fit, and flat-like surface geometry. The orientation of water molecules in the vicinity of surface depends strongly on the surface structure. Especially, the difference is significant in the case of negatively charged surface. At Au (111)-like surface with negative charges, angles between the surface normal and both of the two O-H vectors are around 108 degree. The result agrees with that proposed experimentally by surface enhanced infrared absorption spectroscopy (SEIRAS) applied to Au(111) surface in aqueous solution of perchloric acid. On the other hand, in the case of flat-like surface the angle between the surface normal and one of the O-H vector is 180 degree (orientation E in Figure 1), H-atom is available for hydrogen-bonding with bulk water.

In the present study, the hydrogen end of water becomes more oriented toward the solution phase above the potential of zero charge (pzc). Those features qualitatively agree with results proposed by the SEIRAS experiment. However, the orientation of water molecules undergoes significant changes due to the coadsorption of perchlorate ion at a surface with very positive potential.

I-U Theoretical Studies of Low-Dimensional Correlated Electron Systems

Organic materials with very anisotropic electronic conduction show a variety of phases due to the instability of a metallic state described by the Fermi liquid theory. Many of the ground states have been understood within mean-field theories taking account of the nesting property of the Fermi surface. Recently, however, essential importance of electron correlations is recognized in view of incoherent electron motion to the transverse direction(s) in some metallic states, spin gaps in even-leg ladder systems, possibly *d*-wave superconductivity appearing in the neighborhood of antiferromagnetic, spin-density-wave, or even nonmagnetic phases, and Mott insulator phases themselves. Our concerns are (i) Mott transition accompanied with Peierls distortion or $4k_F$ charge-density wave in $(DCNQI)_2M$, (ii) spin-Peierls, spin-density wave, superconductor, and metallic phases and the dimensional crossover in $(TMTCF)_2X$, (iii) spin gap, *d*-wave superconductivity, and one-particle vs. two-particle dimensional crossovers in $Sr_{14-x}Ca_xCu_{24}O_{41}$, (iv) magnetism and possibly exchange-coupling-induced metal-insulator transition in $CoPc(AsF_6)_{0.5}$, and (v) competition between spin-density wave and superconducting phases in $Pd(dmit)_2$ salts.

I-U-1 Various Transitions in Quasi-One-Dimensional Systems under High Pressure

Kenji YONEMITSU, Jun-ichiro KISHINE and Takuhiro OGAWA

[*Special Issue of Rev. High Press. Sci. Tech.* **6**, 360 (1997)]

Different crossovers and transitions are studied for two-band systems by various techniques. Incomplete interference between the Cooper and Peierls channels leads to spin-density wave, *d*-wave superconductor,

and metallic phases with decreasing dominance of the Peierls channel. The discrepancy between the spin gap observed in the static susceptibility and that in the NMR for undoped spin ladder systems is resolved by using free massive Majorana fermions. Metal-insulator transitions in π-d hybrid systems are successfully described by the $1/N$ correction to the mean-field slave-boson approach.

I-U-2 Phonon Effects on Superconducting Phase in Two-Chain Electron Systems

Kenji Yonemitsu

[*Physica C* **282,** 1109 (1997)]

The scaling analysis based on a continuous model shows that superconductivity in a two-band system is broken by sufficiently strong couplings with $2k_F$ and $4k_F$ phonons at quarter filling. Three-dimensionality makes the system an antiferromagnet if the nesting is still perfect and the particle-hole channel becomes dominant in the low-energy limit.

I-U-3 Renormalization-Group Approach to the Metal-Insulator Transitions in (DCNQI)$_2M$ (DCNQI is *N,N'*-Dicyanoquinonediimine and *M*=Ag, Cu)

Kenji Yonemitsu

[*Phys. Rev. B* **56,** 7262 (1997)]

Metal-insulator transitions and different ground-state phases in quasi-one-dimensional materials, (R_1R_2-DCNQI)$_2M$ (R_1=R_2=CH_3, I and M=Ag, Cu), are studied with a renormalization-group method. We use one-dimensional continuum models with backward scatterings, umklapp processes and couplings with $2k_F$ and $4k_F$ phonons (not static lattice distortion). We take a quarter-filled band for M=Ag and a sixth-filled band coupled with a third-filled band for M=Cu. Depending on electron-electron and electron-phonon coupling strengths, the ground-state phase becomes a Tomonaga-Luttinger liquid or a state with a gap(s). For M=Ag, there appear a spin-gap state with a dominant $2k_F$ charge-density-wave correlation, a Mott insulator with a dominant $4k_F$ charge-density-wave correlation, or a spin-Peierls state with different magnitudes of spin and charge gaps. Three-dimensionality is taken into account by cutting off the logarithmic singularity in either the particle-particle channel or the particle-hole channel. The difference between the ground-state phase of the R_1=R_2=CH_3 salt (spin-Peierls state) and that of the R_1=R_2=I salt (antiferromagnetic state) is qualitatively explained by a difference in the cutoff energy in the particle-particle channel. For M=Cu, there appear a Mott insulator with a charge density wave of period 3 and a Peierls insulator with a charge density wave of period 6. The conditions for the experimentally observed, Mott insulator phase are strong correlation in the sixth-filled band, moderate electron-phonon couplings, and finite electron-$4k_F$ phonon coupling. Resistance is calculated as a function of temperature with a memory-function approximation in both cases above.

I-U-4 Spin Gap of *S*=1/2 Heisenberg Ladder: Field Theoretical Study of Magnetic Susceptibility and NMR Relaxation Rate

Jun-ichiro KISHINE and Hidetoshi FUKUYAMA
(Univ. Tokyo)

[*J. Phys. Soc. Jpn.* **66,** 26 (1997)]

The temperature dependence of the static spin susceptibility, c, and NMR relaxation rate, T_1^{-1}, of S=1/2 Heisenberg two-leg ladder systems have been studied based on the Majorana fermion representation of the S=1/2 Heisenberg spin Hamiltonian introduced by Shelton, Nersesyan and Tsvelik. It is shown that, in the case of $SrCu_2O_3$, we can fit the experimental data of c and T_1^{-1} in terms of the massive Majorana fermion excitation with mass m=440K to resolve the apparent discrepancy of the spin gap activation energies between χ and T_1^{-1}.

I-U-5 Nuclear Gaussian Spin Echo Decay in *S*=1/2 Heisenberg Ladder

Jun-ichiro KISHINE

[*J. Phys. Soc. Jpn.* **66,** 1229 (1997)]

Recently it was reported that the Gaussian spin-echo decay rate, T_{2G}^{-1}, of the S=1/2 Heisenberg two-leg ladder $SrCu_2O_3$ reveals a very weak temperature dependence and saturates at T=0. A calculation using a quantum Monte Carlo technique shows reasonable agreement with experimental results. However it remains unclear how the spin echo decay process reflects the magnetic coherence of the system, especially why T_{2G}^{-1} saturates at T=0. To clarify this point without any assumption on the magnetic coherence of the system, we calculated T_{2G}^{-1} based on the Majorana fermion representation of the Heisenberg two-leg ladder Hamiltonian introduced by Shelton *et al.* In conclusion, the magnetic coherence of the system is clearly described in terms of the condensation of the Majorana fermions into the pair condensed phase with gapfull excitations and the saturation of T_{2G}^{-1} at T=0 can be explained by the remaining pair creation process from the condensate.

I-U-6 Spin Fluctuations in Magnetically Coupled Bilayer Cuprates

Jun-ichiro KISHINE

[*Physica C* **282,** 1771 (1997)]

We investigated spin fluctuations in magnetically coupled bilayer cuprates to elucidate anomalous behaviors of the low energy magnetic excitations in a metallic phase of them. We discussed the neutron scattering cross section and NMR relaxation rate of bilayer cuprates within a framework of the Fermi liquid

theory. In conclusion, we showed the intra-layer spin fluctuations enhances the inter-layer coupling in a magnetically coupled bilayer cuprate, that causes the strong attraction for inter-layer spin singlet pair and repulsion for inter-layer spin triplet pair. This tendency leads to the dynamical screening of the total magnetic excitations in the low energy region. Thus so-called pseudo-spin-gap-anomaly can be realized in a magnetically coupled bilayer cuprate.

I-U-7 Quantized Conductance of One-Dimensional Doped Mott Insulator

Michiyasu MORI, Masao OGATA *(Univ. Tokyo)* **and Hidetoshi FUKUYAMA** *(Univ. Tokyo)*

[*J. Phys. Soc. Jpn.* **66**, 11 (1997)]

The possible modification of quantized conductance of one-dimensional doped Mott insulator, where the Umklapp scattering plays an important role, is studied based on the method by Maslov-Stone and Ponomarenko. At T=0 and away from half-filling, the conductance is quantized as $g=2e^2/h$ and there is no renormalization by Umklapp scattering process. At finite temperatures, however, the quantization is affected depending on the gate voltage and temperature.

I-U-8 The Effect of Electron Interaction on the Coherence Length of Polymer

Xin SUN *(Fudan Univ. and IMS)*, **Kenji YONEMITSU and Yunsheng MA** *(Fudan Univ.)*

Every condensed matter system has a characteristic length called the coherence length. In polymer it measures the extent of the bond-bond correlation. What is the effect of the electron interaction on the coherence length is a common interesting problem. Because the Hubbard model is very successful in many systems, it is also used to describe the electron interaction in polymer. Based on this model, the current theories show that the coherence length is exponentially shrunk by the Hubbard repulsion U.[1] But the experimental data of the coherence length is not very different from the value given by the non-interacting theory.[2] As is well known that the Hubbard model is a good approximation for the systems with narrow band width, but the band width of the polymer is over 10 eV, then the overlap between the neighboring sites can not be neglected, and the electron interaction in polymer should be described by a screened Coulomb potential. Our theory shows that the coherence length is dependent on the screening factor. Only in weak screening, it is reduced by the electron interaction. If the screening is strong, it can be extended. In realistic screening it is only moderately changed by the electron interaction, which is consistent with the experimental data.

References

1) E. Jeckelman and D. Baeriswyl, *Synth. Met.* **69**, 651 (1995); V. Kuprievish, *Phys. Rev. B* **40**, 3882 (1989).

2) S. Kuroda, H. Bando and H. Shirakawa, *J. Phys. Soc. Jpn.* **54**, 3956 (1985); H. Kass *et al.*, *Europhys. Lett.* **4**, 947 (1987).

I-U-9 Electron Correlation and SDW in Polymer

Xin SUN *(Fudan Univ. and IMS)*, **Xiaohua XU** *(Fudan Univ.)* **and Kenji YONEMITSU**

Making pure organic ferromagnet with high Curie temperature is a challenging topic.[1] Many programs for designing polymeric ferromagnets have been proposed. One promising idea is to synthesize some polymer with pendent radicals, when a spin density wave (SDW) is built up in the main chain of the polymer, the radicals' spins can orient to form an organic ferrimagnet.[2] The present theoretical works use the extended Hubbard model and the unrestricted HF method to study the criterion for building the SDW. It is needed to consider the electron correlation more seriously. Because p electrons in polymer possess broad band, the off-diagonal part of the electron interaction, which is omitted in the extended Hubbard model, plays an essential role in the competition between the bond order wave (BOW) and SDW, it is better to have a primary description of electron interaction in polymer. Our study, which goes beyond the extended Hubbard model and the HF approximation, tells that this competition depends on the range of electron interaction, shortening of the interaction range favors SDW. It is also shown that the correlation effect is against the exchange effect in building up the SDW.

References

1) Y. V. Korshak *et al.*, *Nature* **326**, 370 (1987); M. Takahashi *et al.*, *Phys. Rev. Lett.* **67**, 746 (1991); R. Chiarelli *et al.*, *Nature* **363**, 147 (1993).

2) A. A. Ovchinnikov and V. N. Krivnov, *Synth. Met.* **71**, 1777 (1995); Z. Fang *et al.*, *Phys. Rev. B* **51**, 1304 (1995); **53**, 8481 (1996).

I-U-10 Off-Diagonal Interation, Bond Density Correlation, and Their Effects on the Excitons in Conjugated Polymers

Xin SUN *(Fudan Univ. and IMS)* **and Hua ZHAO** *(Fudan Univ.)*

[*Phys. Rev. B* **56**, 16 (1997)]

The exciton plays an essential role in the electroluminescence of polymer. But, how big is the binding energy of excitons in polymer is a controversial issue. The binding energy depends on the attractive interaction between electron and hole, and the existing theories use the extended Hubbard model to calculate the binding energy of excitons. However, the polymer is a broad-band system, the off-diagonal part of the electron interaction is effective. Actually, the extended Hubbard model only contains the diagonal part of electron interaction, which is density correlation, while the off-diagonal part reflects the bond correlation, which is a characteristic for the polymer. Therefore it is needed to study the effect of the off-diagonal part of electron interaction on the binding energy of excitons. We particularly studied the

effects from the bond-bond interaction W and the bond-site interaction X, which are the only off-diagonal terms in the nearest neighbor. Our calculation shows that W and X affect the excitons oppositely: the former suppresses the excitation energy of excitons whereas the latter increases it except for the $2A_g$ state. We find that the screening, which controls the bond-bond correlation, is a main reason to reduce the binding energy of the excitons. Our studies also shows that the off-diagonal interactions affect the singlet exciton with small binding energy even in normal screening, but for large exciton energy, such effects are negligible.

I-V Theoretical Studies of Superconductors under Magnetic Field

Under high magnetic field, a superconductor with a short coherence length shows a regular array of vortices where a magnetic flux quantized according to charge 2e penetrates the sample. An electronic state bound to a vortex has overlaps with those bound to neighboring vortices, but its itinerancy is suppressed by the magnetic field. In the high-temperature superconductors, the coherence length is so short that such bound states can propagate due to a magnetic breakdown. The unconventional internal symmetry of the pairing order parameter also makes the vortex dynamics different from the conventional one. It is because the bound states are resonant with some delocalized states. Our goal is to clarify the role of bound states in a core of magnetic flux on the local density of states and magnetization, which have been observed very recently. Since this is a highly nonlinear phenomenon with competing length scales, order parameter, density and current distributions in superconductors are calculated self-consistently with a careful choice of the gauge potential.

I-V-1 Quasi-Particle Band Structure and Gapless Superconductivity in the Vortex-Lattice State

Takayuki NISHIO *(Tohoku Univ.)*, **Kenji YONEMITSU and Hiromichi EBISAWA** *(Tohoku Univ.)*

[*J. Phys. Soc. Jpn.* **66**, 953 (1997)]

The quasi-particle spectrum for s-wave superconductors in the vortex-lattice state remains gapless in magnetic fields much below the upper critical field H_{c2} where the cyclotron frequency is smaller than the amplitude of the pair potential. This is shown through self-consistent solutions of the Bogoliubov-de Gennes equations for the attractive Hubbard model on the square lattice. It has not been predicted in earlier theoretical works based on a continuous model because it is due to the dispersion of Landau subbands in the lattice model.

RESEARCH ACTIVITIES II
Department of Molecular Structure

II-A Laboratory and Astronomical Spectroscopy of Transient Molecules

Vast, cold, and low-density space environment is a unique laboratory, whose physical and chemical conditions are rarely attained in the laboratory on Earth. The unique space laboratory is favorable to the existence of transient molecules such as molecular ions, free radicals, and unstable molecules, most of which are very exotic and nonterrestrial. These exotic transient molecules are generally difficult and challenging problems for laboratory spectroscopy. Laboratory spectroscopy may be enriched by astronomical studies on non-terrestrial transient species which represent new developments in high-resolution molecular spectroscopy. On the other hand, detailed knowledge about new transient molecules obtained by laboratory spectroscopy is essential to a deeper understanding of physical and chemical processes in space. We developed a high-sensitivity submillimeter-wave and far-infrared spectrometers suitable for high-resolution spectroscopy of transient molecules of astronomical interest. We expect that our laboratory spectroscopy may accelerate the mutually beneficial aspect between laboratory spectroscopy, and astrochemistry and astrophysics.

II-A-1 The Microwave Spectrum of the NH_2 Radical: The Hyperfine Structure of the $^2B_1$ Ground State

Mizuho TONOOKA *(Nagoya Univ.)*, **Satoshi YAMAMOTO** *(Univ. Tokyo)*, **Kaori KOBAYASHI and Shuji SAITO**

[*J. Chem. Phys.* **106**, 2563 (1996)]

The NH_2 radical is an important reaction intermediate in the hydrogenation of the nitrogen atom, and its physical and chemical properties have been studied by high-resolution spectroscopy. Among the various high-resolution spectroscopic methods, microwave spectroscopy is essential for precise determination of its hyperfine structure and, furthermore, line frequency determination for astronomical observations. We measured rotational spectra of the NH_2 radical in its $^2B_1$ ground electronic state by microwave spectroscopy in the frequency region of 230-470 GHz. The radical was generated in a free space cell by dc-glow discharge of NH_3. Seventy nine fine and hyperfine components of four rotational transitions were measured and were analyzed by least squares methods. The hyperfine coupling constants for both the nitrogen and hydrogen nuclei were determined, as shown in Table 1, with higher precision than those of the previous analysis for microwave optical double resonance (MODR) data.[1] The nuclear spin-rotation coupling constants for the hydrogen nucleus as well as the nitrogen nucleus were found to be anomalously large. The anomalous constant of $C_{aa}(H)$ is interpreted by the same reason as for the anomalous large value for $C_{aa}(N)$ originating from the large A constant and the relatively low-lying A^2A_1 electronic state, as first demonstrated in the study of ND_2.[2]

References

1) J. M. Cook and R. F. Curl, Jr., *J. Chem. Phys.* **67**, 1450 (1977).
2) M. Kanada, S. Yamamoto and S. Saito, *J. Chem. Phys.* **94**, 3423 (1991).

Table 1. Hyperfine Coupling Constants of the $NH_2(X^2B_1)$ Radical[a]

Constant	Present study	LMR&MODR[b]
$a_F(N)$	28.061(52)	28.2(4)
$T_{aa}(N)$	-43.035(91)	-42.8(13)
$T_{bb}(N)$	-44.630(118)	-44.7(10)
$\chi_{aa}(N)$	0.322(122)	0.1(13)
$\chi_{bb}(N)$	-3.809(141)	-1.6(11)
$C_{aa}(N)$	0.469(28)	
$C_{bb}(N)$	0.114(24)	
$C_{cc}(N)$	0.0228(96)	
$a_F(H)$	-67.182(108)	-67.2(4)
$T_{aa}(H)$	18.217(174)	18.6(13)
$T_{bb}(H)$	-13.05(27)	-13.4(9)
$T_{ab}(H)$	58.5[c]	
$C_{aa}(H)$	0.253(24)	

[a] MHz(3σ)
[b] Reference 1.
[c] T. C. Steimle, J. M. Brown and R. F. Curl, Jr., *J. Chem. Phys.* **73**, 2352 (1980).

II-A-2 Submillimeter-Wave Spectrum of the NH_2 Radical: Line Frequencies for Astronomical Observations in the 900 GHz Region and their Assignment

Shuji SAITO, Hiroyuki OZEKI, Egbert KLISCH *(Univ. Cologne)* **and Gisbert WINNEWISSER** *(Univ. Cologne)*

The NH_2 radical has the lowest rotational transition, 1_{11}-0_{00}, in the 950 GHz region, which is the most important probe for astronomical observations. The transition showing a very complicated hyperfine structure due to the hydrogen and nitrogen nuclei was measured at the University of Cologne by using a recently installed BWO source. The 30 observed hyperfine components are assigned on the basis of the hyperfine coupling constants which were reported in a previous study,[1] and were well explained within microwave spectroscopic measurement errors by the molecular constants given in the II-A-1 section of this

volume. The precise line frequencies of the transition and their relative intensities are now available for astronomical observations.

Reference

1) M. Tonooka, S. Yamamoto, K. Kobayashi and Shuji Saito, *J. Chem. Phys.* **105**, 2563 (1997).

II-A-3 Far-Infrared Spectra of the NH_2 Radical Observed by a Laser Sideband Spectrometer

Hiroyuki OZEKI and Shuji SAITO

There are plenty of spectroscopic works on the NH_2 radical in the ground electronic state, which were carried out mainly in the infrared and optical wave region. The molecular constants determined in these studies are not satisfactory in their accuracy. Recently high resolution microwave spectroscopy was applied to this radical, and hyperfine coupling constants were precisely determined.[1] NH_2 is so light that the number of rotational transitions which conventional microwave spectroscopy can measure is limited. It is impossible to determine all the constants only from its data. Consequently the problems in the accuracy of the rotational, centrifugal distortion and spin-rotation constants still remain. The only way to resolve these by measuring rotational transitions using a light source with a high spectral purity in the far-infrared, where most of main low-N rotational transitions are available. For this purpose, we measured rotational spectra of NH_2 with our far infrared laser sideband spectrometer.[2]

To date, we have measured three rotational lines in the frequency range between 1300 and 2600 GHz. Figure 1 shows an example of the observed spectrum, which is measured in the 1541 GHz region. The hyperfine structure due to the nitrogen nucleus was clearly observed. The center frequency estimated from the observed spectra is 8 MHz deviated from the predicted position in a recent FT-FIR study,[3] which is probably due to inaccuracies of rotational, centrifugal distortion and spin-rotation constants. Further measurements with this laser sideband spectrometer in the far infrared region will enable us to determine all the molecular constants with the same order of microwave spectroscopic precision.

References

1) M. Tonooka, S. Yamamoto, K. Kobayashi and S. Saito, *J. Chem. Phys.* **106**, 2563 (1996), see also II-A-1.
2) H. Ozeki and S. Saito, *Ann. Rev.* Special Research Projects (1997).
3) I. Morino and K. Kawaguchi, *J. Mol. Spectrosc.* **182**, 428 (1997).

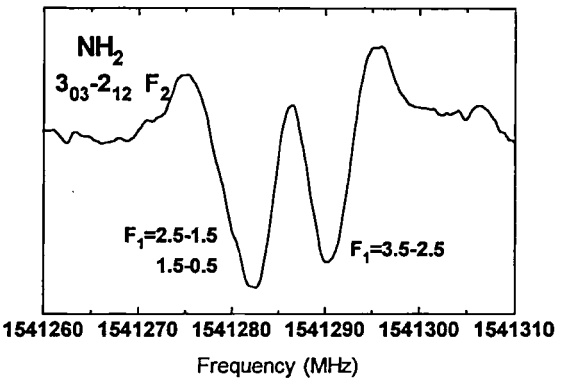

Figure 1. 3_{03}-2_{12} F_2 transition of NH_2 radical at 1541 GHz. Hyperfine splitting due to the nitrogen nucleus is resolved.

II-A-4 The Microwave Spectrum of the NHD Radical in the Ground Electronic State, $^2A''$

Kaori KOBAYASHI, Hiroyuki OZEKI, Shuji SAITO, Mizuho TONOOKA *(Nagoya Univ.)* **and Satoshi YAMAMOTO** *(Univ. Tokyo)*

[*J. Chem. Phys.* **107**, December 8 issue (1997)]

Monodeuterated species of the NH_2 radical has three nonzero spin nuclei and shows an extremely complex hyperfine pattern for each rotational transition, and which has not yet been subjected to microwave spectroscopic study. However, the recent detection of NH_2 toward our Galactic Center and a new finding of highly fractionated deuterium species of several interstellar molecules in the hot regions of the Orion KL source has urged us to study this NHD species in the laboratory. We measured the rotational spectral lines of NHD in the millimeter- and submillimeter-wave region. The NHD radical was produced by a dc-glow discharge through a NH_3 and D_2 mixture at around 220 K. Ten rotational transitions obeying b- and a-type selection rules were observed in the 177-517 GHz region, of which the most important rotational transitions for astronomical observations, 1_{01}-0_{00} and 1_{10}-1_{01}, were included and their detailed fine and hyperfine components were measured with high precision (see Figure 1). The hyperfine interaction of the nitrogen, hydrogen, and deuterium nuclei, which are similar in magnitude, caused complicated hyperfine patterns and made their assignment comparatively difficult. A least-squares analysis of the measured frequencies resulted in the determination of 40 molecular constants including spin-rotation coupling constants of N, H, D and, furthermore, non axial components of magnetic dipolar terms of H and D. The necessity of a higher K-dependent term of the dipole-dipole interaction constant for the hydrogen nucleus relative to the principal axis system reflects the effective geometrical change of the rotational levels.

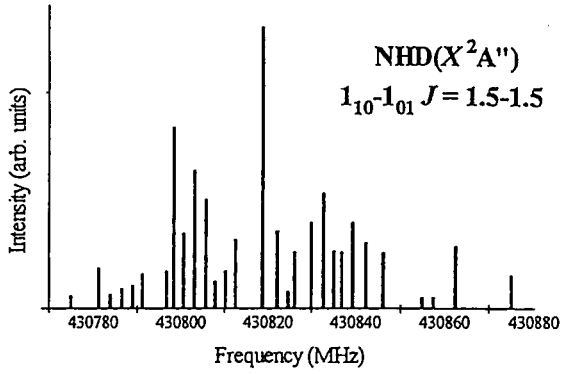

Figure 1. A stick diagram of the 1_{10}-1_{01}, J=3/2-3/2 transition of NHD(X^2A") in the 430 GHz region with observed relative intensities.

II-A-5 Microwave Spectra of the AsH_2 and AsD_2 Radicals in the $^2B_1$ Ground Electronic State

Hideo FUJIWARA, Kaori KOBAYASHI, Hiroyuki OZEKI and Shuji SAITO

The AsH_2 radical is the third member of the fundamental bent-triatomic free radicals starting from NH_2. The former two radicals, NH_2 and PH_2, and their isotopomers have been extensively studied by high-resolution spectroscopy, and their molecular properties are now well characterized. The third one, however, has been investigated only by optical electronic spectroscopy.[1] We detected and measured the pure rotational spectra of AsH_2 and AsD_2 by microwave spectroscopy for the first time. The radicals were generated by the reaction of arsenic powder with $H_2(D_2)$ in dc-glow discharge. Their spectral lines were relatively weak and required long-time averaging for precise frequency measurements. Ten low-N spin-rotational transitions of AsH_2 showing well resolved hyperfine structure due to both the arsenic and hydrogen nuclei were measured and subjected to a least squares fit which determined the following molecular constants: the rotational constants, centrifugal distortion constants, spin-rotation coupling constants with their centrifugal distortion terms, and hyperfine coupling constants for both the nuclei, As and H. Similarly, sixteen transitions of AsD_2 were measured and its molecular constants were precisely determined. The force field analysis has now been carried out using the determined molecular constants. The r_z structural parameters are derived for both the species:

AsH_2: r_z(AsH)=1.5349Å, θ_z(HAsH)=90.69°,

and

AsD_2: r_z(AsD)=1.5293Å, θ_z(DAsD)=90.72°.

Reference

1) R. N. Dixon, G. Duxbury and H. H. Lamberton, *Proc. Roy. Soc. A*, **305**, 271 (1968).

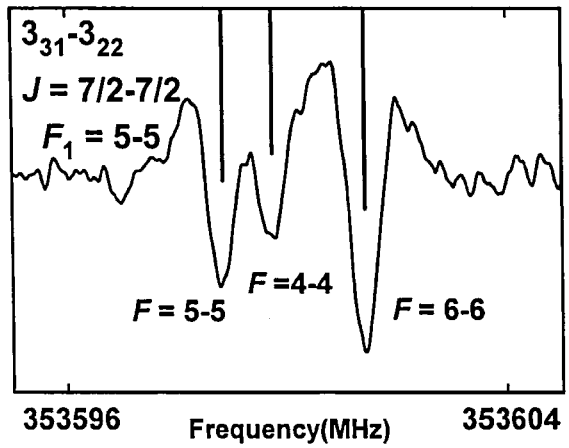

Figure 1. The observed hyperfine structure of the $AsH_2(X^2B_1)$ radical: $N_{KaKc}=3_{31}$-3_{22}, J=7/2-7/2, F_1=5-5. Vertical lines indicate caluculated frequencies and intensities.

II-A-6 Microwave Spectrum of a New Phosphorus Containing Free Radical, $CH_2CP(X^2B_1)$

Imtiaz K. AHMAD, Hiroyuki OZEKI and Shuji SAITO

Carbon-chain molecules, in particular those containing phosphorus, have recently been of interest due to their astrochemical importance and the nature of their molecular structure. To date, the only carbon-phosphorus species to be detected in space is the CP radical, though there are several studies highlighting the possibility of detection of carbon-phosphorus containing compounds in interstellar space. Paucity of precise laboratory data has hindered detections of such species in space. We detected for the first time a completely unknown new carbon-phosphorus free radical, CH_2CP by using microwave spectroscopy. The CH_2CP radicals were successfully generated in a 2 m absorption cell by a dc-glow discharge of an acetylene and phosphine mixture. The same mixture has recently been used to readily produce a linear phospho-allene radical, HCCP.[1] A spectral pattern consisting of several lines showing large Zeeman effects appeared every 10.8 GHz and was assigned to K structures of the a-type R branch transitions of a doublet asymmetric top radical. Intensity alternation between the spectral lines of different K values suggested that the free radical attributed to these spectral lines has C_{2v} symmetry along the a-axis and could be CH_2CP in the $^2B_1$ ground electronic state. This was further supported by the production of chemistry. About hundred spectral lines were measured and were used to determine the following molecular constants: the rotational, centrifugal distortion, and spin-rotation coupling constants, as shown in Table 1. The molecular structure of CH_2CP was tentatively determined from the observed rotational constants.

Reference

1) I. K. Ahmad, H. Ozeki and S. Saito, *J. Chem. Phys.* **107**, 1301 (1997).

Table 1. Molecular Constants of $CH_2CP(X^2B_1)$[a]

Constant	Present study
A	289026(174)
B	5472.284(23)
C	5365.601(22)
Δ_N	0.00108885(144)
Δ_{NK}	0.14994(79)
Δ_K	23.5(fixed)
δ_N	0.0000232(21)
δ_K	0.1086(95)
Φ_{NK}	0.000000714(163)
Φ_{KN}	-0.000413(64)
L_{KKN}	-0.00000757(162)
ε_{aa}	-3272.0(46)
ε_{bb}	-51.167(145)
ε_{cc}	-2.860(129)

[a] MHz(3σ)

II-A-7 Microwave Spectrum of NF in the Second Electronically Excited State, $b^1\Sigma^+$

Kaori KOBAYASHI and Shuji SAITO

In the last Annual Review we reported the detection of NCl in the second electronically excited state, $b^1\Sigma^+$.[1] Generally it is very difficult to observe rotational spectral lines of metastable molecules, especially those in the second electronically excited state, because of their method of production. There are only three examples[2,3] including the case of $NCl(b^1\Sigma^+)$. We improved the production of the NF radical[4] by about ten times by optimizing the production conditions and finally succeeded in detecting for the first time the NF radical in the second electronically excited state by microwave spectroscopy. The NF radical in the $b^1\Sigma^+$ state was generated efficiently by dc-glow discharge of a NF_3 and H_2 mixture. The intensity ratio of a $b^1\Sigma^+$state line to an $a^1\Delta$state line was found to be about 0.006. One of the measured spectral lines is shown in Figure 1. The rotational constant, centrifugal distortion constant, and quadrupole coupling constant of the nitrogen nucleus were determined. The observation of rotational transitions in the vibrational excited state made it possible to derive equilibrium structural parameters. Discussion centered on the change in molecular constants of the electronic states and the internuclear potential of the three lowest states of NF was made.

References

1) K. Kobayashi and S. Saito, *Ann. Rev.* II-A-5 (1996), *J. Phys. Chem. A*, **101**, 1068 (1997).
2) S. Yamamoto and S. Saito, *J. Chem. Phys.* **89**, 1936 (1988).
3) S. Yamamoto, *Chem. Phys. Lett.* **212**, 113 (1993).
4) S. Yamamoto and S. Saito, *J. Chem. Phys.* **86**, 102(1987).

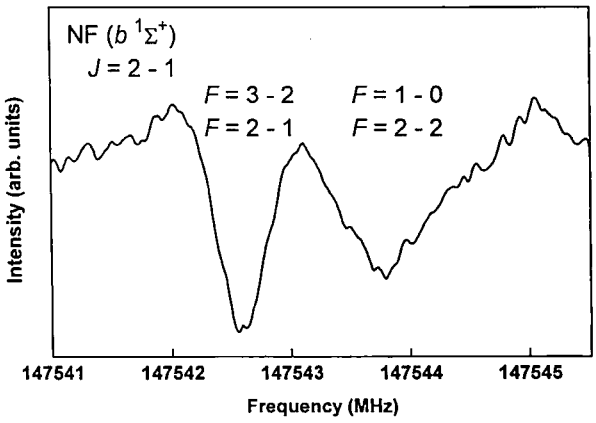

Figure 1. J=2-1 transition of NF ($b^1\Sigma^+$, v=0). The quadrupole hyperfine structure due to nitrogen nucleus is resolved.

II-A-8 The Microwave Spectra of Copper Monoxide, CuO ($^2\Pi_i$) and Silver Monoxide, AgO ($^2\Pi_i$)

Timothy C. STEIMLE *(Arizona State Univ. and IMS)*, **Kei-ichi NAMIKI** *(Grad. Univ. for Advanced Studies)*, **Mitsutoshi TANIMOTO** *(Shizuoka Univ. and IMS)* **and Shuji SAITO**

[*J. Chem. Phys.* **107**, 6109 (1997)]

As discussed in the former Annual Review,[1] spectra of the 3d metal bearing oxides are a good probe in assessing the chemical bonds dependent on the 3d orbital of the metal and the 2p orbital of oxygen, and we reported preliminary results on four microwave spectroscopic studies: $MnO(^6\Sigma^+)$,[2] $CoO(^4\Delta_i)$, $CuO(^2\Pi_i)$, and $TiO(^3\Delta_r)$. Results on the CuO radical have been published in the Journal of Chemical Physics, reporting the determination of the hyperfine coupling constants of the ^{63}Copper nucleus of I=3/2: a=214.1(35), b_F=-483.6(94), c=72.5(95), d=134.5(34), and eQq_0=-16.9(54) MHz. These observed parameters are interpreted by using a plausible molecular orbital configuration made up of a linear combination of atomic orbitals.

Recently we also detected the microwave spectrum of AgO in the $X^2\Pi_i$ state by dc-discharging a mixture of oxygen and a large amount of helium over a silver-plate cathode. The spectral lines of AgO in the $^2\Pi_{3/2}$ state were detected in the frequency region higher than that of the $^2\Pi_{1/2}$ state lines, though the $^2\Pi$ ground electronic state of AgO is claimed to be inverted. This anomalous behavior was explained by a large value of the centrifugal distortion term of the spin-orbit interaction term, A_D, which cancels the change of the rotational constants for both the substates by spin-orbit interaction. A similar anomaly was also found in the case of CuO. The result on the AgO radical will be reported separately.

References

1) K. Namiki, T. C. Steimle and S. Saito, *Ann. Rev.* II-A-6 (1996).

2) K. Namiki and S. Saito, *J. Chem. Phys.* **107**, December 1 issue (1997).

II-A-9 Microwave Spectra of Molecular Ions: Monodeuterated $HCNH^+$ and SD_3^+

Mitsunori ARAKI *(Graduate Univ. for Advanced Studies)*, **Hiroyuki OZEKI and Shuji SAITO**

Simple molecular ions play a crucial role in interstellar chemistry. Accordingly several molecular ions have been identified in interstellar space and their spectral lines have been used to probe molecular clouds. A recent finding of highly fractionated deuterium species of several main interstellar molecules in the hot molecular clouds has urged us to study various deuterium species of known interstellar molecular ions in the laboratory. We measured spectral lines of $HCND^+$ and $DCND^+$ by dc discharging a mixture of HCN and DCN and pure DCN, respectively, in a 2 m free space cell maintained at -100 to 140 °C, where a magnetic field of 110 to 160 G was applied for magnetic confinement of the discharge plasma.[1] Five rotational lines were measured for $HCND^+$ in the 190 to 450 GHz region and eight lines for $DCND^+$ in the 110-480 GHz region. The rotational constants and centrifugal distortion constants were determined precisely by a least squares fit of the measured frequencies. Spectral lines of $DCNH^+$ were looked for but without success. This supports the ab inito results which predict a very small dipole moment for this species.[2]

Similarly we measured spectral lines of perdeuterated species of SH_3^+, SD_3^+, by microwave spectroscopy in the 150-610 GHz region, and its molecular constants were determined with high precision. Since there has been no accurate determination of the structure of SH_3^+, the physically significant r_z structure of SH_3^+ is evaluated from the rotational constants of SH_3^+ and SD_3^+.

References

1) F. C. DeLucia, E. Herbst, G. M. Plummer and G. A. Blake, *J. Chem. Phys.* **78**, 2312 (1983).
2) P. Botschwina *et al.*, *J. Chem. Phys.* **85**, 5107 (1986).

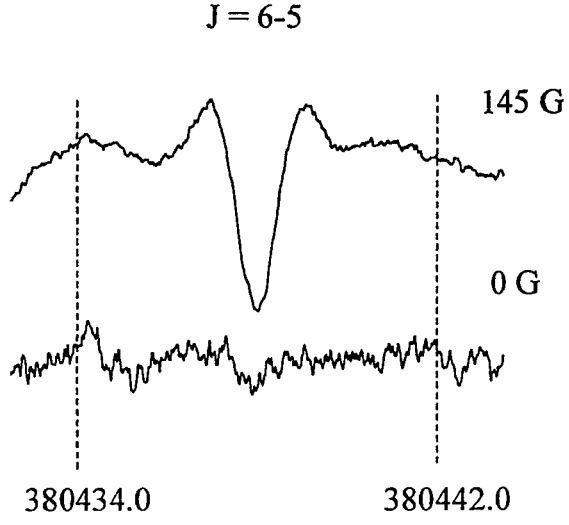

Figure 1. The J=6-5 transition of $HCND^+$. The upper trace shows the enhancement of line intensity by the magnetically confined discharge.

II-B Development of a Mt. Fuji Submillimeter-Wave Telescope

Shuji SAITO, Hiroyuki OZEKI, Hideo FUJIWARA, Satoshi YAMAMOTO *(Univ. Tokyo)*, **Yutaro SEKIMOTO** *(Univ. Tokyo)*, **Junji INATANI** *(National Astronomical Observatory)*, **Masatoshi OHISHI** *(National Astronomical Observatory)* **and Norio KAIFU** *(National Astronomical Observatory)*

In recent years the submillimeter-wave to far infrared region has attracted much attention in the field of astronomy because the initial stage of star forming activity or in other words, the final stage of molecular cloud contraction shows various physical and chemical phenomena in the energy region of this wavelength. Several submillimeter-wave telescopes have now been developed to study astrophysics and astrochemistry of the star-forming regions through atomic and molecular spectral lines. Since atmospheric attenuation, mainly due to water vapor, becomes high in the submillimeter-wave to far infrared region, astronomical observations should be made at a high-altitude site with a cold environment.

We plan to build a submillimeter-wave telescope at the summit of Mt. Fuji. The main scientific purpose of our project is (1) a survey of the neutral carbon line at 492 GHz, and (2) a search for new simple and fundamental molecules, especially related to interstellar dust chemistry, which will help us to understand evolutionary physical and chemical processes of molecular clouds as a whole.

II-B-1 Development of a Wide-Band Acousto Optical Spectrometer(AOS) for the Mt. Fuji Telescope

Hiroyuki OZEKI, Hideo FUJIWARA, Hisashi YOSHIDA, Toshio HORIGOME, Keisuke MIYAZAWA *(National Astronomical Observatory)* **and Shuji SAITO**

The acousto optical spectrometer (AOS) constitutes a central part of the back end system of the radio telescope, which converts RF signals of a receiver system to a spectral image. Construction of an efficient AOS system is one of the most crucial systems in the Mt. Fuji submillimeter-wave telescope project because a wideband AOS operating in such a severe environment as the summit of Mt. Fuji requires additional efforts to realize high stability and reliability over a long period. In order to evaluate the system

performance and its stability over a long accumulation time, we have adopted a method of spectroscopic Allan variance measurement. A dummy noise source was installed, which simulated an output from SIS mixer for the measurement. The dummy noise source consists of a noise diode, amplifiers and other components, and is able to generate up to 18 dBm per 700 MHz band (1.8~2.5 GHz) within 0.1 dB gain compression. Computer programs calculating spectroscopic Allan variance were developed.[1] Figure 1 depicts one of the measurements of the Allan variance of our AOS, which shows its minimum time is around 60 seconds. The current result is well qualified for the level of stability that is required for real operation.

We also installed an automatic frequency calibration system utilizing a frequency comb generator, which will work when the system performance is changed by an ambient temperature change. The frequency comb signal will couple to IF line, and hence the frequency axis will be calibrated. All the processes and status are monitored and controlled by remote workstations.

Reference

1) R. Schieder, private communication.

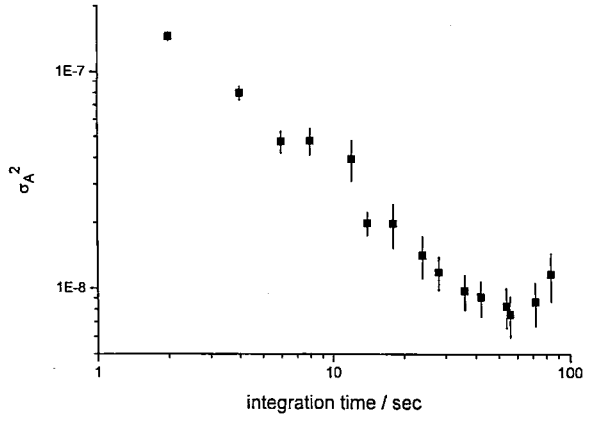

Figure 1. Allan variance of the AOS for the Mt. Fuji telescope. The minimum time is around 60 seconds.

II-C Laser Investigation of Antiproton-Helium Compounds

A recent discovery of anomalous survival of antiprotons in dense helium media suggested the creation of an antiproton-helium compound. If the creation of such an unusual compound is true, it is the first long-lived exotic atom containing hadrons other than the normal protons and neutrons. Moreover, from the viewpoint of atomic and molecular spectroscopy, this new compound is a very attractive object of study, because it has characters of both atoms and molecules; in other words, it is neither an atom nor a molecule, but a completely new entity. Therefore, we started the laser spectroscopic investigation of this compound in order, first, to get a definite evidence of the creation, second, to study its properties and dynamics, and finally to explore the possibility of its applications.

II-C-1 Observation of Double-Resonant Laser-Induced Transitions in the v=n-l-1=2 Metastable Cascade of Antiprotonic ^{4}He Atoms

R. S. HAYANO*, T. ISHIKAWA*, H. TAMURA*, H. A. TORII*, M. HORI*, F. E. MAAS* *(*Univ. Tokyo)*, N. MORITA, M. KUMAKURA, I. SUGAI *(**INS, Univ. Tokyo)*, F. J. HARTMANN†, H. DANIEL†, T. von EGIDY†, B. KETZER†, R. POHL† *(†Munchen Tech. Univ.)*, D. HORVATH *(KFKI Inst.)*, J. EADES††, E. WIDMANN†† and T. YAMAZAKI†† *(††CERN)***

[*Phys. Rev. A* **55**, R1 (1997)]

Another laser-induced resonant transition in the v =n-l-1=2 metastable cascade of antiprotonic ^{4}He atoms has been found by using a double-resonance technique. This was done by setting the first laser to the already known 470.724 nm resonance [(n,l) = (37,34) → (36,33)], while the (38,35) → (37,34) transition was searched for with the second laser. The resonant transition was found at a wavelength of 529.622 ±0.003 nm, showing excellent agreement with a recent prediction of Korobov.

II-C-2 Laser Resonance Studies of the Interactions of Metastable Antiprotonic Helium Atomcules $\bar{p}^4He^+$ with Surrounding H_2 Molecules

T. YAMAZAKI*, B. KETZER, E. WIDMANN*, J. EADES* *(*CERN)*, H. DANIEL**, F. J. HARTMANN**, M. HASINOFF**, R. POHL**, R. SCHMIDT**, T. von EGIDY** *(**Munchen Tech. Univ.)*, D. HORVATH *(KFKI Inst.)*, M. KUMAKURA, N. MORITA, I. SUGAI†, Y. FUJITA† *(†INS, Tokyo Univ.)*, H. A. TORII††, M. HORI††, T. ISHIKAWA††, F. E. MAAS††, H. TAMURA†† and R. S. HAYANO†† *(††Univ. Tokyo)***

[*Chem. Phys. Lett.* **265**, 137 (1997)]

We have employed a laser resonance method to study the interactions of individual states of metastable antiprotonic atomcules $\bar{p}^4He^+$ with surrounding H_2 molecules. We have found that the lifetime of the (n,l) = (37,34) → (39,35) states are shortened by small admixtures of H_2 molecules in quite different ways; the observed quenching cross section for the upper (39,35) state in helium medium at 1 bar and 30K is (2.4 ±1.0) $\times 10^{-15}$cm^2, a factor of 24 larger than that for the lower (37,34) state.

II-C-3 Hydrogen-Assisted Laser-Induced Resonant Transitions between Metastable States of Antiprotonic Helium Atoms

B. KETZER*, F. J. HARTMANN*, T. von EGIDY*, C. MAIERL*, R. POHL* *(*Munchen Tech. Univ.)*, J. EADES, E. WIDMANN**, T. YAMAZAKI** *(**CERN)*, M. KUMAKURA, N. MORITA,**

R. S. HAYANO†, M. HORI†, T. ISHIKAWA†, H. A. TORII† (†*Univ. Tokyo*), I. SUGAI (*INS, Univ. Tokyo*) and D. HORVATH (*KFKI Inst.*)

[*Phys. Rev. Lett.* **78,** 1671 (1997)]

Laser resonance transitions between normally metastable states of antiprotonic helium atoms were observed making use of state dependent quenching effects caused by small admixtures of H_2 molecules. By selectively shortening the lifetimes of states with higher principal quantum number n as compared to those of lower n, this method for the first time provides access to all initially populated metastable states of $\bar{p}He^+$ atoms. This was demonstrated by observing the transitions $(n, l) = (38, l) \rightarrow (39, l + 1), l = 35, 36, 37$ and $(n, l) = (37, l) \rightarrow (38, l + 1), l = 34, 35, 36$.

II-C-4 High-Precision Structural Studies of the Antiprotonic Helium Atom $\bar{p}^4He^+$ by Observing Laser Resonances with $\Delta v = \Delta(n\text{-}l\text{-}1)=2$

T. YAMAZAKI*, E. WIDMANN*, J. EADES* (**CERN*), M. KUMAKURA, N. MORITA, H. A. TORII**, M. HORI**, T. ISHIKAWA**, F. E. MAAS**, H. TAMURA**, R. S. HAYANO** (***Univ. Tokyo*), I. SUGAI†, Y. FUJITA† (†*INS, Univ. Tokyo*), B. KETZER†††, H. DANIEL††, F. J. HARTMANN††, M. HASINOFF††, R. POHL††, R. SCHMIDT††, T. von EGIDY†† (††*Munchen Tech. Univ.*) and D. HORVATH (*KFKI Inst.*)

[*Phys. Rev. A* **55,** R3295 (1997)]

Very weak laser resonances of unfavoured transitions $(n, l) \rightarrow (n+1, l\text{-}1)$ have been observed in metastable $\bar{p}^4He^+$ atoms by using a pulsed antiproton beam. The observed wavelengths (713.578 ± 0.006 nm for $l = 34$ and 726.095 ± 0.004 nm for $l = 35$), as well as those of the known favoured transitions, are to a few ppm accounted for by a recent variational calculation of Korobov [*Phys. Rev. A* **54,** R1749 (1996); and (unpublished)] which includes the relativistic correction to the motion of the electron.

II-D Laser Cooling and Trapping of Neutral Atoms

When an atom absorbs or emits a photon, the atom is accelerated or decelerated because a photon has momentum. On the other hand, a strong radiation field modifies the internal energy of an atom, so that an atom in an inhomogeneous radiation field receives a force from the field. The former mechanism allows us to cool the translational temperature of neutral atoms to an extremely low temperature by laser radiation, and the latter enables the spatial control of neutral atoms with lasers. As the translational temperature goes down to nano kelvin region, the atomic de Broglie wavelength becomes a macroscopic size, and macroscopic quantum-mechanical collective motion of atoms can then be expected to occur. The long de Broglie wavelength also enables us to realize an atomic interferometry. On the other hand, the easy control of atomic spatial position and velocity with lasers is expected to open the possibility of various applications. For these reasons, we have been studying the laser cooling and trapping of neutral atoms.

II-D-1 Branching Ratio of Penning and Associative Ionization Processes due to Ultracold Collision between Laser-Trapped He* Atoms

Mitsutaka KUMAKURA and Norio MORITA

For an isotope effect on ultracold collisions of He* atoms, we previously showed that, in the trap laser field, the total ionization cross section for $^3He^*(2s^3S_1)$ + $^3He^*(2p^3P_2)$ collision is about 1.5 times larger than for $^4He^*(2s^3S_1)$ + $^4He^*(2p^3P_2)$ collision at the same temperature (about 600μK). It is also interesting to study an isotope effect on the competition between Penning and associative ionization processes at an extremely low temperature, because it is expected that even a very small isotope effect can cause a relatively large difference at a sufficiently low temperature. Therefore, by monitoring He^+ and He_2^+ ions resulting from collisions between laser-trapped He* atoms, the branching ratio of Penning and associative ionization processes has been determined for $^3He^*(2s^3S_1)$ + $^3He^*(2p^3P_2)$ and $^4He^*(2s^3S_1)$ + $^4He^*(2p^3P_2)$ ultracold collisions.

The experiment was carried out separately for $^4He^*$ and $^3He^*$ under the same condition that the number of trapped He* atoms was about 10^5 and the trap temperature was about 700μK. To detect He^+ and He_2^+ ions separately, we placed an ion detector away from the center of the trap and observed the time of flight (T.O.F.) from the trap to the ion detector. Ultracold He* atoms were irradiated by a trap laser for a short time (0.5μs) between two longer periods (20μs) without irradiation. This short irradiation played a role of a start trigger for the T.O.F. measurement, because, as known from the previous experiment, the irradiation made the ionization rate more than 100 times larger. Therefore a number of ions was generated during this short irradiation and these ions were immediately pulled to the detector by the electric field. Through this T.O.F. measurement, T.O.F. distributions of He^+ and He_2^+ ions were separately observed, examples of the distributions for $^4He^*$ and $^3He^*$ being shown in Figure 1. Two peaks corresponding to He^+ and He_2^+ ions were clearly seen and the branching ratio was calculated for each species. The obtained ratio of He_2^+ to He^+ was about 2% and 5% for $^4He^*$ and $^3He^*$, respectively, and the ratio for $^3He^*$ was more than twice larger than for $^4He^*$. This is an clear evidence of the isotope effect on the competition of ionization processes in ultracold collision.

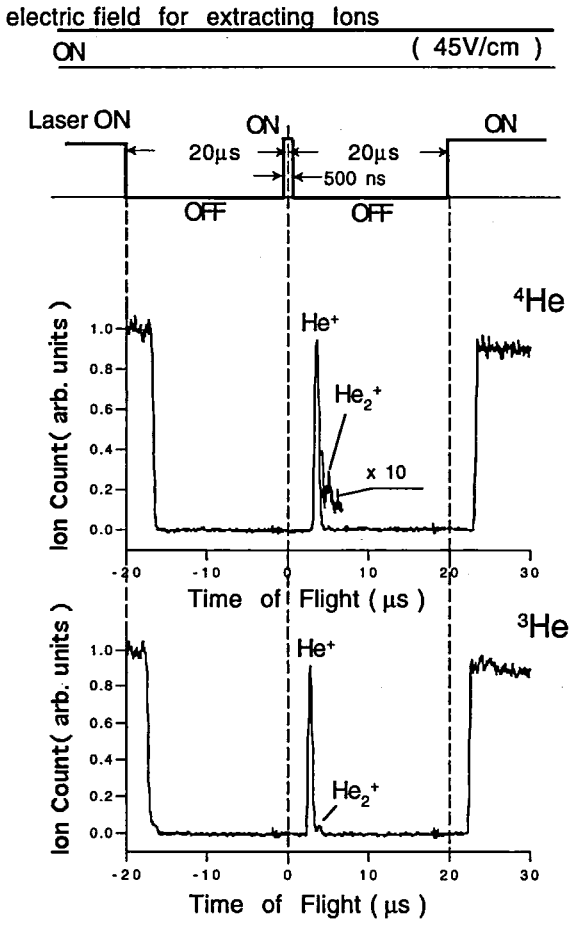

Figure 1. T.O.F. distributions of He^+ and He_2^+ ions resulting from $^4He^*$ + $^4He^*$ and $^3He^*$ + $^3He^*$ ultracold collisions in a magneto-optical laser trap: the peak area ratio of He_2^+ to He^+ is 2% and 5% for $^4He^*$ and $^3He^*$, respectively. The ratio for $^3He^*$ is more than twice larger than for $^4He^*$.

II-D-2 Theoretical Investigation on the He* + He* Ultracold Collision in a Laser Trap

Mitsutaka KUMAKURA and Norio MORITA

Ultracold collision (<1mK) is an interesting subject of study, because, due to the very small initial kinetic energy in atomic collision, unusual or exotic effects, which are of little concern at normal collision energies, can occur. For example, relatively small potential energies that are negligible at a room temperature can strongly modify ultracold collisions, and a long collision time allows a colliding atomic pair to absorb or emit a photon. While ultracold collisions of several kinds of heavier atoms have been studied so far, it is also very interesting to study He* + He* ultracold collisions. Because of its small mass, it is expected to observe remarkable quantum nature of collisions. In fact, even at 700μK, which can easily be attained by a usual laser-cooling technique for He* atoms, the collision de Broglie wavelength is as much as 50nm and is quite long compared with the scale size of the interatomic potential. Moreover, the centrifugal potential is larger than for other atoms, and it forbids ultracold collisions with a large angular momentum L. To investigate such an interesting ultracold collision system, we have studied laser-trapped He* atoms experimentally. In our experiment so far carried out, we obtained two main results as follows; (1) the cross section of collisional ionization in the trap laser field is more than 100 times larger than without the laser field, (2) the cross section of collisional ionization for $^3He^*$ is larger than for $^4He^*$ by about 60%. To interpret these results, we have been trying to estimate the cross sections by a calculation based on moderately long range potentials for $He^*(2s^3S_1)$ + $He^*(2s^3S_1)$ and $He^*(2s^3S_1)$ + $He^*(2p^3P_2)$ collisions. The former collision is mainly due to the centrifugal potential and the dispersion force (short range force). Then, even at about 700μK, except when L = 0, this potential has a centrifugal barrier higher than the initial kinetic energy and any collisional ionization process is prohibited. On the other hand, the latter collision is mainly due to the centrifugal potential and the dipole-dipole force (long range force) and colliding atoms can attract each other through the several potentials with L < 9. Then it is expected that the collisional ionization of $He^*(2s^3S_1)$ + $He^*(2s^3S_1)$ with $0<L<9$, which are forbidden by centrifugal barriers, occurs via the excitation from $2s^3S_1$ to $2p^3P_2$ during a collision and enlarges cross sections by more than 100 times. This conclusion agrees with the experimental result (1). On the isotope effect, theoretical investigations are now in progress.

II-E Spectroscopy of Ions and Atoms in Liquid Helium

Ions and atoms in liquid helium are known to reside in bubble-like cavities due to the Pauli repulsive force between electrons. Physical properties in these exotic surroundings are determined by the potential energy of impurity-He_n system, the surface tension energy of the liquid helium, and the pressure-volume work. Spectroscopic study of ions in liquid helium is expected not only to give information on the structure and dynamics of the bubbles, but also to contribute to the study on the property of superfluid liquid helium. Moreover, if ions are trapped in liquid helium by a radio-frequency trap or just below the liquid helium surface by a static electronic field, this kind of study is expected to break a new ground in the experimental physics of low temperature and low dimensional plasma.

II-E-1 Laser Spectroscopy of Ba Ions in Liquid Helium

Yoshiki MORIWAKI and Norio MORITA

Barium ions have been implanted in liquid helium by laser abration of a barium tip placed in liquid helium. To prevent recombination of the ions and electrons, a high electric field up to 3kV/cm has been applied at the production area. About 10^5 ions thus pro-

duced have been irradiated by a dye laser, and excitation and emission spectra corresponding to the Ba^+ $6s^2S$-$6p^2P_{1/2}$ and $6s^2S$-$6p^2P_{3/2}$ transitions have been observed. Large blue shifts and broadenings seen in the excitation spectra have been assigned to characteristics of the bubble spectra. For further analysis, detailed theoretical calculations of the Ba^+-He potential are necessary.

II-E-2 Laser Spectroscopy of Mg Atoms in Liquid Helium

Yoshiki MORIWAKI and Norio MORITA

Magnesium atoms have been implanted into liquid helium by laser abration of a Mg tip placed in the liquid helium, and excitation and emission spectra of $3s^2\ ^1S$-$3s3p^1P$ and $3s3p^3P$-$3s4s^3S$ transitions have been observed. A bubble model calculation by Tang et al[1] explains the shift and broadening of the excitation spectrum of $3s^2\ ^1S \rightarrow 3s3p^1P$ transition, but does not explain those of the emission spectrum. The emission spectrum of this transition shows extraordinarily large shifts and broadenings compared with the other atomic bubble transition spectra observed. This means that the perturbation energy of the valence electrons in the $3s^2\ ^1S$ state due to the surrounding helium atoms, whose positions are determined by the interaction between $3s3p^1P$ state and helium atoms (the Frank-Condon principle), is not so small as is predicted by the atomic bubble model. Minimizing the total energy of Mg-He_n type excimer and neglecting the rest of the helium atoms around the Mg atom, we have obtained a possible model of Mg-He_{10} system, where helium atoms are placed in the normal plain of the 3p election of Mg atom. Emission spectra from Mg($3s3p^1P$)-He_{10} to the bound-free state Mg($3s^2\ ^1S$)-He_{10} have been found to reproduce the observed spectra.

Another excitation spectrum of $3s3p^3P \rightarrow 3p^2\ ^3P$ has been observed by detecting laser-induced fluorescence of the $3s4s^3S \rightarrow 3s3p^3P$ transition. The direct emission spectra from $3p^2\ ^3P$ state has not been observed yet in the region between 270 and 700nm. The Mg atom in the $3p^2\ ^3P$ state is considered to form Mg-He_2 excimer in liquid helium. The relaxation path from $3p^2\ ^3P$ to $3s4s^3P$ (forbidden transition) is in question.

Reference

1) J.-Z. Tang, M. Kimura and I. Shimamura, *Chem. Phys. Lett.* 256, 327 (1996).

II-F Biomolecular Science

Elucidation of a structure-function relationship of metalloproteins is a current subject of this group. The primary technique used for this project is the stationary and time-resolved resonance Raman spectroscopy monitored by near IR to UV lasers. The main themes that we want to explore are (1) mechanism of oxygen activation by enzymes, (2) mechanism of active proton translocation and its coupling with electron transfer, (3) coupling mechanism of proton- and electron transfers by quinones in photosynthetic reaction center, (4) higher order protein structures and their dynamics, and (5) reactions of biological NO. In category (1), we have examined a variety of terminal oxidases, cytochrome P450s, and peroxidases, and also treated their enzymatic reaction intermediates by using the mixed flow transient Raman apparatus and the Raman/absorption simultaneous measurement device. For (2) the third generation UV resonance Raman (UVRR) spectrometer is under construction and we are going to use it to the peroxy and ferryl intermediates of cytochrme c oxidase. In (3) we succeeded in observing RR spectra of quinones A and B in bacterial photosynthetic reaction centers for the first time and in assigning them with Raman spectra of electronically reduced isotope-labeled quinones. For (4) we developed a novel technique for UV resonance Raman measuremnts based on the combination of the first/second order dispersions of gratings and applied it successfully to 235-nm excited RR spectra of several proteins including mutant hemoglobins and myoglobins. Nowadays we can carry out time-resolved UVRR experiments with nanosecond resolution to discuss protein dynamics. We have succeeded in isolating the spectrum of β37-Trp and α42-Tyr of Hb A separately and their changes upon quaternary structure transition. For (5) we purified soluble guanylate cyclase from bovine lung, characterized it and observed its RR spectra.

II-F-1 Purification of Bovine Soluble Guanylate Cyclase and ADP-Ribosylation on Its Small Subunit by Bacterial Toxins

Takeshi TOMITA *(Grad. Univ. for Advanced Studies)*, **Shingo TSUYAMA** *(Osaka Prefecture Univ.)*, **Yoshio IMAI** *(Osaka Prefecture Univ.)* **and Teizo KITAGAWA**

[*J. Biochem.* (Tokyo) **122**, 531 (1997)]

Soluble guanylate cyclase (sGC) consisting of two different subunits (α; M_r=74,000, β; M_r = 69,000) was purified from bovine lung by more than 12,000-fold in terms of specific activity than that of the supernatant of homogenates and characterized. The heme content determined with the pyridine hemochromogen method and Bradford's protein assey was 0.8 heme per dimer. Cholera-, pertussis-, and botulinum C3 toxins modified exclusively the β-subunit of sGC, yielding ADP-ribose-bound compound with 1:1 stoichiometry, and V_{max} for the cyclase reaction increased by 10 times owing to this modification. When the ADP-ribosylation of sGC was performed simultaneously with two or three bacterial toxins which have distinct amino acid specificities, the resultant enzyme had only one ADP-ribose, and the activity was the same as that of the enzyme modified with one toxin. When NO was incorporated into the reaction mixture containing the ADP-ribosylated sGC, the cyclase activity noticeably increased approximately by the same amount as that seen for the unmodified enzyme. Such effects were not seen with CO. When ADP-ribosylated sGC was incubated with Mn^{2+}, the enzyme activity was synergistically increased. The

heme-deleted sGC was also ADP-ribosylated by bacterial toxins and its activity was raised. These findings suggest that sGC has an ADP-ribosylation site in the proximity of the GTP binding site similar to other GTP-binding proteins and that the β-subunit regulates the activity.

II-F-2 Tyrosine Phosphorylation-Induced Changes in Absorption and UV Resonance Raman Spectra of Src-Peptides

Nobuyuki OKISHIO *(Kanazawa Univ.)*, **Ryuji FUKUDA** *(Kanazawa Univ.)*, **Masako NAGAI** *(Kanazawa Univ.)*, **Yukifumi NAGAI** *(Fukui Medical School)*, **Shigenori NAGATOMO and Teizo KITAGAWA**

[*J. Raman Spectrosc.* in press]

To get insight into possible conformational changes of proteins induced by tyrosine phosphorylation, we investigated the phosphorylation-induced changes in absorption and UV resonance Raman (UVRR) spectra for the two kinds of 13-residue peptides in $pp60^{c\text{-}src}$ protein containing either Tyr^{416} (autophosphorylation site) or Tyr^{527} (C-terminal phosphorylation site), and compared them with the changes of free L-tyrosine. Phosphorylation caused blueshift and marked decrease in the 275 nm-absorption band (L_b transition) for both peptides and L-tyrosine. In UVRR spectra, while frequency downshifts of several modes were observed upon phosphorylation, the most pronounced change is the distinct intensity reduction of the Y1 band around 850 cm^{-1} and appearance of the Y13 band around 760 cm^{-1}. These phosphorylation-induced changes were totally restored upon dephosphorylation by an alkaline phosphatase. A Raman band characteristic to the Tyr^{527}-peptide was also detected. A band at 1461 cm^{-1}, which appeared regardless of the phosphorylation state, was assigned to amide IIp from the comparison with the spectra of other peptides containing proline residues. The effects of H/D exchange in the UVRR spectra were also examined. This is the first application of UVRR spectroscopy to detect possible structural changes of the tyrosine residue by its phosphorylation.

II-F-3 Resonance Raman, Infrared and EPR Investigation on the Binuclear Site Structure of the Heme-Copper Ubiquinol Oxidases from *Acetobacter Aceti*: Effect of the Heme Peripheral Formyl Group Substitution

Motonari TSUBAKI *(Himeji Inst. Tech.)*, **Kazunobu MATSUSHITA** *(Yamaguchi Univ.)*, **Osao ADACHI** *(Yamaguchi Univ.)*, **Shun HIROTA** *(Nagoya Univ.)*, **Teizo KITAGAWA and Hiroshi HORI** *(Osaka Univ.)*

[*Biochemistry* **36**, 13034 (1997)]

Acetobacter aceti produces two different terminal ubiquinol oxidases (cytochromes a_1 and *o*) depending on the culture conditions. Two types of oxidases share a common protein moiety but with different heme components at the binuclear center (heme A for cytochrome a_1 and heme O for cytochrome *o*). We investigated the structure of the binuclear site of the two oxidases using resonance Raman, Fourier transform-infrared (FT-IR), and EPR spectroscopies to clarify the interactions of heme A formyl group with protein moiety. We found that the overall architecture and the electronic configuration at the binuclear center in the oxidized state seem to be well-conserved irrespective of the heme peripheral group at position 8, except for the azide-inhibited state. In contrast, we observed great variations in the C-N stretching frequency and cyanide-binding affinity in the CN-reduced state, in addition to multiple C-O stretching bands in the CO-reduced state. Present and previous studies suggest that the conformational flexibility of the binuclear center in the reduced ligand-bound state may be a common feature among the heme-copper oxidase superfamily. In the CN-reduced state, a hydrogen bond network may be formed among the formyl group, water molecule(s), and the surrounding amino acid residue(s). This network may be very important to maintain proper orientations of the distal amino acid residues and/or the Cu_B^{1+} ion relative to the cyanide ion bound to the ferrous heme iron and could play a critical role for the high-affinity in cyanide-binding.

II-F-4 Solvent Effects of 1,4-Benzoquinone and Its Anion Radicals Probed by Resonance Raman and Absorption Spectra and Their Correlation with Redox Potentials

Xiaojie ZHAO and Teizo KITAGAWA

[*J. Raman. Spectrosc.* submitted]

Resonance Raman (RR), absorption spectra, and cyclic voltammograms were measured for 1,4-benzoquinone (BQ) and its anion radical ($BQ^{-\cdot}$) in various solvents. The absorption maxima of $BQ^{-\cdot}$ around 440 and 320 nm exhibit a good linear correlation both with acceptor numbers (AN) of solvents and the standard reduction potentials of BQ. The frequencies of ν_{8a} (Wilson's notations, C=C stretch) and ν_{9a} (C-H in-plane deformation) of BQ show linear correlation with polarizabilities and dielectric constants of solvents, respectively. The ν_{8a} and ν_{7a} (C=O stretch) frequencies of $BQ^{-\cdot}$ can be linearly correlated with solvent AN. In addition, the standard reduction potentials of BQ also show good linear correlation both with solvent AN and frequencies of ν_{8a} of $BQ^{-\cdot}$. These results cannot be interpreted by simple hydrogen bonding interactions of carbonyl oxygen with solvent but rather sugggest that π-electrons of $BQ^{-\cdot}$ and BQ serve as a H-bond acceptor, forming novel H-bonds with solvent. The magnitude of the novel H-bond interaction is estimated to be ~7 and ~3.5 kcal/mol or less for water.

II-F-5 UV Resonance Raman Studies of Quaternary Structures of Nitrosyl Hemoglobin

Shigenori NAGATOMO, Masako NAGAI *(Kanazawa Univ.)*, **Antonio TSUNESHIGE** *(Univ.*

Pennsylvania), **Takashi YONETANI** *(Univ. Pennsylvania)* **and Teizo KITAGAWA**

Human α-nitrosyl β-deoxy hemoglobin A ($\alpha^{NO}\beta^{deoxy}$HbA) is considered to adopt the superT state with extremely low O_2 affinity, but its structure remains to be clarified. Recently it has been demonstrated that ultraviolet resonance Raman (UVRR) spectrosco-py, which detects UVRR bands of Tyr and Trp residues on the α_1-β_2 subunit interface, distinguishes the T and R quaternary structures of HbA. Accordingly, quaternary structures of nitrosyl HbA were investigated by UVRR spectra excited at 235 nm. The UVRR spectra of deoxyHbA and carbonmonoxyHbA (COHbA) excited at 235 nm were used as the standard spectra of the T and R states, respectively. The fully nitrosyl HbA (NOHbA) at pH 7 gave the UVRR spectrum of the R structure, but in the presence of inositol-hexakisphosphate (IHP), an effector, it exhibited appreciable difference from the R spectrum; Tyr bands were of R-type but Trp bands were of half T type. For the half ligated $\alpha^{NO}\beta^{deoxy}$ state at pH 5.6 in the presence of IHP, the Tyr bands became also T-type and a whole spectrum bares close similarity to the T spectrum. Thus, from UVRR point of view, $\alpha^{NO}\beta^{deoxy}$ at pH 5.6 in the presence of IHP assumes an ordinary T structure. When CO was bound to it, that is, $\alpha^{NO}\beta^{CO}$, spectra of Tyr and Trp were of half T type despite of a fully ligated state. However, when pH was raised to 7.5 and IHP was removed, it gave the R spectrum. EPR and visible RR studies of these samples indicated that the α^{NO} heme adopts the five coordinate structure in the presence of IHP. Consequently it is concluded that the quaternary structure sensitive UVRR bands arising from the α_1-β_2 interface have strong correlation with the presence or absence of the Fe-His bond of the α heme.

II-F-6 A Third-Generation UV Resonance Raman Spectrophotometer Using a Solar-Blind ICCD and a Quasi-CW UV Light Source for Biological Applications

Takashi OGURA, Michihiko AKI and Teizo KITAGAWA

A new type of ultraviolet Raman spectrophotometer for resonance Raman spectroscopy of proteins is reported. In order to avoid interference of visible emission from the sample, a solar-blind multichannel detector was employed. For a highest throughput, a single spectrograph is used and to minimize the sample damage caused by high power flux of excitation light, a frequency-doubled mode-locked Ar^+ laser is employed as the excitation source. Construction and performance of the UV Raman spectrophotometer are described.

II-G Fast Dynamics of Photoproducts in Solution Phases

Picosecond time-resolved resonance Raman (ps-TR³) spectroscopy is a promising technique to investigate ultrafast structural changes of molecules. However, this technique has not been used as widely as nanosecond TR³ spectroscopy, mainly due to the lack of light source which has suitable repetition rates of pulses and wavelength tunability. In order to obtain qualified TR³ spectra, first we need two independently tunable light sources for pump and probe pulses. Second, the repetition rate should be higher than kilohertz to keep a moderate average laser power without allowing the photon density of probe pulse too high. We succeeded in developing light sources for ps-TR³ spectroscopy having wide tunability and kHz repetition, and applied them to study fast dynamics of photoexcited molecules. For carbonmonoxy myoglobin (MbCO), vibrational relaxation with the time costant of 1.9 ps was observed for CO-photodissociated heme. For Ni-octaethylporphyrin in benzene, different population rises in vibrationally excited levels were observed in the anti-Stokes spectra for different vibrational modes. For the same molecule in piperidine, coordination of two solvent molecules was observed in the transient (d,d) excited state. Nanosecond time-resolved Raman spectra were investigated for photodissociation of various mutant myoglobins. The UV ns-TR³ experiments on MbCO demonstrated the presence of a transient open form of the ligand pathway.

II-G-1 Direct Observation of Cooling of Heme upon Photodissociation of Carbonmonoxy Myoglobin

Yasuhisa MIZUTANI and Teizo KITAGAWA

[*Science* **278**, 443 (1997)]

The formation of vibrationally excited heme upon photodissociation of carbonmonoxy-myoglobin and its subsequent vibrational energy relaxation was monitored by picosecond anti-Stokes resonance Raman spectroscopy. The anti-Stokes intensity of the ν_4 band showed immediate generation of vibrationally excited hemes and biphasic decay of the excited populations. The best fit to double exponentials gave time constants of 1.9 ± 0.6 and 16 ± 9 ps for vibrational population decay and 3.0 ± 1.0 and 25 ± 14 ps for temperature relaxation of the photolyzed heme when a Boltzmann distribution is assumed. The decay of the ν_4 anti-Stokes intensity is accompanied by narrowing and frequency-upshift of the Stokes counterpart. These are the first direct monitoring of cooling dynamics of the heme cofactor within a globin matrix which would lead to characterization of how vibrational energy flows through the protein moiety and to the water bath.

II-G-2 Developments of Widely Tunable Light Sources for Picosecond Time-Resolved Resonance Raman Spectroscopy

Yuki UESUGI *(Grad. Univ. for Advanced Studies)*, **Yasuhisa MIZUTANI and Teizo KITAGAWA**

[*Rev. Sci. Instrum.* in press]

Two systems of widely tunable light sources for picosecond time-resolved resonance Raman (ps-TR³)

spectroscopy have been constructed using a 1 kHz ps-Ti: sapphire laser/regenerative amplifier system. Performance of the systems was examined in terms of pulse duration, spectral width, pulse energy and shot-to-shot stability. One system, consisting of white light continuum seeder and β-barium borate optical parametric amplifier, demonstrated tunability in the 500-660 nm range with 1.3-2.1 ps pulse duration and 15 μJ pulse energy. The other system, consisting of a lithium triborate optical parametric generator in type-II noncritical phase matching configuration and β-barium borate optical parametric amplifier, was found to yield visible pulses as high as 18 μJ with 1.5-2.4 ps of pulse duration in the 520-630 nm region. The shot-to-shot stability of generated pulses is less than 10 % for both systems. Capability of the present systems is demonstrated by observing ps-TR^3 spectra of nickel octaethylporphyrin in coordinating and non-coordinating solvents.

II-G-3 Time-Resolved UV Resonance Raman Detection of a Transient Open Form of the Ligand Pathway in Tyr64(E7) Myoglobin

Masahiro MUKAI, Satoru NAKASHIMA *(Osaka Univ.)*, **John S. OLSON** *(Rice Univ.)* **and Teizo KITAGAWA**

[*J. Phys. Chem.* submitted]

X-ray crystallographic analyses of myoglobin (Mb) in the deoxy- and CO-bound states noted the absence of a preformed pathway for ligand movement from the heme iron to the solvent. To explore a mechanism of ligand entry, time-resolved UV resonance Raman experiments have been carried out, using a mutant with tyrosine at the distal histidine position. The results indicate the presence of a transient, open pathway which is generated after photodissociation of CO in the H64Y mutant. The Raman spectra were probed at 235 and 416 nm with a time resolution of 7 ns in the range from -100 ns to 10 ms following photolysis at 532 nm. In the 235-nm excited spectra, the tyrosine bands of H64Y Mb at 1618 (Y8a) and 1176 cm^{-1} (Y9a) are noticeably intensity-enhanced shortly after photolysis but the original intensity is restored by 5 ms. The time range in which the Tyr bands are intensified is prolonged by addition of glycerol to the solvent. This intensity change is not seen with the native Mb which has three naturally occurring Tyr residues. Thus, the intensity increase observed for the mutant Mb is attributed to Tyr64. The corresponding bands of paracresol derivative exhibit greater intensity in polar (H-bond forming) solvents than in nonpolar solvents. This result suggests that the increase in intensity of the Tyr bands in the transient form of the mutant myoglobin compared to that in the equilibrium form is due to exposure of Tyr64 to solvent water. Increased solvation indicates an outward movement of the phenol side chain and formation of an open channel to the distal pocket.

II-G-4 Time-Redolved Resonance Raman Study of Intermediates Generated After Photodissociation of Wild-Type and Mutant CO-Myoglobins

Satoru NAKASHIMA *(Osaka Univ.)*, **Teizo KITAGAWA and John S. OLSON** *(Rice Univ.)*

[*Chem. Phys.* in press]

Time-resolved resonance Raman (TR^3) spectroscopy was applied to elucidate transient structures of myoglobin (Mb) involved in its ligand binding. Pump/probe Raman measurements of the Fe-CO stretching bands (ν_{Fe-CO}) were carried out for various delay times (Δt=-20 ns - 1 ms with a time resolution of 7ns) after laser photolysis of native and mutant COMb complexes. His64(E7) and Leu29(B10) were replaced with an aliphatic and aromatic residues. The static ν_{Fe-CO} frequencies of the mutants depended strongly on the environments around the bound CO and correlated more with the hydropathy indices of the replaced residues than with their sizes. The kinetics of bimolecular CO recombination correlate with the static ν_{Fe-CO} frequencies; a lower–frequency generally results in faster rebinding. Despite these differences, all the proteins exhibited a transient Raman band at ~497 cm^{-1}, which occurred before recovery of the original ν_{Fe-CO} band, and the shift of a porphyrin band from 370 to 379 cm^{-1}. This frequency was unaffected by isotopically labeling the ligand with $^{13}C^{18}O$. The 497 cm^{-1} band was absent in the spectrum at Δt = 0 ns for all of the myoglobins examined except for the His64->Leu (H64L) mutant which shows the band immediately after photolysis. The 370 and 497 cm^{-1} bands are associated with the $C_\beta C_c C_d$ in-plane bending of the propionic side chains and the out-of-plane γ_{12} containing pyrrole swiveling and propionic bending motions, respectively. The 497 cm^{-1} transient band appears to reflect a deoxyheme intermediate in which the hydrogen bonding lattice between Arg45(CD3), His64(E7), the heme-6-propionate, and an external distal pocket water molecule is temporarily disrupted. This disruption allows larger movements of the propionate side chain, explaining intensity enhancement of the 497 cm^{-1} band. Recovery of the hydrogen bonding lattice dampens the movements of the propionate $C_\beta C_c C_d$ bond system, causing the frequency shift of the bending mode from 370 cm^{-1} back to 379 cm^{-1}. In the Leu64 mutant, the external water molecule is already absent, facilitating rapid movement of the heme-6-propionate after photolysis. Larger scale movements of all three side chains could create an open conformation with a channel from the heme iron to the solvent, allowing ligand escape and/or rebinding.

II-G-5 Picosecond Time-Resolved Stokes/Anti-Stokes Resonance Raman Study of Non-Planar Nickel-Octaethyltetraphenylporphyrin in Solution

Sergei G. KRUGLIK, Yasuhisa MIZUTANI and Teizo KITAGAWA

Excited-state dynamics, photoinduced structural transformations and vibrational relaxation have been

studied for highly non-planar Ni-octaethyltetraphenylporphyrin (Ni(OETPP)) in benzene using two-color pump-probe time-resolved resonance Raman (TR^3) technique with 2-ps time resolution both in Stokes and anti-Stokes spectra. The excited (d,d) state, the key excited state for all Ni-porphyrins, was found to be instantly populated following photoexcitation to a (π,π^*) state, gradually evolving in 10-15 ps and then slowly decaying to the ground state. The (d,d)-state lifetime of 490±100 ps was estimated from anti-Stokes Raman intensity kinetics of the prominent transient band at ~258 cm^{-1} (ν_9*), which became the most intense band in the low-frequency range during the action of laser pulse. This time constant is ca. twice longer than that for Ni-octaethylporphyrin (Ni(OEP)). Low-frequency out-of-plane bands γ_{16} (~314 cm^{-1}) and δ_4 (~474 cm^{-1}), which are very strong in the ground-state Raman spectrum because of the saddle distortion of macrocycle, were observed also in the excited-state spectra although being much less pronounced. This indicates that the excited porphyrin structure retains non-planarity to some extent. In the high-frequency range, structure-sensitive Raman bands ν_2, ν_3, ν_{11} and ν_4 experience moderate low-frequency shifts by 8-11 cm^{-1} in the excited (d,d) state. On the contrary, modes ν_{28} and ϕ_5' (B_{2g} symmetry group) containing significant contribution from the C_α-C_m stretch, show shifts by ~17-20 cm^{-1}. In general, the excited-state Raman spectra of Ni(OETPP) bare definite similarity to the ground-state spectra of Cu(OETPP). TR^3 spectra of Ni(OETPP), recorded at first several ps, reveal very complex broad contours reflecting processes of both vibrational heating and structural rearrangements shortly after photoexcitation. Raman manifestations of vibrational cooling of saddle-shaped Ni(OETPP) are distinctly different from that of almost planar Ni(OEP). Kinetics of anti-Stokes ν_4* mode displays an unusual plateau within 4 to 10 ps, presumably reflecting strong influence of structural rearrangements in this time scale.

II-H Molecular and Electronic Structures of Metallofullerenes and the Fullerene Radical Anions

The continued interest in radical ions of fullerenes and metallofullerenes has resulted from the discovery of superconductivity in the CT complexes of alkali metals with fullerenes. Spectroscopic information concerning the electronic structure of C_{60}^- isolated in a single crystal salt has been obtained by EPR measurements at low temperature. Some experimental results were well explained theoretically by the ab initio MO calculation.

II-H-1 Theoretical Prediction on the Molecular Structure of C_{60}^-

Tatsuhisa KATO, Koichi MOGI, Mutsumi AOYAGI, and Takeshi KODAMA *(Tokyo Metropolitan Univ.)*

[*The Molecular Physics Report* in press]

We performed the geometry optimization of C_{60}^- at the level of UHF/6-31G and the vibrational analysis of C_{60}^- in D_{2h}, C_{2h}, and C_i symmetry at an UHF/3-21G level. One point of the result is that the optimized energy level of C_{60}^- in the structure of D_{3d} symmetry is higher than those of D_{5d} and D_{2h}, and that the energy levels of D_{2h}, C_{2h}, and C_i are isoenergetic and much lower than that of D_{3d}. The other is that the structures of D_{2h} and C_{2h} symmetries are not the local minimum of the potential surface. The calculation of D_{2h} and C_{2h} structures gave one normal mode with the imaginary frequency, as shown in the figure. The normal coordinate is denoted as b_{1g} mode of the $^2B_{3u}$ ground electronic state in the D_{2h} structure, and as b_g mode of the A_u state in the C_{2h} structure. These vectors destroy the molecular structure from the higher symmetry to the lower symmetry, that is D_{2h} to C_{2h} and C_{2h} to C_i. The result obtained by the calculation indicates that the most stable structure for C_{60}^- should be the C_i symmetry. Our experimental analysis of the anisotropic components of g factor based on symmetry leads the conclusion that the structure of C_{60}^- should be distorted to the lower symmetry of C_{2h} or C_i, and this conclusion is supported by the theoretical analysis.

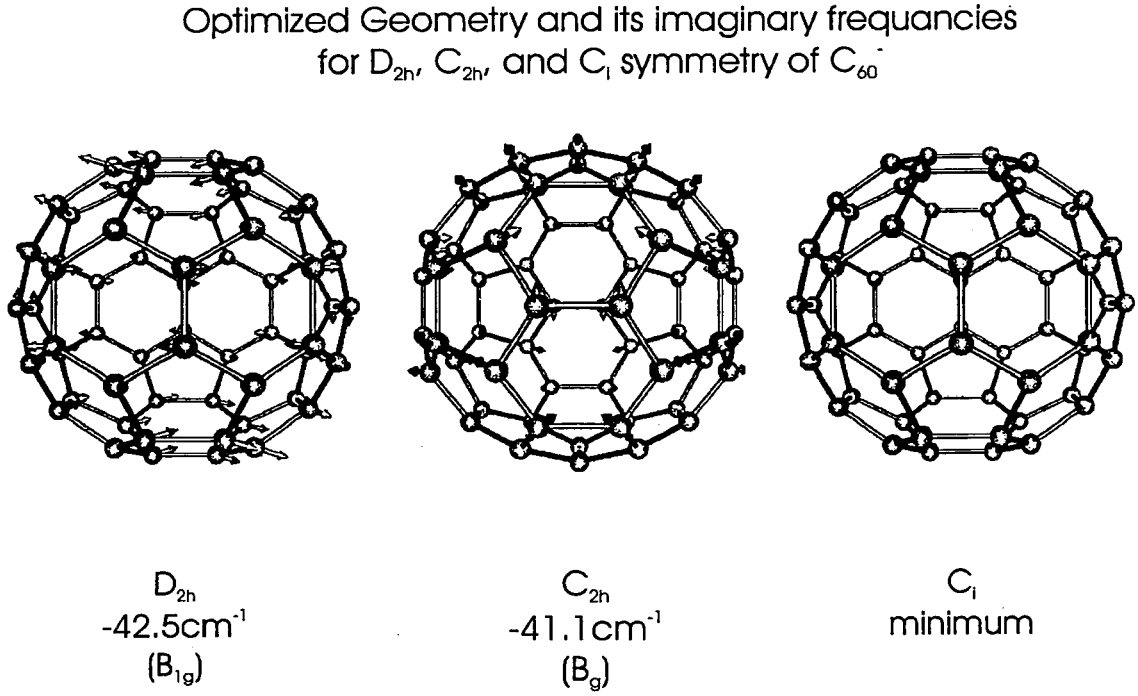

Figure 1. B_{1g} vibrational mode of the $^2B_{3u}$ ground electronic state in the D_{2h} structure and b_g mode of the A_u state in the C_{2h} structure.

II-I Site Selective Spectroscopy in Solid Crystals

The line broadening due to the variation of the environment over the some sites in the crystal structure prevents from determining small energy splitting between pair of closely spaced levels with high accuracy. However the broadening effects give a nice prove to investigate the intermolecular interaction in the crystal structure. On the other hand some techniques of the site selective spectroscopy to eliminate the disturbance were proposed. We are applying the technique of the heterodyne detection of optical magnetic double-resonance to some systems of crystal.

II-I-1 Nuclear Quadrupole Resonance of ^{139}La around Pr^{3+} Doped in LaF_3. Raman Heterodyne Detection Using Optical Transition of Pr^{3+} Ions

Michio MATSUSHITA and Tatsuhisa KATO

[*Chem. Phys. Lett.* **273**, 291 (1997)]

The nuclear quadrupole transitions of ^{139}La around Pr^{3+} doped in LaF_3 have been detected as an optical-rf induced coherent Raman beat on the Pr^{3+} $^3H_4$ - $^3P_0$ transition (20925 cm^{-1}) at 1.5 K. Because the effective ^{141}Pr nuclear magnetic moment is smaller in the excited $^3P_0$ state than in the ground state, the Pr - La interaction decreases upon Pr^{3+} optical excitation, which makes the La NQR transitions couple with the Pr optical transition. Four magnetically inequivalent La nuclei were observed, revealing different local environments of La atoms around impurity Pr^{3+} ions.

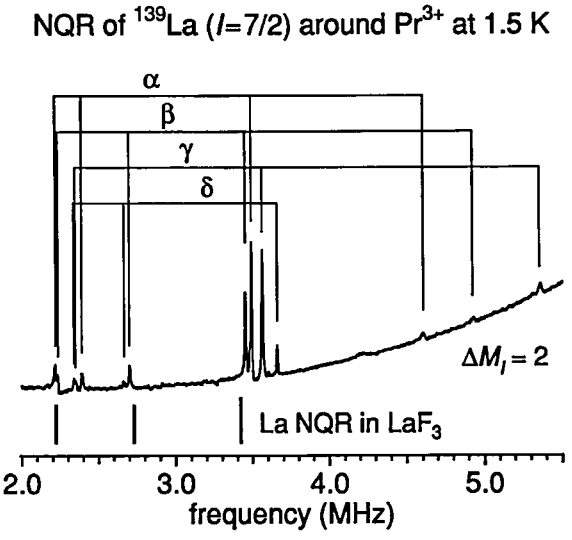

Figure 1. Raman heterodyne detected NQR of La around Pr^{3+} in LaF_3 at 1.5 K. Labels α through δ assign the transitions to four different nearest neighbour La sites around Pr^{3+}. A forbidden $\Delta M_I = 2$ transition is observed for sites α, β, and γ. The NQR frequencies of bulk La at 88 K are also indicated in the figure.

II-J State Correlated Raman Spectroscopy

The vibrational Raman polarizability tensor responds to molecular reorientational relaxation process, and the structural environment in condensed media. The measurement of Raman scattering is a powerful technique for the study of molecular motion and of the mechanism of phase transition. We've built up the system of multichannel type detection of Raman scattering combined with the temperature controlled cell.

II-J-1 Ordering of Liquid Crystals Studied by Polarized Vibrational Raman Spectroscopy

Naoki HAYASHI and Tatsuhisa KATO

The polarized vibrational Raman scattering were measured for the homogeneous oriented nematic liquid crystals of 5CB (4-n-pentyl-4'-cyanobiphenyl) and D302 (cyclohexanecarboxylate). The parallel and perpendicular polarized components of the Raman intensities of several vibrational modes were measured with changing the angle of the polarization of the incident laser against the director of the partial orientation of the nematic liquid crystal. The angular dependence of the intensity for each vibrational line exhibited the specific feature, which reflects the orientational situation of the principal axis of the Raman tensor for the each vibratinal line as well as the retardation effects due to the anisotropy of the macroscopic dielectric constant of liquid crystal. From the analysis of the angular dependence with taking account of the retardation effect, it is possible to evaluate order parameters of not only a dipole term P2 but also a quadrupole term P4. This procedure turned out to be more accurate than the previous methods. For 5CB with 50μm thickness at 25 °C, P2 and P4 for the vibrational line of the ciano group are 0.52 and 0.02, those of phenyl group are 0.52 and 0.12 respectively. This result suggests that distributions of phenyl and ciano groups are almost the same and the core part of molecule is rigid.

II-J-2 The Analysis of the Vibrational Raman Lines of the Pyridine-Water System Measured by a Tandem Type Spectrograph

Tatsuhisa KATO and Akiko MUTO *(Kitasato Univ.)*

A tandem type spectrograph, which is a CCD spectrograph combined with a Fabry-Perot interferometer, was constructed for the highly resolved line shape analysis of scattering light from condensed media. Some local structure of the hydration has been reported for the pyridine-water system, which was investigated by Rayleigh scattering and NMR measurements. The formation of some aligned aggregation of pyridine molecules supported by the hydration has been suggested for the interpretation of the experimental results. The hydrated local structure between pyridine and water might reflect on the line shape of the vibrational Raman lines of pyridine. The extent of the effect of the hydration on Raman lines depends upon the vibrational mode in question. The overview of the changing of the line shape over various vibrational modes would give some key to obtain a clear image of the hydrated local structure of pyridine-water system. The tandem type spectrograph has the advantage of the synchronous recording of highly resolved spectra for several lines, and it's possible to simultaneously analyze the line shape of several lines which are changing with the external condition, temperature, pressure, or concentration of the solution.

II-K Double Resonance Spectroscopy Using Two Phase-Locked Lasers

Optical-Optical double resonance (OODR) is one of the most sophisticated techniques in high resolution spectroscopy. It is as precise as microwave spectroscopy and provides detailed information which is often complementary to other spectroscopic information. Most of OODR experiments observe change of the population induced by irradiation of two laser fields resonant with two transitions of a three level system. However, if we could control the phase relation between the two laser fields and could detect phase dependent signals, it would give direct information on the phase in the quantum state excited by two phase-controlled coherent radiations. In order to perform this coherent OODR experiment, we are developing a light source system where the difference frequency between two lasers is kept phase-locked to a microwave frequency standard.

II-K-1 Development of a Phase-Locking System between Two Single Mode Lasers

Motohiro KUMAGAI *(Tokyo Inst. Tech.)*, **Hideto KANAMORI** *(Tokyo Inst. Tech. and IMS)*, **Michio MATSUSHITA and Tatsuhisa KATO**

The feedback system illustrated in Figure 1 has been constructed to stabilize the difference frequency between two titanium:sapphire ring lasers (Coherent 899-29, 899-21). Two laser lights are mixed in a ultrafast photo-detector (New Focus 1534) and the difference frequency between them is obtained as an electric signal in microwave region. This beat signal is down-converted into a radio frequency by mixing with a frequency standard generated by a synthesized sweeper (HP 83752B). A phase synchronizer (Micronow 215) produces an phase error signal with respect to an rf standard. The error signal is fed back to one of the lasers so that the optical difference follows the microwave standard. With this set-up the frequency jitter of 10 MHz in free-running condition has been considerably reduced down to 500 kHz. By changing the microwave frequency the optical difference frequency can

be scanned from 0.1 to 7 GHz. It is also possible to scan the frequencies of the two lasers while keeping the difference constant. Although further refinement of the feedback circuit is necessary to achieve our ultimate aim of phase-lock, this highly stable and tunable light source system will be an ideal spectroscopic tool for optical-optical double resonance and resonance Raman experiments.

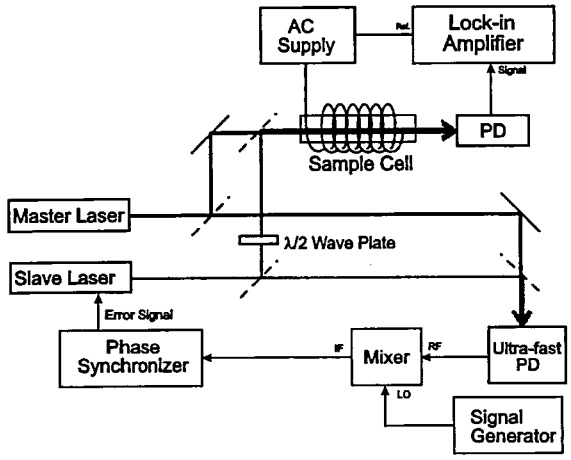

Figure 1. Block diagram of the phase-locking system between two single mode lasers and an OODR detection system using Zeeman modulation.

II-K-2 Optical-Optical Double Resonance Study on the D_2 Line of Rubidium Atom

Motohiro KUMAGAI *(Tokyo Inst. Tech.)*, **Hideto KANAMORI** *(Tokyo Inst. Tech. and IMS)*, **Michio MATSUSHITA and Tatsuhisa KATO**

The hyper-fine structures in the D_2 line of Rubidium atom was studied by optical-optical double resonance (OODR) spectroscopy, using our newly developed phase-locking system between two single mode lasers. High stability of the difference frequency of the two lasers made it possible to observe the hyper-fine structures in the sub-Doppler condition. As an example, Figure 2 represents the double resonance signal of the hyper-fine structure in the ground state of ^{87}Rb (see Figure 1). A sub-structure was observed in the center of the resonance signal, which is considered to be a kind of quantum interference effect between two excitation paths of (F=2-1,F=2-2) and (F=1-1, F=1-2).

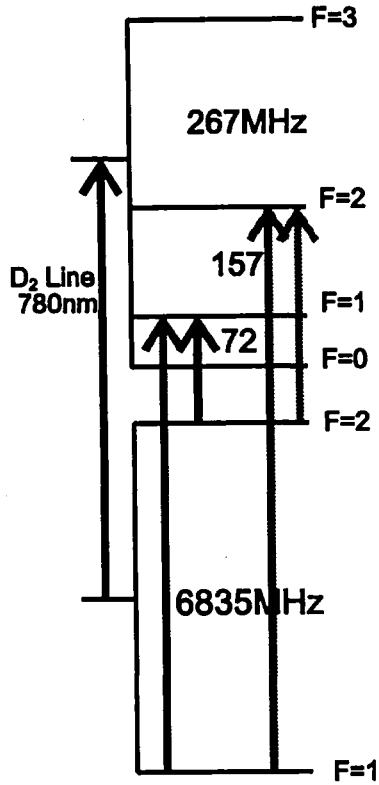

Figure 1. The hyper-fine structures in the D_2 line of ^{87}Rb.

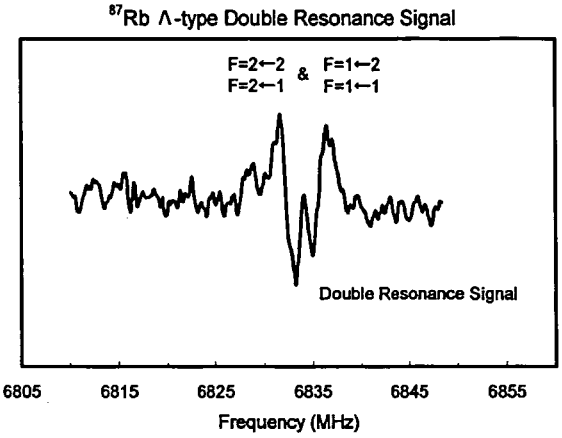

Figure 2. OODR spectrum of ^{87}Rb around 6.835 GHz.

RESEARCH ACTIVITIES III
Department of Electronic Structure

III-A Ultrafast Intermolecular Electron Transfer

Ultrafst fluorescence quenching of the excited dye molecule in neat electron-donating solvent is attributed to intermolecular electron transfer (ET). Accurate measurements of the fluorescence decay are made with coumarins in anilines (aniline, N-monoalkylanilines, and N,N-dialkylanilines), hydrazines (aromatic hydrazines and aliphatic hydrazine), and some of deuterated analogues. We have also performed a transient absorption study on the coumarin-aniline system. To understand the role of solvenit dynamics and intramolecular motion in ET, it is important to study the time dependence of the reaction in detail. An interesting system of studying an ultrafast ET is an electron donor-acceptor (EDA) complex. An oscillatory fluorescence decay has been observed and assigned to a vibrational coherence of the excited-state of EDA complex.

III-A-1 Substituent Effect and Deuterium Isotope Effect of Ultrafast Intermolecular Electron Transfer: Coumarin in Electron Donating Solvent

Hideaki SHIROTA *(Grad. Univ. for Advanced Studies)*, **Haridas PAL, Keisuke TOMINAGA and Keitaro YOSHIHARA**

We have studied the roles of the substitution of electron donating solvent molecules in the ultrafast electron transfer (ET) dynamics which occurs faster than the solvation dynamics. We have used aniline, N-monoalkylanilines, and N,N-dialkylanilines as electron donating solvents and five 7-amino-coumarins as acceptor molecules. The experimental results indicate that the ET rate depends largely on the substitutions of solvent molecules (Scheme 1). In N,N-dialkylanilines the ET rate gets smaller as the size of the alkyl substituent group becomes larger. For N-monoalkylanilines, however, the ET dynamics are not changed by the different alkyl substituent groups. From the both results of the cyclic voltammetric measurement and simulations by the two-dimensional ET model with solvent and nuclear coordinates, the N-alkyl substituent effect on the ET rate appears to be due to the changes in the electronic matrix element. We have also investigated the deuterium isotope effect on the ET dynamics using N-deuterated N-monoalkylanilines as donor solvents. For the fastest ET the isotope effect is hardly observable, whereas the effect is quite large (~ 20 %) for slower ET. The deuterium isotope effect seems to mainly come from the change of stabilization energies in intermolecular hydrogen-bonding interaction by deuteration. The extent of deuterium isotope effect on ET is similar for all N-monoalkylanilines used. This result indicates that the size of the alkyl groups does not affect much the hydrogen-bonding interaction.

$$k_{ET}(\text{Aniline}) \gg k_{ET}(N\text{-methylaniline}) \sim k_{ET}(N\text{-ethylaniline}) \sim k_{ET}(N\text{-}n\text{-propylaniline}) \sim k_{ET}(N\text{-}i\text{-propylaniline}) \ll k_{ET}(N,N\text{-dimethylaniline}) > k_{ET}(N,N\text{-diethylaniline}) > k_{ET}(N,N\text{-di-}n\text{-propylaniline})$$

Scheme 1. The relationship of the ET rate of the electron donating solvents.

III-A-2 Ultrafast Intermolecular Electron Transfer Dynamics in Coumarin-Hydrazine System

Hideaki SHIROTA *(Grad. Univ. for Advanced Studies)*, **Haridas PAL, Keisuke TOMINAGA and Keitaro YOSHIHARA**

Ultrafast intermolecular electron transfer (ET) from electron donating solvents (hydrazines) to the excited coumarin dyes has been investigated using the femtosecond fluorescence up-conversion technique. In this work we have used hydrazine derivatives as the electron donating solvents because hydrazines are well-known electron donating molecules having very low ionization potentials. The oxidation potential of the aliphatic hydrazine used in this study is lower than that of the aromatic hydrazine used. But the ET rate with aromatic hydrazines are seen to be much faster (subpicoseconds) than that with aliphatic hydrazine (a few tens of picoseconds) (Figure 1). The phenyl group of the electron donor hydrazine molecules has thus played an important role in the ET dynamics in the present systems.

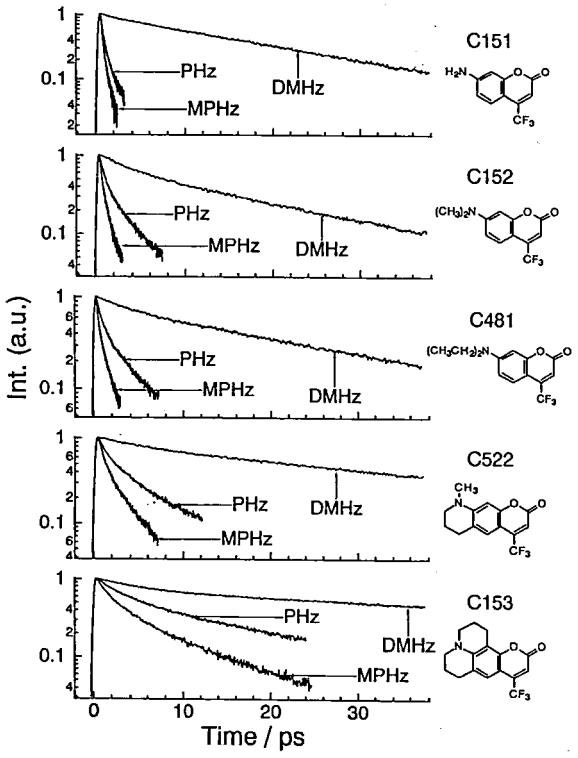

Figure 1. Fluorescence decays of coumarins in phenylhydrazine (PHz), 1-methyl-1-phenylhydrazine (MPHz), and 1,1-dimethylhydrazine (DMHz).

III-A-3 Ultrafast Intermolecular Electron Transfer and Back Electron Transfer in Coumarin-Aniline System

Hideaki SHIROTA *(Grad. Univ. for Advanced Studies)*, **Yukito NAITOH, Keisuke TOMINAGA and Keitaro YOSHIHARA**

We have investigated the ultrafast intermolecular electron transfer and back electron transfer in coumarin 152(C152)-aniline(AN) system by the femtosecond transient absorption spectroscopy using 400 nm pump and visible probe. The fluorescence decay of C152 in AN has already been determined by a fluorescence up-conversion method, which consists of two component 2.4ps (40%) and 10.7ps (60%).[1] These decays are caused by ultrafast intermolecular electron transfer between C152 and AN. The main purposes of this study are as follows: (1) Direct observation of the reaction products such as anion radical of C152 and cation radical of AN. (2) Measurements of the back electron transfer rate. (3) Comparison between both data obtained by the transient absorption and fluorescence up-conversion. The transient absorption signal at 680 nm, which is considerd to be the absorption of the anion radical of C152, consists of a rise with a time constant of 1.7 ps and a decay with 2.9 ps as shown in Figure 1. These rise and decay represent the production of C152 anion radical by electron transfer and the disappearance of the anion by the back electron transfer, respectively. The contribution of slow component measured in the fluorescence up-conversion is not observed in this transient absorption.

Reference

1) H. Shirota, H. Pal, K. Tominaga and K. Yoshihara, *J. Phys. Chem.* submitted.

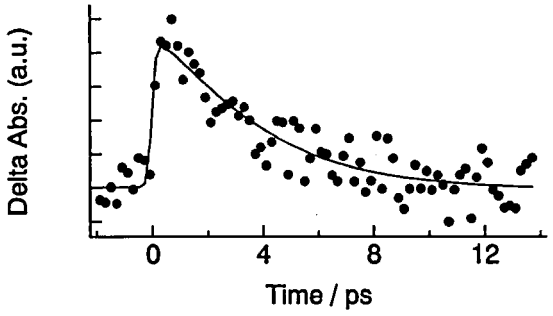

Figure 1. The transient absorption signals at 680 nm originated from C152 in AN, which is obtained by subtracing signals by neat AN from those by C152 - AN system.

III-A-4 Oscillatory Fluorescence Decay of Electron-Donor-Acceptor Complex

Igor V. RUBSTOV *(IMS and JAIST)* **and Keitaro YOSHIHARA** *(IMS and JAIST)*

[*J. Phys. Chem.* **101**, 6138 (1997)]

We observed an oscillatory fluorescence decay dynamics of electron-donor-acceptor complex of hexamethylbenzene and tetracyanoethylene in CCl_4 at room temperature. A fast spontaneous fluorescence decay with a characteristic time of 105 ± 20 fs was measured (Figure 1). An under-damped oscillation of fluorescence is overlapped with this fast decay. The period of the oscillation is 209 ± 4 fs which corresponds to a frequency of 159 ± 3 cm^{-1}. The oscillation is tentatively assigned to an intermolecular vibration in the excited state. The damping time of the oscillations is 280 ± 30 fs.

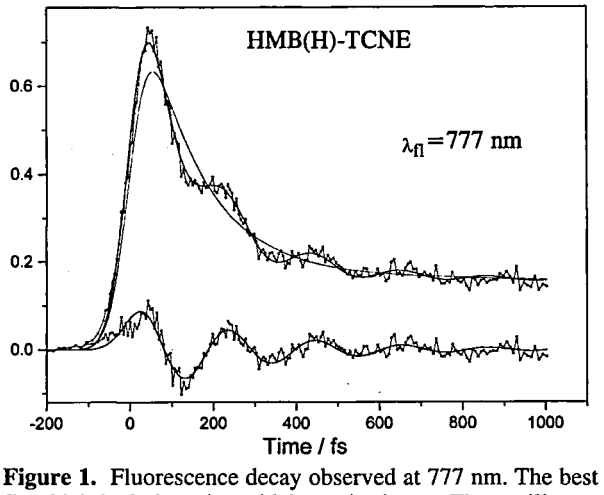

Figure 1. Fluorescence decay observed at 777 nm. The best fit which includes sinusoidal part is shown. The oscillatory part is also shown separately.

III-B Liquid Dynamics Studied by Higher Order Nonlinear Spectroscopy

Vibrational spectra get broadened extensively and often shifted in liquids compared to those in the gas phase. This is because the solute molecule interacts with solvent molecules in a complex manner, and consequently molecular spectra can, in principle, serve as probes to obtain information about the structure and dynamics of molecular liquids. One traditional approach to investigate microscopic details in liquids from molecular spectra is the lineshape analysis. On the theoretical side, a wide variety of sophisticated theories and models have been developed and critically compared with experimental results. However, the lineshape analysis sometimes requires certain amount of fitting parameters, especially in cases of complex microscopic models, and due to a large number of fitting parameters, the lineshape analysis always carries some ambiguity. In recent five years, however, new ultrafast spectroscopies based on higher-order nonlinearity have been developed to make more rigorous approach to the vibrational dynamics than the lineshape analysis. Raman echo is the seventh order experiment, which corresponds to photon echo of the electronic spectroscopy. One of the advantages of the higher-order experiment is that a wide variety of the nonlinear technique can be designed by choosing proper experimental conditions such as phase-matching. Two-dimensional impulsive stimulated Raman scattering (fifth order) and one- and two-dimensional overtone vibrational dephasing (fifth order) fall into this category. These experiments have been providing unique information on microscopic details in liquids which are not available by the conventional techniques.

III-B-1 Overtone Vibrational Dephasing in Chloroform and Deuterated Chloroform

Keisuke TOMINAGA and Keitaro YOSHIHARA

The vibrational dephasing of overtone bands (v= 2 and v = 3) of the C-H stretching of $CHCl_3$ and the C-D stretching of $CDCl_3$ has been studied by higher-order nonlinear spectroscopies. The v = 2 and v = 3 signals are based on fifth and seventh order nonlinear phenomena, respectively. The overtone signals as well as the fundamentals of $CHCl_3$ and $CDCl_3$ are shown in Figure 1. Decay time constants of the signals are shown in the figure. The vibrational dephasing processes of the overtone and fundamental bands cannot be explained by the stochastic theory which is exact for a diatomic molecule with an anharmonic coupling. This deviation from the theoretical prediction may come from a polyatomic nature of the molecule such as off-diagonal anharmonicity and/or coupling with combination bands.

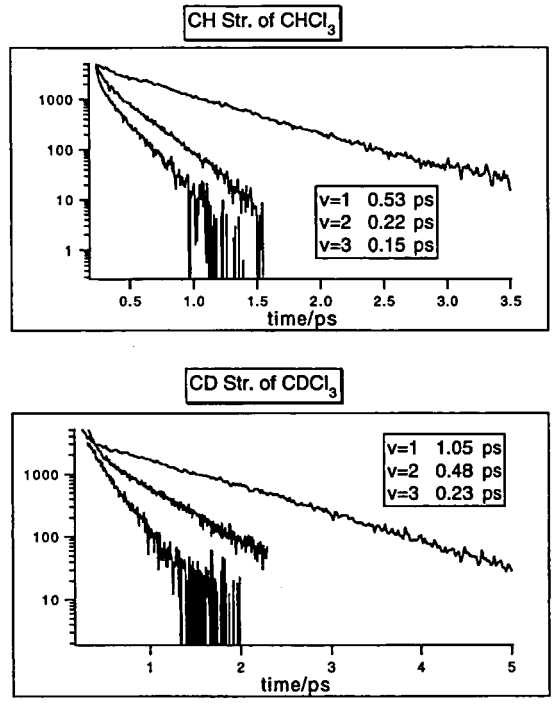

Figure 1. Vibrational dephasing signals of overtone (v = 2 and v = 3) and fundamental bands of the C-H stretching of $CHCl_3$ and the C-D stretching of $CDCl_3$.

III-C Studies on Ultrafast Solvent Dynamics by Optical Kerr Effect

Studies on primary chemical reactions in solution require detail knowledge of solvent dynamics. One of the relevant methods is the measurement of optical Kerr effect (OKE) in the femtosecond-picosecond timescale. We have studied OKE of anilines, which are often used as electron-donating solvent for our works of ultrafast intermolecular electron transfer. In relation to the deuterium isotope effect on solvation dynamics, we have also studied ultrafast polarizability anisotropy relaxation of methanol.

III-C-1 Ultrafast Optical Kerr Effect and Solvation Dynamics of Liquid Aniline

[*J. Phys. Chem. A* **101,** 3641 (1997)]

Neil A. SMITH *(Univ. East Anglia)*, **Shujie LIN** *(Univ. East Anglia)*, **Stephen R. MEECH** *(Univ. East Anglia)* **and Keitaro YOSHIHARA**

Femtosecond optically heterodyne detected optical Kerr effect (OHD-OKE) measurements have been made on liquid aniline. The OHD-OKE data in the fre-

quency domain can be analyzed in terms of three components: a low-frequency diffusional part; a collisional part and an underdamped intermolecular mode. The pure solvent relaxation is also compared with the solvation dynamics measured by the fluorescence dynamic Stokes shift.

III-C-2 Ultrafast Dynamics of Liquid Anilines Studied by the Optical Kerr Effect

Neil A. SMITH *(Univ. East Anglia)*, **Shujie LIN** *(Univ. East Anglia)*, **Stephen R. MEECH** *(Univ. East Anglia)*, **Hideaki SHIROTA** *(Grad. Univ. Advanced Studies)*, **and Keitaro YOSHIHARA**

[*Chem. Phys. Lett.* submitted]

The femtosecond dynamics of liquid aniline, its N methylated derivatives, two deuterium isotopes, and some mixtures are studied by means of the optically heterodyne detected optical Kerr effect. The data are well described by an instantaneous electronic response, and a sum of a librational component, an ohmic lineshape and a two exponential component relaxation. The measured pure liquid dynamics are used to calculate the solvation time correlation function, which is compared with the solvation dynamics of anilines obtained by the dynamic fluorescence Stokes shift measurement.

III-C-3 Deuterium Isotope Effect on Ultrafast Polarizability Anisotropy Relaxation in Methanol

Hideaki SHIROTA *(Graduate Univ. Advanced Studies)*, **Keitaro YOSHIHARA, Neil A. SMITH** *(Univ. East Anglia)*, **Shujie LIN** *(Univ. East Anglia)* **and Stephen R. MEECH** *(Univ. East Anglia)*

We have investigated the ultrafast polarizability anisotropy relaxation of methanol and three deuterated derivatives by the optically heterodyne detected optical Kerr effect. On the picosecond timescale the effect of deuteration is to slow the relaxation (Figure 1). The deuterium isotope effect on the picosecond dynamics is quite similar to the solvation dynamics. On the subpicosecond timescale the deuterium isotope effect is very small. The data are discussed with reference to recent MD simulations of methanol.

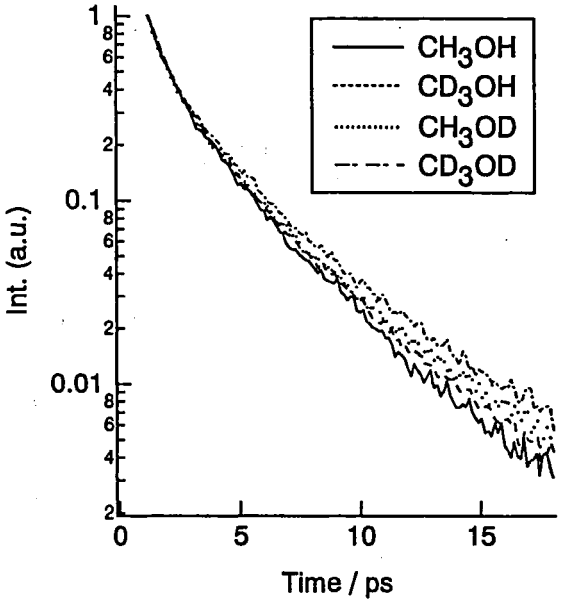

Figure 1. OKE signals for methanol and three different isotopic substituent methanols.

III-D Ultrafast Dynamics of UV-Photoexcited Simple Molecules in Solution by Femtosecond Transient Absorption Spectroscopy

The photoinduced primary processes of simple molecules in solution have been investigated by the femtosecond transient absorption spectroscopy using a regeneratively amplified Ti:Sapphire laser system, which operates on the conditions of 120 fs pulse duration, 900 μJ pulse energy , and 1 kHz repetition rate at around 800 nm. We generated second harmonic and/or third harmonic using BBO crystals for a pump pulse and the white light continuum for a probe pulse, the latter being obtained by focusing a fundamental or second harmonic pulse on a flowing cell of H_2O. Throughout the studies on photodissociation of alkyl halides, isomerization of simple polyenes, ionization of benzene, and so on, we have learnt that the interactions between solutes play the main role for reaction dynamics as described in the later section. For example, in the case of photodissociation of CH_2I_2, the aggregate of solutes causes a specific subsequent reaction which is not seen in an isolated system. Quantitative discussion about the relationship between the structure and dynamics is needed to precisely understand the chemical reaction in the solution phase.

III-D-1 The Polarization Response of I_2 Produced by Photoinduced Chemical Reaction in Neat CH_3I

Yukito NAITOH and Keitaro YOSHIHARA

In order to investigate the dynamics of bimolecular chemical reaction in solution, we have studied I_2 formation process in neat CH_3I by UV excitation. This process starts from photodissociation of CH_3I followed by the reaction between a photofragment $I^*(^2P_{1/2})$ and another CH_3I as solvent. Accordingly, this reaction does not require the translational diffusion before the encounter between two reactant molecules. We have already reported the transient absorption of I_2 formation from UV to visible region and found they consisted of a very fast rise and a slow decay with a time constant of ca. 15 ps. The latter is regarded as disappearance of

I_2 by the reverse reaction between I_2 and CH_3 radical in the solvent cage. For the fast formation of I_2, the photochemistry of CH_3I dimer in the gas phase suggests that this reaction is not stepwise, but a concerted one in the dimer. We have ascertained whether this scheme can be applied for the neat liquid condition by measuring the time-resolved anisotropy, R. Figure 1(a) represents the difference in the rise observed at 580 nm between the parallel and perpendicular configurations of the polarization in the pump and probe pulses. In Figure 1(b), the time-resolved anisotropy R decays from a positive value to zero with a time constant of 960 fs. This means that the nascent I_2 has a given alignment to the laboratory frame and reduces R due to the rotational diffusion. If the structure of neat liquid were random and/or the reaction proceeded stepwise, we would not have non-zero R. This result indicates that on neat liquid condition, the orientation between neighbor CH_3I molecules is responsible for this reaction.

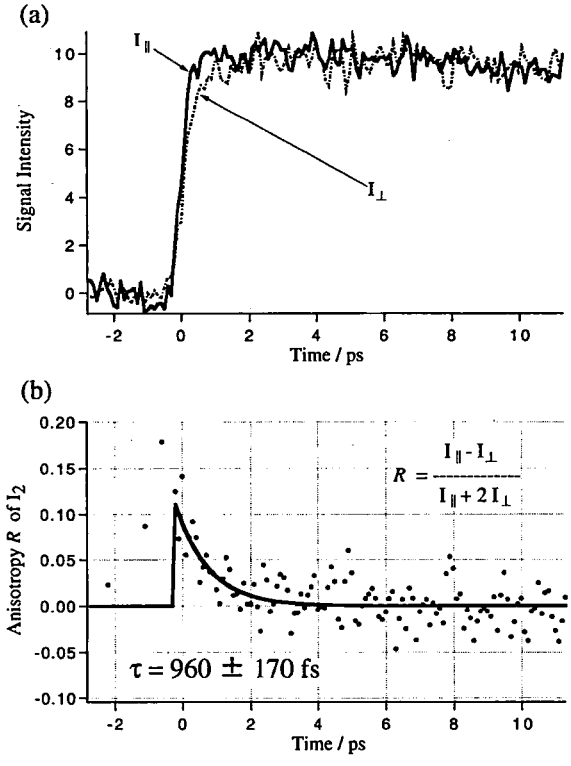

Figure 1. (a) The transient absorption signals in neat CH_3I observed at 580 nm in two different configurations of the polarization in pump and probe pulses. $I_{//}$ and $I_{\perp}$ represent two polarizations are parallel and perpendicular to each other. (b) The time-resolved anisotropy R is equal to $(I_{//} - I_{\perp})/(I_{//} + 2I_{\perp})$. The decay time constant of 960 fs is similar to 1.4 ps of the rotational diffusion time of I_2 in n-hexane.

III-D-2 The I_2 Formation by UV Excitation in CH_3I/CH_3CN System

Yukito NAITOH and Keitaro YOSHIHARA

We have measured I_2 formation process in CH_3I/CH_3CN system and in neat CH_3I by UV excitation. Figure 1 shows the transient absorptions in 2 mol% and 10 mol% CH_3I/CH_3CN observed at 460 nm and in neat CH_3I observed at 480 nm, which almost correspond to the peak position of static I_2 absorption in CH_3I/CH_3CN mixed solutions and in neat liquid. These three signals indicates similar behavior of fast rise. If CH_3I molecules are homogeneously dissolved in CH_3CN solution, the photofragment I should diffuse until it encounters with another reactant CH_3I. This requires a long reaction time. The observed fast rise of I_2 indicates that two or more CH_3I molecules are in contact to one another in CH_3CN solution. Moreover, as discussed in the former section, it is expected that the aggregate of CH_3I molecules forms a given structure in CH_3CN solution. In order to examine this assumption, we plan to measure the time resolved anisotropy R in CH_3I/CH_3CN system.

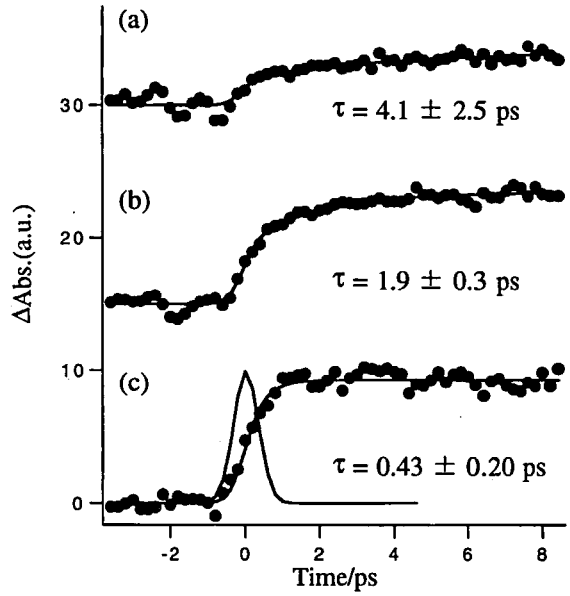

Figure 1. The transient absorption signals observed at 460 nm in (a) 2 mol% CH_3I/CH_3CN and (b) 10 mol% CH_3I/CH_3CN, and at 480 nm in (c) neat CH_3I, respectively.

III-D-3 Solute Concentration Dependence of Complex Formation I and CH_2I_2 by Photodissociation of CH_2I_2 in Solution

Ken-ichi SAITOW *(Grad. Univ. for Advanced Studies)*, **Yukito NAITOH, Keisuke TOMINAGA and Keitaro YOSHIHARA**

We have studied the photoinduced reaction of methylene iodide (CH_2I_2) upon excitation at 268 nm in CH_3CN and hexane solutions. This reaction gives three kinds of photoproducts in femto to picosecond time region based on the transient absorption spectra, and they are assigned to a photofragment: CH_2I radical, the charge transfer (CT) complex between a photofragment I and another parent molecule CH_2I_2: $CH_2I_2^{\delta+}\bullet\bullet\bullet I^{\delta-}$, and the final product: $CH_2I_2^{+}$.[1] The rate of formation of the CT complex significantly depends on the solute concentrations and this rate is much greater than in the case assuming the translational diffusion in homogeneous solution in the experimental concentration range (10^{-4}~10^{-2}M). We consider that this is caused by the formation of solute aggregates in solutions. The degree of solute aggregates is analyzed in both solutions by

solving the rate equations, and the relative relationship between bulk and local concentrations are shown in Figure 1. The local concentration means the number of CH_2I_2 around the fragment I. Figure 1 shows that the local concentration gradually saturates as the bulk concentration increases and the saturation in CH_3CN starts at lower concentration than in hexane solutions. This means that CH_2I_2 in the neighboring region of initially photoexcited CH_2I_2 can participate in CT-complex formation and such a condition is achieved at lower concentration in CH_3CN than in hexane.

Reference

1) K. Saitow, Y. Naitoh, K. Tominaga and K. Yoshihara, *Chem. Phys. Lett.* **262**, 621 (1996).

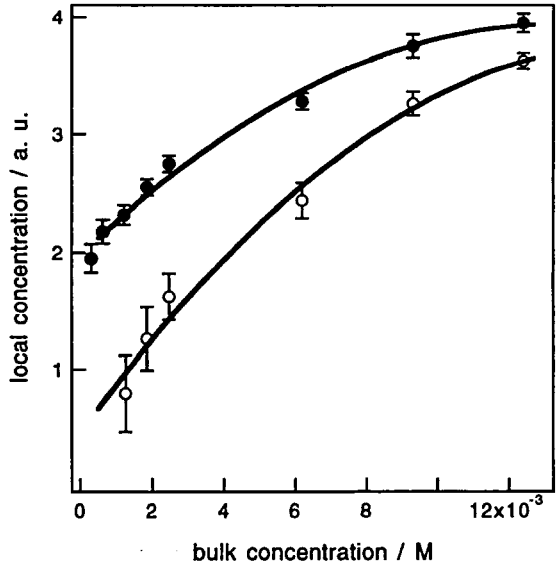

Figure 1. The relative relationship between the local and the bulk concentration of CH_2I_2 in CH_3CN (●) and hexane (○)

III-D-4 Ultrafast Dynamics of Photoexcited *trans*- and *cis*-1,3,5-Hexatriene in Solution

Kaoru OHTA *(Kyoto Univ. and IMS)*, **Yukito NAITOH, Keisuke TOMINAGA, Noboru HIROTA** *(Kyoto Univ.)* **and Keitaro YOSHIHARA**

The electronic, vibrational and conformational relaxations of trans- and cis-1,3,5-hexatriene in solution have been investigated by femtosecond transient absorption spectroscopy. Upon excitation to the 1B state, the transient absorption is observed in the visible region, which mainly consists of the instantaneous rise (<150 fs) and a subpicosecond decay. For trans isomer, the decay of the transient absorption signals becomes faster at longer wavelengths. On the other hand, for cis isomer, the decay of the signals does not depend on the probe wavelength significantly, as shown in Figure 1. For both isomers, these temporal profiles of signals show that the internal conversion from the S_2 to S_1 state occurs within 100 fs and the lifetime of the S_1 state is less than 500 fs. The observed dependence of the decay on the probe wavelengths for trans isomer is ascribed to the vibrational energy redistribution in the S_1 state. We also measured the bleach recovery signals by the one-color pump-probe method in the UV region. The bleach recovers in several time scales. The temporal profiles of trans isomer in the first 20 ps are similar to those of cis isomer, which come from the vibrational relaxation in the ground state. However, in a longer time scale, these signals are quite different to each other. While trans isomer takes 150-300 ps to fully recover the bleach, cis isomer requires no more than 100 ps. These slow components are attributed to the conformational relaxation around C-C single bond to the original forms. The different behavior between trans and cis isomer reflects different product distribution and dynamics among the isomers around the C-C single bonds.

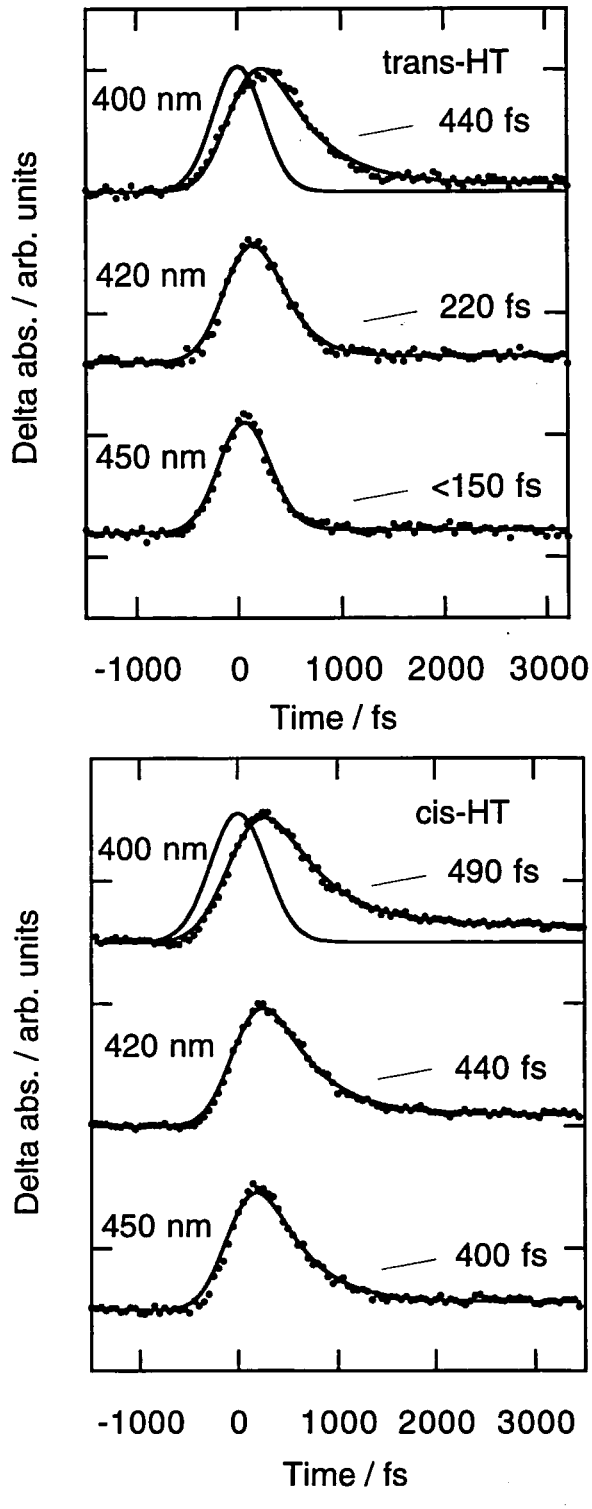

Figure 1. Transient absorption signals trans- and cis-hexatriene observed at three different wavelengths in cyclohexane. The instrument response function is shown in the top decay curve. The solid lines represent the best fits to the data by the convolution of the instrument response function with a exponential function.

III-D-5 Formation of Benzene Dimer Cations in Neat Liquid Benzene

Yoshiya INOKUCHI *(Kyusyu Univ. and IMS)*, **Yukito NAITOH, Kazuhiko OHASHI** *(Kyusyu Univ. and IMS)*, **Ken-ichi SAITOW** *(Grad. Univ. for Advanced Studies)*, **Keitaro YOSHIHARA and Nobuyuki NISHI** *(Kyusyu Univ. and IMS)*

[*Chem. Phys. Lett.* **269**, 298 (1997)]

We have investigated a formation process of benzene dimer cation in neat liquid benzene by using a femtosecond pump-probe laser system. Third harmonic of a regeneratively amplified Ti:Sapphire laser was focused on a flow jet of neat benzene with a thickness of 100 μm at room temperature. The absorption changes from visible to near IR are measured. Figure 1 shows the transient absorption signals at (a) 580 nm and (b) 920 nm. The rise curve at 580 nm is analyzed as two composites of (1) a slowly rising component with a time constant of 14 ps, and (2) a component with a fast rise within the time resolution of apparatus and a slow decay. Based on the pump power dependence of the signal intensity and transient absorption spectrum, we attribute the component (1) to benzene excimer and (2) to the S_1 state of monomer benzene produced by one-photon absorption. The transients observed at 920 nm having a fast rise (< 1 ps) is assigned to benzene dimer cation formed by two-photon absorption. The most reasonable configuration of neat liquid benzene is perpendicular just between the nearest neighbors. The benzene excimer and the dimer cation, however, have a parallel structure. Therefore, the formation times include reorientation from a perpendicular to a parallel configuration. The difference in the appearance times can be rationalized by an effect of a positive charge created in the liquid. Since π electrons of a neighboring benzene feel a strong attractive force from the positive charge, the reorientation to the parallel structure must occur much faster than the rotational motion of neutral species. This causes the fast formation of benzene dimer cation.

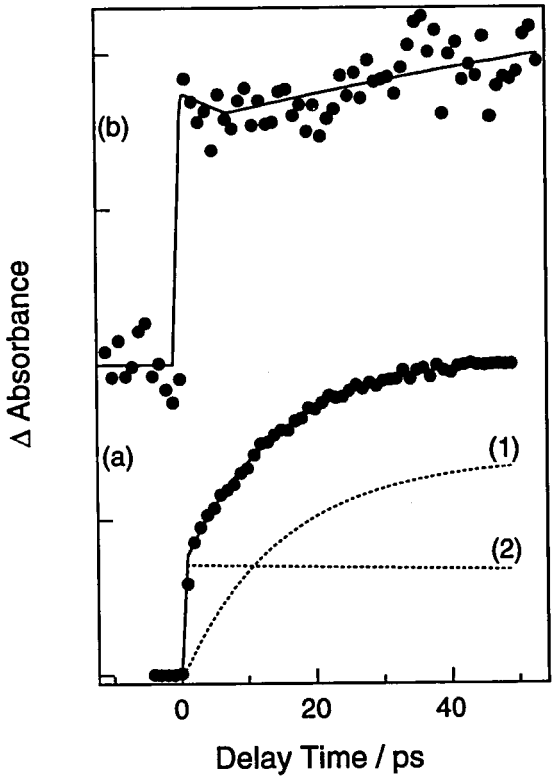

Figure 1. Transient absorption signals measured at (a) 580 nm and (b) 920 nm.

III-E Dynamical Behavior of Electronically Excited States

Understanding the dynamics of photoexcited dye molecules in solution, such as the intra- and intermolecular vibrational energy relaxation, solvation dynamics and electron transfer reaction, has been an area of intense research in recent years. If the excited molecules have an excess vibrational energy, vibrational relaxation should affect the spectral evolution of the solvation dynamics within a few picosecond time scale. We investigated the internal conversion (IC) and intramolecular vibrational energy redistribution process (IVR) of coumarin 481 (C481) in solutions with a large excess energy in order to reveal how the vibrational relaxation is coupled to the solvation process.

III-E-1 Relaxation Processes from a Higher Excited State of a Dye Molecule in Solution Studied by Femtosecond UV Fluorescence Up-Conversion Method

Kaoru OHTA *(Kyoto Univ. and IMS)*, **Tai Jong KANG** *(Taegu Univ. and IMS)*, **Keisuke TOMINAGA, Noboru HIROTA** *(Kyoto Univ.)* **and Keitaro YOSHIHARA**

We investigated the internal conversion (IC) and intramolecular vibrational energy redistribution process (IVR) of coumarin 481 (C481) in solutions with a large excess energy in order to study how the vibrational relaxation is coupled to the solvation process. C481 molecule was excited to a higher electronic excited state (S_n) by the third harmonic (267 nm) of a mode-locked Ti:Sapphire laser. In this case, C481 has an excess energy of > 10000 cm^{-1} from the S_1 state. The fluorescence from the S_1 state was probed by the up-conversion method. We measured time-resolved fluorescence signals of C481 in cyclohexane observed at several wavelengths. The 200-300 fs rising components were observed at all wavelengths. This result suggests that the observed dynamics are mainly controlled by

the IC from S_n to S_1 state, i.e. IC occurs in a 200-300 fs time scale and IVR takes place much faster than the former process. We also observed a blue shift of the spectrum in a 10-ps time scale. The 10-ps components of the up-converted signals are tentatively attributed to the vibrational cooling process in the S_1 state.

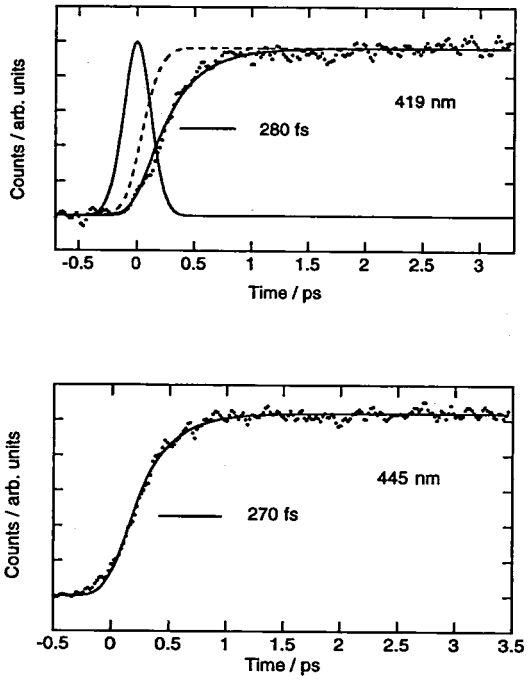

Figure 1. Fluorescence rises and decays of coumarin 481 in cyclohexane observed at two different wavelengths.

III-F Photochemistry on Well-Defined Surfaces

Upon the irradiation of light in the wavelength range from visible to ultraviolet, a number of adsorbed molecules on metal surfaces reveal variety of photochemical processes, including photo-stimulated desorption, rearrangement of adsorbed states, photodissociation, and photo-initiated reactions with coadsorbates. A central and fundamental question in the surface photochemistry is to clarify how adsorbate-substrate systems are excited by photon irradiation. In addition, since photo-initiated reactions can be induced without any thermal activation of reactants, they may provide good opportunities for studying a new class of surface reactions which may not be induced thermally. We have studied photochemistry of various adsorption systems on well-defined metal and semiconductor surfaces mainly by temperature-programmed desorption (TPD), x-ray photoelectron spectroscopy (XPS), work function measurements, near edge x-ray absorption fine structure (NEXAFS) and angular-resolved time-of-flight (TOF) spectroscopy of photodesorbed species associated with pulsed laser irradiation. In this year, we have focused on how uv-photochemistry of methane on Pd(111) is different from that on Pt(111).

III-F-1 Comparative Study of Photochemistry of Methane on Pt(111) and Pd(111) Surfaces

Kazuo WATANABE and Yoshiyasu MATSUMOTO

[*Surf. Science* in press]

Adsorption states and photochemistry of methane physisorbed on Pd(111) have been investigated by temperature-programmed desorption and X-ray photoelectron spectroscopy and compared with those on Pt(111). On both of the surfaces, methane is either dissociated into a hydrogen atom and a methyl radical, or molecularly desorbed by 6.4-eV photon irradiation. In the photochemistry, the direct electronic excitation of the adsorbate-substrate complex plays an important role. Different features observed for Pd(111) compared with Pt(111) are: (1) the adsorbate-substrate interaction is slightly stronger, (2) methane adsorbates show a ($\sqrt{3} \times \sqrt{3}$)R30- LEED pattern at 40 K, (3) the photochemical cross section is larger by 60%, (4) the photochemistry is not self-quenched at prolonged irradiation. The origins of these features are discussed in terms of the differences in the electronic structure between the two surfaces.

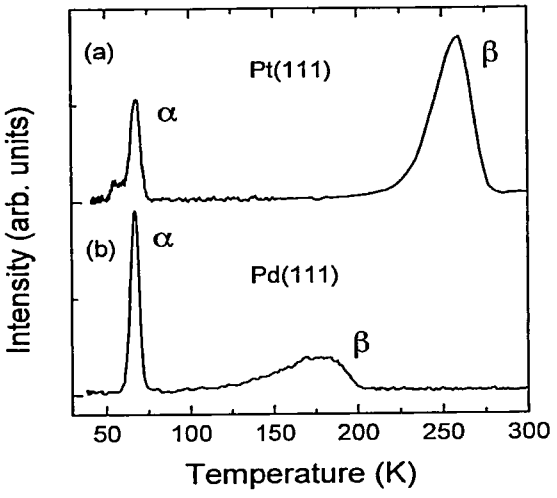

Figure 1. Post-irradiation TPD results of CH_4 (m/e=13) from (a) Pt(111) and (b) Pd(111). Initial CH_4 coverage and the number of accumulated photons were 0.33 ML and 6×10^{18} cm^{-2} for Pt(111) and 0.31 ML and 1.5×10^{19} cm^{-2} for Pd(111), respectively. The peak denoted as α originates from CH_4 molecular desorption, and β from H + CH_3 associative desorption. The heating rate for Pd(111) is 1.1 Ks^{-1} in the entire temperature range, but 0.3 and 5.0 Ks^{-1} below and above 164 K for Pt(111).

III-F-2 Photodesorption Dynamics of Methane on Pd(111)

Kazuo WATANABE and Yoshiyasu MATSUMOTO

[PhD thesis of K. Watanabe]

We have observed photodesorption of CH_3 and CH_4 photodesorbed from a clean and a H-covered Pd(111) surfaces under 193 nm photon irradiation. While the CH_3 TOF distributions could be fitted by single Maxwell-Boltzmann distribution with speed ratio S close to unitiy, the CH_4 TOF distribution consists of three velocity components denoted as P_1 (fast), P_2 (medium) and P_3 (slow). The P_1 component originates from direct molecular desorption, whereas the P_2 component from associative desorption between H* (photofragment of CH_4) and CH_3(a). The remarkable differences between the CH_4 TOF distributions from Pt(111) and Pd(111) surfaces are in the following: (1) The translational energy of the direct molecular desorption from Pd(111) is substantially larger than that from Pt(111). (2) The translational energy of associatively desorbing methane from Pd(111) is smaller than that from Pt(111). The latter suggests that the activation energy of dissociative adsorption of methane is smaller on Pd(111) than on Pt(111). The present TOF results, together with the LEED observation of methane superstructures and the photoreaction cross section measurements, agrees with the model in which the surface states play important roles to determine the interaction between adsorbates and substrates.

III-G Reaction Dynamics on Well-Defined Surfaces

Vast majority of surface reactions studied so far has been interpreted in terms of a Langmuir-Hinshelwood mechanism; reactants are first adsorbed on a surface and a reaction takes place between two chemisorbed species. Although reactants are in equilibrium with surface atoms, the energetics of desorbed products are determined by potential energy surfaces along reaction coordinates. In particular, associative desorption, which is often a reversed process of activated dissociative chemisorption, shows interesting features manifested by a potential barrier near the exit channel. In this year, we demonstrated for the first time that CO_2 is effectively converted to surface carbonate by thermal dissociation of N_2O on Si(100).

III-G-1 Effective Carbonate Formation Induced by Thermal Dissociation of N_2O on Si(100)

Hiroyuki KATO *(Grad. Univ. for Advanced Studies)*, **Kazuya WATANABE and Yoshiyasu MATSUMOTO**

[*Surf. Sci. Lett.* submitted]

Thermal reactions of CO_2 with N_2O on a clean Si(100) surface have been studied by temperature-programmed desorption and X-ray photoelectron spectroscopy. CO_2 physisorbed on Si(100) exclusively desorbs at ~75 K. However, when CO_2 is coadsorbed with N_2O on the clean surface, CO_2 is converted very effectively into a surface carbonate species below 140 K. The carbonate species is dissociated to produce desorbed species of CO or CO_2 in the temperature range of 200 -600 K. For the coadsorbates of $C^{18}O_2$ and $N_2{}^{16}O$, the CO_2 species produced from the carbonate show statistical mixing of oxygen isotopes. The reactions between the coadsorbates do not occur on a fully-oxidized Si(100) surface. Since N_2O does not dissociate on the oxidized surface, thermal dissociation of N_2O adsorbates is essential to form the carbonate species.

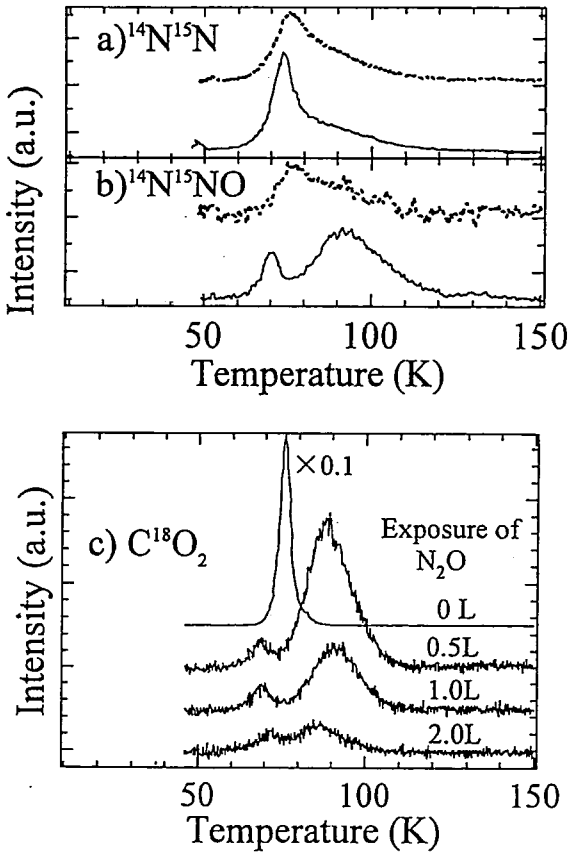

Figure 1. TPD results measured at (a) m/e=29 ($^{14}N^{15}N$) and (b) m/e=45 ($^{14}N^{15}NO$). Dotted curves are signals from neat N_2O (1.0 L) adsorbed on Si(100), and solid curves are from CO_2 (0.4 L) and N_2O (1.0 L) coadsorbed on Si(100). (c) Series of the TPD results measured at m/e=48 ($C^{18}O_2$) from CO_2 and N_2O coadsorbed on Si(100) as a function of N_2O exposure as indicated in the figure. The exposure of CO_2 was 0.4 L. The sample at 45 K was exposed to the gases. The heating rate was 0.4 K/s.

III-H Multiphoton Photoelectron Spectroscopy of Electronic States at Metal Surfaces

A central and fundamental question in surface photochemistry is to clarify how adsorbate-substrate systems are excited with photon irradiation. Two different excitation mechanisms have been frequently discussed : (1) indirect excitation via substrate-mediated charge transfer and (2) direct excitation within adsorbate. In the former mechanism electrons or holes created by photon absorption of metal and semiconductor substrates are attached resonantly to adsorbates. In any case, it is crucial to obtain information on electronic excited states of adsorbate-substrate systems. One of the best methods, and most relevant to surface photochemical measurements, is multiphoton photoelectron spectroscopy. We have applied this photoelectron spectroscopy to probe electronic structures of clean and CO-covered Pt(111) surfaces in this year.

III-H-1 Angle-Resolved Multiphoton Photoelectron Spectroscopy of a Clean Pt(111) Surface

Ikuo KINOSHITA *(Yokohama City Univ.)*, **Toshihisa ANAZAWA and Yoshiyasu MATSUMOTO**

The surface state and image-potential state (IPS) on Pt(111) have been studied by angle-resolved multiphoton photoemission spectroscopy. The three-photon photoelectron spectrum by fs pulses shows two peaks: photoemission from the n=1 IPS populated by nonresonant transitions and that from the sp-derived surface state. Both of the states show free-electron like parabolic dispersion curves. With adsorption of oxygen, the photoemission peak from the surface state disappears, but the peak from IPS still remains.

III-H-2 Two-Photon Photoemission Study of CO adsorbed on Pt(111)

Toshihisa ANAZAWA, Ikuo KINOSHITA *(Yokohama City Univ.)* **and Yoshiyasu MATSUMOTO**

[*J.Electron Spectrsc. and Related Phenomena* in press]

When a molecule chemisorbs on a metal surface, the electronic structure of the molecule is significantly modified by hybridization with substrate electronic states. Thus, measurements of adsorbate-induced electronic states are of primary importance for understanding chemical bondings on metal surfaces. CO chemisorbed on transition metal surfaces provides a good opportunity for this purpose. In this study, unoccupied electronic states induced by CO chemisorbed on a Pt(111) surface have been investigated by two-photon photoelectron (2PPE) spectroscopy. The 2PPE spectra obtained by the excitation with $4.3 \leqq h\nu \leqq 5.4$ eV indicates that photoemission peaks prominent in the 2PPE spectra from the CO-covered Pt(111) surface originate from normally unoccupied CO-induced states above the Fermi level (E_F), which are transiently

occupied in the 2PPE process. The energy of the CO-induced unoccupied state depends on the adsorption site of CO. Below 0.17 ML where CO is adsorbed at the on-top site, the CO-induced state is located at 4.5 eV above E_F. With increase of the coverage to 0.5 ML where CO is adsorbed at the bridge site in addition to the on-top site, a new photoemission peak from the state at 4.3 eV grows. This state is assigned to the unoccupied state of bridge-bonded CO. From the polarization dependence of the 2PPE spectra, these CO-induced states are assigned to the hybridized states of a CO $2\pi^*$ orbital with substrate electronic states.

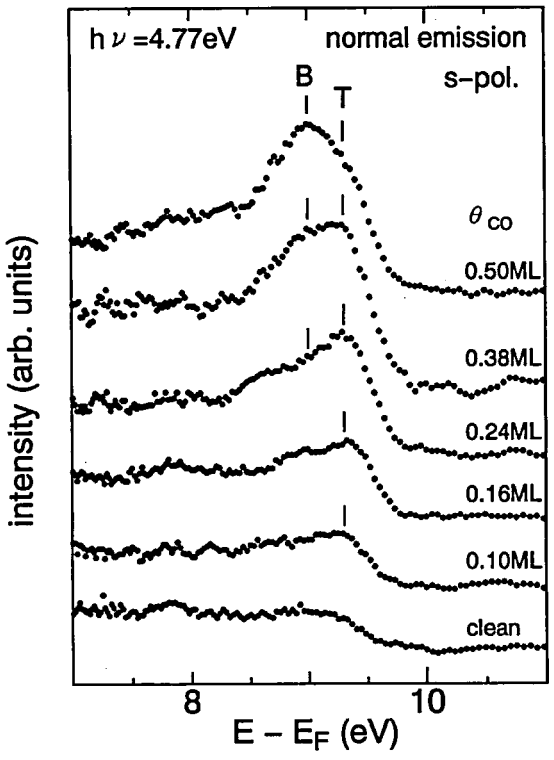

Figure 1. Coverage dependence of 2PPE spectra of CO adsorbed on Pt(111). The spectra were recorded at hν = 4.77 eV with s-polarization. The energy of photoelectrons is referenced to E_F. Note that adsorbate-induced photoemission peaks denoted by T and B grow with increase of CO coverage.

III-I Potentials for Large-Amplitude Vibrations of Molecules in van der Waals Complexes

Large-amplitude vibrations of molecules are considered to play an important role in dynamics. The determination of their potentials, therefore, is of great importance. The potentials are so shallow and flexible that they are strongly dependent on the electronic state in which molecule stays as well as molecular environments. In this project, the change of potentials for large-amplitude internal rotations upon the complex formation has been studied in detail with the molecular beam technique and the laser spectroscopies.

III-I-1 Electronic Spectra of the 2,2'-Bithiophene·Ar Complex

Masao TAKAYANAGI *(Tokyo Univ. Agric. Tech. and IMS)*, **Umpei NAGASHIMA** *(Ochanomizu Univ.)* **and Ichiro HANAZAKI**

Fluorescence-excitation and holeburning spectra were measured for 2,2'-bithiophene monomer and its 1:1 complex with Ar in a supersonic jet. The frequency of the 0-0 transition was found to shift by 85 cm^{-1} upon the complex formation. The shift is larger than those for the 1:1 complexes of substituted benzene and Ar, suggesting the type of intermolecular interaction between 2,2'-bithiophene and Ar is different from that between an substituted benzene and Ar. Harmonic progressions due to the torsional motion around the single bond between two thiophene rings were observed for both of the monomer and complex. Observed torsional frequencies are different greatly for the two species: 186 cm^{-1} for the monomer and 96 cm^{-1} for the Ar complex. This suggests the great change in the structure of 2,2'-bithiopene upon the complex formation. In the previous work,[1] the torsional potentials in the ground electronic state were determined for the monomer. It was found that the equilibrium structure of the 2,2'-bithiophene monomer in a supersonic jet is non-planar with a trans configuration. In contrast, an ab initio calculation predicts that the Ar atom in the complex stays between the S atom in one of the thiophene rings and the H atom at the 4-position in the other thiophene ring, and that the S•••Ar and H•••Ar attractive force makes 2,2'-bithiophene in the complex planar in the ground electronic state.

Reference

1) M. Takayanagi, T. Gejo and I. Hanazaki, *J. Phys. Chem.* **98**, 12893 (1994).

III-J Self-Organization in Chemical Reactions

The self-organizing process in chemical systems is known to occur as a result of nonlinear chemical processes. This kind of chemical systems exhibit sustained temporal chemical oscillations and spatial pattern formation. Moreover, they sometimes exhibit more complicated nonlinear phenomena such as bistability, excitability, multi-frequency oscillations, and the chaotic behavior. They have received attention for their close relation to the activity of living systems in the spontaneously-organized dynamic behavior. Possible applications of such phenomena to the sensing- and image storage devices have also been interested in. We have paid a special attention to the response of chemical oscillator systems to photo-illumination, which is very important in view of the above-mentioned interests but have not been studied so far in any systematic manner. The topics among our results in this year include the study of dynamical response of the Belousov-Zhabotinsky (BZ) system and the minimal bromate oscillator system to a pulsed light perturbation.

III-J-1 Photo-Induced Excitability in the *Tris*-(bipyridyl)ruthenium(II)-Catalyzed Minimal Bromate Oscillator

Akiko KAMINAGA and Ichiro HANAZAKI

The *tris*-(bipyridyl)ruthenium(II)-catalyzed minimal bromate oscillator (MBO) in its reduced steady state (SSI) was found to exhibit an excitable pulse response to the pulsed light perturbation in the visible region, while the oxidized steady state didn't respond to the light pulse. Figure 1 illustrates some typical responses of MBO in SSI for a single light pulse of duration τ = 1.0 s. The system exhibits a pulse response only for light power $P > P_c$, where P_c is a certain critical value of P, and its amplitude is independent of P, suggesting that the system exhibits an excitable character. The threshold is not determined by the peak power but determined by the total pulse energy. These results are successfully accounted for by the reaction scheme in which the photo-excited metal complex produces additional $HBrO_2$ to induce the autocatalytic oxidation:

$$Ru(bpy)_3^{2+*} + Ru(bpy)_3^{2+} + BrO_3^- + 3H^+ \rightarrow 2Ru(bpy)_3^{3+} + HBrO_2 + H_2O \quad (1)$$

where $Ru(bpy)_3^{2+*}$ stands for the photo-excited catalyst. If excess $HBrO_2$ photo-produced by (1) reduces [Br$^-$] below $[Br^-]_{th}$, the autocatalytic process starts to give a sharp rise in the redox potential. The threshold in the light energy corresponds to the number of photons required to produce a sufficient amount of $HBrO_2$ to reduce [Br$^-$] below $[Br^-]_{th}$. The independence of peak height of the response on the light energy is also understandable since, once the autocatalysis starts, the system would experience a single turn along the limit cycle for the dark oscillations.

On the other hand, the system in oxidized steady state under the continuous illumination was found to be insensitive to a pulse perturbation. No evidence was found to support the photo-production of Br$^-$ in the minimal bromate oscillator.

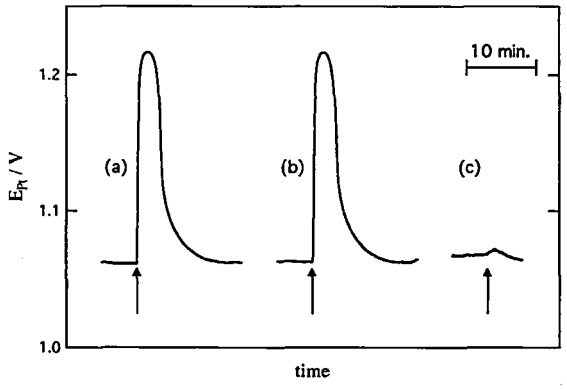

Figure 1. Time profile of the redox potential for the MBO system in SSI after a single pulse light irradiation. The arrows indicate the time of pulse illumination with duration τ = 1.0 s. P = 1.3 W (a), 0.65 W (b), and 0.33 W (c). Initial concentrations are $[Ru(bpy)_3^{2+}]_0$ = 0.10 mM, $[BrO_3^-]_0$ = 25 mM, $[Br^-]_0$ = 0.25 mM, and $[H_2SO_4]_0$ = 0.80 k_0 = 1.05 $\times 10^{-3}$ s^{-1}.

III-J-2 Pulse-Light Induced Phase Shifts of Oscillations in the Minimal Bromate Oscillator

Akiko KAMINAGA and Ichiro HANAZAKI

The phase shift due to a pulse light perturbation in chemical oscillations of the $Ru(bpy)_3^{2+}$-catalyzed minimal bromate oscillator has been examined to exhibit a phase advance. Figure 1(A) illustrates the observed response to a single light-pulse perturbation for the system in the oscillatory state (OSC). The phase and the phase shift of oscillations is defined as $\phi = 2\pi t/T$ and $\Delta\phi = 2\pi(T\text{-}T')/T$, respectively, where T, T' and t are defined in Figure 1(A-d). The observed phase shift $\Delta\phi$ is shown in Figure 1(B) as a function of ϕ. There are the "excitable" phase ($\Delta\phi > 0$; phase advanced) for $\phi/2\pi \geq 0.45$ and the "refractory" phase ($\Delta\phi \approx 0$) for $0 < \phi/2\pi < 0.4$, clearly separated by a narrow region of $\Delta\phi < 0$ (phase delayed) at $\phi/2\pi \approx 0.4$. In the excitable region, the photo-production of $HBrO_2$ triggers autocatalytic oxidation immediately to induce the second peak in advance of the expected time in the dark oscillations. On the other hand, in the refractory region, the photo-produced $HBrO_2$ is immediately consumed by Br$^-$ before the autocatalysis starts, since [Br$^-$] is still higher in this region.

Entrainment of oscillations is observed when a periodic light-pulse train is applied to the system in OSC. Entrainment occurs if the ratio of period of light-pulse

to that of the system under the dark condition falls into the excitable phase in Figure 1(B).

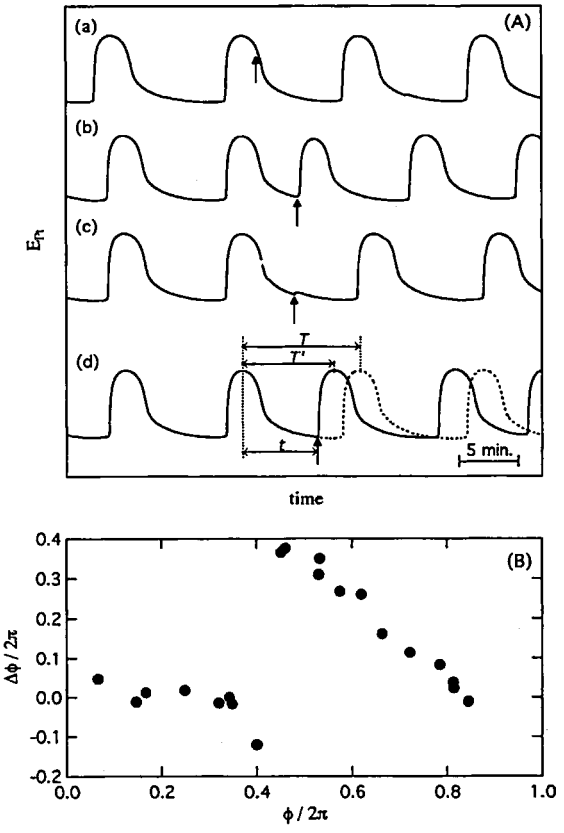

Figure 1. (A) Single light-pulse perturbation on the oscillatory MBO system. The time of application of the pulse with a duration of $\tau = 1.0$ s is indicated by an arrow. Initial concentrations are $[Ru(bpy)_3^{2+}]_0 = 0.10$ mM, $[BrO_3^-]_0 = 25$ mM, $[Br^-]_0 = 0.18$ mM and $[H_2SO_4]_0 = 0.80$ M. $k_0 = 0.92 \times 10^{-3}$ s^{-1}. (a) No response, (b) Oscillation-phase advanced, and (c) Oscillation-phase delayed. (d) Definitions of T, T' and t. (B) Phase shift $\Delta\phi$ *vs.* the phase ϕ of application of a pulse light. Experimental conditions are the same as those for (A) except for $[Br^-]_0 = 0.25$ mM and $k_0 = 0.78 \times 10^{-3}$ s^{-1}.

III–K Spectroscopy and Dynamics of Vibrationally Excited Molecules and Clusters

This research group, which started in April 1997, is planning to study spectroscopy and dynamics of molecules and clusters in higher vibrational state by two-color double resonance spectroscopy. New spectroscopic methods will also be developed to observe the higher vibrational state under collision-free condition.

III-K-1 Nonresonant Ionization Detected IR Spectroscopy for the Vibrational Study in a Supersonic Jet

Takuichiro OMI *(Grad. School Waseda Univ.)*, **Hiroshi SHITOMI** *(Grad. School Waseda Univ.)*, **Nobutake SEKIYA** *(Grad. School Waseda Univ.)*, **Ken TAKAZAWA** *(National Research Institute for Metals)* **and Masaaki FUJII**

[*Chem. Phys. Lett.* **252,** 287 (1996)]

A spectroscopic technique for the measurement of the IR transition in a supersonic jet has been developed. This spectroscopy, the nonresonant ionization detected IR spectroscopy (NID-IR), detects the IR transition by the selective ionization of the vibrationally excited molecule. Because of the ionization detection, it has high sensitivity. Furthermore, the ionization detection allows us to observe the IR spectrum of a specific molecular species by selecting mass of the corresponding cation. The advantage of the NID-IR spectroscopy has been demonstrated by the observation of the IR spectra of phenol, *o*-fluorophenol, acetylene and 7-azaindole in a supersonic jet. The assignments of cis and trans rotational isomers in *o*-fluorophenol are also discussed.

III-K-2 Overtone Spectroscopy of Phenol Studied by the Nonresonant Ionization Detected IR Spectroscopy

Shun-ichi ISHIUCHI *(Grad. School Waseda Univ. and IMS)*, **Hiroshi SHITOMI** *(Grad. School Waseda*

Univ.), **Ken TAKAZAWA** *(National Research Institute for Metals)* **and Masaaki FUJII**

Vibrational transition of jet-cooled phenol has been measured from 3400 cm^{-1} to 14000 cm^{-1} by nonresonant ionization detected IR spectroscopy. Nonresonant ionization detected IR spectroscopy is IR-UV double resonant spectroscopy which detects vibrational transition by nonresonant two-photon ionization due to UV laser. The spectrum shows well-resolved structure due to the first to the fourth quantum of OH stretching vibration, CH vibrations and various kinds of combination vibrations. It is found that the band width decreases in going from lower to higher overtones. The decrease of the band width in the higher overtone has been discussed.

III–L Large Amplitude Motion in Molecular Cation Studied by Pulsed Field Ionization Zero Kinetic Energy Photoelectron Spectroscopy

Large amplitude motion is important subject in spectroscopy, and is a fundamental model to understand non-rigid motion in biological systems and that in chemical reaction. In this project, large amplitude motion, such as internal rotation, intermolecular vibration in cation radicals will be observed by using PFI-ZEKE photoelectron spectroscopy, and its change by ionization will be discussed.

III-L-1 Internal Rotation of Methyl Group in *o*- and *m*-Toluidine Cations as Studied by Pulsed Field Ionization-Zero Kinetic Energy Spectroscopy

Hideyuki IKOMA *(Grad. School Waseda Univ.)*, **Ken TAKAZAWA** *(National Research Institute for Metals)*, **Yuji EMURA** *(Grad. School Waseda Univ.)*, **Shigeru IKEDA** *(Inst. Phys. Chem. Research)*, **Haruo ABE** *(National Research Institute for Metals)*, **Hisaharu HAYASHI** *(Inst. Phys. Chem. Research)* **and Masaaki FUJII**

[*J. Chem. Phys.* **105**, 10201 (1996)]

Internal rotational levels of the methyl group in *o*- and *m*-toluidine cations have been observed by Pulsed Field Ionization-Zero Kinetic Energy photoelectron spectroscopy. Level energies and transition intensities were reproduced by a one-dimensional rotor model with a free-rotor basis set, and the potential curves of the internal rotation in the cations have been determined. Aanalysis for *m*-toluidine shows a drastic increase of the barrier height for internal rotational motion from the neutral to the corresponding cation. On the other hand, the barrier in *o*-toluidine slightly decreases by ionization. The mechanism of the change in barrier height will be discussed in terms of geometrical and electrical change by ionization. It is suggested that the drastic change of internal rotational motion is mainly determined by the electronic structure.

III-M Laser Investigation of Molecular Photodissociation Dynamics

Detailed studies on photodissociation (half collision) dynamics provides the basis for understanding molecular photochemistry and also bimolecular reactions (full collisions). Experimental and theoretical studies must be extended beyond the well-studied triatomic systems (A+BC) in order to understand more complicated reactions encountered in upper atmosphere, interstellar space, and other environment. This project aims at, (1) the development of new experimental techniques to obtain complete information on quantum state distributions of reaction products, and (2) the elucidation of dissociation dynamics of polyatomic molecules. Lasers with high intensity, good monochromaticity, and well-defined polarization provide extremely sensitive detection methods of reaction products with the capability of examining their scalar (*e.g.* energy) and vector (*e.g.* linear and angular momenta) quantities. The extensive use of laser-based techniques is the key for the elucidation of complicated dynamics. Our major effort has been directed to the development of two and three dimensional imaging techniques to visualize the scattering of atoms and molecules and also the development of theoretical treatment of vector correlation observed by imaging. By coupling the laser and imaging techniques, differential cross section (product velocity distribution) can be measured with complete internal state selection. In our project, the imaging method has been applied to direct photodissociation that occurs faster than molecular rotation. Predissociation of acetylene has been studied by more conventional action spectroscopy, and the quantum state dependence of the reaction rate has been examined in detail.

III-M-1 Quantal and Semiclassical Analysis of Vector Correlation in Molecular Photodissociation

Yuxiang MO and Toshinori SUZUKI

[*J. Chem. Phys.* submitted]

General semiclassical expressions of state multipole and multipole moment have been obtained by using the correspondence principle and the vector model of angular momentum. The expression of low rank multipole moment, formerly obtained by comparing the classical and quantum absorption formulae of di-

atomics [D. A. Case, G. M. McClelland and D. R. Herschbach, *Mol. Phys.* **35**, 541 (1978)], has been derived more rigorously. Quantal and semiclassical expressions of multipole moments in space-fixed frame have been obtained by assuming a fixed vector correlation in velocity-fixed (*VF*) frame. The expressions were also obtained for absorption dipole moment fixed (μF) frame. The two expressions can be transformed each other, thus are equivalent. The quantal formulae are suitable for obtaining the vector correlation of small angular momentum such as electronic orbital angular momentum of atoms, while semiclassical ones are practical and satisfactory for large rotational angular momentum, such as molecular rotation of diatomics. The semiclassical formula from (μF)-frame formerly reported [R. N. Dixon, *J. Chem. Phys.* **85**, 1866 (1986)] has been reproduced, while the expression in the *VF* is provided for the first time.

III-M-2 A Test of Semiclassical Analysis of Vector Correlation in Photofragment Imaging: 355 nm Photodissociation of NO_2

Yuxiang MO, Hideki KATAYANAGI and Toshinori SUZUKI

A semiclassical theory to treat vector correlation in molecular photodissociation is tested by photofragment imaging of 355 nm photodissociation of NO_2. A new velocity mapping technique is employed to obtain high-resolution 2D ion image of NO fragments. [2+1] REMPI via C state allowed, for the first time, simultaneous measurements of recoil velocity vector and alignment of state-selected NO. Alignment of NO is treated by semiclassical multipole moments in the velocity-fixed frame, and the geometrical factors P_k were derived for two-photon transition of diatomics with intermediate coupling case between Hund's case (a) and Hund's case (b). Excellent agreement has been obtained between the experiment and theory, thus establishing the methodology. From the simulation of ion images, we obtained a new ratio of the contribution of different virtual states in two-photon transition which turned out to reproduce two-photon absorption spectrum better than the previous value.

III-M-3 Non-Adiabatic Bending Dissociation of OCS

Toshinori SUZUKI, Hideki KATAYANAGI, Yuxiang MO, Shinkoh NANBU and Mutsumi AOYAGI

[*J. Chem. Phys.* submitted]

The simultaneous measurements of speed, angular and alignment distributions of atomic fragment has been made, for the first time, in ultraviolet photodissociation of OCS by photofragment ion imaging technique. From the excitation wavelength dependence of the scattering distribution of $S(^1D_2)$ fragments, the excited states accessed by the photoabsorption were assigned to A' Renner-Teller component of $^1\Delta$ and A"($^1\Sigma^-$) states. It was found that dissociation from A' state gives rise to high and low recoil speed fragments, while A" state only to the high speed fragment. For elucidating the dissociation dynamics, two-dimensional potential energy surfaces of OCS for the C-S stretch and bending coordinates were calculated by ab initio method (MCSCF/SDCI/DZP). Avoided crossings between A'($^1\Delta$) and A"($^1\Sigma^-$) with A'($^1\Pi$) and A"($^1\Pi$), respectively, were found as adiabatic dissociation pathways. Wave packet calculations on these adiabatic surfaces for the total angular momentum J = 1, however, reproduced only the fast speed component. The discrepancy about the slow S atoms between the theory and experiment was attributed to the non-adiabatic transition from A'($^1\Delta$) to A'($^1\Sigma^+$) in the bending coordinate in the course of dissociation. Thus, wave packet calculations including non-adiabatic transition were made using diabatic surfaces and non-adiabatic coupling matrix elements obtained by *ab initio* method. Qualitative agreement between non-adiabatic wave packet calculations and the experimental result confirmed the occurrence of non-adiabatic transition in the bending coordinate. The slow recoil speed of S atom corresponding to the higher rotational excitation of CO in the non-adiabatic dissociation channel is due to more efficient conversion of bending energy into fragment rotation than the adiabatic dissociation channel. Quantitative estimation of non-adiabatic transition probability was made by the analysis of experimental data by taking into account the alignment of $S(^1D_2)$ atoms. The yield of non-adiabatic dissociation from A' state has been calculated to be as large as 35% in the dissociation at 223 nm.

III-M-4 C-Cl Bond Rupture in Ultraviolet Photodissociation of Vinyl Chloride

Kenichi TONOKURA, Lizla B. DANIELS, Toshinori SUZUKI and Koichi YAMASHITA *(Univ. Tokyo)*

[*J. Phys. Chem.* **101**, 7754 (1997)]

Cl atomic elimination in ultraviolet photodissociation of vinyl chloride at 193 and 210 nm has been studied by photofragment ion imaging. The translational energy and angular distributions of the Cl fragments were measured for the two spin-orbit states of ^2P_J (J = 1/2, 3/2). The translational energy distributions of both of the ^2P_J fragments consist of two components; one is a Gaussian-like translational energy distribution with high anisotropy, $\beta = 1.0 \pm 0.2$, while the other is a statistical distribution with low anisotropy, $\beta = 0.3 \pm 0.2$. These features were almost identical for the two photoexcitation wavelengths. The anisotropy parameter, β, of the Gaussian translational energy component is in good agreement with the value predicted for the $\pi^* \leftarrow \pi$ transition by ab initio calculations. The high translational energy component of the Cl fragment is assigned to a prompt dissociation induced by the electronic relaxation from the (π,π^*) to (π(Cl),σ^*(C-Cl)) repulsive state, while the low translational energy component is assigned to a slow dissociation induced by the relaxation to the ground state. The [Cl*]/[Cl] fine structure branching has been found to be almost

identical for the two dissociation pathways despite the large difference of the recoil velocities of the Cl atoms, suggesting an important role of the motion along the coordinate perpendicular to the C-Cl stretching in the non-adiabatic transition.

III-M-5 C-Br Bond Rupture in 193 nm Photodissociation of Vinyl Bromide

Hideki KATAYANAGI, Nobuaki YONEKURA and Toshinori SUZUKI

[*Chem. Phys.* submitted]

Photofragment ion imaging has been applied to 193 nm photodissociation of vinyl bromide. Speed and angular distributions of $Br(^2P_j)$ fragments have been measured state-selectively. The major components in these distributions were the ones with high anisotropy and high translational energy. These are assigned to dissociation by rapid electronic relaxation from the optically-excited (π,π^*) state to (n(Br) or π(Br), σ^*(C-Br)) repulsive states. From anisotropy parameters, 1.2 for Br and 1.25 for Br* channels, the direction of the transition dipole moment for $\pi^* \leftarrow \pi$ transition was calculated to be 26° from the C=C bond axis. The peak of $P(E_t)$ was found to be higher in Br* than Br channel, despite that the available energy is 10.5 kcal/mol smaller in the Br* channel, suggesting that the (π,π^*) state crosses with the repulsive state leading to the $^2P_{1/2}$ at higher energy than those leading to $^2P_{3/2}$. Low energy component with smaller anisotropy ($\beta < 0.8$) has been observed only for the Br channel, which is attributed to the dissociation via the ground state.

III-M-6 Detection of Metastable Triplet Acetylene Produced by Intersystem Crossing from the Excited $A(^1A_u)$ State

Toshinori SUZUKI, Yang SHI and Hiroshi KOHGUCHI

[*J. Chem. Phys.* **106,** 5292 (1997)]

Triplet metastable species produced by intersystem crossing from the $A(^1A_u)$ state of acetylene has been detected by the sensitized phosphorescence method. A sensitized phosphorescence signal was observed from vibronic levels lying lower than the potential energy barrier for dissociation in the a state suggested previously [N. Hashimoto and T. Suzuki, *J. Chem. Phys.* **104,** 6070 (1996)], but was not observed from levels higher than this barrier. The lifetimes of triplet states produced by intersystem crossing from the $V^3K^1(J'=2)$ and $V^4K^1(J'=2)$ levels were estimated to be 100 and 80 ms.

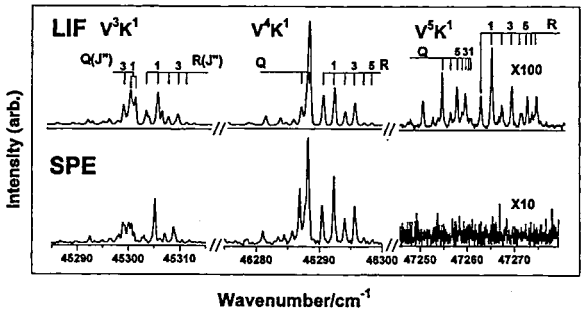

Figure 1. Laser induced fluorescence (LIF) and sensitized phosphorescence excitation (SPE) spectra simultaneously measured for C_2H_2 in supersonic jet. C_2H_2 was seeded in He, and the flight time from the laser-molecular beam to the sensitized phosphorescence detector was 40 μs.

III-M-7 Pump-Probe Measurements of the Predissociation Reaction Time of C_2H_2 from $\tilde{A}(^1A_u)$ State

Nobuhisa HASHIMOTO *(Grad. Univ. for Advanced Studies)*, **Nobuaki YONEKURA and Toshinori SUZUKI**

[*Chem. Phys. Lett.* **264,** 545 (1997)]

The predissociation reaction time from $\tilde{A}(^1A_u)$ state of acetylene has been measured by a pump-probe method. The H-atom signal was found to decay in 69 ns at V^5K^1, $J' = 2$ (E_{excess} = 1192.6 cm^{-1}) and 38 ns at V^6K^1, $J' = 2$ (E_{excess} = 2168.3 cm^{-1}) levels. These values are considered to be the upper bounds for the lifetime of a metastable doorway state for dissociation at these energies.

III-M-8 Dissociation of Metastable CH_3CO Radical Observed by Subpicosecond Time-Clocked Imaging

Takeshi SHIBATA *(Grad. Univ. for Advanced Studies)*, **Haiyang LI, Hideki KATAYANAGI and Toshinori SUZUKI**

[*J. Phys. Chem.* submitted]

An experimental technique to measure energy-dependent dissociation rate k(E) of radical species is presented. Internally-excited CH_3CO radicals were formed by 253 nm photodissociation of CH_3COCl and detected by multiphoton ionization at 760 nm with a variable pump-probe time delay. By resolving the translational energy of CH_3CO^+ ions by 2D ion imaging, the decays of energy-selected radicals were measured for each internal energy. The dissociation rates of CH_3CO radicals determined were an order of magnitude smaller than those calculated by Rice-Ramsperger-Kassel-Marcus theory, thus indicating non-statistical behavior.

III-M-9 2D Imaging of Dissociative Ionization of Molecules in Intense Laser Fields

Haiyang LI, Takeshi SHIBATA *(Grad. Univ. for Advanced Studies)* **and Toshinori SUZUKI**

The behavior of molecules in intense electromagnetic fields is a subject of wide interest and active research with the advent of powerful picosecond and femtosecond lasers. In an intense laser field, the bonding electrons in molecules could be removed, the Coulomb repulsion in a resultant multiply-charged molecular ions undergo rapid dissociation. So far, time-of-flight mass analysis in conjunction with covariance mapping has been employed to study the dynamics of these multielectron dissociative ionization process, this study aims at a new approach by measuring angular-velocity correlation of the fragments by two-dimensional imaging method. In preliminary experiments on OCS performed with the laser pulse, 150 fs, 760 nm, and 10^{15} W/cm^2, it was observed that the multiply-charged ions S^{3+}, S^{4+} are ejected along the polarization of the laser with high degree of angular anisotropy. 2D ion imaging of these fragment is in progress to obtain the dynamics of alignment and dissociation in the intense laser field.

III-N One Atom Cage Effect and a Search for Dynamical Resonance

The modification of dissociation dynamics caused by the presence of a rare gas atom in a binary complex (often referred to as the one atom cage effect) has attracted the attention of both experimentalists and theorists for many years. This problem is of interest because it may ultimately yield insights concerning the role of solvent effects in condensed phase chemistry. Theoretical analyses conclude that the rare gas atom-hydrogen halide (Rg-HX) complexes provide good model systems for exploration of the cage effect. Through photolysis of the HX bond, the signatures of trapped H-atom trajectories should be evident in the H atom scattering distributions and the absorption spectra.

III-N-1 Detection of Ar-HI by (2+1) REMPI

Toshinori SUZUKI, Hideki KATAYANAGI and Michael C. HEAVEN

[*J. Phys. Chem.* **36**, 6697 (1997)]

ArHI was detected by spectroscopic means for the first time. Analysis of the $g^3\Sigma^-(0^+)$-$X^1\Sigma^+(0^+)$ band system yielded estimates for the van der Waals bond lengths in the g and X states. The molecular constants obtained for the g state are T_{e0} = 65698.7(5), D_0 = 393(12), D_e = 417(12), ω_e = 49.0(2) and $\omega_e x_e$ = 1.44(3) cm^{-1}. The implication s of the results for studies of the one-atom cage effect in RgHX complexes are considered.

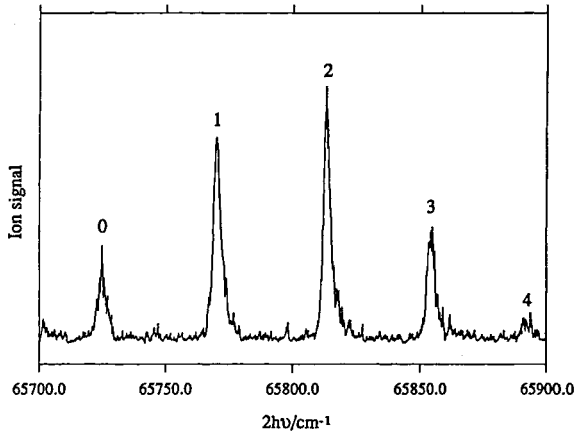

Figure 1. (2+1) REMPI spectrum of the ArHI g-X transition. This trace was obtained by integrating the ion signal for both $ArHI^+$ and ArI^+.

III-O Laser Investigation of Bimolecular Reaction Dynamics

In order to understand chemical reactions, detailed knowledge of the dynamics of atomic and molecular collisions is needed. Crossed molecular beams provide a powerful and versatile approach for the study of reactive and inelastic encounters. However, with the conventional detection technique using electron impact ionization, differential cross sections were hardly measured with rotational resolution. This project aims at the measurement of fully state-resolved differential cross sections for reactive scattering processes via two-dimensional ion imaging. The reaction of $O(^1D_2)$ atoms will be investigated because of their importance in atmospheric chemistry.

III-O-1 Testing Crossed Beam Imaging Apparatus by Observing Inelastic Scattering of NO with Ar at E_{coll} = 70 meV

Hiroshi KOHGUCHI, Christian GEBAUER and Toshinori SUZUKI

We have constructed a crossed molecular beam machine with a 2D ion imaging detector. Each of the two beam sources are pumped by two diffusion pumps (2 × 2000 l/s) backed by roots blowers (250 and 500 m^3/h), while the main chamber is pumped by tandem turbo molecular pumps (1500 l/s and 500 l/s). Two pulsed supersonic beams generated by piezoelectric valves are crossed at the right angle at about 50 mm downstream from the nozzle, and the scattered products are interrogated by a probe laser by resonance-enhanced multiphoton ionization. The subsequent ions are accelerated by an electric field in the direction perpendicular to relative velocity vector and projected

onto a gated two-dimensional position sensitive ion detector. The angular and speed distribution of state-selected products are thus observed.

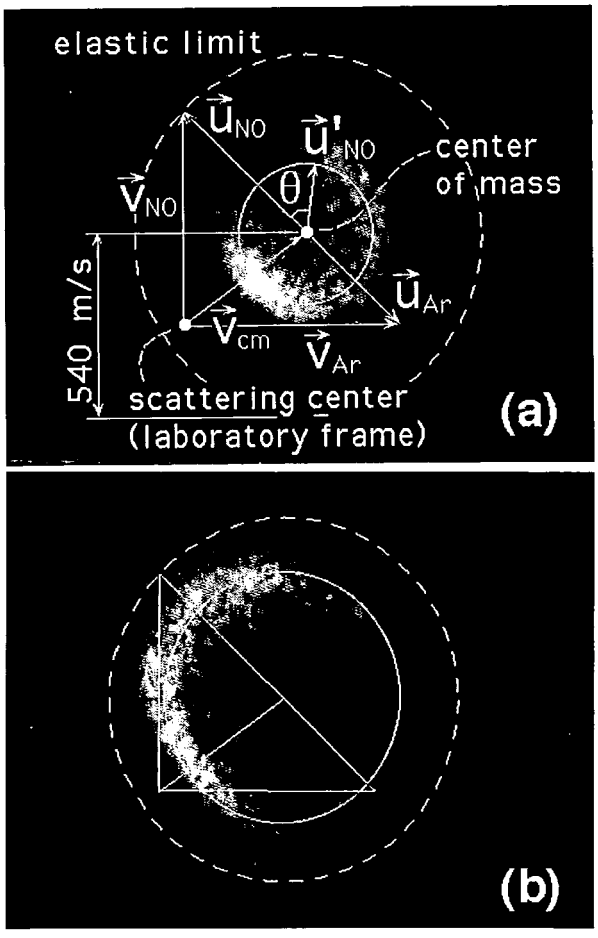

Figure 1. Two-dimensional images of NO scattered by Ar, (a) Ω'= 3/2, v'=0, J'=12, and (b) Ω'= 3/2, v'=0, J'=5. A Newton circle for elastic scattering limit is overlayed. The vectors v are the velocity in the laboratory frame, while the vectors u are the ones in the center-of-mass frame. It is celaly seen that the collisions leading to higher rotational states show smaller Newton circles. Larger J' states appear as more backward scattering (larger θ), while smaller J' states as forward scattering (smaller θ). The images were integrated for 15000 laser shots (10 minutes) each.

III-P Jet Spectroscopy of Free Radicals

Vibrationally resolved LIF spectra of *p*-cyanobenzyl and benzophenone ketyl radicals are measured in a supersonic free jet. Molecular constants are obtained and vibronic coupling is discussed.

III-P-1 Jet Spectroscopy of the $D_1\ ^2B_1$ - $D_0 1^2B_1$ Transition of the *p*-Cyanobenzyl Radical

Masaru FUKUSHIMA *(Hiroshima City Univ.)*, **Kazuhito SAITO** *(Idemitsu Kosan Co. Ltd.)* **and Kinichi OBI** *(Tokyo Inst. Tech. and IMS)*

[*J. Mol Spectrosc.* **180**, 389 (1996)]

We have generated the *p*-cyanobenzyl radical in supersonic free expansion, and measured the vibronically and rotationally resolved laser induced fluorescence excitation and dispersed spectra from single vibronic levels in green-blue region. The lowest energy band at 20738 cm^{-1} with the strongest intensity in the excitation spectrum has been assigned to the 0_0^0 band of the visible spectrum from the vibronic structures in the dispersed spectra. Based on the band type of the 0_0^0 band, a-type, determined from the rotationally resolved excitation spectrum, we have definitely assigned the visible band to the $D_1\ ^2B_1$ - $D_0\ ^1D_1$ transition. The vibronic structure of the $D_2\ ^2B_1$ - $D_0\ ^1D_1$ transition of the benzyl type is characterized by totally symmetric fundamental modes, 1, 8a and 9a.

III-P-2 Laser Induced Fluorescence Spectroscopy of Jet Cooled Benzophenone Ketyl Radical

Shin-ichi WADA *(Tokyo Inst. Tech.)*, **Yoshihisa MATSUSHITA** *(Tokyo Inst. Tech.)* **and Kinichi OBI** *(Tokyo Inst. Tech. and IMS)*

[*J. Phys. Chem. A* **101**, 2423 (1997)]

The $D_1 \leftarrow D_0$ transition of jet-cooled benzophenone ketyl radical (BPK) and its deuteride was studied by using laser induced fluorescence (LIF) spectroscopy. BPK was generated by the 248 nm photolysis of α-phenylbenzoin and its vibrationally resolved LIF excitation and emission spectra were obtained for the first time. The 18 451 cm^{-1} band was assigned to the 0_0^0 band of the $D_1 \leftarrow D_0$ transition of BPK. Two vibrational modes of BPK with 65 and 84 cm^{-1} in the first excited state were assigned to the in-phase and out-of-phase torsional motions of the phenyl rings, respectively. The vibrational mode with 980 cm^{-1} was tentatively assigned to the C-O stretching mode. The mode of 74 cm^{-1} in the ground state was assigned to the in-phase torsional mode. It was confirmed that the torsional motions do not couple with the C-O stretching and O-H rotational motions. The force field analysis and the simple Franck-Condon calculation were made. The measured fluorescence lifetimes of BPK and its deuteride are short and consistent with those in the gas and liquid phases at room temperature.

III-Q Photochemistry in Molecular Clusters

Photochemical reaction in the neutral molecular clusters of benzophenone with hydrogen donors formed in a supersonic free jet expansion has been studied.

III-Q-1 Photochemical Reaction in the Neutral Molecular Clusters of Benzophenone with Hydrogen Donors Formed in a Supersonic Free Jet Expansion

Yoshihisa MATSUSHITA *(Tokyo Inst. Tech.)*, **Shogo NOGUCHI** *(Tokyo Inst. Tech.)*, **Naotaka OHIWA** *(Tokyo Inst. Tech.)* **and Kinichi OBI** *(Tokyo Inst. Tech. and IMS)*

[*J. Photochem. and Photobio. A: Chem.* **102**, 93 (1996)]

Photochemical reaction in the neutral molecular clusters of benzophenone with hydrogen donors formed in a supersonic free jet expansion has been studied. It has been found that intracluster hydrogen abstraction reaction takes place to form benzophenone ketyl radical in the benzophenone-1,4-cyclohecadiene mixed cluster. On the contrary, no ketyl radical has been detected when ethanol, 2-propanol, or several kinds of amine are used as a hydrogen donor. Excitation and emission spectra of the benzophenone-*N,N*-dimethylaniline cluster have suggested that benzophenone and *N,N*-dimethylaniline form a ground state charge transfer complex. The excitation of the benzophenone-tri-n-butylamine cluster promotes the transformation to the van der Waals complex to an exciplex. The reactivity of the clusters on hydrogen abstraction and charge transfer reactions has been discussed on the basis of the nature of hydrogen donors.

III-R Photochemical Processes Studied by Time-Resolved ESR

Photochemical processes generate abnormal electron spin polarization on excited molecules and free radicals, which is called as chemically induced dynamic electron polarization (CIDEP). We have studied photochemical reactions by probing CIDEP. We succeeded in detection of singlet oxygen molecules by monitoring spin polarization generated on free radicals in the singlet oxygen-free radical systems.

III-R-1 The First Observation of CIDEP Generated through the Interaction between an Excited Singlet Oxygen Molecule and a Free Radical

Masaaki MITSUI *(Kyoto Univ.)*, **Keizo TAKEDA** *(IBM)*, **Yasuhiro KOBORI** *(Tohoku Univ.)*, **Akio KAWAI** *(Tokyo Inst. Tech.)* **and Kinichi OBI** *(Tokyo Inst. Tech. and IMS)*

[*Chem. Phys. Lett.* **262**, 125 (1996)]

CIDEP generated through the interaction between the lowest excited singlet oxygen molecule and 2,2,6,6-tetramethylpiperidinyl-1-oxyl (TEMPO) radical was observed by time-resolved ESR technique. Excited singlet oxygen molecules were produced by the triplet sensitized reaction. Absorptive electron spin polarization was generated on the free radical in the excited singlet oxygen molecule-free radical system, in which the CIDEP generation was interpreted by the radical-triplet pair mechanism with doublet precursor (DP-RTPM). The CIDEP time profile was successfully analyzed by using the Bloch equations. Quenching of singlet oxygen with β-carotene provides further evidence for DP-RTPM in the $^1O_2$-TEMPO system.

III-S Magnetic Behavior of Stable Radical Crystals with Delocalized Spin Structures and Electronic Excited States of Stable Radicals and Their Molecular Crystals

In order to find out novel molecule-based magnets, we have investigated the magnetic properties of a series of thioaminyl radical crystals. The thioaminyls have a delocalized unpaired electron in the molecule which leads to relatively large intermolecular exchange interaction compared with the nitroxide or nitronyl nitroxide radicals. The magnetic properties and the electronic structures of the thioaminyls with pyridine derivatives are also examined as a candidate of the spin coupler in the hybrid systems consisting of transition metal ions and stable organic radicals. In addition, to study the novel spin alignment control in the organic open-shell spin systems using the excited molecular field, we investigate the optical properties and the spin states of a series of stable free radicals and their radical crystals.

III-S-1 Magnetic Properties of Stable N-[(Dichlorophenyl)thio]-2,4,6-tri-phenylphenyl-aminyl and N-[(Dichlorophenyl)thio]-2,4,6-tris(chloro-phenyl)phenylaminyl Radical Crystals

Yoshio TEKI *(IMS and Osaka City Univ.)*, **Koichi ITOH** *(Osaka City Univ.)*, **Atsuhiko OKADA** *(Osaka Univ.)*, **Hirokazu YAMAKAGE** *(Osaka Univ.)*, **Tatsuo KOBAYASHI** *(Osaka Univ.)*, **Kiichi AMAYA** *(Osaka Univ.)*, **Sinya KUROKAWA** *(Osaka City Univ.)*, **Sadaharu UENO** *(Osaka City Univ.)* **and Yozo MIURA** *(Osaka City Univ.)*

[*Chem. Phys. Lett.* **270,** 573 (1997)]

The magnetic properties of N-[(dichlorophenyl)thio]-2,4,6-triarylphenyl-aminyl radical crystals are reported. The tree stable thioaminyls show ferromagnetic behaviors described using the on-dimentional Heisenberg model with the large ferromagnetic interaction of $2J/k_B$ = 28.0, 11.4 and 3.6 K. The other two radicals show the antiferromagnetic alternating chain behaviors with $2J/k_B$ = -16.8 K, α = 0.55 and $2J/k_B$ = -128.8 K, a = 0.90. The low-temperature susceptibility and heat capacity measure-ments of the crystal showing $2J/k_B$ = 28.0 reveals a magnetic phase transition at 0.4 K. The ordered phase shows spin-flop transition which reveals an antiferromagnetic long range order.

III-S-2 Magnetic Properties of Stable Pyridyl-Thioaminyl Radical Crystals

Yoshio TEKI *(IMS and Osaka City Univ.)*, **Kenjiro ANDO** *(Osaka City Univ.)*, **Koichi ITOH** *(Osaka City Univ.)*, **Sinya KUROKAWA** *(Osaka City Univ.)* **and Yozo MIURA** *(Osaka City Univ.)*

Novel pyridyl thioaminyls have synthesized and isolated as a candidate of a novel spin coupler in the hybrid systems consisting of transition metal ions and stable organic radicals. N-[(2,4-dichlorophenyl)thio]-4-phenyl-2,6-(3-pyridyl)phenylaminyl radical crystal (Figure 1) shows ferromagnetic behaviors described using the on-dimensional Heisenberg model with the large ferromagnetic interaction of $2J/k_B$ = 22.4 K. The other two radicals show the low-dimensional antiferromagnetic behaviors. The ESR and ENDOR experiments and the ab-initio MO calculations based on a DFT method have been also carried out in order to study their electronic structures. The construction of the organic-inorganic hybrid-type systems consisting of transition metal ions and stable pyridyl thioaminyl radicals are now challenged.

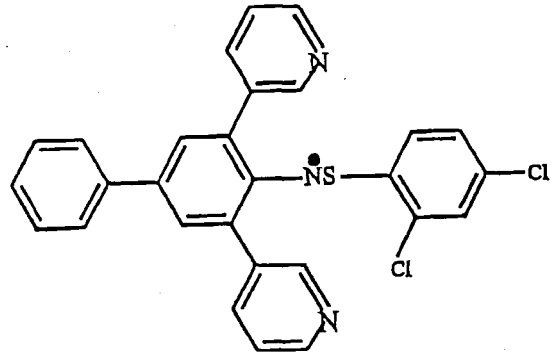

Figure 1. N-[(2,4-dichlorophenyl)thio]-4-phenyl-2,6-(3-pyridyl)phenylaminyl radical.

III-S-3 Electronic Excited States of Stable Radicals and Their Molecular Crystals

Yoshio TEKI *(IMS and Osaka City Univ.)*

In order to examine the spin alignment control in the organic open-shell spin systems and organic magnetic materials using the excited molecular field, we investigate the optical properties and the spin states of a series of stable free radicals and their radical crystals. The absorption, emission spectra have been measured for a series of stable radicals as a candidate of such photo-induced organic magnetic materials. Their spin states and the spin alignments are now investigated by the ODMR (Optically Detected Magnetic Resonance) spectroscopy.

III-T Conformation, Photoisomerization and Solvent Effect of Merocyanine Dyes

There has been increasing interest in the use of merocyanine dyes for photoelectric and photochemical devices. Although there have been a great deal of reports on the application of merocyanine dyes for devices, many questions still remain unanswered. For example, little has been known about the rotational isomerism of possible conformers in relation to the conjugated system. Although some merocyanine dyes show great solvent effects in their electronic absorption spectra, the effects have not been clearly interpreted in terms of the intermolecular interaction and the structural change of dye molecules induced by solvent. In this study, resonance Raman and infrared absorption spectra of merocyanine dyes are measured in various solvents and in the low-temperature Ar matrices to clarify the conformation and the mechanism of photoisomerization and solvent effect.

III-T-1 Conformational Analysis and Photoisomerization of Merocyanine Dyes Studied by Visible Absorption, Resonance Raman and IR Spectroscopies

Masao TAKAYANAGI *(Tokyo Univ. Agric. and Tech. and IMS)*, **Munetaka NAKATA** *(Tokyo Univ. Agric. and Tech.)*, **Yukihiro OZAKI** *(Kwansei-Gakuin Univ.)*, **Keiji IRIYAMA** *(The Jikei Univ. School of Medicine)* **and Mitsuo TASUMI** *(Univ. Tokyo)*

[*J. Mol. Struct.* **405**, 239 (1997)]

The photoisomerization of the merocyanine dyes, 5-[2-(3-ethyl-2-benzothiazolylidene)-1-methyl-ethylidene]-3-ethyl-2-thioxo-4-thiazolidinone [Et(Me)MD] and 5-[2-(3-ethyl-2-benzothiazolylidene)ethylidene]-3-ethyl-2-thioxo-4-thiazolidinone [EtMD], in solution was studied by visible absorption, resonance Raman and IR spectroscopies. It was found that the most stable conformers for Et(Me)MD and EtMD of the four possible isomers A-D were different. For Et(Me)MD, isomer A, which was stable in cyclohexane and carbon tetrachloride, was photoisomerized to isomer C by 514.5 nm laser irradiation. Isomer C returned to isomer A slowly in the dark or rapidly on 488.0 nm laser irradiation. In contrast, Isomer C for EtMD, which was stable in the solvents, was photoisomerized to Isomer A by 488.0 nm or 457.9 nm laser irradiation. Isomer A returned to Isomer C slowly in the dark or rapidly on 514.5 nm laser irradiation in cyclohexane. Possible photoisomerization mechanisms are discussed based on the rotational motions around the two C=C double bonds of the central conjugated system.

III-T-2 Intermolecular Interaction of Merocyanine Dyes Studied by Visible Absorption, Resonance Raman and Infrared Spectroscopies

Masao TAKAYANAGI *(Tokyo Univ. Agric. and Tech. and IMS)*, **Munetaka NAKATA** *(Tokyo Univ. Agric. and Tech.)*, **Yukihiro OZAKI** *(Kwansei-Gakuin Univ.)*, **Keiji IRIYAMA** *(The Jikei Univ. School of Medicine)* **and Mitsuo TASUMI** *(Univ. Tokyo)*

[*J. Mol. Struct.* **407**, 85 (1997)]

Intermolecular interactions of merocyanine dyes, 5-[2-(3-ethyl-2-benzothiazolylidene)-1-methyl-ethylidene]-3-ethyl-2-thioxo-4-thiazolidinone [Et(Me)MD] and 5-[2-(3-ethyl-2-benzothiazolylidene)ethylidene]-3-ethyl-2-thioxo-4-thiazolidinone [EtMD], in various solvents were studied. The spectra of the dyes in an argon matrix-isolated state and in a thin-film state were also measured. In addition to the well-known solvent effects appearing in visible absorption spectra, the solvent dependence of resonance Raman and infrared absorption spectra was examined. The visible absorption bands shift to the longer wavelength region as the polarity of the solvent increases, while the C=O and C=C stretching bands shift to the lower frequency region. Correlation between the visible absorption maximum and C=C stretching vibrational frequency was found, for the first time. The solvent effects on the spectra are explained in term of intermolecular interactions between merocyanine dyes and solvent molecules.

RESEARCH ACTIVITIES IV
Department of Molecular Assemblies

IV-A Solid State Properties of Phthalocyanine Salts and Related Compounds

Some phthalocyanine molecules contain unpaired d-electrons in the conjugated π-electron system. Due to this special nature, the itinerant π-electrons and localized unpaired d-electrons coexist in solid phthalocyanine salts, in which a one-dimensional double-chain system (metal and ligand chain) is formed. Furthermore these chains make up wide (π-band) and narrow (d-band) one-dimensional bands, the energy of the narrow band being close to the Fermi energy of the wide band. The phthalocyanine conductor is thus a two-chain and two-band system. These band structure and exchange interaction of itinerant π-electrons with localized magnetic moments are new aspects in the field of organic metals. For the basic understanding of these materials and to search for a new phenomenon, where a magnetic interaction takes an important role, we prepare and characterize solid phthalocyanine salts and related compounds.

IV-A-1 High-Pressure Study of One-Dimensional Phthalocyanine Conductor, $NiPc(AsF_6)_{0.5}$

Yukako YONEHARA* and Kyuya YAKUSHI
*(*Grad. Univ. Adv. Studies)*

[*Synthetic Metals*, in press]

$NiPc(AsF_6)_{0.5}$ is a two-band system, in which a narrow 3-d band is located just below the Fermi level of the wide p-band. This compound undergoes a metal-insulator transition at ca. 50 K. The nonmetallic state below 50 K is regarded as the localized state caused by a small amount of randomly distributed 3d-holes (Ni^{3+}). High-pressure diffraction experiment shows that a hydrostatic pressure produces an effective uniaxial stress around the Ni^{2+} ions. This uniaxial stress along the chain axis (*z*-axis) lifts up the $3d_{z^2}$-band and causes the gradual charge transfer from 3d- to π-band, which provides 3d holes and thus enhances the randomness of Ni^{3+} distribution. The electrical resistivity, and thermopower show that high pressure expands this nonmetallic phase to the high-temperature region in the *P-T* phase diagram. This extension is consistent with the enhancement of the randomness of Ni^{3+} distribution.

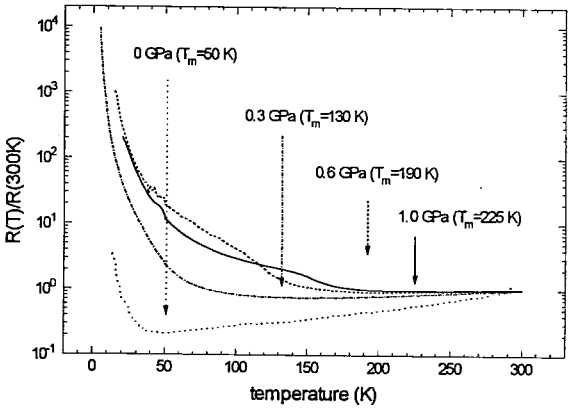

Figure 1. Pressure dependence of the normalized electrical resistance. T_m denotes the resistivity minimum temperature, which increases upon applying pressure.

IV-A-2 New Conducting Composite Material Based on a Platinum Phthalocyanine (PtPc) Charge Transfer Salt and Poly-bisphenol-A-carbonate (PBC). Electrochemical, Optical, Magnetic, and Structural Properties

Iakov L. KOGAN and Kyuya YAKUSHI

[*J. Mat. Chem.* in press]

Electrochemical doping of PF_6^- anion into the solid platinum phthalocyanine (PtPc) has been attempted using poly-bisphenol-A-carbonate (PBC) as a binder of PtPc particles. This $PtPc(PF_6)_x$-PBC composite material has a specific conductivity of 0.5 - 1 Scm^{-1}, the positive value of thermopower 10 μV/K at 300 K, and the ESR signal with Pauli-paramagnetism like behavior in the temperature range 100 - 300 K. These metal-like properties suggest the formation of the charge-transfer salt $PtPc(PF_6)_x$. The ESR principal g-values $g_{//}$=2.0165 and $g_{\perp}$=1.989 and lattice parameters a=b=14.11(2), c=6.491(8) Å which were obtained from the least-squares calculation of the powder X-ray diffraction are very close to those of the charge-transfer salt $PtPc(ClO_4)_{0.5}$ the single crystal of which was prepared by an electrochemical crystallization and characterized before. These data unambiguously show that PF_6^- anions are electrochemical doped into solid PtPc. Three electrochemical oxidation reduction peaks and in situ optical absorption spectra at different potentials have been registered.

The goal of this research is to develop the method to control the band-filling factor of molecular conductors using the electrochemical method. In contrast to the inorganic materials, the control of the band-filling factor is very difficult, since it is usually not possible to control the stoichiometry of organic charge-transfer salts. In this solid electrochemistry, we found the way to dope and dedope the counter anions such as PF_6 by changing the electrochemical potential. Detailed studies on the potential dependence of the stoichiometry, structural change, ESR property, spectroscopic change are in progress.

IV-A-3 Electrochemical and Spectroelectrochemical Properties of a New Stable Composite Film Electrode. Platinum Phthalocyanine — Poly-bisphenol-A-carbonate

Iakov L. KOGAN and Kyuya YAKUSHI

[*Electrochim. Acta* in press]

A new composite electrode PtPc—Poly-bisphenol-A-carbonate of reticulate structure is characterized by two anodic and four cathodic red-ox transitions in propylene carbonate electrolytes. Investigation of the anodic part of CV at slow scan rate 0.02 mV/s displays very narrow peaks 25—50 mV at half height with a large constant potential difference (*pd*) ~0.4—0.5 V between anodic and relevant cathodic maxima. The oxidation at relatively high scan rates results in a new peak, which is interpreted as the dispersion of PtPc in the polymer matrix. The incorporation of carbon into the composite significantly improves the performance of electrode, but does not influence on *pd*. Electrochemical oxidation in tetrabuthylammonium-PF_6 at 0.5 V leads to the transformation from the monoclinic to tetragonal crystal lattice, the growth of electronic conductivity to ~0.1—1 $S \cdot cm^{-1}$, positive thermopower ~10 μV/K, a new absorption band at 553 nm and uniaxial ESR signal at helium temperatures.

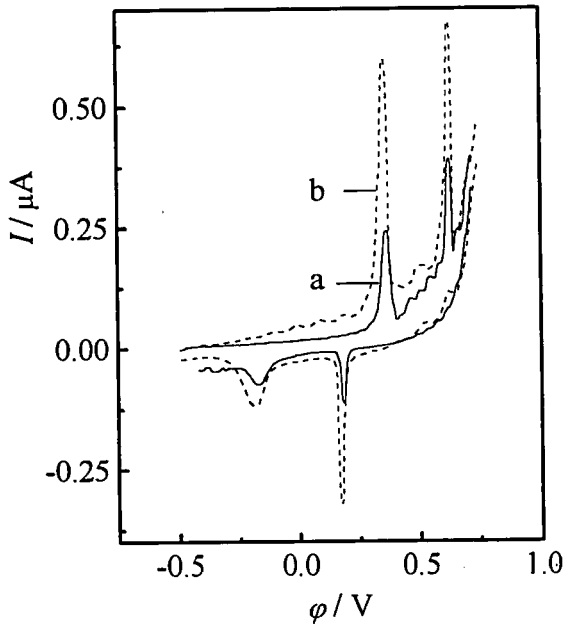

Figure 1. Cyclic voltammogram of the solid PtPc-PBC-Carbon composite in 0.1 M tetrabuthylammonium PF_6 propylene carbonate solution at the scan rate of a) 0.02 and b) 0.05 mV/s. The narrow wave can be obtained with a very slow scan rate and suggests the phase change at the specific electrochemical potential.

IV-A-4 Magnetic Susceptibility of Oriented Single Crystals of $CoPc(AsF_6)_{0.5}$

Mkhital SIMONYAN and Kyuya YAKUSHI

The charge-transfer salts $CoPc(AsF_6)_{0.5}$ is the two-band system, which constitutes of a wide quarter-filled π-band and narrow half-filled d-band. The d-electron in the narrow band is expected to have a magnetic moment and to couple with the itinerant π-electron. Phenomenologically $CoPc(AsF_6)_{0.5}$ shows different physical properties from the non-magnetic $NiPc(AsF_6)_{0.5}$. To understand the role of the magnetic moment at Co site, the magnetic susceptibility of the oriented single crystals of $CoPc(AsF_6)_{0.5}$ was measured with the magnetic field parallel and perpendicular to the conducting axis. The susceptibility is much more suppressed than that of CoPc which conforms the Curie law, but significantly larger than $NiPc(AsF_6)_{0.5}$ which conforms the Pauli paramagnetism. A large anisotropy was observed in the magnetic susceptibility of the oriented crystals. The susceptibilities with H//c and H⊥c constitute of the Curie component and the T-linear component. The observed anisotropy ($\chi_\perp > \chi_{//}$) turns to be reverse ($\chi_\perp < \chi_{//}$) after the correction of the large anisotropic diamagnetic susceptibility coming from the ring current of the large p-conjugated system and the large spin-orbit coupling of cobalt ion. The Curie component was assigned to $(CoPc)_2^+$ doublet. From the comparison with an XY model and the analysis of the spin structure of $(CoPc)_2^+$ doublet, the linearly increasing component seems to be interpreted based on the $(CoPc)_2^+$ quartet.

IV-B Structure and Properties of Organic Conductors

The study of organic metals rapidly developed when the dimensionality of an intermolecular charge-transfer interaction is expanded. This expansion of dimensionality has been brought about by the discovery of new molecules such as BEDT-TTF or C60. In this project we treat one-, two-, and three-dimensional organic metals and superconductors to know what is most important for stabilizing a metallic state and for designing new superconducting materials. The most basic physical parameters are the transfer integrals which represent the dimensionality and itinerancy of the electron, and the on-site Coulomb energy and coupling constants with molecular vibration which represent the localized character of the electron. We systematically determine these parameters by polarized reflection spectroscopy assembling a microscope, multi-channel detection system, FT-IR, and liquid helium cryostat.

Another ongoing program is to look for negative-*U* organic charge-transfer compounds, the strategy of which is described in the special research project of this issue. In this research program, the most important parameter is the charge or valence of the molecule in a mixed valent state. The examination of the electronic and vibrational transitions at low temperature or high pressure is most effective to characterize the valence.

IV-B-1 Peierls Transition of DMTSA-BF_4 Having a Half-Filled Quasi-One-Dimensional Band

Jian DONG, Kyuya YAKUSHI, Kazuo TAKIMIYA* and Tetsuo OTSUBO* *(Hiroshima Univ.)*

A quasi-one-dimensional charge-transfer salt with a half-filled band usually becomes a Mott insulator. In contrast to this general property, DMTSA-BF_4 having a half-filled band shows a metallic conductivity down to *ca.* 180 K and undergoes metal-insulator transition. The enhancement of the vibornic modes below 100 K in the //c polarized reflection spectrum provides evidence of the Peierls transition for this metal-insulator transition. Comparing with the vibronic structure of dimerized DMTSA-ClO_4, the Peierls energy gap was estimated to be less than 90 meV which is consistent with the activation energy (30 meV) of the electrical resistivity below 150 K. From the analysis of the vibronic modes based on the dimer model, the coupling with molecular vibration turns out to be much weaker than TCNQ-, TTF-, and ET-based molecular conductors. It is surprising that the screened electron-electron correlation is so weak in half-filled pseudo-one-dimensional organic compound. This is attributed to the large transfer integral ($t_{//}$=0.33 eV) and weak coupling with molecular vibration. In the isostructural compound DMTTA-BF_4, the electron-electron correlation effect is more remarkable than DMTSA-BF_4, which is related to the small transfer integral ($t_{//}$=0.16 eV).

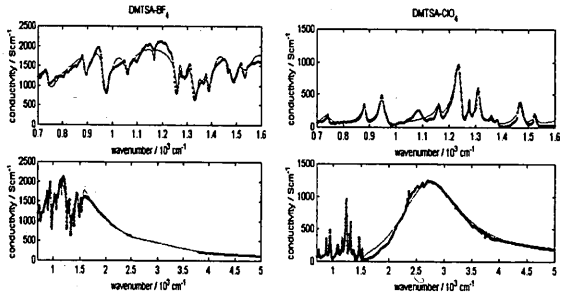

Figure 1. Conductivity spectra of DMTSA-BF_4 at 10 K and DMTSA-ClO_4 at 297 K which are observed by the electric field of the light parallel to the pseudo-one-dimensional chain. The dots are the experimental data and solid line is the best-fit curve based on the dimer vibronic model.

IV-B-2 Electronic Structure of κ-ET_2X salts, Where "ET" is Bis(ethylenedithio) tetra-thiafulvalene (BEDT-TTF) Molecule

Valery A. IVANOV, Kyuya YAKUSHI and Elena UGOLKOVA* *(*N.S. Kurnakov Inst. of General and Inorg. Chem. of RAS)*

[*Physica C* **275,** 26 (1977)]

The electronic structure of κ-ET_2X salt is studied on the basis of the tight-binding approach for correlated electrons. The uncorrelated energy band constitutes of 4 branches. The analytical formula of the partial and total density of states are derived. The upper two branches which is partially filled is split into two by the introduction of the electron-electron correlation. These correlated energy dispersion and energy gap was calculated to be

$$\Delta_s = \frac{1}{2}\left[\sqrt{9+(\frac{2\varepsilon}{t})^2}+\sqrt{(\frac{3}{2})^2+(\frac{2\varepsilon}{t})^2}-\frac{9}{2}\right]t$$

where $\varepsilon=U/2$ is the half of the on-site Coulomb energy ant t is the interdimer transfer integral. Variations of ET donor arrangements at a fixed hole concentration lead to a variation of an energy scale and to a variety of properties. When the correlated bands widen, the insulator-metal transition occurs due to an electron scattering on spin and charge fluctuations. For this triangular lattice, this phase transition occurs at the following critical point

$$\left(\frac{t}{\varepsilon}\right)_{crit} = \frac{4\pi}{\sqrt[4]{3}\sqrt{15\pi^2+64}} = 0.66$$

IV-B-3 Charge-Transfer Salts of $M(mnt)_2$ (M=Ni, Pd, Pt, Au) with BDNT: Ferromagnetic Interaction in Conductive $(BDNT)_2$-$[Ni(mnt)_2]$

Mikio URUICHI, Kyuya YAKUSHI, Yoshiro YAMASHITA and Jingui QIN

[*J. Mater. Chem.* in press]

Charge-transfer salts between BDNT and $M(mnt)_2$ (M=Ni, Pd, Pt, and Au) were prepared by mixing $BDNT(SbCl_6)_2$ and $TBA_2[M(mnt)_2]$ and by electrochemical oxidation of BDNT in the $TBA[M(mnt)_2]$ solution. Almost all powdery samples of (1:1) salts show a high electrical conductivity. The valence of $M(mnt)_2$ was determined to be 1- by the CN stretching mode, which means that the valence of BDNT is 0.5+, 1+, or 2+. Their crystal structures are not known except low-conductive BDNT-$[Au(mnt)_2]_2$, in which $Au(mnt)_2$ makes a dimer and the dimer is stacked in a crisscross way. Among these compounds, $(BDNT)_2$-$[Ni(mnt)_2]$ exhibits a ferromagnetic interaction with J=3.4 K. It is concluded from the ESR experiment that $[Ni(mnt)_2]^{1-}$ is responsible to the ferromagnetic interaction. The unpaired electrons on BDNT are not interacting with Ni(mnt)2 and the quarter-filled BDNT band is responsible to the high conductivity.

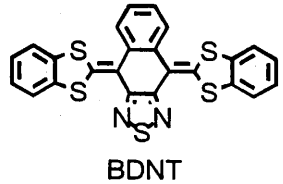

BDNT

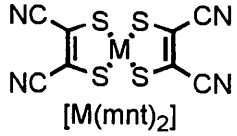

$[M(mnt)_2]$

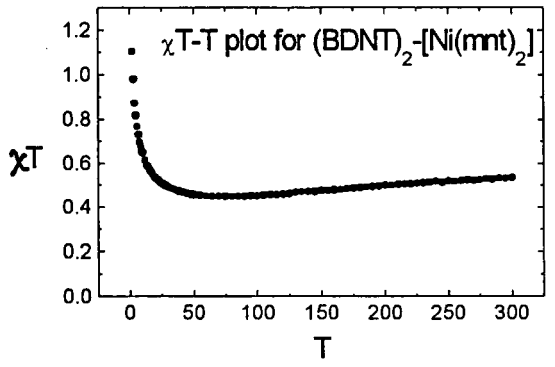

Figure 1. χT curve of $(BDNT)_2$-$[Ni(mnt)_2]$. The rise-up below 50 K indicates the ferromagnetic interaction in this compound.

IV-C Development of a Spiro-Conjugated Donor System: a New Type Donor able to form Charge-Transfer Salts with a 2-D or 3-D Electronic Conduction Band

The study of organic conductors has been rapidly developed after the finding of TTF-TCNQ, and is still progressing mainly on TMTSF, BEDT-TTF, DCNQI, and $M(dmit)_2$ systems. The basic concepts for how to design organic donor or acceptor to get metallic compound were presented already in early periods of this field, all of which concepts request a plane-conjugated molecular structure. The seek for new material is considered to be continued within this old framework as yet. We here mention the possibility of non-planner donor having a spiro-conjugated molecular structure, to yield charge-transfer salts with a multi-dimensional conduction band under less dependence of donor packing motif. The model molecule having a D_{2d} symmetry, its highest occupied molecular orbitals (HOMOs) are degenerated, and hence, we expect ferromagnetic interaction as well as metallic behavior in its radical salt.

IV-C-1 New Spiro Donor Molecules: Bis(tetrathiafulvalenyldithio)-Methane and -Germane

Kazumasa UEDA, Masaru YAMANOHA, Toyonari SUGIMOTO *(Osaka Pref. Univ.)*, **Hideo FUJITA** *(Kyoto Univ.)*, **Akito UGAWA, Kyuya YAKUSHI and Kenji KANO** *(Kyoto Univ.)*

[*Chem. Lett.* 461 (1997)]

As a new tetrathiafulvalene (TTF)-based donor molecule were synthesized spirocarbon and germanium compounds substituted with two tetrathiafulvalenyldithiolate groups. The redox processes were composed of two pairs of broad and reversible waves, each of which involves two electron transfer. The radical cations or bis(radical cation)'s generated by one- or two-electron oxidation were characterized by ESR.

IV-D NMR Study of Organic Conductors

The nuclear magnetic resonance (NMR) is a powerful method to examine electronic state of condensed matters. With this microscopic method, one can get further insight into nature of the metallic, superconducting and magnetic natures of materials. In this research project, we aim at getting a comprehensive understanding of a variety of electronic phases in several organic materials by the NMR experiments.

IV-D-1 ^{13}C NMR Study of Nesting Instability in α-$(BEDT\text{-}TTF)_2RbHg(SCN)_4$

Kazuya MIYAGAWA, Atsushi KAWAMOTO *(Ochanomizu Univ.)* **and Kazushi KANODA**

[*Phys. Rev. B* **56** (1997) in press]

The low-temperature nesting instability in the quasi-two-dimensional organic conductor, α-$(BEDT\text{-}TTF)_2RbHg(SCN)_4$, has been investigated by ^{13}C NMR. Below 12 K, drastic decreases in the Knight shift and $1/(T_1T)^{-1}$ were observed with neither splitting nor broadening in the NMR spectra, as shown in Figures. 1 and 2. The $1/(T_1T)^{-1}$ shows no enhancement around the nesting instability, unlike the conventional spin-density-wave (SDW) transition. The present ^{13}C NMR data are suggestive of nonmagnetic transition but allow only an unusual case of mobile state in the SDW scenario.

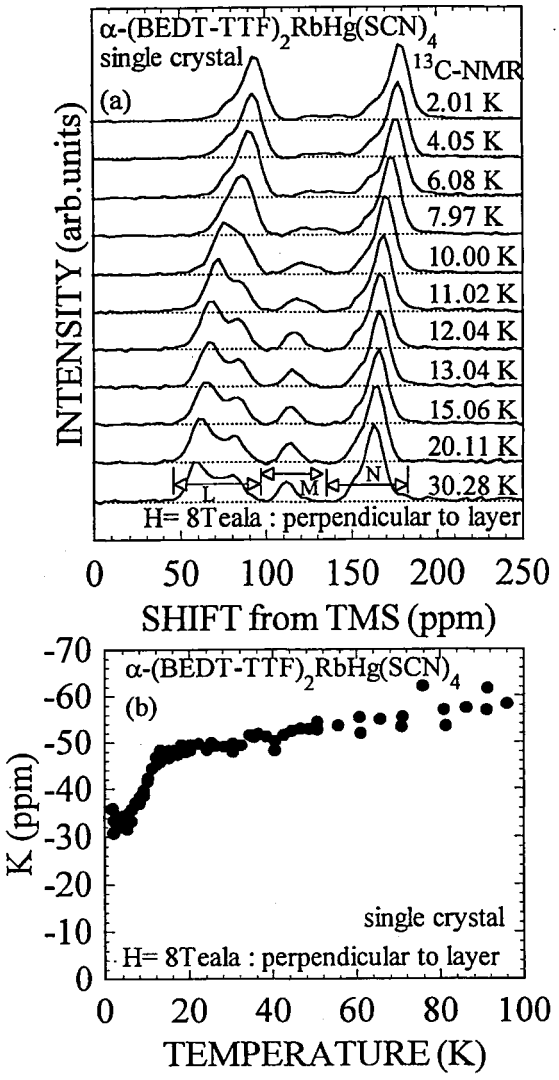

Figure 1. (a) ^{13}C NMR spectra and (b) averaged Knight shift of a single crystal under a perpendicular field of 8 T.

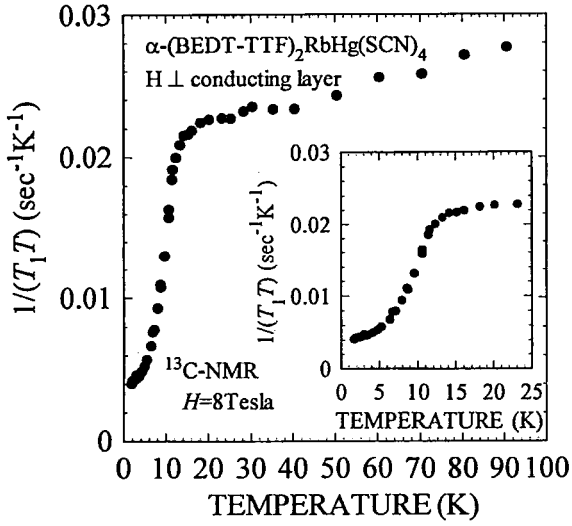

Figure 2. ^{13}C nuclear spin-lattice relaxation rate. The low-temperature region is expanded in the inset.

IV-D-2 Deuterated κ-(BEDT-TTF)$_2$Cu[N(CN)$_2$]Br: a System on the Border of the Superconductor/ Magnetic-Insulator Transition

Atsushi KAWAMOTO *(Ochanomizu Univ.)* **Kazuya MIYAGAWA and Kazushi KANODA**

[*Phys. Rev. B* **55,** 14140 (1997)]

The electronic state of the deuterated salt of the organic system, κ-(BEDT-TTF)$_2$Cu[N(CN)$_2$]Br, has been investigated by dc/ac susceptibility and $^1H/^{13}C$ NMR measurements. We found that the system is situated in the critical region of the transition between a superconducting phase with T_C of ~ 11.5 K and an antiferromagnetic phase with T_N of 14 ~ 15 K. It was also found that the rapid cooling through 80 K drives the superconducting phase into the magnetic phase, as is shown in Figure 1. That is considered to come from introduction of some lattice disorder to the system near the Mott transition.

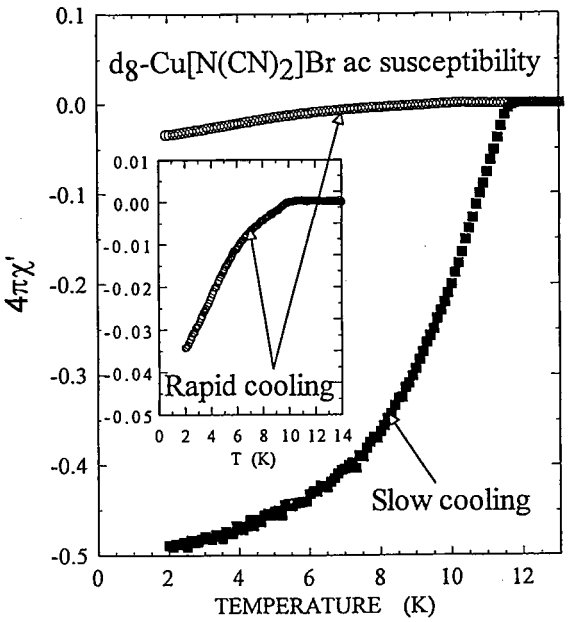

Figure 1. ac susceptibility of deuterated κ-(BEDT-TTF)$_2$Cu[N(CN)$_2$]Br crystal after slow or rapid cooling. The ac field is applied perpendicular to the layer. The results after rapid cooling are expanded in the inset.

IV-D-3 ^{13}C NMR Study on Deuterated κ-(BEDT-TTF)$_2$Cu[N(CN)$_2$]Br

Kazuya MIYAGAWA, Atsushi KAWAMOTO *(Ochanomizu Univ.)* **and Kazushi KANODA**

[*Phys. Rev. Lett.* submitted]

A family of κ-(BEDT-TTF)$_2$X show superconducting and insulating ground states, depending on the anion, X. The salts with X=Cu(NCS)$_2$ and Cu[N(CN)$_2$]Br are superconductors with T_c ~ 10 K and 12 K, respectively, while the isostructural X=Cu[N(CN)$_2$]Cl salt is an insulator, which undergoes an antiferromagnetic transition at T_N ~27 K. The ^{13}C and ^1H NMR studies on these salts revealed that the X=Cu[N(CN)$_2$]Cl salt is a Mott insulator and that the electron-electron correlation plays an important role in appearance of different ground states and lead us to propose a conceptual phase

diagram, which is divided into the superconducting and insulating phases by a line characterizing the Mott transition.

The deuterated X=Cu[N(CN)$_2$]Br (d8-Br) salt was found to be situated just on this border by our previous study of polycrystals. In order to investigate the electronic states of this salt in more detail, ^{13}C NMR measurements using a single crystal have been performed. The external field was applied to parallel to the a-axis, which is in the conducting plane.

While the spectrum seems to consist of one component at room temperature, they start to split into two components around 30 K, which become well separated at lower temperatures, showing that two phases, the metallic and insulating phases, exist in separate regions in the crystal. We have measured the spectra and the spin-lattice relaxation time, T_1, of each phase below 30 K.

In the insulating phase, the divergence of $1/(T_1T)$ and the onset of broadening of the spectra around 16 K indicates a magnetic ordering. The spectrum shifts only to the higher frequency side by 0.9 MHz at 6 K. This behavior can be explained by a simply commensurate antiferromagnetic configuration of the spin localized on the dimer with a moment of ~0.3μ_B/dimer. Associated with the spectral separation at 30 K, the line with smaller shift, which comes from the metallic phase, has a sudden decrease in $1/(T_1T)$ around 30K, suggesting a suppression of magnetic fluctuations. It is noted that $1/(T_1T)$ starts to decrease again below 20 K, which is higher than T_c determined by ac susceptibility measurement. This behavior is reminiscent of the spin-gap discussed in high-T_c cuprats and spin-ladder systems.

IV-D-4 Electron Correlation, Metal-Insulator Transition and Superconductivity in Quasi-2D Organic Systems, (ET)$_2$X

Kazushi KANODA

[*Physica C* (1997) in press]

A family of quasi-two-dimensional organic systems, (ET)$_2$X, have been studied by NMR, susceptibility and specific heat measurements in the light of role of electron correlation. A systematic variation of antiferromagnetic spin fluctuations toward metal-(superconductor)-to-insulator transition and the ordered spin structure in the insulating phase are uncovered. Based on the results, we propose a conceptual phase diagram for (ET)$_2$X as shown in Figure 1, where the κ-type of family span a critical region of Mott transition. The superconductivity, which is enhanced near the Mott transition, is suggested to have line nodes in gap parameter by NMR relaxation and specific heat profiles.

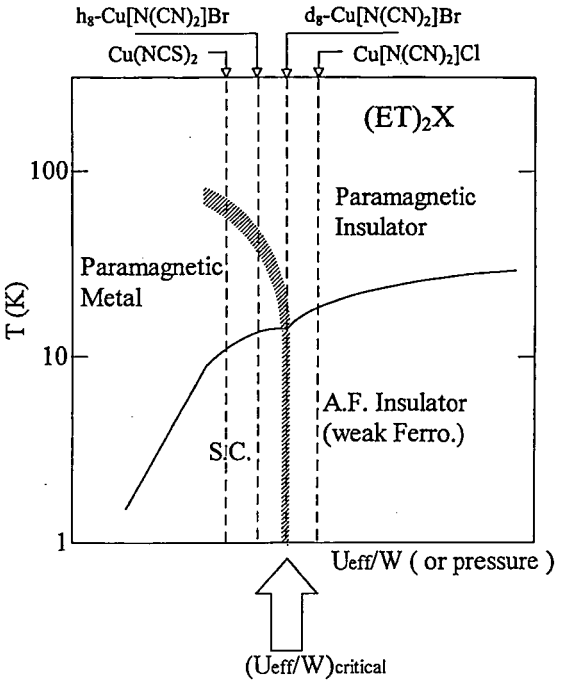

Figure 1. Conceptual phase diagram of (BEDT-TTF)$_2$X.

IV-D-5 ^{13}C and ^{1}H NMR Study of Vortex Dynamics in a Layered Organic Superconductor at Selective Nuclear Sites

Kazushi KANODA, Kazuya MIYAGAWA and Atsushi KAWAMOTO *(Ochanomizu Univ.)*

[*Physica C* (1997) in press]

The dynamics of the vortices in the quasi-two-dimensional superconductor, κ-(BEDT-TTF)$_2$Cu(NCS)$_2$, under a perpendicular field was investigated by NMR relaxation rate measurements at the three different nuclear sites; namely the central carbon, ethylene carbon and ethylene proton sites. The two carbon sites were enriched by ^{13}C isotope separetely for ^{13}C NMR. The vortex dynamics contribution to the relaxation rate was separated from the quasiparticle contribution and found to show a peak formation around 2 K with a site-dependent peak height, as shown in Figure 1. The analysis supports that the peak behavior does not come from the simple crossover but from some qualitative change in the vortex dynamics.

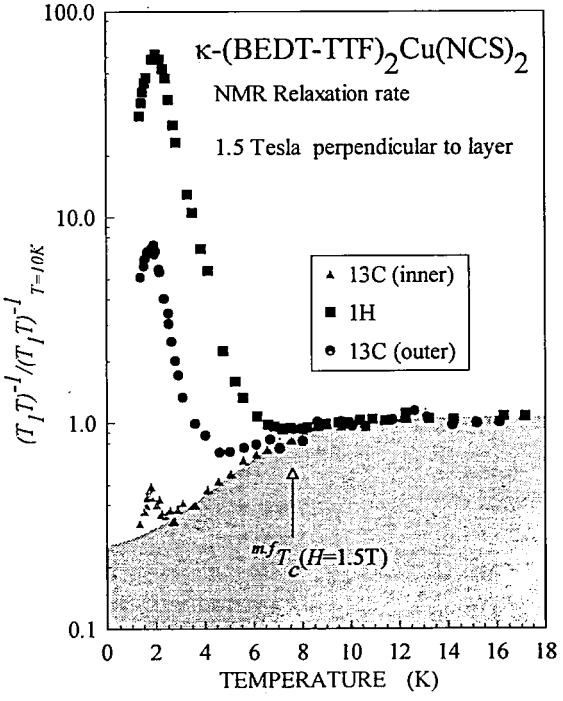

Figure 1. $(T_1T)^{-1}$ normalized to the values at 10 K.

IV-E Electron Transport and Magnetic Study of Anisotropic Superconductors

There are increasing interests in anisotropic transport and magnetic properties of layered superconductors, because their low-dimensional fluctuations around the transition temperature and dynamic properties of vortex motion are center of unsolved problems in physics of superconductors. In addition to this, such layered superconductors have some possibilities to be used as electronic devices. BEDT-TTF based organic charge transfer salts are typical examples for inquiry of such problems and possibilities, because of their structural peculiarity that the conducting donor layers are separated by thick anion layers. In some BEDT-TTF salts extremely two-dimensional characters than that of Bi-based high-T_c oxide have so far been reported.

IV-E-1 Phase Diagram of Vortices in the Quasi-Two-Dimensional Organic Superconductor, α-(BEDT-TTF)$_2$NH$_4$Hg(SCN)$_4$; a System of Pancake Vortices with Out-of-Plane Coupling Dominated by the Electromagnetic Energy

Hiromi TANIGUCHI, Yasuhiro NAKAZAWA and Kazushi KANODA

[*Phys. Rev. B* in press]

The Anisotropy and field-temperature (*H-T*) phase diagram of the quasi-two-dimensional superconductor, α-(BEDT-TTF)$_2$NH$_4$Hg(SCN)$_4$, were investigated through the specific heat, ac complex susceptibility, $\chi=\chi'-i\chi''$ and resistivity measurements under zero and dc fields normal to the conducting plane. The anisotropy ratio of resistivity and penetration depth has given an anisotropy parameter, γ, of as large as ~10^3. In the vortex state, the onset of the in-plane and out-of-plane ac susceptibility is found to form a characteristic line well below the H_{c2} line determined by the specific heat measurements, as shown in Figure 1. The absence of the frequency dependence in the out-of-plane susceptibility suggests that this is a melting line of vortices, rather than a crossover of vortex dynamics. The behavior of out-of-plane resistivity, of which the onset is shown in Figure 1, implies that the interlayer coherence between pancake vortices is established well above the melting line. Considering the anisotropy parameter obtained in the present study, the pancake vortices in this superconductor is viewed as an assembly coupled mainly through the electromagnetic energy in the out-of-plane direction. According to this feature, the two characteristic lines in the *H-T* diagram were qualitatively explained by the recent melting and decoupling theories taking account of the electromagnetic coupling. The solid curves in Fig. 1 are the results of fitting based on these theories.

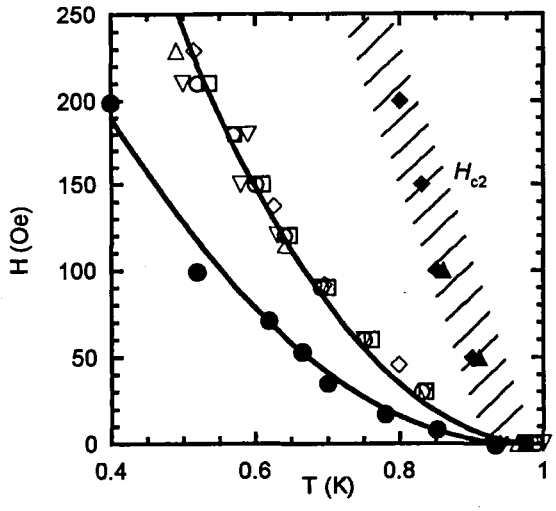

Figure. 1. *H-T* phase diagram of α-(BEDT-TTF)$_2$NH$_4$Hg-(SCN)$_4$. The onset temperatures of the inductive transition (closed circles) and the offset ones of the out-of-plane resistive transition (open symbols) are plotted along with the mean-field H_{c2} line in *H-T* plane and are fitted to the functional forms in the melting theory and the out-of-plane decoupling theory.

IV-F Thermodynamic Study of Organic Conductors

In order to get reliable information on absolute values of electron density of states and on the entropy distribution around the phase transition, specific heat studies are inevitable. In this project, we constructed several calorimeters available at low-temperature region and also in magnetic fields and performed a systematic investigation on organic materials from a thermodynamic viewpoint.

IV-F-1 Reply to the "Comment on 'Electronic Structure of Insulating Salts of the κ-(BEDT-TTF)$_2$X Family Studied by Low-Temperature Specific Heat Measurements'"

Yasuhiro NAKAZAWA and Kazushi KANODA

[*Phys. Rev. B* **56**, 951 (1997)]

The ac and dc susceptibility data of the identical sample of κ-(BEDT-TTF)$_2$Cu[N(CN)$_2$]Cl that we have used for the previous low-temperature specific heat experiment [Phys. Rev. B **53**, R8875 (1996)] is presented. As we have shown in Figures 1, 2, we observe neither appreciable depression of the magnetic transition temperature nor appearance of superconductive phase due to the grease effect in our experimental configuration, which excludes the interpretation that the absence of the γ term in our specific heat data in zero magnetic field is due to the pressure induced superconductivity.

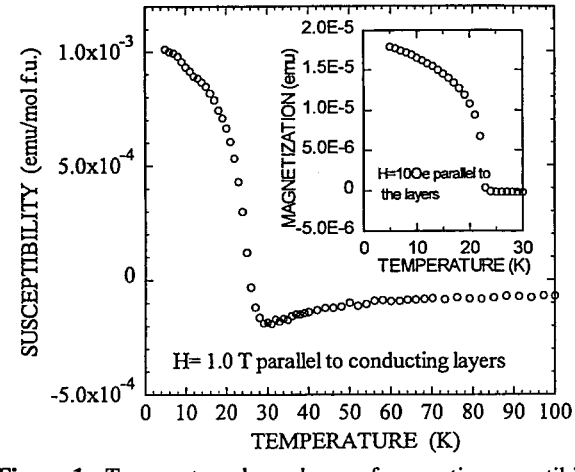

Figure 1. Temperature dependence of magnetic susceptibility of κ-(BEDT-TTF)$_2$Cu[N(CN)$_2$]Cl obtained in the external field of 1T. The inset shows M vs T curve around the weak ferromagnetic transition in a field of 10Oe.

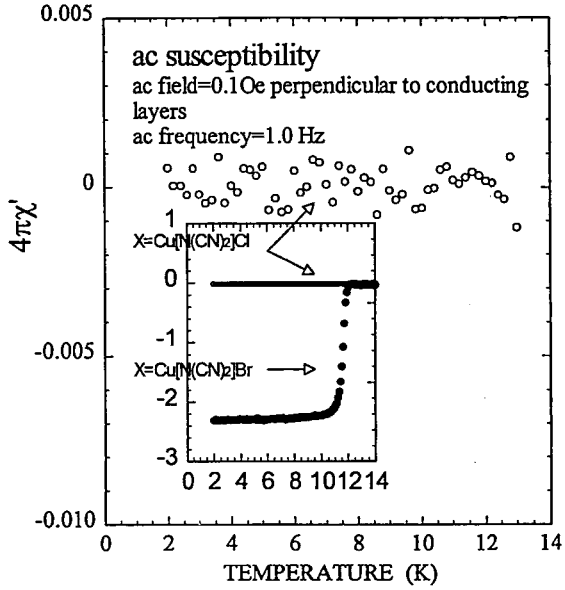

Figure 2. Temperature dependence of ac susceptibility of κ-(BEDT-TTF)$_2$Cu[N(CN)$_2$]Cl.

IV-F-2 Low-Temperature Specific Heat of κ-(BEDT-TTF)$_2$Cu[N(CN)$_2$]Br in the Superconducting State

Yasuhiro NAKAZAWA and Kazushi KANODA

[*Phys. Rev. B* **55**, R8670 (1997)]

The low-temperature specific heat of single crystals of κ-(BEDT-TTF)$_2$Cu[N(CN)$_2$]Br was studied in a

temperature range between 0.11K and 4.5K and in magnetic fields up to 2T. The electronic specific heat C_{el}, in the superconducting state shows a quadratic temperature dependence. As is shown in Figure 1, the magnetic-field dependence of the temperature-linear term (γ) obeys $\gamma=k\gamma_n(H/H_{c2})^{1/2}$ relation, where H_{c2}=10T, γ_n=22mJ/molK^2, and k=0.80. These results support the existence of line-nodes in the superconducting gap and therefore suggests that the symmetry of electron pairs in this material is unconventional with anisotropic wave function. The existence of line nodes is most reasonably attributable to the two-dimensional $d_{x^2-y^2}$ wave model or anisotropic d+s wave model recently discussed for high-T_c cuperates.

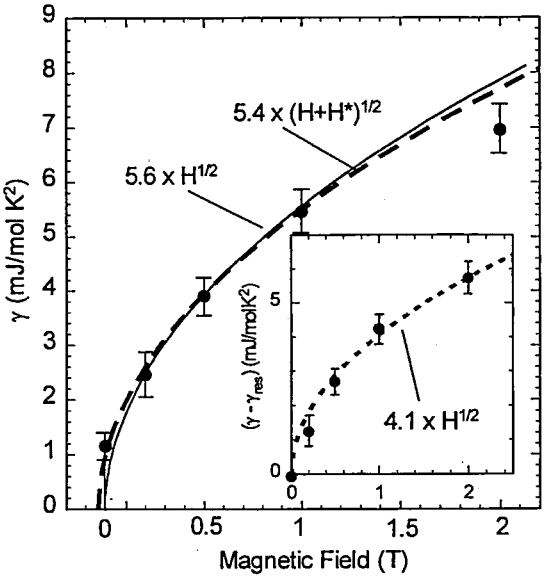

Figure 1. Field dependence of the γ term in the electronic specific heat.

IV-F-3 Thermodynamic Property of Organic Superconductor κ-(BEDT-TTF)$_2$X

Yasuhiro NAKAZAWA and Kazushi KANODA

[*Physica C* (1997) in press]

The low-temperature specific heat data of superconductive phase and insulating phase in the κ-(BEDT-TTF)$_2$X system are compared. We show in Figure 1, C_p/T vs T^2 plot for X=Cu(NCS)$_2$ sample in fields of H=0Oe, 200Oe and 300Oe applied perpendicular to the conducting layer. By fitting the data of H=0Oe to the form mentioned above, we get the values of α=3.53mJ/molK^3, β=12.5mJ/molK^4, γ=2.84mJ/molK^2. Although we do not know why this salt gives a slightly larger γ value than X=Cu[N(CN)$_2$]Br salt, it is appreciable from the figure that the quadratic term is gradually diminished and replaced by γ term with increasing external magnetic fields . The fitting of the data gives α=1.21mJ/molK^3, β=13.6mJ/molK^4, γ=5.19 mJ/molK^2 for H=200Oe and α=0.77mJ/molK^2, β=13.9mJ/molK^4, γ=6.68mJ/molK^2 for H=300Oe. The abrupt increase of γ values in such low-magnetic fields, in spite of a relatively higher H_{c2} value of about 6T in this material, is also consistent with the picture of unconventional pairing.

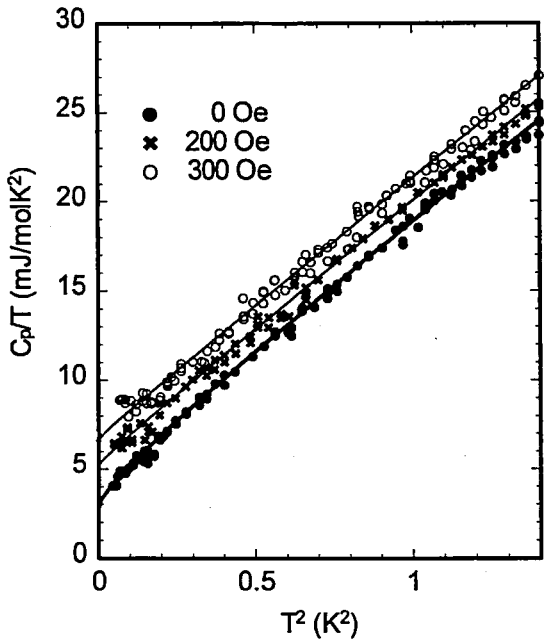

Figure 1. Magnetic fields dependence of C_p/T vs T^2 curve for X=Cu(NCS)$_2$ salt.

IV-G Novel Electronic States of d-π System of (DCNQI)$_2$M

The hybrid electronic systems composed of itinerant and nearly localized electrons are new frontiers of materials. The DCNQI-metal complexes are one promising family of materials along this line. The members of this family can be nearly pure π electron systems or π-d interacting electronic systems, depending on the metal ions. In this research project, we aim at developing a new member of DCNQI-metal complexes with novel electronic properties and getting a comprehensive understanding of a rich variation of the electronic phases in this family.

IV-G-1 Wigner-Crystal Type of Charge Ordering in an Organic Conductor with a Quarter-Filled Band; (DI-DCNQI)$_2$Ag

Ko-ichi HIRAKI and Kazushi KANODA

[*Phys. Rev. Lett.* submitted]

^{13}C-NMR measurements have been performed to investigate the nature of the insulating state of a quasi-one-dimensional conductor, (DI-DCNQI)$_2$Ag, with a quarter-filled band. At higher temperatures above 220

K, ^{13}C-NMR spectra are single lines because all of ^{13}C sites are crystallographically equivalent. Below 220 K, however, the spectra get split into two lines with different shift and width. Since the shift is proportional to the local electron density of LUMO at ^{13}C site, the line separation in the paramagnetic state indicates the disproportionality of the electron density. This result is an evidence of $4k_F$ charge density wave with two-fold charge-density modulation along the c-axis. It is emphasized that the $4k_F$ CDW in this system is the charge modulation type rather than the lattice modulation type, which is widely observed in many organic systems with quarter filled bands.

The 1D π band of this system is much narrower than those of other Ag salts of DCNQI such as (DMe-DCNQI)$_2$Ag according to the band structure calculation. So, it is reasonable to consider that the screening between the electrons is weak and the long range Coulomb interaction, V, plays a crucial role in the charge ordering. The present case is essentially viewed as the Wiger-Crystalization of electrons in the charge transfer salt.

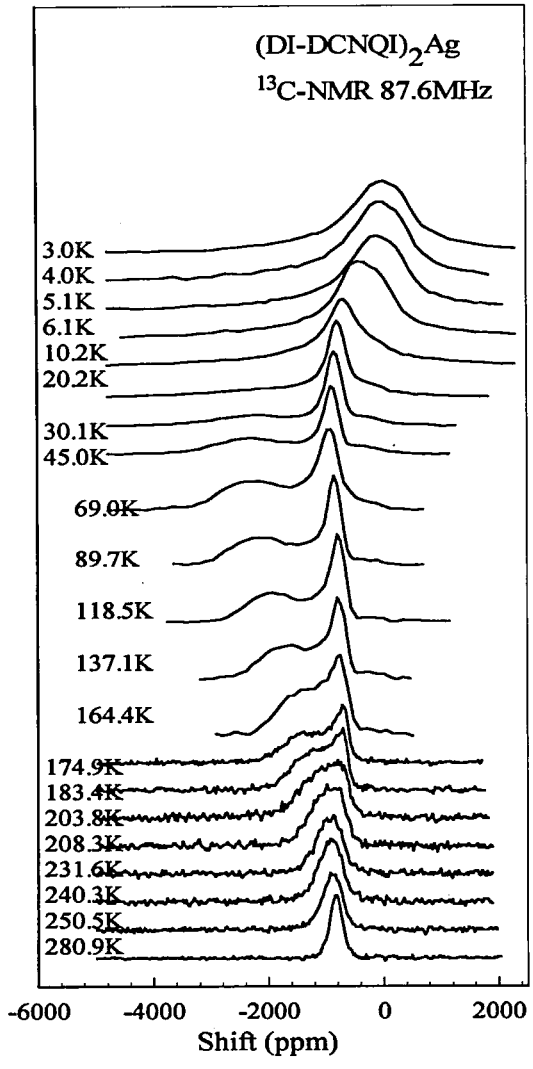

Figure 1. ^{13}C-NMR spectra of the cyano carbon in the DI-DCNQI molecule of (DI-DCNQI)$_2$Ag at various temperatures.

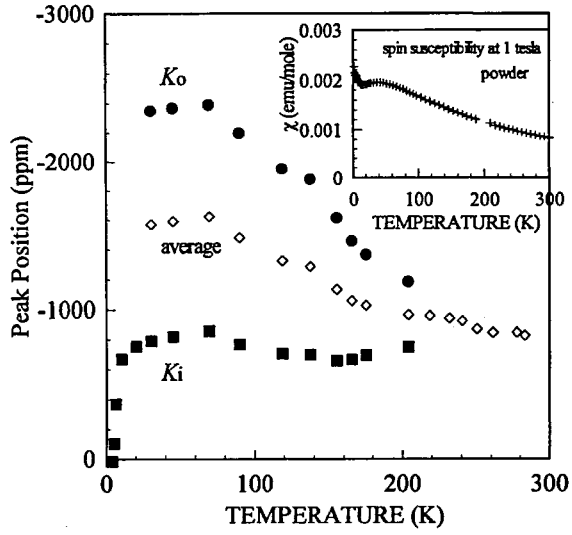

Figure 2. Temperature dependence of the peak positions of the inner and outer lines, K_i and K_o, and the averaged one, $(K_i+K_o)/2$. The susceptibility, χ, with correction of core diamagnetism is shown in the inset.

IV-G-2 ^{13}C-NMR Study of Metal-Insulator Transition in (DMe-DCNQI)$_2$Cu with Partial Deuteration

Atsushi KAWAMOTO *(Ochanomizu Univ.)* **Kazuya MIYAGAWA and Kazushi KANODA**

[*Phys. Rev. B.* submitted]

The electronic states of a series of (DMe-DCNQI)$_2$Cu systems with non-deuterated and partially deuterated methyl groups in DMe-DCNQI molecule have been investigated by ^{13}C NMR measurements at the cyano carbon sites. The Knight shift of the non-deuterated specimen, which is metallic in the whole temperature range, is not scaled to the total spin susceptibility, demonstrating that the metallic state consists of several electronic bands with different local spin susceptibility due to the π-d hybridization. In the insulating phases of the partially deuterated specimens, the ^{13}C NMR spectra are splitted into two lines, one of which has nearly zero shift and the other has large positive shift with a Curie-Weiss temperature dependence. The former line comes from the cyano group coordinated to the nonmagnetic Cu^+ ion, while the latter comes from that coordinated to the magnetic Cu^{2+} ion. The sign of the shift and intensity analysis provide an evidence that there is no spin fraction in DCNQI molecules in the insulating phases. The low-temperature re-entrant metallic state is found to be just the same as that in the non-deuterated system through the shift and relaxation rate behaviors. No fluctuations are observed in the vicinity of the metal-insulator and insulator-metal re-entrant transitions. This shows that the transitions are of the first order.

IV-H Electric and Magnetic Properties of a Series of λ-Type BETS Conductors and Related Organic Conducting Systems

Since the discoveries of new types of two-dimensional BEDT-TTF superconductors β- and κ-BEDT-TTF$_2$I$_3$ and the first molecular superconductors based on transition metal complex molecules in 1984-1987 (Russia, Japan and France), more than ten years have passed. In the last decade, Japanese chemists have contributed greatly to develop new molecular superconductors. One of the recent main topics is a paramagnetic organic superconductor discovered in 1995 (UK). Although the number of organic superconductors is increasing year by year, κ-BEDT-TTF$_2$Cu[N(CN)$_2$]Cl still keeps the highest T_c record since 1990 (USA). Undoubtedly, the structure-chemical concept of design of two-dimensional stable metal band by using multi-chalcogen π molecules, which was promoted by us in 1980s, was a backbone of the studies in developing new conducting systems. Although this concept was useful to search for new molecular metals, it cannot tell anything about the superconducting transition and of course about T_c. There seems to be no reliable idea to develop new organic superconductor with elevated T_c at present. Probably the magnitude of T_c is less important in the studies of physics of organic superconductors. And the recent interest seems to be concentrated on the establishment of the general comprehension on the low-temperature phase diagram of the organic superconductors from the viewpoint of the highly correlated low-dimensional metal systems.

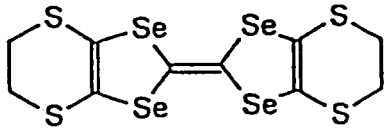

BETS(=bis(ethylenedithio)tetraselenafulvalene)

IV-H-1 Low-Temperature Phase Diagram of λ-Type Organic Superconductor

Hayao KOBAYASHI, Hiroki AKUTSU, Emiko ARAI, Hisashi TANAKA *(Univ. Tokyo)* **and Akiko KOBAYASHI** *(Univ. Tokyo)*

[*Phys. Rev.* **B56**, R8526 (1997)]

The physical properties of a new series of organic superconductors with fourfold quasi-stacking structures, λ-BETS$_2$GaX$_z$Y$_{4-z}$ (BETS=bis(ethylenedithiotetraselena-fulvalene; X, Y=F, Cl, Br; 0<z<2) are changed continuously by tuning z-value. λ-BETS$_2$GaBr$_z$Cl$_{4-z}$, takes a superconducting ground state at 0<z<z_c (≈0.8) and a semiconducting state at z_c<z<2.0. The maximum T_c is about 10 K, showing the existence of "10 K-class non-ET organic superconductors" (ET= bis(ethylenedithio)tetrathiafulvalene (BEDT-TTF)). The temperature dependence of the resistivity resembles closely that of κ-type ET superconductor but the susceptibility behavior is different. The susceptibility of λ-BETS$_2$GaBr$_{1.5}$Cl$_{2.5}$ is isotropic and decreases fairly sharply below 30 K. No indication of spin flop transition was observed at 10 K, suggesting that the insulating phase neighboring on the superconducting phase is not antiferromagnetic down to at least 10 K.

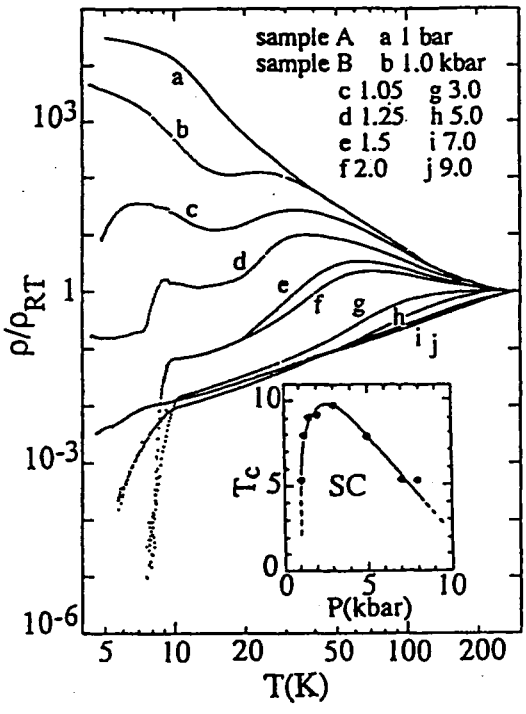

Figure 1. Pressure dependence of the resistivity and T_c (inset) of λ-BETS$_2$GaBr$_{1.5}$Cl$_{2.5}$

IV-H-2 The First Organic Superconductor Exhibiting a Superconductor-to-Antiferromagnetic Insulator Transition, λ-BETS$_2$(Fe$_x$Ga$_{1-x}$)Cl$_4$

Hayao KOBAYASHI, Akane SATO, Emiko ARAI, Hiroki AKUTSU, Akiko KOBAYASHI *(Univ. Tokyo)* **and P. CASSOUX** *(CNRS)*

An unprecedented superconductor-to-antiferromagnetic insulator transition was observed in an organic conductor, λ-$BETS_2$ $(Fe_xGa_{1-x})Cl_4$ (x ≈ 0.55 and 0.43), where magnetic Fe^{3+} ions play a crucial role. At ambient pressure, the phase with x ≈ 0.55 undergoes a metal-to-insulator transition at 4.5 ± 0.5 K. At a pressure of 1 kbar, it undergoes a superconducting transition with a critical temperature of 4.6 ± 0.5 K. A subsequent superconductor-to-insulator transition is observed below 3.6 K. At 1.5 kbar, the system remains superconducting down to 2 K. The phase with x ≈ 0.43 exhibits a superconducting (SC) transition and a subsequent superconductor-to-insulator (SC-I) transition at ambient pressure (T_c = 4.0-4.5 K and T_{SC-I} = 3.0-3.6 K). The magnetic susceptibility of this phase (χ) shows a sharp decrease at T_c and becomes anisotropy below T_{SC-I}. The anisotropy and field dependence of χ indicate the insulating state below T_{SC-I} to be antiferromagnetic. This finding suggests a possibility of the future development of magnetic organic superconductors.

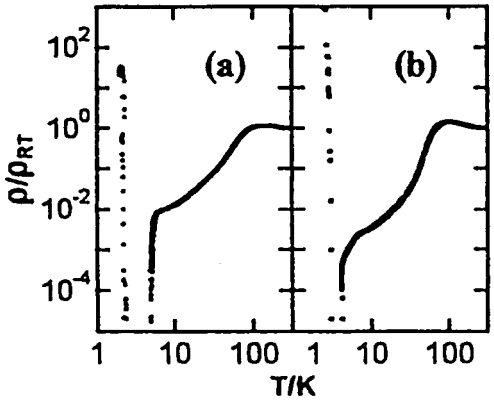

Figure 1. Resistivity of λ-$BETS_2(Fe_xGa_{1-x})Cl_4$ (a) x=0.55 at 1 kbar (b) x=0.43 at 1 bar

IV-H-3 The Origin of the π-d Coupled Metal-Insulator Transition in Highly Correlated Organic Conductor with Magnetic Anions, λ-$BETS_2FeCl_4$

Hiroki AKUTSU, Emiko ARAI, Hayao KOBAYASHI, Hisashi TANAKA *(Uni. Tokyo)*, **Akiko KOBAYASHI** *(Univ. Tokyo)* **and P. CASSOUX** *(CNRS)*

Recently, the organic ferromagnetic metal has become an attractive target in the development of new organic conducting systems. In order to find a clue to design such novel systems, organic conductors with interaction between metal electrons and magnetic moments must be developed as the first step. The unique metal-insulator (MI) transition of λ-$BETS_2FeCl_4$ is of special interest because the magnetic moments of high-spin Fe^{3+} ions are ordered antiferromagnetically below T_{MI}. The most characteristic feature of the magnetic behavior of this system is the discontinuous magnetization drop at T_{MI} when magnetic field is parallel to the *c* axis (//easy axis of AF structure). The magnitude of $\Delta M/M$ (=0.07-0.08) and the resistivity behavior of the metallic state indicating the strong correlation of π conduction electrons suggest a crucial role of the S=1/2 spins of π electron system. Below T_{MI}, the system will have two types of spin systems, that is, *d* and π spin systems. The MI transition of this complex might be a unprecedented cooperative AF transition of π and *d* spin systems.

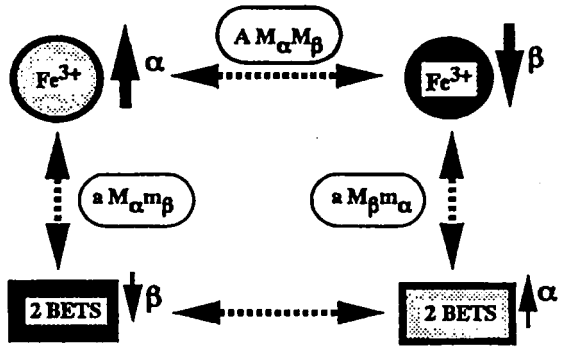

Figure 1. Schematic drawing of the Antiferromagnetically coupled two spin system in λ-$BETS_2FeCl_4$

IV-H-4 Three-Dimensional (T-P-H) Phase Diagram of λ-$BETS_2$ $FeCl_4$

Hiroki AKUTSU, Kiyonori KATO, Emiko ARAI, Hayao KOBAYASHI, Akiko KOBAYASHI *(Univ. Tokyo)*, **Madoka TOKUMOTO** *(ETL)*, **Luc BROSSARD** *(CNRS)* **and P. CASSOUX** *(CNRS)*

Magnetoresistance of λ-$BETS_2FeCl_4$ was measured along the needle axis of the crystal to determine the pressure and magnetic field dependencies of the coupled metal-insulator and antifferromagnetic transition temperature (T_{MI} (=T_N)). T_{MI} is lowered by applying pressure and/or magnetic field. The T_{MI} vs. H curve gives two flection points (H_1, H_2). The anomaly observed around 1 T (H_1) corresponds to the spin-flop transition observed by the SQUID measurements. T_{MI} is slightly dependent on H between H_1 and H_2. Magnetization (M) of the oriented polycrystalline sample of λ-$BETS_2FeCl_4$ was measured at 2-15 K in the magnetic field of 0.01-7 T. The magnitude of the characteristic drop of M observed for the field parallel to the c axis ($\Delta M//$) becomes small above 1.2 T but remains almost constant above 4.5 T.

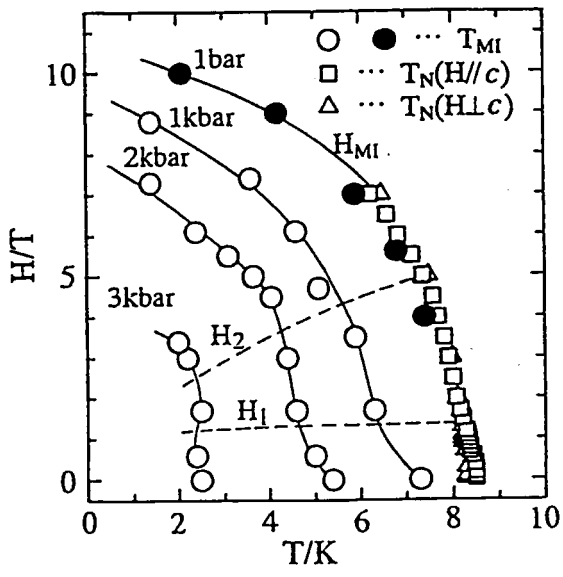

Figure 1. Pressure dependence of T_{MI}-H curve of λ-$BETS_2FeCl_4$.

IV-H-5 Electrical and Structural Properties of κ-Type BETS Conductors

Hisashi TANAKA *(Univ. Tokyo)* **Akiko KOBAYASHI** *(Univ. Tokyo)* **and Hayao KOBAYASHI**

Until recently, the development of κ-type organic conductors based on TTF-like donor molecules has been considered to be a shortcut to get new organic superconductors. However, no superconducting system has been found in κ-type BETS salts. We have prepared the crystal of κ-$BETS_2InBr_4$ and measured the resistivity down to 4.2 K. A small but distinct anomaly was observed at 150 K. The low-temperature crystal structure analysis revealed that this resistivity anomaly is related to the change in the coordination structure of $InBr_4^-$ anions. The $InBr_4^-$ ion takes a tetrahedral structure at room temperature but transforms into pseudo-five coordinated one below 150 K. Since the similar resistivity anomaly has been also observed in κ-$BETS_2InCl_4$, the transformation of the coordination geometry will be the nature of the In complex.

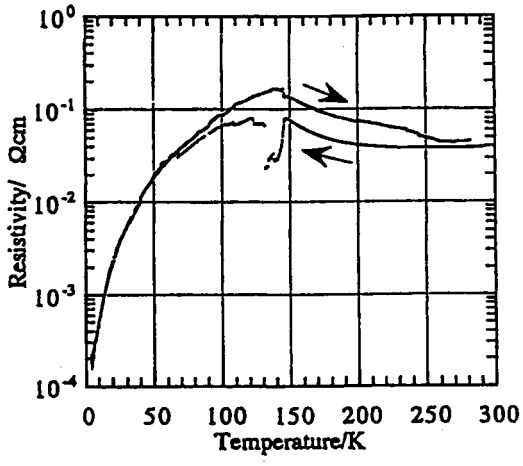

Figure 1. Resistivity of κ-$BETS_2InBr_4$.

IV-H-6 Structural, Electric and Magnetic Properties of EDT-XYF_2Z (X,Y=S or Se; Z=PF_6, TaF_6, ClO_4, $GaCl_4$, $FeCl_4$,..)

Akane SATO, Hayao KOBAYASHI and Akiko KOBAYASHI *(Univ. Tokyo)*

We have synthesized simple asymmetrical π donor EDT-TTF and the related molecules. Many 2:1 complexes were prepared electrochemically by using octahedral and tetrahedral anions. The room-temperature and low-temperature crystal structures, electrical resistivities and magnetic susceptibilities were examined. The simple extended Huckel tight-binding band calculation gave quasi-one-dimensional Fermi surfaces. Figure 1 shows the temperature dependencies of resistivity (ρ) and susceptibility (χ) of EDT-TTF_2PF_6. The system was metallic down to about 50 K and around 40 K the drop of χ was observed. X-Ray diffraction experiments showed that the twofold structure develops below T_{MI}, suggesting the insulating state to be non-magnetic.

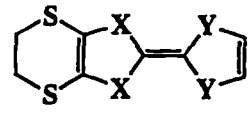

X= Y= S : EDT-TTF or EDT
X= Se, Y= S : EDT-DSDTF or EDST
X= S, Y= Se : EDT-DTDSF or EDTS
X= Y= Se : EDT-TSF or EDS

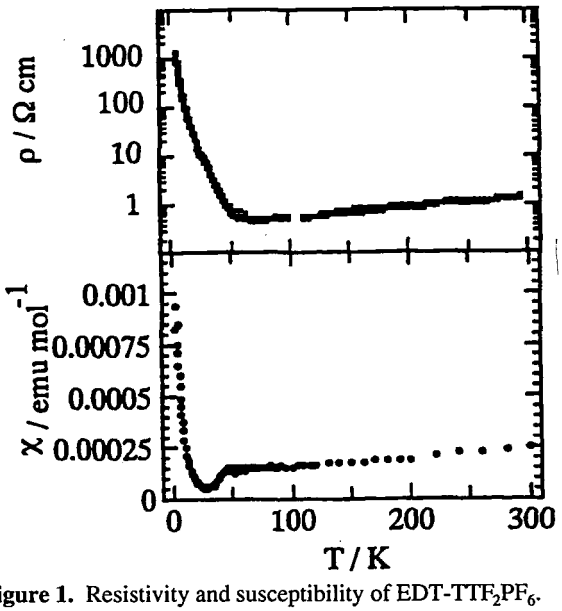

Figure 1. Resistivity and susceptibility of EDT-TTF_2PF_6.

IV-I Electric and Magnetic Properties of Ni(dmix)$_2$ (x= t, se) Complexes

Among about 80 molecular superconductors ever reported, 7 superconductors are systems based on transition metal complex molecules. The first superconducting transition metal complex [TTF][Ni(dmit)$_2$]$_2$ was discovered under pressure in 1986 (France) and the first ambient-pressure Ni(dmit)$_2$ superconductor was found in 1993 (Japan). They are composed of TTF-like π donor and π acceptor (Ni(dmit)$_2$) molecules. Although three "pure M(dmit)$_2$ superconductors" without TTF-like donors have been found in Japan, there is no ambient-pressure "pure π acceptor superconductor" based on M(dmit)$_2$ and closed shell cations. Therefore such a system still remains to be a target in the development of new conductors. Recently many trials have been made to prepare new transition metal complex molecules with extended π ligands and planar binuclear metal complexes with the purpose of using them as building units of new conducting crystals. However, no molecule exceeding M(dmit)$_2$ seems to have been obtained until now.

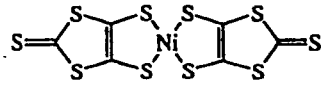

Ni(dmit)2

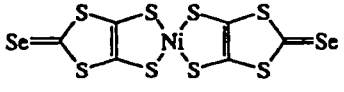

Ni(dmise)2

IV-I-1 Magnetic Properties of Ni(dmit)$_2$ Conductors with Stable Metallic States

Akiko KOBAYASHI *(Univ. Tokyo)*, **Akane SATO and Hayao KOBAYASHI**

The first "pure π acceptor conductor" retaining the metallic state down to liquid He temperature at ambient pressure is α-[(CH$_3$)$_2$(C$_2$H$_5$)$_2$N][Ni(dmit)$_2$]$_2$ discovered in 1986. The stability of the metallic state of this system is originated from the unique two-dimensional molecular arrangement called "spanning overlap arrangement." Considering the large efforts paid to develop various conductors, it is surprising that besides the recently developed two Ni(dmise)$_2$ conductors and three Ni(dmit)$_2$ systems obtained by us, there is no conductors based on transition metal complexes exhibiting stable metallic states down to low temperatures. We have recently examined resistivity of these systems down to very low temperature (0.5 K in α-[(CH$_3$)$_2$(C$_2$H$_5$)$_2$N][Ni(dmit)$_2$]$_2$ and 0.05 K in γ-[(CH$_3$)$_2$(C$_2$H$_5$)$_2$N][Ni(dmit)$_2$]$_2$) and found that these systems cannot be the ambient-pressure "pure π acceptor superconductor." It is very interesting that α-[(CH$_3$)$_2$(C$_2$H$_5$)$_2$N][Ni(dmit)$_2$]$_2$ and analogous system [(CH$_3$)$_2$(C$_5$H$_{10}$)N][Ni(dmit)$_2$]$_2$ exhibit anomalously large and temperature-dependent paramagnetic susceptibility (χ(dia)~-4.5x10^{-4} emu/mol) similar to that of semiconducting α-[(CH$_3$)$_4$N][Ni(dmit)$_2$]$_2$.

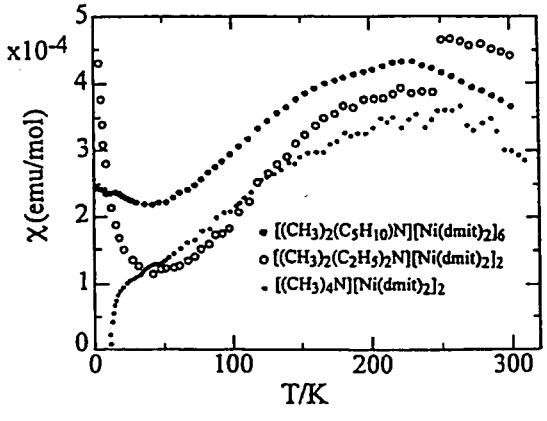

Figure 1. Susceptibilities of Ni(dmit)$_2$ conductors.

IV-I-2 New Metallic Ni(dmise)$_2$ Complex

Akane SATO, Hayao KOBAYASHI and Akiko KOBAYASHI *(Univ. Tokyo)*

A new Ni(dmise)$_2$ conductor N,N-dimethylpiperidinium [Ni(dmise)$_2$]$_2$ (dmise=4,5-dimercapto-1,3-dithie-2-selone) was prepared. The resistivity measurement showed the system to be metallic down to 2 K (ρ(RT)=0.02 Ωcm). In contrast to the normal metallic nature of this complex, the magnetic susceptibility was unexpectedly large and temperature dependent (χ(RT)=8.4 x10^{-4} emu mol^{-1}). This system is the first M(dmise)$_2$ conductors with stable metallic state, whose crystal structure has been determined. Ni(dmise)$_2$ molecules are arranged in so-called "spanning overlap mode."

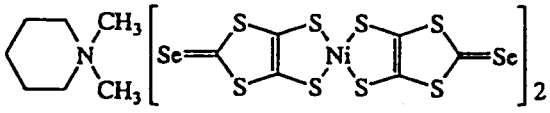

N,N-dimethylpiperidinium[Ni(dmise)$_2$]$_2$

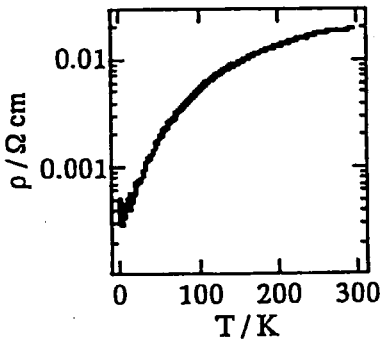

Figure 1. Resistivity of $[(CH_3)_2(C_2H_5)_2N]$ $[Ni(dmise)_2]_2$

IV-J X-Ray Studies at Low Temperature and High Pressure

The molecular crystal is rich in the structural freedom and therefore frequently undergoes a structural phase transition at low temperature and/or high pressure. In addition, the electronic properties is very sensitive to the structural modification. For example, even the small conformational disorder of the constituent molecules can destroy the metallic state. Furthermore, it is well known that even a small pressure less than 1 kbar produces a crucial effect on the low-temperature electronic properties. Therefore, the crystal structure determination at low temperature and/or high pressure is inevitable for the studies on the molecular conducting systems.

(I) Low-temperature studies: Several years ago we have developed a low-temperature X-ray imaging plate systems. The same type of low-temperature X-ray system becomes to be used in some laboratories in Japan. (II) High-pressure studies: Almost two decades ago, we (H. K and A. K.) tried to make crystal structure analyses of partially oxidized platinum complexes at high pressure by using diamond anvil cell. Since the rotating anode X-ray generator and diffractometor were not available at that time, we used a 2kW X-ray generator, precession camera and X-ray films. The X-ray intensities were visually estimated. However, in spite of the very hard works required, the insufficient quality of the X-ray intensity data prevented us to continue the single crystal structure determination at high pressure. Nowadays the diamond anvil high-pressure cell is commercially available. But we designed two types of high pressure cells: (1) beryllium cylinder cell for low-pressure region (<5 kbar) (2) diamond anvil cell for high pressure region (>20kbar). We have made preliminary high-pressure diffraction experiments on two molecular conductors by using beryllium cell and X-ray imaging plate system. We considered these experiments to be a necessary step for higher pressure studies by diamond anvil cell.

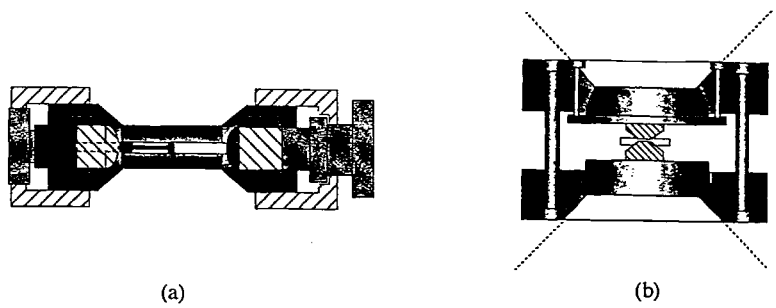

(a) (b)

High-pressure X-ray cell. (a) beryllium cylinder cell (b) diamond anvil cell

IV-J-1 Low-Temperature X-Ray Diffraction Studies on Molecular Conductors

Akane SATO, Hayao KOBAYASHI and Akiko KOBAYASHI *(Univ. Tokyo)*

We have recently examined low-temperature Crystal structures of two Pd(dmit)$_2$ superconductors, one Ni(dmise)$_2$ conductor and a series of EDT-TTF$_2$X (X=TaF$_6$, GaCl$_4$) systems. [R][Pd(dmit)$_2$]$_2$ (R=$(CH_3)_4N$, $(CH_3)_2(C_2H_5)_2N$) is the high-pressure superconductor. At ambient pressure, any distinct structural phase transition was not observed down to 10 K. In $[C_5H_{10}N(CH_3)_2][Ni(dmise)_2]_2$, the satellite X-ray reflections showing the development of fivefold superstructure were observed below 250 K. EDT-TTF$_2$TaF$_6$ showed X-ray $2k_F$ diffuse streaks below 250 K indicating one-dimensional lattice instability. Below 50 K which is

nearly equal to the MI transition temperature (60 K), $2k_F$ spots were observed. However, the $2k_F$ diffuse streaks observed below 250 K were almost unchanged at T_{MI}. Considering the simplicity of the crystal structure of this system, the coexistence of $2k_F$ streaks and $2k_F$ spots below T_{MI} seems to be very puzzling.

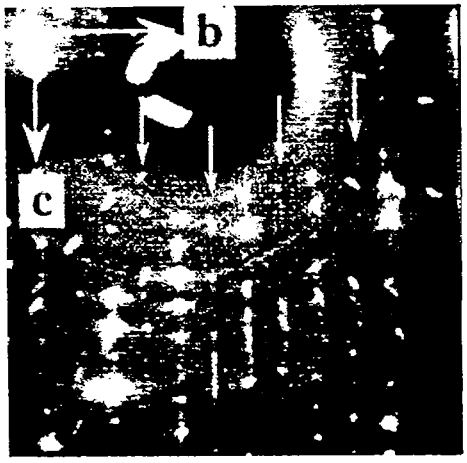

Figure 1. X-ray diffraction pattern of EDT-TTF_2TaF_6 at 13 K.

IV-J-2 High Pressure X-Ray Crystal Structure Analyses of Molecular Conductors

Takafumi ADACHI, Hayao KOBAYASHI and Akiko KOBAYASHI *(Univ. Tokyo)*

By using Be cylinder cell, the crystal structures of two molecular conducting systems, α-BEDT-TTF_2I_3 and $[(CH_3)_2(C_2H_5)_2N][Pd(dmit)_2]_2$ were examined up to 5 kbar. The pressure medium was the silicone oil. The diffraction patterns were detected by Weissenberg type X-ray imaging plate. The lattice constants and X-ray intensities of diffraction spots were determined at various pressures by the usual procedure. The crystal structures were refined by usual least-squares refinement programs. The R-values were about 10 %. The suitable correction of X-ray absorption is essential to improve the intensity data. The tight-binding band parameters were calculated on the basis of the high-pressure structures. The compressibilities of these two crystals were fairly different. The solid lines are those of Birch-Murnaghan equation, whose validity for the molecular crystals will be examined in future by using higher-pressure data to be obtained with diamond anvil cell.

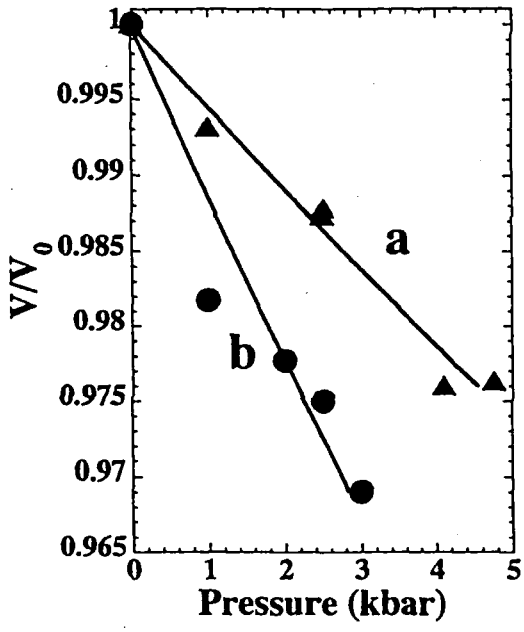

Figure 1. Pressure dependence of the unit cell volume (a) $[(CH_3)_2(C_2H_5)_2N][Pd(dmit)_2]_2$ (b) a-BEDT-TTF_2I_3

IV-K Development of New Molecular Conductors

The development of new materials is the most important driving force for the field of solid state chemistry. The idea of the molecular design of stable two-dimensional π metal band pushed forward by us in the middle of 1980s contributed greatly to produce various types of molecular metals and superconductors, which have aroused increasing interest of chemists and physicists. However, we must now grow out of the conventional concept of the design of molecular conductors toward the future development. From this point of view we have performed the development of several types of new component molecules of conducting systems. It will be imagined that the crystal structures of organic conductors composed of π donor molecules such as polythio-substituted TTF and ditellurium bridged polyacene have an organic/inorganic hybrid nature. By examining these structures, a guiding principle to design new organic conductors will be obtained.

IV-K-1 Development of New Selenium Containing Metal Complex $M(ddds)_2$

Hideki FUJIWARA, Emiko ARAI and Hayao KOBAYASHI

[*J. Chem. Soc., Chem. Commun.* 837 (1997)]

The selenium substitution of inner sulfur atoms of $M(dddt)_2$ is expected to increase the transverse intermolecular interaction and therefore to stabilize metallic state. From this viewpoint, we synthesized novel metal complex $[M(ddds)_2]^{n-}$ (M=Ni, Au; n=0, 1). The crystal structures of tetraalkylammonium salts of $M(ddds)_2$ were determined. There is no stack of $M(ddds)_2$ anions. The anions and the cations are alternately arranged. The intraligand Se-Se length is longer than that of inner sulfur atoms of $M(dddt)_2^-$ and is almost equal to the S-S length in the six-membered ring. Therefore, two-dimensional intermolecular close contacts can be expected in $M(ddds)_2$ complexes. Neutral $M(ddds)_2$ (M = Ni, Au) were synthesized by chemical and electrochemical oxidation from monoanionic $M(ddds)_2$. The neutral molecules pack as parallel crosses. $Ni(ddds)_2$

dimer has intradimer Ni-Se bond (2.496(1)Å) and forms a $[Ni(ddds)_2]_2$ molecule. The $Bu_4N[Ni(ddds)_2]$ shows two pairs of reversible redox waves (-0.60, +0.16 V vs. Ag/AgCl), which correspond to the two redox processes through its dianion to neutral state, and one irreversible redox wave. The room temperature magnetic susceptibility measurement showed that $Bu_4N[Ni(ddds)_2]$ is paramagnetic with μ_{eff} = 1.77 μ_B corresponding to one unpaired electron per molecular formula.

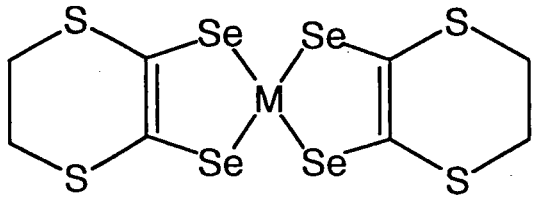

IV-K-2 Synthesis of Novel Extended Fulvalene-Metaldithiolene Complexes and Mixed Ligand Metal Complexes

Akiko KOBAYASHI *(Univ. Tokyo)*, **Mieko KUMASAKI** *(Univ. Tokyo)*, **Hisashi TANAKA** *(Univ. Tokyo)*, **Taro SAITO** *(Univ. Tokyo)*, **Hideki FUJIWARA, Emiko ARAI and Hayao KOBAYASHI**

Recent preparation of transition metal complex with extended tatrathiafulvalenedithiolato ligand has been of much interest because they have expanded π-conjugated electron system and low on-site Coulomb repulsion on the molecule and sufficient potentials to yield highly conducting metals or superconductors. Furthermore they have possibility to produce new stacking arrangements in the crystal due to the elongated molecular structures. We have prepared novel tetraphenylphosphonium (TPP) salts of nickel and copper complexes of extended TTF dithiolate, propylenedithio tetrathiafulvalenedithiolate ($C_9H_6S_8^{2-}$, $ptdt^{2-}$) and we have determined crystal structures of TPP $[Ni(ptdt)_2](acetone)_{1.4}$ and $TPP_2[Cu(ptdt)_2](acetone)_{1.2}$. The spanning overlap arrangement is the only type of molecular arrangement, which can make the metallic state of dithiolene complex stable. But the structures based on the molecules with extended π-ligands suggest the possibility of new two-dimensional (2D) or 3D molecular arrangement. In addition to the symmetrical extended ligand metal complexes, we have examined the mixed ligand systems and prepared new metal dithiolene complex $(TTP)_2[Ni(dmit)(ttc)]$ and clarified the crystal structure of this complex.

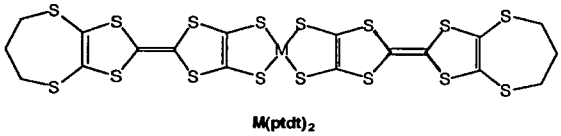

IV-K-3 Synthesis, Structure and Properties of New Sulfur-Bridged TTF Dimer

Hideki FUJIWARA, Emiko ARAI and Hayao KOBAYASHI

Development of TTF dimer and oligomer has much interest for the synthetic chemistry of new organic donors because of reduction of the on-site Coulomb repulsion in its dication state and enhancement of intermolecular interaction. We synthesized new sulfur-bridged tetrathiafulvalene (TTF) dimer molecule **1** in which two TTF moieties are connected to each other by two trithio chains. X-Ray crystal structure analysis revealed that the molecule has cyclophane-like structure and interplanar distance in the dimer is 3.86 Å. The TTF dimers form stacking structure and the electrochemical property was investigated by cyclic voltammetry technique. The dimer shows two pairs of reversible one-electron redox waves (+0.57, 0.67 V vs. Ag/AgCl in PhCN) and one pair of reversible two-electron redox wave (+1.15 V). Preparation of cation radical salts was performed by electrochemical oxidation. The structure of ClO_4 salt was determined. When the electrocrystallization was performed in chlorobenzene, ClO_4 salt with composition of 1:2:1 (Donor:Anion:PhCl) was obtained. On the other hand, 1:2 salt was obtained in THF. In both cases, each dimer is separated by anions and solvents.

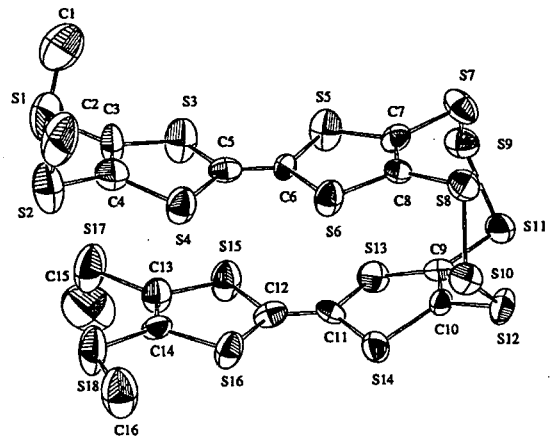

Figure 1. Molecular structure of **1**.

IV-K-4 Synthesis, Structure and Physical Properties of Pentathio-Substituted TTF Derivative; Ethylenedithio(pentathio)tetrathiafulvalene

Emiko ARAI, Hideki FUJIWARA and Hayao KOBAYASHI

We focused on the pentathio group as substituent to realize a novel intermolecular network by S-S contacts of pentathio group and we synthesized the pentathio-substituted TTF derivative; ethylenedithio-(pentathio)tetrathiafulvalene. X-Ray structure analysis of the neutral molecule revealed that there are many intermolecular S-S contacts less than the sum of the van der Waals radii (3.7 Å) and two-dimensional network through sulfur atoms is developed between the pentathio groups and TTF moieties. Therefore two-dimensional intermolecular interaction requested for realization of stable metallic state is expected in its conducting solids. CV result indicates that **1** shows two pairs of reversible redox waves (+0.69 and +1.06 V versus Ag/AgCl) and electron-donating ability of **1** is

lower than that of BEDT-TTF by condensation of pentathio group. Furthermore we prepared the ClO_4 salt of this donor. X-Ray structure analysis of the salt revealed that there is no intermolecular S-S contacts between donor columns owing to the anions and crystal solvents located between them, but there is several short intermolecular contacts (3.560 and 3.598 Å) mediated by sulfur atoms of TTF moieties in the dimer. Electrical conductivity measurement revealed that the ClO_4 salt is semiconducting with an activation energy of 0.12 eV and room temperature electrical conductivity is comparatively high (4-0.5 x 10^{-1} S cm^{-1}) for 1:1 salt because of tight one-dimensional stacking.

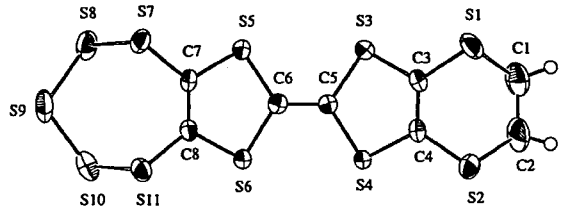

Figure 1. Molecular structure of ethylenedithio (pentathio)tetrathiafulvalene

IV-K-5 Crystal Structures and Electrical Conductivities of Cation-Radical Salts of a Tellurium-Containing Donor: 2,3-DMTTeA

Akiko KOBAYASHI *(Univ. Tokyo)*, **Masahiro NAKATA** *(Univ. Tokyo)*, **Hayao KOBAYASHI, Kazuo TAKIMIYA** *(Hiroshima Univ.)*, **Tetsuo OTSUBO** *(Hiroshima Univ.)* **and Fumio OGURA** *(Kinki Univ.)*

[*J. Chem. Soc., Chem. Commun.* 837 (1997)]

In the field of molecular conductors, systems based on tellurium-containing donor molecules have not received as much attention as systems based on sulfur- or selenium-containing donors. By incorporating heavy chalcogen atoms such as tellurium into donor molecules, a new metallic system with a wider bandwidth and a higher dimensionality is expected to appear. We report here the first examples of cation radical salts of a polyacene donor with peri-ditellurium bridges, 2,3-DMTTeA. The resistivities of all the salts showed semiconducting temperature dependence. However, the Br- salt has quite a high room temperature conductivity (1.3 X 10^3 S cm^{-1}) and a very low activation energy (0.010 eV). The common feature to all the structures of the salts is the disorder of the donor molecules caused by their unsymmetrical shape. One possible reason why the donor molecules have this orientational disorder may be that the Te ••• Te network is dominant in the construction of the crystal structures.

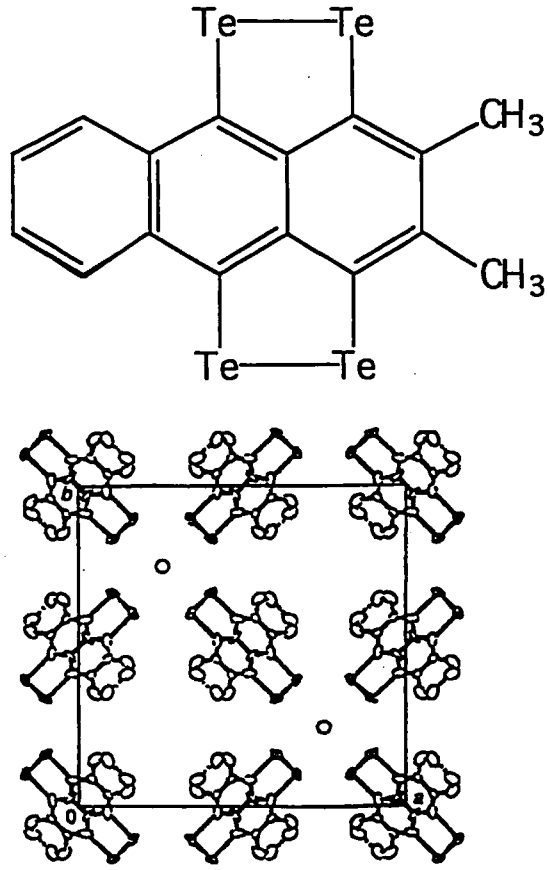

Figure 1. 2,3-DMTTeA structure and Crystal structure of the Br salt.

IV-K-6 Development of Novel Organic Conductors Based on Tellurium Containig Electron Donors

Akiko KOBAYASHI *(Univ. Tokyo)*, **Emiko ARAI, Hideki FUJIWARA, Hayao KOBAYASHI, Kazuo TAKIMIYA** *(Hiroshima Univ.)*, **Tetsuo OTSUBO** *(Hiroshima Univ.)* **and Fumio OGURA** *(Kinki Univ.)*

In the course of the studies on molecular conductors of 2,3-DMTTeA donor, we were faced on the problem of disorder derived from its unsymmetrical molecular structure because tellurium network is dominant in the construction of the crystal structure. This disorder has exerted a harmful influence upon the transport properties of the salts. In order to avoid the disorder of donor we focused on the symmetrical polyacene donor with peri-ditellurium bridges, 2,3,6,7-TMTTeN and prepared the cation-radical salts of this donor. The resistivities of almost all the salts showed semiconducting temperature dependence similar to the case of 2,3-DMTTeA. However, all the salt obtained so far have a high room temperature conductivity (10^1 - 10^2 S cm^{-1}) and a very low activation energy compared to the 2,3-DMTTeA salts. X-ray crystal structure analysis revealed that all the salts have high symmetry with tetragonal lattices. In these crystals ditellurium bridges are situated in four-fold symmetry. Anions are on the four-fold axis and disordered due to the disagreement of the periodicity with the stacking period of

DMTTeA. On the other hand we also make an attempt to produce new tellurium containing donor molecules because tellurium based organic conductors may give us new guidelines for realization of new organic conductors and new physical properties.

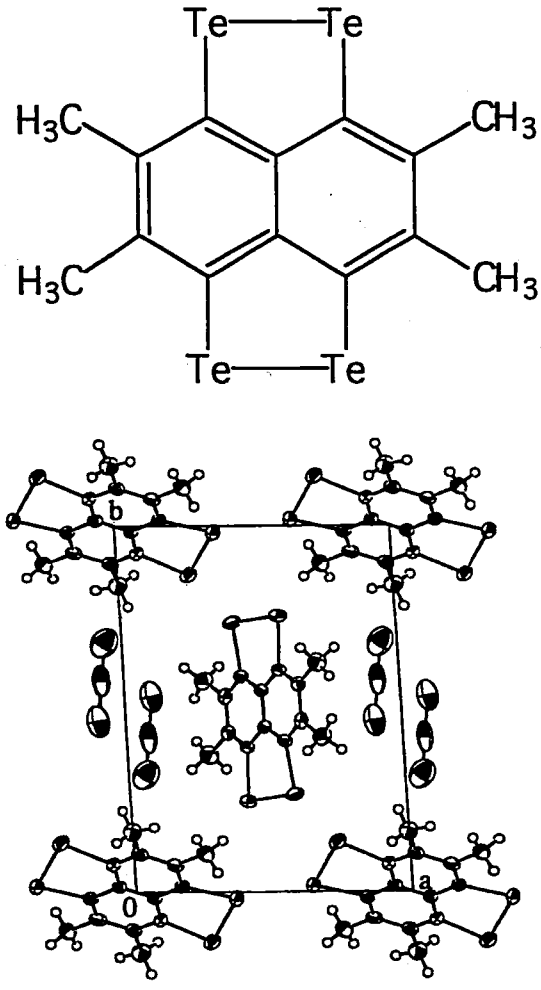

Figure 1. 2,3,6,7-TMTTeN structure and crystal structure of 2,3,6,7-TMTTeN•CS_2

IV-K-7 Development of New Donor Components with Magnetic Moiety

Hideki FUJIWARA, Emiko ARAI, Akane SATO and Hayao KOBAYASHI

Molecular conductors with π-d electron systems have attracted a considerable attention for these years because it is expected that electron conduction of π-electron systems and magnetic moments of transition metals may interact to each other to yield novel electric and magnetic properties. However the conduction electrons and magnetic moments are separated and the interaction between them are weak in the systems studied so far. Therefore we intend to develop new electron donors having the magnetic moiety such as stable organic radical, magnetic transition metal atom in one molecule. In these systems conduction electrons will strongly interact with magnetic moments. We hope that in near future these study will tell us the way to realize the organic magnetic metal desired for long time.

IV-L Development of Pulsed Field Gradient NMR Spectroscopy

Pulsed field gradient spin echo (PGSE) nuclear magnetic resonance (NMR) is a powerful method for the study of dynamics in condensed matter because it probes transitional motion of molecules selectively, without being affected by vibrational or rotational motions. Advantage of the method lies also in that incorporation of impurity probe is unnecessary. However, applications of this technique to strongly dipole-coupled spin systems with short T_2 or to the study of slow and anisotropic self-diffusion are challenging problems for modern NMR spectroscopy because combined techniques of line-narrowing, pulsing of sharp and intense field gradients, and multi-dimensional field-gradient generation are necessary. In the present study we developed a new pulse current driver for very intense magnetic field gradient of 11.3 T m^{-1}, and a versatile pulse generator for slow and anisotropic self-diffusion dynamics in strongly dipole-coupled spin systems.

IV-L-1 High Speed Controller for Very Intense Magnetic Field Gradient Pulses in PGSE-NMR

Osamu OISHI and Seiichi MIYAJIMA

Pulsed field gradient current controller was improved for the slower dynamics measurements in solids or liquid crystals. Figure 1 shows the schematic circuit diagram of the apparatus. Higher voltage and larger current performances were made possible by using 2SK1527 (Hitachi) high speed power MOS-FETs in the place of the former ones.[1] The field gradient (FG) pulse of a TTL level transferred from the pulse generator (IV-L-2) is photo-coupled with TLP-2631 (Toshiba) and amplified by DS-0026 (National Semiconductors) to drive the MOS-FETs. FG intensity is controlled by

setting a reference level by TL317LP (Texas Instruments) voltage regulator. Well-balanced field gradient pulses of intensity as large as 11.3 T m^{-1} was realized by applying a current of 45 A on a single MOSFET. The rising and fallng times are *ca.* 10 μs.

Reference

1) O. Oishi and S. Miyajima, *J. Magn. Reson.* **123 A**, 64 (1996).

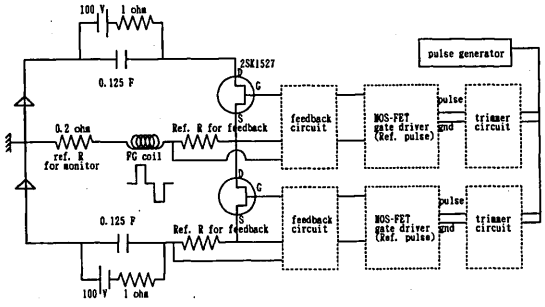

Figure 1. Schematic diagram of the FG current controller

IV-L-2 Personal Computer-Controlled 16 Channel Versatile Pulse Generator for Nuclear Magnetic Resonance

Tomonori TOYODA, Hisashi YOSHIDA, Osamu OISHI and Seiichi MIYAJIMA

[*Rev. Sci. Instrum.* **68**, 3140 (1997)]

Fully-digitized automatic pulse generator for general NMR purposes was designed and constructed [Figure 1]. The following features were realized: (i) Pulse sequence is constructed in a standard 32 bit personal computer rather than on-board microprocessors. (ii) 16 independent channels are controlled by identifying each of the binary states by 16 bit codes. (iii) The single time periods of 0.1 μs to *ca.* 7 min are obtained in 0.1 μs step by using 10 MHz master clock and 32 bit time data. The period longer than above is obtained by repetition. (iv) To realize the high speed control and high time-resolution, the pulse generator hardware is separated from the host computer. Once the pulse sequence is transferred from the computer to the pulse generator, the pulse sequence is synthesized within the pulse generator hardware, and then output to the main spectrometer console. (v) The hardware consists of basic TTL devices without resorting to custom LSIs. (vi) Centronics printer interface, which is already installed in a commercial personal computer, is used for data transfer. Laboriousness in making a custom interface board or the cost in purchasing the commercial interface boards are thus avoided. On the other hand, a technique is necessary in constructing the pulse sequence data because only 3 bus lines are available for the 16 channel data. The present pulse generator design does not depend on the models of personal computers, and the devices used are readily available worldwide. The present equipment was successfully used for the PGSE anisotropic self-diffusion experiment in liquid crystal.

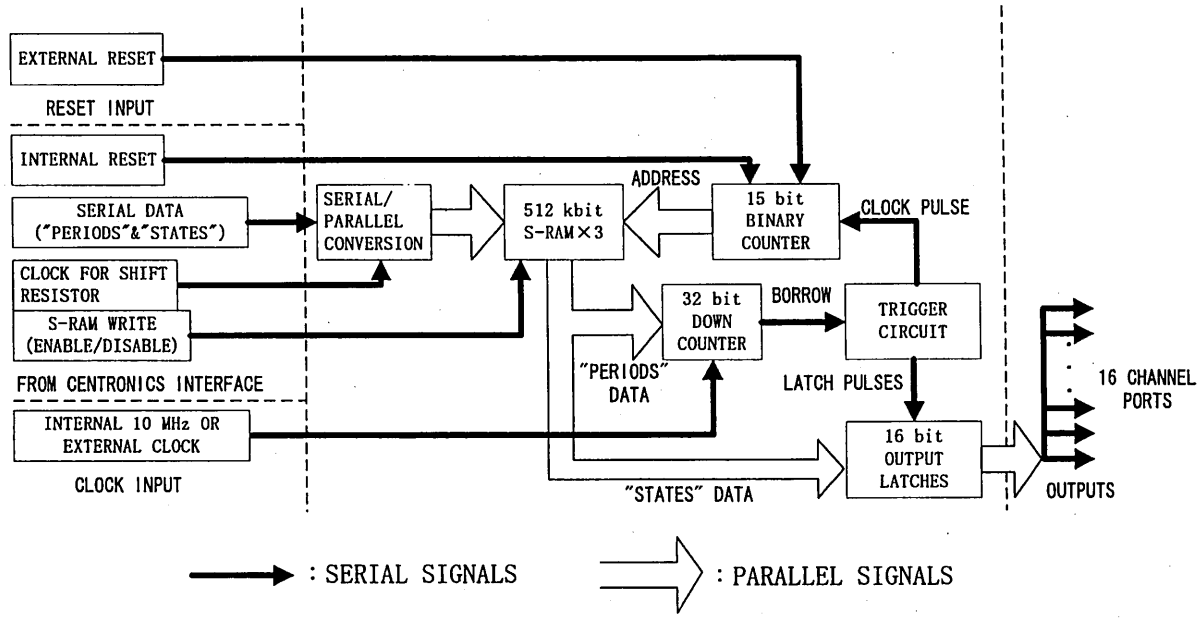

Figure 1. Block diagram of the pulse generator

IV-M Phase Transitions and Dynamical Ordering in Liquid Crystals

Extensive NMR studies are conducted for the dynamical ordering of liquid crystals. Field-alignment-induced shift of the ^{13}C resonance lines, transient oscillation of the ^{13}C magnetization during cross-polarization, and natural abundance ^{2}H NMR experiments were conducted. Theoretical basis for the spectral analysis was also developed. Special emphasis was placed on the microscopic origin of antiferroelectricity in chiral smectic liquid crystal. Doubly reentrant liquid crystal and the newly synthesized nematic liquid crystals with flexible poly(oxyethylene)

chains were also studied. New instrumental development is being made for the NMR of liquid crystal at high hydrostatic pressures.

IV-M-1 General Theory for the NMR Spectra of Liquid Crystals

Toshihito NAKAI *(Univ. Tsukuba)* **and Seiichi MIYAJIMA**

General theoretical framework is developed for the NMR spectrum to analyze the molecular structure, dynamics, and order in liquid crystals including intramolecular degrees of freedom. NMR spectrum for the magnetically aligned specimen is described by a projection of the local magnetic interaction tensor onto the magnetic field axis. Intramolecular segmental order parameter is described by corresponding Wigner rotation matrix elements. By introducing an idea of *molecule as a rigid body* which results from consideration of all the internal motion, the orientational characteristics of liquid crystal is described by four effective order parameters; (i) S_{00}, the uniaxial order parameter identical with the classical Maier-Saupe parameter, (ii) $(S_{20}+S_{-20})/2$, a difference in orientational characteristics of the two molecular short axes with respect to the main director, which originates from the molecular biaxiality, (iii) $(S_{02}+S_{0-2})/2$, a difference in orientational characteristics of the molecular long axis with respect to the secondary and the tertiary directors, and represents the phase biaxality, and (iv) $(S_{22}+S_{2-2}+S_{-22}+S_{-2-2})/4$, which is a coupled quantity between molecular biaxiality and phase biaxiality. The first two are nonzero even in uniaxial liquid crystal, but the latter two are nonzero only in biaxial phases. Field-aligned ^{13}C NMR spectra of MHPOBC were analyzed by using the present theoretical approach, and the preliminary calculation gave a result that the molecular long axis tilts from the para-axes of the phenylene and the biphenylene axes as much as 7.3 and 8.0 deg., respectively. Most probably, both cores are executing 180 deg. flip motion, and the S_{00} was 0.75 in the S_A phase.

IV-M-2 Complete Assignment of the ^{13}C NMR Lines in Antiferroelectric MHPOBC

Hiroki FUJIMORI, Toshihito NAKAI *(Univ. Tsukuba)*, **Daisuke KUWAHARA and Seiichi MIYAJIMA**

We are developing extensive NMR investigations into the microscopic origin of antiferroelectricity in chiral smectic liquid crystal. In this paper we report complete assignment of the ^{13}C NMR lines for both isotropic and oriented samples of the prototypical compound MHPOBC [Figure 1]. To this goal two-dimensional double quantum coherence spectroscopy (INADEQUATE) in the isotropic phase, analysis of the alignment-induced shifts and their temperature-dependences, cross-polarization efficiencies, chemical substitution, *i.e.*, trifluorination of the 1-methyl group, were employed. The assignment for the isotropic (a) and oriented (b) spectra of the core part is shown in Figure 2. The assignment for the chain part is given in Ref. 1).

Reference

1) T. Nakai *et al.*, *Phys. Rev. E* submitted.

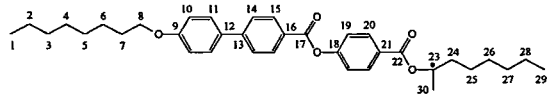

Figure 1. Numbering of the carbons in MHPOBC.

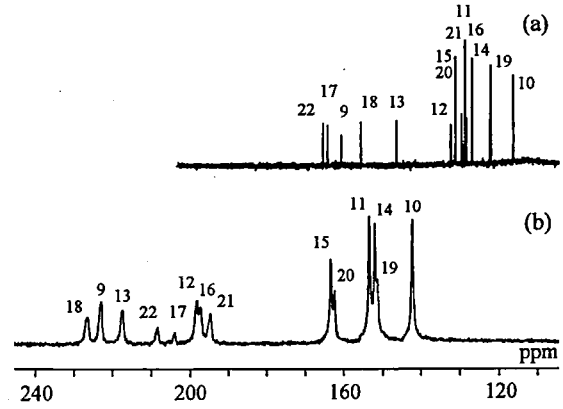

Figure 2. Assignment of the high resolution ^{13}C NMR spectra for the core part of MHPOBC. (a) isotropic and (b) oriented spectra.

IV-M-3 Natural Abundance ^2H NMR Spectroscopy: Anomalous Deuteration Effect on the Chain Dynamics of a Doubly Reentrant Liquid Crystal

Hiroki FUJIMORI, Daisuke KUWAHARA and Seiichi MIYAJIMA

Deuterium quadrupole spectrum gives detailed feature of structure and molecular motion in condensed matter. When natural abundance ^2H NMR is employed, ^2H spin (I=1) behaves as a test probe to detect the dynamics of *protonated* compounds or segments because of very small natural abundane (0.015 %) of deuterium. In this paper we studied the dynamics of the octyl chain in the doubly reentrant liquid crystal, 4-cyanobenzoyloxy-[4-octylbenzoyloxy]-*p*-phenylene (CBOBP).[1] The chain-deuterated homologue CBOBP-*d*17 was also studied, and the comparison of the two gave an interesting insight into the mass effect on the chain dynamics and its relationship with this unusual phase transition phenomenon (*i.e.*, lattice melting on lowering the temperature). Most significant feature was the anomalous enhancement of the segmental order parameter at low temperature which was found only for the deuterated chain [Figure 1]. This must be related with the anomalous deuteration effect, *i.e.*, a significant shift as large as 5 K of the reentrant phase transition temperature. It is thus proved that comparative study of ^2H NMR of the natural sample and the sample with specifically deuterated segments gives valuable information on the mass effect on the molecular dynamics and related phase transitions.

Reference

1) S. Miyajima and T. Hosokawa, *Phys. Rev. B* **52**, 4060 (1995).

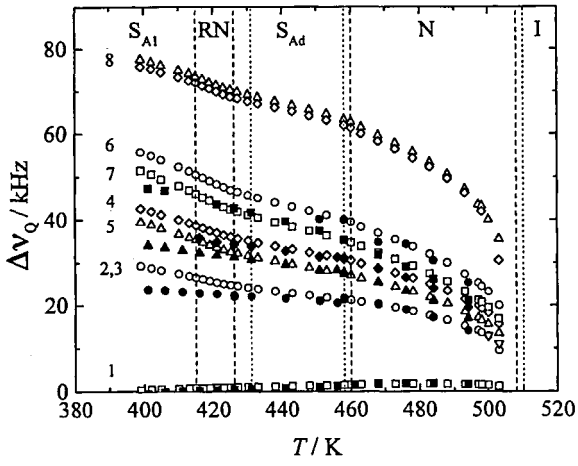

Figure 1. Temperature dependence of the deuterium quadrupole splittings for individual methylene segments in natural CBOBP (●) and chain-deuterated CBOBP-*d*17 (○).

IV-M-4 Transient Oscillation of Magnetization in ^{13}C-^{1}H Dipole Coupled Spin Systems in Liquid Crystal

Philippe BERDAGUE *(Univ. Paris)*, **Jean-Pierre BAYLE** *(Univ. Paris and IMS)*, **Hiroki FUJIMORI and Seiichi MIYAJIMA**

^{13}C spin magnetization exhibits transient oscillation when the ^{13}C is dipole-coupled with ^{1}H in double resonance experiment in the rotating frame. This is possible when the individual ^{13}C spin is strongly coupled with the nearest small number of ^{1}H spins and the relevant interaction is much stronger than the ^{1}H spin diffusion. The oscillation experiment first demonstrated for rapidly rotating molecule in solid state[1] was recently applied to liquid crystal.[2] In this paper we applied the technique to evaluate the local ^{13}C-^{1}H dipole interaction in newly synthesized nematic liquid crystals [Figure 1]. In spite of the complex molecular structure, the well resolved lines exhibited very strong transient oscillation, *e.g.*, for C(1) and C(1') as shown in Figure 2. The obtained dipole coupling constants were 2.33 and 1.39 kHz, respectively. The significantly small value for C(1') proved that a strong folding, *i.e.*, unusual conformation of the oxymethylene unit, is occurring in the laterally substituted chain to maintain the rodlike molecular structure in the liquid crystalline state. The transient dipolar oscillation was thus shown to be useful in structural and dynamical analysis of liquid crystal.

References

1) L. Mueller et al., Phys. Rev. Lett. **32**, 1402 (1974).
2) R. Pratima and K. V. Ramanathan, J. Magn. Reson. **118 A**, 7 (1996).

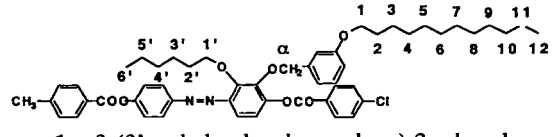

Figure 1. 3-(3'-*n*-dodecyloxybenzoyloxy)-2-*n*-hexyloxy-4-(4'-chlorobenzoyloxy)-4'-(4'-methylbenzoyloxy)azobenzene

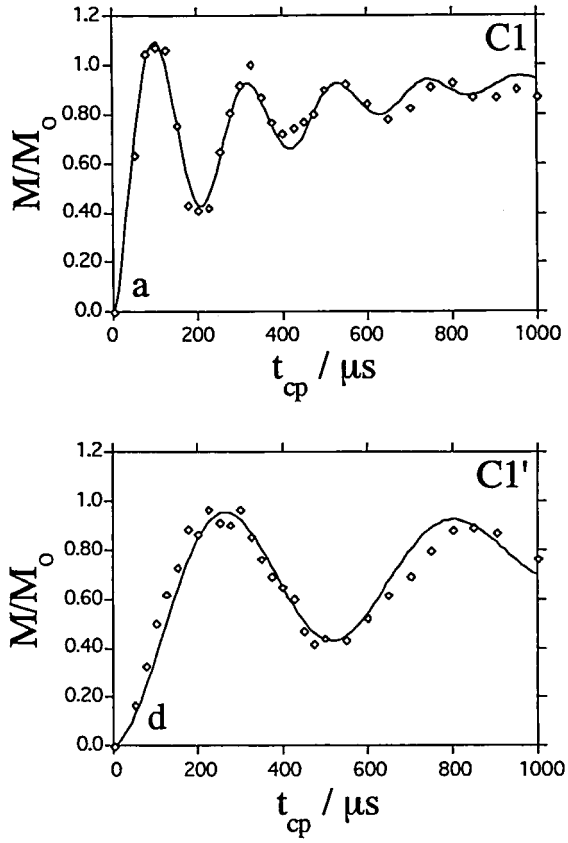

Figure 2. Transient oscillation of the cross-polarized ^{13}C magnetization for C(1) and C(1').

IV-M-5 Unusual Ordering of a Di(oxyethylene) Chain in a Dialkoxy Laterally Substituted Nematogen as Evidenced by ^{13}C NMR

Vincent RAYSSAC*, Philippe LESOT*, Jean-Pierre BAYLE and Seiichi MIYAJIMA** *(*Univ. Paris, **Univ. Paris and IMS)*

[*J. Mater. Chem.* submitted]

Poly(oxyethylene) chain was incorporated at one end of a four-ring core, and a nematic liquid crystal existing at almost room temperature was obtained [Figure 1]. The orientational and conformational characteristics were studied by ^{13}C NMR spectroscopy. Field-alignment-induced shift and transient oscillations of ^{13}C magnetization observed during variable contact-time cross-polarization experiment revealed a novel feature of di(oxyethylene) chain dynamics. The C-H bond order parameters [Figure 1] deduced from the effective C-H dipolar coupling constants were noticeably small compared with those of conventional alkyl chain, and showed monotonical decrease along the chain without exhibiting even-odd oscillation. These features were discussed on the basis of the gauche-rich conformational characeristics of the poly(oxyethylene) chain.

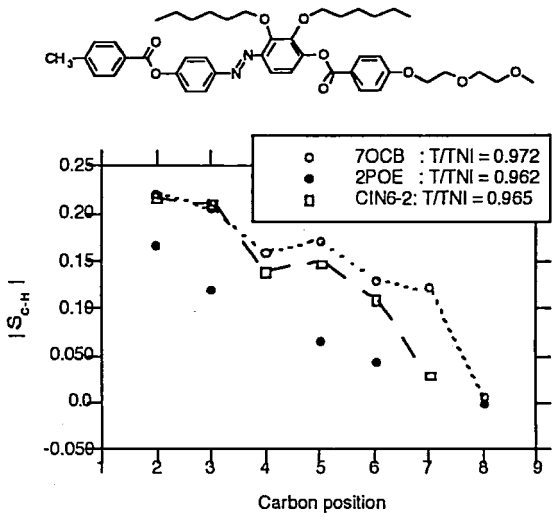

Figure 1. C-H order parameter variation along the chain (●), in comparison with those of conventional alkyl chains (○ and □).

IV-M-6 Low Melting Point Nematic Liquid Crystals with Oxyethylene Units: ^{13}C NMR Study of the Unusual Conformation

Vincent RAYSSAC*, Patrick JUDEINSTEIN*, Jean-Pierre BAYLE, Daisuke KUWAHARA and Seiichi MIYAJIMA** *(*Univ. Paris, **Univ. Paris and IMS)*

Four new nematic liquid crystals were synthesized which bear zero, one, two, or three oxyethylene units at one end of the molecular core. It was found that poly(oxyethylene) units act to lower the melting point [Figure 1], and stabilize the nematic liquid crystal because of their flexibility. The tri(oxyethylene) homologue was found to be nematic at room temperature. The segmental order was studied by ^{13}C NMR spectroscopy, and the strongly temperature-dependent conformational change was suggested.

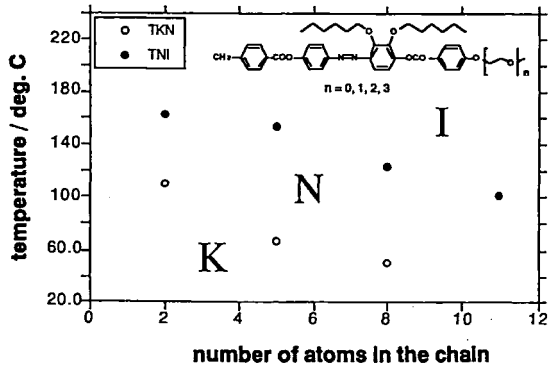

Figure 1. Crystal-nematic (○) and nematic-isotropic (●), transition temperatures as a function of the number of segments in the poly(oxyethylene) terminal chain.

IV-M-7 Design and Construction of Hydrostatic Pressure NMR Probehead

Hironori OGATA, Seiichi MIYAJIMA, Toshio HORIGOME, Tatsuharu TORII and Michio WATANABE

We have designed and constructed a hydrostatic pressure NMR probehead for the study of liquid crystal. Figure 1 shows the cross-sectional view of the hydrostatic pressure NMR probehead. It is designed for the ^{13}C and ^{2}H NMR measurements at pressures up to 4.1 kbar and at temperatures ranging from 300 to about 530 K. This probehead is inserted into a superconducting magnet of 6.34 T and is connected with the NMR spectrometer (JEOL GSX270WB). The hydrostatic pressure is produced in a commercial high pressure generator and transmitted with a low viscosity silicone oil to the NMR tube made with SUS316, whose cross-section is given in Figure 2. The sample is separated from the silicone oil with a Teflon sample cell. The saddle-type NMR coil is mounted on plug 5 which contains the radio frequency feedthrough that is connected to the tuning and matching capacitors. Temperature of the sample is controlled by changing the temperature of the dried air passing through the glass dewer, and is measured by the four-wire technique and monitored by a platiuum-resistor. The pressure applied to the sample is monitored by the change in resistivity of a manganin wire.

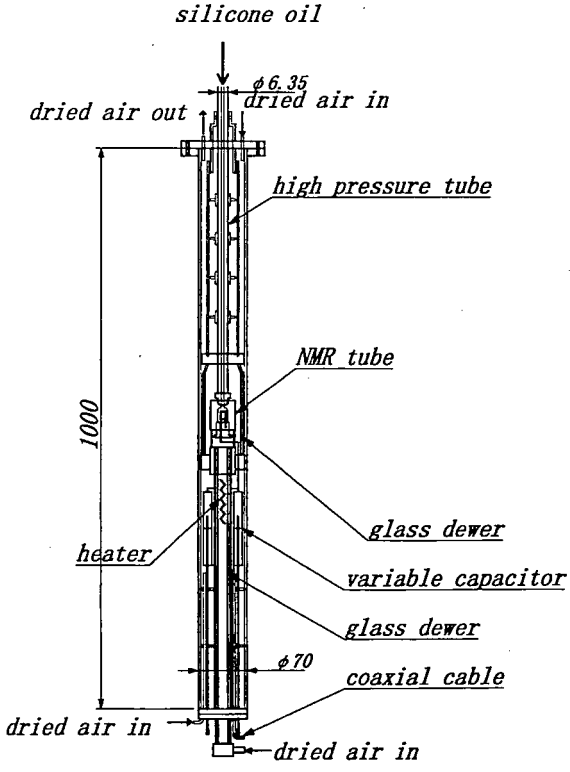

Figure 1. Cross-sectional view of the hydrostatic pressure NMR probehead.

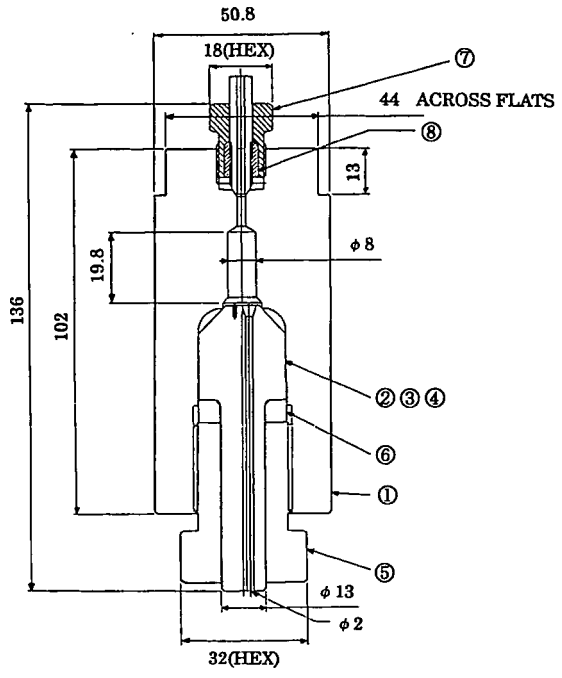

Figure 2. Cross-sectional view of the hydrostatic pressure NMR tube.

IV-N Hydrogen/Deuterium Dynamics in Organic Hydrogen-Bonded Solids

Hydrogen-bonded materials exhibit various dielectric phenomena and phase transitions related to hydrogen/deuterium dynamics. Among them, we focus on 9-hydroxyphenalenone derivatives, which show significant dielectric response caused by intramolecular hydrogen transfer coupled with tautomerization. These compounds show a variety of dielectric ordering phenomena, and are regarded as zero-dimensional hydrogen-bonded dielectrics. Nature of the phase transitions and hydrogen/deuterium dynamics in these compounds are investigated by means of solid state NMR spectroscopy. The origin of the deuterium-induced phase transition found in 5-bromo derivative is of special interest. New 9-hydroxyphenalenone derivatives are also synthesized to search for novel functionality of tautomeric molecules.

IV-N-1 Phase Transitions and Hydrogen/Deuterium Ordering in 9-Hydroxyphenalenone Derivatives in the Solid State

Tomoyuki MOCHIDA, Daisuke KUWAHARA, Seiichi MIYAJIMA and Tadashi SUGAWARA
(Univ. Tokyo)

Temperature dependence of the ^{2}H NMR spectra for single crystals of 5-methyl-9-deuteroxyphenalenone show that the phase transition at T_c = 44 K accompanies doubling of resonance lines, thus the transition is shown to accompany an antiferroelectric deuteron ordering. On the other hand, a powder ^{2}H NMR study on methyl-deuterated 5-methyl-9-deuteroxyphenalenone showed that the methyl group rotates rapidly even at 5 K. Thus the motion of the methyl group is not related to the antiferroelectric phase transition, but the ordering of the locally hydrogen-bonded deuteron is the microscopic origin of this phase transition.

5-Bromo-9-hydroxyphenalenone behaves as a quantum paraelectric material based on hydrogen tunneling. The deuterated derivative, 5-bromo-9-deuteroxyphenalonenone, exhibits deuterium-induced phase transitions; ^{2}H NMR studies on single crystals show that the resonance lines split into two doublets at T_I = 34 K, which indicates that the deuteriums are antiferroelectrically ordered below T_I (Figure 2). With further lowering the temperature, each line becomes broadened and finally splits into four doublets at T_C =22 K. The result supports a model that the incommensurate feature[1] between T_I and T_C originates from an incommensurate tilt of the molecules, which becomes commensurate below T_C to give four crystallographically independent molecules. Thus it is demonstrated that the deuterium-induced phase transition is related to the deuteron ordering, while proton in the hydrogenated compound cannot be ordered due to tunneling motion.

Reference
1) Y. Noda *et al.*, *J. Phys. Soc. Jpn.* **63**, 4286 (1994).

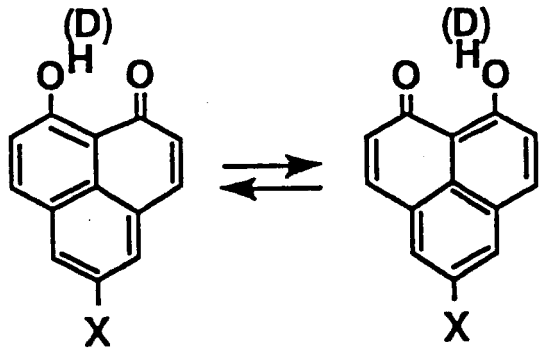

Figure 1. Tautomerization of 9-hydroxyphenalenone derivatives.

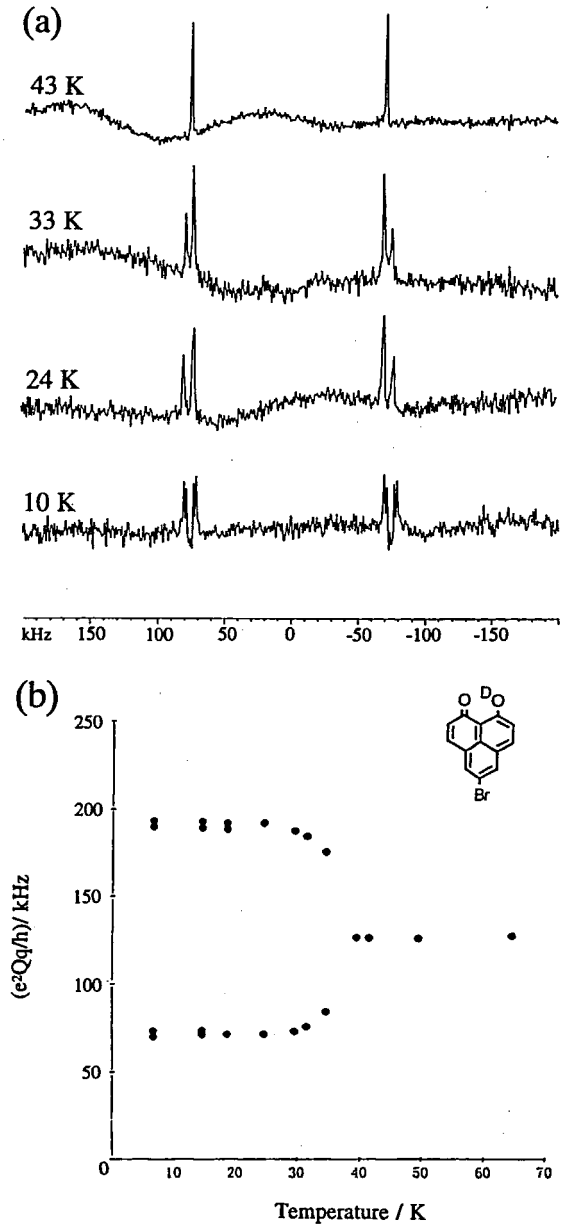

Figure 2. (a) ^{2}H NMR spectrum of a single crystal of 5-bromo-9-deuteroxyphenalenone as function of temperature. (b) Temperature dependence of the quadrupole splitting in the ^{2}H NMR spectrum of a single crystal of 5-bromo-9-deuteroxyphenalenone.

IV-N-2 Structures and Hydrogen Dynamics in 9-Hydroxyphenalenone Derivatives with Additional Hydrogen-Bonding Site at the 5-Position

Tomoyuki MOCHIDA, Daisuke KUWAHARA, Seiichi MIYAJIMA and Tadashi SUGAWARA
(Univ. Tokyo)

In order to control tautomerization by introducing secondary hydrogen dynamics, 9-hydroxyphenalenones with additional hydrogen-bonding substituents at the 5-position are synthesized. The 5-hydroxy derivative forms an infinite ribbon structure through bifurcated hydrogen bond between the 5-hydroxyl group and the β-diketone moiety. A similar ribbon structure was found in the crystals of 5-carboxy derivative (Figure 1(a)). This crystal contained the solvent molecule as a guest in-between the molecular ribbons. In both crystals, ^{13}C CP/MAS NMR spectra showed absence of tautomerization dynamics, which is ascribed to an asymmetric perturbation to the intramolecular hydrogen-bond potential. On the other hand, rapid tautomerization was observed in the crystals of 5-carboxy derivative obtained by sublimation. The structure is characterized by the dimeric structure joined by the carboxyl group (Figure 2(c)). Thus the coupling of the intermolecular proton jump in the carboxylic acid dimer and the intramolecular tautomerization dynamics is of special interest, and is under investigation by means of ^{2}H and ^{17}O NMR spectroscopies.

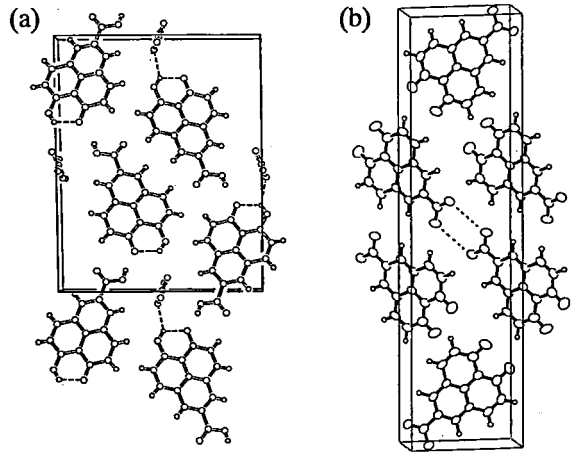

Figure 1. Crystal structures of 5-carboxy-9-hydroxyphenalenone — acetic acid 3:1 inclusion compound (a) and 5-carboxy-9-hydroxyphenalenone (b).

IV-O Electronic Properties of Alkali-Hydrogen-Carbon Systems

In alkali-hydrogen-carbon ternary systems, hydrogen or alkali metal elements exhibit a variety of electronic states when doped or intercalated in the host crystal lattice. An interesting feature is how the hydrogen 1s state contribute to the bulk electronic properties. Structural and electronic properties were studied for sodium-hydrogen-graphite and sodium-hydrogen-C_{60} ternary compounds by means of solid state NMR spectroscopy and the first principle local density functional calculation of the electronic state.

IV-O-1 Theoretical Study on Electronic States of Sodium-Hydrogen-Graphite Ternary Intercalation Compounds

Shin'ichi HIGAI*, Shugo SUZUKI*, Kenji NAKAO*, Seiji MIZUNO, Hironori OGATA and Seiichi MIYAJIMA** *(*Univ. Tsukuba and **Hokkaido Univ.)*

The electronic states of sodium-hydrogen-graphite ternary intercalation compounds (NaH-GICs) have been studied from first principles by constructing several simple structural models based on the experimental results. For all the structural models, the 3s charge of sodium is transferred to hydrogen and carbon, and NaH-GICs are classified into the donor type. Since the charge transfer to hydrogen is incomplete, hydrogen 1s band with small dispersion forms the Fermi surface together with graphite p band.

IV-O-2 ^{13}C NMR Study in Na_4HC_{60} Superconductor

Hironori OGATA, Seiichi MIYAJIMA, Kenichi IMAEDA and Hiroo INOKUCHI

^{13}C NMR studies have been carried out for the Na_4HC_{60} superconductor. The motionally narrowed NMR line at 184 ppm from tetramethyl silane (TMS) observed at room temperature proves that C_{60} molecules are rotating rapidly with respect to the NMR time scale(10^{-4}s). As the temperature is reduced, a powder pattern is observerd. Figure 1 shows the temperature dependence of spin-lattice relaxation rates ($1/T_1$). Below about 150 K, the obtained $1/T_1$ shows Korringa-like temperature dependence (T_1T=280 sK) within experimental accuracy. At about 260 K, a large jump of $1/T_1$ is observed, which is caused by the increase of the density of states at Fermi level, $N(E_F)$, above this temperature. This first order phase transition is observed also by the magnetic susceptibility, ^{23}Na NMR shift and the ^1H spin-lattice relaxation rates. The hyperfine value is expected to be 70 sK above 260 K from the magnetic susceptibility data. The observed $1/T_1$ data in Figure 1 reveals that additional contribution to $1/T_1$ exists both below and above 260 K. They may be attributed to the modulation of the chemical shift anisotropy and the ^{13}C-^1H dipole interaction due to the motions of C_{60} and hydrogen. Figure 2 shows the relationship between the superconducting transition temperature, T_c, and $(T_1T)^{-0.5}$ observed for K_3C_{60} and Rb_3C_{60}, as well as for the present Na_4HC_{60}. The dotted line shows the predicted relationship by the weak-coupled BCS theory extrapolated by the data of K_3C_{60} and Rb_3C_{60}. A slightly less value of $(T_1T)^{-0.5}$ for Na_4HC_{60} suggest that H 1s and/or Na 3s orbitals contribute to the electronic state on the Fermi surface.

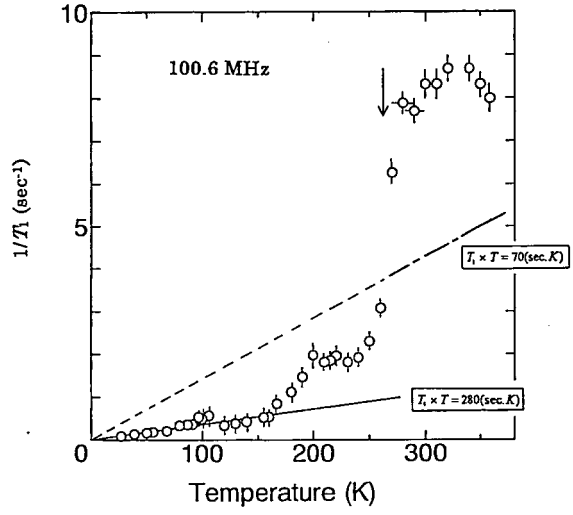

Figure 1. Temperature dependence of $1/T_1$ in Na_4HC_{60} superconductor.

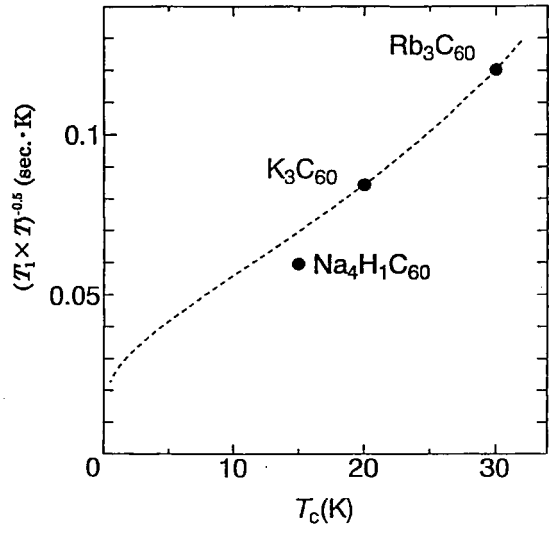

Figure 2. Relationship between $(T_1T)^{-0.5}$ and T_c for K_3C_{60}, Rb_3C_{60} and Na_4HC_{60} superconductors.

IV-P Search for Novel Charge Transfer Complexes Based on BEDT-TTF Type Organic Donors

To search for novel electronic phenomena based on organic donors, we have undertaken systematical investigations into charge transfer complexes based on BEDT-TTF type organic donors and various TCNQ derivatives. In these two component systems, novel electronic phenomena based on BEDT-TTF systems are to be realized by tuning the sizes and/or electron affinities of the acceptors. We focused further on the correlation between the properties of the acceptor and those of the resultant assemblies to obtain hints for designing novel functional materials.

IV-P-1 Synthesis and Properties of CT Complexes of BMDT-TTF Involving Double-Chain Donor Arrangements

Tomoyuki MOCHIDA, Tatsuo HASEGAWA*, Seiichi KAGOSHIMA* and Yoshihiro IWASA**
*(*Univ. Tokyo and **JAIST)*

The structures and properties of unique CT complexes based on bis(methylenedithio)-tetrathiafulvalene (BMDT-TTF) are investigated. Figure 1 shows the crystal structure of (BMDT-TTF)$_2$(ClMe-TCNQ). The complex has a segregated stack structure, characterized by a double-chain conduction column composed of a BMDT-TTF dimer. It is interesting to note that the (BMDT-TTF)$_2$(R_1R_2-TCNQ) [R_1, R_2=Cl, Me; = Cl, H; = Br, Me; = Br, H] series are isostructural. All the complexes are metallic, though they show metal-insulator transitions at low temperatures due to the one-dimensionality of the conduction electronic systems. The magnetic susceptibilities tend to decrease with decreasing temperature after experiencing a broad enhancement.

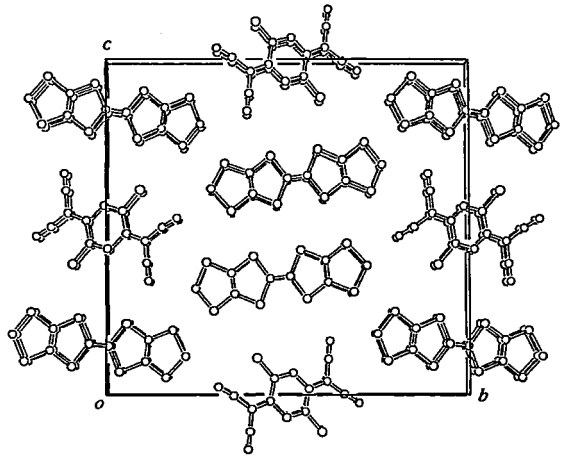

Figure 1. Crystal structure of (BMDT-TTF)$_2$(ClMe-TCNQ), viewed along the stacking axis.

IV-P-2 Electronic States and Anti-Ferromagnetic Order in Mixed-Stack Charge Transfer Compound (BEDT-TTF)(F_2TCNQ)

Tatsuo HASEGAWA*, Seiichi KAGOSHIMA*, Tomoyuki MOCHIDA, S. SUGIURA and Yoshihiro IWASA**** *(*Univ.Tokyo and **JAIST)*

[*Solid State Commun.* **103**, 489 (1997)]

Crystal structure, optical, and magnetic properties are investigated for a unique class of donor-acceptor charge-transfer complex, (BEDT-TTF)(F_2-TCNQ). Charge-transfer from the donor to the acceptor is complete, forming an ionic mixed-stack CT crystal. "Side-by-side" interaction between BEDT-TTF molecules results in a one-dimensional correlated electronic system, which is perpendicular to the donor-acceptor mixed-stack column. Consequently, F_2-TCNQ radical spins are strongly isolated from neighboring molecules, showing Curie-like behavior in magnetic susceptibility followed by an anti-ferromagnetic order at around T_N = 30 K.

IV-Q Photoelectron Spectroscopy of Organic Solids in Vacuum Ultraviolet Region

The works of ultraviolet photoelectron spectroscopy (UPS) and also of UPS with synchrotron radiation light-source (UVSOR-UPS) of organic materials have been proceeded to find their quantitative electronic structures.

IV-Q-1 Ultraviolet Photoemission Spectra of Perchlorate-Doped *cis*- and *trans*-Polyacetylene

Koji KAMIYA,* Takayuki MIYAMAE, Makoto OKU, Kazuhiko SEKI,** Hiroo INOKUCHI, Chizuko TANAKA*** and Jiro TANAKA*****
*(*Chiba Univ., **Nagoya Univ., ***Kanagawa Univ.)*

[*J. Phys. Chem.* **100**, 16213 (1996)]

The UPS spectra of *cis*- and *trans*-polyacetylene were measured by careful treatment of fresh samples. This is the first UPS measurement of *cis*-polyacetylene (*cis*-transiod). Assignments of the observed spectra are given by comparing with energy levels of *cis*- and trans-$C_{20}H_{20}$ obtained by ab initio MO calculation. The change of UPS spectra upon stepwise perchlorate doping was measured; at first the intensity of C2pπ band decreased and the whole band shifted to higher binding energy. By further doping, a new C2pπ band appeared close to the Fermi level E_F when the conductivity reached 11000 S/cm. These change show insulator to metal transition accompanied with structural transformation. The UPS spectrum near E_F showed a strong correlational effect characteristic of a low-dimensional conductor. The spectra of heavily perchlorate-doped and potassium-doped polyacetylene near E_F are analyzed by a theory of Kopietz, Moden and Schönhammer (*Phys. Rev. Lett.* **74**, 2997 (1995)).

IV-R Electrical Conduction and its Related Properties of Organic Solids

Two major categories of organic solids are known to offer the prospect of good electrical conduction. The first group comprises single-component materials; typical examples are polycyclic aromatic compounds and also phthalocyanines. The second group consists of charge-transfer complexes such as the perylene-bromine complexes (donor-acceptor complexes). After the accumulation of large number of works on those charge-transfer complexes, their conductivity ranges from semiconductivity to superconductivity.

To expand the research field of molecular conductors, we always consider to introduce a new category. Recently, with the introduction of gaseous elements such as hydrogen and nitrogen to the charge-transfer complexes, we are finding the third category to produce a new type of molecular conductors.

In this section, therefore, we present the works on the electronic properties of single component organic semiconductors, charge-transfer complexes and also three components organic superconductor based on C_{60}.

IV-R-1 Crystal Structure and Thermodynamic Behavior of Tetrabenzo[*de,hi,op,st*]pentacene Endoperoxide

Akira IZUOKA,* Tomohide MURASE,* Mitsuyoshi TSUKADA,* Yuko ITO,* Tadashi SUGAWARA,* Akira UCHIDA, Naoki SATO*** and Hiroo INOKUCHI** (**Univ. of Tokyo, **Toho Univ., ***Kyoto Univ.)*

[*Tetrahedron Lett.* **38**, 245 (1997)]

Crystal structure of an endoperoxide of tetrabenzo[*de,hi,op,st*]pentacene (TBPA-O_2) was accurately determined by X-ray crystallography (see Figure 1). The unusually long O-O and C-O bonds was rationalized by the characteristics molecular structure of TBPA-O_2. The thermodynamical behavior of addition of oxygen to TBPA and elimination of oxygen from TBPA-O_2 was discussed based on the enthalpy difference between TBPA-O_2 and TBPA + O_2 and the thermodynamic parameters of the extrusion reaction of oxygen from TBPA-O_2.

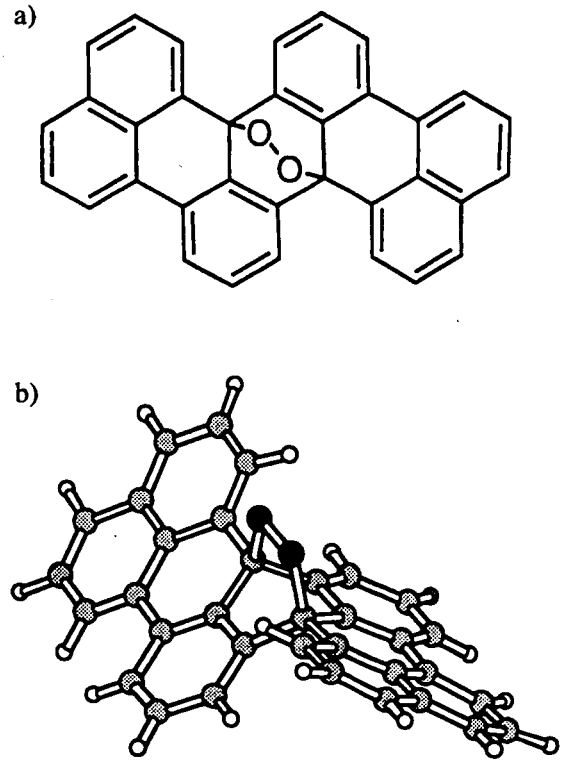

Figure 1. a) TBPA-O_2 and b) its molecular structure.

IV-R-2 Calorimetric Studies of Tetrakis(alkylthio)tetrathiafulvalene, TTC_n-TTF (n=3,8)

Toshiaki TANAKA,* Tooru ATAKE,* Zurong SHI, Chikako NAKANO, Toshiaki ENOKI,* Gunzi SAITO and Hiroo INOKUCHI** (**Tokyo Inst. Tech., **Kyoto Univ.)*

[*J. Phys. Chem. Solids* **58**, 295 (1997)]

The heat capacity of tetrakis(alkylthio)tetrathiafulvalenes (TTC_n-TTF, n=3,8) was measured by adiabatic calorimetry between 10 and 330 K. TTC_3-TTF and TTC_8-TTF had melting points at 306.58 and 322.51 K with enthalpy of fusion of 42.7 and 89.3 kJ mol^{-1}, respectively. The liquid phase of TTC_3-TTF could be cooled down to liquid helium temperature without crystallization, and a glass transition was observed at about 205 K. In the heating run, the supercooled liquid transformed into a metastable solid phase at about 225 K, and then it transformed into the stable solid phase at about 270 K. In the case of TTC_8-TTF (Form II), two solid-solid phase transitions of the first-order type were found at 94.3 and 215.8 K with enthalpy of transition of 0.16 and 4.92 kJ mol^{-1}, respectively. Some thermodynamic functions were derived from the present data, and the numerical tables were given.

IV-R-3 Superconductivity in Sodium-Hydrogen-C_{60} Ternary Compound

Kenichi IMAEDA, Jonas KRÖBER, Hiroo INOKUCHI, Yukako YONEHARA* and Kenji ICHIMURA* *(*Kumamoto Univ.)*

[*Synth. Met.* **85**, 1575 (1997)]

The magnetic properties of the superconducting sodium-hydrogen-C_{60} ternary compound have been investigated by means of SQUID and ESR. The superconducting parameters (the penetration depth λ and the coherence length ξ) are estimated to be λ=2800 Å and ξ=38 Å using $H_{c1}(0)$=90 G and $H_{c2}(0)$=22 T. The spin susceptibility and the ESR linewidth decrease sharply below ~250 K, suggesting the presence of some phase transition.

IV-R-4 Rietveld Analysis of the Superconducting $Na_xH_yC_{60}$

Chikako NAKANO, Kenichi IMAEDA, Jonas KRÖBER and Hiroo INOKUCHI

[*Chem. Lett.* 343 (1997)]

The room temperature structure of a superconducting phase of $Na_xH_yC_{60}$ was determined from the analysis of its powder X-ray diffraction pattern by the Rietveld method. The space group is $Fm\bar{3}m$, with Z=4, and the refined cell parameter a is 14.406(1) Å. Na^+ ions in the octahedral and tetrahedral sites are off-centered. From their occupancies, the composition x is estimated at 3.6.

IV-R-5 Recovery and Enhancement of Superconductivity in the Sodium-Hydrogen-C_{60} Ternary System

Kenichi IMAEDA, Jonas KRÖBER, Chikako NAKANO, Hiroo INOKUCHI and Kenji ICHIMURA *(Kumamoto Univ.)*

[*J. Phys. Chem.* in press]

Sodium-hydrogen-C_{60} ternary compounds have been prepared by intercalation of sodium hydride (NaH) into C_{60}. This method afforded a high-quality superconducting (SC) sample with a large volume fraction, but on the other hand, only a few high-quality SC samples were obtained and most of the samples were nonsuperconducting. However, we have succeeded in transforming a non-SC sample into an SC sample and further in enhancing superconductivity. The Rietveld analysis clarifies that the non-SC phase (α-phase) has an orthorhombic structure, in contrast to a cubic structure for the SC phase (β-phase). The absence of superconductivity in the α-phase will be understood by the broken symmetry.

IV-R-6 Phase Transition and Isotope Effect in $Na_xH_yC_{60}$ Superconductor

Kenichi IMAEDA, Chikako NAKANO and Hiroo INOKUCHI

[*Proceedings of the 23rd Biennial Conf. on Carbon*]

The temperature dependence of powder X-ray diffraction measurement for the superconducting $Na_xH_yC_{60}$ was carried out between room temperature and 100 K. The face centered cubic profile at room temperature starts to be deformed below about 240 K. The 100 K profile can be assigned to a simple cubic with space group $Pa3$ and a lattice constant a=14.185(5) Å by Rietveld analysis. T_c of the deuteride compound prepared by NaD was observed at 12 K, which is a 3 K lower than the hydride compound. The 3 K shift will be explained with the isotope effect ($T_c \propto M^{-0.5}$; M being the ionic mass) predicted by the BCS theory.

IV-R-7 Electronic Structure Calculations of $Na_xH_yC_{60}$

Shugo SUZUKI*, Kenji NAKAO*, Kenichi IMAEDA, Chikako NAKANO and Hiroo INOKUCHI *(*Univ. Tsukuba)*

The electronic structure of a novel compound, $Na_xH_yC_{60}$,[1] is studied by the first-principles calculations based on the density-functional theory within the local-density approximation. It has been elucidated by the Rietveld analysis that x is about 3~4. Also, the results of the thermal desorption spectroscopy have shown that y is about 1. Then, we study the electronic structures of Na_3HC_{60} and Na_4HC_{60}, assuming one Na atom per site for the tetrahedral sites and one H atom per site for the octahedral sites in both Na_3HC_{60} and Na_4HC_{60}, while one Na atom per site for the octahedral sites of Na_3HC_{60} in contrast with two Na atoms per site for the octahedral sites of Na_4HC_{60}.

The results of the electronic structure calculations are shown in Figure 1: (a) for Na_3HC_{60} and (b) for Na_4HC_{60}. The Fermi levels are shown by the dashed

lines. It is found that new bands shown by open circles in the figure appear in addition to the bands derived from the lowest unoccupied molecular orbitals (LUMO) of the C_{60} molecules shown by closed circles in the figure. The new bands are found to be mainly composed of the 1*s* orbitals of the H atoms. It is, however, shown that, because of considerably large mixing between the LUMO of the C_{60} molecules and the 1s orbitals of the H atoms, the H atoms are in the negatively charged state of $H^{0.2-} \sim H^{0.3-}$. This means that the conduction electrons exist on the H atoms in agreement with the experimental observations such as large isotope effects on the superconducting transition temperatures by the substitution of deuterium for hydrogen.

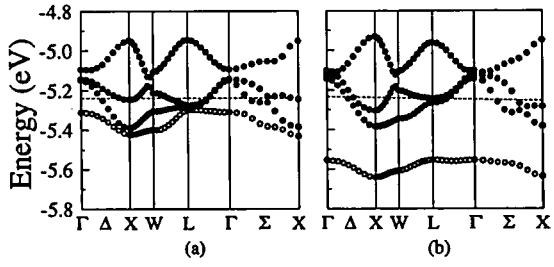

Figure 1. Electronic structures of (a) Na_3HC_{60} and (b) Na_4HC_{60}. The open circles show new bands derived from the 1*s* orbitals of the H atoms and the closed circles show the bands derived the lowest unoccupied molecular orbitals of the C_{60} molecules. The dashed lines show the Fermi levels.

Reference

1) K. Imaeda, J. Kröber, H. Inokuchi, Y. Yonehara and K. Ichimura, *Solid State Commun.* **99**, 479 (1996).

IV-S NMR Study of Functional Interactions in Molecular Based Solids: Magnetic, Electronic, and Dynamic Interactions

Control of functional interactions such as magnetic, electronic and dynamic one is a key to produce new functional materials. It is important to study the possibility of the functional interactions. The nuclear magnetic resonance provides microscopic aspects of the functional interactions in the solid state. Hydrogen bond has a great capability for mediating a variety of functional interactions. For example we found the magnetic interaction through the hydrogen bond for several organic ferromagnetic materials. And proton transfer tunneling in the interacting hydrogen bonds, which are connected by organic π-conjugated system, was also found. This interaction is a key point for propagating information of one hydrogen bond to the other hydrogen bond through molecular frame. The organic π-conjugated system with metallic ions is also expected to produce a new function. Organometallic conjugated system was investigated, i.e. magnetic property of linear multinuclear metal complexes and thermochromism of organometallic complex.

IV-S-1 Solid State ^{1}H-MAS-NMR and Spin Densities on Protons of the Organic Ferromagnetic Tempo Derivatives

Goro MARUTA *(Osaka Univ.)*, **Sadamu TAKEDA** *(Gunma Univ. and IMS)*, **Takashi KAWAKAMI** *(Osaka Univ.)*, **Wasuke MORI** *(Kanagawa Univ.)*, **Ron IMACHI** *(Univ. Electro-Commun.)*, **Takayuki ISHIDA** *(Univ. Electro-Commun.)*, **Takashi NOGAMI** *(Univ. Electro-Commun.)* **and Kizashi YAMAGUCHI** *(Osaka Univ.)*

[*Mol. Cryst. Liq. Cryst.* in press]

Ferromagnetism in purely organic materials attracts a grate interest, since Kinoshita *et al.* reported a molecular ferromagnet at low temperature.[1] Most examples of organic ferromagnetic crystals are based on nitroxide (N-O) radicals. Main interest of this field is to control the intermolecular magnetic interaction between N-O radical groups in crystal to produce the ferromagnetic ordering. As a possible intermolecular ferromagnetic interaction path, a close contact of methyl and/or methylene protons to N-O radical group of adjacent molecules in crystal has been proposed from X-ray diffraction experiment.[2] The methyl and methylene protons are expected to be intermolecular ferromagnetic exchange coupler via spin polarization mechanism (NO(↑)-C(↓)-C(↑)-H(↓)•••NO(↑)). The electron spin polarized on the proton is a key point.

Electron spin densities on hydrogen atoms of 4-(arylmethyleneamino)-2,2,6,6-tetramethylpiperidin-1-oxyls (abbreviated as Ar-CH=N-TEMPO), which show ferromagnetic behavior at low temperatures, were determined in their crystal phases from the temperature dependence of the Fermi contact shift measured by high speed magic angle spinning proton nuclear magnetic resonance. This method revealed a large negative hyperfine coupling constant for the methyl and methylene protons, A = -1.0 MHz for Ar = *p*-Cl-ph and A = -1.3 MHz for Ar = ph, and very small one for the aryl group protons, |A| < 0.01 MHz for p-Cl-ph and A = +0.1 MHz for ph. The observed negative hyperfine coupling constant (negative spin density) of methyl and methylene protons matches with spin alternation for the intermolecular spin polarization mechanism through the contact of methyl and/or methylene protons to adjacent N-O radical group. This contact potentially contributes to the intermolecular ferromagnetic interaction.

References

1) M. Kinoshita, P. Turek, M. Tamura, Y. Nozawa, D. Shiomi, Y. Nakazawa, M. Ishikawa, M. Takahashi, K. Awaga, T. Inabe and Y. Maruyama, *Chem. Lett.* 1225 (1991).
2) T. Nogami, T. Ishida, M. Yasui, F. Iwasaki, N. Takeda, M. Ishikawa, T. Kawakami and K. Yamaguchi, *Bull. Chem. Soc. Jpn.* **69**, 1841 (1996).

IV-S-2 Thermochromism and Dynamics of Organometallic Conjugated System:

Zirconocene Complex of 1,4-Diphenyl-1,3-butadiene

Sadamu TAKEDA *(Gunma Univ. and IMS)*, **Hiroki FUKUMOTO** *(Osaka Univ.)*, **Kazushi MASHIMA** *(Osaka Univ.)*, **Goro MARUTA** *(Osaka Univ.)*, **Kizashi YAMAGUCHI** *(Osaka Univ.)* **and Akira NAKAMURA** *(Osaka Univ.)*

[*J. Phys. Chem.* **101**, 278 (1997)]

Conjugation in organic compounds is represented by extended pπ-pπ interactions. Trans-polyacetylene is typical and fascinating one-dimensional conjugated system. Many interesting physical and chemical properties have been found for this pπ conjugated system upon doping. A modified conjugation and/or doping category can be seen in organometallic systems, in which extended π-interaction involving metal-carbon bonding is realized.[1] The uniqueness of the organometallic π-systems containing various transition metals exists because of their large variety of the electronic and molecular structures. An example is metal π-complexes of organic conjugated systems. Particularly polyene complexes of early transition metals such as zirconium are interesting, since these electron-deficient metal ions are highly reactive and thus the polyene system may be largely perturbed by the bonding with zirconium which is both electron-donating (π-type) and -attracting (σ-type) in varying degrees. The situation is basically different from the simple doping of conventional conjugated systems.

We observed the thermochromism of the deeply colored zirconocene complex of 1,4-diphenyl-1,3-butadiene (DPBD) in the solid state. The color of the polycrystals of this complex is in between deep red and deep purple and changes continuously as the temperature is decreased from room temperature to liquid nitrogen temperature, while the precursors of the complex, $ZrCp_2Cl_2$ and 1,4-diphenyl-1,3-butadiene, are almost colorless. Variable temperature ^{13}C-CP/MAS NMR spectroscopy revealed that a remarkable change of the electronic structure of the DPBD molecule by constructing the complex propagates all over the carbon sites and that the distortion of the electronic structure of the complex becomes continuously large as temperature is decreased. This phenomenon is closely related to the thermochromism. The mechanism of the temperature variation of the electronic structure of the complex was attributed to the dynamics of phenyl ring and cycropentadienyl ring of the complex. Fast rotation of the cyclopentadienyl ring around its five fold axis with the extremely small activation energy of 28 meV (= 2.6 kJ/mol) and 180°-flip rotation of the phenyl ring about the C-C bond with the activation energy of 84 meV (= 7.7 kJ/mol) were recognized by the measurement of the spin-lattice relaxation rate of proton NMR. Quasielastic neutron scattering experiment suggests a small angle flipping of the phenyl ring, which is much faster than the two motional modes mentioned above. Semiempirical ZINDO molecular orbital calculation revealed that the deep color of the complex originates in the HOMO-LUMO and HOMO-LUMO+1 transitions. These molecular orbitals consists of d-orbitals of zirconium and π-orbital of organic components and are sensitive to the orientation of the π-orbital of cycropentadienyl rings, suggesting that the dynamic perturbation is operative for the transition energies.

Reference

1) A. Nakamura, *Bull. Chem. Soc. Jpn.*, **68**, 1515 (1995).

IV-S-3 Synthesis and Gas-Occlusion Property of Dinuclear Molybdenum (II) Dicarboxylates

Satoshi TAKAMIZAWA *(Osaka Univ.)*, **Masatoshi FURIHATA** *(Kanagawa Univ.)*, **Wasuke MORI** *(Kanagawa Univ.)*, **Sadamu TAKEDA** *(Gunma Univ. and IMS)* **and Kizashi YAMAGUCHI** *(Osaka Univ.)*

[*Inorg. Chim. Acta* submitted]

Molybdenum (II) ions form anti-ferromagnetically coupled dinuclear complexes with a variety of carboxylate anions. The dinuclear complex has four carbxylate ligands in a plane perpendicular to the axis of dimuclear metal ions. Employing dicarboxylate dianions as ligand, we obtained new complex with super structure, in which dinulear complexes were linked together by dicarboxylate dianions to form infinite squared lattice plane and the planes were stacked to construct micropore or channel structure. We also found that gas molecules, such as butane and neopentane, were greatly adsorbed in this channel. The gas occlusion property of several newly constructed complexes were investigated by solid state NMR technique. The ^{13}C-CP/MAS NMR probes the local structure of the host lattice complexes and the environment of the guest molecules. For terephthalate complex, the ^{13}C-CP/MAS NMR signal of 2,3,5,6- phenyl carbons significantly shifted to lower field by 0.8 ppm with adsorbing n-butane, while other signals including carboxyl carbon remained almost constant. This result indicate that the occluded molecules apparently interact with 2,3,5,6-phenyl carbons. The line width showed no significant broadening, suggesting homogeneous change of the environment of the benzene ring of all the terephthalate ligands which construct the channel lattice. The chemical shift returned to the original one, as the occluded n-butane molecules were removed by evacuation. The change of the local structure of the host lattice due to the occlusion of n-butane is reversible. Two additional peaks corresponding to the methyl and methylene groups of n-butane appeared at 24.8 and 13.4 ppm, respectively. The line width of the n-butane is small, suggesting rapid motion of the molecule in the host lattice. In case of other gas molecules such as neopentane, very similar behavior was observed.

IV-S-4 Determination of the Electron Spin Density Distribution and Magnetic interaction Path in 4-(Hydroxyimino)-TEMPO Crystal by Solid State High Speed Magic Angle Spinning D-NMR

Goro MARUTA *(Osaka Univ.)*, **Sadamu TAKEDA** *(Gunma Univ. and IMS)*, **Ron IMACHI** *(Univ. Electro-Commun.)*, **Takayuki ISHIDA** *(Univ. Electro-Commun.)*, **Takashi NOGAMI** *(Univ. Electro-Commun.)* **and Kizashi YAMAGUCHI** *(Osaka Univ.)*

Electron spin densities on hydrogen atoms of 4-(hydroxyimino)-TEMPO, which has been recently found to be a molecular ferromagnet at low temperature, were determined in the crystalline phase from the temperature dependence of the Fermi contact shift measured by D-MAS-NMR. Large negative hyperfine coupling constant, A_D (A_D= –0.55MHz), observed for the NOD group implies that spin polarization mechanism works via intermolecular hydrogen bond. Positive hyperfine coupling constant (A_D= +0.12MHz) for axial CD_3 groups indicates that single occupied MO spreads out toward the direction of axial methyl groups by hyperconjugation, while the equatorial methyl groups show negative coupling constant (A_D= –0.24MHz). From these direct observation of the spin density distribution on the magnetically coupled molecules in crystalline phase, the magnetic interaction path for the ferromagnetic coupling was discussed. MAS heating problem and the calibration of the thermometer which we employed were also discussed.

IV-S-5 Proton Dynamics in Interacting Hydrogen Bonds in Crystals: Proton Tunneling in the NHO Hydrogen Bonds of N,N'-Di(2-hydroxy-1-naphthylidene)-*p*-phenylenediamine

Sadamu TAKEDA *(Gunma Univ. and IMS)*, **Tamotsu INABE** *(Hokkaido Univ.)*, **C. BENEDICT** *(Freie Univ. Berlin)*, **U. LANGER** *(Freie Univ. Berlin)* **and H. H. LIMBACH** *(Freie Univ. Berlin)*

Knowledge of proton-transfer quantum dynamics in hydrogen bonds is necessary for understanding many important chemical and biological processes. An effect of interaction between two hydrogen bonds on the proton transfer dynamics is also important for propagation of information through molecular frame. N,N'-Di(2-hydroxy-1-naphthylidene)-p-phenylenediamine, which is abbreviated by DNP, has two NHO hydrogen bonds in the molecule and may be a candidate of a system of interacting hydrogen bonds. Combination of the two possible forms, OH and NH forms, of the two hydrogen bonds in DNP molecule leads to four tautomeric forms, i.e. [OH, OH], [OH, NH], [NH, OH] and [NH,NH]. Proton-transfer quantum tunneling in NHO hydrogen bonds was investigated by ^{1}H-NMR relaxation and ^{15}N-CP/MAS NMR spectrum which was measured down to 26 K with ultra-low temperature CP/MAS probe for ^{15}N-enriched DNP. Temperature variation of ^{15}N chemical shift indicates the fast exchange between NH form (-NH-) and OH form (=N-) even at 26 K. T_1 of ^{1}H and ^{15}N chemical shift were analyzed by four-site exchange model with tunneling effects. The result suggests that the form of one hydrogen bond, OH or NH form, affects the potential energy function hindering the proton transfer motion in the other hydrogen bond of DNP molecule. The information of one hydrogen bond propagates to the other hydrogen bond through the molecular frame.

IV-S-6 Solid State High Resolution 2H-NMR Study of Spin Density Distribution in Hydrogen-Bonded Organic Ferromagnet HQNN

Goro MARUTA *(Osaka Univ.)*, **Sadamu TAKEDA** *(Gunma Univ. and IMS)*, **Akifumi ODA** *(Osaka Univ.)*, **Michio M. MATSUSHITA** *(Univ. Tokyo)*, **Akira IZUOKA** *(Univ. Tokyo)*, **Tadashi SUGAWARA** *(Univ. Tokyo)* **and Kizashi YAMAGUCHI** *(Osaka Univ.)*

Spin density distribution in the organic magnetic crystals, α-HQNN, β-HQNN and RSNN were determined from the temperature dependence of the contact shifts in solid state ^{1}H-MAS-NMR and ^{13}C-CP/MAS-NMR spectra. Solid state ^{2}H-MAS-NMR of deuterated hydrogen bonds revealed remarkably large spin density on hydroxyl groups which were considered to mediate the intermolecular magnetic interaction. On the basis of the experimental results, the microscopic intermolecular magnetic interaction path in the crystals were discussed in conjunction with the quantum chemistry calculations.

IV-T Electronic Structures and Physical Properties of Quasi-One- Dimensional Halogen-Bridged Mixed-Valence Metal Complexes

Recently quasi-one -dimensional halogen-bridged mixed-valence compounds (MX-chains) have been extensively investigated because they show very interesting physical properties such as an intense intervalence charge transfer band, an overtone progression in resonance Raman spectra, a luminescence with Stokes-shift, midgap absorptions attributable to solitons or polarons, large third-order nonlinear optical susceptibilities, one-dimensional model compounds of high Tc copperoxide superconductivities, etc,. These compounds are considered as Peierls-Hubbard system where the electron-phonon interaction (S), the electron transfer (T), the on-site and inter-site Coulomb interactions (U and V) are cooperated or competed with one another. Compared with other inorganic and organic compounds, these MX-chains have characteristic points as follows; (1) The magnitudes of the physical parameters (S,T,U and V) and/or the band gaps can be tuned by substituting the metal ions, bridging halogens, in-plane ligands, and counteranions; (2) The interchain interactions can be controlled by using the hydrogen-bonds from one- to three-dimensionally. Therefore we can anticipate the interesting physical properties in these compounds.

IV-T-1 Electronic Structure of the Quasi-One-Dimensional Halogen-Bridged Ni Complexes

Hiroshi OKAMOTO, Yuji SHIMADA, Yasuo OKA, Ashish CHAINANI, Takashi TAKAHASHI *(Tohoku Univ.)*, **Hiroshi KITAGAWA, Tadaoki MITANI** *(JAIST)*, **Koshiro TORIUMI** *(Himeji Inst. Tech.)*, **Kazuo IOUE, Toshio MANABE** *(Nagoya Univ.)* **and Masahiro YAMASHITA** *(Nagoya Univ. and IMS)*

[*Phys. Rev. B* **54**, 8438 (1997)]

The electronic structure of the one-dimensional Ni complexes, $[Ni(chxn)_2X]X_2$(X=Cl, Br, (chxn)=1R,2R-cyclohexanediamine), is studied by using optical spectroscopy, x-ray photoelectron spectroscopy (XPS) and Auger electron spectroscopy. The optical spectra show that the Br compounds have a smaller gap as compared with the Cl compounds. An analysis using a simple X-Ni-X trimer model on the optical spectra and the Ni 2p XP spectra yields quantitative estimates for the charge transfer (CT) energy Δ and the transfer energy T for discrete and one-dimensional Ni complexes. The analysis on the Ni LVV Auger spectra in conjunction with the valence XP spectra indicates that the average on-side d-d Coulomb energy U in the one-dimensional and discrete Ni complexes is about 5 eV, quite similar to the case of the Ni dihalides. The obtained results demonstrate that the one-dimensional Ni complexes are CT insulators. We discuss the differences in the electronic structures of the one-dimensional Ni complexes with the Ni dihalides and the one-dimensional Pt complexes on the basis of the estimated parameter values of Δ, T, and U.

IV-T-2 Dynamics of Photoinduced Gap States and Self-Trapped Excitons in the MX Chain Compounds with Degenerate and Non-Degenerate CDW Ground States

Hiroshi OKAMOTO, Yuji SHIMADA Yoshio KAGA, Yasuo OKA *(Tohoku Univ.)*, **Masahiro YAMASHITA** *(Nagoya Univ. and IMS)*, **Toshio MANABE** *(Nagoya Univ.)* **and Tadaoki MITANI** (JAIST)

[*Synth. Met.* **86**, 1293 (1997)]

We have characterized the photoinduced gap states from the photoinduced absorption (PA) spectroscopy in the halogen (X)-bridged metal (M) complexes having degenerate CDW state, $([Pt(en)_2][Pt(en)_2X_2](ClO_4)_4$: X=Cl, Br) and those having non-degenerate CDW state, $([Pt(en)_2][Pt(en)_2X_2](ClO_4)_4$: X=Br, I). In the former complexes, observed are the two midgap bands named as A and B, which have been assigned to spin-solitons, while in the latter complexes,photogenerations of solitons are suppressed. Photogenerations of polarons have been detected in both types of complexes. We have also investigated the excitation profiles of the luminescence from the self-trapped excitons, which are compared with those of the PA signals due to the gap states. The results demonstrate that the luminescence process strongly competes with the dissociation process to spin-soliton pairs followed by nonradiative recombinations.

IV-T-3 Determination of the Electronic Structure in the Strongly Correlate 1-D Electron Systems: X-Ray Photoelectron and Auger Spectroscopy of Halogen-Bridged Nickel Complexes

Hiroshi OKAMOTO, Ashish CHAINANI, Takashi TAKAHASHI *(Tohoku Univ.)*, **Hiroshi KITAGAWA, Tadaoki MITANI** *(JAIST)*, **Toshio MANABE** *(Nagoya Univ.)* **and Masahiro YAMASHITA** *(Nagoya Univ. and IMS)*

[*Synth. Met.* **86**, 2136 (1997)]

The electronic structure of the 1-D Ni complexes, $[Ni(chxn)_2X]X_2$ (X=Br, Cl) is studied together with discrete Ni complexes, $[NiX_2([14]aneN_4)]ClO_4$ (X=Br, Cl), using X-ray photoelectron spectroscopy (XPS) and Auger electron spectroscopy (AES). An analysis using a simple X-Ni-X trimer model on the Ni 2p XP spectra yields quantitative estimates for the charge transfer (CT) energy Δ and the transfer energy T. An analysis on the Ni LVV Auger spectra indicates that the average on-site Coulomb energy U in these Ni complexes is about 5 eV. The obtained results demonstrate that the 1-D Ni complexes are CT insulators.

IV-T-4 The Metallic State in a MMX-Chain Complexes, Pt2(dta)4I

Hiroshi KITAGAWA, Noriaki ONODERA, Jeung-SUN ANN, Tadaoki MITANI *(JAIST)*, **Koshiro TORIUMI** *(Himeji Inst. Tech.)* **and Masahiro YAMASHITA** *(Nagoya Univ. and IMS)*

[*Synth. Met.* **86**, 1977 (1997)]

Transport, optical, magnetic, and structural properties of MMX-type halogen-bridged mixed-valence complex, $Pt_2(dta)_4I$(dta=CH_3CS_2) were investigated. This complex exhibits metallic conduction between 300 K, which is the first observation in halogen-bridged 1-D transition-metal complexes. Below 300 K, a metal-semiconductor transition was observed. This salt undergoes an order-disorder phase transition at 340 K. The mixed-valence state is discussed.

IV-T-5 Competition between Electron-Correlation in Ni(III) and Electron-Lattice Interaction in Pd(II)-Pd(IV) in Mixed-Metal MX-Chain, $Ni_{1-x}Pd_x(chxn)_2Br_3$

Toshio MANABE, Takuya KAWASHIMA *(Nagoya Univ.)*, **Masahiro YAMASHITA** *(Nagoya Univ. and IMS)*, **Hiroshi OKAMOTO** *(Tohoku Univ.)*, **Hiroshi KITAGAWA, Tadaoki MITANI** *(JAIST)*, **Makoto INOKUCHI and Kyuya YAKUSHI**

[*Synth. Met.* **86**, 2233 (1997)]

The electrical conductivities, IR, XPS and resonance Raman spectra of a series of Ni-Pd mixed-metal MX-chain compounds, $Ni_{1-x}Pdx(chxn)_2Br_3$ have been measured in order to investigate the competition be-

tween the electron-correlation in Ni(III) and the electron-lattice interaction in Pd(II)-Pd(IV) states. In these compounds, at x=0.4, the activation energy in electrical conductivity is minimized. And at x=0.4 or below, the ν N-H does not split, while at x with larger than 0.5, ν N-H shows triplet. This result suggests that the Pd(II)-Pd(IV) mixed-valence states are effectively influenced by Ni(III) states, approaching toward the Pd(III) states.

IV-T-6 Dynamics of Solitons and Polarons in the Quasi-One-Dimensional MX Chain Compound $[Pt(en)_2][Pt(en)_2I_2](ClO_4)_4$

Hiroshi OKAMOTO, Yasuo OKA *(Tohoku Univ.),* **Tadaoki MITANI** *(JAIST)* **and Masahiro YAMASHITA** *(Nagoya Univ. and IMS)*

[*Phys. Rev. B* **55**, 6330 (1997)]

The dynamics of solitons and polarons have been studied in a $[Pt(en)_2][Pt(en)_2I_2](ClO_4)_4$ single crystal using photoinduced infrared absorption measurements. The annihilation process of the gap states is well explained by the bimolecular recombination model. Both carriers are long lived at low temperatures due to their finite pinning energies, and their decay characteristics are strongly temperature dependent. The temperature dependences of the rate constant of recombination for both carriers clearly show a crossover of the transport mechanism from hopping to tunneling with decrease of temperature. This behavior of the gap states is in contrast to that observed in transpolyacetylene.

IV-U Low-Dimensional Magnetic Systems

Low-dimensional magnetic systems are of current interest because they show peculiar quantum effects. A striking phenomenon is the strong spin-dependent behavior at T=0, of the one-dimensional Heisenberg antiferromagnet (1D-HAF). Haldane predicted that for the integer spin values S ,1D-HAF exhibits a singlet ground states separated from the first triplet excited state with an energy gap Eg (Haldane gap), while for the half-integer spin values S, the 1D-HAF has a gapless spectrum of the excitation. Although there have been many theoretical works on low-dimensional magnetic systems, only a few systematic works on syntheses and measurements have been carried out.

IV-U-1 S=1 New Haldane Gap Systems and Spin Glass Behaviors: Syntheses, Structures and Magnetic Properties of Linear-Chain Ni(II) Complexes

Toshio MANABE, Tachi. OHISHI *(Nagoya Univ.),* **Masahiro YAMASHITA** *(Nagoya Univ. and IMS),* **Tetsuya TAKEUCHI** *(Osaka Univ.),* **Taturu YOSHIDA** *(Nakanihon Automotive College),* **Yan YU, Zentaro HONADA and Koichi KATSUMATA** *(RIKEN)*

[*Synth. Met.* **85**, 1717 (1997)]

A series of compounds, $[Ni(AA)_2X]Y$ (AA= diamines etc; X=N_3 and NO_2; Y=ClO_4, PF_6 etc) with S=1 have been synthesized, and their magnetic properties and crystal structures have been investigated. They have linear-chain structures. It has been found that the magnitude of the Haldane gaps can be controlled by substituting the bridging groups (X) and in-plane ligands (AA). On the other hand, $[Ni([15]aneN_4)N_3]$-PF_6, $[Ni([14]aneN_4)N_3]ClO_4 \cdot H_2O$ and $[Ni(en)_2NO_2]BF_4$ show spin glass behaviors.

IV-U-2 Inducing a Magnetic Ordering in the Haldane Material $Ni(C_5H_{14}N_2)_2N_3(ClO_4)$ by Magnetic Field

Zentaro HONDA, Koichi KATSUMATA *(RIKEN),* **Tachi OHISHI, Toshio MANABE** *(Nagoya Univ.)* **and Masahiro YAMASHITA** *(Nagoya Univ. and IMS)*

[*J. Phys. Condens. Matter* **9**, L83 (1997)]

From a heat capacity measurement in high magnetic fields and low temperatures, we have obtained evidence for a magnetic ordering in the S =1 quasi-one dimensional Heisenberg antiferromagnet $Ni(C_5H_{14}N_2)_2$-$N_3(ClO_4)$. The transition temperature is ~0.6 K at 12 T parallel to the chain axis.

IV-V Organic-Inorganic Hybrid-Type Charge Transfer Complexes

Organic-inorganic hybrid-type charge transfer complexes have been the forcus of much recent research . In these complexes, it is expected that two different electronic states of d and π are coupled to each other, which may provide a unique opportunity for constructing of novel electronic systems.

IV-V-1 Physical Properties of Quasi-One-Dimensional Charge-Transfer Metal Complexes; $[M(HBQD)_2]TCNQ$(M=Ni, Pd; H_2BQD=1,2-Benzoquinoedioxime)

Yuka KAGAMI, Fumiyasu IWAHORI, Tachi OHISHI, Tetsuo HAMA, Toshio MANABE *(Nagoya Univ.),* **Masahiro YAMASHITA** *(Nagoya Univ. and IMS),* **Hiroshi KITAGAWA, Ken-ichi SAKAI and Tadaoki MITANI** *(JAIST)*

[*Synth. Met.* **86**, 1803(1997)]

We have investigated the physical properties of $[M(HBQD)_2]TCNQ$ (M=Ni, Pd; H_2BQD=1,2-benzoquinonedioxime) which consist of alternating -D-A-D-A- type stackings of transition-metal-complex donors and organic TCNQ acceptors. The degree of charge-transfer for each sample was estimated to be -0.1 from the results of IR, Raman spectra, and bond length of TCNQ. From XPS measurements, the valence state of Ni or Pd was found to be transformed at low temperature from +II to the mixed valency of +II, +III or +II,+IV, respectively. This behavior can be considered to be due to the charge-transfer from d-orbital of the transition metal to π–antibonding orbital of the HBQD ligands, which was comfirmed by lower-energy shift of IR stretching modes of C=N in HBQD. This temperature-induced charge-transfer between transition metal and ligand is the first observation in the transition-metal-complex assemblies.

RESEARCH ACTIVITIES V
Department of Applied Molecular Science

V-A Molecular Mechanisms of Oxygen Activation by Heme Enzymes

By sharing a common prothetic group, the heme enzymes such as cytochromes P450, peroxidases, and catalases catalyze their own unique biological functions; monooxygenation, hydrogen peroxide dependent oxidation, and dismutation of hydrogen peroxide, respectively. Our efforts have been focused on the elucidation of the structure-biological function relationship of those heme enzymes by employing both enzymic systems including mutants and their synthetic model systems.

V-A-1 Effects of Concerted Hydrogen Bonding of Distal Histidine on Active Site Structures of Horseradish Peroxidase. Resonance Raman Studies with Asn70 Mutants

Masahiro MUKAI, Shingo NAGANO *(Kyoto Univ.)*, **Motomasa TANAKA** *(Kyoto Univ.)*, **Koichiro ISHIMORI** *(Kyoto Univ)*, **Isao MORISHIMA** *(Kyoto Univ.)*, **Takashi OGURA, Yoshihito WATANABE and Teizo KITAGAWA**

[*J. Am. Chem. Soc.* **119**, 1758 (1997)]

Effects of a highly conserved hydrogen bond between the distal histidine (His) and a nearby aspargine residue (Asn) of peroxidases upon the active site structures were investigated using resonance Raman (RR) and EPR spectroscopy. Although there is no crystallographic data for horseradish peroxidase (HRP), Asn70 is deduced to be the hydrogen bond acceptor for HRP. Accordingly, site-directed mutagenesis of Asn70 to Val (N70V) and to Asp (N70D) was carried out with HRP, and their RR spectra were compared with those of native and wild type (WT) enzymes in the resting, reduced, CN-bound ferric and compound II states. In the resting state, the six-coordinate high-spin structure is the main component for N70V and N70D mutants, while the five-coordinate high-spin structure is dominant for the native and WT HRPs. This was confirmed with EPR spectra. The Fe^{III}-CN stretching (ν_{Fe}-CN) and bending RR bands for the linear and bent forms were identified using $^{12}C^{15}N$ and $^{13}C^{14}N$ isotopes. The ν_{Fe}-CN frequency of the linear form is lower for the mutants than for native enzyme, and the spectral patterns of the mutants at pH 7.0 resemble that of the basic form of native HRP. The Fe-histidine stretching bands of reduced HRPs exhibit pH dependent frequency shifts, and the midpoint pH values were 7.2, 5.9, and 5.5 for native, N70V, and N70D, respectively. This change is ascribed to the acid-base transition of the distal His. While the Fe^{IV}=O stretching (ν_{Fe}=O) frequency of compound II at pD 7.0 is lower than that at pD 10.0 for native enzyme, the ν_{Fe}=O band of the mutants show no pH dependent frequency shifts between pD 7.0 and pD 10.0. However, the H_2O/D_2O frequency change of ν_{Fe}=O and the oxygen atom exchange with bulk water suggested the presence of the hydrogen bond between the oxygen ligand of the ferryloxo heme and distal His for these mutants at pD 10.0. On the basis of these observations, it is proposed that the hydrogen bond between the N_δ-proton of distal His and Asn70 regulates the p*K*a of the N_ε-proton (and thus the reactivity of compound II at the distal side) and also affects the Fe-His bond at the proximal side via tertiary structure changes.

V-A-2 Conversion of Myoglobin into a Highly Stereospecific Peroxygenase by L29H/H64L Mutation

Shin-ichi OZAKI, Toshitaka MATSUI and Yoshihito WATANABE

[*J. Am. Chem. Soc.* **118**, 9784 (1996)]

Myoglobin (Mb), normally a carrier for molecular oxygen can catalyze hydrogen peroxide supported peroxygenation of a variety of substrates, including olefin epoxidation and thioether sulfoxidation. However, the turnover numbers for sulfoxidation by Mb are lower than the values obtained by the incubation with peroxidases. Catalysis by Mb is presumably associated with an intermediate equivalent to compound I of peroxidase; however, the exact location of one of the two oxidation equivalents has not clearly been defined yet. To identify active site residues controlling ferryl oxygen transfer reactions, we have performed site-directed mutagenesis studies of sperm whale Mb. Mutating Leu29 to a histidine residue improves the rate and enantioselectivity for the oxidation of thioanisole. The rate increases versus wild type Mb are 15-fold and 22-fold for L29H and L29H/H64L Mb, respectively. On the contrary, the elimination of His64 in the distal pocket causes about 70% decrease in the oxidation rate with respect to the recombinant wild type Mb. The dominant formation of *R* by the mutation is in contrast with 97% ee for S enantiomer given by F41L HRP. The extremely high stereoselectivity with 97% incorporation of ^{18}O from $H_2{}^{18}O_2$ into the sulfoxide for L29H/H64L Mb clearly indicates the ferryl oxygen transfer to thioanisole and rules out the involvement of molecular oxygen and hydroxyl radical. Regardless of the size and electronic properties for *para* substituents of thioanisole, the L29H/H64L mutant oxidizes sulfides faster than the wild type with higher enantioselectivity.

V-A-3 Catalytic Intermediates of Polyethylene Glycolated Horseradish Peroxidase in Benzene

Shin-ichi OZAKI, Yuji INADA *(Toin Univ. Yokohama)* **and Yoshihito WATANABE**

[*Keio J. Med.* **45**, S68 (1996)]

Horseradish peroxidase (HRP) catalyzes the oxidation of a variety of aromatic substrates utilizing hydrogen peroxide, and it is found to be catalytically active in not only aqueous but also nonaqueous media. However, the reaction intermediates in organic solvents have not been clearly defined. Thus, we report here the UV-visible spectra of compound I and II for HRP dissolved in benzene by rapid scanning spectroscopy. HRP is solubilized in benzene homogeneously by the covalent modification of lysine residues with polyethylene glycol. The addition of a stoichiometric quantity of hydrogen peroxide to polyethylene glycolated horseradish peroxidase (PEG-HRP) in benzene gave the compound I chromophore. In the presence of a large excess of guaiacol, compound I is first reduced to compound II, then to the ferric enzyme. Thus, catalytic intermediates in benzene are the ferryl species as established in aqueous buffer. The slower compound I reduction with guaiacol in benzene than in buffer suggests that the accessibility of the active site for the substrates decreases in benzene.

V-B Molecular Mechanism of Substrate Metabolisms by Heme Enzymes

Heme enzymes oxidize a wide variety of substrates, however, the detailed molecular mechanisms for many types of reactions including *N*-demethylation of amines, hydroxylation, NO synthesis, heme oxygenation, etc. are still obscure. Thus, we have started the mechanistic studies on *N*-demethylation of amines and heme oxygenation.

V-B-1 Mechanistic Studies of *N*-Demethylation of Dimethylaniline Derivatives by O=Fe^{IV} Porphyrin π-Cation Radicals of Peroxidases and Their Synthetic Models

Yoshio GOTO, Joseph P. DINNOCENZO *(Univ. Rochester)*, **Jeffrey P. JONES** *(Univ. Rochester)*, **Shun-ichi FUKUZUMI** *(Osaka Univ.)* **and Yoshihito WATANABE**

Heme enzymes such as Horseradish peroxidase (HRP) and Cytochrome P450 are known to catalyze oxidative *N*-demethylation of amines. On the basis of deuterium isotope effects on the *N*-demethylation, the reactions have been considered to proceed by the initial electron transfer followed by deprotonation and oxygen rebound mechanisms. However, deuterium isotope effects obtained on the basis of internal competitive isotope effects can be rationalized by both the initial electron transfer and direct hydrogen abstract mechanisms. Thus, we have started the direct observation of the reactions of the reactive intermediate of heme enzymes (compound I) and a series of substituted dimethylaniline by stopped flow measurements. At the same time, we have prepared an O=Fe^{IV}TMP π-cation radical complex in methylene chloride at -50°C and examined its reactions with the anilines. In the case of HRP compound I reactions with anilines, the rate constants are independent to either the substrate is deuterated or not, while the *N*-demethylated products apparently show a large isotope effects. Thus, the reaction mechanism is consistent with the initial rate determining electron transfer followed by product determining deprotonation. On the other hand, the reactions by the O=Fe^{IV}TMP π-cation radical complex show that the reaction rate correlate to the redox potential of the dimethylaniline derivatives. At the same time, the deuteration of the substrates slows down the oxidation rates. Deuterium isotope effects on the basis of the products formed are under investigation.

V-B-2 Mechanistic Studies of a Suicidal *meso*-Oxidation of Novel Iron Porphyrin Complexes as a Model of the Formation of α-*meso*-Hydroxyheme by Heme Oxygenase

Tatsuya MURAKAMI *(Kyoto Univ.)*, **Shin-ichi OZAKI, Toshitaka MATSUI, Yoshihito WATANABE and Isao MORISHIMA** *(Kyoto Univ.)*

A suicidal *meso*-oxidation of novel iron porphyrin complexes has been investigated in order to gain mechanistic insights into the generation of α-*meso*-hydroxyheme catalyzed by Heme Oxygenase (HO). We have prepared a novel iron porphyrin complex, in which less hindered *p*-chlorophenyl groups were introduced to two *meso*-positions and the other two *meso*-positions were protected by mesityl groups; Fe^{III}BMB*p*CPP (**1a**) [BMBpCPP: 5,15-bis(mesityl)-10,20-bis(*p*-chlorophenyl)porphyrin]. The reaction of **1a**-trifluoroacetate (Tfa) and a small excess of *p*-nitroperbenzoic acid (*p*NPBA) was carried out in dichloromethane containing 4 equiv of trifluoroacetic acid at -70°C. The oxidation product (**2a**) showed two intense absorption in the near-IR region, and g values (6.18, 5.68, and 1.98) typical of an iron(III) rhombic high spin complex. In NMR measurements, four-splitting resonances were assigned to β-pyrrole H of **2a**, suggesting the ring structure with *C*s symmetry. These spectroscopic features readily lead us to identify **2a** as a ferric isoporphyrin complex. Further, IR and electrospray ionization (ESI) mass spectral measurements indicated **2a** bearing a *p*-nitrobenzoyloxy group at a *meso*-position. On the basis of the kinetic profile of the reaction between **1a**-tfa and *p*NPBA, the reaction was concluded to proceed *via* the formation of a *p*-nitroperbenzoate-iron(III) complex followed by an O-O bond cleavage, and more importantly, the generation of an intermediate (**3a**) was transitionally observed. To elucidate the way of the O-O bond cleavage associated with an electronic structure of **3a**, effects of the substituents of perbenzoic acids on the rate of the O-O bond cleavage were examined. Electron-withdrawing ability was found to accelerate the reaction, indicative of heterolysis of the O-O bond. The *meso*-addition of the releasing group followed an intramolecular manner.

These results demonstrate that this suicidal *meso*-oxidation, which eventually gives the iron(III) isoporphyrin complex (**2a**), proceeds via the formation of a *p*NPBA-iron(III) porphyrin complex and the following intermediate (**3a**) yielded by the heterolytic O-O bond cleavage coupled with a intramolecular migration of *p*-nitrobenzoyloxy group to the *meso*-position.

V-C Model Reactions of Non-Heme Proteins

Monomeric and dimeric non-heme iron proteins play important roles in biological redox processes. Many reactions catalyzed by the non-heme enzymes are quite similar to those by hemoproteins. We are interested in the active intermediates responsible for oxidation and oxygenation by non-heme enzymes, especially the similarity and differences.

V-C-1 A Model for Lipoxygenases: Synthesis, Structures, and Reactivity of (Hydroxo) Iron(III) Complexes with a Tetradentate Tripodal Ligand

Seiji OGO, Masakazu IWASE,* Senji WADA, Koichiro JITSUKAWA,* Hisahiko EINAGA,* Hideki MASUDA* and Yoshihito WATANABE
*(*Nagoya Inst. Tech.)*

Mononuclear non-heme iron enzymes, lipoxygenases (LO) catalyze the peroxidation of polyunsaturated fatty acids and fatty acid esters. Synthesis, structure, and reactivity of $[Fe^{III}(TNPA)(OH)(p\text{-}X\text{-}PhCOO)]^+$ (**1**, X = H or Me, TNPA = tris-(6-neopentylamino-2-pyridylmethyl)amine) as models for the active species in the catalytic cycle of LO have been studied. Reactions of **1** with H_2O_2 caused the oxidation of one N-H group of TNPA ligand of 1 to afford $[Fe^{III}(TNPA)(N\text{-}O)(p\text{-}X\text{-}PhCOO)]^+$ (2); the structure of **1** and **2** were unequivocally determined by single-crystals X-ray structural analysis. A presence of (hydroperoxo)iron(III) intermediate species before **2**, and after **1**, has been indicated by trap experiments using thioanisole, but not directly observed. Moreover, complex **2** reacts with excess H_2O_2 to form $[Fe^{III}(TNPA)(N\text{-}O)(OOH)]^+$ (3) which was identified by electrospray ionization mass spectrometry (ESI-MS).

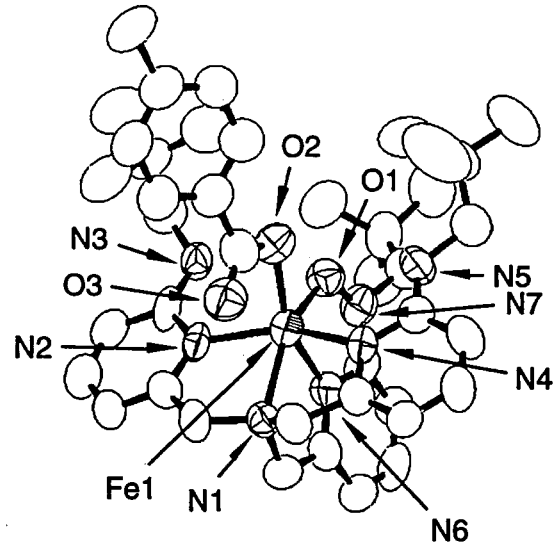

Figure 1. ORTEP drawing of $[Fe^{III}(TNPA)(N\text{-}O)(p\text{-}X\text{-}PhCOO)]^+$ (**2**).

V-D Aqueous Organometallic Chemistry

Aqueous organometallic chemistry is a relatively new and exciting area that has primarily focused on the reactions of organometallic compound with water soluble substrates in aqueous solution. We have discovered that a supramolecular host, $[Cp^*Rh(2'\text{-deoxyadenosine})]_3(OTf)_3$, has utility as a new aqueous ^1H NMR shift reagent, via a host-guest molecular recognition process, with a wide variety of water soluble organic substrates.

V-D-1 A New, Aqueous ^1H NMR Shift Reagent Based on Host-Guest Molecular Recognition Principles for Organic Compound Structural Analysis: Non-Covalent π-π and Hydrophobic Interactions Using a Supramolecular Host, $[Cp^*Rh(2'\text{-deoxyadenosine})]_3(OTf)_3$

Seiji OGO, Shigeyuki NAKAMURA,* Kiyoshi ISOBE,* Richard H. FISH and Yoshihito WATANABE** *(*Osaka City Univ., **Lawrence Berkeley National Lab., University of California)*

A supramolecular host, $[Cp^*Rh(2'\text{-deoxyadenosine})]_3(OTf)_3$ (**1**, $Cp^* = \eta^5\text{-}C_5Me_5$, $OTf = CF_3SO_3^-$), has utility as a new aqueous ^1H NMR shift reagent, via a host-guest molecular recognition process that occurs by non-covalent π-π and hydrophobic interactions, with a wide variety of H_2O soluble organic substrates. These organic compound guests encompass examples such as aromatic carboxylic acids, phenylacetic acid (**G1**), 1-naphthoic acid (**G2**), and 2-naphthoic acid (**G3**), an aliphatic carboxylic acid, cyclohexylacetic acid (**G4**), as well as biological compounds, a di and a tetrapeptide containing terminal L-tryptophan (Trp) or L-phenylalanine (Phe) groups, L-Trp-L-Phe (**G5**) and L-Trp-L-Met-L-Asp-L-Phe amide (**G6**) in the pH range of 5-10. The molecular recognition parameters that effect the ^1H NMR shifts of the organic guests and a comparison with the water soluble lanthanide shift reagents (LSRs) have been studied to demonstrate the usefulness of this aqueous molecular receptor as an aid for organic compound structural analysis.

V-E New High-Dimensionality Molecule-Based Magnets

Organic free radicals with unpaired electrons serve as exceptions to typical organic molecules that are characterized by their closed-shell electronic structure in which all the even number of electrons are paired. When a molecule is endowed with two or more degenerate or nearly degenerate orthogonal orbitals and the equal number of electrons, Hund's rule dictates that the Coulombic repulsion between the electrons will be minimized by allocating one electron to each MO all with parallel spins. On the basis of this principle, quite a few organic molecules with high spin ground states have been prepared. Some of the highlights are a nonacarbene with eighteen parallel spins ($S = 9$) characterized at cryogenic temperature and some triradicals with three parallel spins ($S = 3/2$) among which trinitroxide radical is noted for its high stability at room temperature under air. Efforts to increase the number of the aligned spins have, however, been hampered by difficulty in assembling the radical centers in higher concentration; the higher series of the carbenes, for example, are not only difficult to prepare but also start to recombine chemically or intrachain and/or intermolecular interactions become antiferromagnetic if not strongly enough to form a chemical bond.

In order to overcome these difficulties, we have made recourse to a strategy of assembling the organic radical centers by means of complexation with paramagnetic transition metal ions. The dimensionality of the complex, the sign of exchange coupling and the magnitude of the exchange coupling between the neighboring spins may be readily tuned by this strategy.

V-E-1 Spontaneous Magnetization in a 2 : 3 Complex Formed by 3,4',5-Tris(N-oxy-*tert*-butylamino)biphenyl and Manganese(II) bis(hexafluoro-acetylacetonate)

Katsuya INOUE and Hiizu IWAMURA *(Kyushu Univ.)*

[*Adv. Matter.* **8**, 73 (1996)]

Black powders of $\mathbf{1}_2$•[Mn(II)(hfac)$_2$]$_3$ were obtained by mixing the entitled tris(nitroxide) (**1**) and bis(hexafluoroacetylacetonato)manganese(II) {Mn(II)•(hfac)$_2$} in a mixed solvent acetone/*n*-heptane. As the temperature was lowered, the observed molar susceptibility times temperature increased, gave a maximum at 10 K. The magnetization versus T plots for the complex measured at a magnetic field of 5 Oe showed a sharp rise at $T_C = 9.5$ K. The saturation magnetization value was 9 μ_B at 20000 Oe and 5 K in good agreement with a model in which a perfect 2-D ferrimagnetic sheet with heterospin ferromagnetic - antiferromagnetic network stack ferromagnetically across the layer.

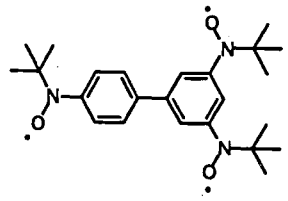

1

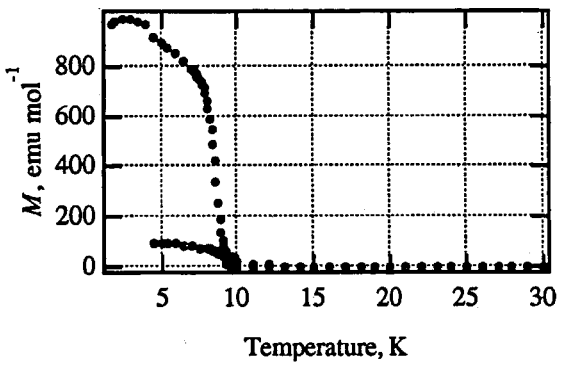

Figure 1. Magnetization vs. T plots for the complex $\mathbf{1}_2$•[Mn(II)(hfac)$_2$]$_3$ measured in a field of 5 Oe and spontaneous magnetization.

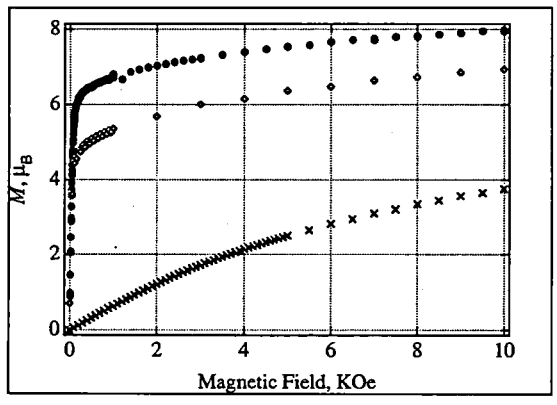

Figure 2. Field dependence of the magnetization of $\mathbf{1}_2$•[Mn(II)(hfac)$_2$]$_3$ measured at 1.8 K (●), 5.0 K (A), and 15.0 K (X).

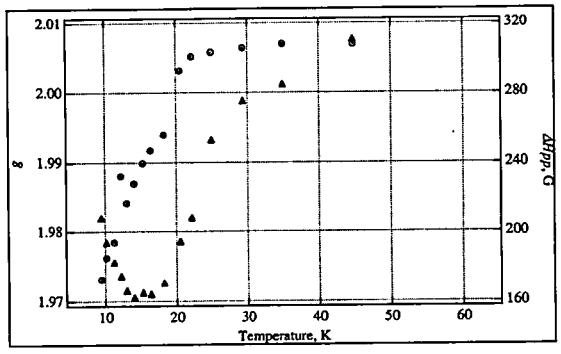

Figure 3. The temperature dependence of g (○) and ΔHpp (K) values for $\mathbf{1}_2$•[Mn(II)(hfac)$_2$]$_3$.

V-E-2 High-Spin Polynitroxide Radicals as Versatile Bridging Ligands for Transition Metal Complexes with High Ferri/Ferromagnetic T_C

Hiizu IWAMURA *(Kyushu Univ.)*, **Katsuya INOUE and Takashi HAYAMIZU** *(Kyushu Univ.)*

[*Pure Appl. Chem.* **68**, 243 (1996)]

π-Conjugated di- and trinitroxide radicals with triplet and qualtet groung states, respectively, were react with manganese(II) bis(hexafluoroacetylacetonate) to give polymer complexes having well-defined structures. While a 1:1 1-D complex from m-phenylenebis (nitroxide) was found to be a metamagnet (T_C = 5.5 K), 2:3 2-D and 3-D complexes from the trinitroxides become ferri/ferro-magnets with T_C in the range 3.4 - 46 K. Design of these self-assembled heterospin systems with tailored dimensions and the sign and magnitude of the exchange coupling will serve as a useful strategy for exploring higher T_C molecule based magnets.

V-E-3 Magnetic Characterization of One-Dimensional Molecule-Based Metamagnet made of Mn(II)(hfac)$_2$ and 1,3-Bis(*N*-oxy-*tert*-butylamino)-benzene

Katsuya INOUE and Hiizu IWAMURA *(Kyushu Univ.)*

[*Mol. Clyst. Liq. Cryst.* **286**, 133 (1996)]

Manganese bis(hexafluoroacetylacetonate), Mn(hfac)$_2$, reacts with 1,3-bis-(*N*-oxy-*tert*-butylamino)benzene, **2**, to give a 1:1 polymeric complex of formula [Mn(hfac)$_2$•**2**]$_n$. An X-ray crystal structure analysis reveals that the manganese(II) ion and the molecule of **1** makes one-dimensional chains by ligation of the latter serving as a bis(monodentate) ligand to the former. A crystalline sample of the complex undergoes transition to a metamagnet at 5.5 K. In the ordered phase, it exhibits a large uniaxial magnetic anisotropy with the uniaxial anisotropy constant, K_{u1}, of 8.3 × 10^6 J m^{-3} by single crystal magnetic measurements.

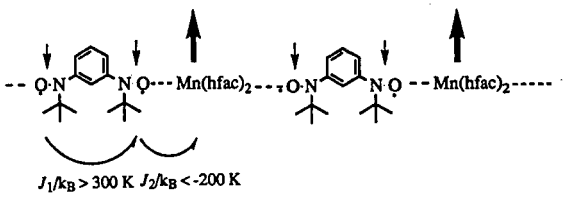

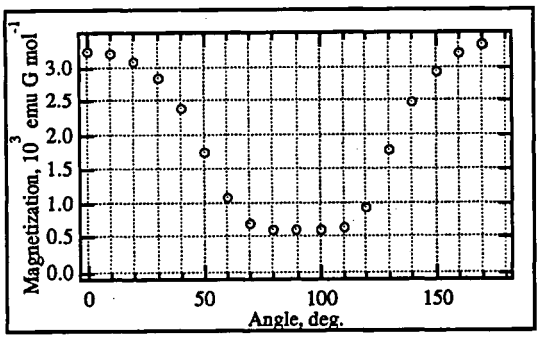

Figure 1. The angle dependence of the magnetization of a single crystal of this complex. Rotated along crystal *a* axis (○).

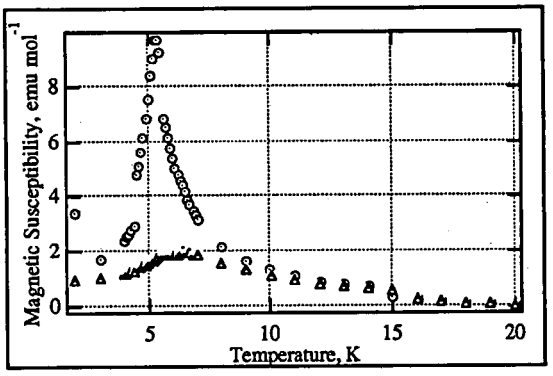

Figure 2. The temperature dependencies of the magnetic susceptibility of a single crystal of [Mn(II)(hfac)$_2$•**2**] along (○) and perpendicular to (△) the crystal *c* axis measured in 5 Oe.

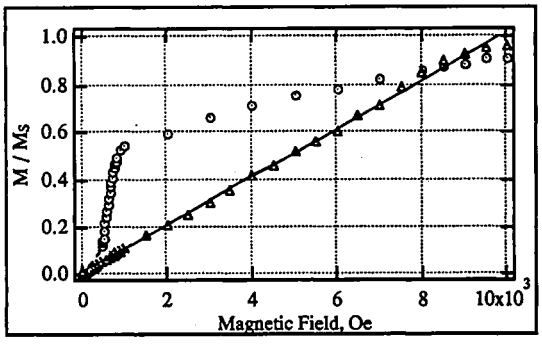

Figure 3. Field dependencies of the magnetization of a single crystal of [Mn(II)(hfac)$_2$•**2**] with the field applied along (○) and perpendicular to (△) the *c* axis at 1.8 K.

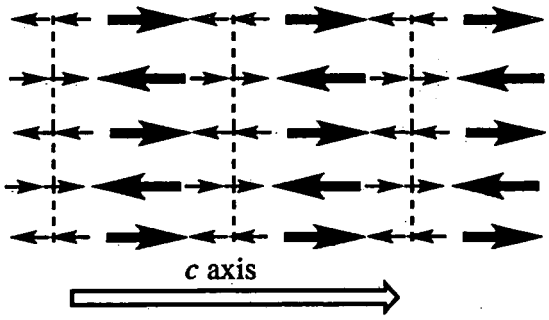

Figure 4. A schematic drawing of the magnetic structure of [Mn(II)(hfac)$_2$•**2**]. Broken lines show the N(*tert*-Bu)O• - F - N(*tert*-Bu)O• antiferromagnetic interaction between the ferrimagnetic 1-D chains. Solid lines show the ferromagnetic interchain interaction through the ligands.

V-E-4 Ferrimagnets Made By Assembling High-Spin Organic Polyradicals By Mean of Complexation With Magnetic Metal Ions. VII. One-Dimensional Chains Made by an Alternating Array of Mn(II)(hfac)$_2$ and 1,3-Bis-(N-oxy-tert-butylamino)benzenes

Katsuya INOUE and Hiizu IWAMURA *(Kyushu Univ.)*

[*Proc. Mater. Res. Soc.* **413**, 313 (1996)]

A strategy of assembling and aligning spins of organic free radicals by means of complexation with magnetic metal ions has been pursued for obtaining ferro/ferrimagnets with high phase-transition temperature (T_C). Triplet m-phenylenebis(*t*-butylnitroxide) and 2,4-bis(4,4,5,5-tetramethyl-4,5-dihydro-1-oxido-3-oxyimidazol-2-yl)thiophene formed with d^5 bis(hexafluoroacetylacetonato)manganese(II) {Mn(hfac)$_2$} a 1D chain and a ladder-type polymer that proved to be a metamagnet (5.5 K) and a ferro/ferrimagnet (11 K), respectively. Quartet 1,3,5-tris{*p*-(N-oxy-tert-butylamino)phenyl}benzene and the lower analogs formed with {Mn(hfac)$_2$} 2D network structures with T_C in the range 3.4-9.3 K. Bis-{3-*tert*-butyl-5-(*N*-oxy-*tert*-butylamino)phenyl} nitroxide with a quartet ground state formed a 2:3 complex with Mn(hfac)$_2$. The terminal two nitroxide groups of the trinitroxide radicals are ligated to two different Mn ions to form a zigzag chain. The middle nitroxide group is used to cross-link the adjacent chains through a third Mn ion, resulting in the formation of a parallel-crosses-shaped 3D structure. The temperature dependence of the magnetization at 5 Oe revealed a transition to the spin-ordered phase at 46 K. Efforts are in progress to make organic polyradical/magnetic ion hybrid-spin systems with higher T_C and endow the magnetic materials with photoresponsiveness and other functionality.

V-F Magnetism in Quantum Spin Systems

Quantum nature in low-dimensional Heisenberg systems has attracted much interests in recent decades. We focus on the isotropic nature of electron spins in organic radicals consisting only of light elements. We have constructed some low-dimensional systems such as a honeycomb lattice and a linear chain containing both ferromagnetic and antiferromagnetic interactions. The magnetic couplings can be controlled by chemical modifications. The ground state properties were examined by the temperature dependence of the susceptibilities and the field dependence of the magnetization down to 0.5 K.

V-F-1 Construction of spin-1/2 Heisenberg Chains with Ferromagnetic and Antiferromagnetic Interactions

Yuko HOSOKOSHI, Kohichi TAKIZAWA,* Hiroki NAKANO,* Tsuneaki GOTO,* Minoru TAKAHASHI* and Katsuya INOUE *(*ISSP, Univ. Tokyo)*

[*J. Mag. Mag. Mater.* in press]

Magnetic properties of spin-1/2 Heisenberg chains with ferromagnetic and antiferromagnetic couplings have been investigated. Three related organic biradicals with intramolecular ferromagnetic couplings (J_F's) were synthesized. The magnitude of J_F can be controlled by chemical modifications. All of them crystallize to form chain structures with intermolecular antiferromagnetic couplings (J_{AF}'s). The exchange couplings are estimated to $2J_F/k_B$=638 K and $2J_{AF}/k_B$=-14.5 K for PNNNO, $2J_F/k_B$=387 K and $2J_{AF}/k_B$=-43 K for F_2PNNNO, and $2J_F/k_B$=216 K and$2J_{AF}/k_B$=-12 K for PIMNO, where PNNNO=2-[*p*-(N-*tert*-butyl-*N*-oxyamino)phenyl]-4,4,5,5-tetramethyl-4,5-dihydro-1*H*-imidazol-1-oxyl-3-oxide, F_2PNNNO=2-[*o*-difluoro-*p*-(*N*-*tert*-butyl-*N*-oxyamino)phenyl]-4,4,5,5-tetramethyl-4,5-dihydro-1*H*-imidazol-1-oxyl-3-oxide, and PIMNO =2-[*p*-(N-*tert*-butyl-*N*-oxyamino)phenyl]-4,4,5,5-tetramethyl-4,5-dihydro-1*H*-imidazol-1-oxyl.

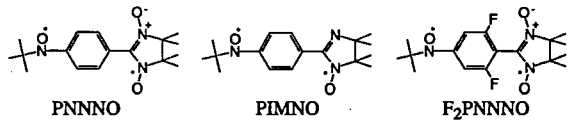

V-F-2 Magnetic Properties of spin-1/2 Heisenberg Honeycomb Lattice with Ferro-magnetic and Antiferromagnetic Interactions

Yuko HOSOKOSHI, Mitsue TAKAHASHI,* Tsuneaki GOTO* and Katsuya INOUE *(*ISSP, Univ. Tokyo)*

[*J. Mag. Mag. Mater.* in press]

The magnetic properties of 2-iodo, 2-bromo and 2-cyclopropyl nitronyl nitroxide radicals (abbreviated to INN, BrNN and C_3H_5NN, respectively) are presented. All these compounds construct a honeycomb lattice with ferromagnetic and antiferromagnetic interactions; S=1/2 spins form a uniform ferromagnetic chain which

couples antiferromagnetically with neighbouring two chains to form a honeycomb lattice in a plane including chains. The exchange couplings are estimated to $2J_F/k_B$=8.0 K and $2J_{AF}/k_B$=-10.5 K for INN, $2J_F/k_B$=2.6 K and $2J_{AF}/k_B$=-9.1 K for BrNN, and $2J_F/k_B$=0.8 K and $2J_{AF}/k_B$=-3.6 K for C_3H_5NN. The magnetization and susceptibility of each compound was studied down to 0.5 K and up to 9 tesla. For C_3H_5NN,, the antiferromagnetic order was observed at 1.5 K.

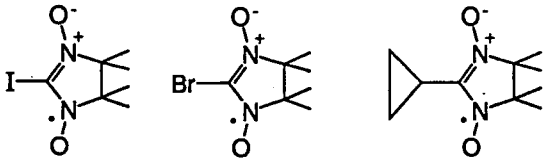

INN BrNN C_3H_5NN

V-F-3 Spin-1/2 Heisenberg Model with Ferromagnetic and Antiferromagnetic Interactions on a Honeycomb Lattice

Hiroki NAKANO,* Yuko HOSOKOSHI and Minoru TAKAHASHI* *(*ISSP, Univ. Tokyo)*

[*J. Mag. Mag. Mater.* in press]

The ground state of spin-1/2 Heisenberg ferromagnetic chains coupled by antiferromagnetic interactions on a honeycomb lattice, which describe properties of 2-iodo, 2-bromo and 2-cyclopropyl nitronyl nitroxides, is studied by mean-field approximations with a help of numerical diagonalizations. We obtain the critical ratio of the ferromagnetic interaction to the antiferromagnetic one between ordered and disordered phases to be 0.784 ± 0.001. It is found that, in the cases corresponding to the three materials, the ground state of the system is not ordered.

V-G Pressure Effect on Molecular Magnetism

Organic radicals are 'soft' magnetic materials and pressure effect is attractive and undeveloped subject. We have studied the pressure effect through the magnetic and heat capacity measurements.

V-G-1 Magnetic Properties of Pure Galvinoxyl under Pressure—Suppression of the Structural Change and Observation of the Magnetic Ordering

Yuko HOSOKOSHI, Masaki MITO,* Masafumi TAMURA *(Toho Univ.)*, **Kazuyoshi TAKEDA,* Minoru KINOSHITA** *(Sci. Univ. Tokyo in Yamaguchi)* **and Katsuya INOUE** *(*Kyushu Univ.)*

[*The Review of High Pressure Science and Technology* in press]

We have already discovered that the structural change of organic radical, galvinoxyl is suppressed by pressurization. At ambient pressure, a structural change occurs at 85 K and the system falls into a diamagnetic state. On the other hand, magnetism under 7 kbar down to 1.8 K obeys the one dimensional Heisenberg ferromagnet with $2J/k_B$=25 K. In this report, magnetic and thermal properties under 6.4 kbar down to 0.5 K are described. Under the zero field, the χac value takes a maximum at around 0.7 K. This maximum temperature decreases with applied fields, which suggests an antiferromagnetic phase transition. In the heat capacity measurement, a λ-shaped peak was observed at 0.72 K and the bulk nature of the phase transition is confirmed. We also observe the broad peak at around 10 K which is characteristic to the one-dimensional Heisenberg ferromagnet. We analyse the the field dependence of this broad peak on the basis of the one-dimensional Heisenberg ferromagnet and obtained $2J/k_B$=18 K. Thus, we conclude that galvinoxyl is a quasi-one dimensional Heisenberg ferromagnet with $2J/k_B \approx 20$ K with weak antiferromagnetic interchain interactions, which results in the three-dimensional antiferromagnetic phase transition at 0.72 K.

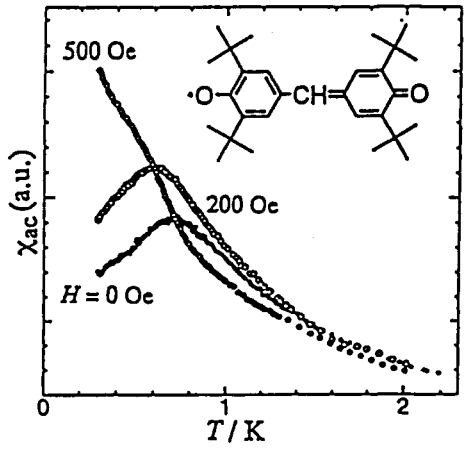

Figure 1. Temperature dependence of the ac susceptibility of galvinoxyl under 6.4 kbar.

V-H New Charge-Transfer Complexes Exhibiting Novel Magnetic Properties

In 3d transition metals of iron, cobalt and nickel ferromagnetic state can be maintained at extremely high temperature. In contrast, even a highest critical temperature (Tc) of ferromagnetic phase transition is 1.48 K in entirely s/p orbital-based organic ferromagnets, of which the first one has been discovered in a nitronylnitroxide radical crystal and successively about twenty ones have till now been prepared by using other radical crystals and charge-

transfer (CT) complxes. In the present study we investigated the synthesis and magnetic properties of new CT complexes with aim at achieving purely organic ferromagnets with high *Tc*.

V-H-1 1:2 TCNQ/TCNQ$^{-\bullet}$ Mixed Salts Exhibiting Ferromagnetic Behavior at Room Temperature

Kazumasa UEDA *(Osaka Pref. Univ.)*, **Toyonari SUGIMOTO** *(Osaka Pref. Univ. and IMS)*, **Satoshi ENDO, Naoki TOYOTA, Masakado KOHAMA, Koji YAMAMOTO** *(Osaka Pref. Univ.)*, **Yusaku SUENAGA, Hiroshi MORIMOTO, Toshiyuki YAMAGUCHI, Megumu MUNAKATA** *(Kinki Univ.)*, **Nobuyoshi HOSOITO** *(Kyoto Univ.)*, **Nobuko KANEHISA, Yoshiyuki SHIBAMOTO and Yasushi KAI** *(Osaka Univ.)*

[*Chem. Phys. Lett.* **261**, 295 (1996)]

Ferromagnetic behavior at room temperature was observed in the tetramethylammonium (NMe_4^+) (Figure 1) and cesium (Cs^+) salts of tetracyanoquinodimethane (TCNQ) and its radical anion ($TCNQ^{-\bullet}$) in a molecular ratio of 1:2, as is shown in Figure 2. The saturation magnetizations and coercive forces are 0.79 emu/mol and ca. 300 Oe for (NMe_4^+•$TCNQ^{-\bullet}$)•/2TCNQ, and 1.46 emu/mol and ca. 100 Oe for (Cs^+•$TCNQ^{-\bullet}$)•1/2TCNQ, respectively. In contrast, the 1:1 TCNQ/$TCNQ^{-\bullet}$ mixed tetraethylammonium (NEt_4^+) salt, (NEt_4^+•$TCNQ^{-\bullet}$)•TCNQ exhibited no ferromagnetic behavior at room temperature nor at lower temperatures.

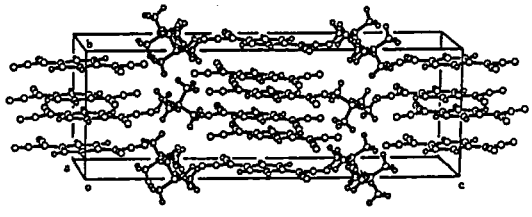

Figure 1. The crystal structure of (NMe_4^+•$TCNQ^{-\bullet}$)•1/2TCNQ.

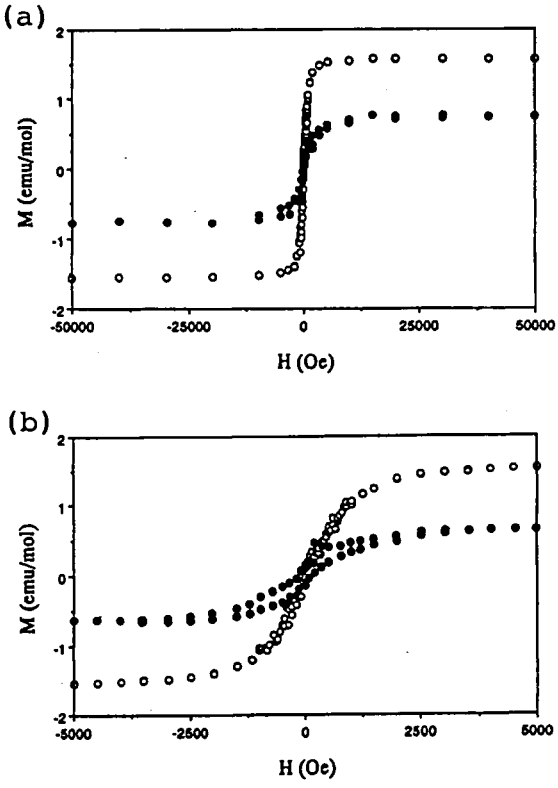

Figure 2. The magnetization curves of (NMe_4^+•$TCNQ^{-\bullet}$)•1/2TCNQ (●) and (Cs^+•$TCNQ^{-\bullet}$)•1/2TCNQ (○) in the applied field ranges of (a) ±50 kOe and (b) ±5 kOe at room temperature.

V-H-2 Temperature Dependence of Crystal Structures, and Electrical Conducting and Magnetic Properties in Plate Crystals of 1:2 Tetrafluorotetracyanoquinodimethane /Tetrafluorotetracyano-quinodimethanide Mixed Tetramethyl-ammonium and -Phosphonium Salts

Kazumasa UEDA *(Osaka Pref. Univ.)*, **Toyonari SUGIMOTO** *(Osaka Pref. Univ. and IMS)*, **Toshiharu TADA, Kei-ichiro NISHIMURA, Satoshi ENDO, Naoki TOYOTA, Masakado KOHAMA, Koji YAMAMOTO** *(Osaka Pref. Univ.)*, **Toshiyuki YAMAGUCHI, Yusaku SUENAGA, Megumu MUNAKATA** *(Kinki Univ.)*, **Nobuko KANEHISA, Yoshiyuki SHIBAMOTO, Yasushi KAI** *(Osaka Univ.)* **and Nobuyoshi HOSOITO** *(Kyoto Univ.)*

[*Mol. Cryst. Liq. Cryst.* **296**, 323 (1997)]

The room-temperature crystal structure of a plate of (PMe_4^+•$TCNQF_4^{-\bullet}$)•1/2$TCNQF_4$ was analyzed (Figure 1) and very similar to that of the corresponding NMe_4^+ salt. However, significant difference was recognized between the two crystals in the structures of $TCNQF_4$ and $TCNQF_4^{-\bullet}$ molecules, and in the contacts between the dimerized $TCNQF_4^{-\bullet}$ molecules and between the $TCNQF_4$ and $TCNQF_4^{-\bullet}$ molecules. The change in both molecular structure and contact as

above was also observed at a lowering temperature. The magnitude in change was larger in the NMe_4^+ salt than in the PMe_4^+ salt. However, such a change in the crystal structure by temperature exerted no special influence on the electrical conducting and magnetic properties.

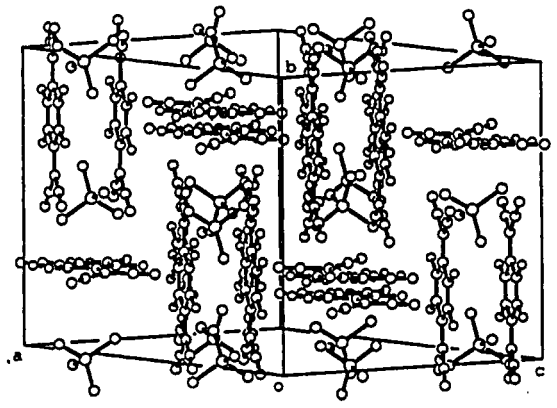

Figure 1. The room-temperature crystal structure of a plate of $(PMe_4^+ \cdot TCNQF_4^{\cdot-}) \cdot 1/2TCNQF_4$.

V-H-3 Synthesis, and Electrical Conducting and Magnetic Properties of a Neutral Bis-(dimethylthiotetrathiafulvalenyldithiolate)-copper Complex

Kazumasa UEDA, Makoto GOTO *(Osaka Pref. Univ.)*, **Toyonari Sugimoto** *(Osaka Pref. Univ. and IMS)*, **Satoshi ENDO, Naoki TOYOTA** *(Osaka Pref. Univ.)* **and Hideo FUJITA** *(Kyoto Univ.)*

[*Synth. Metals* **85**, 1679 (1997)]

A neutral copper complex (**1**) substituted with two tetrathiafulvalenyldithiolato groups was successfully synthesized by the iodine oxidation of the corresponding monoanionic complex (**2**) obtained by the reaction of bis(tetramethylammonium) bis(dimethylthio-tetrathiafulvalenyldithiolato)zinc complex with $CuCl_2$. The complex **1** showed a high electrical conductivity (7.8 x 10^{-2} S·cm^{-1}) on the compressed pellet at room temperature. On the other hand, a very low value (1.0 x 10^{-6} S·cm^{-1}) was obtained for **2**. The ESR and SQUID measurements suggest significant interaction between the copper d spin and conducting tetrathiafulvalenyl π electron in **1**.

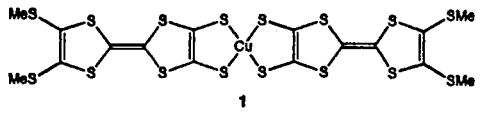

1

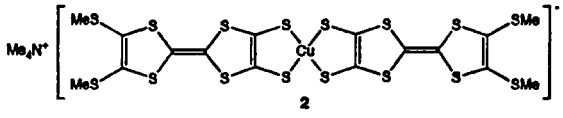

2

V-H-4 Highly-Conducting Neutral Copper Complexes Substituted with Two Tetrathiafulvalenyldithiolato Groups

Kazumasa UEDA, Makoto GOTO, Masaki IWAMATSU *(Osaka Pref. Univ.)*, **Toyonari SUGIMOTO** *(Osaka Pref. Univ. and IMS)*, **Koji YAMAMOTO** *(Osaka Pref. Univ.)* **and Hideo FUJITA** *(Kyoto Univ.)*

The neutral bis(tetrathiafulvalenyldithiolato)copper complexes, $Cu(R_2C_6S_8)_2$ (**Ia**: R=Me; **Ib**: R=Et; **Ic**: R,R=-CH_2CH_2-) were synthesized by the reaction of bis(tetramethylammonium or tetraethylammonium) bis(tetrathiafulvalenyldithiolato)zincates with $CuCl_2$ in DMF, followed by the oxidation with iodine. The room-temperature electrical conductivities were 7.8 x 10^{-2}, 5.0 x 10^{-4}, and 3.7 S·cm^{-1} on the compressed pellets for **Ia**, **Ib** and **Ic**, respectively. The magnetic susceptibility measurements (Figure 1) showed that the remaining spin amounts on the copper atom are very small in all complexes as a result of large electron-transfer from the copper(II) atom to the tetrathiafulvalenyl ligands.

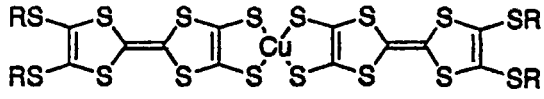

Ia R = Me
Ib R = Et
Ic R,R = -CH_2CH_2-

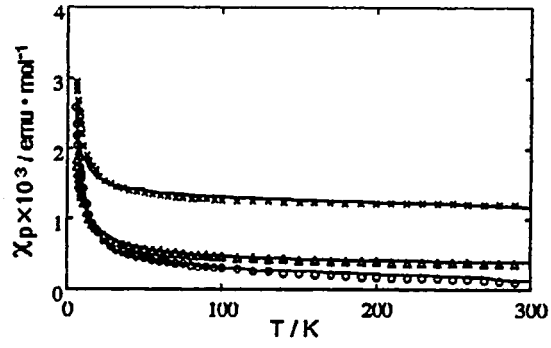

Figure 1. The temperature dependences of the paramagnetic susceptibilities (χ_p's) obtained for **Ia** (×), **Ib** (○) and **Ic** (△). The solid lines are reproduced by using appropriate C, θ and χ_p values in the equation of $\chi_p(T) = C/(T-\theta) + \chi_p$.

V-H-5 New Spiro Donor Molecules: Bis(tetrathiafulvalenyldithio)-methane and -germane

Kazumasa UEDA, Masaru YAMANOHA *(Osaka Pref. Univ.)*, **Toyonari SUGIMOTO** *(Osaka Pref. Univ. and IMS)*, **Hideo FUJITA** *(Kyoto Univ.)*, **Akito UGAWA, Kyuya YAKUSHI** *(IMS)* **and Kenji KANO** *(Kyoto Univ.)*

[*Chem Lett.* 461 (1997)]

As a new tetrathiafulvalene-based donor molecule were synthesized spiro carbon and germanium comounds substituted with two tetrathiafulvalenyldithiolate groups (**1**: M=C; **2**: M=Ge) The redox processes were composed of two pairs of broad and reversible

waves, each of which involves two electron transfer. The radical cation or bis(radical dication)'s generated by one- or two-electron oxidation of **1** and **2** were characterized by ESR.

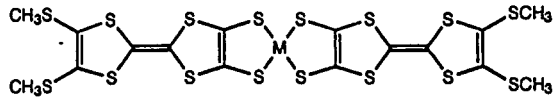

1 : M = C, 2 : M = Ge

V-H-6 A Novel Tetrathiafulvalenoquinodimethane Derivatives Exhibiting Strong Electronic Absorption in a Near-Infrared Region

Kazumasa UEDA, Masaki IWAMATSU *(Osaka Pref. Univ.)*, **Toyonari SUGIMOTO** *(Osaka Pref. Univ. and IMS)* **and Hideo FUJITA** *(Kyoto Univ.)*

[*Chem. Lett.* in press]

Organic compounds possessing both electron-donating and electron-accepting moieties within them, are much expected as components for the preparation of organic materials with novel functions such as intrinsic electrical conductivity, non-linear optics, near-infrared absorption and so on. In the course of our attempts to get donor/acceptor spiro compounds, we could accidentally obtain a novel tetrathiafulvaleno-quinodimethane derivative (**1**), in which a dihydrotetrathiafulvalene group contributes as an electron-donating moiety, while an ethanediylidene-2,2'-bis(indane-1,3-dione) group as an electron-accepting moiety. We now show the molecular (Figure 1) and crystal structures, and electrochemical, optical and electrical conducting properties of **1**. Among them it should be noted that **1** exhibits its longest wavelength electronic absorption till a near-infrared region (>800 nm) and there is no significant absorption in the visible region of 400 to 800 nm (Figure 2).

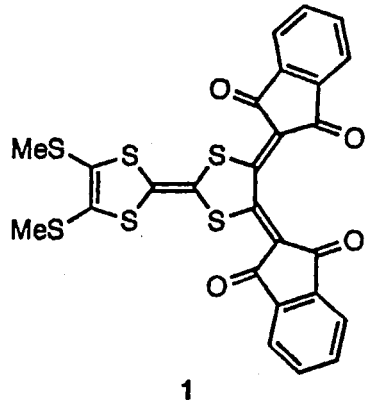

1

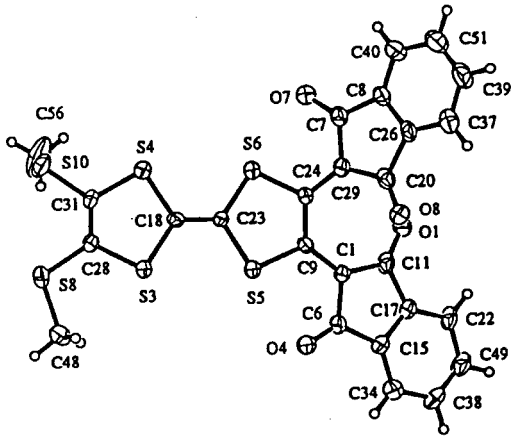

Figure 1. The molecular structure of **1**.

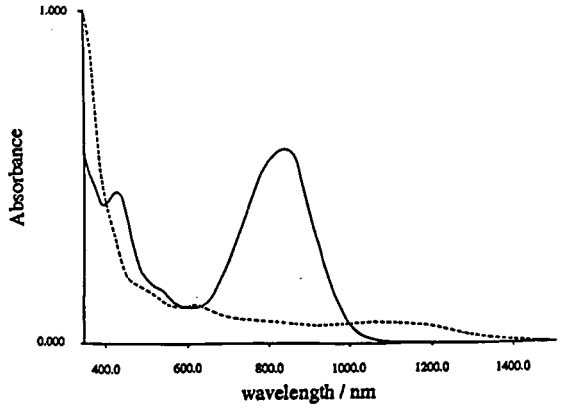

Figure 2. Absorption spectra of **1** in benzene (4.05×10^{-5} mol·l^{-1}) and of its radical anion in DMF (4.05×10^{-5} mol·l^{-1}).

V-I Syntheses, Crystal Structures, and Solid State Properties of Halogen-Bridged Metal Complexes with Linear Chain Structures

Halogen-bridged one-dimensional metal complex consisted from Pt dimer complex, $Pt_2(dta)_4I$ (dta=$CH_3CS_2^-$), is of interest from valence fluctuation, since several electronic states are possible for the many electrons - many atoms system compared to the well-known Pt^{II}-X-Pt^{IV} mixed valence compounds.

V-I-1 Intramolecular Twisting Motion and Phase Transition of Halogen-Bridged One-Dimensional Compound, $Pt_2(dta)_4I$

K. TORIUMI,[a] K. TAKATA,[b] Y. OZAWA,[b] H. KITAGAWA,[c] N. ONODERA,[c] T. MITANI[c] and

M.YAMASHITA,[d] *([a]Himeji Inst. Tech. and IMS, [b]Himeji Inst. Tech., [c]JAIST., [d]Nagoya Univ.)*

The electronic conductivity measurement for the single crystal of $Pt_2(dta)_4I$ revealed semiconductor → metal → semiconductor transitions at the temperature range 300—350K.[1] Temperature dependence of the lattice parameters was measured by single crystal X-ray diffraction method. Anomalous negative hysteresis for the cell volume was observed in the temperature range -20—100°C. In order to reveal the transition phenomena, single crystal structure analyses were made at various temperatures. By comparing the structures at -89°C and 130°C, it was revealed that the first order phase transition was occurred at ca. 90°C from the low-temperature phase with space group C2/c to the high-temperature phase of A2/m. The helical arrangement of the four dta ligand planes around the central Pt–Pt axis is ordered in the low-temperature phase, but it is disordered in the high-temperature phase. From the detailed structure analyses at 20°C—90°C corresponding to the metallic behavior, it has become apparent that new conformation of $Pt_2(dta)_4$ unit appears, in which four dta ligand planes are almost parallel to the Pt-Pt axis (Figure 1). This conformation is forced to elongate the Pt-Pt distance and also change the electronic structure from Pt^{3+}-Pt^{3+} to Pt^{2+}-Pt^{2+}. This indicates that intramolecular twisting motion should be coupled with the change of electronic states of $Pt_2(dta)_4$ units.

Reference

1) H. Kitagawa, N. Onodera, J.-S. Ahn, T. Mitani, M. Kim, Y. Ozawa, K. Toriumi, K. Yasui, T. Manabe and M. Yamashita, *Mol. Cryst. Liq. Cryst.* 285, 311 (1996).

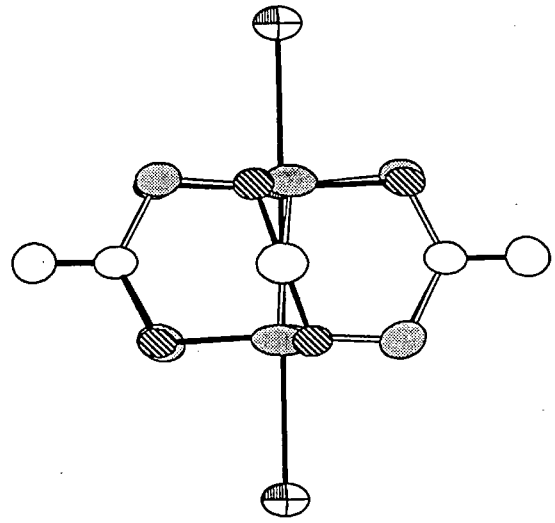

Figure 1. Disordered structure of $Pt_2(dta)_4I$ at 49.5°C.

V-J Spectroscopic Studies on Charge Delocalization and Charge Transfer in Molecular Clusters and in Pure Liquids

Charge transfer processes resulting in dynamical charge delocalization such as consecutive proton or electron hopping in molecular clusters and even in pure liquids are highly interesting in relation to the charge transportation in insulating materials. Not only in aromatic molecular liquids but also in pure water itself electric conductivity is very low when they do not contain impurities of ionic atoms or molecules. We demonstrated that a positive charge in a pure benzene cluster is localized in a dimer unit where the charge resonance (CR) interaction makes the two molecules share an electron forming an intermolecular bond. One of the hot topics in this project is the finding of the charge hopping in vibrationally excited benzene trimer cations. This means the dimer cation core in the trimer is switching, probably periodically concerted with an asymmetric stretching motion of the three benzene molecules.

V-J-1 Infrared Photodissociation Spectroscopy of Benzene Trimer Ions. Switching of the Dimer Ion Core in Vibrationally Excited States

Yoshiya INOKUCHI *(Kyusyu Univ.)*, **Kazuhiko OHASHI and Nobuyuki NISHI**

[*Chem. Phys. Lett.* in press]

A vibrational spectrum of benzene trimer ion, $(C_6H_6)_3^+$, was investigated in the 2900-3100 cm^{-1} region by infrared (IR) photodissociation spectroscopy. Mass-selected trimer ions were irradiated with an IR laser beam from an optical parametric oscillator system (Continuum Mirage 3000) pumped with an injection-seeded Nd:YAG laser. Resultant fragment dimer ions were mass-analyzed and detected by a secondary electron multiplier tube. We obtained an IR photodissociation spectrum of the trimer ions by plotting the yields of the fragment dimer ions against the frequencies of the IR laser. Two distinct maxima are seen at 2986 and 3047 cm^{-1} as shown in Figure 1. The 2986-cm^{-1} band looks asymmetric in shape. The intensity of this band is about eight times as strong as that of the 3047-cm^{-1} one. The intense band at 2986 cm^{-1} was attributed to a C–H stretching vibration of the dimer ion core in $(C_6H_6)_3^+$. The spectra of isotopically mixed benzene trimer ions, $(C_6H_6)(C_6D_6)_2^+$ and $(C_6H_6)_2(C_6D_6)^+$, were also obtained in the main band region. In both cases, two types of fragment dimer ions were observed: $(C_6H_6)(C_6D_6)^+$ and $(C_6D_6)_2^+$, and $(C_6H_6)(C_6D_6)^+$ and $(C_6H_6)_2^+$, respectively. The shapes of the main bands change dependent on the observed fragment ions. All of the spectra showed asymmetric band shapes except for the spectrum of $(C_6H_6)(C_6D_6)_2^+$ monitored at $(C_6D_6)_2^+$ mass position. Asymmetric band shapes can be decomposed into two or three components, which are due to the benzene molecules in the different sites of the trimer ions. We can reasonably explain the rela-

tive abundance of the components in the spectra by considering a core switching in advance of the dissociation. Thus the evidence of the core switching is obtained for the trimer ions in the vibrational excited levels of the ground electronic state.

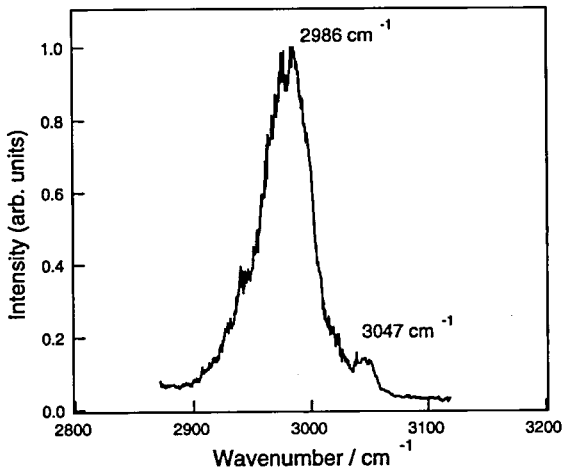

Figure 1. IR photodissociation spectrum of $(C_6H_6)_3^+$. The ordinate stands for the yields of $(C_6H_6)_2^+$. Two maxima emerge at 2986 and 3047 cm^{-1}.

V-J-2 Charge Delocalization in Benzene-Naphthalene Hetero-Dimer Cation

Masaki MATSUMOTO *(Kyushu Univ.)*, **Yoshiya INOKUCHI** *(Kyusyu Univ.)*, **Kazuhiko OHASHI and Nobuyuki NISHI**

[*J. Phys. Chem.* **101**, 4574 (1997)]

The electronic spectrum of the benzene-naphthalene hetero-dimer cation is measured in the 400-1200 nm region by photodissociation spectroscopy. Figure 1 shows the photodissociation spectra of benzene-naphthalene hetero-dimer cation $(BzNp)^+$ in the middle. On the top and the bottom, those of naphthalene dimer cation $(Np)_2^+$, and benzene dimer cation $(Bz)_2^+$ are shown for the references. The most intense band at 580 nm in the middle spectrum is assigned to a local excitation (LE) band of the naphthalene cation chromophore. In addition to this band, an LE band of the benzene cation chromophore of the hetero-dimer is observed at nearly the same position (430 nm) as that of the benzene homo-dimer cation. The observation indicates that the positive charge stays on the benzene molecule in some probability, although the ionization potential of benzene is by 1.10 eV higher than that of naphthalene. The spectrum of the hetero-dimer cation also shows an intermolecular charge transfer(CT) band around 920 nm. On the basis of the position of the CT band as well as the intensity of the LE band relative to that of the homo-dimer, the probability of finding the charge on the benzene molecule is analyzed to be approximately 9 %.

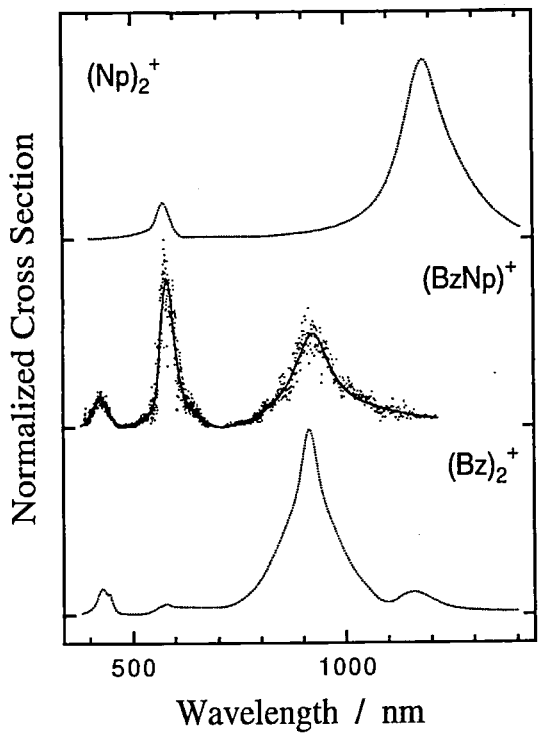

Figure 1. Photodissociation spectra of $(Np)_2^+$(top), $(BzNp)^+$(middle), and $(Bz)_2^+$. Amplitudes of the three spectra are normalized independently; relative intensities of them are just arbitrary to one another.

V-J-3 Electronic Structures and Photo-evaporation Dynamics of Benzene Cluster Ions

Yasuhiro NAKAI *(Kyushu Univ.)*, **Kazuhiko OHASHI and Nobuyuki NISHI**

[*J. Phys. Chem.* **101**, 472 (1997)]

The electronic spectra of benzene cluster ions, $(C_6H_6)_n^+$ with n=3-6, are measured through mass-selected photodissociation spectroscopy. The spectra in the 400-1100-nm region show three distinct absorption maxima centered around 430, 590-620, and 950 nm, which are analogous to the spectrum of $(C_6H_6)_2^+$. The 950-nm band is assigned to a charge resonance (CR) band characteristic of the dimer ion, while the other two bands are attributed to local excitation bands. The position of the CR band is found to be almost independent of cluster size. The result suggests that the cluster ions have a charge-localized structure involving a strongly bound dimer ion core. In addition, the number and translational energy of neutral molecules ejected following photoexcitation are measured for $(C_6H_6)_n^+$ with n=3-8 in the photon energy range of 0.5-3.0 eV. The average number of ejected molecules increases linearly with increasing photon energy, suggesting that the fragmentation proceeds via the sequential ejection of neutral monomers. The average translational energy carried by one monomer is determined to be 50-70 meV, which is comparable with the calculated value according to a statistical theory. A large part of the imparted photon energy is partitioned into internal energies of the products. These results indicate that the photofragmentation of $(C_6H_6)_n^+$ can be regarded as a

unimolecular decay of vibrationally hot clusters, despite the promotion of the chromophoric dimer core to the repulsive excited state.

V-J-4 Pump-Probe Photodepletion Spectroscopy of $(C_6H_6)_2^+$. Identification of Spectrum in the Charge Resonance Band Region

Kazuhiko OHASHI, Yoshiya INOKUCHI *(Kyusyu Univ.)* **and Nobuyuki NISHI**

[*Chem. Phys. Lett.* **263**, 167 (1996)]

A pump-probe technique has been developed to study mass-selected cluster ions in the gas phase. The approach allows one to address the question of existence of a number of isomeric forms of cluster ions. Photodissociation of mass-selected ions is used as both pump and probe method. The probe laser is fixed at a wavelength resonant with a transition of an isomer. The intensity of the fragment ion signal generated by the probe laser (probe-laser signal) is proportional to the population of the isomer. The pump laser, preceding the probe laser in time, is capable of reducing the population of the isomer selected by the probe laser. The depopulation is seen as a depletion of the probe-laser signal.

Figure 1 shows the photodissociation spectrum of $(C_6H_6)_2^+$ (dotted curve) in near-infrared region. Both the main band at 920 nm and relatively weak one at 1160 nm are assigned to charge resonance (CR) bands. The issue is whether the two bands are due to two isomers of $(C_6H_6)_2^+$. The pump-probe experiment is performed by fixing the pump-laser wavelength at 920 nm and changing the probe-laser wavelength from 850 to 1210 nm. The intensity of the pump laser is kept at a constant value in a series of the measurement. The depletion yield of the probe-laser signal is plotted against the probe-laser wavelength in Figure 1. The pump laser reduces the intensities of the probe-laser signals by 55-60 % at all wavelengths studied. This finding rules out the possibility that two isomers of $(C_6H_6)_2^+$ are responsible for the appearance of the two CR bands. If the two CR bands were due to different isomers, the depletion yields would be zero at wavelengths in the 1160-nm band region. We therefore conclude that two distinct transitions of a single isomer are responsible for the two CR bands. No evidence is found for the existence of other isomers of $(C_6H_6)_2^+$.

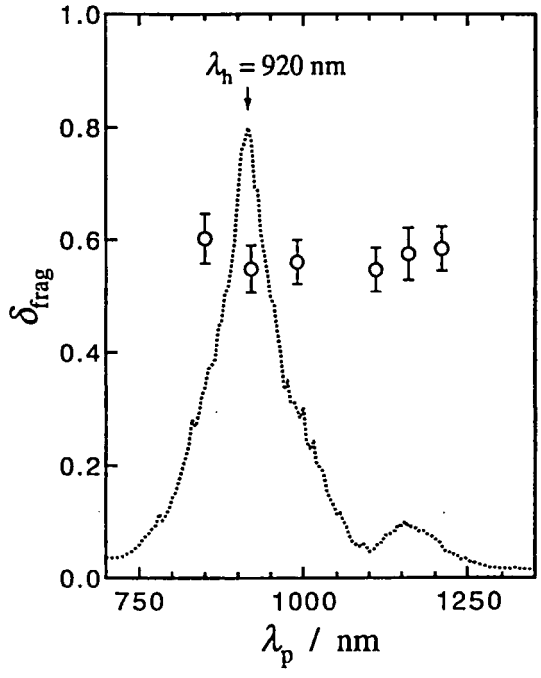

Figure 1. Plots of the depletion yield of the probe-laser signal against the wavelength of the probe laser (open circles). The pump-laser wavelength is fixed at 920 nm. The dotted curve stands for the photodissociation spectrum of $(C_6H_6)_2^+$.

V-J-5 Formation of Benzene Dimer Cations in Neat Liquid Benzene Studied by Femtosecond Transient Absorption Spectroscopy

Yoshiya INOKUCHI *(Kyusyu Univ.)*, **Yukito NAITOH, Kazuhiko OHASHI** *(Kyusyu Univ. and IMS)*, **Ken-ichi SAITOW** *(Graduate Univ. for Advanced Studies)*, **Keitaro YOSHIHARA, and Nobuyuki NISHI** *(Kyusyu Univ. and IMS)*

[*Chem. Phys. Lett.* **269**, 298 (1997)]

Photoionization of neat liquid benzene has been studied by femtosecond pump-probe experiments in the near infrared (IR) region. Third harmonic of a regeneratively amplified Ti:Sapphire laser was focused on a flow jet of neat liquid benzene with a thickness of 100 μm at room temperature. The absorption changes were measured in the region from visible to near IR. Figure 1 shows the transient absorption spectrum at 2 ps delay time. A transient species is formed within 1 ps following two-photon excitation of liquid benzene at 268 nm, which shows a broad absorption band with a peak at 920 nm and extended intensities at wavelengths around 1000 nm. Since the band position of the transient absorption spectrum nicely coincides with that of the photodissociation spectrum of benzene dimer cation in the gas phase, this band is attributed to a charge resonance band of a localized dimer cation created in neat liquid benzene. The asymmetric band shape may suggest that appreciable amount of the dimer cores are dressed in various sizes of benzene molecules.

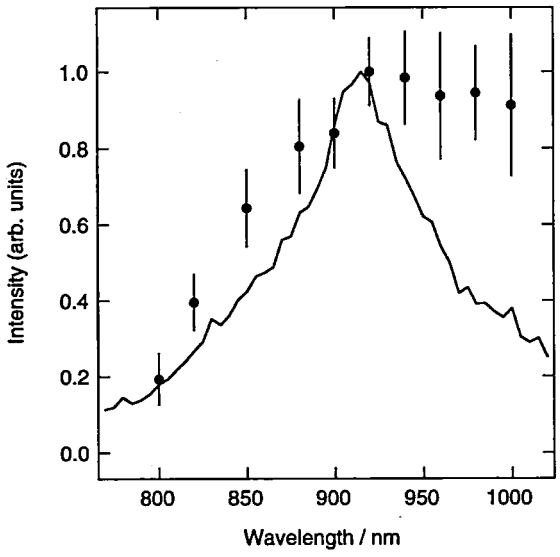

Figure 1. Transient absorption spectrum of neat liquid benzene in a near infrared region (solid circles). Solid curve shows photodissociation spectrum of mass-selected benzene dimer cation in the gas phase.

V-J-6 Nanosecond Time-Resolved Study on the Electronic Spectra of Jet-Cooled Anthracene Dimer

Hiroshi SEKIYA *(Kyushu Univ.)*, **Kentaro KOSUGI** *(Kyusyu Univ.)*, **Norihiro MATSUOKA** *(Kyushu Univ.)*, **Masaharu NISHIGUCHI, Kazuhiko HINO** *(Kyushu Univ.)*, **Kaori NISHI** *(Kyushu Univ.)*, **Kazuhiko OHASHI, and Nobuyuki NISHI**

Excimer emissions from jet-cooled anthracence dimer are studied in the excitation energy region from 362 nm to 376 nm, where the dual emission is observed. Mass selected resonance enhanced two-photon ionization of the anthracene molecular beams with various beam conditions, such as stagnation pressures and nozzle temperatures, revealed that the most part of the excited species are the same dimer. The $S_1 \leftarrow S_0$ absorption spectrum shows the strongest sharp origin band at 26630 cm^{-1} accompanied with 7 side bands and a weak intramolecular n_{12} band is also seen at 390 cm^{-1} higher than the origin band. This series is designated as Dimer L system. At 367.5 nm (580 cm^{-1} higher than the sharp $S_1 \text{-} S_0$ origin band), a very board band appears with a 370 cm^{-1} vibronic band. This broad band system are designated as Dimer H system. The sharp band (Dimer L system) excitation causes a very broad emission with relatively steep rise at 420 nm and a peak at 465 nm. The lifetime of this emission is, however, as short as 15±5 ns, shorter than that of the monomer (25 ns). On the basis of the band position and its broadness we attributed this emission to an excimer $(A^*A) \leftrightarrow (AA^*)$. The broad band (Dimer H system) excitation provides dual emission composed of high energy fluorescence with a bandwidth of 15 nm(FWHM) and a short lifetime 15±5 ns and a very broad emission with a width of ~100 nm and lifetimes of 300-800 ns (variable with observing wavelengths of the emission). Although the some part of it can be contaminated with the emission from higher polymers, the very broad emission is attributed to an excimer with a charge resonance configuration of $(A^+A^-)^* \leftrightarrow (A^-A^+)^*$.

V-K Molecular Clusters Formed in Aqueous Solutions

Alcohols and carboxylic acids with methyl, ethyl, and propyl groups mix with water at any ratio. Because the mixtures look transparent to the eye, we have believed these molecules are dissolved homogeneously in water. Our previous X-ray diffraction and mass spectrometric study of ethanol-water mixtures with ethanol mole fractions $0.0002 < \chi_e < 0.02$ suggested that cohesion of ethanol molecules are quite dominant even in such low concentrations. Low frequency Raman spectroscopy or Rayleigh wing spectroscopy is very much suited for studying intermolecular bindings in solutions, since Raman scattering activity arises from the autocorrelation of the induced polarizability which is expressed in terms of a sum of the dipole induced dipole contributions mostly from neighboring molecules because they are inversely proportional to the sixth powers of intermolecular distances. *Ab initio* calculation of a gas phase water dimer in an optimized geometry provided a vibrational frequency of a Raman active intermolecular mode to be 205 cm^{-1} (MP2/6-31G**) which is coincident with the peak frequency observed in an ice spectrum demonstrating the calculated frequencies can be reliably used for the assignment of the observed Raman spectra of these mixtures.

V-K-1 Low Frequency Raman Spectroscopy of Ethanol-Water Mixtures: Evidence for Self-Association of Solute and Solvent Molecules

Kazuhiro EGASHIRA *(Kyoto Univ.)* **and Nobuyuki NISHI**

Low frequency region Raman spectra of ethanol-water binary solutions are measured and presented in the form of the relative scattering activities, the $R(\nu)$ spectra. Raman signals originating from dipole-induced dipole interaction are dominated with the interaction between the neighboring molecules. Figure 1 shows the $R(\nu)$ spectra of pure water, pure ethanol, and their mixtures. Since the hydrogen bonding energy between water and ethanol molecules is nearly the same as those between either two water molecules or two ethanol molecules, one can expect the appearance of water-ethanol pair signals with intensities stronger than that of the weaker homogeneous pair signal (water-water or ethanol-ethanol). The observation of an isosbestic point for the spectral change indicates that the change is apparently elucidated by a two state model: water-water pair sate and ethanol-ethanol pair state. What is happening for ethanol-water pairs. Our previous X-ray diffraction and mass spectrometric study demonstrated that in aqueous mixtures ethanol molecules are prone to show cohesion forming ethanol polymers in water.

Ethanol polymers are formed not only by hydrogen bondings but also hydrophobic interaction between ethyl groups. The hydrophobic interaction is stabilized in an aqueous environment. The $R(\nu)$ spectra were found to be decomposed into linear combination of the $R(\nu)$ spectra of pure water and pure ethanol. The plots of the coefficients of linear combination exhibited an inflection point at x_E(ethanol molar fraction) = 0.2, where the integrated intensity of clusters showed maximum in the mass spectrometric observation and excess enthalpy of mixing showed the largest negative value. These observations may suggest that the molecules in each group of ethanol associates and water media exhibit almost independent motional activities in the binary solutions. Such group motions of massive ethanol clusters and water media may result in the dissociation of ethanol-water bonds.

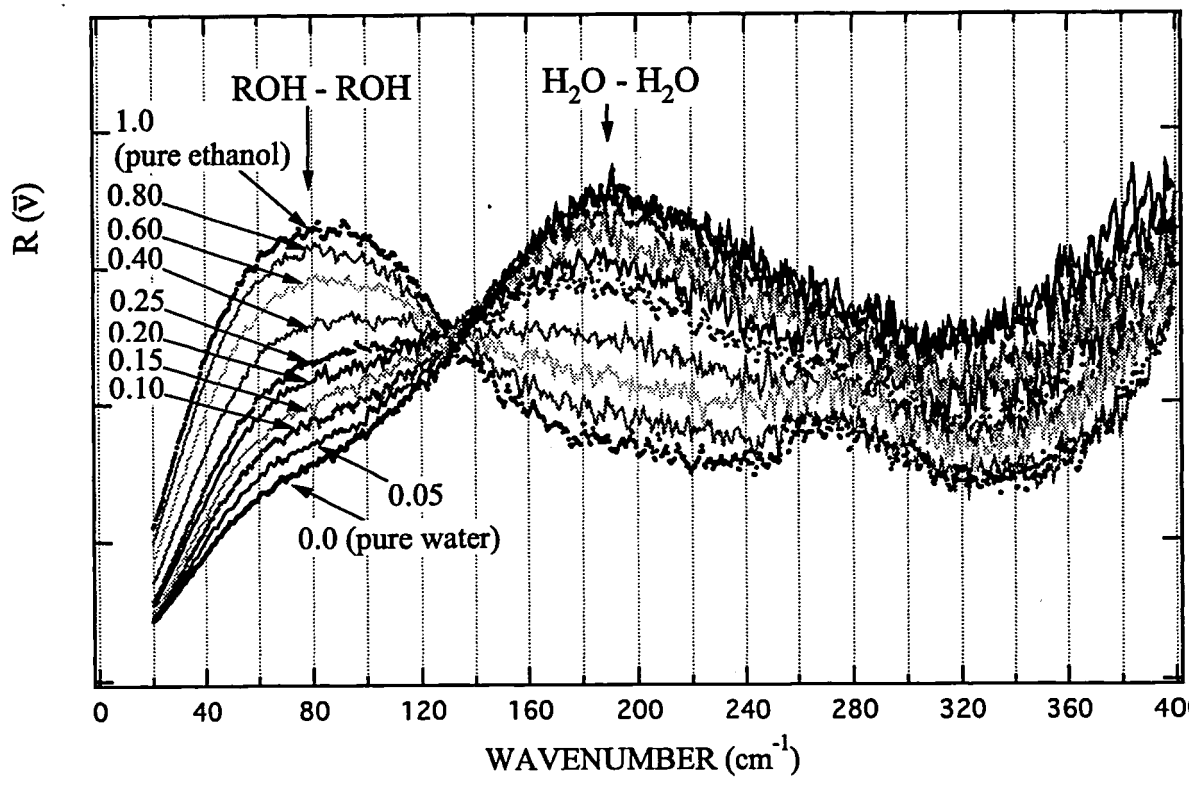

Figure 1. Mixing ratio dependence seen in the $R(\nu)$ representation of low frequency Raman spectra of ethanol-water binary solutions and the pure liquids. One can see an isosbestic point at 132 cm^{-1} where we expected the appearance of strong signals due to ethanol-water pairs. Notice that the ethanol-ethanol pair signal appears to be active even in a low ethanol concentration of x_E= 0.05.

V-K-2 Cohesion of Alcohols in Propanol-Water Mixtures

Kentaro KOSUGI *(Graduate Univ. for Advanced Studies)*, **Masaki ASATO** *(Kyushu Univ.)* **and Nobuyuki NISHI**

Propanol has two isomers with a liner propyl and isopropyl groups. Both are miscible in water at any ratio, while addition of one more methylene to the linear chain causes phase separation. Mass spectrometric study of propanol-water mixture showed preferential cohesion of propanol molecules in water. With increasing alcohol molar fraction (x_A) up to 0.09, propanol polymer signals showed dynamical growth in intensities. Although the intensities of larger polymers decreased, attachment of small but increasing numbers of water molecules were observed with increasing polymer size. The numbers of water molecules for 2-propanol are more than twice as large as those of 1-propanol and increased quadratic to the polymer size in contrast with the linear increase for 1-propanol. This may suggest difference of the polymer structures of the two isomers. Hydration curves showed inflection points at x_A=0.08- 0.09, where the excess enthalpies of mixing of the two compound show the largest negative values.

Low frequency Raman spectra of the two propanols and their mixtures with water at various mixing ratios were observed in the region of 14-400 cm^{-1}. Some of the spectra are shown in Figure 1. A broad peak at 70 cm^{-1} is considered to be composed of two origins: ROH-ROH intermolecular stretching vibration and bending motion of stacked molecules. All alcohols of methanol to propanol and water showed the bending signals in the region of 40-60 cm^{-1}. The spectra of two mixture solutions with x_A =0.05 and 0.19 are shown in the figure. The two mixtures and the two pure liquids show an isosbestic point at 122 cm^{-1} indicating the negligible contribution of propanol-water pairs to the association process. Noticeable intensity increase at 70 cm^{-1} is seen in the x_A =0.05 spectrum. This shows that

the alcohol-alcohol interaction becomes dominant in the solution even in this concentration.

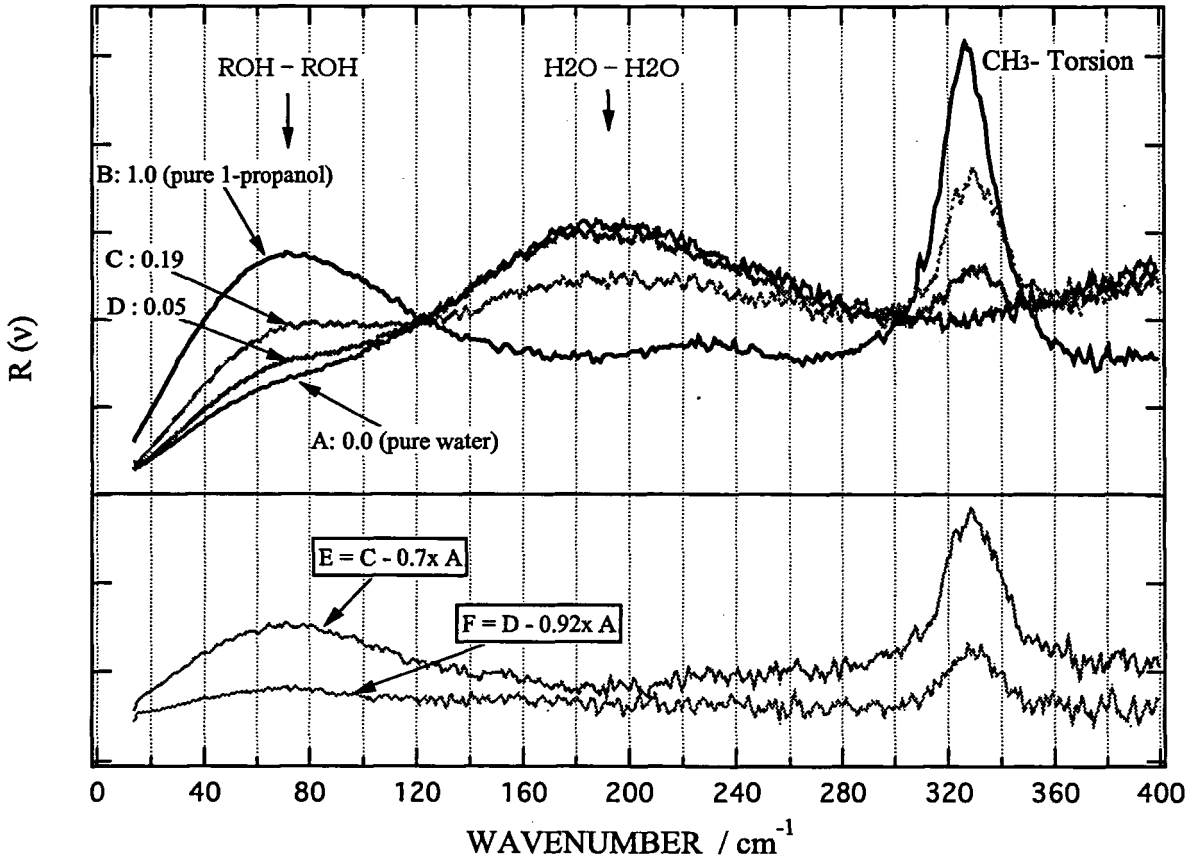

Figure 1. Low frequency Raman spectra of pure water(A), pure 1-propanol(B), and their mixtures with x_A =0.19(C) and 0.05(D). The spectra (E) and (F) are obtained by subtracting 70% and 92% contributions of water spectrum (A) from spectrum C and spectrum D, respectively. E and F are almost identical to the spectrum of pure 1-propanol (B).

V-L Structures and Dynamics of Negatively-Charged Molecular Clusters

One of the fundamental issues regarding the properties of negatively-charged molecular clusters concerns their electronic structures: namely, how the aggregates of molecules bind the excess electrons and how the electronic structures evolve with cluster size. This question is not always easy to answer intuitively, even for the simplest molecular clusters such as $(H_2O)_n^-$, $(CO_2)_n^-$, $(SO_2)_n^-$ ..... etc. To address this issue we have measured the photoelectron spectra to probe the electronic structures of the cluster anions. Of particular interest are (1) the extent of charge localization/delocalization in the negatively-charged clusters, and (2) the existence of "electronic isomers" having different electronic structures. Photofragmentation dynamics and reactivities characteristic of those cluster anions have also been investigated and experimental results are discussed in terms of their electronic properties.

V-L-1 Photoelectron Spectroscopy of $(CO_2)_n^-$: Core Switching in the $2 \leqq n \leqq 16$ Range

Tatsuya TSUKUDA *(Univ. Tokyo)*, **Mark A. JOHNSON** *(Yale Univ.)* **and Takashi NAGATA**

[*Chem. Phys. Lett.* **268**, 429 (1997)]

Since the pioneering work of Klots and Compton[1], a number of experiments have shown that cluster anions of carbon dioxide, $(CO_2)_n^-$, with $n \geqq 3$ are readily formed in the collisions between neutral $(CO_2)_N$ clusters and slow electrons, while a bare CO_2 molecule does not bind an excess electron as long as it retains the linear equilibrium geometry. We have re-investigated photoelectron spectra[2] of $(CO_2)_n^-$ at the photon energy of 4.66 eV (Figure 1), from which the vertical detachment energy (VDE) is determined as a function of cluster size $2 \leqq n \leqq 16$. The n-dependence of VDE exhibits sharp discontinuities between n = 6 and 7, and between n = 13 and 14. This indicates that the anionic core of $(CO_2)_n^-$ changes from CO_2^- to $C_2O_4^-$ at n = 7, and from $C_2O_4^-$ to CO_2^- at n = 14. A hole-burning type of photoelectron measurement has also been performed

revealing that $(CO_2)_6^-$ is flopping between the two isomeric structures, $CO_2^-\cdots(CO_2)_5$ and $C_2O_4^-\cdots(CO_2)_4$.

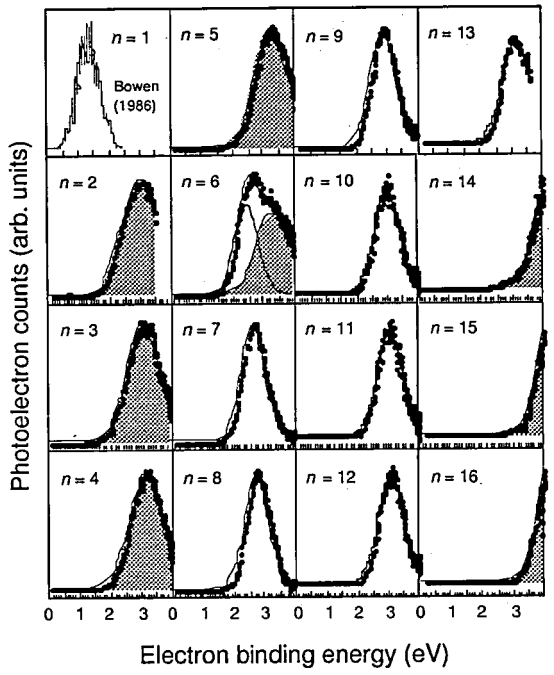

Figure 1. Photoelectron spectra of $(CO_2)_n^-$ with $2 \leqq n \leqq 16$. The photoelectron counts are plotted against electron binding energy defined as $E_b = h\nu - E_k$, where $h\nu$ and E_k represent the photon energy and the kinetic energy of the photoelectrons, respectively. The shaded areas correspond to the band components attributed to the $C_2O_4^- \cdots (CO_2)_{n-2}$ isomers.

References

1) C. E. Klots and R. N. Compton, *J. Chem. Phys.* 67, 1779 (1977); 69, 1636 (1978).
2) M. J. DeLuca, B. Niu and M. A. Johnson, *J. Chem. Phys.* **88**, 5857 (1988).

V-L-2 Photoelectron Spectroscopy of $(CS_2)_n^-$: Coexistence of Electronic Isomers

Tatsuya TSUKUDA *(Univ. Tokyo)*, **Takayuki HIROSE** *(Univ. Tokyo)* **and Takashi NAGATA**

[*Chem. Phys. Lett.* in press]

We have measured the photoelectron spectra of $(CS_2)_n^-$ to explore the isomers having different electronic structures. Figure 1 displays the photoelectron spectra of $(CS_2)_n^-$ with $1 \leqq n \leqq 6$. As the observed band shift lies in the range expected for typical ion–molecule interactions, we infer that the electronic structure of $(CS_2)_n^-$ evolves as an ion-neutral complex, $CS_2^-\cdots(CS_2)_{n-1}$, with increase in the cluster size. A closer examination of the $n = 2$ spectra revealed that non–negligible amount of photoelectrons are detected in the energy range between the lowest band and the high-energy bands. This is most obvious in $n = 2$, which clearly demonstrates the presence of another photoelectron band around 2.7 eV. The 2.7-eV photoelectron band is ascribed to the $C_2S_4^-$ molecular anion. For the larger clusters with $n \geq 3$, the band intensity ascribable to the $C_2S_4^-\cdots(CS_2)_{n-2}$ structure appears slight but significant. This shows the coexistence of "electronic" isomers, $CS_2^-\cdots(CS_2)_{n-1}$ and $C_2S_4^-\cdots(CS_2)_{n-2}$.

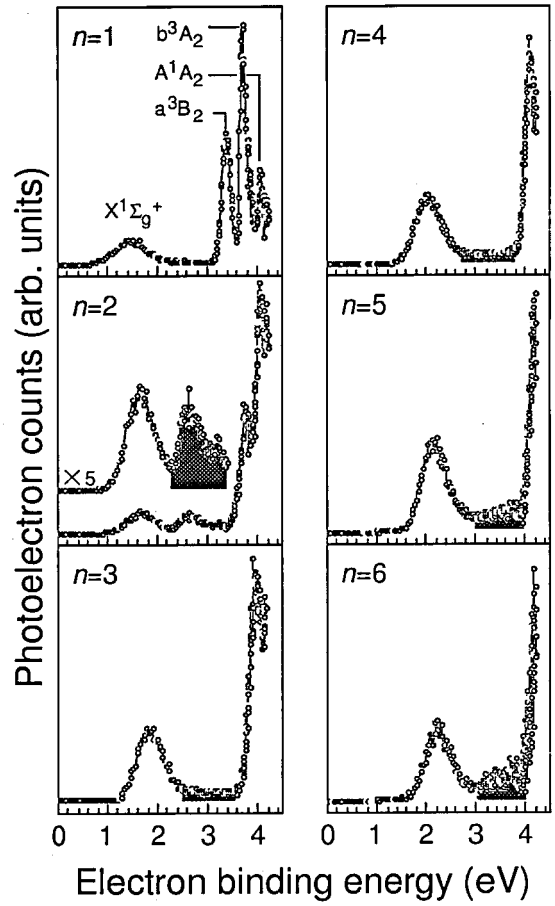

Figure 1. Photoelectron spectra of $(CS_2)_n^-$ measured at the photon energy of 4.66 eV. The shaded areas represent the contributions from the $C_2S_4^-\cdots(CS_2)_{n-2}$ isomers. The high-energy bands appearing in the $n = 1$ spectrum are tentatively assigned to the transitions to a^3B_2, b^3A_2 and A^1A_2 states of CS_2.

V-L-3 Electronic Structures of $(SO_2)_n^-$ as Studied by Photoelectron Spectroscopy

Tatsuya TSUKUDA *(Univ. Tokyo)*, **Takayuki HIROSE** *(Univ. Tokyo)* **and Takashi NAGATA**

[*Int. J. Mass Spectrum. & Ion Processes* in press]

Photoelectron spectroscopy is used to probe the electronic properties of $(SO_2)_n^-$. As shown in Figure 1, the photoelectron band shifts smoothly toward a higher electron binding energy in the $n \geqq 2$ range. The result indicates that $(SO_2)_2^-$ acts as a core in the larger analogues. An S-S bonded structure of $(SO_2)_2^-$, where the excess electron is shared equally between the two SO_2 monomers[1)], is a strong candidate for the anionic core. As the $(SO_2)_n^-$ spectrum contains a single photoelectron band, we can rule out the possibility that isomeric forms of $(SO_2)_n^-$ coexist under our ion-source conditions.

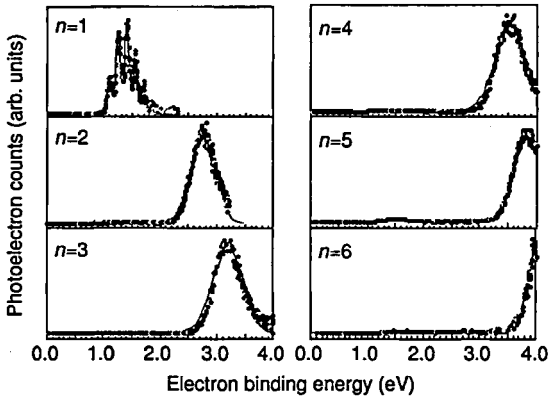

Figure 1. Photoelectron spectra of $(SO_2)_n^-$ with $1 \leqq n \leqq 6$.

Reference

1) N. Berthe–Gaujac, I. Demachy, Y. Jean and F. Volatron, *Chem. Phys. Letters* 221, 145 (1994).

V-L-4 Nucleophilic Reactivity of Gas-Phase Cluster Anions

Tatsuya TSUKUDA *(Univ. Tokyo)*, **Morihisa SAEKI** *(Univ. Tokyo and IMS)* **and Takashi NAGATA**

[*J. Phys. Chem.* **101**, 5103 (1997)]

Since early 1970s, gas-phase S_N2 displacement reactions, $X^- + RY \rightarrow RX + Y^-$, have long been a subject of extensive theoretical and experimental investigations. However, little is known about the reactions of larger analogues; that is, nucleophilic reactions including cluster anions, $M_n^- + RY \rightarrow RM_m + Y^-$, etc. In the present study, we have demonstrated for the first time the chemical reactivity of $(CO_2)_N^-$ as a nucleophile by means of a mass spectrometric technique combined with photoelectron spectroscopy. Negatively-charged clusters of carbon dioxide $(CO_2)_N^-$ react with CH_3I leading to the formation of anions with the formulae $[(CO_2)_nCH_3I]^-$, $[(CO_2)_nCH_3]^-$ and $[(CO_2)_nI]^-$. Photoelectron spectroscopy of the product anions has revealed that an acetyloxy iodide anion, $CH_3CO_2I^-$, is formed in $[(CO_2)_nCH_3I]^-$ with $1 \leqq n \leqq 3$. The $CH_3CO_2I^-$ anion exhibits a large vertical detachment energy (VDE) of 3.53 eV, due probably to delocalization of the excess electron. Ab initio calculations show that the excess electron resides in the O-I anti-bonding orbital of $CH_3CO_2I^-$ (see V-L-7). The reaction is found to be strongly subject to steric hindrance around the carbon site of CH_3I. In fact, the reaction of $(CO_2)_N^-$ with 2-C_3H_7I yields no product cluster anions containing 2-$C_3H_7CO_2I^-$. We infer from this finding that $CH_3CO_2I^-$ is formed via an S_N2 transition state, which is prepared by a nucleophilic attack of CO_2^- on the carbon site of alkyl iodide (Scheme 1).

The overall reaction process can be regarded as carboxylation by the reductive activation of CO_2, which opens up a possibility of studying elementary processes of electrochemical reactions, not in the condensed phase but in the gas phase with a restricted number of solvent molecules.

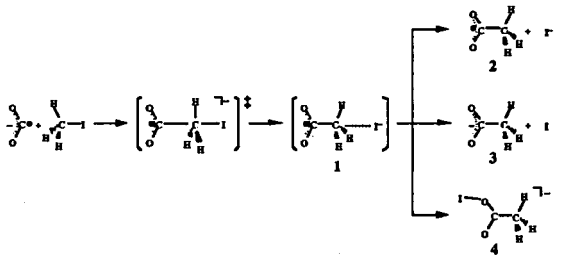

Scheme 1.

V-L-5 Photoabsorption and Photo-fragmentation Studies of Acetyloxy Iodide Anion $CH_3CO_2I^-$

Morihisa SAEKI *(Univ. Tokyo and IMS)*, **Tatsuya TSUKUDA** *(Univ. Tokyo)*, **Suehiro IWATA and Takashi NAGATA**

[*Chem. Phys. Lett.* in press]

Recently we have reported the formation of acetyloxy iodide anion, $CH_3CO_2I^-$, in the gas-phase reactions of $(CO_2)_n^-$ with methyl iodide: $(CO_2)_n^- + CH_3I \rightarrow CH_3CO_2I^- + (n-1)CO_2$. [1), 2)] This was the first observation not only of nucleophilic reactivities of $(CO_2)_n^-$ but also of $CH_3CO_2I^-$ anion. In this study photoabsorption cross sections of newly produced gas-phases anion of acetyloxy iodide, $CH_3CO_2I^-$, are obtained by photofragmentation spectroscopy in the spectral range 2.48 - 3.60 eV. The photoabsorption spectrum is dominated by two broad bands, peaking at 3.0 and 3.2 eV, well below the vertical detachment energy. Photoproducts are found to be $CH_3CO_2^-$ and I^-, for which branching fractions are determined as a function of excitation energy. Base on these experimental findings, we discuss the electronic properties and state correlation in $CH_3CO_2I^-$ in conjunction with the results of ab initio calculations (see V-L-7).

References

1) T. Tsukuda, M. Saeki and T. Nagata, *Chem. Phys. Letters* **251**, 309 (1996).
2) T. Tsukuda, M. Saeki, S. Iwata and T. Nagata, *J. Phys. Chem.* **101**, 5103 (1997).

V-L-6 Photoabsorption and Photo-fragmentation Studies of Nitric Oxide Cluster Anions $(NO)_n^-$

Lei ZHU, Tatsuya TSUKUDA *(Univ. Tokyo)*, **Morihisa SAEKI** *(Univ. Tokyo and IMS)* **and Takashi NAGATA**

Photoabsorption cross sections for $(NO)_n^-$ with $3 \leqq n \leqq 7$ have been measured in the energy range of 2.70 - 3.55 eV. A single broad peak in the visible region was observed, whose blue-shift with growing n is interpreted as a trimer-core chromophore in the cluster anions. The time-of-flight (TOF) spectra of ionic and neutral fragments produced in the photodissociation of $(NO)_n^-$ ($3 \leqq n \leqq 23$) were measured at wavelength of 440 nm with photons of

either parallel ($\Theta = 0°$) or perpendicular ($\Theta = 90°$) polarization with reference to the ion beam direction. For $(NO)_n^-$ with $3 \leqq n \leqq 7$, direct dissociation of the core anion prevails, which gives rise to high kinetic energy release of $(NO)_2^-$ and neutral NO fragments along with anisotropic angular distributions. For $(NO)_n^-$ with $n \geqq 8$, an almost isotropic distribution was observed for the fragments indicating that "evaporation" of the solvent NO neutrals dominates.

V-L-7 *Ab Initio* MO Calculations on Acetyloxy Iodide Anion $CH_3CO_2I^-$

Morihisa SAEKI *(Univ. Tokyo and IMS)*, **Tatsuya TSUKUDA** *(Univ. Tokyo)*, **Lei ZHU, Takashi NAGATA and Suehiro IWATA**

Geometrical and electronic structures of $CH_3CO_2I^-$ were investigated by *ab initio* MO calculations at the MP2 level of theory. The optimized structure is composed of an acetate framework, which binds an I atom through an elongated O-I bond with an internuclear distance of $\approx$ 2.6 Å. Interaction between the HOMO of acetate and the 5*p* orbital of I atom results in the formation of a pair of orbitals with bonding and anti-bonding character, the latter accommodating the excess electron. The MR-CI calculation for excited states indicates the existence of two optical transitions with non-zero oscillator strength. and they are assigned to the $3^2A' \leftarrow 1^2A'$ and $4^2A' \leftarrow 1^2A'$ transitions. While $4^2A'$ incipiently correlates to the $CH_3CO_2 + I^-$ dissociation limit, the interaction with $1^2A'$ causes an avoid crossing at a certain internuclear distance and, as a result, $4^2A'$ adiabaticaly correlates to the $CH_3CO_2^- + I(^2P_{1/2})$ dissociation channel. These theoretical findings well explain the results experimentally obtained in the photoabsorption and photodissociation studies of $CH_3CO_2I^-$(see V-L-5).

RESEARCH ACTIVITIES VI
Department of Vacuum UV Photoscience

VI-A Electronic Structure and Decay Mechanism of Inner-Shell Excited Molecules

This project is being carried out in collaboration with Photon Factory (KEK-PF). We are interested in ionic fragmentations and electron emissions via inner-shell excitation of molecules and in their polarization dependence. Recently we have investigated vibronic couplings in the inner-shell excited states of some polyatomic molecules, and found that the fragmentation takes place during the molecular vibrations. The bending vibration is important in considering angular distribution of fragment ions. We are extending our approaches to other molecules.

VI-A-1 Angular Distribution of the Fragment Ions Following the S 1*s* Photoexcitations of OCS

Jun-ichi ADACHI, Yasutaka TAKATA, Nobuhiro KOSUGI, Atsunari HIRAYA,* Eiji SHIGEMASA, Akira YAGISHITA** and Yoshinori KITAJIMA****
*(*Hiroshima Univ., *KEK-PF)*

We have measured angle-resolved ion-yield spectra for the S 1*s* excited states of OCS using linearly polarized synchrotron radiation. The intense peak (**A**) in the ion-yield spectrum observed in the 90° direction to the electric vector of the incident light (I_{90}) is assigned to the 1σ (S 1*s* → 4π* (π*) excited state. The fragment ions emitted following the π* excitation is also observed in the 0° direction (I_0) and the peak top in the I_0 spectrum is slightly lower (0.09 eV) in energy than in the I_{90} spectrum. These results mean that the π* excited state is affected with the Renner-Teller effect as observed in the O 1*s* → π* excitation of N_2O [J. Adachi *et al.*, *J. Chem. Phys.* **102**, 7369 (1995)]. The intense peak (**B**) in the I_0 spectrum is assigned to the 1σ → 10σ* (σ*) excited state. The width of Peak B is larger than that of Peak A. This indicates that the 10σ* orbital is of anti-bonding character and the equilibrium bond distances are elongated in the 1σ → 10σ* excited state. The present spectra reveal that Peak **D** includes the 1σ → 4*p*σ and 4*p*π Rydberg excited states.

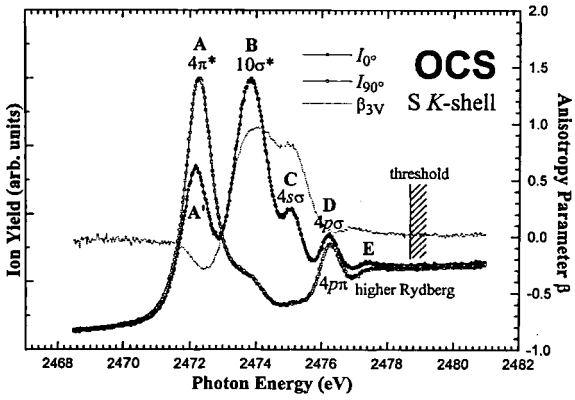

Figure 1. Angle-resolved ion-yield spectra and anisotropy parameter on fragment ions for the S *K*-shell excited states of OCS. The dotted (I_0) and solid lines (I_{90}) show the ion yields in the 0° and 90° directions to the electric vector of the incident light, respectively. The thin broken line shows the observed anisotropy parameter $\beta_{3V} = 2\cdot(I_0 - I_{90}) / (I_0 + 2\cdot I_{90})$ for the fragment ions with the kinetic energy of more than 3 eV.

VI-A-2 Angular Distribution of the Fragment Ions following the S 1*s* Photoexcitations of CS_2

Jun-ichi ADACHI, Yasutaka TAKATA, Nobuhiro KOSUGI, Atsunari HIRAYA,* Eiji SHIGEMASA, Akira YAGISHITA** and Yoshinori KITAJIMA****
*(*Hiroshima Univ., **KEK-PF)*

We have measured angle-resolved ion-yield spectra for the S 1*s* excited states of CS_2 using linearly polarized synchrotron radiation. The intense peak (**A**) in the ion-yield spectrum observed in the 90° direction to the electric vector of the incident light (I_{90}) is assigned to the S 1*s* → π* excited state. The intense peak (**B**) in the ion-yield spectrum in the 0° direction (I_0) is attributed to two excited states: the $1\sigma_u$ (S 1*s*) → $7\sigma_g$* (σ_g*) valence and $4s\sigma_g$ Rydberg excited states. The fragment ions emitted following the σ* excitation is also observed in the I_{90} spectrum and the peak top in the I_{90} spectrum (**B'**) is slightly higher (0.07 eV) in energy than in the I_0 spectrum (**B**). Peak **B'** is attributed to the vibronically induced transition; that is, the $1\sigma_g$ (S 1*s*) → σ_g* excitation borrows the intensity from the S 1*s* → π* transition (**A**) through the bending mode. Peak **D** in the I_0 spectrum is probably assigned to $5s\sigma_g$ Rydberg excited states mixed with the $7\sigma_g$* excited state. Peaks **E** and **E'** near the ionization threshold are attributed to higher members of Rydberg excited states.

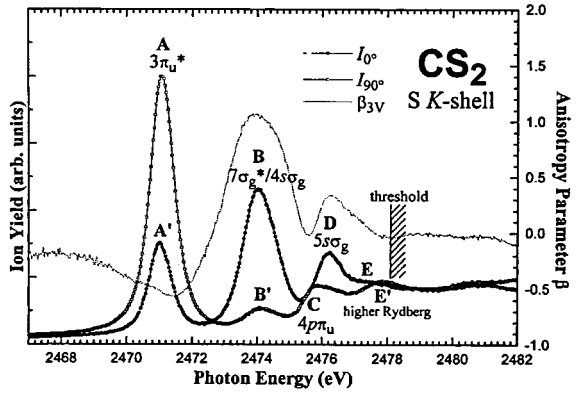

Figure 1. Angle-resolved ion-yield spectra and anisotropy parameter on fragment ions for the S *K*-shell excited states of CS_2. The dotted (I_0) and solid lines (I_{90}) show the ion yields

in the 0° and 90° directions to the electric vector of the incident light, respectively. The thin broken line shows the observed anisotropy parameter $\beta_{3V} = 2\cdot(I_0 - I_{90}) / (I_0 + 2\cdot I_{90})$ for the fragment ions with the kinetic energy of more than 3 eV.

VI-A-3 Vibronic Couplings in the C 1*s* → *ns* σ_g Rydberg Excited States of CO_2

Jun-ichi ADACHI, Nobuhiro KOSUGI, Eiji SHIGEMASA* and Akira YAGISHITA* *(*KEK-PF)*

[*J. Phys. Chem.* **100**, 10783 (1996)]

Fragment ion yields in the C 1*s* → Rydberg excitation region of CO_2 were measured in the 90° and 0° directions relative to the electric vector of the linearly polarized light. The C 1*s* → *ns* (*n* = 3 and 4), *npσ* and *npπ* (*n* = 3 – 7), and *nd* (*n* = 3 and 4) Rydberg transitions are clearly observed and show some vibrational structures. The dipole-forbidden C 1*s* (σ_g) → 3*s*σ_g Rydberg transition is the strongest of all the Rydberg transitions, and the ion yield in the 90° direction is dominant. This indicates that the bending vibration is predominantly coupled with the 3*s*σ_g Rydberg state and the intensity-lending dipole allowed state is a very strong π^* resonance, only 2 eV lower than the 3*s*σ_g state. On the other hand, in the 4*s*σ_g Rydberg state the vibronic coupling through the antisymmetric stretching mode is strongly observed in the 0° direction. This is probably because the 4*s*σ_g state approaches another intensity-lending state with Σ_u^+ symmetry and goes away from the π^* resonance. The angle-resolved ion-yield technique is very powerful for elucidating the vibronic coupling mechanism.

VI-A-4 Fixed-Molecule 1*s*$\sigma_{g,u}$ Photoelectron Angular Distributions as a Probe of σ_g^* and σ_u^* Shape Resonances of CO_2

Naoki WATANABE,* Jun-ichi ADACHI, Koichi SOEJIMA, Eiji SHIGEMASA,*** Akira YAGISHITA,*** N. G. FOMINYKH**** and A. A. PAVLYCHEV****** *(*Hokkaido Univ., **Niigata Univ., ***KEK-PF, ****St. Petersburg Univ.)*

[*Phys. Rev. Lett.* **78**, 4910 (1997)]

Angular distributions of 1*s*$\sigma_{g,u}$ photoelectrons from CO_2 molecules, oriented parallel to the electric vector of incident light, have been measured. The angular distribution patterns at σ_g^* and σ_u^* shape resonances are significantly different from those expected in the virtual molecular orbitals concept. The analyses of the patterns have made it clear that the mixing of outgoing photoelectron partial waves and the interference between them are responsible for the observed patterns, unlike N_2 photoionization. Calculations based on a quasiatomic model have reproduced the observed patterns fairly well.

VI-A-5 Soft X-ray Absorption and X-ray Photoelectron Spectroscopic Study of Tautomerism in Intramolecular Hydrogen Bonds of *N*-Salicylideneaniline Derivatives

Eisuke ITO,* Hiroshi OJI,* Tohru ARAKI,* Kazuyoshi OICHI,* Hisao ISHII,* Yukio OUCHI,* Toshiaki OHTA, Nobuhiro KOSUGI, Yusei MARUYAMA,*** Toshio NAITO,**** Tamotsu INABE**** and Kazuhiko SEKI*** *(*Nagoya Univ., **Univ. Tokyo, ***Hosei Univ., ****Hokkaido Univ.)*

[*J. Am. Chem. Soc.* **246**, 475 (1997)]

The tautomerism for five *N*-salicylideneaniline derivatives in solid phase was studied by near-edge X-ray absorption fine structure (NEXAFS) spectroscopy at the N K- and O K-edges as well as X-ray photoelectron spectroscopy (XPS) in the N 1s and O 1s regions. The NEXAFS spectral features were assigned by the comparison with the core excitation spectra of reference compounds and ab initio MO calculations of the core-excited states by the improved virtual orbital method using the relaxed Hartree-Fock orbitals. The tautomeric structures were deduced by the intensity of peaks characteristic of the tautomers in OH- and NH-forms. These results demonstrate the usefulness of NEXAFS as well as XPS for studying the tautomerism in hydrogen bonded systems.

VI-B Soft X-ray Photoelectron-Photoabsorption Spectroscopy and Electronic Structure of Transition Metal Compounds

We are measuring inner-shell photoabsorption and photoelectron spectra by using a high-performance electron energy analyzer connected to the soft X-ray double crystal monochromator of the beamline BL1A at the UVSOR facility. Last year we started to investigate electronic structures of molecular Ni complexes with planar structure. This year strong metal-to-ligand charge transfer (MLCT) bands in the Ni 2p photoabsorption are found by successfully measuring their polarization dependence; furthermore, several forbidden satellite features are also found in the Ni 3d-valence and 3p/3s-core photoelectron spectra, which are resonantly allowed via the Ni 2p excitation. We have discussed characteristic one-electron features in inner-shell excited states of the molecular Ni complexes.

VI-B-1 Polarization Dependence of Ni 2*p* Photoabsorption of $K_2Ni(CN)_4 \cdot H_2O$

Takaki HATSUI *(Grad. Univ. Adv. Studies)*, **Yasutaka TAKATA and Nobuhiro KOSUGI**

To elucidate the origin of characteristic satellite peaks, polarized Ni 2p photoabsorption spectra were measured on the single crystal of $K_2Ni(CN)_4 \cdot H_2O$ as shown in Figure 1. Transitions are classified into three types: (i) isotropic (E⊥z ≒ E//z), (ii) in-plane (E⊥z), and (iii) dominant out-of-plane (E⊥z < E//z). The dipole-allowed states from Ni 2p should have d and/or s components; (i) 2p-4s*, (ii) 2p-$3d_{x2-y2}$* or L_{x2-y2}*, (iii) 2p-L_{xz}* or L_{yz}*, where Ni has two unoccupied orbitals, $3d_{x2-y2}\sigma$* and 4s*, and the unoccupied ligand orbitals (L*) have $d_{xy}\sigma$*, $d_{z2}\sigma$*, $d_{xz}\pi$* and $d_{yz}\pi$* symmetries. Peaks A and C should be forbidden in the E // z considering the disorder induced by dehydration under vacuum, and are attributable to the transition to Ni $3d_{x2-y2}(b_{1g})$ and L_{xy}*(b_{2g}), respectively. The results of ab initio SCF calculations of Ni 2p excited states revealed that the peak B and D are attributable to the transitions to the Ni 4s*(a_{1g}) and $L_{xz,yz}$*(e_g) orbital, respectively.

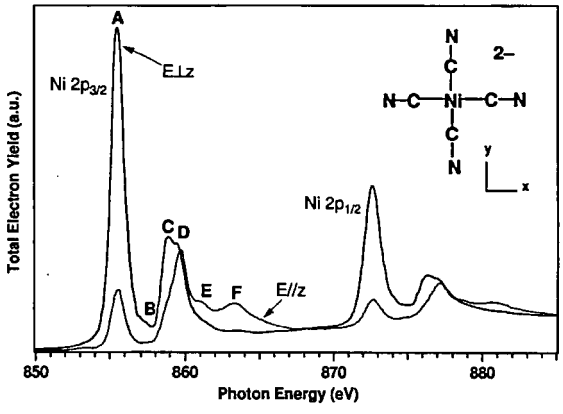

Figure 1. Polarized Ni 2p photoabsorption spectra of $K_2Ni(CN)_4 \cdot H_2O$.

VI-B-2 Polarization Dependence of Ni 2*p* Photoabsorption of Ni Dimethyl-glyoxime

Takaki HATSUI *(Grad. Univ. Adv. Studies)*, **Yasutaka TAKATA, Nobuhiro KOSUGI, Kaoru YAMAMOTO*, Toshihiko YOKOYAMA* and Toshiaki OHTA*** *(*Univ. Tokyo)*

Polarized Ni 2p photoabsorption spectra were measured on the single crystals of nickel dimethylglyoxime, $Ni(Hdmg)_2$ as shown in Figure 1. The planar $Ni(Hdmg)_2$ molecules are aligned exactly parpendicular to the c axis, and are alternately rotated 90° about the c axis. Therefore, the E⊥z, or E⊥c, spectrum corresponds to an average of the E//x and E//y spectra, where E is the electric vector of incident light. In this molecule, there is no in-plane ligand π* orbital with hybridization with Ni $3d_{x2-y2}$; therefore, we cannot expect strong satellites in E⊥z. This expectation is in good agreemnt with the obsevation. The lowest peak A is attributable to the transition to Ni $3d_{xy}$*. Peak C does not show a significant polarization dependence and is assigned to the transition to the Ni 4s* (a_g) orbital. Peaks B and D are stronger in the E//z spectra and are attributable to the transitions to the L_{xz}*(b_{2g}) and L_{yz}*(b_{3g}) orbital, respectively.

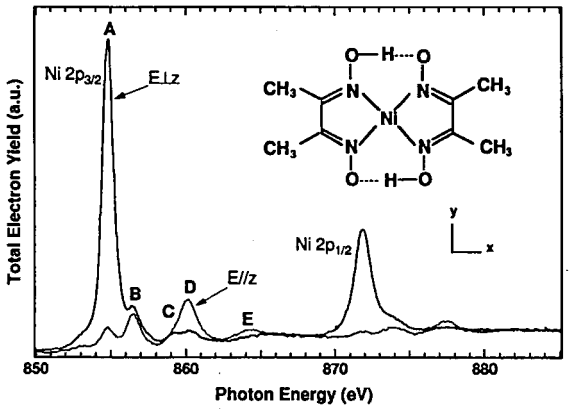

Figure 1. Polarized Ni 2p photoabsorption of $Ni(Hdmg)_2$.

VI-B-3 Resonant Behavior in Ni 3d, 3p and 3s Photoelectron Spectra at the Ni 2p Excitation of Planar Molecular Complex $Ni(Hdmg)_2$

Yasutaka TAKATA, Takaki HATSUI and Nobuhiro KOSUGI

[*J. Electron Spectrosc.* in press]

Resonant photoelectron spectra of the Ni 3d valence and Ni 3p and 3s core were measured for nickel dimethylglyoxime [$Ni(Hdmg)_2$] in the Ni 2p excitation region. Figure 1 shows photoelectron spectra in the valence band region at the off-resonance (0), Ni $2p_{3/2}$ (1-6), and $2p_{1/2}$ (7-9) resonance excitations together with the normal Auger spectrum. The highest peak labeled sharp (#), which arises in the Ni 3d ionized states with constant binding energy, is enhanced by the resonance excitation. The satellite bands labeled f and f', which are weak or forbidden in the off-resonance spectrum, are also enhanced and lower the kinetic energies with the higher photon energies; that is, the satellites have neither constant binding energy nor constant kinetic energy. In the Ni 3s and 3p ionization region, the satellites are enhanced but the Ni 3s and 3p primary ionized states are not enhanced at all. Similar resonant behaviors of the satellites have not been reported in solid systems, except for $K_2Ni(CN)_4$. In the oxides and halides, the satellites observed in the off-resonance spectrum are enhanced and show constant binding energies in a wide photon energy region. The satellite features arise in $2p\ \varphi_i - 3d3d\ \psi_f$, $2p\ \varphi_i - 3p3d\ \psi_f$, $2p\ \varphi_i - 3s3d\ \psi_f$, and $2p\ \varphi_i - 3p3p\ \psi_f$, where ψ_f behaves as an exciton converging to the doubly ionized state with $\underline{3d}\ \underline{3d}$ and so on, and has a larger bound-state energy than φ_i converging to the $2p_{3/2}/2p_{1/2}$ singly ionized state.

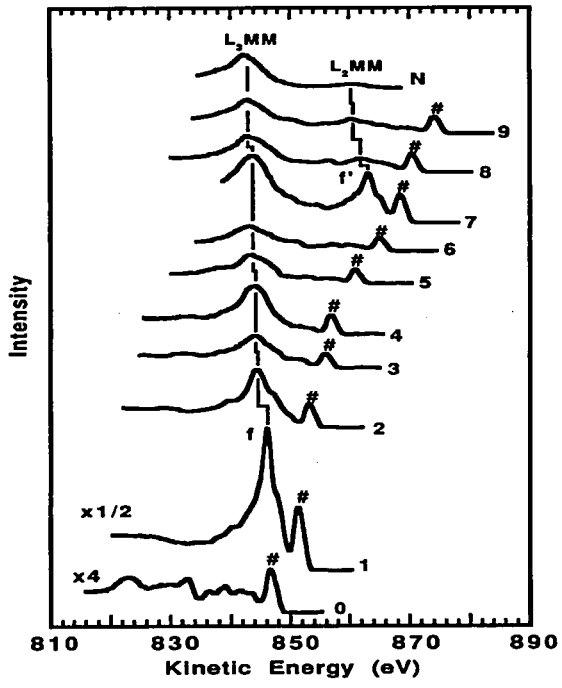

Figure 1. Photoelectron spectra in the Ni 3d valence ionization regions of $Ni(Hdmg)_2$. The off-resonance spectrum (0) was measured at 849.9 eV. The Ni $2p_{3/2}$ resonance spectra were measured at 854.7 eV (1), 856.4 eV (2), 859.1 eV (3), 860.1 eV (4), 864.2 eV (5), 868.2 eV (6), and the Ni $2p_{1/2}$ resonance spectra were measured at 868.2 eV (7), 871.5 eV (8), 877.2 eV (9). The normal Auger spectrum at the photon energy of 899.6 eV is also shown.

VI-C Studies on Primary Photochemical/physical Processes using Femtosecond Time-Resolved Electronic Spectroscopy

Ultrafast spectroscopy is playing an essential role in the elucidation of photochemical reactions. Thanks to recent advances of the laser technology, we are now even able to observe wavepacket evolution in the course of chemical reactions with femtosecond time-resolution. In this project, we are studying primary photochemical/physical processes in the condensed phase using several types of femtosecond time-resolved spectroscopy. We already constructed two experimental setups in the last year; a femtosecond time-resolved fluorescence up-conversion spectrometer and a femtosecond optical heterodyne detected impulsive stimulated Raman scattering (OHD-ISRS) spectrometer. In this year, while continuing research with these setups, we have also constructed a setup for femtosecond time-resolved absorption spectroscopy which covers the wavelength region from near-uv to near-ir.

VI-C-1 Observation of Dimer Excited-State Dynamics in the Double Proton Transfer Reaction of 7-Azaindole by Femtosecond Fluorescence Up-Conversion

Satoshi TAKEUCHI and Tahei TAHARA

[*Chem. Phys. Lett.* in press]

Femtosecond time-resolved fluorescence of 7-azaindole dimer in hexane was measured at room temperature by using the up-conversion method (Figure 1). The measurements covering a wide visible wavelength region revealed that the fluorescence consists of two rapid decay components (τ_1 = 0.2 ± 0.1 ps, τ_2 = 1.1 ± 0.1 ps) and a long-lived component attributable to the tautomeric fluorescence (τ_3 = 3.2 ns and λ_{max} = 490 nm). The two decay components were assigned to the fluorescences from two dimeric excited states which are successively populated in the relaxation process prior to the double proton transfer reaction. The dynamics of the excited-state proton transfer as well as assignments of the dimeric excited states is discussed.

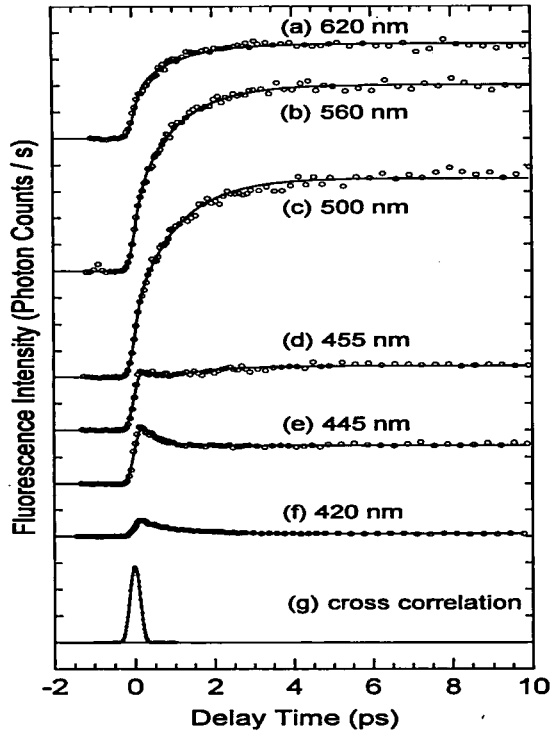

Figure 1. Time-resolved fluorescence signals obtained from

7-azaindole dimer in hexane (10^{-2} mol dm^{-3}, 270 nm excitation). Fluorescence signals at 620 nm (a), 560 nm (b), 500 nm (c), 455 nm (d), 445 nm (e), 420 nm (f), and a typical cross-correlation trace between the excitation and the gate pulses (g). The open circles are experimental data points, and the solid curves are results of the fitting analysis. The instrumental time-resolution given by the fwhm of the cross-correlation trace is 280 fs.

VI-C-2 Construction of a Femtosecond UV-VIS-NIR Transient Absorption Spectrometer

Satoshi TAKEUCHI and Tahei TAHARA

We have constructed an experimental setup for femtosecond transient absorption measurements with a pump-probe scheme (Figure 1). The light source of this system is a regeneratively amplified output of Ti:sapphire laser (1 mJ/pulse, 100 fs duration @800 nm). This fundamental output is divided into two parts to generate pump and probe pulses. One is frequency-doubled in a LBO crystal (1mm thickness), and the produced second harmonic (SH) is further mixed with the residual fundamental in a BBO crystal (0.5 mm thickness) to generate the third harmonic (TH). One of these harmonics (SH : 400 nm, 150 μJ: TH : 267 nm, 30 μJ) is used as a pump pulse. The other fundamental is focused into a quartz cell containing water to generate a femtosecond white light continuum covering a wide spectral region from near-UV to near-IR. The continuum is divided into two, and is used as a probe pulse and a reference pulse. The probe and reference pulses transmitting the sample are fiber-coupled into an imaging spectrograph (500 mm focal length), and their spectral intensities are simultaneously detected by a CCD camera. Pump-induced absorbance change signal at a certain delay time is calculated from these spectral data with and without the pump. The time-resolution of the instrument was estimated as 200 fs and 350 fs for photoexcitation with the SH and TH pulses, respectively. The data can be collected at a 100 Hz repetition rate synchronized with the light source. This spectrometer enables us to detect the absorbance change as small as 1 mO.D. in several seconds.

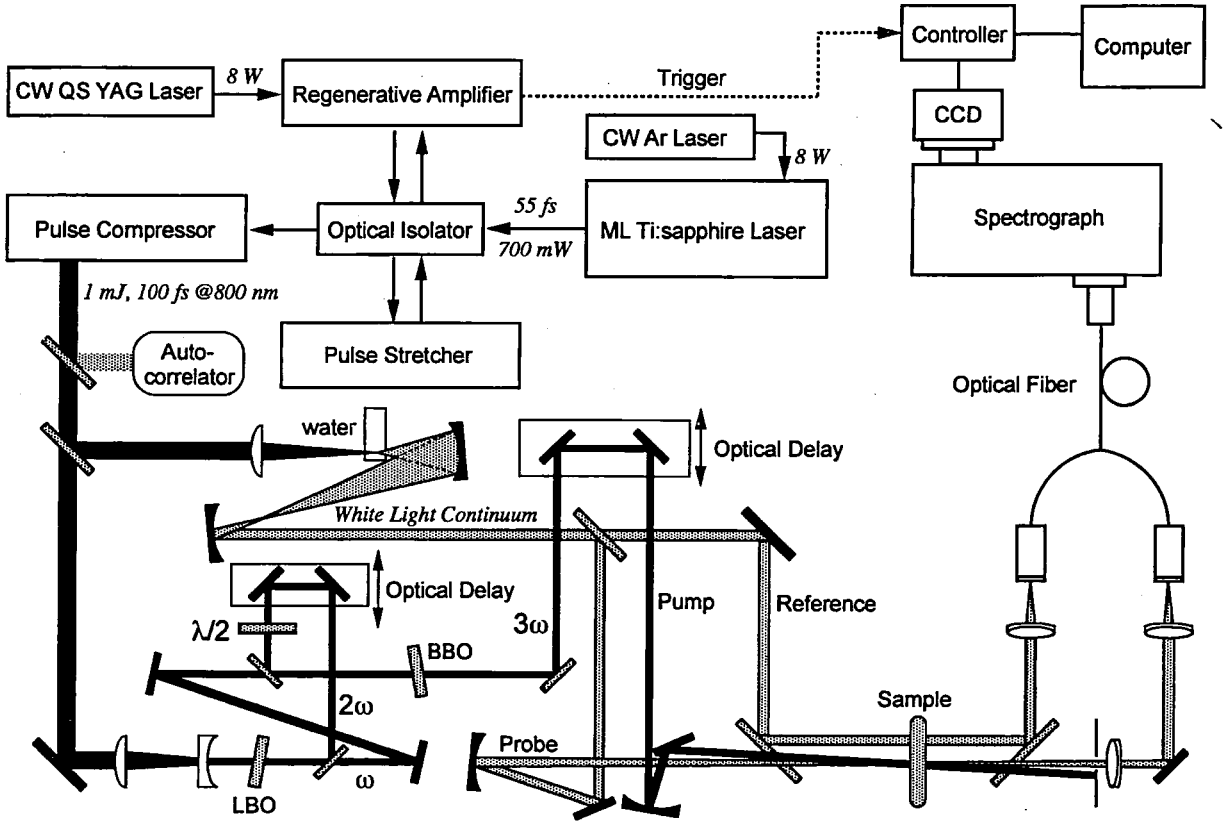

Figure 1. Experimental setup for femtosecond transient absorption measurements.

VI-C-3 Construction of a Flow System of Supercritical Fluids for Ultrafast Spectroscopy

Misa KAYAMA *(Grad. Univ. for Advanced Studies)* **and Tahei TAHARA**

Recently, supercritical fluids are attracting much interest in many research fields because of their unique hybrid nature of gas and liquid. Their physicochemical properties (density, viscosity and dielectric constant) can be continuously adjusted without passing through a phase boundary. Supercritical fluids can be considered a continuously tunable solvents which allow intensive investigation of solvent effects on photochemical processes. However, when we apply ultrafast spectroscopy to supercritical fluids, the irradiation of intense laser pulses sometimes causes troubles, such as local heating, accumulation of photoproducts, and burning of the sample. They prevent us from getting reliable spectroscopic data. In order to solve these problems, we constructed a flow system of supercritical fluids (figure 1). The apparatus consists of a cell, a high pressure pump

and a water circulator. The cell is made of stainless steel and is equipped with two sapphire windows (0.5 mm thick) for laser irradiation and signal light collection. The temperature and pressure of the fluid are monitored by a thermocouple and a pressure gauge, respectively, inserted into the fluid. Supercritical fluid is circulated with use of a commercial HPLC pump with a typical flow rate of 7 ml/min. The temperature of the system is adjusted and maintained with accuracy of ±0.1 °C by circulating temperature-controlled water.

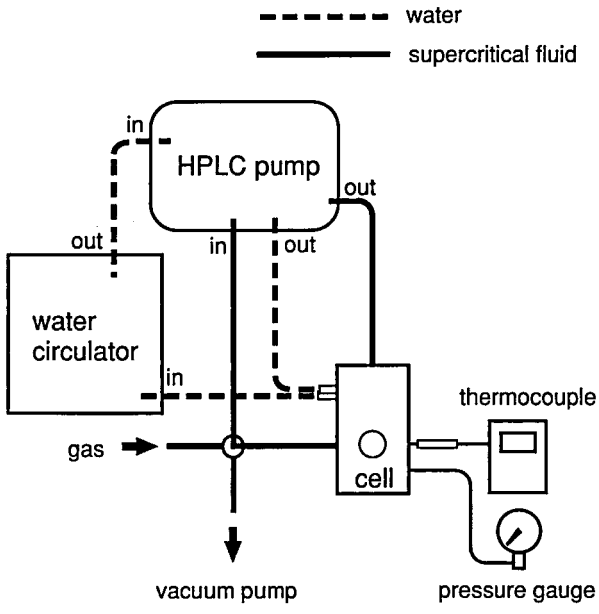

Figure 1. A schematic diagram of a flow system of supercritical fluids

VI-C-4 Femtosecond Time-Resolved Fluorescence Measurements of Coumarin153 in Supercritical Fluids

Misa KAYAMA *(Grad. Univ. for Advanced Studies),* **Satoshi TAKEUCHI and Tahei TAHARA**

Elucidation of the solvation dynamics has been one of the central subjects in ultrafast spectroscopic study on solution-phase chemistry. Measurements of dynamic Stokes shift (temporal shift of the fluorescence spectrum) of dye molecules have been widely carried out to investigate the ultrafast dynamics of polar solvation. Supercritical fluids, on the other hand, are unique solvents whose physicochemical properties can be continuously adjusted by controlling pressure and temperature, and the solvation in supercritical fluids is attracting much interest. The time-resolved study on the solvation dynamics in supercritical fluids is expected to shed new light on our understanding of the solute - solvent interaction. We measured femtosecond time-resolved fluorescence of coumarin 153 dissolved in supercritical fluoroform at several fluorescence wavelengths. The measurements were carried out using the up-conversion method with time resolution as high as 200 fs. In the early delay time region (~ a few picoseconds), fast decaying feature is observed for the blue side of the fluorescence while rising feature is found for the red side, which corresponds to dynamics Stokes shift of coumarin 153 in supercritical fluoroform. The measurements with change of the pressure and temperature of the fluid are under way to clarify the dependence of the solvation dynamics on the condition of supercritical fluoroform.

VI-D Studies on Photochemical Reactions using Picosecond Time-Resolved Vibrational Spectroscopy

Time-resolved vibrational spectroscopy is a very powerful tool for the study of short-lived intermediates appearing in chemical reactions. It often affords detailed structural information which is not obtainable with time-resolved electronic spectroscopy. However, for molecules in the condensed phase, we need energy resolution as high as 10 cm^{-1} in order to obtain well-resolved vibrational spectra. This energy resolution is compatible only with time-resolution slower than picosecond because of the limitation of uncertainty principle. In this sense, picosecond measurements can be regarded as the best compromise between energy resolution and time resolution for time-resolved frequency-domain vibrational spectroscopy. In this project, we study photochemical processes and short-lived transient species by means of picosecond time-resolved vibrational spectroscopy.

VI-D-1 Construction of a Picosecond Time-Resolved Raman Spectrometer

Atsuhiko SHIMOJIMA and Tahei TAHARA

An apparatus for picosecond time-resolved Raman scattering measurements was constructed. The system is based on a picosecond mode-locked Ti:sapphire laser. The output of the oscillator laser is regeneratively amplified (> 600 mW, 760~840 nm, 1 kHz, ~2 ps), and is used as the pump and probe pulses after adequate wavelength conversion. The second and the third harmonics are generated in nonlinear crystals(LBO,BBO). Raman cells(H_2 and D_2 gas, ~30 atm) are also used to convert the photon energy. The optical configuration for the measurement with 266 nm-pump and 400 nm-probe is shown in Figure 1. Only minor change in optical configuration is required with change of the pump and probe color, and it can be made very easily. The pump and probe beams are separated by a dichroic mirror or a Pellin Brocka prism, and are introduced to each optical path to generate time delay between them. Then they are recombined at a dichroic mirror, and are focused on a thin film-like jet stream of sample solution. Raman scattering is collected and focused onto the entrance slit of a polychromator by a camera lens, and is detected by a CCD camera cooled with liquid nitrogen. The delay time between the pump and probe pulses is changed by a computer-driven mechanical stage. In order to determine the time origin and to estimate the time resolution, we measure the optical Kerr effect of hydrocarbon, which is very useful and easy method applicable to any combination of the pump and probe wavelengths.

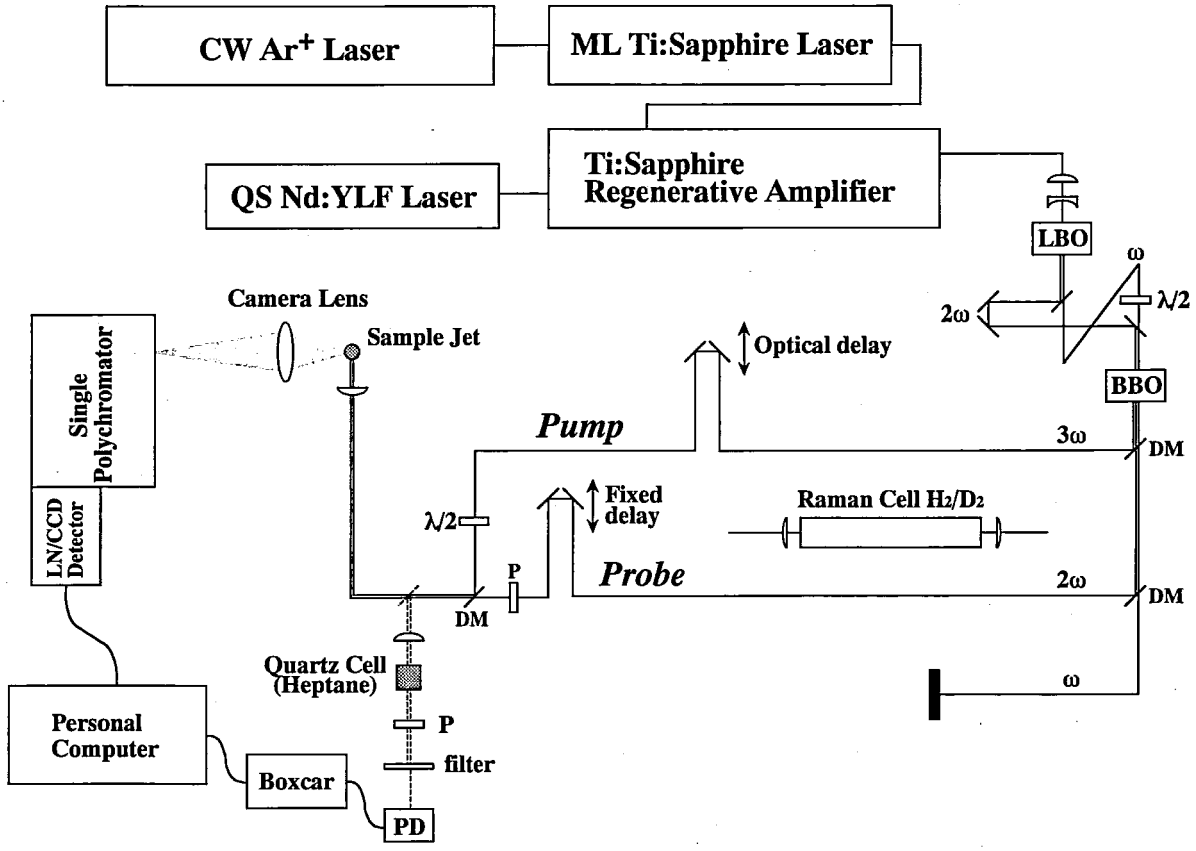

Figure 1. An apparatus for the time-resolved Raman spectroscopy. λ/2: half wave plate, P: Glan laser prism, DM: dichroic mirror. Dashed line indicates the optical path for the optical Kerr effect measurement.

VI-D-2 Observation of the Picosecond Dynamics of Photoexcited *all-trans* Retinal by Time-Resolved Spontaneous Raman Spectroscopy

Atsuhiko SHIMOJIMA and Tahei TAHARA

Picosecond time-resolved spontaneous resonance Raman spectra of *all-trans* retinal were measured in hexane (Figure 1). The pump pulse (385 nm) was the second harmonic of the regeneratively amplified output of a Ti:sapphire laser. The first Stokes line (435 nm) of a D_2 Raman shifter excited by the second harmonic was used as the probe. The frequency resolution of the measurement was approximately 10 cm^{-1} and time resolution was about 2 ps. The Raman bands due to the ground state of *all-trans* retinal were observed at negative delay time and they disappeared with photoexcitation. Then Raman bands due to the lowest excited triplet (T_1) state appeared with a time constant of 30 ps. The probe wavelength is in regorous resonance with T-T absorption, so that we were able to obtain reliable Raman spectra even though the intensity of the fluorescence background was still ~20 times higher than those of Raman signals. The obtained time constant of the rise of the T_1 state is in good agreement with the reported values which were determined by time-resolved absorption and fluorescence spectroscopies. The present experiment clearly demonstrated that time-resolved spontaneous Raman spectroscopy is applicable to the study of the picosecond dynamics of retinal photoisomerization, and is expected to afford detailed information about its reaction mechanism.

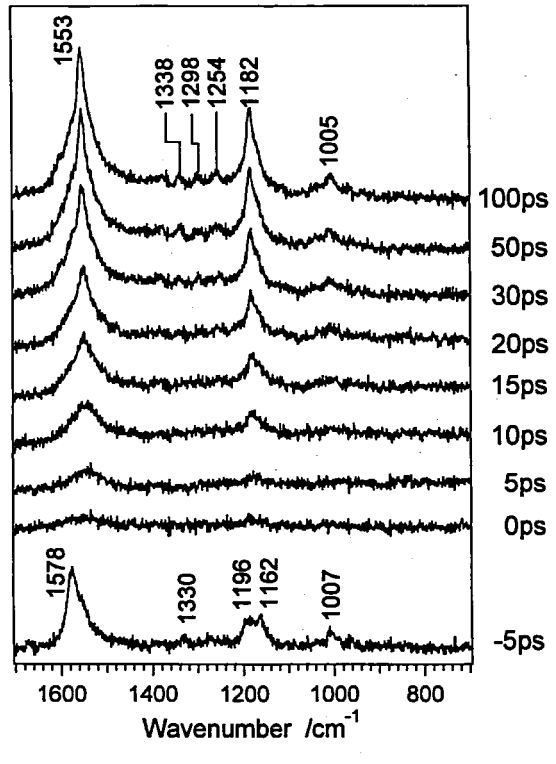

Figure 1. Picosecond time-resolved resonance Raman spectra of *all-trans* retinal in hexane (10^{-3} mol dm^{-3}, pump 385 nm, probe 435 nm). Solvent Raman bands were subtracted from the spectra.

VI-E Development of Time-Resolved Spectroscopy using Synchrotron Radiation

Synchrotron radiation affords photons in a wide energy region from X-ray to far-infrared, and is intrinsically produced in the form of a picosecond pulse train. The unique characteristics of synchrotron radiation are very attractive for time-resolved spectroscopy. In this project, by utilizing the combination of laser and synchrotron radiation, we attempt time-resolved measurements in energy regions which are not accessible with the existing lasers. A key development of this type of spectroscopy is the synchronization between picosecond lasers and synchrotron radiation. We have already achieved synchronization between a mode-locked Nd:YAG laser and synchrotron radiation. We have also constructed a laser pulse transportation system using optical fibers. In this year, we constructed a setup for subnanosecond time-resolved measurements in far-infrared region at beamline BL6B in UVSOR.

VI-E-1 Construction of a Setup for Subnanosecond Time-Resolved Far-Infrared Measurement using Synchrotron Radiation

Tahei TAHARA, Akito UGAWA and Kyuya YAKUSHI

Far-infrared spectra contain much information about low-frequency motion in the material including intermolecular vibrations in liquid and phonons in solid. It is highly desirable to develop time-resolved far-infrared spectroscopy, since it is expected to afford unique information on photo-induced processes in the material. In order to examine potentiality of synchrotron radiation for time-resolved far-infrared measurements, we constructed a setup at beamline BL6B in our synchrotron radiation facility (UVSOR). The schematic diagram of the setup is shown in Figure 1. In this setup we use picosecond laser pulses for the excitation of the sample, and utilize far-infrared synchrotron radiation for probing. Picosecond laser pulses are generated from a mode-locked Nd:YAG laser, and are transported to the beamline by using an optical fiber. A full one-to-one synchronization between the laser pulse and synchrotron radiation is achieved by applying the synchrotron RF signal to the mode-locker of the laser. Far-infrared/infrared synchrotron radiation is introduced to a Michelson-type Fourier Transform spectrometer through a Si or KRS-5 optical window. The pumping laser pulses and the probing synchrotron radiation pulses are focused and overlapped on the sample, and the reflected synchrotron radiation beam is detected with a bolomer. In this pump-probe scheme, no time-resolution is required for the detector. Time-resolution of this apparatus is predominantly determined by the duration of synchrotron radiation which is about 1 ns. The change in the sample reflectivity smaller than 10^{-3} can be observed regardless of the slowly decreasing intensity of the synchrotron radiation.

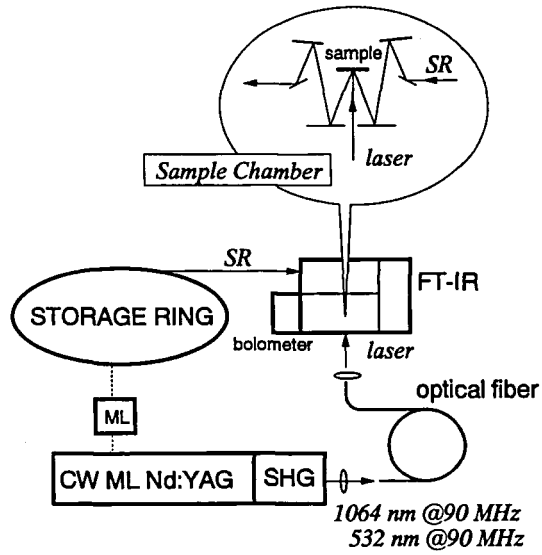

Figure 1. A schematic diagram of a setup for subnanosecond time-resolved measurement at BL6B in UVSOR.

VI-F Synchrotron Radiation Stimulated Surface Reactions

Study of synchrotron radiation (SR) stimulated surface reaction is a promising topic in fundamental science, because dynamical processes induced by the photostimulated core-electron excitations on surfaces are scarcely explored so far. This field is important also in applied science, since the fundamental study is expected to develop the new techniques for material processing.

VI-F-1 Potential of Site Specific Photo-chemical Processing Using Synchrotron Radiation

Tsuneo URISU, Toshio IBUKI *(Kyoto Educational Univ.)*, **Yoshiaki IMAIZUMI and Masahiro KAWASAKI** *(Hokkaido Univ.)*

[*Nuclear Instruments and Method* in Phys. Res. B **122**, 364 (1997)]

An absorption spectrum in the vacuum ultra violet region and a photoelectron spectrum for the valence-electron-states of the gas phase dimethyl aluminum hydride (DMAH) were measured and the energy levels of the DMAH electronic states were determined. Using

this result, it was concluded that the difference of the carbon contamination in photo-stimulated Al deposition between white beam synchrotron radiation and MgK α line irradiation excites valence electron-states, mainly π_{CH3} state, and breaks the C-H bond. On the other hand, in the case of SR irradiation, not only valence-electron-states, but also Al 2*p* and Al 2*s* core-electron states are excited and the Al-C bond is broken. This indicates the usefulness of the photochemical site-specific processing.

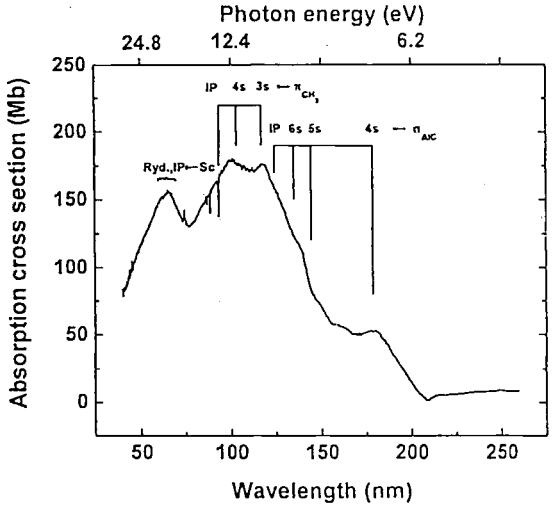

Figure 1. Photoabsorption cross sections of DMAH observed at 1×10^{-2} Torr. The spectral resolution is 0.2 nm. The Rydberg assignments are indicated.

VI-F-2 Structural Changes of Silicon Dioxide Films Caused by Synchrotron Irradiation

Y. PARK, S. RHEE *(Pohang Univ. Sci. Tech.)*, **Y. IMAIZUMI and T. URISU**

[*J. Appl. Phys.* **80**, 1236 (1996)]

Effects of synchrotron radiation (SR) on silicon oxide films, deposited with remote plasma-enhanced chemical vapor deposition, has been investigated. SR irradiation had an effect on the silicon dioxide structure which was confirmed by *in situ* infrared reflection absorption spectroscopy. As the substrate temperature was increased to 373 K, the SiO_2 structure become loose by irradiation led to the increase of surface roughness and also the formation of hemispherical bubbles on the film surface, which was confirmed by atomic force microscope. Generation of oxygen-related paramagnetic defect was observed by electron spin resonance.

VI-F-3 Extremely High Quantum Yield of Thin Film Deposition Reaction by Core Electron Excitations

Yoshiaki IMAIZUMI and Tsuneo URISU

The excitation energy dependence of the reaction quantum yield and the carbon contamination with synchrotron radiation stimulated Al thin film deposition using the low temperature condensed layer of dimethyl aluminum hydride (DMAH) were evaluated quantitatively in the vacuum ultra violet region for the first time. It has been found that the core electron excitation gives a few tens to hundreds times higher reaction quantum yield than the valence electron excitations. It is quantitatively explained by the Auger stimulated desorption model. The carbon contamination decreases due to site specific effect by the core electron excitations.

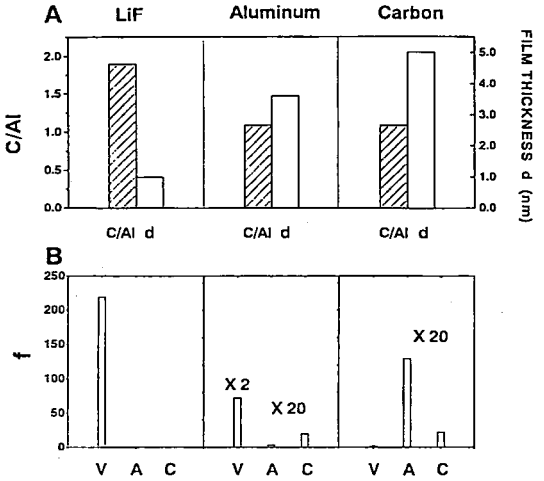

Figure 1. (A) Composition ratio (C/Al) of the condensed layer just after the filtered SR beam irradiations, and the deposited film thickness (d) are given by bar graphs, for the cases of LiF (left), aluminum (center) and carbon (right) filters. (B) The dependence on the excitation energy off (the number of absorbed photons per one DMAH molecule during the irradiation in each energy region of V; valence , A;aluminum core, and C; carbon core electron excitation regions) when using LiF (left), aluminum (center) and carbon (right) filters.

VI-F-4 Growth Mechanisms in the Synchrotron Radiation-Assisted Silicon Gas Source Molecular Beam Epitaxy Using Disilane

Akitaka YOSHIGOE *(Toyohashi Univ. Tech.)*, **Shinya HIRANO and Tsuneo URISU**

Growth mechanisms on the Si(100) surface in the synchrotron radiation (SR) assisted gas source molecular beam epitaxy (SR-GSMBE) are investigated in the low temperature region by *in-situ* monitoring the surface silicon hydrides (deuterides) during the epitaxial growth by means of an infrared reflection absorption spectroscopy using a $CoSi_2$ buried metal layer substrate. It is concluded that the chemisorption of gas phase active species such as SiH_n and H including their ions following the hydrogen desorption is a key mechanism in the SR-GSMBE at low substrate temperatures. It is also concluded that the decomposition of surface higher hydrides (SiH_2, SiH_3) by SR makes the surface more reactive for the chemisorption of the gas phase active species than the non irradiated surface and improve the crystallinity.

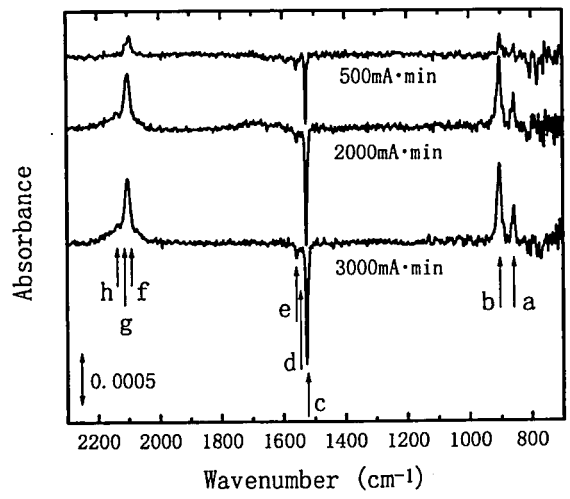

Figure 1. Change of the IRRAS spectrum during SR-GSMBE with increasing SR dose (mAmin unit) at 140 °C. The Si(100) BML substrate was initially terminated by deuterium atoms with saturatiion coverage. The assignments of peaks are; a: SiH_3 symmetric deformation (960 cm^{-1}), b: SiH_2 bending scissors (908 cm^{-1}), c: SiD stretching (1525 cm^{-1}), d and e: SiD_3 stretching (1542 and 1554 cm^{-1}), f: SiH symmetric stretching (2100 cm^{-1}), g: SiH_2 symmetric stretching (2113 cm^{-1}), h: SiH_3 symmetric and asymmetric stretching (2140 cm^{-1}).

VI-F-5 Infrared Reflection Absorption Spectrum of Silicon Deuterides on Si(100) Surface

Shinya HIRANO, Akitaka YOSHIGOE *(Toyohashi Univ. Tech.)*, **Syed Irfan GHEYAS, Takayuki MIYAMAE, Kazuhiko MASE and Tsuneo URISU**

Many investigations about hydrogen surface reaction and hydrogen thermal desorption mechanisms on the Si(100) had been carried out both experimentally and theoretically. However, these interpretations are so inconsistent that the desorption mechanisms are yet unresolved problems. In order to understand the thermal desorption mechanisms of deuterium on Si(100) surfaces, the high resolution IRRAS spectrum of surface chemisorbed deuterium on Si(100) as a function of surface temperature have been investigated by BML-IRRAS. Figure 1 displays the changes in the IRRAS spectrum for Si(100) surfaces with atomic deuterium saturation exposure at 400 K as a function of annealing temperature. It is clearly observed that the peak intensity of SiD increases with increasing substrate temperature up to around 650 K keeping the peak frequency at 1525 cm^{-1} and its slight asymmetric shape. So, we considered the desorption pathway of D_2 from dideuteride phase corresponding to the β 2-H_2 TPD desorption state is mainly $2SiH_2 \rightarrow 2SiH + H_2(g)$. The peak shift by the temperature increase 670 K → 690 K is due to the decrease of dipole-dipole coupling interaction, since the population of SiD significantly decreases above 670 K. These results support the preparing or isomerization mechanisms.

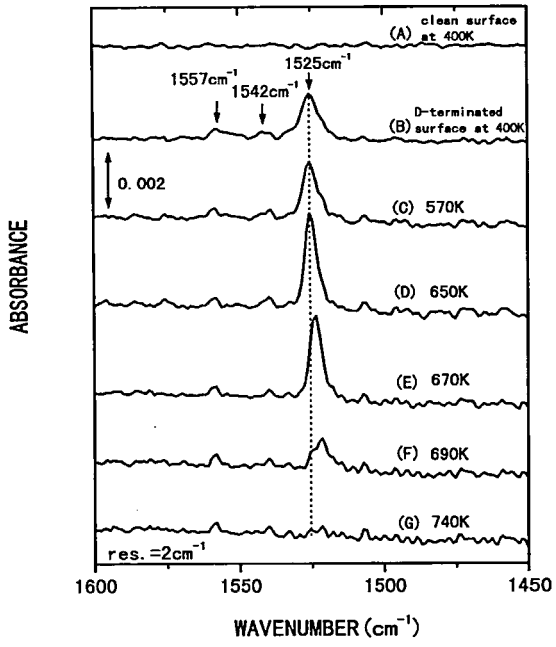

Figure 1. IRRAS spectrum of Si(100) (1×1):D surfaces with atomic deuterium saturation exposure at 400 K as a function of annealing temperature.

VI-F-6 Chemisorption of Deuterium on Ultrathin Ge Film Deposited over Si(100)-2x1: Existence of Dideuteride Phase

Syed Irfan GHEYAS, Tsuneo URISU, Shinya HIRANO, Hidekazu WATANABE, Suehiro IWATA, Mutsumi AOYAGI, Mitsuhiro NISHIO *(Saga Univ.)* **and Hiroshi OGAWA** *(Saga Univ.)*

[*Phys. Rev. B* submitted]

Adsorption of atomic deuterium on ultrathin Ge film deposited over Si(100) has been studied using Fourier-Transformed Reflection Absorption Spectroscopy (FT-IRAS), Reflection High Energy Electron Diffraction (RHEED) measurements and *ab initio* cluster calculation. We have established that chemisorption of atomic deuterium on Ge/Si(100) forms a previously unreported dideuteride phase, in addition to the already well known monodeuteride phase, 2x1. Also etching of the Ge atoms by deuteriums, never reported before, has clearly been observed. As far as etching mechanism is concerned, we have found the dideuteride species to be relatively stable and does not lead to etching of surface Ge atoms. However, the dideuteride structure is vulnerable in the presence of incoming deuterium atoms and spontaneously etches.

VI-F-7 Design and Performance of a Multilayered Mirror Monochromator in the Low Energy Region of Vacuum Ultra Violet

Harutaka MEKARU, Tsuneo URISU, Yoshiyuki TSUSAKA *(Himeji Inst. Tech.)*, **Shin MASUI** *(Sumitomo Heavy Industries Ltd.)*, **Eijiro TOYOTA** *(Sumitomo Heavy Industries Ltd.)* **and Hisataka TAKENAKA** *(NTT-AT)*

For the energy region from tens to hundreds of electron volts, the multilayered mirror (MLM) monochromator has not ever been realized due to the difficulty of reducing the background noise of the total reflection component. In this work, a double-crystal-type MLM monochromator equipped with a thin-film filter has been designed on the basis of trial fabrication of the mirror-driving system and of Mo/Si and Mo/C MLMs, and its performance has been evaluated by calculating its output photon flux. It is shown in figure 1 that by using the MLMs at low incident angles combining with an appropriate thin-film filter, it is possible to make a practical monochromator with high output photon fluxes and the low background noise.

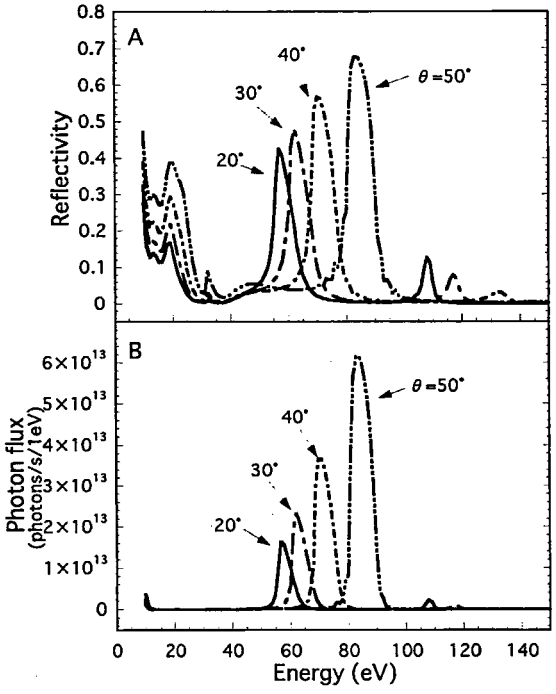

Figure 1. (A) The calculated reflectivity for the Mo/Si MLM and (B) the output photon flux of the monochromator using Mo/Si MLMs + C filter for 100 mA ring current and the 16.56 mrad by 12.79 mrad acceptance angle of the pre-mirror, assuming that the monochromator is set up in the beamline BL-4A1 of the UVSOR.

VI-F-8 Double MultiLayered Mirror Monochromator Beamline BL-4A1 for Synchrotron Radiation Stimulated Processing Study

Harutaka MEKARU, Yoshiyuki TSUSAKA *(Himeji Inst. Tech.)*, **Takayuki MIYAMAE, Eiken NAKAMURA** *(JAIST)*, **Toyohiko KINOSHITA and Tsuneo URISU**

We developed a double multilayered mirror monochromator to get high photon flux and to scan wide wavelength regions. Figure 1 shows the drawings of BL-4A1, which consists of a pre-mirror chamber, a double MLM monochromator, a white beam chamber, a differential pumping chamber, a filter box, a current monitor and an X-ray photoelectron spectrometer (XPS). When the multi-layered mirror is not used, the SR beam is reflected by a pairs of Pt coated plain mirrors with grazing incident angle of 2 degrees in the white beam chamber to keep the output beam at the same height as that of the multi-layered mirror monochromator output. The pre-mirror is a elliptically-bent cylindrical mirror which is set at a distance of 2345.4 mm from the light source point and focuses the beam at the point of 6100 mm downstream from the center of the pre mirror with a spot size of about 5 mm by 2 mm.

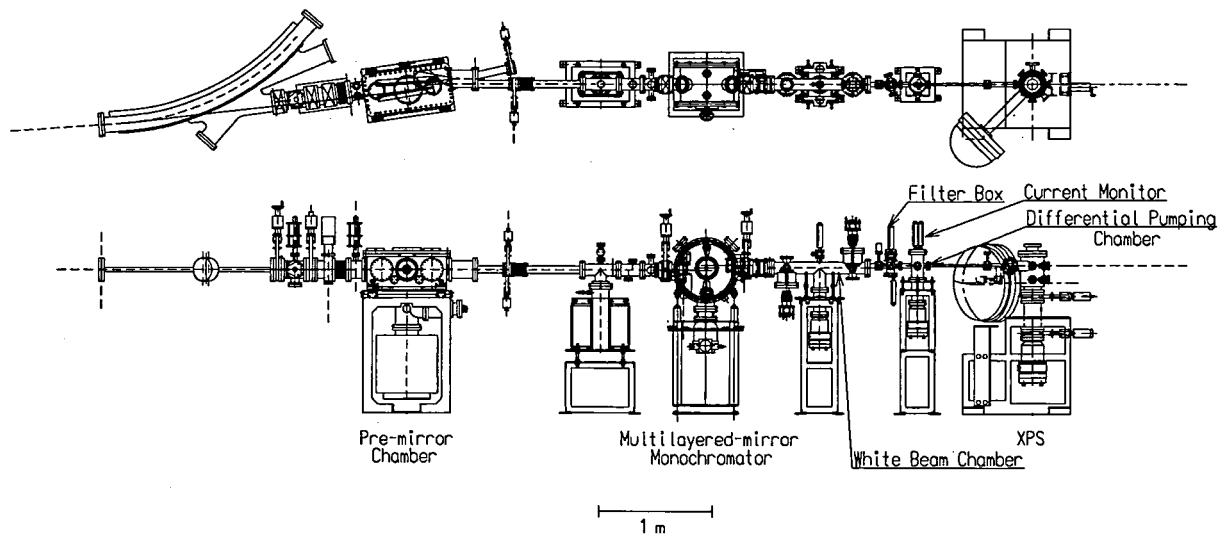

Figure 1. The drawings of the beamline BL-4A1 of the UVSOR.

VI-G Ion Desorption Induced by Core-Electron Transitions Studied by Electron-Ion Coincidence Spectroscopy Combined with Synchrotron Radiation

Ion desorption induced by core-electron transitions has been studied using energy-selected electron ion coincidence spectroscopy combined with synchrotron radiation. Auger electron photoion coincidence (AEPICO) and photoelectron photoion coincidence (PEPICO) spectroscopies proved to be an ideal tool for investigations of the ion desorption induced by core-level excitations. AEPICO results show that the character of the orbitals where holes are created as well as the effective hole-hole Coulomb repulsion are important factors in the Auger-stimulated ion desorption from covalent molecules. The PEPICO spectroscopy, on the other hand, provided direct evidences of site-specific ion fragmentation induced by core-level excitations.

VI-G-1 Study of Ion Desorption Induced by a Resonant Core-Electron Transition of Condensed H_2O by Using Auger Electron Photo-Ion Coincidence (AEPICO) Spectroscopy Combined with Synchrotron Radiation

Kazuhiko MASE, Mitsuru NAGASONO, Shin-ichiro TANAKA, Tsuneo URISU, Eiji IKENAGA,* Tetsuji SEKITANI* and Ken-ichiro TANAKA*
*(*Hiroshima Univ.)*

[*Surf. Sci.* in press]

Ion desorption induced by a resonant excitation of O 1*s* of condensed amorphous H_2O has been studied by total ion and total electron yield spectroscopy, non-derivative Auger-electron spectroscopy (AES), and Auger-electron photoion coincidence (AEPICO) spectroscopy. The spectrum of total ion yield divided by total electron yield exhibited a characteristic threshold peak at $h\nu$ = 533.4 eV, which is assigned to the $4a_1 \leftarrow$ O 1*s* resonant transition. The AES at the $4a_1 \leftarrow$ O 1*s* resonance is interpreted as composed of the spectator-AES of the surface H_2O, and the normal-AES of the bulk H_2O where the $4a_1$ electron is delocalized before Auger-transitions. H^+ is found to be the only ion species in AEPICO spectra measured at the $4a_1 \leftarrow$ O 1*s* resonance and at the O 1*s* ionization ($h\nu$ = 560 eV). The electron kinetic energy dependence of the AEPICO yield (AEPICO yield spectrum) at the $4a_1 \leftarrow$ O 1*s* resonance is found to be greatly different from that at the O 1*s* ionization. The peak positions of the AEPICO yield spectrum at the $4a_1 \leftarrow$ O 1*s* resonance are found to correspond to those of the spectator-AES of the surface H_2O which was extracted from the AES at the $4a_1 \leftarrow$ O 1*s* resonance. Furthermore, the AEPICO yield is greatly enhanced at the $4a_1 \leftarrow$ O 1*s* resonance as compared with that at the O 1*s* ionization. On the basis of these results, spectator-Auger-stimulated ion desorption mechanism and/or ultrafast ion desorption mechanism are concluded to be responsible for the H^+ desorption at the $4a_1 \leftarrow$ O 1*s* resonance. The enhancement of the H^+ yield is ascribed to the O-H anti-bonding character of the $4a_1$ orbital.

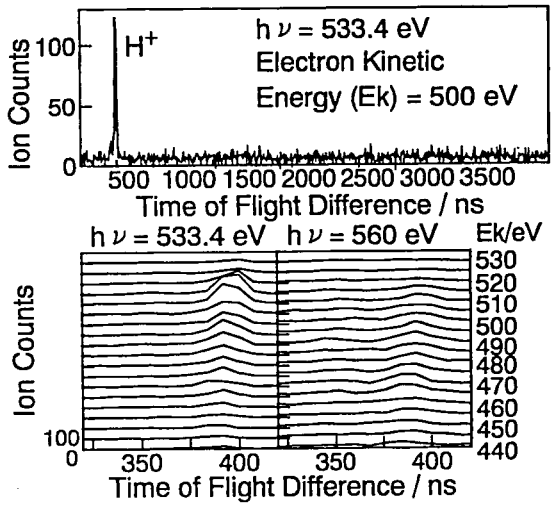

Figure 1. (a) AEPICO spectrum of condensed H_2O at $h\nu$ = 533.4 eV in coincidence with electrons at a kinetic energy of 500 eV. The intense peak at 384 - 408 ns was assigned to the H^+ signal. (b) AEPICO spectra of condensed H_2O at $h\nu$ = 533.4 and 560 eV in coincidence with electrons at kinetic energies of 440 - 530 eV corresponding to the O KVV Auger region.

VI-G-2 Study of Ion Desorption Induced by a Resonant Core-Electron Transition of Condensed NH_3 Using Auger Electron Photo-Ion Coincidence (AEPICO) Spectroscopy Combined with Synchrotron Radiation

Mitsuru NAGASONO, Kazuhiko MASE, Shin-ichiro TANAKA and Tsuneo URISU

[*Surf. Sci.* in press]

Photostimulated ion desorption at the $4a_1 \leftarrow$ N 1*s* resonant transition of condensed NH_3 was studied using electron emission spectroscopy and Auger electron photo-ion coincidence (AEPICO) spectroscopy. The total ion yield divided by the Auger electron yield exhibited a threshold peak at $h\nu$ = 399 eV, which is ascribed to the resonant transition from the N 1*s* to the N-H antibonding $4a_1$ orbital. The electron emission spectrum at the $4a_1 \leftarrow$ N 1*s* resonance is decomposed into three components, i.e., a valence photoelectron emission spectrum, and normal- and resonant-Auger electron emission spectra. We ascribe the resonant-Auger electron emission spectrum mainly to spectator-

Auger transitions on the basis of the peak assignment. A series of AEPICO spectra at the $4a_1 \leftarrow$ N $1s$ resonance was also measured as a function of the Auger electron kinetic energy. The electron kinetic energy dependence of the H^+ AEPICO yield displays a shape approximately similar to that of the mixed spectrum of normal- and spectator-Auger electron emission spectra. Based on this result the H^+ desorption at the $4a_1 \leftarrow$ N $1s$ resonance is concluded to originate from the spectator-Auger transitions and from the normal-Auger transitions following the delocalization of the excited electron.

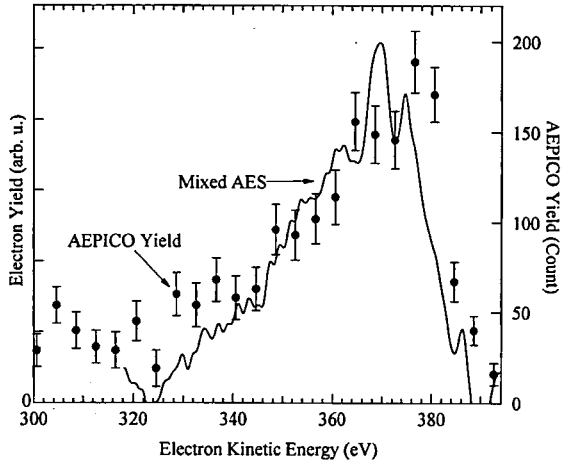

Figure 1. AEPICO yield spectrum (closed circles) and the mixed spectrum of normal- and spectator-Auger electron emission spectrum as a function of the electron kinetic energy.

VI-G-3 Photon Stimulated Ion Desorption of Condensed Acetonitrile Induced by Carbon Core Excitation

Tetsuji SEKITANI,* Eiji IKENAGA,* Hideki Matsuo,* Kenichiro TANAKA* *(*Hiroshima Univ.),* **Kazuhiko MASE, Mitsuru NAGASONO, Shinichiro TANAKA and Tsuneo URISU**

[*Surf. Sci.* in press]

A study of surface photochemical reaction induced by core excitation has been developed with the advance of synchrotron radiation technique. Inparticular, site-specific reaction has been found in photon stimulated ion desorption (PSID) following core electron excitation. Auger stimulated ion desorption (ASID) mechanism is widely proposed as a model of PSID. In this model, the ion desorption is directly related to the Auger final state. In the present study, we have investigated PSID of condensed acetonitrile molecules induced by carbon core excitation to reveal the desorption mechanism related to the Auger process using the total electron yield, total ion yield, resonant Auger electron, and Auger electron-photoion coincidence (AEPICO) spectroscopies. We have mainly used AEPICO apparatus. This apparatus detects the energy selected electron and the ion produced simultaneously by a single excitation event. H^+ ion was only detected in AEPICO spectra. Total ion yield spectrum divided by total electron yield shows that the desorption efficiency is largely increased at resonant excitation of carbon $1s$ electron in the CH_3 group to C-H* orbital. We have measured Auger spectrum and AEPICO yield spectrum at C-H* excitation. AEPICO yield spectrum shows that H^+ ion is desorbed via spectator Auger processes leaving two-hole one-excited-electron states. We have also measured similar spectra at other resonant excitations (π^*_{CN}, σ^*_{CC}, σ^*_{CN}). The results indicate that ion desorption depends strongly on the bonding/antibonding character and localized character of the excited state.

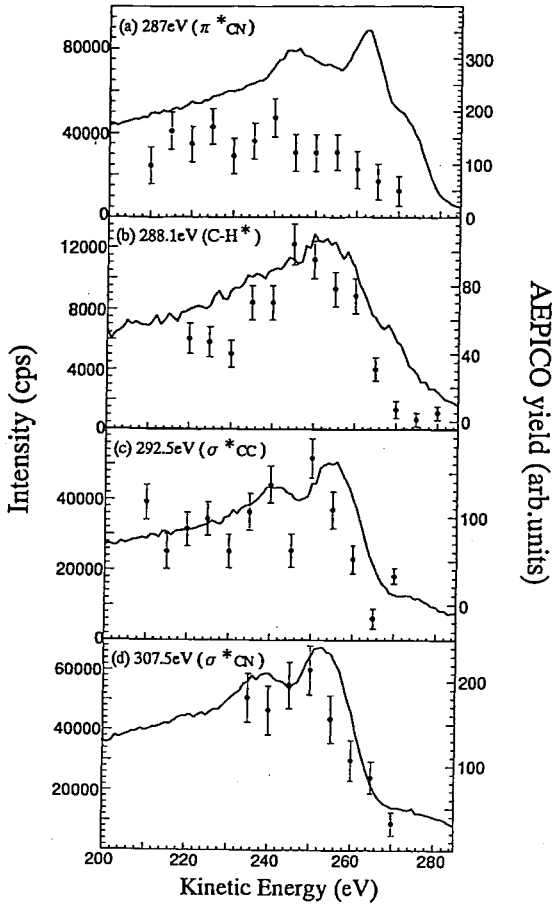

Figure 1. The AEPICO yield spectrum of condensed CH_3CN as a function of C(KVV) Auger-electron kinetic energy (closed circles) at $h\nu$ = 287, 288.1, 292.5 and 307.5 eV, respectively. Solid line shows the non-derivative Auger-electron spectrum.

VI-H Photoionization Dynamics Studied by Electron Spectroscopy Combined with a Continuous Synchrotron Radiation Source

Molecular photoionization is a major phenomenon in vacuum UV excitation and provides a large amount of information on fundamental electron-core interactions in molecules. Especially, autoionizing and shape resonances become of main interest, since they often dominate photoabsorption cross sections and lead to various vibronic states which are inaccessible in direct ionization. In order to elucidate dynamical aspects of photoionization, we have developed a versatile machine for photoelectron spectroscopy. Introduction of a new methodology, two-dimensional photoelectron spectroscopy, allows us to investigate autoionization and predissociation of superexcited states of acetylene, nitric oxide, carbonyl sulfide, sulfur dioxide and so on. In this method, the photoelectron yield is measured as a function of both photon energy and electron kinetic energy (binding energy). The spectrum, usually represented as a contour plot, contains rich information on photoionization dynamics.

VI-H-1 Two-Dimensional Photoelectron Spectroscopy of Acetylene: Rydberg-Valence Interaction between the $(3\sigma_g)^{-1}(3p\sigma_u)^1$ and $(3\sigma_g)^{-1}(3\sigma_u)^1$ States

Hideo HATTORI, Yasumasa HIKOSAKA *(Tokyo Inst. Tech. and IMS)*, **Takumi HIKIDA** *(Tokyo Inst. Tech.)* **and Koichiro MITSUKE**

[*J. Chem. Phys.* **106**, 4902 (1997)]

Two-dimensional photoelectron spectroscopy is performed for studying autoionization of acetylene in the Franck-Condon gap between the $X\ ^2\Pi_u$ and $A\ ^2A_g$ states of $C_2H_2^+$. The photoelectron spectrum in the photon energy range from 12.8 to 13.6 eV shows exclusive vibrational excitation of the symmetric C-H stretching mode ν_1 of $C_2H_2^+(X\ ^2\Pi_u)$, which results from autoionization of the valence state $(3\sigma_g)^{-1}(3\sigma_u)^1$. Vibrational frequencies with anharmonicities of the ν_1 and ν_2 (the symmetric C-C stretch) modes are determined by a least-squares fit of the ionization energies of the observed peaks to a second order expansion. At the photon energy of 14.120 eV autoionization of the Rydberg state $(3\sigma_g)^{-1}(3p\pi_u)^1$ leads to a complicated photoelectron spectrum where probably the *trans*-bending mode ν_4 of $C_2H_2^+(X\ ^2\Pi_u)$ as well as ν_1 is excited, reflecting a substantial geometrical change during autoionization. Furthermore, a similar excitation of the ν_4 mode is observed at ~13.8 eV. An excellent agreement in positions of the vibrational levels between the spectra at 13.821 and 14.120 eV suggests the presence of the Rydberg state $(3\sigma_g)^{-1}(3p\sigma_u)^1$ at ~13.8 eV which has not been identified previously in the photoabsorption or photoionization cross section curves. The constant-ionic-state spectra for the $\nu_1 = 0$ - 4 levels of $C_2H_2^+(X\ ^2\Pi_u)$ show two spectral features: (a) a weak shoulder ($\nu_1 = 0$) or a small maximum ($\nu_1 = 1$ - 4) at 13.8 eV and (b) two groups of peaks in the range of 14.0 - 14.4 eV. The ratio of the integrated intensity of the 13.8 eV maximum to that of the two groups differs from level to level. This observation is interpreted in terms of a strong interaction between the Rydberg $(3\sigma_g)^{-1}(3p\sigma_u)^1$ and valence $(3\sigma_g)^{-1}(3\sigma_u)^1$ states.

VI-H-2 Superexcited States of OCS Probed by Using Photoelectron Spectroscopy for Autoionizing Atomic Sulfur

Yasumasa HIKOSAKA *(Tokyo Inst. Tech. and IMS)*, **Hideo HATTORI, Takumi HIKIDA** *(Tokyo Inst. Tech.)* **and Koichiro MITSUKE**

[*J. Chem. Phys.* **107**, 2950 (1997)]

Neutral dissociation of superexcited states of OCS has been studied by two-dimensional photoelectron spectroscopy using synchrotron radiation in the photon energy range of 14.2 - 16.8 eV. A two-dimensional spectrum exhibits noticeable features which are assigned as resulting from autoionizing transitions of excited atomic sulfur S* from Rydberg states converging to $S^+(^2D^o)$ to $S^+(^4S^o)$. The precursor molecular states leading to S* + CO are considered to be multiple-electron-excited Rydberg states, OCS*(*Dis*), converging to OCS^+ with $^2\Sigma^-$ and/or $^2\Delta$ symmetry. The electron signal counts due to autoionization of S* show enhancement at excitation photon energies for the Rydberg states OCS*(R_B) converging to $OCS^+(B^2\Sigma^+)$. These results support a predissociation mechanism for the formation of S*: conversion from OCS*(R_B) to OCS*(*Dis*).

VI-H-3 Branching Ratios from a Rydberg State Converging to $OCS^+(B^2\Sigma^+)$ to Probable Decay Pathways

Yasumasa HIKOSAKA *(Tokyo Inst. Tech. and IMS)*, **Hideo HATTORI, Takumi HIKIDA** *(Tokyo Inst. Tech.)* **and Koichiro MITSUKE**

We have proposed the following mechanism for the formation and autoionization of S* from OCS*(R_B) in the preceding theme:

$$OCS(X^1\Sigma^+) + h\nu \rightarrow OCS^*(R_B) \rightarrow OCS^*(Dis)$$
$$\rightarrow S^*[\text{converging to } S^+(^2D^o)] + CO(X^1\Sigma^+)$$
$$\rightarrow S^+(^4S^o) + CO(X^1\Sigma^+) + e^-.$$

Previous studies in the literature have revealed that OCS*(R_B) is deactivated through several pathways, apart from the above conversion process. Combining the present results on two-dimensional photoelectron spectroscopy with the reported data of photoabsorption and photoionization cross sections allows us to evaluate the quantum yield η of every pathway. In the case of the $5s\sigma$ state at $E_{h\nu}$ =15.17 eV, η for formation of autoionizing S* is estimated to be ~1%. Further-

more, the $5s\sigma$ state suffers conversion to any neutral superexcited state (η = 67%) more efficiently than simply autoionizes into $OCS^+(X^2\Pi)$ (η = 12%). This leads to a conclusion that the autoionization lifetime of the $5s\sigma$ state is of the same order as or longer than a vibrational period of the antisymmetric stretch mode.

VI-I Vacuum UV Spectroscopy Making Use of the Combination of Synchrotron Radiation and a Mode-Locked UV Laser

An ultraviolet laser system has been developed which synchronizes precisely with the undulator radiation from the storage ring of the UVSOR facility. A mode-locked Ti:sapphire laser is made to oscillate at the frequency of the ring in a multibunch operation mode. The delay timing between undulator and laser pulses can be changed from 0 to 11 ns. The following two synchrotron radiation-laser combination studies have been performed. (1) Two-photon ionization of helium atoms studied as the prototype of the time-resolved experiment, and (2) fluorescence excitation spectroscopy of $N_2^+(X^2\Sigma_g^+)$ ions produced by synchrotron radiation photoionization of N_2 or N_2O. In the near future, similar combination techniques will be widely available in the study of photodissociation and photoionization dynamics of gaseous molecules in the VUV and soft X-ray regions.

VI-I-1 Development of a Tunable UV Laser System Synchronizing Precisely with Synchrotron Radiation Pulses from UVSOR

Masakazu MIZUTANI, Manabu TOKESHI *(Kyusyu Univ.),* **Atsunari HIRAYA** *(Hiroshima Univ.)* **and Koichiro MITSUKE**

[*J. Synchrotron Rad.* **4**, 6 (1997)]

A mode-locked Ti:sapphire laser is made to oscillate at the frequency of the UVSOR storage ring, 90.115 MHz, in a multi-bunch operation mode. The third harmonic of the laser is available in the wavelength range 243-280 nm. Synchrotron radiation from an undulator is monochromatized by a grazing-incidence monochromator and introduced coaxially with the laser. The temporal profile of the photon pulses is monitored *in situ* by a luminescing substance/photomultiplier combination. The delay timing between the laser and synchrotron radiation can be changed from 0 to 11 ns by adjusting an electronic module that provides phase-locked loop stabilization of the laser pulse. The reliability and feasibility of this laser-synchrotron radiation combination technique are demonstrated by applying pump-probe experiments to two physical systems. The first system is photodissociation of iodomethane (CH_3I) with a laser photon, followed by photoionization of I and CH_3 fragments with synchrotron radiation. The second, two-photon ionization of He atoms, is studied as the prototype of a time-resolved experiment. The He^+ signals as a function of the laser-synchrotron radiation delay are found to be enhanced in a narrow time window, which can be interpreted in terms of a short lifetime of the resonant state, $He^*(1s2p\ ^1P)$, produced by primary synchrotron radiation excitation.

VI-I-2 Apparatus for Laser Induced Fluorescence Spectroscopy of Ions or Neutral Fragments Prepared by VUV Photoexcitation

Masakazu MIZUTANI, Hiromichi NIIKURA *(Graduate Univ. for Advanced Studies),* **Atsunari HIRAYA** *(Hiroshima Univ.)* **and Koichiro MITSUKE**

[*J. Synchrotron Rad.* in press]

Figure 1 shows the experimental set up for laser induced fluorescence excitation spectroscopy of ions produced by synchrotron radiation photoionization. A mode-locked Ti:sapphire laser generates its second harmonic in the wavelength range of 365-420 nm. The spectral and temporal resolution of the laser are estimated to be 9.2 cm^{-1} and 1.2 ps. Monochromatized undulator radiation is supplied from beam line BL3A2 of the UVSOR storage ring. The two light beams are introduced coaxially into a photoionization vacuum chamber. A molecular beam of a sample gas crosses at right angles with the light beams. The fluorescence is collected with an input optics perpendicularly to the photon and molecular beams, dispersed by a monochromator, and detected by a photomultiplier. The output of the photomultiplier is processed by a preamplifier and a constant fraction discriminator, and fed into the input of a dual-channel gated photon counter. An optical chopper modulating the laser beam is used to alternate the data acquisition cycle of the laser on and off at 400 Hz in combination with the photon counter. We are thus able to compensate transient changes or long term drifts in various experimental conditions.

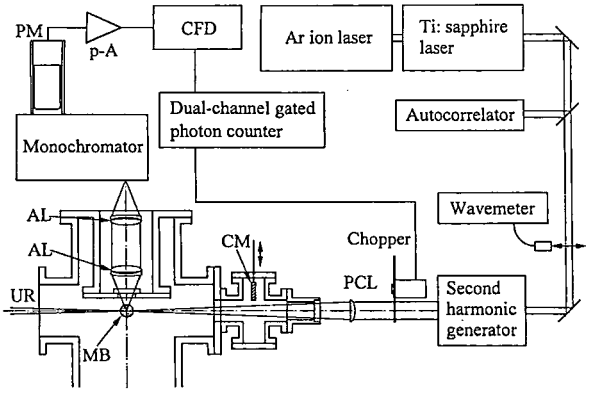

Figure 1. Schematic diagram of the apparatus for the laser-synchrotron radiation combination experiment. UR, monochromatized undulator radiation; MB, cross section of the molecular beam expanded from a nozzle; AL, achromatic lens; CM, gold-mesh photocurrent monitor; PCL, plano-

convex lens; PM, photomultiplier; p-A, pre-amplifier; CFD, constant fraction discriminator.

VI-I-3 Laser Induced Fluorescence Excitation Spectroscopy of N_2^+ Produced by Photoionization of N_2 and N_2O with Synchrotron Radiation

Hiromichi NIIKURA *(Graduate Univ. for Advanced Studies)*, **Masakazu MIZUTANI, Atsunari HIRAYA** *(Hiroshima Univ.)* **and Koichiro MITSUKE**

Measurements are carried out of the laser induced fluorescence (LIF) excitation spectra of N_2^+ ($X\,^2\Sigma_g^+$, v'' = 0) produced from N_2 and N_2O. This experiment is the first case for LIF excitation spectroscopy of molecules in the gas phase by utilizing the synchrotron radiation-laser combination. The experimental details are described in the preceding theme. The laser wavelength is scanned in the region of the 0_0^0 band, i.e., the ($B\,^2\Sigma_u^+$, v' = 0) ← ($X\,^2\Sigma_g^+$, v'' = 0) transition of N_2^+ at 389-392 nm. The fluorescence dispersed by the second monochromator is monitored at ~425 nm which corresponds to the ($B\,^2\Sigma_u^+$, v' = 0) → ($X\,^2\Sigma_g^+$, v'' = 1) transition. Figure 1 shows LIF excitation spectra of N_2^+ which is prepared either (a) by potoionization of N_2 with the undulator photon energy at 18.0 eV or (b) by that of N_2O at 18.60 eV. Data points are obtained from the difference between the signal counts with and without the laser as a function of the laser wavelength. Two maxima in Figure 1(a) are ascribed to the *P* and *R* branches arising from a primary rotational distribution of N_2^+ ($X\,^2\Sigma_g^+$), though the rotational bands are not resolved. The rotational temperature is estimated to range from 250 to 300 K by simulation of the LIF excitation spectrum using a laser spectral width of 9.2 cm^{-1}. This indicates that no marked rotational excitation occurs in N_2^+ ($X\,^2\Sigma_g^+$, v'' = 0) produced from N_2.

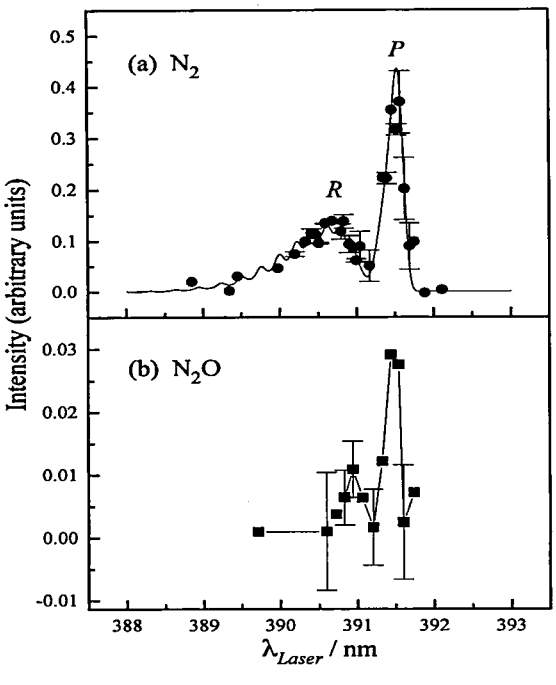

Figure 1. Laser induced fluorescence excitation spectra of the ($B\,^2\Sigma_u^+$, v' = 0) ← ($X\,^2\Sigma_g^+$, v'' = 0) transition of N_2^+ which is produced from (a) N_2 and (b) N_2O. The solid line in (a) represents a spectrum at T = 300 K calculated by using the theoretical intensity distribution of rotation bands. The solid line in (b) is a guide to the eye.

VI-I-4 Time-Resolved Fluorescence Spectroscopy of the Products Resulting from VUV Excitation by Using a Streak Camera

Masakazu MIZUTANI, Hiromichi NIIKURA *(Graduate Univ. for Advanced Studies)* **and Koichiro MITSUKE**

An apparatus for time-resolved fluorescence spectroscopy has been developed at beamline BL3A2 on the UVSOR storage ring in order that the decay dynamics of the molecules produced by VUV excitation can be investigated. The molecular beam expanded from a nozzle made of a multi-channel capillary array plate intersects at 90° with the undulator light supplied from the beamline. The fluorescence is collected with an input optics perpendicularly to the photon and molecular beams, and detected by a streak camera which operates in a synchroscanning mode. The frequency of the streak camera is set to 45.058 MHz, a half of that of the main radio-frequency cavity on UVSOR. The feasibility of the time-resolved experiment is examined by observing radiative transitions from the $CF_4^+(C\,^2T_2)$ state produced by photoionization of CF_4 with a monochromatized undulator light in the photon energy range of 21.2 to 25.1 eV. A measured total fluorescence cross section curve shows an onset at 21.6 eV, which is consistent with the value previously reported. Figure 1 is a time-resolved spectrum of the fluorescence from $CF_4^+(C\,^2T_2)$ obtained by using the streak camera. Since the repetition rate of the fluorescence is twice as high as the sweeping cycle of the streak camera, Figure 1 is composed of a pair of decay curves of the fluorescence at the falling and rising phases of the sweeping cycle. The dashed curve is a time-resolved spectrum calculated by assuming the lifetime of 10 ns and temporal resolution of 0.444 ns. By simulation, the fluorescence lifetime is estimated to be 10±2.5 ns which is in fair agreement with the reported value of 8.75 ns.

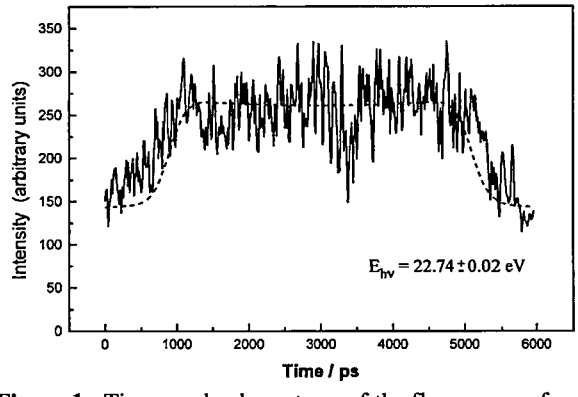

Figure 1. Time-resolved spectrum of the fluorescence from $CF_4^+(C\,^2T_2)$ measured with the streak camera.

VI-J Rebuilding the Monochromator on Beamline BL2B2 in UVSOR

On beamline BL2B2, a grazing incidence monochromator has been constructed which supplies photons in the energy region from 20 to 200eV. This monochromator will bridge the energy gap between beamlines BL3A2 and BL8B1, thus providing for an accelerating demand for the high-resolution and high-flux photon beam from the research field of photoexcitation of inner-valence electrons or *L*-shell electrons in the third-row atom.

VI-J-1 Design of an 18 m Spherical Grating Monochromator at UVSOR

Hiroaki YOSHIDA *(Hiroshima Univ. and IMS)* **and Koichiro MITSUKE**

[*J. Synchrotron Rad.* submitted]

An 18m spherical grating monochromator (SGM) with high resolution and high flux has been developed at the bending-magnet beamline BL2B2 of the UVSOR facility. The schematic layout of the beamline is shown in Figure. 1. The monochromator is designed to cover the energy range of 20 - 200 eV by using three gratings: G1 (2400 lines mm^{-1}, R = 18m) at 80 - 200 eV, G2 (1200 lines mm^{-1}, R = 18 m) at 40 - 100 eV, and G3 (2400 lines mm^{-1}, R = 9.25 m) at 20 - 50 eV. A resolving power ($E/\Delta E$) of 5000 and photon flux of more than 10^{10} photons s^{-1} are expected at a 100mA ring current. A small including angle of 140° is adopted for G3 and two plane mirrors coated with aluminum are located between G3 and the exit slit as optical filters. These geometrical devices may contribute significantly to reduction of the high-order lights.

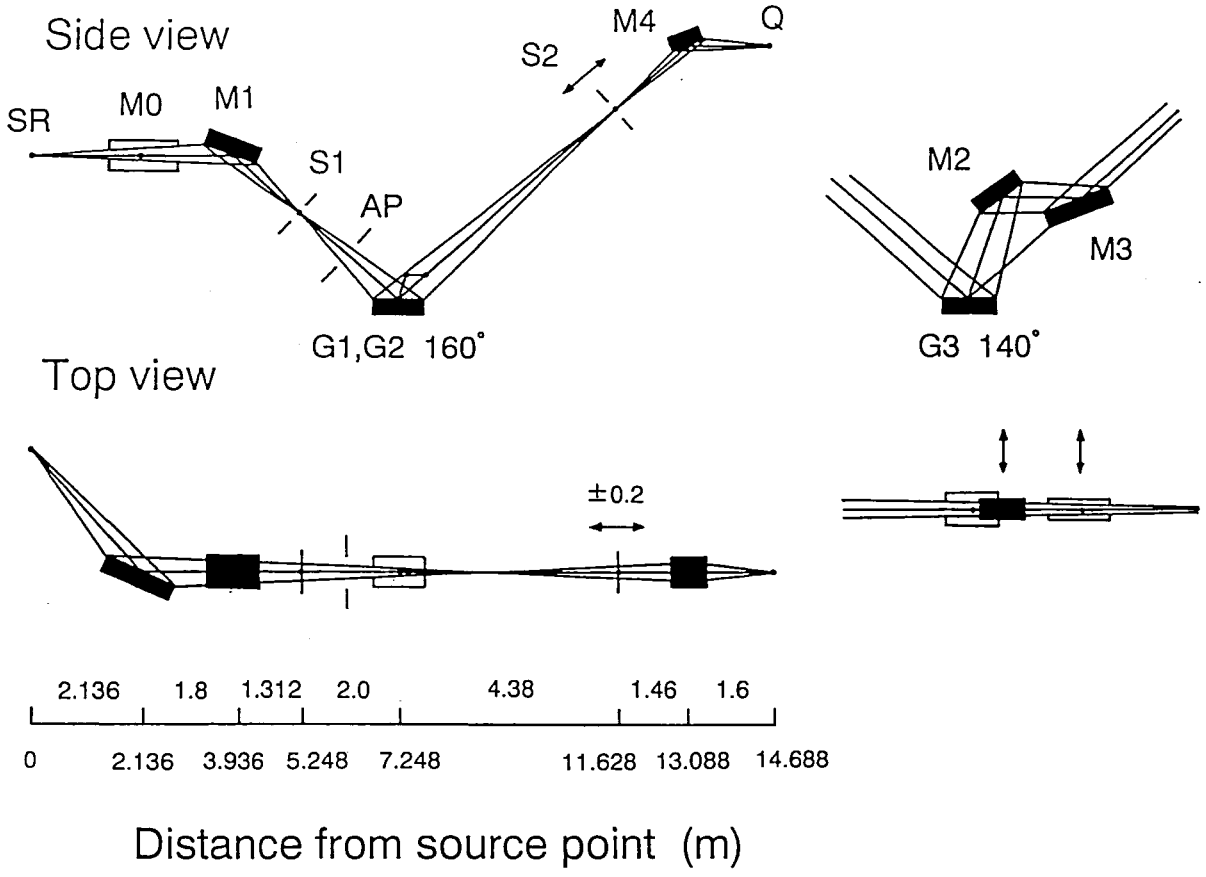

Figure 1. Schematic diagram of the renewed BL2B2 beamline with an 18 m SGM. Two optical paths with including angles of 160° for G1 and G2 and 140° for G3 are indicated. SR, synchrotron radiation source point; M0, elliptically bent plane mirror; M1, spherical mirror; S1, entrance slit; AP, aperture; G1, G2, and G3, spherical gratings; M2 and M3, plane mirrors; S2, exit slit; M4, toroidal mirror; Q, sample point.

VI-K Absolute Photoabsorption Cross Section and Radiative Dissociation of Polyatomic Molecule Excited at Valence Shell

Determination of total photoabsorption cross section in a wide energy region is the fundamental step for physical and chemical investigation of material. Most of oscillator strengths(Photoabsorption cross sections) of molecule are distributed in the energy region up to ~50 eV, in which the Rydberg, superexcited and ionized states are produced. Absolute photoabsorption cross section and dissociative excitation process of the electronically excited photofragment(s) have been studied in the valence excitation region using synchrotron radiation on the BL2A beamline of UVSOR facility.

VI-K-1 C_6F_5X (X = H, F, Cl, Br, and I) Radical Cation Formation in the 10-40 eV Region

Takumi HIKIDA *(Tokyo Inst. Tech.)*, **Toshio IBUKI** *(IMS and Kyoto Univ. Educ.)* **and Kazumasa OKADA** *(IMS and Hiroshima Univ.)*

In excitation energy region 10-40 eV, the emission spectra of corresponding radical cations were observed in the photolysis of C_6F_5X (X = H, F, Cl, Br, and I). Thresholds for the emission from the photoproducts coincide well with the ionization energies of C_6F_5X to form the excited π^{-1} radical cations. Emission efficiency curves were found to be composed of three parts. The first portions (13-16 eV) which start right after the thresholds showed high and nearly constant efficiencies. This excitation area is largely comprised of the benzenic π orbital excitation. The second parts (18-24 eV) of the curves where the efficiencies were constant but less than an half of the first parts were the same energy region as the absorption by the halogen lone pairs. The efficiencies gradually decreased to the last parts where the efficiencies were very low were the energy region of the inner shell excitations. The absolute values were determined to be 20, 4, 2, 0.2, and 0.05 % for X= Cl, F, H, Br, and I, respectively, for the 13-16 eV excitation. The efficiencies of Br- and I-derivatives were the much less among others, probably because of the presence of the dark σ^{-1} levels below the emissive π^{-1} states.

VI-K-2 Photodissociation Spectroscopy of Some Small Nitriles in the Vacuum Ultraviolet Region

Kazuhiro KANDA *(Iwaki Meisei Univ.)*, **Takashi NAGATA** *(IMS)* **and Toshio IBUKI** *(IMS and Kyoto Univ. Educ.)*

Photoabsorption cross sections of RCN (R=CH_3, C_2H_5, n-C_3H_7 and C_6H_5) molecules and the cross sections for the production of the $CN(B^2\Sigma^+\text{-}X^2\Sigma^+)$ and the $CN(A^2\Pi_i\text{-}X^2\Sigma^+)$ were determined in the excitation wavelength region 30-150 nm. The measurements were performed by using a window-less experimental configuration at BL2A, where a gas filter was employed in the wavelengths shorter than the LiF cut-off. In the absorption spectrum of CH_3CN, numerous peaks, which are assignable to Rydberg transition and intravalence transition, have been observed in the wavelength region $\lambda > 95$ nm. The first and second ionization potentials of CH_3CN are reported to be 12.21 eV (101.5 nm) and 13.14 eV (94.4 nm). No structural band was observed below 95 nm, where the excitation energy was beyond second ionization potential. The quantum yields for the $CN(B^2\Sigma^+)$ and $CN(A^2\Pi_i)$ production drastically decrease from 102 to 95 nm. This decrease is due to the preferential operation of the ionization of CH_3CN in the energies above the first ionization potential.

In contrast with CH_3CN, the absorption spectra of other molecules, C_2H_5CN, n-C_3H_7CN and C_6H_5CN, show broad bands. These bands are assignable to the Rydberg transitions converging to the low ionization potential limits. The cross sections for the production of the excited CN radicals from these molecules are much smaller than that of CH_3CN. The observed cross section for producing excited CN radicals has negative dependence on the size of hydrocarbon group. This dependence can be interpreted in terms of the dissipation of the available excess energy to the hydrocarbon group. The quantum yield decreases with the excitation wavelength in the region $\lambda > 100$ nm. The decrease of yield for the production of the $CN(B^2\Sigma^+)$ is larger than that of $CN(A^2\Pi_i)$. The drastical drop of the quantum yield corresponding to the opening of the ionization channel was not observed in the photoexcited fluorescence spectra of these molecules.

VI-K-3 Photoabsorption and Fluorescence Cross Sections of $SiCl_4$ in the Region of 6.2-31 eV

Toshio IBUKI *(IMS and Kyoto Univ. Educ.)*, **Mitsuhiko KONO** *(IMS and Univ. Tokyo)*, **Yukiko ASARI** *(Kyoto Univ. Educ.)*, **Atsunari HIRAYA** *(IMS and Hiroshima Univ.)* **and Kosuke SHOBATAKE** *(Nagoya Univ.)*

[*J. Chem. Phys.* **106**, 4853 (1997)]

Absolute photoabsorption and fluorescence cross sections of gaseous $SiCl_4$ have been measured in the energy region 6.2-31 eV by using synchrotron radiation as a light source. Higher order light from a 1-m Seya monochromator has been suppressed by use of an Ar gas filter in the range of 11.3-15.5 eV (110-80 nm) and a LiF window at $h\nu < 11.8$ eV (105 nm). Emissions have been observed for the $\tilde{C}\,^2T_2 \rightarrow \tilde{A}\,^2T_2$ and $\tilde{C}\,^2T_2 \rightarrow \tilde{X}\,^2T_1$ processes of $SiCl_4^+$ molecular ion and the $\tilde{A}\,^1B_1 \rightarrow \tilde{X}\,^1A_1$ and $^3B_1 \rightarrow \tilde{X}\,^1A_1$ of $SiCl_2$ radical. Total fluorescence cross section has been determined to be 22.4 ± 1.0 Mb at 21.22 eV. By comparing with the par-

tial formation cross section of the $\tilde{C}\ ^2T_2$ ionic state [Carlson *et al.*, *J. Chem. Phys.* **84**, 641 (1986)], it has been concluded that the $SiCl_4^+(\tilde{C}\ ^2T_2)$ formed decays through radiative processes with quantum yield $\phi_f \sim 1$. The experimental results provide information on the breakdown pathways of the $SiCl_4^+(\tilde{C}\ ^2T_2)$ state ion. The bands observed in photoabsorption and fluorescence excitation spectra have been assigned as the (4*s*, *np*, and *np'*) $\leftarrow 3t_2$, (4*s* and *np*) $\leftarrow 1e$, (4*s* and 4*p*) $\leftarrow 2t_2$, and (*np* and *nd*) $\leftarrow 2a_1$ Rydberg series. The ionization energies for $(2t_2)^{-1}$ and $(2a_1)^{-1}$ have been found to be 15.04±0.03 and 18.17±0.03 eV, respectively.

VI-K-4 Dissociative Excitation Cross Section of Formic Acid in the 105 - 155 nm Region

Kiyohiko TABAYASHI, Takashi HINO, Koh SAITO *(Hiroshima Univ.),* **Kazumasa OKADA** *(IMS and Hiroshima Univ.)* **and Toshio IBUKI** *(IMS and Kyoto Univ. Educ.)*

In a previous measurement for the dispersed fluorescence spectrum of formic acid, emission from OH(A) and HCOO* has been observed upon photoexcitation at an intense absorption peak of 110 nm. Here the cross sections for the following dissociative excitation processes have been measured in the excitation wavelength range 105 - 155 nm,

$$HCOOH + h\nu \rightarrow HCO + OH(A) \quad (1)$$
$$\rightarrow HCOO^* + H \quad (2)$$

The cross sections were separately obtained by detecting the emission intensities of the OH(A) bands in the 280-325 nm region and the HCOO* bands in the 330-500 nm region using the optical filters. Although both cross sections are essentially a function of the excitation wavelength, the branching ratio of the reaction (1) increases with decreasing the excitation wavelength, i.e. from ~0 at 138 nm to ~0.4 at 110 nm. Total fluorescence quantum yield also increases with decreasing the excitation wavelength with a maximum of 5.4 % at 106 nm. The dissociative excitation measurements were repeated for the D-substituted formic acid and the cross sections for the similar reactions to the (1) and (2) have been determined. From the analysis of the quantum yields, it has been shown that the deuterium isotope enhancement of the cross section is prominent for both excitation processes when the hydrogen on the C atom is replaced by deuterium in HCOOH.

VI-L Creation of High-Sensitive Photorefractive Glasses and Photoinduced Structural Changes

Photorefractive effect,"photosensitivity", has great practical value in that it makes possible a family of novel passive filter devices that have application in optical optical communications and optical sensors. In this project the goal is to create highly sensitive photorefractive thin films. We examined the photoinduced index changes in Ge-doped silica glasses by excimer laser irradiation.

VI-L-1 Preparation of Bragg Gratings in Sputter-Deposited GeO_2-SiO_2 Glasses by Excimer-Laser Irradiation

Junji NISHII *(Osaka National Research Institute),* **Hiroshi KAWAZOE** *(Tokyo Inst. Tech.)* **and Hideo HOSONO** *(IMS and Tokyo Inst. Tech.)*

GeO_2-SiO_2 thin glass films were prepared by the rf sputtering deposition method. Changes in the refractive index of -3% and in the volume of +18% were induced in the film by irradiation with excimer-laser pulses. Bragg gratings a (periodic surface-relief pattern with a sinusoidal wave) have been written in the film by irradiation through a phase mask.

VI-L-2 Defect Formation in SiO_2:GeO_2 Glasses Studied by Irradiation with Excimer Laser Light

Hideo HOSONO *(IMS and Tokyo Inst. Tech.),* **Hiroshi KAWAZOE** *(Tokyo Instit. Tech.)* **and Junji NISHII** *(Osaka National Research Institute)*

The formation of germanium electron centers in $[SiO_2]_9[GeO_2]$ glasses by irradiation with excimer laser light was found to occur via two-photon absorption processes for ArF, KrF, and XeCl lasers. Although the wavelength of KrF laser light corresponds to the absorption band of preexisting oxygen-deficient defects associated with Ge ions, no significant difference in the formation efficiency was seen between ArF and KrF laser lights. The efficiency for XeCl laser light was smaller by four orders of magnitude than that for ArF or KrF light, but was still larger by an order of magnitude than the formation efficiencies of Si E' centers in SiO_2 glasses with ArF laser light. It was shown that defect-formation efficiencies for the case where the two-photon energy is close to the optical band gap are much lower than for that when the two-photon energy is enough to exceed the band gap.

VI-M Creation of Amorphous Metallic Conducting Amorphous Oxides

High transparency to visible radiation is incompatible with high electrical conductivity in most solid crystalline materials. This is also true for amorphous materials. Existing amorphous (a-) semiconductors are classified into two categories, a tetrahedral system represented by amorphous silicon and the chalcogenide system by a-As_2S_3.

However, neither system possesses both high transparency and high conductivity. We have explored new materials which meet both property requirements and found novel oxides with different crystal structures, i.e., $MgIn_2O_4$(spinel), $ZnGa_2O_4$(spinel), $Cd_{1-x}Y_xSb_2O_6$ (pyrochlore) and $AgSbO_3$ (defect pyrochlore). If transparent and conducting materials are realized, they should have the dual merits of transparent conductors and amorphous materials. In this project, we set up a working hypothesis to explore novel wide-gap oxide amorphous semiconductors on the basis of a consideration concurring the chemical bonding and approach this issue.

VI-M-1 Working Hypothesis to Explore Novel Wide Band Gap Electrically Conducting Amorphous Oxides and Examples

Hideo HOSONO *(IMS and Tokyo Inst. Tech.)*, **Naoto KIKUCHI** *(Tokyo Inst. Tech)*, **Naoyuki UEDA** *(IMS and Tokyo Inst. Tech.)* **and Hiroshi KAWAZOE** *(Tokyo Inst. Tech.)*

A working hypothesis for exploring optically transparent and electrically conducting amorphous oxides is proposed on the basis of simple considerations concerning chemical bonding. The hypothesis predicts that amorphous oxides composed of heavy metal cations with an electronic configuration of (n-1) $d^{10}ns^0$ may be converted into transparent conducting amorphous oxides when doped by Li ion implantation or heating at temperatures below crystallization. Three new materials, amorphous Cd_2GeO_4, $AgSbO_3$ and Cd_2PbO_4, have been prepared as examples.

VI-M-2 Novel Oxide Amorphous Semi-conductors: Transparent Conducting Amorphous Oxides

Hideo HOSONO *(IMS and Tokyo Inst. Tech.)*, **Masahiro YASUKAWA** *(Tokyo Inst. Tech.)* **andHiroshi KAWAZOE** *(Tokyo Inst. Tech.)*

A working hypothesis to find wide gap oxide semiconductors was proposed on the basis of simple considerations. The hypothesis predicts that amorphous double oxides composed of heavy metal cations (HMCs) with an electronic configuration (n-1) $d^{10}s^0$ are promising candidates for a novel class of amorphous semiconductors. Electrical and optical properties of three amorphous double oxides composed of the HMCs, a-$AgSbO_3$, C d_2GeO_4 and Cd_2PbO_4, were examined, following this hypothesis. It was found that when carrier electrons are generated via the formation of oxygen vacancies or doping of excess cations by ion implantation, these three wide band gap amorphous oxides show high electrical conductivities of 10^{-1} to 10^2 S cm^{-1} at ~300K and the conductivity remains almost constant down to 77 or 4 K for high carrier concentrations ($>10^{18}cm^{-3}$). This high conductivity originates primarily from a large Hall mobility of ~$10cm^2V^{-1}s^{-1}$, which is higher by several orders of magnitude than that in amorphous transition metal oxides, Si:H and chalcogenides. A variety of chemical compositions for a novel oxide amorphous semiconductor are suggested.

VI-N Ultraviolet Photoelectron Spectroscopy of Organic and Inorganic Solids

Work of ultraviolet photoelectron spectroscopy (UPS) of organic solids and inorganic compounds have been proceeded. We investigated their quantitative electronic structures using photoelectron spectrometer combined with synchrotron radiation light source (UVSOR-UPS).

VI-N-1 Angle-Resolved UPS of Ultrathin Films of Functional Organic Molecules with Synchrotron Radiation: Determination of Molecular Orientation by Quantitative Analysis of Photoelectron Angular Distribution

Nobuo UENO

[*J. Electron Spectr. Relat. Phenom.* **78**, 345 (1996)]

This paper describes the determination of the molecular orientation of functional organic molecules in their ultrathin films deposited on crystal surfaces by the quantitative analysis of photoelectron angular distribution observed with synchrotron radiation. The examples of the results are presented for phthalocyanine and bis(1,2,5 thiadiazolo)-*p*-quinobis (1,3-dithiole), a new type of organic emiconductor. Further, the first theoretical simulation of the valence-band spectrum is also shown for oriented thin films of naphthacene, a conventional organic semiconductor. These analyses were based on the independent-atomic-center approximation (IAC) and single scattering theory (SS) combined with molecular orbital (MO) calculation. It is shown that even the simple IAC/MO model can simulate the photoelectron angular distribution very well for a π band at near flat-lie orientation of planer molecules. Further we found that the SS/MO calculations can give the full valence band spectra of large organic molecules, which are in excellent agreement with observed ones.

VI-N-2 Angle-Resolved Ultraviolet Photo-electron Spectroscopy of Thin Films of Bis(1,2,5 Thiadiazolo)-*p*-Quinobis (1,3-Dithiole) on the MoS_2 Surface

Nobuo UENO, Akinori KITAMURA *(Chiba Univ.)*, **Koji K. OKUDAIRA** *(Chiba Univ.)*, **Takayuki MIYAMAE, Yoshiya HARADA** *(Chiba Univ.)*, **Shinji HASEGAWA, Hisao ISHII, Hiroo INOKUCHI, Takafumi MIYAZAKI** *(Toyama Univ.)* **and Kazuhiko SEKI** *(Nagaya Univ.)*

[*J. Chem. Phys.* **107**, 2079 (1997)]

In this paper, we report on the angle-resolved ultraviolet photoelectron spectroscopy on ultrathin films of bis(1,2,5-thiadiazolo)-*p*-quinobis(1,3-dithiole) [BTQBT] deposited on a MoS_2 surface with synchrotron radiation, and describe the quantitative analysis of the angular distribution of photoelectron from the highest occupied state. The observed angular distributions were better explained by those calculated with the single-scattering approximation combined with molecular orbital calculation considering intramolecularly scattered waves than the previously used independent-atomic-center approximation combined with molecular orbital calculation. Further the low-energy-electron diffraction measurements were performed on the film. From the low-energy electron diffraction, the two-dimensional lattice of the ultrathin film on the MoS_2 was found to be $MoS_2(0001)$-($\sqrt{13}\times\sqrt{13}$, R=±13.9°)-BTQBT, and from the analysis of the photoelectron angular distributions, it was found that at the lattice points the molecules lie flat with azimuthal orientations of 19 and 47° with respect to each surface crystal axis of MoS_2. On the basis of these results, the full structure of the thin film, the two-dimensional lattice and full molecular orientations at the lattice points, is proposed.

VI-N-3 Ultraviolet Photoelectron Spectroscopy of N-Type Conducting Polymers

Takayuki MIYAMAE, Daisuke YOSHIMURA *(Nagoya Univ.)*, **Hisao ISHII, Yukio OUCHI** *(Nagoya Univ.)*, **Takafumi MIYAZAKI** *(Toyama Univ.)*, **Tsuneaki KOIKE** *(Mitsui Petrochem. Inductries LTD)*, **Takakazu YAMAMOTO** *(Tokyo Inst. Tech.)*, **Yukiko MURAMATSU** *(Tokyo Inst. Tech.)*, **Hideki ETORI** *(Tokyo Inst. Tech.)*, **Tsukasa MARUYAMA** *(Tokyo Inst. Tech.)* **and Kazuhiko SEKI** *(Nagoya Univ.)*

[*Synth. Met.* **84**, 939 (1997)]

Ultraviolet Photoelectron Spectra were measured using synchrotron radiation for four kinds of π-conjugated polymers, poly(pyridine-2,5-diyl)[Ppy], poly(2,2'-bipyridine-5,5'-diyl)[Pbpy], poly(2-methylantraquinone-1,4-diyl)[P(2Me-1,4-AQ)], and poly(antraquinone-1,5-diyl)[P(1,5-AQ)], which exhibit n-type electrically conducting polymers. The spectra were analyzed with MO calculations of the oligomers. Upon potassium doping of Pbpy, two new states, which can be assigned to bipolaron bands, appeared in the originally empty energy gap. While Ppy shows similar gap states, it requires higher dopant concentration to create bipolaron bands than in the case of K-doped Pbpy. Ppy shows a weak coordinating ability toward the alkaline-metal than in the case of Pbpy, because of the mainly head-to-tail structure of Ppy. The UPS spectra of K-doped P(2Me-1,4-AQ) and K-doped P(1,5-AQ) also shows similar gap states. The changes in electronic structure of these polymers are discussed based on the conformational difference between these polymers.

VI-N-4 Photoelectron Spectra of Metallofullerenes, GdC_{82} and La_2C_{80}: Electron Transfer from Metal to the Cage

Shojun HINO *(Chiba Univ.)*, **Kentaro IWASAKI** *(Chiba Univ.)*, **Kazunori UMISHITA** *(Chiba Univ.)*, **Takafumi MIYAZAKI** *(Toyama Univ.)*, **Takayuki MIYAMAE, Koichi KIKUCHI** *(Tokyo Metropol. Univ.)* **and Yohji ACHIBA** *(Tokyo Metropol. Univ.)*

[*Chem. Phys. Lett.* in press]

Ultraviolet photoelectron spectra of metal fullerenes, GdC_{82} and La_2C_{80} are measured with the synchrotron orbital radiation. Though the specimens for the photoemission measurement are not commonly adopted sublimed films but dried up films prepared from its solution, GdC_{82} gives structure rich spectra to reflect its electronic structure while La_2C_{80} gives a spectrum poor in structure. The intensity of bands in the GdC_{82} spectra depends on the incident photon energy, as are observed in other fullerenes. The spectra of GdC_{82} resemble those of LaC_{82}, which indicate their analogous electronic structure. The spectrum of La_2C_{80} does not show characteristic structures that have been observed in those of other fullerenes and it resembles that of amorphous carbon. C 1s core photoelectron spectra of these metal fullerenes obtained with the MgKα radiation are also presented.

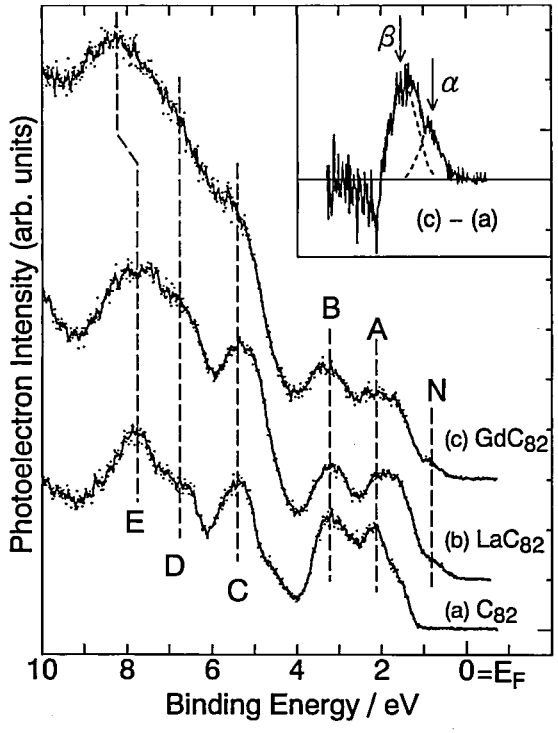

Figure 1. Photoelectron spectra of C_{82}, LaC_{82} and GdC_{82} obtained with hn = 20 eV excitation energy. Inset is the differece spectrum obtained by substracting the C_{82} spectrum from the GdC_{82} spectrum (the intensity of both of them is normalized at 3.2 eV peak that seems to have been less suffered from the effect of superposition of the secondary electrons). The difference spectrum can be deconvoluted into two peak components α and β with intensity ratio 1:2.

VI-N-5 Structure and Catalysis of $Li_xNi_{2-x}O_2$ Oxide Systems for Oxidative Coupling of Methane

Takafumi MIYAZAKI *(Toyama Univ.)*, **Takao DOI** *(Tosoh Corp.)*, **Takayuki MIYAMAE and Ikuya MATSUURA** *(Toyama Univ.)*

[*Stud. Surf. Sci. Catal.* in press]

Photoelectron spectroscopy (XPS and UPS) studies have been applied to the investigation of active oxygen species of solid solution series $Li_xNi_{2-x}O_2$ with wide range of $0<x=1$ for understanding the origin of high activity and C_2-selectivity of the oxidative coupling of methane.

From the comparison of these spectral features, the surface oxygen of $Li_{0.3}Ni_{1.7}O_2$ with a cubic structure was assigned to O^{2-} species, while that of $LiNiO_2$ with a hexagonal structure was attributed to O^- species associated with the catalytic activity for the oxidative coupling of methane.

From the relationship between these structures and the catalytic activity, it was inferred that the anisotropic layered superstructure of $LiNiO_2$ largely affected the formation of the active oxygen species for the oxidative coupling reaction.

VI-N-6 Resonant Photoemission Study of Ladder Compound $Sr_{14}Cu_{24}O_{41}$

Osamu AKAKI *(Tohoku Univ.)*, **Ashish CHAINANI** *(Tohoku Univ.)* **and Takashi TAKAHASHI** *(Tohoku Univ.)*

There is increasing interest in one-dimensional cuprates because of their peculiar electronic and magnetic properties as well as its relation to the superconducting mechanism in two-dimensional cuprates. In this report, we present results of resonant photoemission spectroscopy (PES) on $Sr_{14}Cu_{24}O_{41}$, which was recently found to show superconductivity below 12K under high pressure (3.5-4 GPa) by substituting Sr with Ca atoms.[1] $Sr_{14}Cu_{24}O_{41}$ consists of Cu_2O_3 planes with two-leg ladders and CuO_2 chains (Figure 1). $(Sr, Ca)_{14}Cu_{24}O_{41}$ is regarded as a "self-doped" ladder material with the Cu formal valence of 2.25. However, $Sr_{14}Cu_{24}O_{41}$ is an insulator and substitution of Sr atoms with Ca gradually increases its metallic conductivity. The superconductivity is observed in a heavily substituted sample $Sr_{0.4}Ca_{13.6}Cu_{24}O_{41}$ under high pressure. It is still unknown at present where doped holes are and what role the Ca substitution plays in the crystal. In order to study the charge distribution in $Sr_{14}Cu_{24}O_{41}$, we have performed a resonant photoemission spectroscopy.

Photoemission measurements were performed at BL8B2 with $Sr_{14}Cu_{24}O_{41}$ single crystals at room temperature. Samples were repeatedly scraped by a diamond file to obtain a fresh and clean surface. Figure 2 shows PES spectra of $Sr_{14}Cu_{24}O_{41}$ measured at various photon energies across the Cu3p-3d core threshold (about 74 eV). We find that a new structure emerges around 13 eV binding energy at the core-threshold excitation (~ 74 eV). This new structure in the PES spectrum is ascribed to the so-called two-hole bound state, which is known to resonantly enhanced at the photon energy of Cu 3p-3d core excitation. The appearance of two hole-bound state in the resonant PES spectrum indicates that there is a substantial number of Cu^{2+} ions with Cu $3d^9$ configuration in the compound. At the present stage, it is unknown whether these Cu^{2+} ions are located on ladders or chains in the crystal. However, it is at least obvious that both (ladder and chain) are not doped and either of them should have almost no holes. This finding establishes the starting point to elucidate the electronic structure of "doped" superconducting $(Sr, Ca)_{14}Cu_{24}O_{41}$.

We thank Prof. Akimitsu at Aoyama-Gakuin University for providing the single crystals.

Reference

1) M. Uehara *et al.*, *J. Phys. Soc. Jpn.* 65, 2764 (1996).

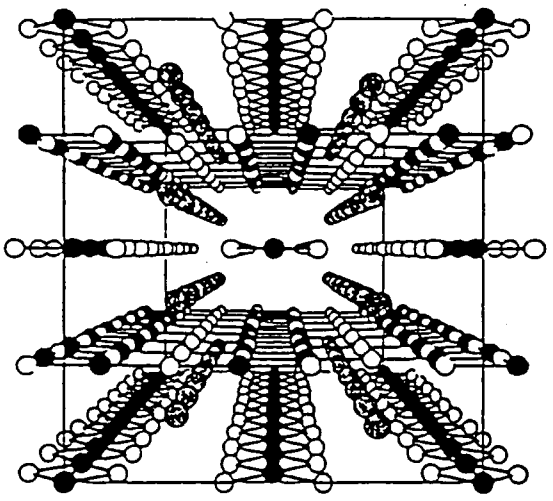

Figure 1. Crystal structure of $Sr_{14}Cu_{24}O_{41}$

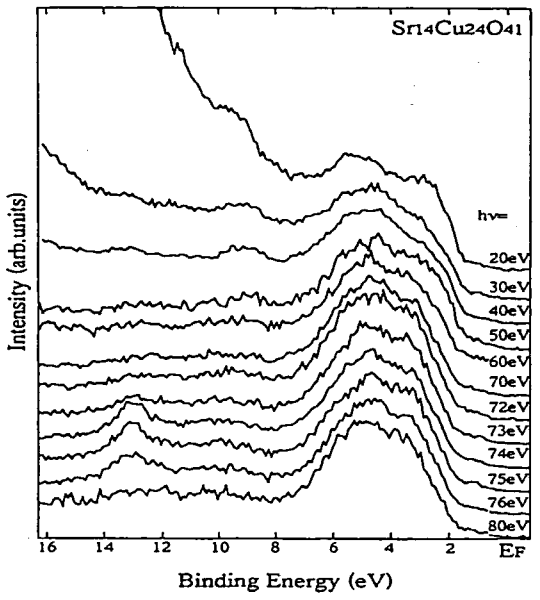

Figure 2. Photoemission spectra of $Sr_{14}Cu_{24}O_{41}$ at various photon energies across the Cu 3p-3d core threshold (~74 eV).

VI-O Desorption Induced by Electronic Transitions from Cryogenic Surfaces

Desorption processes of particles from cryogenic surfaces are studied using synchrotron radiation in vacuum ultraviolet region. As a result of decay processes after an electronic excitation of surface layers by synchrotron radiation, various kinds of particles are released from the surface. Cryogenic substrates such as solid rare gases have particular excitation channels for the desorption of electronically excited neutral particles that are pronounced at the creation energy region of exciton. Experiments are performed at BL5B of UVSOR. We use an UHV chamber with liquid-He cryostat and particle detectors sensitive for excited neutral species, which is connected to the monochromator of the beamline via differential pumping stages. We discuss the mechanisms of excitation, energy transfer and desorption phenomena induced by electronic transitions by measuring the kinetic energy and angular distributions of desorbed species, incident energy dependence of desorption yield, correlation between particle emission and photon emission, and so on.

VI-O-1 Excitonic Energy Transfer Process in Ne-Kr Alloy Studied by Photon Stimulated Desorption of Metastable Atoms

Takato HIRAYAMA*, Toshihiro NAGAI*, Munehide ABO*, Ichiro ARAKAWA*, Koichiro MITSUKE and Makoto SAKURAI *(*Gakushuin Univ.)*

[*J. Electron Spectrosc.* **80**, 101 (1996)]

Metastable atom desorption from a pure solid Ne and a solid Ne-Kr alloy has been systematically studied using a monochromatic synchrotron radiation. Refined time-of-flight spectrometer enabled us to investigate the desorption mechanism in more detail. Metastable Ne atoms desorbed through cavity ejection mechanism by the excitation of the first order surface, and the first and the second order bulk excitons are found to have almost the same kinetic energy, E_k = 0.18±0.02 eV, while by $2p^53p$ type surface exciton, E_k = 0.21±0.02 eV. By the excitation of Ne bulk exciton in Ne-Kr alloy, effective excitonic energy transfer process has been observed, which results in the decrease of the Ne* desorption yield by the bulk excitation.

VI-O-2 Absolute Desorption Yield of Meta-stable Atoms from the Surface of Solid Rare Gases Induced by Exciton Creation

Takato HIRAYAMA*, Akira HAYAMA*, Toshihiro KOIKE*, Takafumi KUNINOBU*, Ichiro ARAKAWA*, Koichiro MITSUKE, Makoto SAKURAI and E. V. SAVCHENKO** *(*Gakushuin Univ. **B. Verkin Inst. for Low Temp. Phys. and Eng.)*

[*Surf. Sci.* in press]

Absolute yields of the metastable excited atoms desorbed from the surfaces of solid Ne and Ar by the creation of surface and bulk excitons have been measured using monochromatized synchrotron radiation as a selective excitation source. We have obtained the absolute yields of (2.3±0.7) × 10^{-3}, (1.4±0.4) ×10^{-3}, and (7.8±2.3) × 10^{-4} (atoms/photon) at the excitation of S1, B1 and S' exciton for Ne, respectively, and 1 x 10^{-5} (atoms/photon) at S1 excitation for Ar. The probability for metastable atom desorption is found to be about 2 to 10% at the excitation of S1 exciton on the surface of solid Ne.

VI-O-3 Long Lifetime Emission of the Excited Species Ejected from the Surface of Solid Ne

E. V. SAVCHENKO*, Takato HIRAYAMA, Akira HAYAMA**, Toshihiro KOIKE**, Takafumi KUNINOBU**, Ichiro ARAKAWA**, Koichiro MITSUKE and Makoto SAKURAI** *(*B. Verkin Inst. for Low Temp. Phys. and Eng. **Gakushuin Univ.)*

[*Surf. Sci.* in press]

Desorption of long-lived neutral particles from solid Ne is studied using selective photoexcitation and time of flight (TOF) technique. The luminescence due to direct light from the sample surface is blocked by rotating the sample. Two new prominent features are revealed in the TOF spectra measured at a special geometry: a prominent long tail and a maximum at the delay time of ~0.5ms. From the analysis of the excitation spectra recorded by the time window technique and the TOF spectra at selective excitation it is assumed that the new features are closely related to Ne_2* excimer desorption. Analysis of probable mechanisms of the long lifetime emission is presented.

VI-P Structure and Vibrational Spectra of Molecules Physisorbed on Metal Surfaces

Molecular layers physisorbed on metal surfaces at low temperature show specific structures which depend on the interaction between molecules and substrate, and vibrational spectra for physisorbed molecules reveal the details of the interaction. We use dynamical analysis of low-energy electron diffraction (LEED) to investigate the structure of adsorbed layers, and high-resolution electron energy loss spectroscopy has been utilized for vibrational spectroscopy for adsorbed molecules. As a complemental method for vibrational spectroscopy of surfaces, infrared

reflection absorption spectroscopy will be combined with our experimental system. A new cryogenic sample holder for surface vibrational spectroscopy is also under development in order to provide a substrate at less than 4.2K.

VI-P-1 Upgraded Infrared Beamline BL6A1 at UVSOR

Makoto SAKURAI, Hidekazu OKAMURA*, Katsumi WATANABE*, Takao NANBA*, Shin-ichi KIMURA and Masao KAMADA *(*Kobe Univ.)*

BL6A1, a far-infrared (FIR) beamline at UVSOR originally built in 1986, has been upgraded recently. The upgrade included the introduction of a second FT-IR spectrometer, and now it is possible to cover the entire FIR-IR range (3 cm^{-1} to 10000 cm^{-1}) in one sequence of measurements, without having to open the sample chamber; the beamline has become a more convenient and powerful experimental station than before. The upgrade is also expected to enable such experiments as IR studies of molecules adsorbed on the solid surfaces, and time-resolved IR spectroscopies.

VI-P-2 Development of the Cryogenic Sample Holder for Low Energy Electron Diffraction and Electron Energy Loss Spectroscopy

Masuaki MATSUMOTO, Tamotsu MAGOME*, Makoto SAKURAI and Tatsuo OKANO* *(*IIS, Univ. Tokyo)*

Most of the gases can be condensed or physisorbed as the multilayer solid films on surfaces cooled below 10K. The nature of the physisorbed molecules is different from that of both the chemisorbed and the gas phase molecules. We develop the cryogenic sample holder in order to study the structure and the vibrational state of the physisorbed molecules. Sample is cooled with the liquid helium transfer type cryostat and can be cooled to the temperature about 10K. In order to reduce the radiation from room temperature, the sample is surrounded by the shield which is cooled with closed cycle refrigerator. Sample can be heated with tantalum heater to temperature above 1200K in the cleaning procedure. Temperature of the sample is measured with Pt/PtRh thermocouple which is calibrated with Si diode thermometer. We are now designing the new cryostat in order to cool the sample below 4.2K.

VI-P-3 Structure of the NO Molecule on the Pt(111) Surface at Low Temperature

Masuaki MATSUMOTO, Natsuo TATSUMI*, Katsuyuki FUKUTANI*, Makoto SAKURAI and Tatsuo OKANO* *(*IIS, Univ. Tokyo)*

Platinum is one of the most useful catalyst and adsorption of NO molecule on the Pt(111) was studied by various techniques. The previous results of EELS and RAIRS show two different vibrational state depending on the exposure. They were assigned to the bridge site molecules at low exposure region and on-top site molecules at high exposure region. However, the recent result of the structural analysis with LEED dynamical calculation is inconsistent with these results. They only measure the LEED pattern in high exposure region and the structure of this system is controversial yet. For the purpose of the determination of the structure of this system, we develop the high sensitive automated LEED system combined with RAIRS. We use the computer controlled cooled CCD camera in order to measure the diffuse and weak LEED pattern in low exposure region and use the DLEED theory to analyze these patterns. We also study the change of the structure by irradiation of ultraviolet laser.

VI-Q Electronic Structures of Functional Organic Materials Studied by Spectroscopies Using Synchrotron Radiation

Recently functional organic materials have attracted much attention in close relation to their possible applications such as molecular devices, organic electroluminescent devices, and organic solar cells. The elucidation of electronic structures of functional organic materials is indispensable for understanding and development of such a function. With photoelectron spectroscopy (PES), VUV absorption and reflection spectroscopy, and near-edge X-ray absorption fine structure (NEXAFS), we have investigated the electronic structures of various organic materials such as (I) materials and their interfaces of organic electroluminescent devices and organic solar cells, (ii) silicon-based organic compounds, (iii) basic oligomers as a model compound of polymers, and (iv) salicylideneaniline derivatives with tautomerism in intramolecular hydrogen bonds, which can be regarded as proton transfer system.

VI-Q-1 Energy Level Alignment a t Organic /Metal Interfaces Studied by UV Photoemission: Breakdown of Traditional Assumption of a Common Vacuum Level at the Interface

Hisao ISHII, Daisuke YOSHIMURA,* Kiyoshi SUGIYAMA* and Kazuhiko SEKI* *(* Nagoya Univ.)*

[*IEEE transactions on electron devices, in press, J. Electron Spectrosc. Relat. Phenom.* **78**, 359 (1996); *Syn. Metals* **86**, 2399 (1997)]

Electronic structures of model interfaces of organic electroluminescent (EL) devices and porphyrin/metal interfaces were investigated by UV photoemission spectroscopy (UPS). At all the measured interfaces, shift of the vacuum level was observed, showing the formation of an interfacial electric dipole layer. For Alq_3 (tris(8-hydroxyquinolino)aluminum), TPD (*N,N'*-diphenyl-*N,N'*-(3-methylphenyl)-1,1'-biphenyl-4,4'-diamine), and DP-NTCI (*N,N'*-diphenyl-1,4,5,8- naphtyl-tetracarboxylimide)/metal interfaces, interfacial energy

diagrams determined by UPS correspond well with the actually observed carrier-injecting character at the interfaces. For ZnTPP (5,10,15,20-zinc-tetraphenylporphyrin), H_2TPP (5,10,15,20-tetraphenylporphyrin), and H_2T(4-Py)P (5,10,15,20-tetra(4-pyridyl) porphyrin) / metal interfaces, the shifts of the vacuum level as well as the energies of the levels in porphyrins could be expressed as a linear function of work function of the metal substrate. The slope of the linear function depended on the compound. These findings are in contrast to the traditional assumption of common vacuum level at the interfaces. For ZnTPP/metal interfaces, sample exposure to oxygen induced energy level shift in close relation with the change of the substrate work function at oxygen exposure. The present results have clearly demonstrated that direct observation of the interfacial electronic structure by microscopic method such as UPS is necessary for understanding the organic electronic devices such as EL devices and organic solar cells.

VI-Q-2 Electronic Structures Of Polysilanes And Related Compounds

Kazuhiko SEKI[a], Hisao ISHII, Akira YUYAMA[a], M.WATANABE[b], K.FUKUI[c], E.ISHIGURO[d], J.YAMAZAKI, S.HASEGAWA, K.HORIUCHI[e], T. OHTA[f], H.ISAKA[g], M.FUJINO[g], M.FUJIKI[g], K.FURUKAWA[g] and N.MATSUMOTO[g] *([a]Nagoya Univ., [b]Tohoku Univ., [c]Fukui Univ., [d]Univ. Ryukyus, [e]Hiroshima Univ., [f]Univ. Tokyo and [g]NTT)*

[*J. Electron Spectrosc. Relat. Phenom.* **78**, 403 (1996), *Mol. Cryst. Liq. Cryst.* **285**, 205(1996)]

UPS and Si K- and $L_{II,III}$-edge NEXAFS spectra of various polysilanes, poly(dimethylsiloxane), and octakis(t-butyl)octa-silacubane(OTBOSC) were measured for elucidating their occupied and vacant electronic structures, in comparison with the results for polysilazane. The results revealed that the electronic structures are sensitive for the main chain structure, pendant, and the dimensionality of the Si-containing backbone.

VI-Q-3 Polarized VUV Absorption and Reflection Spectra of Oriented Films of Poly(tetrafluoroethylene) $(CF_2)_n$ and its Model Compound

Kohei NAGAYAMA,* Takayuki MIYAMAE, Ryuichi MITSUMOTO,* Hisao ISHII, Yukio OUCHI* and Kazuhiko SEKI* *(*Nagoya Univ.)*

[*J. Electron Spectrosc. Relat. Phenom.* **78**, 407 (1996)]

Polarized vacuum-UV absorption and reflection spectra were measured for oriented films of plytetrafluoroethylene(PTFE)$(CF_2)_n$ and its model compound perfluorotetracosane (PFT) n-$C_{24}F_{50}$. The lowest energy excitation leading to an intense peak was found to be polarized along the molecular chain, and its energy decreases with the chain length (8.05eV for PFT and 7.66eV for PTFE). The polarization and chain-length dependence are discussed with the aid of information by theoretical calculation, NEXAFS, and electron transmission spectroscopy.

VI-Q-4 Soft X-ray Absorption and X-ray Photoelectron Spectroscopic Study of Tautomerism in Intramolecular Hydrogen Bonds of N-Salicylideneaniline Derivatives

Eisuke ITO[a], Hiroshi OJI[a], Tohru ARAKI[b], Kazuyoshi OICHI[a], Hisao ISHII, Yukio OUCHI[a] Toshiaki OHTA[c], Nobuhiro KOSUGI, Yusei MARUYAMA[d], Toshio NAITO[e], Tamotsu INABE[e] and Kazuhiko SEKI[a] *([a]Nagoya Univ.y, [b]KEK, [c]Univ. Tokyo, [d] Hosei Univ. and [e]Hokkaido Univ.)*

[*J. Am. Chem. Soc.* **119**, 6336 (1997)]

The tautomerism in solid phase was studied by near-edge X-ray absorption fine structure (NEXAFS) spectroscopy at the N K- and O K-edges and X-ray photoelectron spectroscopy (XPS) in the N1s and O1s regions for five N-salicylideneaniline derivatives: N,N'-disalicylidene-1,6-pyrenediamine (DSPY), N,N'-disalicylidene-p-phenylenediamine (BSP), N-(2-hydroxy-1-naphthylidene)-1-pyrenylamine (NPY), N,N'-di(2-hydroxy-1-naphthylidene)-p-phenylenediamine (DNP), and the complex between DNP and 7,7,8,8-tetracyanoquinodimethane (DNP-TCNQ). The NEXAFS spectral features were assigned by (1) the comparison with the core excitation spectra of reference compounds and (2) *ab initio* MO calculations of the core-excited states by the improved virtual orbital method using the relaxed Hartree-Fock orbitals. The tautomeric structures were deduced by the intensity of peaks characteristic of the tautomers in OH- and NH-forms. The XPS spectra gave structures consistent with those by NEXAFS, and also allowed quantitative estimation of the relative tautomer populations. The results range from the dominance of the OH-form in DSPY and BSP to comparable mixture of the OH- and NH-forms in DNP and DNP-TCNQ. These structures are consistent with the previous estimation by X-ray diffraction (XD), except for DNP-TCNQ where XD suggested the NH-form dominance. The good correlation of the population by XPS with the C-O bond length by XD supports the present conclusion for DNP-TCNQ. These results demonstrate the usefulness of NEXAFS as well as XPS for studying the tautomerism in hydrogen bonded systems.

VI-R Growth and Characterization of InAs Nanometer-Scale Island on InP (001) Substrate

For three-dimensional confinement of electrons and holes, new physical phenomena and improvement of optoelectronic devices, such as extremely sharp emission line, phonon relaxation bottleneck, and temperature-independent threshold current density for lazing, have been predicted. We have studied InAs quantum dots on InP, since they are expected to emit radiation in technologically important 1.3 - 1.5 μm region.

VI-R-1 Formation of InAs Islands on InP (001) by Droplet Hetero-Epitaxy

Youichi NONOGAKI, Tadashi IGUCHI *(Nagoya Univ.)*, **Yasufumi FUJIWARA** *(Nagoya Univ.)* **and Yoshikazu TAKEDA** *(Nagoya Univ.)*

[*Appl. Surf. Sci.* **117/118**, 665 (1997)]

We have successfully obtained InAs islands on InP (001) by a novel droplet hetero-epitaxy using low-pressure organometallic vapor phase epitaxy. The island growth sequence was initiated by trimethylindium (TMIn) supply in H_2 atmosphere which was intended to form In droplets and followed by tertiarybutylarsine (TBAs) supply after the TMIn supply was stopped at a growth temperature. By this process, large islands of which height was above 100 nm with clear facets were observed under atomic force microscope. Using a modified sequence in which the TMIn supply was stopped and the substrate temperature was lowered before the TBAs supply, the appearance of the islands was drastically changed. In the specimen prepared by this sequence at the same substrate temperature, small islands of about 10 nm in height were observed together with the large islands. In order to form smaller islands and to suppress formation of the large islands, the substrate temperature dependence of the islands from 530 to 610 °C were investigated. The smallest islands with the height of 5 nm were obtained at the substrate temperature of 565 °C.

VI-R-2 InAs Dots Grown on InP (001) by Droplet Hetero-Epitaxy Using OMVPE

Youichi NONOGAKI, Tadashi IGUCHI *(Nagoya Univ.)*, **Shingo FUCHI** *(Nagoya Univ.)*, **Yasufumi FUJIWARA** *(Nagoya Univ.)* **and Yoshikazu TAKEDA** *(Nagoya Univ.)*

[*J. Mat. Sci. & Eng. B* submitted]

We have successfully obtained InAs dots on InP (001) by droplet hetero-epitaxy and observed room-temperature photoluminescence (PL) spectrum with a peak at around 1.6 μm. Dependencies of the surface morphology on the substrate temperature and on the TMIn-supply time were investigated. From atomic force microscope (AFM) images of the samples prepared by varying the TMIn-supply time a critical coverage for supplied In to form droplets was found to exist between 1.5 monolayer (ML) and 3 ML. This result was confirmed by low-temperature PL measurement. At the TMIn supply of 3 ML which was above the critical coverage, small dots of which height about 5 nm were formed at the density of 9.8×10^9 cm^{-2}. PL spectrum of the sample grown using the same sequence followed by growth of a 10 nm InP cap-layer exhibited 1.6 μm emission with full width at half maximum of 150 meV at room temperature.

RESEARCH ACTIVITIES VII
Coordination Chemistry Laboratories

Prof. Masa-aki Haga, Prof. Takeshi Sakurai and Dr. Hideaki Monjushiro continued their position of Synthetic Coordination Chemistry. Dr. Sadamu Takeda moved to Gunma University as an Assoc. Prof. and Dr. Hidemi Nagao joined to Synthetic Coordination Chemistry as the Assist. Prof. of Synthetic Coordination Chemistry. Assoc. Prof. Makoto Fujita joined to Functional Coordination Chemistry and Dr. Takahiro Kusukawa took the position of Assist. Prof. of the laboratory. Prof. Megumu Munakata (Kinki University) and Assoc. Prof. Naohide Matsumoto (Kyushu University) finished their term as Adjunct Prof. in March 1997 in the Laboratory of Coordination Bond. Their effort during their term is gratefully appreciated. Prof. Ginya Adachi (Osaka University and Assoc. Prof. Hiromi Tobita (Tohoku University) are newly appointed as Adjunct Prof. of Laboratory of Coordination Bond. Prof. Yuzou Yoshikawa (Okayama University) and Assoc. Prof. Hiroshi Nakazawa (Hiroshima University) continued their position as Adjunct Prof. of the laboratory of Complex Catalysis.

VII-A Surface Coordination Chemistry towards Molecular Protonic Devices

Supramolecular metal complexes as precursors for molecular devices have attracted much attention in recent years. A molecular switching by an external stimulus is one of fundamental functions in the supramolecular complexes. Protonation can act as an external trigger in complexes containing basic sites. We have developed the chemical principle underlying the proton-induced switching in 2-(2-pyridyl)benzimidazole Ru complexes. In order to achieve the proton-induced switching systems, the interlocking between the potential change by protonation/deprotonation and the pKa change by Ru(II) to Ru(III) oxidation is responsible. The judicious molecular design of the Ru complexes containing benzimidazole ligands allows us to synthesize the novel supramolecular metal complexes with bistable property not only in solution but also at the surface. Our synthetic strategy is the following: (1) The intrinsic properties of molecular inorganic complex are thoroughly examined from the viewpoint of photoactive, electroactive, or proton-responsive building blocks for molecular devices. (2) The molecular inorganic complex modules are organized or integrated for building up the molecular assemblies. Particularly, "complexes-as-ligands" method is useful to synthesize the supramolecular systems.

Our final goal of this "surface coordination chemistry" project is to construct the supra- or supermolecular assembly in the controlled manner through the coordination bond at the interface, and to find a molecular function as a molecular protonic devices.

VII-A-1 Synthesis of pH-Response Dinuclear Ru Complexes with an Internal Reference

Masa-aki HAGA, Hatsuko MAEKAWA and Md. Delower HOSSAIN

Reversible protonation of uncoordinated nitrogen site in 2-(2-pyridyl)benzimidazole Ru complexes induces the change of redox potential, while the complexes with 1-methyl-2-(2-pyridyl) benzimidazole does not show any pH responses. The incorporation of these two benzimidazole ligands makes it possible to synthesize novel Ru dinuclear complexes with a pH internal reference. This chemical principle has been applied to synthesize novel Ru dinuclear complexes with an internal standard. Two $Ru(bpy)_2$ dinuclear complexes with new novel bridging ligands in Scheme 1 were synthesized. The pKa value of dinuclear Ru complex, $[\{Ru(bpy)_2\}_2(L)]^{4+}$, is 5.43 for L = L1 and 5.91 for L2. The cyclic voltammogram of the complex $[\{Ru(bpy)_2\}_2(L1)]^{4+}$ in CH_3CN/buffer(1 : 1 v/v) at pH 2.2 shows two oxidation waves centered at +1.00 and +1.40 V vs Ag/AgCl, which are assigned to $Ru^{II/III}$ oxidation for benzimidazole side and (2-pyridyl)-pyrazine side, respectively. At pH 7.9, the separation of these two waves became larger, and they are shifted to +0.77 V and +1.39 V vs Ag/AgCl. The $E_{1/2}$-pH diagram revealed the pH dependence of oxidation potential only for the first oxidation process, but not for the second one. This result strongly suggests that these dinuclear Ru complexes are regarded as a pH probe with an internal reference at the molecular level.

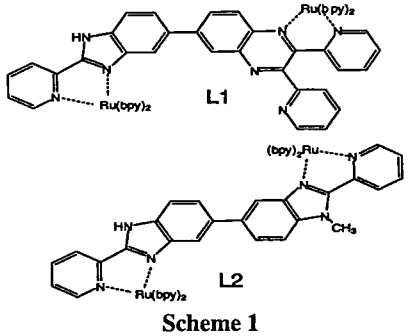

Scheme 1

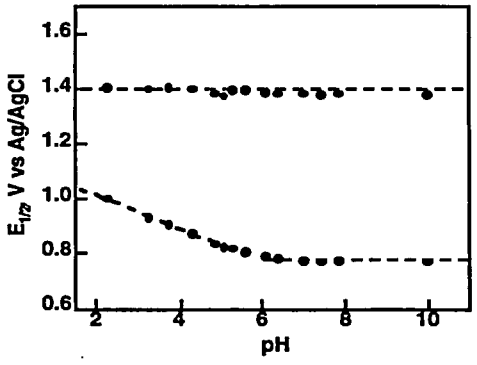

Figure 1. The $E_{1/2}$-pH diagram of $[\{Ru(bpy)_2\}_2(L_1)]^{4+}$ in CH_3CN/buffer

VII-A-2 pH-Sensitive Self-Assembled Monolayer Based on Ru Complexes Containing 2,6-Bis(N-(1-mercaptooctyl)-benzimidazolyl)-pyridine on the Au Surface: Synthesis and Proton-Coupled Redox Properties

Yasushi KAWATA, Hideaki MONJUSHIRO and Masa-aki HAGA

New anchoring ligand, 2,6-bis(N-(1-mercaptooctyl)-benzimidazolyl)-pyridine, and its Ru complex (**1**) in Scheme 1 were synthesized. A gold surface was modified with the Ru complex (**1**) by the self-assembling method. A symmetrical reversible redox peak due to immobilized Ru(II/III) couple was observed in Britton-Robinson buffer(pH 1.9). The oxidative peak potential of the Ru complex modified on Au is linearly dependent on the solution pH. Both XPS and FTIR measurements confirmed the chemical composition of SAM monolayer and orientation of the complex at the Au surface.

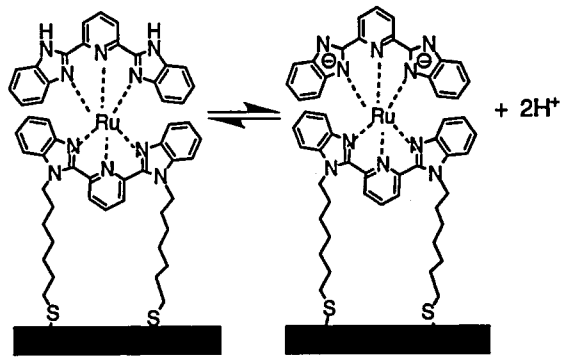

Scheme 1. Structure of Ru Complex (**1**)

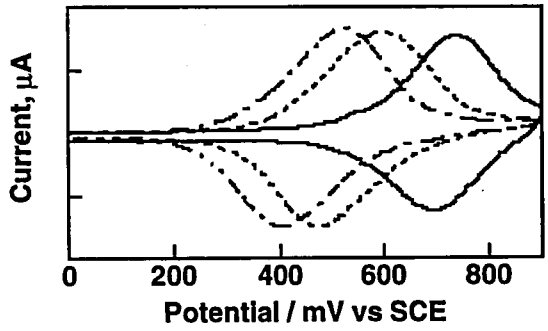

Figure 1. Cyclic voltammograms of the Ru complex modified on Au at various pH (From right to left, pH 2.80, 3.77, 4.51)

VII-B Synthesis and Characterization of Self-Assembled Organic Ligands and Metal Complexes on Surface Towards Solution-Phase Molecular Epitaxy

The assembling of polynuclear metal complexes at the interface is one of the potential synthetic routes to realize the solution-phase molecular epitaxy towards molecular electronic devices. In order to control the molecular ordering in two dimensions, the incorporation with coordination bond has advantage compared to the other molecular interactions such as hydrogen bonding and electrostatic interaction from the viewpoint of strength of interaction and molecular geometry around mental ion. However, the incorporation with coordination bond at the interface has not extensively studied so far. We intended to examine the applicability of "metal complex as a ligand" strategy at the interface by using the Ru complexes. This layered architecture of metal complexes provides the capability of studying the novel properties on nanometer scale. Thus, we examined two methodologies to build up the multilayer films on solid surface; one is the Langmuir-Blodgett(LB) techniques, and the other is self-assembled monolayer(SAM) method on gold or silicon wafer.

VII-B-1 Preparation of Surfactant Ruthenium Complexes Containing (Benzimidazolyl)-pyridine Derivatives With Long Alkyl Chains

Hideaki MONJUSHIRO, Kazumasa HARADA, Miho NAKAURA, Noriaki KATO, Masa-aki HAGA, Matthew RYAN *(York Univ.)* **and A. B. P. LEVER** *(York Univ.)*

[*Mol. Cryst. Liq. Cryst.* **294**, 15 (1997)]

In order to study the controlled ordering of the metal complex in two dimensions, we have synthesized new surfactant ruthenium complexes containing 6,6'-bis(N-octyl- or laurylbenzimidazolyl)-2,2'-bipyridine(L = L8 or L12) by the reaction of $[RuCl_2(\eta^6\text{-}\pi\text{-cymene})]_2$ with L in methanol and DMSO. The Ru complexes formed a stable monolayer film on the Langmuir trough air-water interface. The isotherm indicates the complex begins to pack into the expanded state at an area/molecule of approximately 110 Å/molecule. As compression continues, a plateau region occurs at 20.5 mNm^{-1}. The isotherm then becomes steeper with a limiting molecular area of about 52 Å/molecule and a collapse pressure of 42 mNm^{-1}. This behavior suggests that at low surface pressure the plane of the complex are lying flat on the surface with the alkyl chains protruding away from the surface. At higher pressure, the complex is packed and oriented almost perpendicular to the surface. In the LB monolayer films, the signals for cyano groups were split into two peaks with equal height at 397.0 and 397.9 eV, even the N1s peaks on tetradentate ligand remain identical, which is distinct from those for the powder sample. This spectral difference indicates that the complex is oriented almost perpendicular to the surface and two cyano groups possess

different chemical environments; i.e., one of axial cyano groups will be weakly interacted to the surface, probably to the hydroxy group on the glass surface through hydrogen bonding. This XPS results are consistent with the hypsochromic spectral shift on the UV spectra.

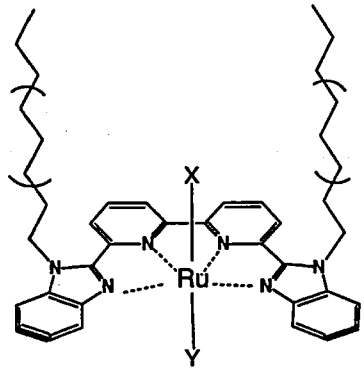

$[Ru(X)(Y)(L8 \text{ or } 12)]^{n+}$
n = 0; X = Y =Cl or CN
n = 0; X = Cl, Y = DMSO

Scheme 1. Structure of Ru complexes

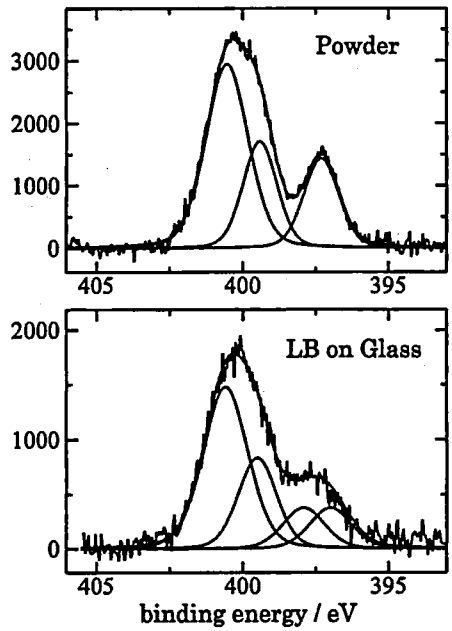

Figure 1. XPS N1s spectra of *trans*-$Ru(CN)_2(L12)$ for both the powders and LB films on glass plate.

VII-B-2 Ultraviolet Photoelectron Emission from Langmuir Monolayer of Ru Complex at the Air-Water Interface

Hideaki MONJUSHIRO, Kazumasa HARADA, Noriaki KATO and Masa-aki HAGA

Ultraviolet photoelectron yield (UPY) spectra of Langmuir layer of amphiphilic Ru complex, trans-$RuCN_2(C_{12}$-bpybim) (C_{12}-bpybim = 6,6'-bis(N-lauryl-benzimidazoil)-2,2'-bipyridine), at the air/water interface were measured in ambient conditions. It was observed that photoelectron emission threshold energy, *Et*, depends on the surface concentration of the complex. The *Et* value is constant at lower surface concentration but decreased abruptly at the concentration where surface pressure begins to rise. The change in *Et* of the complex on water surface is considered to be due to the two-dimensional aggregation of the complex. The difference in *Et* between in dilute surface concentration phase and in compressed monolayer phase could be understood by considering the polarization effect on the photo-ionization final state. It is concluded that UPYS is very sensitive technique and gives new information about the aggregation state of molecules on water surface in monolayer or submonolayer level.

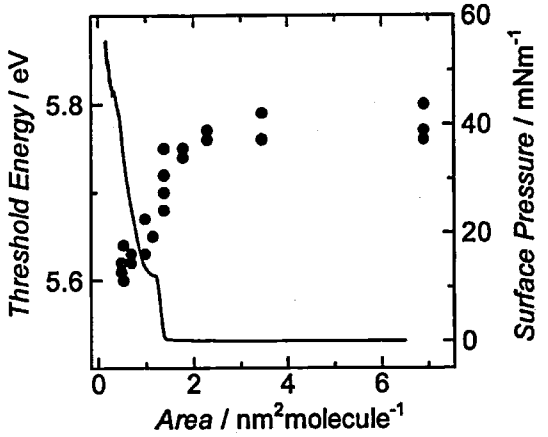

Figure 1. Dependence of photoelectron emission threshold energy, *Et*, on molecular area for $Ru(CN)_2(C_{12}$-bpybim) at air/water interface.

VII-B-3 Metal Coordination Incorporating with Amphiphilic Ru Complexes at the Air-Water Interface

Masa-aki HAGA, Noriaki KATO, Hideaki MONJUSHIRO and Kezhi WANG

The assembling of polynuclear metal complexes at the interface is one of the potential synthetic routes to realize the solution-phase molecular epitaxy towards molecular electronic devices. In order to control the molecular ordering in two dimensions, the incorporation with coordination bond has advantage compared to the other molecular interactions such as hydrogen bonding and electrostatic interactions from the viewpoint of strength of interaction and molecular geometry around mental ion. However, the incorporation with coordination bond at the interface has not extensively studied so far. In the present study, new amphiphilic ruthenium complexes containing 2,6-bis(N-octadecyl-benzimidazolyl)-pyridine (L) was synthesized, which leads to a stable Langmuir-Blodgett(LB) film formation and the incorporation of metal ion from subphase.

Figure 1 shows a π-A isotherm of $[Ru(L)(tppz)]^{2+}$ complex (tppz = tetra(2-pyridyl)pyrazine), spread on pure water and 10^{-4} M Cu^{2+} ion in water subphase. Considering the molecular size of $[Ru(L)(tppz)]^{2+}$ from molecular modeling, the complex is densely packed with the tppz group facing towards water subphase. The X-ray diffraction patterns of mononuclear Ru LB films(23 layers) transferred onto a hydrophilic glass plate at 20 mNm^{-1} revealed relatively sharp peaks at 2θ

=2.1°, 4.2°, and 6.2°, which indicates the existence of a organized Y-type multilayer structure. When the subphase contains Cu^{2+} ion, a large expansion of liquid phase was observed in the π-A isotherm for $[Ru(L)(tppz)]^{2+}$ complex. The electrostatic repulsion between Ru ions is responsible for this expansion. This result indicates that the incorporation of Cu^{2+} ion to the amphiphilic Ru complex occurred at the interface. Other metal dication such as Zn^{2+} and Cd^{2+} can also bind the amphiphilic $[Ru(L)(tppz)]^{2+}$ complex from the subphase. This film was transferred to the hydrophilic glass surface, which was examined by angular dependence of XPS method. The deeper location of Cu^{2+} ion compared to Ru ion was confirmed by the angular dependence on the ratio of $Ru3d_{5/2}$ vs Cu2p signal intensities. Therefore, the "metal complex as a ligand" strategy can be employed in the air-water interface by using the amphiphilic Ru complexes with coordination site.

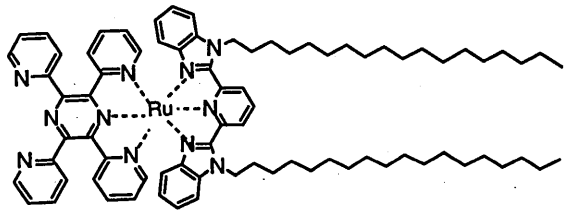

Scheme 1. Structure of amphiphilic Ru complex

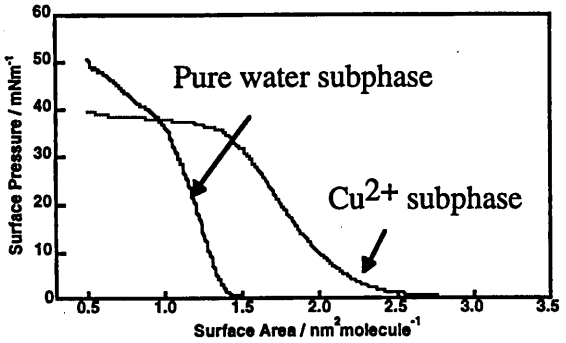

Figure 1. π–A isotherms of $[Ru(L)(tppz)]^{2+}$ complex on pure water subphase and Cu^{2+} subphase

VII-C Redox Chemistry of Inorganic Metal Complexes

The fundamental understanding and deeper knowledge of the redox processes in inorganic metal complexes are needed in order to build in the supramolecular inorganic complexes as components of molecular based devices. Molecular electrochemistry of inorganic and organometallic metal complexes in solution has been investigated in order to elucidate the redox chemistry of metal complexes and get relationships between structure and electrochemical behavior.

VII-C-1 Trinuclear Ruthenium Complex with Face Capping Benzene Ligand. Hapticity Change Induced by Two Electron Redox Reaction

Akiko INAGAKI *(Tokyo Inst. Tech)*, **Yoshiaki TAKAYA** *(Tokyo Inst. Tech)*, **Toshifumi TAKEMORI** *(Tokyo Inst. Tech)*, **Hiroharu SUZUKI** *(Tokyo Inst. Tech)*, **Masako TANAKA** *(Tokyo Inst. Tech)* **and Masa-aki HAGA**

[*J. Am. Chem. Soc.* **119**, 625 (1997)]

Transition metal complexes with facial arene ligands have been of great interest since these compounds may be reasonable models of arenes chemisorbed at a three-fold site on the surface of a close-packed metal lattice. We recently synthesized a novel facial benzene complex $\{(C_5Me_5)Ru\}_3(\mu\text{-}H)_3(\mu^3\text{-}\eta^2\text{:}\eta^2\text{:}\eta^2\text{-}C_6H_6)$ (**1**)by the reaction of $\{(C_5Me_5)Ru\}_3(\mu\text{-}H)_3(\mu^3\text{-}H)_2$ with 1,3-cyclohexadiene during studies of substrate activation on di- and trinuclear polyhydride complexes of ruthenium. The μ^3- η^2:η^2:η^2-coordination of the benzene ring was confirmed by X-ray diffraction. Average "coordinated" and "uncoordinated" C-C distances of C_6H_6 ligand are almost equal within the experimental error. In the cyclic voltammogram recorded in tetrahydrofuran, two reversible one-electron oxidation were observed at -490 and -224 mV vs Ag/AgCl. In view of the interest in the correlation between oxidation state and structure of the face-capping benzene complex, oxidation with 1 and 2 equiv of ferricinium salt gave monocation and dication, respectively, in which the structure of dication was determined by X-ray crystallography of a single crystal of $\{(C_5Me_5)Ru\}_3(\mu\text{-}H)_3(\mu^3\text{-}\eta^3\text{:}\eta^3\text{-}C_6H_6)(BPh_4)_2$(**2**)(Scheme 1). The most striking structural feature is the μ^3-η^3:η^3-coordination of the C_6 ring. An allyoiety is coordinated to one of three ruthenium centers, and another allyl moiety bridges two ruthenium centers. Therefore, complex **2** is the first example of the hapticity change in face-capping benzene ligand induced by a redox process. This dication **2** is reduced stepwise to form complex **1** quantitatively via the monocation by treatment with sodium naphthalide.

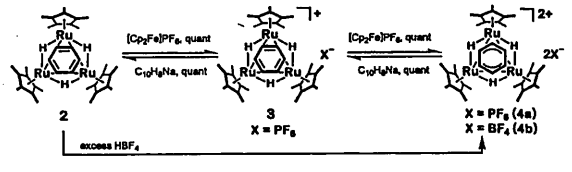

Scheme 1

VII-C-2 Synthesis and Crystal Structure of A Cationic Trinuclear Ruthenium(II) Complex $[Ru_3(\mu_2\text{-}Cl)_3(\mu_3\text{-}Cl)_2\{1,2\text{-bis(diphenylphosphino)-benzene}\}_3]PF_6$

Kazushi MASHIMA *(Osaka Univ.)*, **Naoki KOMURA** *(Osaka Univ.)*, **Tsuneaki YAMAGATA** *(Osaka Univ.)*, **Kazuhide TANI** *(Osaka Univ.)* **and Masa-aki HAGA**

[*Inorg. Chem.* **36**, 2908 (1997)]

Treatment of $[RuCl_2(\eta^6\text{-}C_6H_6)]_2$ with two equiv of 1,2-bis(diphenylphosphino)benzene (dpb) in methanol at room temperature afforded a cationic mononuclear complex $[RuCl(\eta^6\text{-}C_6H_6)(dpb)]Cl$ (**2**). When complex **2** in methanol was heated at 50 °C for 13 h, a cationic trinuclear complex $[Ru_3(\mu_2\text{-}Cl)_3(\mu_3\text{-}Cl)_2(dpb)_3]Cl$ (**3a**) was obtained in 75% yield with a liberation of the benzene ligand. The cationic trinuclear core was revealed by X-ray analysis of $[Ru_3(\mu_2\text{-}Cl)_3(\mu_3\text{-}Cl)_2(dpb)_3]PF_6$ (**3b**). The triangle of three ruthenium atoms were linked by three μ_2-bridging chloride atoms and two face-capped μ_3-chloride atoms. Each ruthenium was surrounded with four chloride atoms and two phosphorus atoms in cis positions and thus adopted pseudo octahedral geometry as expected for Ru(II) complexes. The interatomic Ru—Ru distances (3.219(3)—3.234(3) Å) of **3b** are out of the Ru—Ru single bond distance.

Cyclic voltammetry of **3b** in THF (0.1 M $TBABF_4$) showed the reversible one-electron oxidation process at + 0.75 V *vs* Fc^+/Fc. In addition, the irreversible reduction occurred at - 1.92 V. The oxidation potential of complex **3b** is almost comparable to face-sharing bioctahedral Ru complexes such as $[Ru_2Cl_3(PEt_2Ph)_6]^+$ (+0.78 and +1.33 V *vs* Fc^+/Fc). In the case of face-sharing bioctahedral Ru complexes, two oxidation processes were observed with the potential separation of ~ 0.5 V, indicating the strong interaction of Ru-Ru ions through strong delocalization of the charge. In the present trinuclear complex, attempts to measure the additional oxidation waves in more positive potential region were unsuccessful because of the experimental limit for available potential window. However, the substantial charge delocalization will be expected in **3b**. A wide gap between oxidation and reduction indicates the strong interaction between metal ions and the stabilization of oxidation state of all Ru(II) ions in complex **3b**, which is attributed to the coordination of the chelating triaryl phosphine ligand.

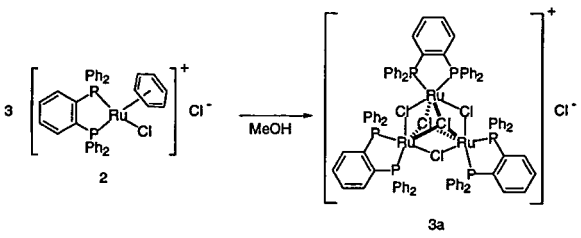

VII-C-3 1,8-Diphenyl-octa-1,3,5,7-tetraene Complexes of Ruthenium(II): Crystal Structures of [μ-(s-*cis*-1,2,3,4-η:s-*cis*-5,6,7,8-η-PhCH=CHCH=CHCH=CHCHPh)(RuClCp*)2] and [μ-(s-*trans*-1,2,3,4-η:s-*trans*-5,6,7,8-η-PhCH=CHCH=CHCH=CHCHPh)-{Ru(acac)$_2$}$_2$]

Kazushi MASHIMA *(Osaka Univ.)*, **Hiroki FUKUMOTO** *(Osaka Univ.)*, **Kazuhide TANI** *(Osaka Univ.)*, **Masa-aki HAGA and Akira NAKAMURA** *(Osaka Univ.)*

[*Organometallics* submitted]

Reaction of 1,8-diphenyl-1,3,5,7-octatetraene with $[Ru(\mu\text{-}Cl)Cp^*]_4$ (**1**) ($Cp^* = \eta^5$-pentamethylcyclopentadienyl) gave [μ -(s-*cis*-1,2,3,4-η:s-*cis*-5,6,7,8-η-PhCH=CHCH=CHCH=CHCHPh)$(RuClCp^*)_2$] (**2**), whose crystal structure revealed that **2** has a planar tetraene backbone coordinated by two Cp*RuCl moieties in s-cis-η^4-fashion; while the reaction with $Ru(acac)_3$/Zn system resulted in the formation of [μ-(s-*trans*-1,2,3,4-η:s-*trans*-5,6,7,8-η-PhCH=CHCH=CHCH=CHCHPh){$Ru(acac)_2$}$_2$] (3), where both of the two $Ru(acac)_2$ moieties prefer s-*trans* coordination and thus the plane of the octatetraene backbone of **3** is deformed into an S-shape. Electrochemical studies for complexes **2** and **3** revealed that complex 3 has a strong coupling between the two ruthenium centers and is a conjugatively interacted dπ-pπ organometallic system, whereas complex **2** has a longer π-conjugation of the tetraene backbone without electronic communication between the two RuClCp* moieties

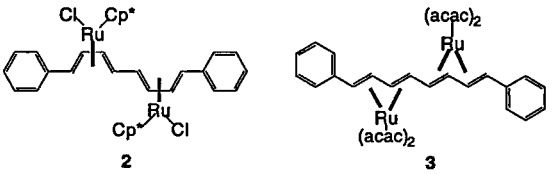

VII-C-4 Synthesis and Redox Properties of Ruthenium(II) Complexes with Tetradentate 6,6'-Bis(benzimidazolyl)-2,2'-bipyridine Ligand

Kazumasa HARADA, Hideaki MONJUSHIRO and Masa-aki HAGA

New ruthenium complex, *trans*-[RuCl(DMSO)(L)](BF_4) (L = 6,6'-bis(benzimidazolyl)-2,2'-bipyridine, DMSO = dimethyl sulfoxide) (**1**) was synthesized from the reaction of $[RuCl_2(\pi\text{-cymene})_2]_2$ with tetradentate ligand L in DMSO, which becomes a good starting compound for the preparation of *trans*-$[Ru(X)_2(L)]$ complex(L = 4-methylpyridine). The crystal structure of complex 1 were determined by X-ray analysis. Crystal data for complex **1**: monoclinic, space group *P21/c* with $Z = 4$ in a unit of dimension, a = 14.709(2) Å, b = 28.573(3) Å, c = 7.985(2) Å, and β = 96.42(2)°. The crystal structure of complex **1** displays an octahedral geometry around Ru ion with S-coordinated DMSO and chloride anion at the apical positions(Figure 1). Cyclic voltammogram shows the redox-induced linkage isomerization of Ru-DMSO bond: i.e., S- coordination for Ru(II) and O-coordination Ru(III) states, which was interconverted by the redox reaction on the time scale of cyclic voltammetry. The apical ligand substitution of *trans*-[RuCl(DMSO)(L)](BF_4) by 4-methylpyridine leads to complex, $[Ru(py)_2(L)]^{2+}$ (**2**). The complex **2** showed a reversible oxidation process and a reversible reduction at +0.70 and -1.56 V vs Fc+/Fc. The slow photosubstituiton of apical pyridine with chloride anion on complex **2** in acetonitrile was observed under the photoirradiation.

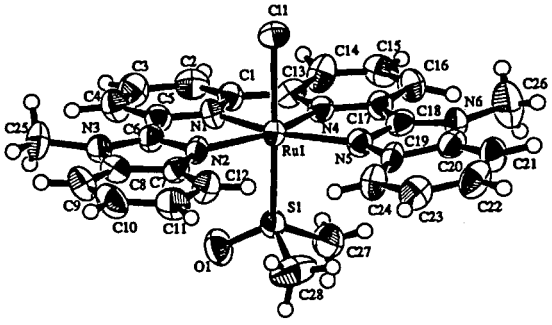

Figure 1. X-ray structure of *trans*-[RuCl(DMSO)(L)]Cl $\cdot 3H_2O$

VII-C-5 Synthesis and Photoinduced Electron Transfer Processes in Ru(II)(bpy)$_2$/Os(III)(bpy)$_2$-Based Triad Complexes Containing Functionalized Diimide Ligands

Md. D. HOSSAIN, Masa-aki HAGA, Hideaki MONJUSHIRO, B. GHOLAMKHASS *(Osaka Univ.)*, **Koichi NOZAKI** *(Osaka Univ.)* **and Takeshi OHNO** *(Osaka Univ.)*

[*Chem. Lett.* 573 (1997)]

The photoinduced electron transfer processes in novel Ru(II)(bpy)$_2$/Os(III)(bpy)$_2$-based triad complexes containing functionalized diimide ligands in Scheme 1 were investigated by the picosecond time-resolved absorption(TA) spectra. The picosecond time-resolved absorption(TA) spectra of homodinuclear Ru(II)-L1-Ru(II) complex **3** in CH_3CN observed at 15ps after excitation exhibits the bleaching of an MLCT band at 459 nm and the rise of absorption around 400 and 550 nm due to the anion radical of bpy ligand, indicating the formation of an MLCT triplet excited state of the Ru(II) moiety. In 200 ps, several absorption peaks appeared at 470, 610, 682, and 756 nm, which are characteristics of the L1 anion radical. These new TA peaks then disappeared with a single exponential decay (rate constant = 2.9×10^9 s^{-1}) through back electron transfer to reproduce the original form. The yield of formation of the CS state (Ru(III)-(L1$^-$)-Ru(II)) is calculated as 80-100% and the rate constants of the photoinduced electron transfer between the Ru(bpy)$_2$ and L1 for complex **3** are determined as $(1.1 \pm 0.1) \times 10^{10}$ s^{-1} and 2.9×10^9 s^{-1} from the excited state decay and the charge separation yield. The Ru(II)-L1-Os(III) mixed-valent complex **1** was selectively formed by one-electron oxidative electrolysis of Ru(II)-L1-Os(II) complex (3×10^{-4} mol dm^{-3}) at +0.5V in CH_3CN. The TA spectrum of complex **1** immediately after the excitation shows the formation of Ru(II)-MLCT excited state as shown in Figure 1. The fast electron transfer from L1$^-$ anion to Os(III) site gave a CS Ru(III)-L1-Os(II) state, which is the redox isomer state of the starting complex. The back electron transfer from L1$^-$ anion to Ru(III) site would reduce the production yield of the CS state that was estimated 75%. By considering the similarity of TA spectra for the early stage in both homodinuclear Ru complex **3** and mixed-valence complex 1, the electron transfer occurred from Ru(II) to L1 at first, followed by rapid electron transfer from L1 anion radical to Os(III). The rate of charge recombination(CR) from Os(II) to Ru(III) is calculated as 9.1×10^6 s^{-1} (τ =110 ns). This slow CR rate implies the diimide unit keeps the Ru(III) and Os(II) moieties apart from each other even though three donor or acceptor units are connected by a somewhat flexible propane linker. The direct photoinduced electron transfer process from Ru(II)-MLCT excited state to Os(III) is much slower compared to the stepwise electron transfer.

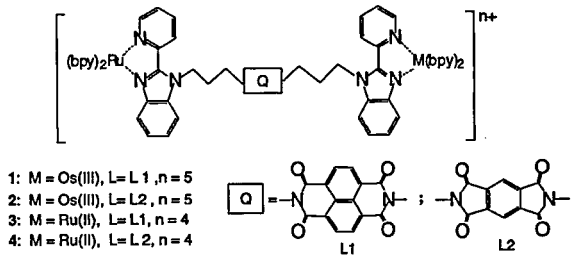

Scheme 1. Newly synthesized Ru(II)(bpy)$_2$/Os(III)(bpy)$_2$-based triad complexes containing functionalized diimide ligands

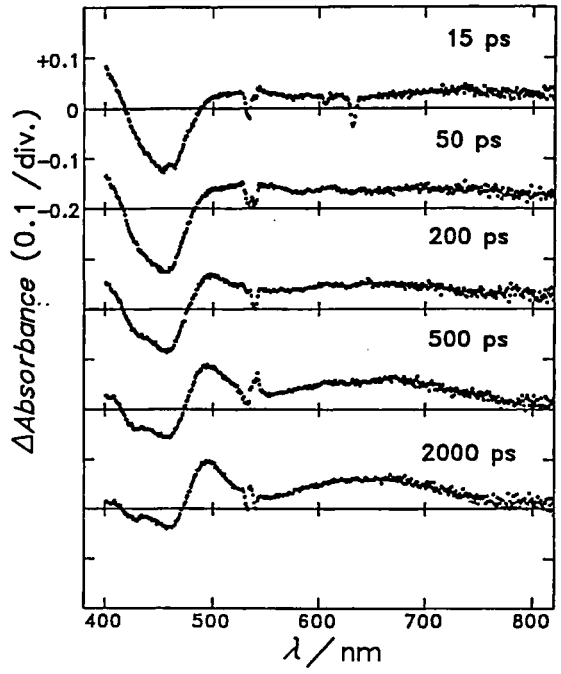

Figure 1. Picosecond time-resolved transient absorption spectra of complex **1**, [Ru(bpy)$_2$(L1)Os(bpy)$_2$](ClO$_4$)$_5$, in CH_3CN (3×10^{-4} mol dm^{-3}) at room temperature.

VII-C-6 Ruthenium(II) Complexes with Tetradentate 6,6'-Bis(oxazolinyl or benzimidazolyl)-2,2'-bipyridine Ligand: Synthesis, Electrochemical Properties, and Catalytic Reactivities

Kazuya MIZUSHIMA *(Mie Univ.)*, **Miho NAKAURA** *(Mie Univ.)*, **Soon-Bong PARK** *(Toyohashi Inst. Tech.)*, **Hisao NISHIYAMA** *(Toyohashi Inst. Tech.)*, **Hideaki MONJUSHIRO, Kazumasa HARADA and Masa-aki HAGA**

[*Inorg. Chim. Acta* **261**, 175 (1997)]

New ruthenium complexes, *trans*-[$RuX_2(L)$] (L = tetradentate 6,6'-bis(oxazolinyl or benzimidazolyl)-2,2'-bipyridine; X = halide or cyanide ion) have been synthesized. The present Ru complexes reveal a stable Ru(II/III) oxidation process and exhibit strong MLCT bands around 450 - 600 nm. The oxidation potential depends on the axial halogeno ligand; the potential increases in the order of X = Cl < Br < CN. The complexes possess the catalytic activity for oxidation of styrene and 1-phenylethanol. The bis(benzimidazolyl)-bipyridine complex has stronger oxidizing power compared to analogous bis(oxazolinyl)bipyridine complex.

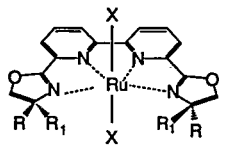

X = Cl, Br, CN

L

bpyox; R = R_1 = CH_3
bpymox; R=*iso*-Pr, R_1 =H

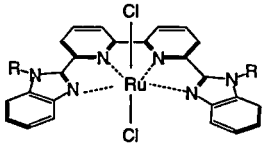

L

bbbpyH_2; R = H
dmbbbpy; R = CH_3

VII-C-7 Spectroelectrochemical Analysis of Intervalence Band in Mixed-Valence Di- and Tetranuclear Ru Complexes by Flow-Through Method

Masa-aki HAGA, Md. Meser ALI *(Mie Univ.)*, **Hiroyasu SATO** *(Mie Univ.)*, **Hideaki MONJUSHIRO, Koichi NOZAKI** *(Osaka Univ.)* **and Kenji KANO** *(Kyoto Univ.)*

[*Inorg. Chem.* submitted]

Novel dendritic tetranuclear Ru and Os-2,2'-bipyridine complexes bridged by 2,2'-bis(1-methyl-benzimidazo-2-yl)-4,4'-bipyridine (Scheme 1) showed four closely spaced one-electron oxidation processes; i.e., the central one-electron oxidation occurs first, followed by three peripheral metal oxidations at almost same potentials. During the progress of electrochemical oxidation, a characteristic near-infrared(NIR) band was observed, which can be assigned to intervalence charge transfer(IT) transition within the mixed-valence state. Since the potential separations among these three processes are generally small, the selective oxidation could not be achieved and even the one-electron oxidized species might be easily disproportionated into the original and two electron oxidized species. Therefore, the accurate determination of the absorption spectra for the mixed valence complexes should be determined by considering the comproportionation equilibria. In order to reconstruct the corrected absorption spectra of each mixed-valence complex, we have developed a new spectral analysis method based on the combination of digital simulation analysis of the reversible CV curves(Figure 1) and the electrochemical titration by flow-through cell(Figure 2), which gives the complete spectra of IT band for the partially oxidized species in the dendritic tetranuclear complexes. This method can be applicable not only for the dendritic Ru tetranuclear complexes but also dinuclear Ru complexes.

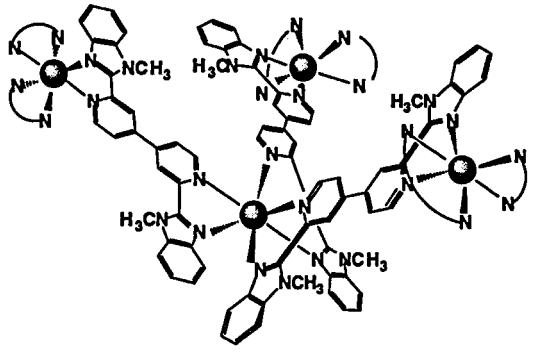

Scheme 1. Structure of dendritic tetranuclear Ru/Os-2,2'-bipyridine complexes

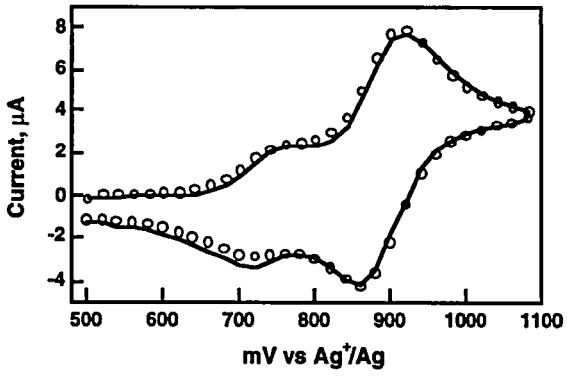

Figure 1. Cyclic voltammogram of [{$(bpy)_2$Ru(dmbbbpy)}$_3$-Ru]$^{8+}$ in CH_3CN at the platinum working electrode: Scan rate = 50 mV/s and its digital simulation result shown as a solid line.

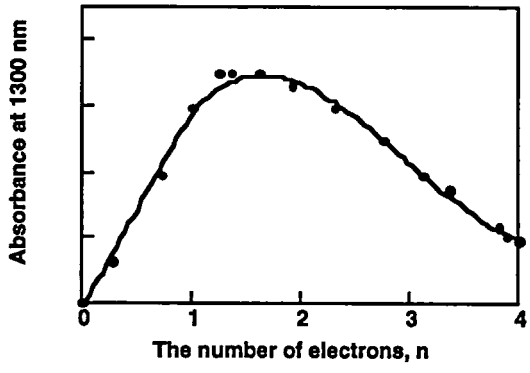

Figure 2. A plot of absorbance at 1300 nm vs the number of electrons, n,obtained from the current ratio for the complex, [{$(bpy)_2$Ru(dmbbbpy)}$_3$Ru]$^{8+}$ (2.3×10^{-4} M)

VII-D Metal Ions in Biological Systems

In order to reveal the biological roles of transition metal ions, structures and reactions of metalloproteins and metalloenzymes such as NO reductase, laccase, ascorabte oxidase, and several blue copper proteins have been studied by absorption, CD, MCD, and EPR spectroscopies and by magnetic susceptibility measurements. V-haloperoxidase has also been isolated and characterized.

VII-D-1 Reduction and Oxidation Processes of Blue Copper Proteins, Azurin, Pseudoazurin, Umecyanin, Stellacyanin, Plantacyanin, And Plastocyanin Approached by Cyclic and Potential Step Voltammetries

Takeshi SAKURAI, Fumitaka NOSE, Takayuki FUJIKI and Schinnichiro SUZUKI *(Osaka Univ.)*

[*Bull. Chem. Soc. Jpn.* **69**, 2855 (1996)]

Direct electrochemistry of a series of blue copper proteins: azurin, pseudoazurin, umecyanin, stellacyanin, plantacyanin, and plastocyanin has been performed at a gold electrode modified with di-4-pyridyl disulfide and/or at a bare glassy carbon electrode. Well-resolved cyclic voltammograms with peak separation, ΔE_p = 55 - 100 mV were obtained. Protein molecules associate with the electrode surface through both electrostatic and hydrophobic interactions, of which the predominant one differs according to the combination of protein and electrode. Double-step voltammetry showed that redox processes of blue copper proteins depend profoundly on the translocation of the molecules (diffusion and/or change of orientation) at the electrode surface. The heterogeneous rate constants at pH 6.0 and 25 °C for both reduction and oxidation processes were independently determined to be the order of 10^{-3} to 10^{-4} cms^{-1} by single-step voltammetry and were compared with those determined by cyclic voltammetry. Further, activation parameters for redox processes of some blue copper proteins have been determined from temperature dependence studies. The reaction pathway of blue copper proteins was discussed.

VII-D-2 Intracomplex Quenching by Copper(II) Ion of Exited Singlet and Triplet States of Zinc Myoglobin Modified with Diethylenetriaminepentaacetic Acid

Keiichi TSUKAHARA *(Nara Women's Univ.)*, **Chieko KIMURA** *(Nara Women's Univ.)* **and Takeshi SAKURAI**

[*Chem. Lett.* 601 (1996)]

Both excited singlet and triplet states of zinc myoglobin, whose lysine residue was modified with diethylenetriaminepentaacetic acid, were quenched by copper(II) ions bound at the modified site.

VII-D-3 Isolation and Characterization of Nitric Oxide Reductase from Paracoccus halodenitrificans

Nobuhiko SAKURAI and Takeshi SAKURAI

[*Biochemistry* **36**, in press]

Nitric oxide reductase was isolated from the membrane fraction of a denitrifying bacterium, Paracoccus halodenitrificans, in the presence of n-dodecyl-β-D-maltoside. A relatively simple and effective procedure to purify NO reductase using DEAE-Toyopearl and hydroxyapatite (ceramic) chromatographies has been developed. The enzyme consisted of two subunits with molecular masses of 20 and 42 kDa associated with the *c* type heme and two *b* type hemes, respectively. The optical and MCD spectra of the oxidized (as isolated) and reduced enzymes indicated that the heme *c* is in the low spin state and the hemes *b* are in the high and low spin states. The EPR spectrum also showed the presence of the split high spin component ($g_\perp$ = 6.6, 6.0) and two low spin components ($g_{z,y,x}$ = 2.96, 2.26, 1.46, g_z = 3.59). Although the presence of an extra iron was suggested from atomic absorption spectroscopy, a non-heme iron could not be detected by colorimetric titrations using ferene and nitro-PAPS. One of extra signals at g = 4.3 and 2.00 might come from a non-heme iron, while they may originate from an adventitious iron and a certain non-metallic radical, respectively. When CO acted on the reduced enzyme, both of the low spin hemes were not affected, and when NO acted on the reduced enzyme, the optical and MCD spectra were of a mixture of the oxidized and reduced enzymes. Consequently, the reduction of NO was supposed to take place at the high spin heme *b*. The heme *c* and the low spin heme *b* centers were considered to function as electron mediators during the intermolecular and intramolecular processes.

VII-D-4 Spectral Properties of Cytochrome c_{553} and a Membrane-Bound Cytochrome *b* from *Alcaligenes xylosoxidans* GIFU 1051

Nobuhiko SAKURAI, Hideyuki KUMITA *(Nagoya Inst. Tech.)*, **Takeshi SAKURAI and Hideki MASUDA** *(Nagoya Inst. Tech.)*

[*Bull. Chem. Soc. Jpn.* **70**, in press]

Cytochrome c_{553} and cytochrome *b* were isolated from soluble and membrane fractions of *Alcaligenes xylosoxidans* GIFU 1051, respectively, and their spectroscopic characterization has been performed. Cytochrome c_{553} has been shown to be in the low spin state both in the oxidized and reduced forms at room temperature by the absorption and magnetic circular dichroism (MCD) spectra, while the high spin heme has been also observed in the cryogenic electron paramagnetic resonance (EPR) spectra. Exogenous small ligands such as NO and CO bind to cytochrome c_{553} by expelling the axial His ligand. The membrane-bound cytochrome *b* has two heme *b* centers in a protein

molecule which are the active centers of NO reductase, the cytochrome *bc* complex, although the enzyme activity was considerably low. The absorption, MCD, and EPR spectra of the membrane-bound cytochrome *b* showed that two heme *b* centers are in the different electronic states, the high and low spin states. Cytochrome c_{553} is the natural electron donor to the membrane-bound NO reductase, although the interprotein electron-transfer could not been studied because of the low enzyme activity of the cytochrome *b* subunit.

VII-D-5 Observation of Cu-N_3^- Streching and N_3^- Asymmetric Stretching Bands for Mono-Azide Adduct of Rhus vernicifera Laccase

Shun HIROTA *(Nagoya Univ.)*, **Hiroki MATSUMOTO** *(Nagoya Univ.)*, **Hong-wei HUANG, Takeshi SAKURAI, Teizo KITAGAWA and Osamu YAMAUCHI** *(Nagoya Univ.)*

Mono-azide adduct of Rhus vernicifera laccase was investigated with resonance Raman and FT-IR spectroscopies as a step forward elucidation of the structure and function of the trinuclear center. The Cu-N_3^- stretching RR band was observed for azide-bound multicopper oxidases for the first time. The Cu-N_3^- band was located at 400 cm^{-1} for mono-$^{14}N_3^-$ laccase, which shifted to 396 cm^{-1} with the $^{15}N^{14}N^{14}N^-$ analog. The Cu-N_3^- asymmetric stretching band was observed by FT-IR spectroscopy at 2035 cm^{-1} for $^{14}N_3^-$ laccase and at 2025 cm^{-1} with the $^{15}N^{14}N^{14}N^-$ analog. These spectra were comparable with those for hemocyanin with a stronger π bank donation from the copper to the bound N_3^- molecule.

VII-D-6 Magnetic Studies of the Trinuclear Center in Laccase and Ascorbate Oxidase Approached by EPR Spectroscopy and Magnetic Susceptibility Measurements

Hong-wei, HUANG, Takeshi SAKURAI, Hideaki MONJUSHIRO and Sadamu TAKEDA

The trinuclear centers in laccase and ascorbate oxidase have been studied by EPR spectroscopy and magnetic susceptibility measurements over the wide range of temperature, 5 K to 300 K. The EPR spectra showed that type 2 Cu receives increasing tetrahedral distortion with raising temperature. Magnetic susceptibilities of laccase showed that both of type 1 and type 2 Cu's are almost fully paramagnetic since the antiferromagnetic interaction between type 3 Cu's is extremely strong from 5 K to 300 K. On the other hand, the effective magnetic moment of ascorbate oxidase is contributed by ca. 1.7 Cu^{2+} even below ca. 100 K, since type 2 Cu is partly in the reduced form. The effective magnetic moment continuously increased with raising temperature because the antiferromagnetic interaction between type 3 Cu's is not as strong as in the case of laccase. The type 2 Cu EPR signals in laccase and ascorbate oxidase were conspicuously broadened with raising temperature because of the increasing contribution of the triplet state by type 3 Cu's and/or of the rapid relaxation which finally led to only ca. 30 % detection of the type 2 Cu signal at room temperature. The stepwise binding of azide to one of type 3 Cu's made the type 3 Cu to be EPR detectable. According to the SQUID measurements type 2 Cu and one of type 3 Cu's antiferromagnetically coupled through a bridging group, possibly not an azide ion but a hydroxide ion. All these findings indicate that the steric structure and magnetic property of the trinucelar center change depending on temperature and the magnetic data at room temperature reflect the inherent property of the trinuclear center composed of type 2 and type 3 Cu's in multicopper oxidases.

VII-D-7 Isolation and Characterization of Vanadium Bromoperoxidase from a Marine Macroalga, *Ecklonia stolonifera*

Isao HARA and Takeshi SAKURAI

The bromperoxidase has been isolated from the brown seaweed *Ecklonia stolonifera* (83 kDa) and has been characterized. Bromoperoxidase requires vanadium for enzyme activity as has been evidenced by EPR spectroscopy. On addition of V^{5+} to the isolated enzyme, the enzyme activity was increased ca. 250%, indicating that more than 2/3 of the protein molecules were in the apo form. The increases in the enzyme activity was specific to V^{5+}, while Fe^{2+}, Fe^{3+}, and Cu^{2+} inhibited the enzyme activity. This V^{5+} addition effect was inhibited in the phosphate buffer, probably because phosphate and vanadate compete for the active site. The present bromoperoxidase exhibited a high thermostability (Tm = 68 °C) and a high stability in organic solvents (completely intact even in the presence of 50 % of methanol, ethanol and 1-propanol).

VII-D-8 Damping Wave Packet Approach: a Calculation Method of Nonpertubative Nonlinear Optical Susceptibilities Including Effects of nNuclear Motion at Finite Temperatures

Masayoshi NAKANO* *(*Osaka Univ.)*, **Yoichi MATSUZAKI** *(Nippon Steel Corp.)*, **Hidemi NAGAO, Satoru YAMADA*, Isamu SHIGEMOTO* and Kizashi YAMAGUCHI***

[*Chem. Phys. Lett.* **258**, 307 (1996)]

A method is developed for a nonperturbative calculation of nonlinear optical susceptibilities for specific systems such as low-density gases or single molecule systems, including effects of nuclear motion, Nuclear motion is treated quantum-mechanically by wave packet dynamics with population damping effects. As an example, the effects of temperature and mass on the third-order susceptibilities for a three-atom cation model system are examined.

VII-D-9 Calculation of Magnetization by Path Integral Method I

Hidemi NAGAO, Hiroyuki KAWABE *(Kinjo College)*, **Takashi KAWAKAMI*** *(*Osaka Univ.)*, **Mitutaka OKUMURA** *(Osaka Natl. Res. Inst.)*,

Wasuke MORI *(Kanagawa Univ.)*, **Kiyoshi NISHIKAWA** *(Kanazawa Univ.)* **and Kizashi YAMAGUCHI***

[*Mol. Cry. Liq. Cry.* **286**, 171 (1996)]

The path integral method is formulated by means of the extended Thouless parametrization. The ab initio Hamiltonian and the Zeeman Hamiltonian are used in our model systems. Numerical calculation of physical properties of molecules is performed in terms of the Monte Carlo method. The dependence of the magnetization of a hydrogen molecule on the division for the partition function, the temperature and the external magnetic field is discussed.

VII-D-10 Calculation of Magnetization by Path Integral Method II

Takashi KAWAKAMI* *(*Osaka Univ.)*, **Hidemi NAGAO, Kenji UEDA*, Wasuke MORI** *(Kanagawa Univ.)* **and Kizashi YAMAGUCHI***

[*Mol. Cry. Liq. Cry.* **286**, 177 (1996)]

Theoretical treatment based on the path integral method were presented and applied to calculations for the magnetization. Numerical calculation is performed by the Monte Carlo method. In this paper, this method is applied to the simple system, which is methyl and hydrogen redical pair as a extended model from the hydrogen molecule system in the series paper entitled "part I" by Nagao et al. Detailed studies about division number, Monte Carlo active space, magnetic field, temperature and distance dependences were performed in order to clarified the scope and limitation.

VII-D-11 Path Integral Formation for Many-Electron System

Hiroyuki KAWABE *(Kinjo College)*, **Hidemi NAGAO and Kiyoshi NISHIKAWA** *(Kanazawa Univ.)*

[*Intern. J. Quantum Chem.* **59**, 457 (1996)]

The Feynman path integral method is applied to the many electron problem of quantum chemistry. We begin with constructing new closure relations in terms of the LCAO coefficients, and investigate the transition amplitude and the partition function of the system in question, then "a classical path of electron" which is described by the time dependent Hartree-Fock-Roothaan equation is obtained by minimizing the action integral of the system with respect to "the electron coordinate." The next order approximation is obtained by evaluating the deviation from the classical path, which is approximately written by a Gaussian integral. The result is expected to be the random phase approximation.

VII-D-12 Many-Electron-Wavepackets Method

Hidemi NAGAO, Masayoshi NAKANO* *(*Osaka Univ.)*, **Syuusuke YAMANAKA*, Yasuteru SHIGETA** *(Kanazawa Univ.)*, **Satoru YAMADA*, Daisuke YAMAKI*, Isamu SHIGEMOTO*, Shinji KIRIBAYASHI* and Kizashi YAMAGUCHI***

[*Int. J. Quantum Chem.* **60**, 1291 (1997)]

A computational scheme to study the dynamics of many-electrons in molecular systems by wavepackets method is presented. Several approaches to calculation of nonlinear optical properties for molecules under time-independent or time-dependent external electronic fields are presented. Some simple examples of one-dimensional two- or three-electron systems are demonstrated concretely. Implications of these results are discussed in relation to the validity of the many electron wavepackets (MEWP) method.

VII-D-13 Nonadiabatic Treatment of Molecular System by the Wavepackets Method

Hidemi NAGAO, Hiroyuki KAWABE *(Kinjo College)*, **Koichi KODAMA*** *(*Kanazawa Univ.)*, **Yasuteru SHIGETA*, Kiyoshi NISHIKAWA*, Masayoshi NAKANO**** *(**Osaka Univ.)* **and Kizashi YAMAGUCHI****

[*Int. J. Quantum Chemistry* **60**, 1261 (1997)]

We have already developed the many-electron wavepackets (MEWP) method in order to study the dynamics and electronic structure of molecular systems. We extended the MEWP method to study the nonadiabatic effects and formulated a nonadiabatic molecular theory, where both electron and nucleus are treated equivalently. Then we applied our method to the isotope series of hydrogen molecule i.e.,H_2,HD and D_2, and calculated the total energy and the average distance between nucleus-nucleus, electron-electron, and electron-nucleus in order to analyze numerically the nonadiabatic effect in the molecule. Finally, we calculated the real-time evolution of the polarization by means of Chebyshev scheme, and by Fourier transforming this, we found out the excitation spectrum of the system, which corresponds to the electronic excitation and the nuclear vibrational frequency.

VII-D-14 Path Integral Monte Carlo Method for ab Initio cCalculation

Hiroyuki KAWABE *(Kinjo College)*, **Hidemi NAGAO and Kiyoshi NISHIKAWA** *(Kanazawa Univ.)*

[*Int. J. Quantum Chem.* **60**, 1223 (1997)]

The Feynman path integral method is applied to the many electron problem. We first give new closure relations in terms of ordinary complex and real numbers, which could be derived from an arbitrary complete set of state vectors. Then, in the path integral form, the partition function of the system and the ensemble average of energy are explicitly expressed in terms of these closure relations. It is impossible to evaluate the path integral by direct numerical integrations because of its huge amount of integration vari-

ables. Therefore, we develop an algorithm by the Monte Carlo method with constraints corresponding to the normalization condition od states to calculate the required integral. Finally, the ensemble average of energy for the hydrogen molecule is explicitly evaluated by the quantum Monte Carlo method and results are compared with the result obtained from the ordinary full CI method.

VII-D-15 Many-Electron Hyperpolarizability Density Analysis: Application to Dissociation Process of One-Dimensional H_2

Masayoahi NAKANO* *(*Osaka Univ.)*, **Hidemi NAGAO and Kizashi YAMAGUCHI***

[*Phys. Rev. A* **55**, 1503 (1997)]

A method for density analysis of static polarizabilities (α) and second hyperpolarizabilities (γ) on the basis of the finite-field (FF) many-electron wavepackets (MEWP) method is developed and applied to evaluation of the longitudinal α and γ in the dissociation process for a one-dimensional H_2 model.Remarkable increases in α and γ are observed in the intermediate dissociation region. The internuclea distance where the γ is maximized is also found to be larger than that where the α is maximized. In order to elucidate the characteristics of α and γ in the dissociation process, we extract their classical pictures describing displacements of two-electron configurations by using (hyper)polarizability densities on the two-electron coordinate plane. It is suggested from these classical pictures that the polarization in the ionic structure contributes primarily to the enhancement of (hyper)polarizability in the intermediate dissociation region, while the polarization in the diradical structure causes the decrease of the (hyper)polarizability at a large internuclear distance. This implies that the experimental search for species with chemical bonds in the intermediate correlation regime is important and interesting in relation to the molecular design of nonlinear optical materials.

VII-D-16 Theoretical Study on the Second Hyperpolarizability of H_3^+ System by Path Integral Method

Hidemi NAGAO, Masayoahi NAKANO* *(*Osaka Univ.)*, **Satoru YAMADA*, Koji OHTA** *(Osaka Natl. Res. Inst.)* **and Kizashi YAMAGUCHI***

[*Synthetic Metals* **85**, 1159 (1997)]

Based on the path integral method formulated in terms of the Thouless parametrization, numerical calculations of the ensemble average of the polarizability and the second polarizability are carried out by means of the Monte Carlo method. An H_3^+ system is examined to elucidate the performance of the present method. We discuss the dependence of the calculated (hyper)polarizabilities on the number of the division of the partition function and the accuracy of the results obtained by the present method.

VII-D-17 Theoretical studies for second hyperpolarizabilities of alternant and condensed-Ring cconjugated systems II

Shinji KIRIBAYASHI* *(*Osaka Univ.)*, **Masayoshi NAKANO*, Satoru YAMADA*, Isamu SHIGEMOTO*, Hidemi NAGAO and Kizashi YAMAGUCHI***

[*Synthetic Metals* **85**, 1163 (1997)]

Alternant and condensed-ring conjugated systems are expected to have large electron correlation and structure dependencies of the second hyperpolarizabilities (γ). For example, cation radical triafulvalene exhibits a large negative γ at the Hartree-Fock (HF) level contrary to a large positive one at the Moller-Plesset second-order (MP2) level. In this paper, we investigate γ's for different charged states (neutral, ion radical and di-ion states) of pentalene and triafulvalene to reveal their electron correlation dependencies up to the Moller-plesset fourth order.

VII-D-18 Calculation of Magnetization by Path Integral Method

Takashi KAWAKAMI* *(*Osaka Univ.)*, **Hidemi NAGAO, Wasuke MORI** *(Kanagawa Univ.)* **and Kizashi YAMAGUCHI***

[*Synthetic Metals* **85**, 1753 (1997)]

Theroretical studies of magnetic properties have been carried out and we have progressed the numerical treatment of those by the path integral method. In this method, the numerical partition function can be calculated directly and is applied to numerical studies of the magnetization including temperature effect. The path integral method is formulated by means of the Thouless parametrization and progressed with the Monte Carlo method. We present the numerical calculations for a simple molecular system, i.e. the Cu^{2+}-H(d9-s) system, which is related to the Ti^{3+}-H(d1-s) system as discussed previously and considered as a hole doped system. Finally, it is found that our method can lead its magnetic behaviors successfully.

VII-D-19 Path Integral Method by Means of Generalized Coherent States and its Numerical Approach to Molecular Systems. I. Ensemble aAverage of Total Energy

Hidemi NAGAO, Yasuteru SHIGETA* *(*Osaka Univ.)*, **Hiroyuki KAWABE** *(Kinjo College)*, **Takashi KAWAKAMI*, Kiyoshi NISHIKAWA** *(Kanazawa Univ.)* **and Kizashi YAMAGUCHI***

[*J. Chem. Phys.* in press]

A path integral formulation by the generalized coherent states of the Thouless parameterization is presented to apply to molecular systems. Explicit expressions of the ensemble average of the physical property including the spin space is also derived. In order to

compute the ensemble average, a novel calculating scheme is shown. The Monte Carlo method by the metropolis algorithm is used, and in order to avoid the negative sign problem, a reweighting method is attempted. Simple examples are examined to demonstrate performances of calculations. We discussed in relation to the total energy and the number of the division for the partition function or the temperature.

VII-D-20 Theoretical Study of Second Hyperpolarizability by Path Integral Method: Effects of External Magnetic Field

Hidemi NAGAO, Masayoshi NAKANO* *(*Osaka Univ.)*, **Koji OHTA** *(Osaka Natl. Res. Inst.)* **and Kizashi YAMAGUCHI***

[*Int. J. Quantum Chem.* in press]

Explicit expressions of polarizability and hyperpolarizability are formulated by a path integral method in terms of the generalized coherent states of the Thouless parametrization. A novel scheme is shown for calculating the molecular properties including total energy, and the Monte Carlo method using the metropolis algorithm is utilized for performing the actual calculations. As a simple example, the hydrogen molecule is examined to demonstrate performances of the present scheme. We discuss improvement of accuracy of the (hyper)polarizabilities depending on the number of the division for the partition function and also behaviours of the (hyper)polarizability for the external magnetic field. We compare the present results with those obtained by the conventional molecular orbital theory.

VII-D-21 Possibilities of Charge- and/or Spin-Mediated Uperconductors and Photo Induced Superconductor in the Intermidiated Region of Metal-Insulator Transitions

Hidemi NAGAO, Masamichi NISHINO* *(*Osaka Univ.)*, **Masaki MITANI*, Yasuhiro YOSHIOKA* and Kizashi YAMAGUCHI***

[*Int. J. Quantum Chem.* in press]

Magnetism, conductivity and superconductivity of molecular materials are discussed on the basis of extended Hubbard-Peierls Hamiltonians, which involve four parameters; transfer integral (T), electron-lattice interaction (W), on-site and inter-site Coulomb interactions (U, V). The four component spinor is introduced to define order parameters which characterize four different electronic states (charge density wave, spin density wave, singlet and triplet superconductivities) in a unified fashion. Several intermediate regions in these parameters are interesting and important from current theoretical reasons. Many experimental results clearly show importance of intermediate correlation regimes for active controls of these states by chemical modifications and by external fields such as high pressure. Several model Hamiltonians such as CT and t-J models are derived for elucidation of potential electronic properties of molecule-based materials. Recent computational results based on the t-J model are utilized to rationalize our J-model for spin-mediated superconductivity. Possibilities of magnetic conductors, charge- and/or spin-mediated superconductors, and photo-induced superconductor instead of charge-mediated Little model are examined in the intermediate region of several metal-insulator transitions. Possible candidates are also proposed on the basis of various circumstantial experimental results. Implications of the calculated results are finally discussed in relation to recent development of the intersection area between conducting, magnetic and optical molecular materials.

VII-D-22 Finite Temperature ab Initio Calculation by Path Integral Monte Carlo Method

Hiroyuki KAWABE *(Kinjo College)*, **Koichi KODAMA*** *(*Kanazawa Univ.)*, **Hidemi NAGAO and Kiyoshi NISHIKAWA***

[*Int. J. Quantum Chem.* in press]

We develop the path intergal method for quantum chemistry, apply the Monte Carlo method to an evaluation of the path integral, and calculate the ensemble average of the energy. For finite temperature, a simple Monte Carlo eavluation of the path integral brings out the negative sign problem. In this work, to avoid practically this problem on the numerical evaluation, we apply the new reweighting method to the Monte Carlo integration, and calculate effectively the ensemble average of the energy for finite temperature.

VII-D-23 A Theory of High Tc Superconductors via Electron Correlation: I. Superconductive Phase and Spin Gap

Hidemi NAGAO, Hiroyuki KAWABE *(Kinjo College)* **and Kizashi YAMAGUCHI** *(Osaka Univ.)*

[*Phys. Rev. B* submitted]

A theory of high Tc superconductivity via electron-electron interaction is presented in relation to that of cupric superconductors. The theory is constructed by a model hamiltonian for metallic states generated by hole doping into an antiferromagnetic insulator with a square plane lattice. A field theoretical description of quasi-particles by the Bogoliubov transformation is introduced to construct several electronic states such as antiferromagnetic, valence bond and superconductive states. The Hartree-Fock hamiltonian for the lattice is explicitly given under the constraint of no on-site double occupancy. Anormalous and normal Green's functions for the uniform medium with respect to the hole are derived by using a mean-field hamiltonian. Analytical expression of the critical temperature for the superconductive phase, together with that of spin gap, is also derived explicitly. A phase diagram for the superconductivity and the spin gap is depicted against the hole concentration in the lattice, showing the close relationship between the superconductivity and spin gap. Implications of the results obtained from the present model are discussed in relation to several experimantal

results for cupric superconductors, and also other theoretical results obtained by the Hubbard and t-J models.

VII-D-24 A Theory of Symmetry and Model Hamiltonian for High Tc Superconductors

Hidemi NAGAO, Hiroyuki KAWABE *(Kinjo College)*, **Kiyoshi NISHIKAWA** *(Kanazawa Univ.)* **and Kizashi YAMAGUCHI** *(Osaka Univ.)*

[*Phys. Rev. Lett.* submitted]

A theory of the symmetry and a model hamiltonian for the high temperature superconductivity is presented. We discuss that the symmetry is broken for the spin rotation in the antiferromagnetic or the hole-doped state. A Nambu-Goldstone (NG) boson in these states is derived. A picture, which is that the symmetry in the hole-doped state is restored by the NG boson, is presented. In the case, a model hamiltonian for the hole-doped state in copper oxides is also presented, and a reduced hamiltonian for many-electron system is derived. It is shown that the electronic interaction becomes attractive by dopin holes in the reduced hamiltonian.

VII-D-25 Non-Adiabatic Molecular Theory and It's Application

Yasuteru SHIGETA* *(*Kanazawa Univ.)*, **Koichi KODAMA*, Hidemi NAGAO, Hiroyuki KAWABE** *(Kinjo College)* **and Kiyoshi NISHIKAWA***

[*Chem. Phys. Lett.* submitted]

We have developed a new molecular theory which is beyond the Born-Oppenheimer approximation (BOA). The ordinary moldecular theory is based upon the BOA, where electrons and nuclei are not treated equivalently. In order to treat both particles equivalently, we first develop the coupled mean field theory (CMFT). Next, we introduce the generator coordinate method based upon the CMFT to take into account the dynamical correlation between electrons and nuclei, because the CMFT can not treat the correlation. We yield the collective energy and the eigenstate of a molecular system directly, and could project out the vibrational frequency from the resultant eigenvalues. We apply this method to the isotope series of the hydrogen molecule (H_2, HD and D_2), and analyze the isotope and non-adiabatic effects on the energy, expectation values of inter-particle distance and vibrational frequency in detail.

VII-D-26 Non-Adiabatic Molecular Theory and It's Application. II Water Molecule

Yasuteru SHIGETA* *(*Kanazawa Univ.)*, **Koichi KODAMA*, Hiroyuki KAWABE** *(Kinjo College)*, **Hidemi NAGAO and Kiyoshi NISHIKAWA***

[*Int. J. Quantum Chem.* submitted]

We introduce a new molecular theory beyond the Born-Oppenheimer approximation which treats both electrons and nuclei quantum-mechanically and equivalently. First, we develop the coupled mean field theory (CMFT) for both the electronic and nuclear field. Then in order to take account the dynamical correlation between these particles, we develop the new molecular theory applying the generator coordinate method based upon the CMFT. In this method, we calculate directly the molecular eigenstate of a water molecule. We analyze especially the vibrational motion of the water molecule and the isotope effect on the electronic state.

VII-E Metal Assisted Control and Functionalization of Biomolecules

In the control of gene regulation, DNA functions are carried out through interactions with other molecules such as gene regulatory proteins and smaller molecules associated by characteristic conformational changes (curvature, unwinding, melting, etc.). Therefore, molecules that induce structural changes of specific sites of DNA would effect gene expression and could possibly be applicable in the treatment of genetic disorders. The research in our group focuses on the supramolecular chemistry of nucleic acids, peptides, and synthetic metal complexes. Central to this work is the design and synthesis of new metal complexes which can recognize and/or convert the structures of specific sites of DNA. Another goal of our research is to design and synthesize artificial DNA or peptides with tailored functions through the understanding of molecular basis of noncovalent complexes formed cooperatively between biomolecules.

VII-E-1 Macrocyclic Zinc(II) Complexes for Selective Recognition of Nucleic Acid Bases in Single- and Double-Stranded Polynucleotides

Eiichi KIMURA*, Takuya IKEDA*, Mariko MURATA* and Mitsuhiko SHIONOYA *(*Hiroshima Univ.)*

[*Chem. Eur. J.* in press]

Zn-cyclen complex **1**, and Zn-acridine pendant cyclen **2** selectively bind to thymine and uracil nucleosides in aqueous solution at physiological pH. Interactions of these complexes, bis(Zn-cyclen) **3**, and Zn-naphthalene pendant cyclen **4** with a series of polynucleotides have been investigated. These complexes disrupt the A-U (or T) H-bonding to unzip the duplex of poly(A)·poly(U), as demonstrated by lowering melting temperatures of poly(A)·poly(U) and poly(dA)·poly(dT) with an increase in their concentrations. The order of the denaturing efficiency is well correlated with the order of the 1:1 affinity constants for each complex with uracil / thymine; **3 > 2 > 4 > 1**. The comparison of CD spectra of poly(A)·poly(U),

poly(A), and poly(U) in the presence of **3** revealed a structural change from poly(A)·poly(U) to single-stranded poly(A) and poly(U). This can be explained by the exclusive binding of **3** to uracils in poly(U). These Zn complexes, on the other hand, stabilized poly(dG)·poly(dC).

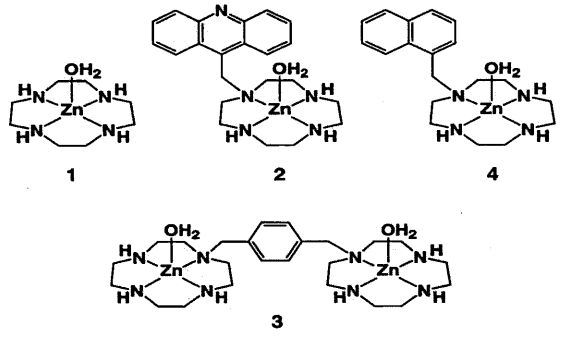

VII-E-2 Denaturation of Double-Stranded Oligonucleotides Containing an AT-Rich TATA-Box Sequence by a Macrocyclic Zinc(II) Complex

Akio OJIDA, Michito SHIOTSUKA, Kentaro TANAKA, Motoyuki TASAKA*, Luigi G. MARZILLI, Patricia A. MARZILLI**, Eiichi KIMURA*** and Mitsuhiko SHIONOYA** *(*Graduate Univ. for Advanced Studies, **Emory Univ. and IMS, ***Hiroshima Univ.)*

AT-rich sequences in transcriptional regulatory domains of DNA are well known to play key roles in the initiation of transcription. Molecules that bind specifically to the AT-clusters with distortion and/or bending of DNA would effect gene expression and could possibly be applicable in the treatment of genetic disorders. We previously demonstrated that a macrocyclic Zn complex, Zn-cyclen, binds reversibly and preferentially to thymine or uracil and inhibits poly(A)·poly(U) hybridization in aqueous solution at physiological pH. In this paper, we describe the interactions between this complex and oligomeric DNA duplexes including an adenovirus TATA-box or other AT-rich sequences. Thermal denaturation experiments (Figure 1) and imino-proton NMR studies (Figure 2) have clearly disclosed that only Zn-cyclen complex induced a stepwise melting of the duplex oligonucleotides while hydrated zinc ion and other metal complexes stabilized their duplex structures.

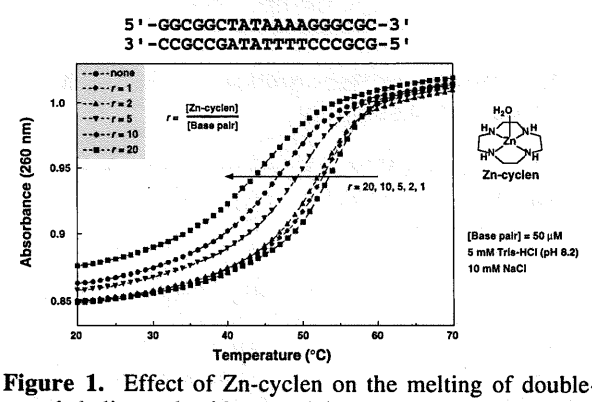

Figure 1. Effect of Zn-cyclen on the melting of double-stranded oligonucleotides containing a TATA-box sequense.

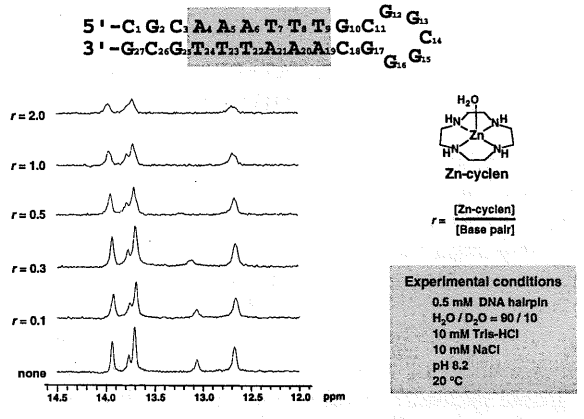

Figure 2. Imino-proton NMR spectra of a 27-mer hairpin-type oligonucleotide in the presence of Zn-cyclen at various concentrations.

VII-E-3 Novel Synthetic Receptors for AT Base Pairs

Akio OJIDA, Motoyuki TASAKA*, Kentaro TANAKA and Mitsuhiko SHIONOYA *(*Graduate Univ. for Advanced Studies)*

We previously demonstrated that a macrocyclic Zn complex induces a melting of AT-rich domains of double-stranded DNA by binding to thymine of AT base pairs. On the basis of this finding, we have designed a novel zinc complex by using a rigid and concave shape of glycouril as a building block. This zinc complex is expected to convert the structure and function of AT-rich sequences such as TATA-box in the transcriptional regulatory domain of a specific gene by binding to both thymine and adenine bases. The ligand moiety was synthesized from benzil and urea in seven steps (Figure 1). The solution behaviors of the metal complexes is now underway.

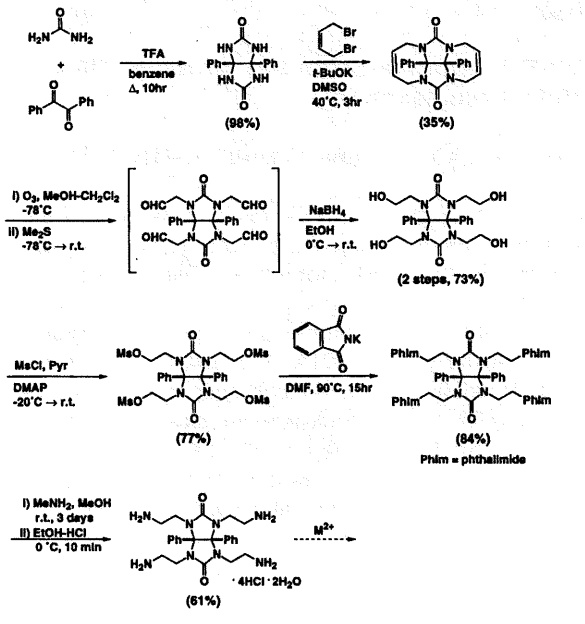

Figure 1. Synthetic route for a newly designed receptor for an AT base pair.

VII-E-4 Design and Synthesis of DNA Binding Metallopeptides

Michito SHIOTSUKA, Kentaro TANAKA, Akio OJIDA and Mitsuhiko SHIONOYA

Regulation of transcriptional processes of DNA depends on the site-specificity of DNA-binding proteins. Structural changes of DNA induced by proteins are important factors controlnig the initiation of transcription. We have synthesized novel peptides, GlyMetGlyGlyMet and $(GlyMetGlyGlyMetCys(s\text{-}s))_2$, as building blocks for DNA-binding metallopeptides, by a solid phase synthetic method. The latter ligand is capable to donate metal ions with four sulfur atoms on methionyl residues to form possibly tetrahedral or square-pyramidal metal complexes. We have isolated the 1:1 Pt(II) complex with $(GlyMetGlyGlyMetCys(s\text{-}s))_2$. The mass spectrum of this complex is shown in Figure 1. Redox-active metal complexes of this ligand would give rise to changes of coordination geometries of the metal ions and subsequently conformations of the peptide moieties, and would be a promising element for DNA-binding metallopeptides with recognition sites.

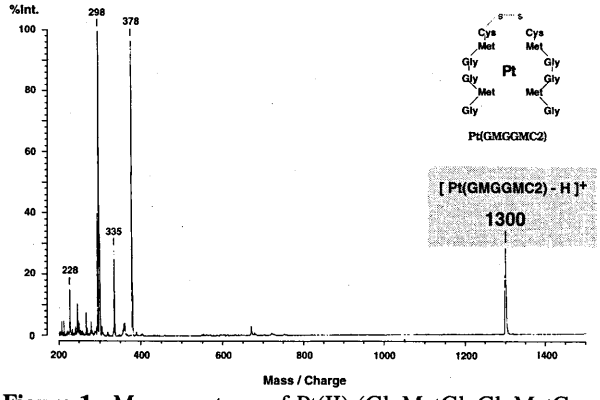

Figure 1. Mass spectrum of Pt(II)-$(GlyMetGlyGlyMetCys(s\text{-}s))_2$.

VII-E-5 Double-Stranded Artificial DNAs by Metal Complexation

Kentaro TANAKA and Mitsuhiko SHIONOYA

For the purpose of utilizing DNA as functionalized materials, natural nucleobases were replaced by artificial nucleobases as metal coordination sites. The artificial DNAs are expected to form double-stranded structures by metal complexation instead of hydrogen bonds at the axis of DNA. We first introduced an *o*-phenylenediamine as a nucleobase to ribose moiety and prepared RNA- and DNA-type nucleosides as shown in Figure 1. Such metal alignments at the axis of ds-DNA with chelating nucleobases could possibly be applicable to molecular wire, optical devices, drugs, etc.

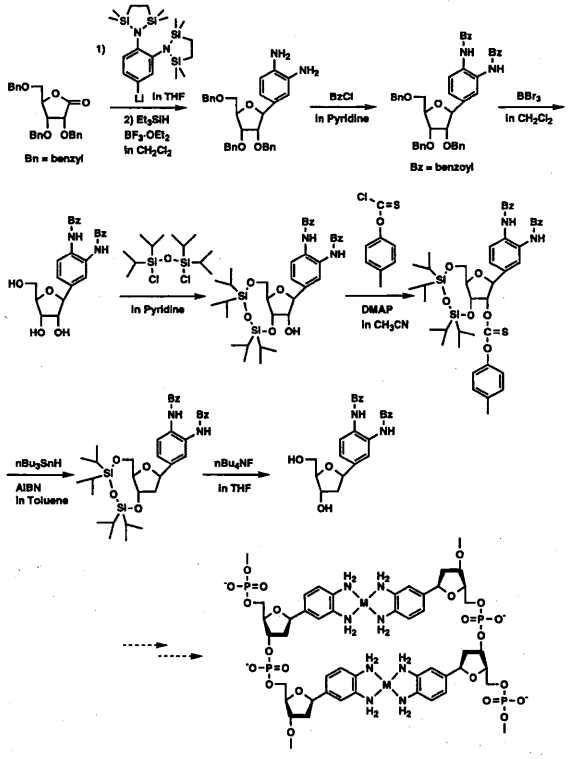

Figure 1. Synthetic route of a new nucleoside bearing an *o*-phenylenediamine nucleobase.

VII-E-6 Artificial Peptides: Alignment of Functionalized Metal Complexes on Peptide Backbone

Kazuki SHIGEMORI*, Kentaro TANAKA and Mitsuhiko SHIONOYA *(*Graduate Univ. for Advanced Studies)*

The rational design of novel proteins and peptides offers a new approach to the study of structure and function, and presents the possibility of constructing new biomaterials such as catalysts and biosensors. We have concentrated our attention on the use of peptides as an efficient tool in the metal alignment. In this project, a cystein hexamer, in which each thiol group coordinates to a terpyridine-Pt(II) complex, was newly designed and synthesized. The cystein hexamer was synthesized by a solid phase synthetic method and the crude product was purified by HPLC. The reaction of this hexadentate ligand with six equivalent terpyridine-Pt(II)-Cl afforded deep red material. The purification and identification of this product are now underway.

VII-E-7 Molecular Recognition of DNA by Metal Assisted Self-Assembly

Akihiko HATANO*, Kentaro TANAKA and Mitsuhiko SHIONOYA *(*Graduate Univ. for Advanced Studies)*

Self-assembly processes are used to create complex functional biological structures of nanoscale dimensions with precision, and are now recognized as efficient tools in the construction of new systems with tailored functions. We have designed a self-assembled

anti-sense DNA which could be built up by molecular subunits with the cooperative participation of many weak, reversible, non-covalent bonding interactions such as hydrogen bonding, metal coordination, hydrophobic interaction, etc. We have synthesized four molecular subunits each of which interacts with one of the four natural nucleobases through hydrogen bonding and metal coordination. By the interactions which would take place between single- or double-stranded DNA (or RNA) and a mixture of these four subunits, a thermodynamically minimized structure with complementarity would be constructed. This self-assembly system could be applicable to anti-sense (or -gene) and furthermore to alignment of functionalized compounds on DNA. The synthesis of the subunits is now underway.

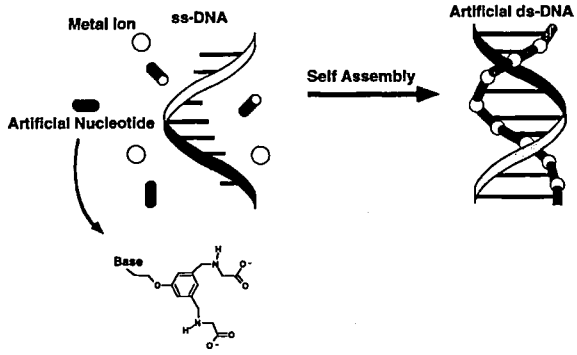

VII-E-8 Alignment of Functionalized Metal Complexes on DNA by Non-Covalent Interactions

Hiromasa MORISHITA*, Kentaro TANAKA and Mitsuhiko SHIONOYA *(*Graduate Univ. for Advanced Studies)*

Self-assembly features the cooperative participation of non-covalent interactions to construct thermodynamically minimized structures. The main purpose of this research is to arrange functionalized molecular subunits on DNA by non-covalent interactions. A key feature of this system is the complimentarity that exists between the molecular subunits and nucleobases of DNA. We have designed novel square-planar metal complexes bearing a functionality for hydrogen bonding with nucleobases and an aromatic moiety for π-π stacking with the neighboring subunit. The synthesis of the subunits is now underway.

VII-E-9 A Model Study for DNA Polymerases using a Newly Designed Dinuclear Metal Complex

Mitsuhiko SHIONOYA, Jik CHIN*, Motoyuki TASAKA and Kentaro TANAKA** *(*McGill Univ. and IMS, **Graduate Univ. for Advanced Studies)*

DNA polymerases are metalloenzymes that catalyze replication of DNA. The enzyme uses one strand of DNA as a template to generate its complimentary sequence from primer molecules and nucleoside triphosphates. At low temperatures, the newly formed double helix is stable, but at elevated temperatures, the DNA molecules can dissociate and repeat the polymerase catalyzed cycles of replication resulting in rapid amplification of DNA. The chemical mechanism of DNA formation involves cleavage of the nucleoside triphosphates at the α position by transesterification. We planed to develop simple metal complexes that can cut nucleoside triphosphates at the α position. The cleavage of the triphosphate by hydrolysis as well as by transesterification to solvent methanol or ethanol will be investigated. It is well known that cis-diaqua metal complexes can coordinate diphosphates to form six-membered rings. It is also well known that cis-diaqua metal complexes can efficiently hydrolyze phosphate diesters. We planed to develop two cis-diaqua metal complexes that are covalently linked to each other that can hydrolyze nucleoside triphosphates at the α position. One metal in the dinuclear complex could coordinate the β and the γ phosphates to form the six-membered ring while the other metal could coordinate the α phosphate and cleave it. Such dinuclear metal complexes may ultimately be developed to have polymerase activity. Furthermore, metal complexes that rapidly hydrolyze triphosphates are of interest to the pharmaceutical or biotech industries for controlling RNA regulation.

VII-E-10 A Novel Macrocyclic Terbium Complex Targeting Telomere DNA

Mitsuhiko SHIONOYA, Yuko HATA*, Tohru KOIKE*, Eiichi KIMURA*, Kimiko KOBAYASHI and Sei TSUBOYAMA**** *(*Hiroshima Univ., **RIKEN)*

Tb(III) ion is known to exhibit a low level of intrinsic fluorescence, which is enhanced many-fold upon interaction with nucleotides and single-stranded nucleic acids. We have examined the effects of several Tb(III) macrocyclic complexes including newly synthesized **1**. This complex displayed a significant fluorescence enhancement only when it interacts with polyG. Fluorescence intensity for **1** in the presence of polyG was 25 times greater than that without nucleic acid. In contrast, almost no fluorescence enhancement was observed with monomeric nucleotides, GMP and GTP, and double-stranded polyG•polyC. Furthermore, the interaction between **1** and G-rich telomere DNA, which is known to form G-quartet, was examined using a 24-mer oligonucleotide, 5'-TTAGGGTTAGGG-TTAGGGTTAGGG-3'. Fluorescent enhancement of **1** was again observed in the presence of this oligonucleotide. Excitation spectra of **1** with this oligonucleotide indicated that the fluorescent enhancement can be explained by energy transfer from nucleobases to **1**. Although the detailed interaction mode between the oligonucleotide and **1** is still unclear, such a compound could possibly be applicable to gene diagnosis related to telomere DNA.

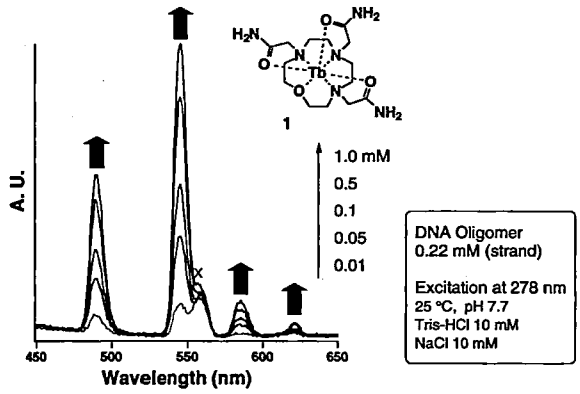

Figure 1. Fluorescent enhancement of the terbium(III) complex **1** in the presence of oligonucleotide, 5'-TTAGGGTTAGGGTTAGGGTTAGGG-3', containing human telomere sequences.

VII-E-11 Structure and O_2–Uptake Properties of a Novel Nickel(II) Complex of Pyridyl–Pendant Dioxocyclam

Eiichi KIMURA*, Masatoshi SASADA*, Mitsuhiko SHIONOYA, Tohru KOIKE*, Hiromasa KUROSAKI and Motoo SHIRO***** *(*Hiroshima Univ., **Kumamoto Univ., ***Rigaku Corp.)*

[*J. Bioinorg. Chem.* **2**, 74 (1997)]

A novel pyridyl-pendant dioxocyclam has been synthesized to study its nickel(II) complexation and reactivity with molecular oxygen. A purple nickel(II) complex with a deprotonated amide and a yellow nickel(II) complex with two deprotonated amides were isolated and the structure of the latter complex was determined by X-ray analysis. It was concluded from the visible absorption and NMR studies of this complex in aqueous solution that the four-coordinate nickel(II) complex is in equilibrium with a five-coordinate square-pyramidal nickel(II) complex with the apical coordination of the pyridyl-pendant. An electrochemical study disclosed a low nickel(II/III) redox potential of +0.29 V *vs* SCE for this complex at pH 9.5 and 25 °C. The nickel(II) complex absorbed an equimolar amount of O_2 at pH 7.9 and 25 °C, and the O_2 was activated to cleave supercoiled pBR 322 DNA.

VII-E-12 Metal Assisted Self-Replicating of Small Molecules and DNA

Mitsuhiko SHIONOYA, Kentaro TANAKA and Jik CHIN* *(*McGill Univ. and IMS)*

We planed to synthesize molecules that, when covalently linked to each other, can form a template for further self-replication with the help of metal ions. One of the signatures of a self-replicating system is a sigmoidal growth curve. Real-time monitoring of the "growth" of the system should be much simpler than in previous systems since formation of the product will be accompanied by a color change due to the release of the *p*-nitrophenoxide group. Metal ions may provide assistance for growth of this system by bringing the two reactants in close proximity to each other thereby increasing the effective molarity of the reacting groups.

VII-F Stereochemistry of Coordination Compounds and Adsorption Phenomena of Various Gases on Inorganic Solids

Several coordination compounds including higher(than four)-coordinate silicon(IV) complexes are going to be synthesized and studied stereochemically. Dielectric properties of inorganic solids adsorbed H_2O, on which the two-dimensional condensation of water occurs, were investigated as a function of surface coverage. Adsorption properties of N_2 on copper-ion-exchanged mordenites were also investigated.

VII-F-1 Stereochemistry and Electrochemistry of Cobalt(II) and Cobalt(III) Complexes Containing Optically Active Tetradentate Schiff Base Ligands

Masakazu HIROTSU,* Masaaki KOJIMA,* Kiyohiko NAKAJIMA,† Setsuo KASHINO* and Yuzo YOSHIKAWA *(*Okayama Univ., †Aichi Univ. Educ.)*

[*Bull. Chem. Soc. Jpn.* **69**, 4925 (1996)]

Cobalt(II) complexes containing tetradentate Schiff base ligands with phenyl substituents, [Co(Schiff base)], have been prepared and the electrochemical properties are reported. The crystal structure of [Co{7-Phsal-(*rac*)-stien}], where the Schiff base ligand was derived from 2-hydroxy-benzophenone and (*rac*)-1,2-diphenylethylenediamine, has been determined by X-ray structure analysis. Crystal data: monoclinic, $P2_1/n$, a = 13.956(2) Å, b =14.703(2) Å, c = 17.808(3) Å, β = 112.21(1)°, V = 3383.0(9) Å^3, Z = 4, and R =0.052 and R_w = 0.039 for 3976 unique reflections with $I > 3\sigma(I)$. The two phenyl groups in the N-N chelate moiety are in the axial positions and block the apical sites. In this complex, the redox potential of the Co(III)/Co(II) couple is 0.20 V *vs.* Ag/Ag$^+$ in acetonitrile and becomes more positive by *ca.* 300 mV than that for [Co(salen)]. This large positive shift is attributed to the steric effect of the two axially disposed phenyl groups. The redox potentials of the analogous cobalt(II) Schiff base complexes, where (*meso*)-1,2-diphenylethylenediamine and (*R*)-1-phenylethylenediamine were used as a diamine, are also explained in terms of the steric effect of the phenyl substituents. The corresponding cobalt(III) Schiff base complexes with two additional axial ligands, [Co(Schiff base)(L)$_2$]ClO$_4$ (L = imidazole (im), 1-methylimidazole (Meim)), have been prepared. The steric interaction between the phenyl groups on the N-N chelate moiety and the axial

ligands is discussed based on the X-ray structure, the circular dichroism (CD) spectra, and the ^{1}H NMR spectra. The crystal structure determination of [Co{sal-(*meso*)-stien}(Meim)$_2$]ClO_4 has been performed. Crystal data: monoclinic, $P2_1/c$, a = 10.789(2) Å, b = 20.512(3) Å, c = 15.330(2) Å, β = 99.88(1)°, V =3342.3(8) Å^3, Z = 4, and R = 0.051 and R_w = 0.049 for 3414 unique reflections with $I > 3\sigma(I)$. In order to study the steric effect of the phenyl substituents, the [Co(Schiff base)(L)$_2$]ClO_4 complexes have been prepared using (*R*)-1,2-propanediamine as a diamine. The different behavior shows that the interaction between the phenyl groups is sensitive to the orientation.

VII-F-2 Interconversion between Polymeric Orange and Monomeric Green Forms of a Schiff Base-Oxovanadium(IV) Complex

Kiyohiko NAKAJIMA,† Masaaki KOJIMA,* Shunryo AZUMA,* Ryuichi KASAHARA, Motonobu TSUCHIMOTO,** Yoshihiro KUBOZONO, Hironobu MAEDA,* Setsuo KASHINO,* Shigeru OHBA,** Yuzo YOSHIKAWA and Junnosuke FUJITA***** *(†Aichi Univ. Educ., *Okayama Univ., **Keio Univ., ***International Christian Univ.)*

[*Bull. Chem. Soc. Jpn.* **69**, 3207 (1996)]

The orange and green forms of the Schiff base-oxovanadium(IV) complex, [VO{sal-(*RR*)-stien }]·MeOH (**1**, green), [VO{sal-(*RR*)-stien}]·2$CHCl_3$ (**2**, green), and [VO{sal-(*RR*)-stien}]·CH_3CN (**3**, orange) (H_2{sal-(*RR*)-stien} =*N*,*N*'-disalicylidene-(*RR*)-I,2-diphenyl-I,2-ethanediamine), have been prepared, and their crystal structures were determined by an X-ray method. The green forms, **1** and **2**, contain mononuclear square pyramidal molecules of the complex, while the orange form **3** consists of individual complexes stacked to give an infinite linear •••V=O•••V=O••• chain. **1**, which crystallizes as monoclinic in space group $P2_1$ with Z=4, has the cell parameters a = 16.684(2), b = 16.923(4), c =9.249(3)Å, β=105.76(2)°, and V =2513(1)Å^3. **2**, which crystallizes as triclinic in space group $P\bar{1}$ with Z = 2, has the cell parameters a =13.187(3), b =13.469(3), c =10.450(3) Å, α=103.72(2), β = 103.20(3), γ=63.03(2)°, and V =1591.2(7) Å^3. **3** crystallizes as triclinic in space group $P\bar{1}$ with Z = 2. The cell parameters are a =13.300(3), b =13.667(4), c = 7.55 1(l) Å, α= 90.44(2), β= 94.51(2), γ= 97.36(2)°, and V =1357(1) Å^3. The final R indices are R =0.059 and R_w=0.062 for **1**, R =0.098 and R_w=0.090 for **2**, and R = 0.053 and R_w=0.042 for **3**. The structural characteristics of these complexes are compared and discussed. **3** shows piezochromism (mechanochromism); its color changes from orange to green upon grinding. **1** and **2** turn orange when heated at 120 °C for a few minutes. The extent of conversion either by grinding or heating was studied by EXAFS (X-ray absorption fine structure) and IR spectroscopy. The orange crystals turn green when exposed to chloroform vapor, and the green crystals turn orange upon exposure to acetonitrile vapor.

VII-F-3 Chromatographic Resolusion Mechanism of a Tris(1,10-phenanthroline)-Silicon(IV) Complex

Yasuharu OHMORI,* Masaaki KOJIMA,* Setsuo KASHINO* and Yuzo YOSHIKAWA *(*Okayama Univ.)*

[*J. Coord. Chem.* **39**, 219 (1996)]

The ion-association constants between the optically active complex cations (Λ-or Δ-[Si(phen)$_3$]$^{4+}$) and the resolving agent anions ([Sb_2{(+)-tart}$_2$]$^{2-}$, tart = tartrate(4-) ion) were determined spectrophotometrically. Ion-association between the complex cation and the eluent anion occurred in two steps and the stereoselective interaction was observed in the second step. The second-step association constant for the Λ-enantiomer (K_2 = 1.41×10^3) is larger than that for the Δ-enantiomer (K_2=1.07×10^3). The second-step association plays a dominant role in determining the elution order in column chromatographic resolution. The molecular mechanics calculations for the ion-associated species were performed to obtain information about the microscopic interaction between the ions. The total strain energy for the species containing the Λ-enantiomer is smaller than that for the Δ -enantiomer and this can explain the experimental finding that the Λ-enantiomer is eluted faster than the Δ-enantiomer.

VII-F-4 Mononuclear and Mixed-Valence Trinuclear Manganese Complexes Containing Tripodal Tetradentate Ligands. Phenolato, Carboxylato, and Alkoxo Bridges

Masakazu HIROTSU,* Masaaki KOJIMA* and Yuzo YOSHIKAWA *(*Okayama Univ.)*

[*Bull. Chem. Soc. Jpn.* **70**, 649 (1997)]

Manganese complexes containing tripodal tetradentate ligands with an N_2O_2 donor set (H_2L^1: *N*,*N*-bis-(2-hydroxybenzyl)-*N*',*N*'-dimethylethylenediamine, H_2L^2: *N* -(3,5-di-t-butyl-2-hydroxybenzyl)-*N*-(2-hydroxybenzyl)-*N*',*N*'-dimethylethylenediamine, H_2L^3: *N*,*N*-bis(3,5-di-*t*-butyl-2-hydroxybenzyl)-*N*',*N*'-dimethylethylenediamine) have been prepared. The mononuclear and trinuclear complexes with the additional carboxylate ligand were isolated. The steric effect of the 3-positioned *t*-butyl groups on the aromatic rings of the tripodal ligand controls the type of the complex structure. The L^3 ligand gave a mononuclear complex, [Mn(L^3)(mcba)(CH_3OH)], where mcba is a *m*-chlorobenzoate anion; the structure has been determined by X-ray analysis. The trinuclear complexes are formulated as [$Mn_3(L^n)_2$(carboxylato)$_2$-(OCH_3)$_2$] (n = 1, 2). For the L^4 and L^5 ligands (H_2L^4: *N*,*N*-bis(5-methoxy-2-hydroxybenzyl)-*N*',*N*'-dimethylethylenediamine, H_2L^5: *N*,*N*-bis(5-chloro-2-hydroxybenzyl)-*N*',*N*'-dimethylethylenediamine), trinuclear complexes were also obtained. Three trinuclear complexes were also structurally characterized by X-ray analysis. The three manganese cores are arranged linearly, and the structural parameters indicate that the

oxidation states are Mn^{III}-Mn^{II}-Mn^{III}. The Mn^{III} and Mn^{II} cores are bridged by phenolate, carboxylate, and alkoxide groups, and the manganese cores are separated in the range of 3.14 and 3.17 Å. The variable-temperature magnetic susceptibility measurements of the mixed-valence trinuclear complexes revealed that the spin exchange coupling constants (J) between Mn^{III} and Mn^{II} ions range from -0.25 to 1.9 cm^{-1}. The exchange interactions are weak, and both antiferromagnetic and ferromagnetic interactions were observed.

VII-F-5 Stabilization of Copper Metal Cluster in Mordenite Nanopores: Water Treatment of Evacuated Copper Ion-Exchanged Mordenite at 300 K

Yasushige KURODA,* Shin-ichi KONNO,* Yuzo YOSHIKAWA, Hironobu MAEDA,* Yoshihiro KUBOZONO,* Hideaki HAMANO,* Ryotaro KUMASHIRO* and Mahiko NAGAO* *(*Okayama Univ.)*

[*J. Chem. Soc. Faraday Trans.* **93**, 2125 (1997)]

The change of the state of copper ion in mordenite due to the heat treatment and subsequent rehydration at 300 K was investigated using electron spin resonance (ESR), X-ray absorption fine structure (XAFS) — both in the extended region (EXAFS) and in the near-edge region (XANES) —, and infrared (IR) spectroscopy techniques. The ESR intensity attributed to Cu(II) species exchanged in mordenite decreased with increasing temperature of the pretreatment in vacuo. The XANES spectra gave a band at 8.976 keV for copper ion-exchanged mordenite evacuated at 300 K and bands at 8.981 and 8.992 keV for the sample evacuated at 873 K. These results are interpreted in terms of a reduction of Cu(II) to Cu(I) species in mordenite nanopores by evacuation at higher temperatures. An increase in intensity of the ESR spectra and a decrease in intensity of the 1s-4p band (8.981 keV) in the XANES spectra proved that treating the 873 K-evacuated sample with H_2O vapour at 300 K brings about a reoxidation of Cu(I) to Cu(II). There is also direct evidence for an existence of the metallic copper clusters with low crystallinity in the cavity of mordenite nanopores, which is formed by ion-exchange procedure, followed by heat treatment at 873 K and subsequent treatment with H_2O vapour at 300 K; the Fourier-transform of EXAFS gave the band at 2.16 Å (without phase-shift correction), being attributable to the scattering from Cu-Cu pair in metal. These results can be interpreted by assuming a disproportionation reaction of cuprous ions to Cu(II) and Cu(0) during a course of such treatments. On the ground of the coordination number calculated from the EXAFS data, the average size of the metal clusters is estimated to be *ca.* 10 Å. The formation of such small metal clusters may be due to a stabilization of small clusters in the zeolite nanopores. The driving force for the disproportionation reaction, which was examined by IR spectroscopy, seems to come from a formation of the Brønsted acid sites on the mordenite lattice through the H_2O treatment. Such an easy conversion of valence state for copper ions may be due to the spatial distribution of ion-exchanged sites in mordenite. In high-silica zeolites, the distance between Al ions is large, and hence the separated two single charges in the mordenite lattice are compensated by two Cu(I) species in the 873 K-treated sample and by $CuOH^+$, H^+, and Cu(0) species upon treating the 873 K-treated sample with H_2O vapour.

VII-F-6 Characterization of Active Sites on Copper Ion-Exchanged Mordenite for Dinitrogen Adsorption by Using CO as a Probe Molecule

Yasushige KURODA,* Hironobu MAEDA,* Yuzo YOSHIKAWA, Ryotaro KUMASHIRO* and Mahiko NAGAO* *(*Okayama Univ.)*

[*J. Phys. Chem.* **B101**, 1312 (1997)]

The peculiar feature of copper ion-exchanged mordenite in dinitrogen (N_2) adsorption has been investigated through the measurements of infrared (IR) and emission spectra (ES), and X-ray absorption fine structure (XAFS). IR spectra provided the definitive evidence for the existence of at least two kinds of adsorption sites on the 873 K-treated copper ion-exchanged mordenite; the absorption bands centered at 2160 and 2150 cm^{-1} appeared when CO molecules were adsorbed. The adsorbed species assigned to the former band was desorbed at 573 K *in vacuo* and that to the latter one at 473 K. It was found that the site responsible for the latter band acts as effective sites for N_2 adsorption. XAFS spectra also showed new bands due to the CO adsorption on copper ion at 1.48 Å, 2.52 Å, and 8.981 keV, together with bands at 1.85 Å and 8.993 keV. The former set of bands was concomitant with the appearance of an IR band at 2150 cm^{-1} due to the adsorbed CO species. The two bands (at 8.981 and 8.993 keV) observed in the XAFS spectra for CO-adsorbed sample are explained in terms of the formation of planar three- or four-coordinate site through the reaction of copper ion with CO molecule. CO adsorption also caused a significant shift of emission band from 470 to 430 nm. This band reverted to the original position by evacuating the sample at 473 K, accompanying by a liberation of CO. It makes possible to interpret that the adsorption site responsible for respective bands at 2150 cm^{-1} in IR, at 430 nm in ES, and at 8.981 keV in XAFS spectra through the interaction with CO molecules is effective one for N_2 adsorption at ambient temperature.

VII-F-7 Specific Feature of Dielectric Behavior of Water Adsorbed on Ag_2O Surface

Yasushige KURODA,* Taisuke WATANABE,* Yuzo YOSHIKAWA, Ryotaro KUMASHIRO,* Hideaki HAMANO* and Mahiko NAGAO* *(*Okayama Univ.)*

[*Langmuir* **13**, 3823 (1997)]

The dielectric behavior of Ag_2O samples with different amounts of adsorbed H_2O was investigated in the temperature range from 308 to 200 K and in the frequency region from 0.1 Hz to 5 MHz. A large relaxation is observed in these ranges, and it is explained by the interfacial polarization due to the heterogeneity of the system. The characteristic frequency (f_m) for this relaxation is lowered with decreasing temperature until a complete monolayer is established. However, such a behavior of f_m in the region beyond the surface coverage of *ca.* 1 reveals a new specific feature; the f_m value gives a maximal frequency at around 278 K. The cause of these behavior is explored through the measurements of the differential adsorption heat, water content, and Clausius-Clapeyron plots ($\ln p$ *vs.* $1/T$). As a result, a new phenomenon observed in the Ag_2O-H_2O system can be explained by considering that the continuous phase change occurs at around 278 K in the adsorbed layer higher than the monolayer; the cluster-like structure formed on the OH groups at a temperature higher than 278 K is transferred to the two- or three-dimensional network structure formed by H-bonding between adsorbed H_2O molecules in the lower temperature region.

VII-G Creation of Complexes Containing New Types of Bonds between a Transition Metal and a Phosphorus

The most typical bond fashion between a transition metal and a phosphorus is a dative bond, where the lone-pair electrons on a phosphorus atom are donated to a vacant d orbital of a transition metal. We focus on rather new types of bond fashion between a transition metal and a phosphorus, such as a covalent bond, a multiple bond, and a hypervalent bond. New preparative methods of complexes containing such bonds have been developed and the reactivities of these complexes have been examined.

VII-G-1 Reactivity of Cationic Phosphenium Complexes of Molybdenum: Migration of OR, SR, and NR_2 on a Tertiary Phosphorus Compound to a Phosphenium Ligand

Yoshitaka YAMAGUCHI, Hiroshi NAKAZAWA *(Hiroshima Univ. and IMS),* **Mitsuru KISHISHITA and Katsuhiko MIYOSHI** *(Hiroshima Univ.)*

[*Organometallics* **15**, 4383 (1996)]

The reaction of a cationic monoaminomonoalkoxy phosphenium complex of Mo, mer-[(bpy)$(CO)_3$Mo-{PN(Me)CH_2CH_2O}]$^+$, with a diamino-substituted phosphorus compound, PN(Me)CH_2CH_2NMe(Y) (Y = OMe, OEt, SEt, N$(CH_2)_3CH_2$), proceeds with substitution for CO and then with the Y group migration to the coordinating phosphenium phosphorus to give [(bpy)$(CO)_2${PN(Me)CH_2CH_2O(Y)}Mo-{PN(Me)CH_2-CH_2NMe}]$^+$, which is also prepared from a cationic diamino phosphenium complex of Mo, *mer*-[(bpy)$(CO)_3$-Mo{PN(Me)CH_2CH_2NMe}]$^+$, and a monoamino-substituted phosphorus compound, PN(Me)CH_2CH_2O-(Y), by a simple CO/PN(Me)CH_2CH_2O(Y) substitution. This migration reaction is irreversible. The migration mechanism is also discussed.

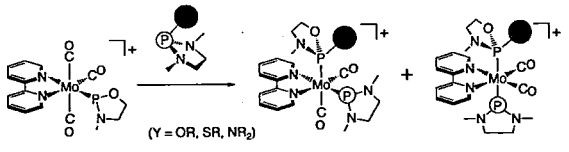

VII-G-2 Formation of a Six Membered Metallacycle Consisting of Iron, Carbon, Phosphorus, Boron, and Two Oxygens: The First Example of Precedence of Migratory Insertion of CO into an M-C Bond over OR Abstraction from Coordinating Phosphite by BF_3

Hiroshi NAKAZAWA *(Hiroshima Univ. and IMS),* **Yoshitaka YAMAGUCHI and Katsuhiko MIYOSHI** *(Hiroshima Univ.)*

[*Organometallics* **15**, 4661 (1996)]

Treatment of Cp(CO)MeFe{$P(OMe)_3$} with BF_3•OEt_2 and then PPh_3 gave a six-membered metallacyclic complex, Cp(PPh_3)FeC(Me)$OBF_2OP(OMe)_2$, which is suggested by its NMR data and X-ray analysis to be best described as a carbene phosphite metallacycle. The reaction mechanism is discussed.

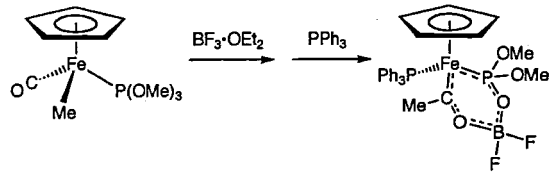

VII-G-3 Reaction of Cationic Piano Stool Iron Complexes Containing Phosphorus Ligands with Phosphorus Ylide

Hiroshi NAKAZAWA *(Hiroshima Univ. and IMS),* **Yoshiko UEDA** *(Hiroshima Univ.),* **Keiichi NAKAMURA** *(Hiroshima Univ.)* **and Katsuhiko MIYOSHI** *(Hiroshima Univ.)*

[*Organometallics* **16**, 1562 (1997)]

Reactions of PF_6- salts of cationic piano stool iron complexes with phosphorus ylide, CH_2PPh_3, were examined. In the reaction of dicarbonyl complex [Cp$(CO)_2$FeL]$^+$ (L = $P(OMe)_3$, $P(OEt)_3$, $PPh_2(OMe)$), Cp(CO)LFe{C(O)CH=PPh_3} is formed by the nucleophilic attack of the carbene carbon of CH_2PPh_3 on the carbonyl carbon of the complex. In contrast, the reaction of monocarbonyl complex [Cp(CO)LFe{P-$(OR)_3$}]$^+$ (L = $P(OMe)_3$, R = Me; L = PMe_3, R = Me; L = $P(OEt)_3$, R = Et) yields Cp(CO)LFe{P(O)$(OR)_2$} by

the Arbuzov-like dealkylation reaction. $[Cp(PMe_3)_2Fe\{P(OMe)_3\}]^+$, having no CO ligand, also exhibits the Arbuzov-like dealkylation reaction under forcing conditions. These results indicate that increasing the back donation ability from a central transition metal to a ligand induces a change in the reaction site from a carbonyl carbon in a CO ligand to an α-carbon in a phosphite ligand. In the reaction of $[Cp(CO)_2Fe\{PPh_2H\}]^+$, proton abstraction from the PPh_2H ligand takes place to give a phosphide complex $Cp(CO)_2Fe\text{-}PPh_2$.

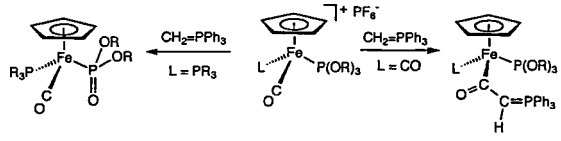

VII-G-4 Comparison of the Reactivity of Cationic Phosphenium Complexes of Iron Containing a Group 14 Element Ligand

Hiroshi NAKAZAWA *(Hiroshima Univ. and IMS)*, **Yoshitaka YAMAGUCHI, Kazumori KAWAMURA and Katsuhiko MIYOSHI** *(Hiroshima Univ.)*

[*Organometallics* in press]

Reactions of $Cp(CO)(EMe_3)Fe\{PN(Me)CH_2CH_2NMe(OMe)\}$ (E = Si (**2a**), Ge (**3a**), and Sn (**4a**)) with a Lewis acid ($BF_3{\bullet}OEt_2$ or $Me_3SiOSO_2CF_3$ (TMSOTf)) have been examined. The silyl complex **2a** reacts with $BF_3{\bullet}OEt_2$ to give a stable cationic phosphenium complex $[Cp(CO)(SiMe_3)Fe\{PN(Me)CH_2CH_2NMe\}]BF_4$ by OMe anion abstraction from phosphorus. This reaction is in contrast to that of the corresponding alkyl complex reported earlier showing that the phosphenium complex once formed undergoes immediately migratory insertion of the phosphenium ligand into the Fe-C bond. The X-ray analysis of $[Cp(CO)(SiMe_3)Fe\{PN(Me)CH_2CH_2NMe\}]BPh_4$ reveals that there is considerable double bond character in the Fe-P bond. The rotation barrier around the Fe-P(phosphenium) bond is estimated ($\Delta G^{\ddagger}$ (248K) = 12.7 kcal/mol) from a variable temperature 1H NMR study. The germyl complex **3a** exhibits the same reactivity as that of **2a**. In contrast, the stannyl complex **4a** reacts with TMSOTf to give a stannylene complex $[Cp(CO)(SnMe_2)Fe\{PN(Me)CH_2CH_2NMe(Me)\}]OTf$ (**4e**). The X-ray analysis reveals that **4e** is regarded as a stannylene iron complex doubly base-stabilized by an oxygen of OTf^- and one nitrogen of the $PN(Me)CH_2CH_2NMe(Me)$ ligand. In solution, there is an equilibrium between a base-stabilized and a base-free stannylene form. The activation parameter ($\Delta G^{\ddagger}$ (188K) = 9.0 kcal/mol) is estimated for the methyl group exchange in the stannylene ligand. The reaction of $Cp(CO)(Sn^nBu_3)Fe\{PN(Me)CH_2CH_2NMe(OMe)\}$ with TMSOTf verifies that a cationic phosphenium iron complex is formed first and that then an alkyl migration from the Sn to the phosphenium phosphorus takes place.

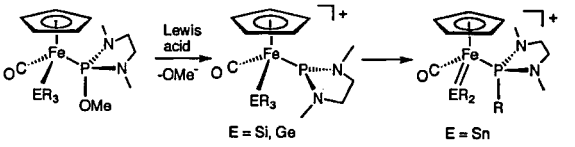

VII-G-5 A Novel Synthesis, X-ray Crystal Structures and Spectroscopic Properties of Metallated Hypervalent Phosphorus Complexes, $Cp(CO)LFe\{P(OC_6H_4Y)(OC_6H_4Z)\}$ (L = CO, $P(OPh)_3$, PMe_3; Y, Z = NH, NMe, O)

Kazuyuki KUBO *(Hiroshima Univ.)*, **Hiroshi NAKAZAWA** *(Hiroshima Univ. and IMS)*, **Tsutomu MIZUTA** *(Hiroshima Univ. and IMS)* **and Katsuhiko MIYOSHI** *(Hiroshima Univ.)*

Iron phosphorane complexes, $Cp(CO)_2Fe\{P(OC_6H_4Y)_2$ (Y = NR, **1a** (R = H), **1b** (R = Me); Y = O, **3**), have been prepared from $[Cp(CO)_2Fe\{P(OPh)_3\}]PF_6$, $o\text{-}HOC_6H_4YH$, and a Lewis base. An unsymmetrical iron phosphorane complex, $Cp(CO)_2Fe\{P(OC_6H_4O)(OC_6H_4NR)\}$ (**2a**, R = H; **2b**, R = Me) has been prepared from $[Cp(CO)_2Fe\{P(OC_6H_4O)(OPh)\}]PF_6$, $o\text{-}HOC_6H_4NRH$, and a Lewis base. These reactions involve a nucleophilic attack of an organic nucleophile at a trivalent phosphorus coordinated to an iron and substitution on the phosphorus. During the course of preparation of **1b**, $[Cp(CO)_2Fe\{P(OC_6H_4NMe)(OC_6H_4NMeH)\}]PF_6$ (**4**) was isolated, which corresponds to one of intermediates on the reaction pathways to give **1** ~ **3**. **4** reacts with a Lewis base to give **1b**. A reaction of hydrophosphorane $HP(OC_6H_4NH)_2$ with *n*-BuLi leads to NH proton abstraction to give an amide $HP(OC_6H_4NH)(OC_6H_4N^-)$, which then reacts with Cp(CO)LFeCl to yield $Cp(CO)LFe\{P(OC_6H_4NH)_2\}$ by an apparent 1,2-proton migration. The X-ray structures of **1b**, **2b**, and **4** were determined. **1b** and **2b** have slightly distorted trigonal-bipyramidal geometries around the phosphorus with the iron fragment in the equatorial position, and have longer $P\text{-}O_{eq}$ bonds than that of an organophosphorane, indicating that the $Cp(CO)_2Fe$ fragment serves as a strong π donor. The Fe-P(phosphorane) bond rotates freely in solution even at -50 °C. A berry pseudorotation around the phosphorane phosphorus does not occur for **1a** ~ **2b** and **5** ~ **7**, whereas it does occur for **3**.

VII-G-6 Migration Reaction of a Hypervalent Fragment: Base-Induced Migration of a Phosphorane Fragment from Iron to the Cyclopentadienyl Ring in $Cp(CO)_2Fe\{P(OC_6H_4Y)(OC_6H_4Z)\}$

Kazuyuki KUBO *(Hiroshima Univ.)*, **Hiroshi NAKAZAWA** *(Hiroshima Univ. and IMS)*, **Kazumori KAWAMURA** *(Hiroshima Univ. and IMS)* **and Katsuhiko MIYOSHI** *(Hiroshima Univ.)*

Iron phosphorane complexes, $Cp(CO)_2Fe\{P(OC_6H_4Y)(OC_6H_4Z)\}$ (Y, Z = NMe, O) react with

lithium diisopropyl amide (LDA) and then MeI to give $\{\eta^5\text{-}C_5H_4P(OC_6H_4Y)(OC_6H_4Z)\}(CO)_2FeMe$, showing the first example of migration of a hypervalent phosphorus fragment. The structure of one of the migration products, $\{\eta^5\text{-}C_5H_4P(OC_6H_4NMe)_2\}(CO)_2Fe\text{-}CH_2Ph$ was determined by X-ray analysis. Monitoring the migration reaction spectroscopically suggests that the reaction is initiated by a proton abstraction on the Cp ring by LDA, followed by migration of the phosphorane fragment to the Cp ring to give $\{\eta^5\text{-}C_5H_4P(OC_6H_4Y)(OC_6H_4Z)\}(CO)_2Fe^-$ which is converted into $\{\eta^5\text{-}C_5H_4P(OC_6H_4Y)(OC_6H_4Z)\}(CO)_2\text{-}FeR$ by the treatment of alkyl halide. The reaction of $Cp(CO)_2Fe\{P(OC_6H_4NH)_2\}$ with LDA proceeds first with NH proton abstraction to give $Cp(CO)_2Fe\{P\text{-}(OC_6H_4NH)(OC_6H_4N^-)\}$, and then with Cp proton abstraction followed by phosphorane migration to give $\{\eta^5\text{-}C_5H_4P(OC_6H_4NH)(OC_6H_4N^-)\}(CO)_2Fe^-$. The complex is converted by the addition of MeI to give $\{\eta^5\text{-}C_5H_4P(OC_6H_4NH)(OC_6H_4NH)\}(CO)_2FeMe$ and $\{\eta^5\text{-}C_5H_4P(OC_6H_4NH)(OC_6H_4NMe)\}(CO)_2FeMe$.

VII-H Activation of Carbon Dioxide on Metal Complexes

An electrophilic attack of CO_2 to coordinatively unsaturated metal complexes produces M-η^1-CO_2 complexes, which work as precursors to CO evolution through M-CO complexes. Metal complexes endowed with an ability of opening a chelate ring only when reduction of CO_2 is taking place, therefore, are highly desired to improve the stability of coordinatively unsaturated metal complexes. Moreover, reduction of M-CO without accompanying CO evolution is an essential factor to make multi-electron reduction of CO_2. Carbon dioxide bonded to strong organic bases is also reductively activated as similar to M-η^1-CO_2 complexes. Taking into account lability of coordinatively unsaturated low valent metal complexes, adduct formation of CO_2 with organic bases is generally much easier than the formation of M-η^1-CO_2 ones. A fundamental difference in the reductive activation of CO_2 on metals and organic bases is that a C-O bond of CO_2 is easily cleaved on metals, while CO_2/CO conversion is practically inhibited on organic bases. Reductive activation of CO_2 on organic bases, therefore, would be utilized in CO_2 fixation without accompanying a C-O bond cleavage. Both acidity and basicity of neighboring groups (ligands) of redox centers are largely influenced by redox reactions so that basic ligands as well as metals provide possible binding sites for the reductive activation of CO_2. The reactivity of the activated CO_2 on both sites are regulated by the redox reaction of the metal complexes. An M-M bond of an $M_3(\mu_3\text{-}S)$ core is subject to fission upon two-electron reduction. As a result, two-electron reduction of the $M_3(\mu_3\text{-}S)$ core provides two reaction sites for an electrophilic attack of CO_2; one is μ_3-S and the other is coordinatively unsaturated metals. Oxalate is selectively produced by a coupling reaction of two molecules of CO_2 activated on the adjacent sulfur and metal sites.

VII-H-1 Seven-Coordinated 2,2':6'2"-Terpyridinemolybdenum(II) Complexes: Synthesis, Structure and Reactivity of [Mo(CO)(C_7H_8)-(4,4',4"-R_3terpy)X]X' (R= H or ^{t}Bu)

Thomas DANIEL, Hirotaka NAGAO, Hiroshi NAKAJIMA, Koji TANAKA and Akira NAKAMURA

[*J. Organometallic Chem.* **509**, 225 (1996)]

A norbornadiene(terpyridine) complex [Mo(CO)-(C_7H_8)(terpy)I]I (**2a**) was prepared in two steps from $[Mo(CO)_4(C_7H_8)]$ (**1**), iodine and 2,2' : 6',2"-terpyridine. On treatment with either KPF6 in methanol or $AgSbF_6$ in CH_2Cl_2 the more soluble salts [Mo(CO)-(C_7H_8)(terpy)I]PF_6 (**2b**) and [Mo(CO)(C_7H_8)(terpy)I]-SbF_6 (**2c**) were isolated with good yields. With 4,4',4"-tri-tert-butyl-2,2' : 6',2"-terpyridine, in similar reactions the tert-butyl-substituted terpyridine compounds [Mo(CO)(C_7H_8)(4,4',4"-^{t}Bu$_3$terpy)I]X (X = I (**3a**), PF_6 (**3b**) or SbF_6 (**3c**)) were obtained, while the oxidation of **1** with two equiv of $CuBr_2$ led to the bromo-(terpyridine) complexes [Mo(CO)(C_7H_8)(terpy)Br]X (X = Br (**4a**), PF_6 (**4b**) or SbF_6 (**4c**)). The X-ray structural analysis for **4c** revealed a triangle formed by the norbonadiene and the halogen is perpendicular to the plane formed by terpyridine and CO. The iodo compound **2a** and the bromo analogue **4a** reacted with two equiv of $AgSbF_6$ to give a complex of the composition $\{[Mo(CO)(C_7H_8)(terpy)]_2(acetone)\}$-$(SbF_6)_4$ (**5**). Treatment of **5** with two equiv of PMe_3 afforded $[Mo(CO)(C_7H_8)(terpy)PMe_3](SbF_6)_2$·acetone (**6**). The similar compound [Mo(CO)(C_7H_8)(terpy)-$NCCH_2CH_3$]$(SbF_6)_2$ (**7**), which can be easily prepared from **5** and a fivefold excess of propionitrile.

VII-H-2 *Cis*-μ-1,2-Peroxo Diiron Complex: Structure and Reversible Oxygenation

Takaharu OOKUBO *(Kanazawa Univ.)*, **Hideki SUGIMOTO, Toshihiko NAGAYAMA** *(Kanazawa Univ.)*, **Hideki MASUDA** *(Nagoya Inst. Tech.)*, **Takahisa SATO, Koji TANAKA, Yonezo MAEDA, Hisashi OKAWA** *(Kyushu Univ.)*, **Yoshihito HAYASHI, Akira UEHARA** *(Kanazawa Univ.)* **and Masatatsu SUZUKI** *(Kanazawa Univ.)*

[*J. Am. Chem. Soc.* **118**, 701 (1996)]

The reaction of 2 equiv of $Fe(BF_4)_2{\cdot}6H_20$ with 1 equiv of HPh-bimp and C_6H_5COONa in EtOH under N_2 gave $[Fe_2(Ph\text{-}bimp)(C_6H_5COO)](BF_4)_2.3H_2O$ (2). Two iron centers in **2** are coordinatively unsaturated and readily react with O_2 in acetonitrile to generate an oxygenated complex $\{Fe_2(Ph\text{-}bimp)(C_6H_5COO)(O_2)\}(BF_4)_2$ $\bullet CH_3CN\bullet C_2H_5OC_2H_5.H_2O$ (**1**). The electronic spectrum of 2 in acetonitrile displays two d-d bands at 853 nm (ε = 12 $dm^3mol^{-1}cm^{-1}$) and 1900 nm (ε = 22 $dm^3mol^{-1}cm^{-}$

[1]), typical of high-spin five coordinate Iron(II) centers. The complex **1** has an intense dark green color, its electronic spectrum in CH_3CN at 20 °C showing a broad absorption band at 800-500 nm (ε = ca. 1700 $dm^3mol^{-1}cm^{-1}$). Boiling the CH_3CN solution of **1** under N_2 resulted in decolorization of the solution. Bubbling of O_2 through the solution restored the original dark green color. Thus, complex **1** is substantially thermally stable toward irreversible oxidation compared to the *p*-peroxo complexes reported so far. A single crystal suitable for X-ray crystallography was obtained by a diffusion of diethyl ether into an acetonitrile solution of **2** under O_2 at -20 °C. The molecular structure of the dinuclear cation of **1** has a triply bridged structure with *cis*-1,2-peroxide, μ-Phenolate of Ph-bimp, and *p*-benzoate, which is quite similar to that of a μ-phenolate dicobalt complex. $[Co_2(bpmp)(C_6H_5COO)(O_2)](BF_4)_2 \cdot H_2O$ (3) Such a *cis*-μ-1,2-peroxo coordination mode has been suggested for $[Fe_2(N\text{-Et-HPTB})(C_6H_5COO)(O_2)]^{2+}$. The equilibrium constant (K) of eq 1 for the oxygenation of 2 was measured by spectrophotometric titration in CH3CN at 20 °C under various partial pressures. $K[P(O_2)_{1/2} = 1/K]$ of **2** was estimated to be ca. 0.5 $Torr^{-1}$.

VII-H-3 Crystal Structure of $[Ru(bpy)_2(CO)(\eta^1\text{-}C(O)OH)]^+$ as a Key Intermediate in CO_2/CO Conversion

Kiyotsuna TOYOHARA, Hirotaka NAGAO and Koji TANAKA

[*Chem. Lett.* 27 (1996)]

The CO_2/CO conversion under protic conditions is explained by an acid-base equilibrium among η^1-CO_2, -COOH and -CO metal complexes (eq 1). The molecular

$$[M\text{-}CO_2]^{n+} \underset{OH^-}{\overset{H^+}{\rightleftharpoons}} [M\text{-}C(O)OH]^{(n+1)+} \underset{OH^-}{\overset{H^+}{\rightleftharpoons}} [M\text{-}CO]^{(n+2)+} \quad (1)$$

structures of both $[Ru(bpy)_2(CO)_2]^{2+}$ and $[Ru(bpy)_2(CO)(CO_2)]$ were already demonstrated by X-ray analysis. The molecular structure of the remaining $[Ru(bpy)_2(CO)((COOH)]^+$ is specially of interest, since the amphoteric reactivity of $[Ru(bpy)_2(CO)((COOH)]^+$ plays the key role in the CO_2/CO conversion in both CO_2 reduction and water gas shift reaction. X-ray analysis of $[Ru(bpy)_2(CO)(C(O)OH)](PF_6)$ revealed that the Ru-COOH bond distance of [Ru(bpy)2(CO)-(C(O)OH)]$^+$ (2.003 Å) is much shorter than the Ru-CO_2 one of $[Ru(bpy)_2(CO)(CO_2)]$ (2.064 Å). The shortening of the former is ascribed to an increase in a π-acceptor ability of the COOH moiety, since the Ru-N bond (*trans* to Ru-C) also show the similar behavior (Figure 1). The smooth conversion of eq. 1 in H_2O, therfore, is assited by synergic σ-donor and π-acceptor chracteristics of bpy ligands.

VII-H-4 Catalytic Generation of Oxalate through Activation of Two CO_2 Molecules on $[(IrCp^*)_2(Ir\text{-}\eta^4\text{-}Cp^*CH_2CN)(\mu_3\text{-}S)_2]$

Koji TANAKA, Yoshinori KUSHI, Kiyoshi TSUGE, Kiyotsuna TOYOHARA, Takanori NISHIOKA *(Osaka city Univ.)* **and Kiyoshi ISOBE** *(Osaka city Univ.)*

[*Inorg. Chem.* in press]

Electrochemical reduction of CO_2 in the presence of $[(IrCp^*)_3(\mu_3\text{-}S)_2](BPh_4)_2$ ($[Ir_3S_2](BPh_4)_2$) in CH_3CN at -1.30 V (*vs.* Ag/AgCl) produced $C_2O_4^{2-}$ with a current efficiency of 60%, and $[(IrCp^*)_2(Ir\text{-}\eta^4\text{-}Cp^*CH_2CN)(\mu_3\text{-}S)_2]^+$ ($[Ir_3S_2CH_2CN]^+$) was isolated from the electrolyte solution. The crystal structure of $[Ir_3S_2CH_2CN](BPh_4)$ by X-ray analysis (Figure 1) revealed that a linear CH_2CN group is linked at the exo-position of a C_p^* ligand, and the $C_p^*CH_2CN$ group coordinates to an Ir atom with an η^4-mode. The cyclic voltammogram of $[Ir_3S_2CH_2CN]^+$ in CH_3CN under CO_2 exhibited a strong catalytic current due to the reduction of CO_2, while that of $[Ir_3S_2]^{2+}$ did not show an interaction with CO_2 in the same solvent. Thus, the reduced form of $[Ir_3S_2CH_2CN]^+$ works as the active species in the reduction of CO_2. The IR spectra of $[Ir_3S_2CH_2CN]^+$ in CD_3CN showed a reversible adduct formation with CO_2. The controlled potential electrolysis of $[Ir_3S_2CH_2CN]^+$ at -1.50 V under CO_2 evidenced the generation of $C_2O_4^{2-}$ through a 1: 2 adduct between $[Ir_3S_2CH_2CN]^0$ and CO_2. A coupling reaction of two CO_2 molecules activated on adjacent μ_3-S and Ir in $[Ir_3S_2CH_2CN]^0$ is proposed for the first selective generation of $C_2O_4^{2-}$.

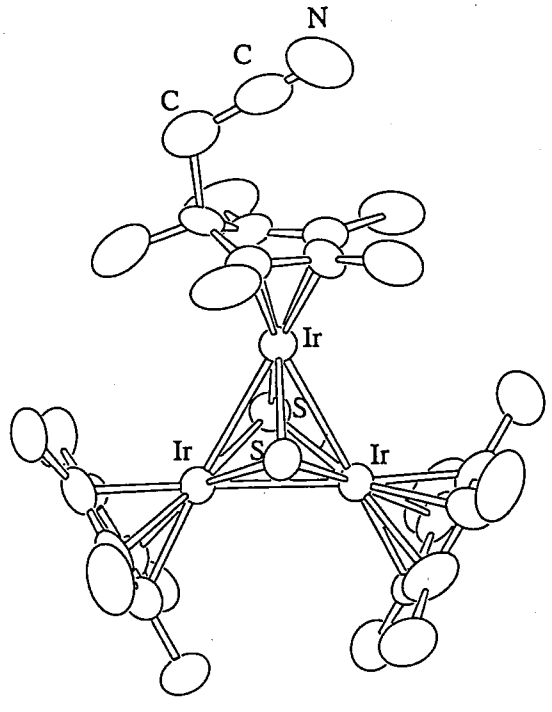

Figure 1. Molecular structure of $[(IrCp^*)_2(IrCp^*CH_2CN)(\mu_3\text{-}S)_2]^+$ as an active species for $C_2O_4^{2-}$ generation.

VII-H-5 Structural and Electrochemical Comparison of Copper(II) Complexes with Tripodal Ligands

Hirotaka NAGAO *(Sophia Univ.)*, **Nobutoshi KOMEDA, Masao MUKAIDA** *(Sophia Univ.)*, **Masatatsu SUZUKI** *(Kanazawa Univ.)* **and Koji TANAKA**

[*Inorg. Chem.* **35**, 6809 (1996)]

A series of copper(II) complexes with tripodal polypyridylmethylamine ligands, such as tris(2-pyridylmethyl)amine (tpa), (6-methyl-2-pyridyl-methyl)bis(2-pyridylmethyl)amine (Me_1tpa), bis(6-methyl-2-pyridylmethyl)(2-pyridylmethyl)amine (Me_2tpa), and tris(6-methyl-2-pyridylmethyl)amine (Me_3tpa), have been synthesized and characterized by X-ray crystallography: $[Cu(H_2O)(tpa)](ClO_4)_2$ (**1**) crystallized in the monoclinic system, space group $P2_1/a$, with a = 15.029(7) Å, b = 9.268(2) Å, c = 17.948(5) Å, β = 113.80(3)°, and Z = 4. $[CuCl(Me_1tpa)]ClO_4$ (**2**) crystallized in the triclinic system, space group $P\bar{1}$, with a = 13.617(4) Å, b = 14.532(4) Å, c = 12.357(4) Å, α = 106.01(3)°, β = 111.96(2)°, γ = 71.61(2)°, and Z = 4. $[CuCl(Me_2tpa)]ClO_4$ (**3**) crystallized in the monoclinic system, space group $P2_1/n$, with a = 19.650(4) Å, b = 13.528(4) Å, c = 8.55(1) Å, β = 101.51(5)°, and Z = 4 (R = 0.071, R_w = 0.050). $[CuCl(Me_3tpa)]$-$[CuCl_2(Me_3tpa)]ClO_4$ (**4**) crystallized in the monoclinic system, space group $P2_1/a$, with a = 15.698(6) Å, b = 14.687(7) Å, c = 19.475(4) Å, β = 97.13(2)°, and Z = 4. **1**-**4** are penta-coordinate geometries with three pyridyl and one tertiary amino nitrogen atoms, and a chloride or aqua oxygen atom. Nitrite ion coordinated to the Cu(II) center of Me_1tpa, Me_2tpa, and Me_3tpa complexes with only oxygen atom to form nitrito adducts, and the catalytic activity for the reduction of NO_2^- increases in the order of Me_3tpa << Me_2tpa << Me_1tpa < tpa complexes.

VII-H-6 Control of Coordination Mode of η^1- and η^2 -1,8-Naphthyridine Ligated to Ru(II)-bis(bipyridine) Complexes

Hiroshi NAKAJIMA, Hirotaka NAGAO and Koji TANAKA

[*J. Chem. Soc. Dalton Trans.* 1405 (1996)]

Both $[Ru(bpy)_2(\eta^1\text{-napy})(CH_3CN)](PF_6)_2$ ([**1**]-$(PF_6)_2$) and $[Ru(bpy)_2(\eta^2\text{-napy})](PF_6)_2$ ([**2**]$(PF_6)_2$) (bpy = 2,2'-bipyridine, napy = 1,8-naphthyridine) were prepared, and thier crystal structures were determined by X-ray analysis. Crystal data for [**1**]$(PF_6)_2$: triclinic, space group $P\bar{1}$ with Z = 2 in a unit of dimension, a = 13.389(5), b = 13.590(2) and c = 10.577(2) Å, a = 104.19(2), b = 109.47(2) and c = 76.48(2)°; for [**2**]$(PF_6)_2$: orthorhombic, space group Pbcn with Z = 2 in a unit of dimension, a = 12.497, b = 15.085 and c = 17.594 Å The crystal structure of $[\mathbf{1}]^{2+}$ displays an octahedral coordination with monodentate napy, acetonitrile and two chelating bpys. Despite the inequivalency of two nitrogens of napy of $[\mathbf{1}]^{2+}$ in the solid state, ^{1}H-NMR spectra of $[\mathbf{1}]^{2+}$ in aromatic region resembles that of $[\mathbf{2}]^{2+}$ in a wide-range of -90 to 60 °C, which implies dynamic behavior of napy in $[\mathbf{1}]^{2+}$ in solutions (Scheme 1). Both $[\mathbf{1}]^{2+}$ and $[\mathbf{2}]^{2+}$ undergo an irreversible reduction at -0.98 V (*vs.* Ag|AgCl) in DMF, and the process gradually becomes a reversible redox reaction on raising temperature up to 30 °C. EPR spectra of $[\mathbf{1}]^{+}$ revealed that one-electron reduction of $[\mathbf{1}]^{2+}$ takes place in the napy localized orbital without an appreciable increase in the electron density on one of the nitrogen of napy. The distinct inequivalence in the charge density between two nitrogen atoms of singly reduced napy results in stabilization of the N rather than N, N' co-ordination mode.

VII-H-7 Resonance Equilibrium between Ru^{III}-(catechol) and Ru^{II}(semiquinone) and Stable Electron Localized Form of RuII(quinone) in Ru-dioxolene-terpyridine Complex

Masato KURIHARA, Stephane DANIELE *(Univ. Nice-Sophia Antipolis)*, **Kiyoshi TSUGE and Koji TANAKA**

A series of ruthenium complexes with terpyridine and substituted dioxolene ligands were prepared. The molecular structure of [Ru(terpy)(dbcat)Cl] was determined by X-ray crystallography, where terpy and dbcat denote terpyridine and 3,5-di-*t*-butylcatecholato, respectively. Crystal data: monoclinic, space group $P2_1/c$, Z = 8, a = 11.548(1) Å, b = 18.224(5) Å, c = 30. 002(8) Å, b = 96.51(2)°, and R = 0.077 (Rw = 0.068). The carbon-oxygen bond lengths of the ligand lie between those of catecholato and semiquinonato ligands. The electronic state of Ru(terpy)(dioxolene)X is represented by Ru^{II}(terpy)(semiquinone)X rather than Ru^{III}(catecolato) on the basis of the electronic absorption spectra, while the reverse relation was deduced from the IR spectra. Furthermore, ESR spectra dermonstrated a resonance equilibrium between Ru^{II}-(semiquinone) and Ru^{III}(catecolato) forms. The above results indicates that Ru^{II}(semiquinone) and Ru^{III}-(catecolato) complexes exist as resonance isomers (eq 1) both in the solid state and solutions.

$$Ru^{II}(\text{semiquinone}) \leftrightarrow Ru^{III}(\text{catecolato}) \quad (1)$$

VII-H-8 Oxide Transfer Reaction from Carbonate to Metal-CO Complex, Affording Metal-η^1-CO_2 Complex and Carbon Dioxide

Hiroshi NAKAJIMA, Kiyotsuna TOYOHARA, Kiyoshi TSUGE and Koji TANAKA

[*Chem. Lett.* 485 (1996)]

Much attention is being devoted to metal-η^1-CO_2 complexes which are the key intermediate for CO_2/CO conversion. In protic media, CO_2/CO conversion on metals takes place through acid-base equilibria among $[M\text{-}\eta^1\text{-}CO_2]^{n+}$, $[M\text{-}\eta^1\text{-}C(O)OH]^{(n+1)+}$ and $[M\text{-}CO]^{(n+2)+}$ (eq 1). In the absence of proton donors, CO_2/CO con-

version is achieved by oxide transfer between metal-CO_2 and CO_2 (eq 2), which may be more

$$[M\text{-}\eta^1\text{-}CO_2]^{n+} \overset{H^+}{\rightleftharpoons} [M\text{-}\eta^1\text{-}C(O)OH]^{(n+1)+} \overset{H^+}{\rightleftharpoons} [M\text{-}CO]^{(n+2)+} \quad (1)$$

$$[M\text{-}CO_2]^{n+} + CO_2 \rightleftharpoons [M\text{-}CO]^{(n+2)+} + CO_3^{2-} \quad (2)$$

useful than that in H_2O (eq 1) from the viepoint of utilizartion of CO_2 as C1 resources. Reversible oxide transfer reactions from CO_3^{2-} to $[Ru(bpy)_2(CO)_2]^{2+}$ and from $Ru(bpy)_2(CO)(\eta^1\text{-}CO_2)$ to CO_2 are established (Scheme 1). The oxide transfer reaction from CO_3^{2-} to $[Ru(bpy)_2(CO)_2]^{2+}$ producing $Ru(bpy)_2(CO)(\eta^1\text{-}CO_2)$ and CO_2 in CH_3CN is ascribed to the less basicity of the Ru-η^1-CO_2 group compared with that of CO_3^{2-}. The reverse oxide transfer from $Ru(bpy)_2(CO)(\eta^1\text{-}CO_2)$ to CO_2 affording $[Ru(bpy)_2(CO)_2]^{2+}$ is assisted by Li^+ due to low solubility of Li_2CO_3 in CH_3CN.

VII-H-9 Determination of Basicity of μ_3-X and η^1-Y Ligands (X, Y = S, Se) of Reduced, Oxidized and Super-Oxidized Forms of $[Fe_4X_4(YAd)_4]^{2-}$ (Ad = 1-Adamantane) in Aqueous Solutions

Masami NAKAMOTO,* Kenji FUKAISHI,* Tsuyoshi TAGATA,* Hide KAMBAYASHI and Koji TANAKA *(* Osaka Municipal Tech. Res. Inst.)*

[*Inorg. Chim. Acta.* in press]

A series of $[Fe_4X_4(YAd)_4]^{2-}$ (X,Y= S, Se; Ad= 1-adamantane) were prepared as a model of high potential iron-sulfur proteins. Hydrolysis of those clusters were efficiently depressed in aqueous poly[2-dimethylamino(hexanamide)] (PDAH) solutions due to the enbedding effect in hydrophobic environment and/or inhibition of dissociation of the terminal ligand into the aqueous media. Cyclic voltammetry of the clusters in aqueous PDAH solutions showed pH dependent redox potentials of not only $[Fe_4X_4]^{+/2+}$ but also $[Fe_4X_4]^{2+/3+}$ (X, Y = S and Se) couples, resulting from redox-linked protonation reactions of three oxidation states of $[Fe_4X_4(YAd)_4]^{n-}$ (n= 1-3). pK Values of the reduced, oxidized, and super-oxidized forms of$[Fe_4X_4(YAd)_4]^{2-}$ were determined by computer simulation of the pH dependent redox potentials. The basicity of the μ_3-X cores (X= S and Se) of three oxidation states of $[Fe_4X_4(YAd)_4]^{n-}$ (n= 1, 2, 3) is stronger than the YAd (Y= S and Se) ligands: in the case of the mono-protonated $[Fe_4X_4(YAd)_4]^{3-}(H^+)$ and $[Fe_4X_4(YAd)_4]^{2-}(H^+)$, basicity of the η^1-Y ligand of $[Fe_4X_4(YAd)_4]^{2-}(H^+)$ becomes stronger than that of μ_3-X cores, although the μ_3-X cores of $[Fe_4X_4(YAd)_4]^{3-}(H^+)$ still show stronger basicity compared with those of η^1-Y ligands.

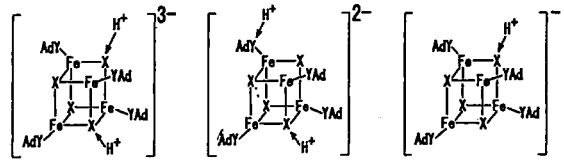

Figure 1. Protonation of reduced, oxidized and super-oxidized $[Fe_4(\mu_3\text{-}X_4)(\eta^1\text{-}YR)]^{2-}$ in aqueous solutions.

VII-I Supramolecular Self-Assembly through Coordination

Supramolecular self-assembly refers to the spontaneous generation of well-defined structures from component molecules under a well-defined set of conditions. Since 1990, we have been studying the self-assembly of finite and infinite structures based on coordination chemistry, where coordinate bonds induce the generation of defined structures. Our studies are focused on the self-assembly of such finite structures as macrocycles, catenanes (interlocked molecules), and cages, as well as infinite network structures. In the construction of the discrete structures, our strategy may be characterized by the use of palladium's 90 degree coordination angle because synthetic chemists have never employed this angle to constructed their target structures.

VII-I-1 On the Structure of Transition Metal-Linked Molecular Squares

Makoto FUJITA, Osamu SASAKI,* Takashi MITSUHASHI,* Toshiyasu FUJITA,* Jun YAZAKI,* Kentaro YAMAGUCHI* and Katsuyuki OGURA* *(*Chiba University)*

[*J. Chem. Soc. Chem. Commun.* **118**, 899 (1996)]

The structure of molecular square **1** assembling from $(en)Pd(NO_3)_2$ and 4,4'-bipyridine was confirmed by X-ray crystallography, whereas squares assembling from $(en)Pd(NO_3)_2$ and larger ligands, py-X-py (py = 4-pyridyl, X = CH=CH, C-C, *p*-C_6H_4) were shown to exist in equilibrium with molecular triangles.

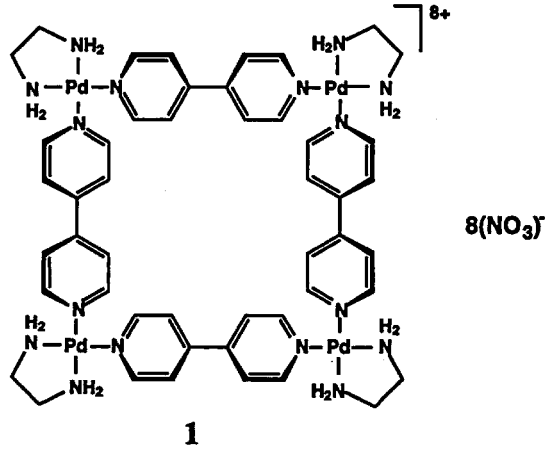

1

VII-I-2 Catenane Formation from Two Molecular Rings through Very Rapid Slippage. A Möbius Strip Mechanism

Makoto FUJITA, Fumiaki IBUKURO,* Hiroko SEKI, Osamu KAMO,*** Mamoru IMANARI*** and Katsuyuki OGURA**** *(*Graduate Univ. for Advanced Studies, **Chiba University, ***JEOL Ltd.)*

[*J. Am. Chem. Soc.* **118**, 899 (1996)]

Catenane **1** exists in rapid equilibrium with monomer ring **2** (eq 1, M. Fujita *et al.*, *Nature* **367**, 720 (1994)). A conventional explanation for the catenane formation involves dissociation of a ring at a Pd-N linkage, threading another ring on the thread, and reconnection of the ends of the thread (mechanism a in Scheme 1). However, the results of the present study negated this simple mechanism and strongly supported an alternative. Here we suggest that the rapid interconversion is explained in terms of ligand exchange between Pd-N bonds. More strictly, our proposed pathway leading to the catenane involves *two sequential ligand exchanges between two molecular rings concomitant with a twisting of the rings around each other* (mechanism b in Scheme 1).

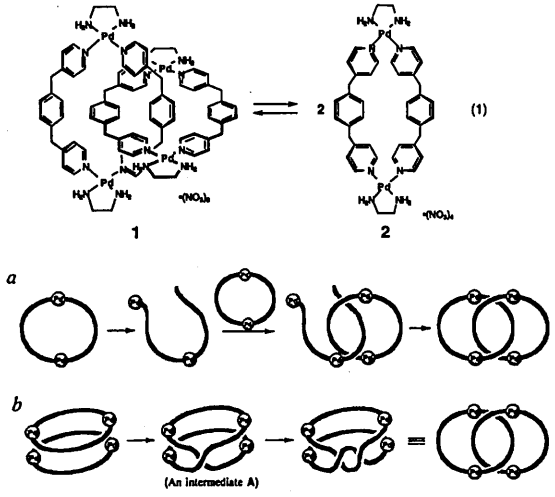

Scheme 1. Possible Mechanisms for the Rapid Slippage of Two Molecular Rings: (a) Conventional Mechanism and (b) Ligand Exchange Mechanism

VII-I-3 Made-to-Order Assembling of [2]-Catenanes from Palladium(II)-Linked Rectangular Molecular Boxes

Makoto FUJITA, Masaru AOYAGI,* Fumiaki IBUKURO,* Katsuyuki OGURA and Kentaro YAMAGUCHI**** *(*Graduate Univ. for Advanced Studies, **Chiba University)*

[*J. Am. Chem. Soc.* submitted]

Linked-ring molecules or catenanes have long intrigued chemists because mechanically connected structures are expected to show unique properties which chemically connected molecules have never possessed. An ideal methodology for catenane synthesis should allow chemists to design and prepare a variety of catenanes in quantitative yields without synthetic difficulties. Here we show such an ideal catenane synthesis can be provided by metal-mediated supramolecular self-assembly. That is, designed molecular boxes composed of transition metals and organic ligands are quantitatively catenated if the boxes involve parallelly arranged aromatic sides with the interplane separation of ca 3.5 Å. Thus eight building blocks - four metals and four ligands - are found to self-assemble into [2]catenanes **1** and **2** consisting of two rectangular molecular boxes.

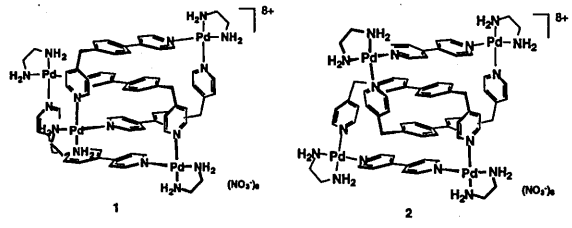

VII-I-4 A Nano-Sized Macrocycle Constructed From Four Organic Ligands Held Together by Six Metal Ions

Makoto FUJITA, Hidenori FUNAKI,* Katsuyuki OGURA* and Kentaro YAMAGUCHI* *(*Chiba Univ.)*

Precise control of nanometer-scale structures has become one of the most important subjects both in physics and chemistry. Here we show the construction of a nano-sized macrocycle through supramolecular self-assembly from ten simple molecules. Thus, macrocyclic supramolecular complex **1** was assembled from six molecules of ethylenediamine-palladium(II) nitrate and four molecules of tris(4-pyridyl)methane. The structure of **1** was confirmed by crystallography and NMR spectroscopy.

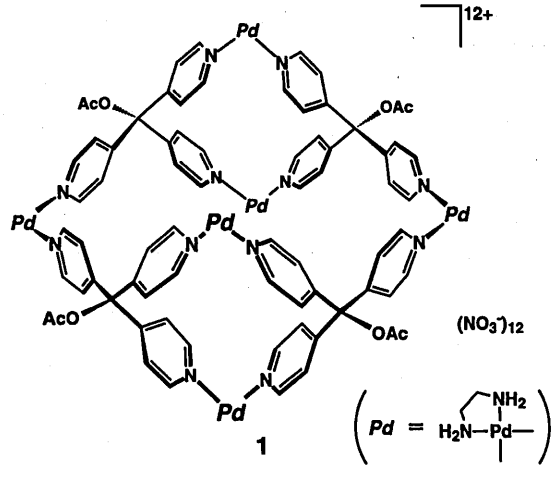

VII-I-5 Binding Property of a Coordination Nanocage Self-Assembling From Ten Components

Makoto FUJITA, Takahiro KUSUKAWA, Tomonori KONDO* and Katsuyuki OGURA* *(*Chiba Univ.)*

The synthesis of hollow, nanometer-scale molecular "container compounds" makes possible the creation of localized chemical micro-environments with properties different from those of the bulk phases. Recently, a hollow, roughly spherical nanocage framework (**1**, ca 2 nm in diameter) was constructed by self-assembly from ten species, four organic ligands held together by six metal ions.[1] Herein reported is binding property of nanocage 1 with large guest molecules. It is shown that self-assembled cage **1** can hold as many as four adamantane molecules inside its nanosized cavity. Thus efficient formation of **1**•G_4 complex (G = adamantane) in a two-phase system was observed when D_2O solution of **1** was stirred with saturated hexane solution of adamantane at 60 °C (Figure 1).

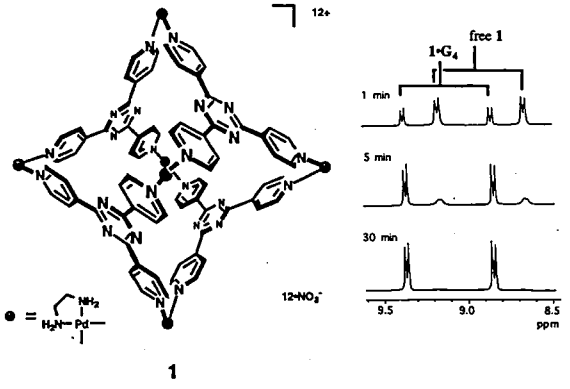

1

Figure1. Time-dependent NMR observation of aq phase in the formation of **1**•G_4 complex through liquid-liquid extraction (aq phase: D_2O solution of **1**; org phase: saturated hexane solution of **G**.

VII-I-6 Coordination Polymers Self-Assembling From Cadmium(II) Ions and Flexible Pyridine-Based Bridging Ligands

Makoto FUJITA, Masaru AOYAGI* and Katsuyuki OGURA** *(*Graduate Univ. for Advanced Studies, **Chiba Univ.)*

This paper describes coordination polymers assembling from cadmium nitrate and flexible bridging ligands, Py-X-Py (Py = 4-pyridyl, **1a**: X = CH_2, **1b**: X = C(=CH_2), **1c**: X = CH_2CH_2). Single X-ray analysis of these complexes showed that their infinite topologies are quite different from each other despite the structural similarity of ligands **1a-1c**. Upon treatment with $Cd(NO_3)_2$, **1a** gave a sheet structure of an infinite two-dimensional network with a stoichiometry of ML_2 (M and L denote metal and ligand, respectively). Ligand **1b** also afforded an infinite polymer possessing the same ML_2 composition. However the polymer structure is characterized by a one-dimensionally bounded macrocyclic frameworks where adjacent Cd ions are linked by two ligand molecules. Interestingly, ligand **1c** gave an infinite polymer of $ML_{1.5}$ composition whose structure was shown to be a unique one-dimensional framework having macrocyclic frameworks (M_2L_2) linked by different L molecules.

VII-I-7 Self-Assembled Molecular Ladders

Makoto FUJITA, Osamu SASAKI,* Kenya WATANABE,* Katsuyuki OGURA* and Kentaro YAMAGUCHI *(*Chiba Univ.)*

[*New. J. Chem.* in press]

Coordination of a pyridine-based bridging ligand, 1,4-bis(4-pyridylmethyl)benzene, with cadmium nitrate afforded an infinite ladder complex, the unit structure of which involves a T-shaped assembly of three pyridine rings about a heptacoordinated Cd(II) atom. The ladder structure was found to expand its cavity volume by enclathrating *p*-dibromobenzene in the cavity. Nearly orthogonal interpenetration of infinite ladders was observed in the solid structure.

VII-I-8 A "Swellable" Two-Dimensional Coordination Network

Makoto FUJITA, Kenya WATANABE,* Yoon-Jung KWON,* Masaru AOYAGI, Katsuyuki OGURA*, Kentaro YAMAGUCHI* and Kayoko KASAI***** *(*Chiba Univ., **Graduate Univ. for Advanced Studies, ***Miyagi Univ. Edu.)*

Controlled synthesis of metal complexes capable of enclathrating organic molecules has been an area of continuous research activity. The enclathration by these complexes with rigid frameworks often shows high shape selectivity. However, if stated reversely, the high selectivity does not lead to the made-to-order synthesis of clathrate complexes with a variety of organic guests. Here, by contrast, we report the enclathration of a relatively wide variety of aromatic guests by a "swellable" two-dimensional (2D) network assembling from cadmium(II) and flexible ligand $PyCH_2C_6F_4CH_2Py$. As schematically illustrated below, this network is constricted if the guest is small, but is expanded if the guest becomes large.

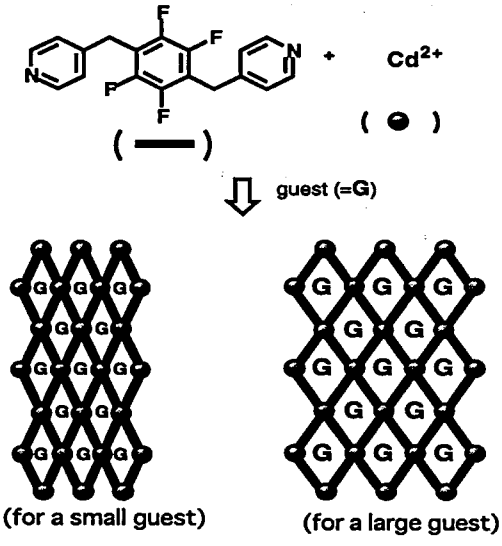

Scheme 1. Schematic presentation of the "swellable" coordination zeolites.

VII-J Multidimensional Crystal Engineering of Supramolecular Metal Complexes

A global persistent searching for new materials with improved properties has led to an extensive investigation into inorganic and organic polymers. The reasoning behind this strategy is that if these new materials possess some properties unique to either organic polymers or inorganic polymers, they may produce revolutionary development in fundamental science and technology. Thus, attention is being focused increasingly on supramolecular metal complexes which possess both properties of inorganic and organic compounds. In order to find new materials we have attempted to synthesize one-, two- and three-dimensional copper and silver complexes with donor organic compounds.

VII-J-1 Double Hydrogen-Bonds and π-π Stacking Assembled Two-Dimensional Copper(I) Complex of 2-Hydroxy- quinoxaline

Jie DAI,[a] Mikiko YAMAMOTO,[a] Takayoshi KURODA-SOWA,[a] Masahiko MAEKAWA,[a] Yusaku SUENAGA[a] and Megumu MUNAKATA
([a]Kinki Univ. and IMS)

[*Inorg. Chem.* **36**, 2688 (1997)]

Copper(I) ethylene complex of 2-hydroxyquinoxaline (Hhq), $[Cu(Hhq)_2(C_2H_4)]ClO_4$, was synthesized and characterized crystallographically. The cations of the complex are linked to each other by head-to-tail double H-bonded, AD:::DA, to form a one-dimensional infinite zig-zag chain structure. Keto form (C=O...H-N) is predominant in these H-bonds and the N-O distance is 2.79 Å. The H-bond assembled Hhq molecule planes are strongly stacked with the distance of 3.30 Å forming a unique two dimensional cooperative system of H-bonds and π-π interactions (Figure 1), which is a fundamental characteristic of proton-electron transition systems. The NMR and IR spectra of this complex are also discussed.

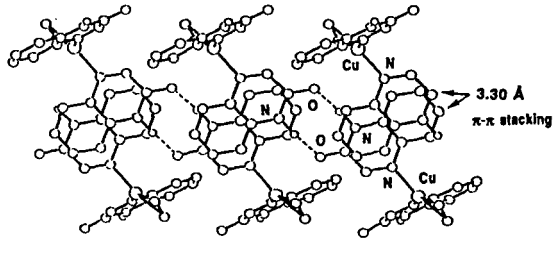

Figure 1. The packing of the coordinarion and H-bond-linked chains in $[Cu(Hhq)_2(C_2H_4)]ClO_4$.

VII-J-2 Assembly of a Mixed-Valence Cu(I/II) System Coupled by Multiple Hydrogen Bondings through Tetrahydroxybenzoquinone

Megumu MUNAKATA *([a]Kinki Univ. and IMS)*, **Liang Ping WU,[a] Takayoshi KURODA-SOWA,[a] Mikiko YAMAMOTO,[a] Masahiko MAEKAWA[a] and Kazuma MORIWAKI[a]**

[*Inorg. Chim. Acta* in press]

The synthesis and characterization of a mixed-valence copper complex $[Cu^{II}(bpy)_2Cl]_2[Cu^{I}Cl_2]_2$-$(C_6O_6H_4)$, where bpy = 2,2'-bipyridine, is described. The structure contains discrete copper(II) cation and copper(I) anion groups. In the cation each divalent copper is linked to two bpy molecules and one chloride ion in a trigonal bipyramidal fashion, whereas in the anion each monovalent copper is linearly bound to two chlorine atoms. The mixed-valence Cu(I/II) system is associated by multiple hydrogen bonding through tetrahydroxybenzoquinone, leading to an infinite chain structure of the complex, Figure 1.

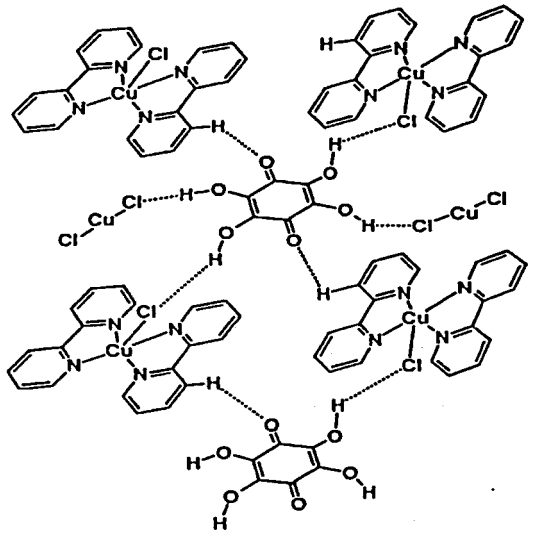

Figure 1. Hydrogen-bonded networks in the mixed-valence copper complex, $[Cu^{II}(bpy)_2Cl]_2[Cu^{I}Cl_2]_2(C_6O_6H_4)$

VII-J-3 S···S Contact Assembled Silver(I) Complexes of 4,5-Ethylenedithio-1,3-dithiole-2-thione Having Unique Supramolecular Networks

Jie DAI,[a] Takayoshi KURODA-SOWA,[a] Megumu MUNAKATA *([a]Kinki Univ. and IMS)*, **Masahiko MAEKAWA,[a] Yusaku SUENAGA[a] and Yasuhiro OHNO[a]**

[*J. Chem. Soc. Dalton Trans.* 2363 (1997)]

Two silver(I) complexes of 4,5-ethylenedithio-1,3-dithiole-2-thione ($C_5H_4S_5$), $\{[Ag(C_5H_4S_5)_3]ClO_4 \cdot CH_3CN\}_2$ and $[Ag(C_5H_4S_5)CF_3SO_3]$ have been synthesized and characterized crystallographically. They are unique dimer and two-dimensional structures respectively and assembled by S···S contacts (Figure 1).

The finding of the shortest S···S contacts (3.284 Å, 3.262 Å) in these complexes indicates that the coordination linkage in metal complexes of organic donor can be expected to control the intra- or intermolecular interactions. The coordination mode of the $C_5H_4S_5$ ligand has also been systematically discussed.

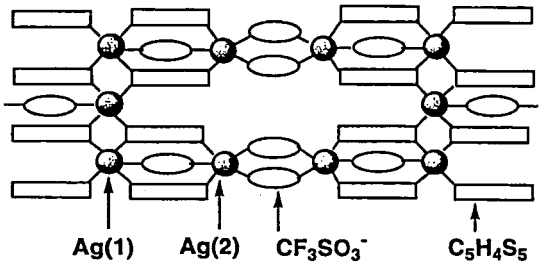

Figure 1. Schematic structure of the two-dimensional network of $[Ag(C_5H_4S_5)CF_3SO_3]$.

VII-J-4 Syntheses, Structures and Properties of Linear Copper(I) Coordination Polymers with Tetrakis(ethylthio)tetrathiafulvalene and Tetrakis(propylthio)tetrathia-fulvalene

Mikiko YAMAMOTO,[a] Xinmin GAN,[a] Takayoshi KURODA-SOWA,[a] Masahiko MAEKAWA,[a] Yusaku SUENAGA[a] and Megumu MUNAKATA *([a]Kinki Univ. and IMS)*

[*Inorg. Chim. Acta* **261**, 169 (1997)]

Linear copper(I) coordination polymers, $[Cu(TTC_2\text{-}TTF)]BF_4$ (**1**) and $[Cu(TTC_3\text{-}TTF)]ClO_4$ (**2**), were synthesized and characterized by spectroscopic and X-ray crystallographic methods. They are 1:1 metal-ligand complexes in which each of the copper(I) ions is tetrahedrally coordinated by four sulfur atoms from the bridging TTC_2-TTF or TTC_3-TTF molecules to form coordination polymeric chains, Figure 1. **1** and **2** were doped with iodine to afford $\{[Cu(TTC_2\text{-}TTF)]BF_4\}(I_3)_{0.33}$ and $\{[Cu(TTC_3\text{-}TTF)]ClO_4\}(I_3)_{0.33}$, which exhibit conductivities of 2×10^{-5} and 4×10^{-5} Scm^{-1} at 25 °C for compacted pellets, respectively.

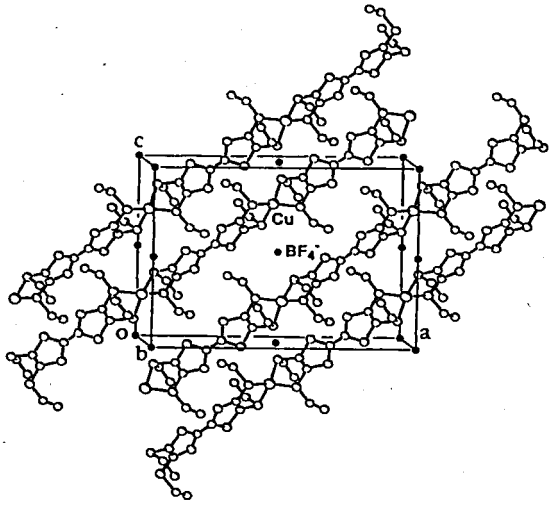

Figure 1. The structure of $[Cu(TTC_2\text{-}TTF)]BF_4$ (**1**).

VII-J-5 Two Types of New Polymeric Copper(I) Complexes of Pyrazinecarboxamide Having Channel and Helix Structures

Megumu MUNAKATA *([a]Kinki Univ. and IMS)*, **Liang Ping WU,[a] Takayoshi KURODA-SOWA,[a] Masahiko MAEKAWA,[a] Kazuma MORIWAKI[a] and Susumu KITAGAWA** *(Tokyo Metropolitan Univ.)*

[*Inorg. Chem.* in press]

This paper reports the syntheses and structures of two polymeric copper(I) complexes of 2-pyrazinecarboxamide, $[Cu_2(pzca)_3](ClO_4)_2(Me_2CO)_2$ (**1**) and $[Cu(pzca)(Me_2CO)_{0.5}](BF_4)$ (**2**). The complexes **1** and **2** form unusual channel and helical structures (Figure 1) based on the hexanuclear circular array of ligand-bridged Cu(I) ionsm, respectively that are of current interest in the design of synthetic, macroporous coordination solids.

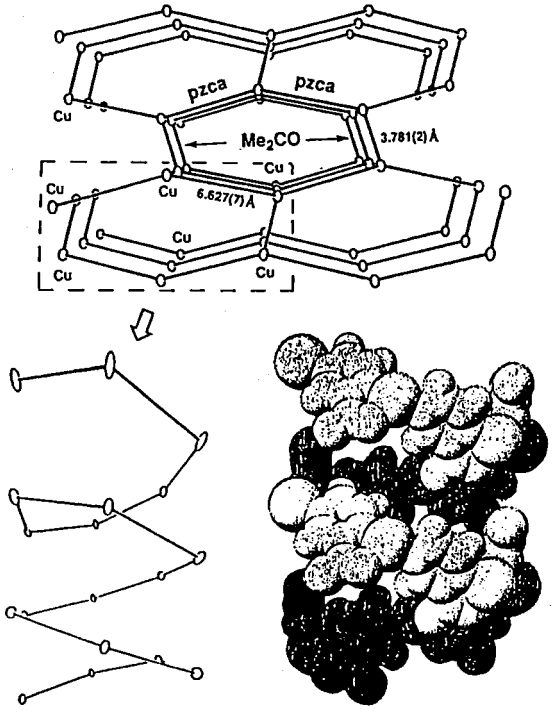

Figure 1. Helical cyclic array in $[Cu(pzca)(Me_2CO)_{0.5}](BF_4)$.

VII-J-6 A S···S Contact Assembled Tetranuclar Copper(I) Complex with Sulfur-Rich Ligand, 4,5-Ethylenedithio-1,3-dithiole-2-thione

Jie DAI,[a] Megumu MUNAKATA *([a]Kinki Univ. and IMS)*, **Liang Ping WU,[a] Takayoshi KURODA-SOWA[a] and Yusaku SUENAGA[a]**

[*Inorg. Chim. Acta* **258**, 65 (1997)]

In copper(I) complex with 4,5-ethylenedithio-1,3-dithiole-2-thione ($C_5H_4S_5$), $[Cu_4I_4(C_5H_4S_5)_4]$, the metal center is a stepped Cu_4I_4 core coordinated by two lig-

ands $C_5H_4S_5$ in different ways. One is bidentate coordinated through thiocarbonyl group and thioether group and the other is monodentate coordinated only through thiocarbonyl group. The Cu_4I_4 clusters are bridged by bidentate $C_5H_4S_5$ molecules to form one dimensional polymeric chains along c axis, and the chains further more form a three-dimensional network assembled by interchain S···S contacts, Figure 1. The shortest S···S contact distance is 3.257(2) Å.

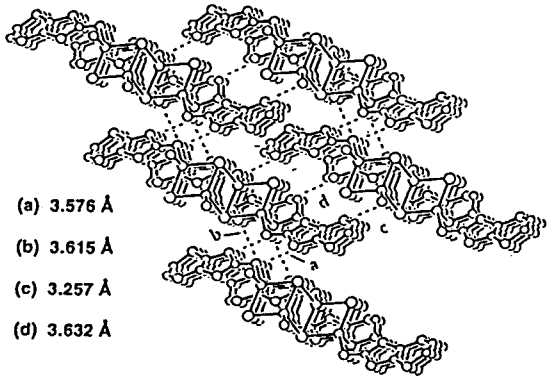

Figure 1. Top view of $[Cu_4I_4(C_5H_4S_5)_4]$ along coordination chains, showing a S····S contact network.

VII-J-7 Construction and Conductivity of W-Type Sandwich Silver(I) Polymers with Pyrene and Perylene

Megumu MUNAKATA *([a]Kinki Univ. and IMS)*, **Liang Ping WU,[a] Takayoshi KURODA-SOWA,[a] Masahiko MAEKAWA,[a] Yusaku SUENAGA[a] and Kunihisa SUGIMOTO[a]**

[*Inorg. Chem.* **31**, 4903 (1997)]

The first organosilver(I) compounds of pylene(pyr) and perylene(per) presented here, $[Ag_2(pyr)(ClO_4)_2]$ and orange prisms of $[Ag_2(per)(ClO_4)_2]$ exhibit an unusual tetra-η^2-coordination fashion bridging four metal centers leading to W-type sandwich polymeric chains and sheets, Figure 1. Both compounds irradiated with light or iodination show typical radical cation ESR signals.

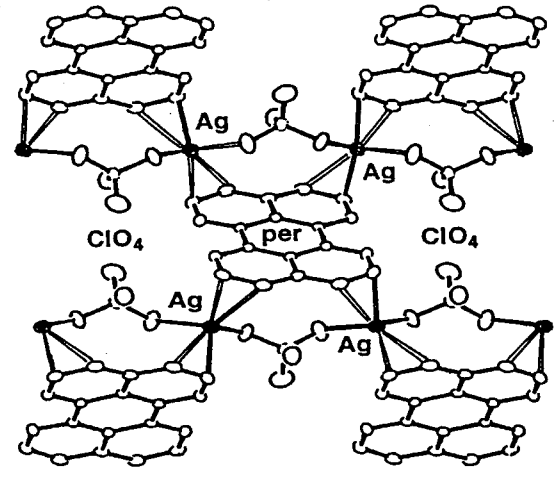

Figure 1. Portion of an infinite 2-D sheet framework in $[Ag_2(per)(ClO_4)_2]$.

VII-J-8 Synthesis and Structure of a Three-Dimensional Copper(II) Coordination Polymer with 1,2-Bis(imidazol-1'-yl)ethane

Liang Ping WU,[a] Yoshiro YAMAGIWA,[a] Takayoshi KURODA-SOWA,[a] Tadao KAMIKAWA[a] and Megumu MUNAKATA *([a]Kinki Univ. and IMS)*

[*Inorg. Chim. Acta* **256**, 155 (1997)]

The synthesis and characterization of the copper(II) complex $[Cu(bim)_{2.5}](ClO_4)_2 \cdot 2MeOH$ (bim = 1,2-bis(imidazol-1'-yl)ethane) is described. The complex contains non-interacting ClO_4^- anions and $\{[Cu(bim)_{2.5}]^{2+}\}_n$ macrocation in which each metal ion involves a distorted square-based pyramidal coordination environment comprising five N atoms from five separate bim molecules. The total structure consists of two alternately stacked 2-D sheets of copper(II) ions bridged through the bidentate imidazole molecules constituting a three-dimensional network (Figure 1).

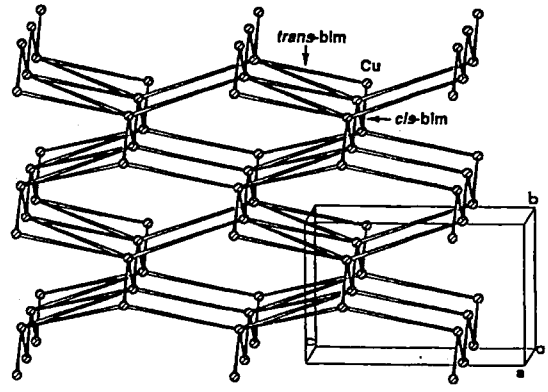

Scheme 1. Perspective view of the $[Cu(bim)_{2.5}]^{2+}$ cation. Circle, white and black rods represent the copper center, bim molecules of *trans* and *cis*-configurations, respectively.

VII-J-9 Crystal Engineering of Multidimensional Copper(I) and Silver(I) Coordination Supermolecules and Polymers with Functions

Megumu MUNAKATA *(Kinki Univ. and IMS)*, **Liang Ping WU** *(East China Normal Univ.)* **and Takayoshi KURODA-SOWA** *(Kinki Univ.)*

[*Bull. Chem. Soc. Jpn.* **70**, 1727 (1997)]

Considerable progress has been made in recent years in controlling the assembly and orientations of individual molecules to create specific aggregates. It is the aim of this review to give an account of the latest developments in our groups with regard to construction of functional crystal metal complex supermolecules from self-assembly of copper(I) and silver(I) coordination compounds by intermolecular interactions such as hydrogen bonding, aromatic stacking and S•••S contacts as well as coordination bonds, Figure 1.

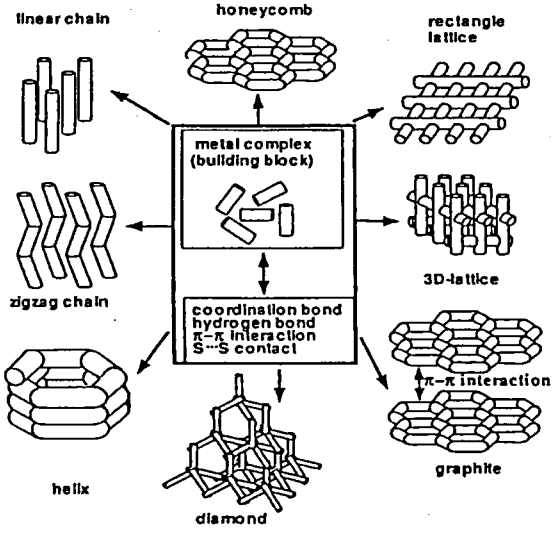

Figure 1. Metal complex supermolecules and polymers.

VII-J-10 The Solid and Solution Structures of Ternary Gold(I) Complexes with Triphenylphosphine and N- Ligands

Megumu MUNAKATA *([a]Kinki Univ. and IMS)*, **Sheng-Gang YAN,[a] Masahiko MAEKAWA,[a] Mamoru AKIYAMA[a] and Susumu KITAGAWA** *(Tokyo Metropolitan Univ.)*

[*J. Chem. Soc. Dalton Trans.* in press]

Twelve gold(I) complexes of $[Au(PPh_3)L]ClO_4$ (L= 2-(2'-pyridyl)benzimidazole and so on) were prepared and characterized. The gold(I) in the complexes is coordinated to one nitrogen atom and one phosphine atom. The most important feature is the preferential coordination of the imidazole group to Au(I) rather than the pyridine group, Figure 1. A rapid intramolecular exchange of coordination site of L to gold(I) was found from the ^1H NMR studies.

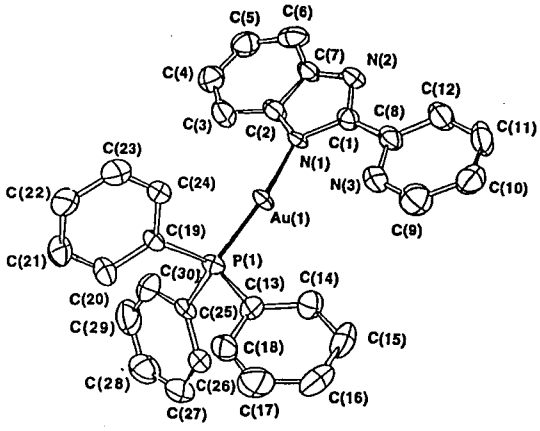

Figure 1. Molecular structure of $[Au(PPh_3)\{2\text{-}(2'\text{-pyridyl})benzimidazole\}]^+$

VII-K Interconversion between Monomeric and its Self-Assembled Oligomeric Metal Complexes

Self-assembly process involving metal ion has attracted much attentions. A feature of self-assembly is the use of modular building blocks which contains sufficient structural information to guide the self-assembly reaction. Metal ion together with ligand contains a variety of structural information to guide the self-assembly reaction. One of the recent interests of the filed of supramolecular chemistry is to design and synthesize supramolecules exhibiting switching ability, whose structure or/and physical and chemical properties change by an input of external information. A supramolecule reversibly interconverting between monomeric modular building block and self-assembled oligomer by an input of an external information would be of the utmost interest. The closest documented reactions which can be considered as interconversions of metal complexes between monomers and self-assembled oligomers are olation and oxolation reactions affording iso- or heteropolyanions. However, these reactions do not allow control of the nuclearity and structure of the generated oligomeric species as they involve only H_2O derived species as ligands. They generally afford several oligomeric species, the equilibrium between them being usually established very slowly (months). From the point of view, we have focused on metal complex with a multidentate ligand containing imidazole moiety, in which an interconversion between monomer and self-assembled oligomer or polymer is available depending on the pH. Such a complex exists as a monomer in the form of the protonated species under acidic condition, while under basic condition the generated imidazolate nitrogen atom can function as a ligand to another metal ion to produce imidazolate-bridged oligonuclear complex. There are many ways to control the characteristics in the self-assembly process. A choice of appropriate ligand framework or/and metal ion would produce a variety of self-assembled structures, because the ligand framework gives a steric restriction to the self-assembly structure and the metal ion gives another restriction due to its preferable coordination geometry. It is also expected that the construction and disconstruction process can be available, if the formation and cleavage of the metal-imidazolate nitrogen coordination-bond between adjacent units is possible depending on the pH.

VII-K-1 Proton-Dependent Monomer ↔ Oligomer Interconversion of Copper(II) Complexes with *N*-(2-Substituted-imidazol-4-ylmethylidene)-2-aminoethylpyridine (2-Substituent = Methyl and Phenyl)

Naohide MATSUMOTO *(Kumamoto Univ. and IMS)*, **Yuri MOTODA, Masaaki MIMURA** *(Kumamoto Univ.)*, **Toshio NAKASHIMA** *(Oita Univ.)*, **Francoise**

DAHAN and Jean-Pierre TUCHAGUES *(CNRS, Toulouse)*

The monomer ↔ oligomer switching of a metal complex is generated by proton abstraction/supply as a common external information input. The Cu(II) complexes with the chemical formula of $[CuCl_2(HL^n)]$ **1** and **2** have been prepared, where HL^n=*N*-(2-substituted-imidazol-4-ylmethylidene)-2-aminoethylpyridine and the 2-substituent is methyl and phenyl group for n=1 and 2, respectively. The protonated complexes **1** and **2** assume a penta-coordinated square pyramidal geometry with N_3Cl_2 donor atoms consisting of three nitrogen atoms of tridentate ligand and two chloride ions in the solid state, while in the aqueous solution the copper(II) ion assumes $[N_3(H_2O)]$ chromophere. When **1** and **2** was treated with an equimolar amount of sodium hydroxide or triethylamine, the deprotonation of the imidazole moiety motivates a self-assembly process, consisting of a formation of coordination bond of the imidazolate nitrogen atom to a copper(II) ion of adjacent modular unit, to give the self-assembled compounds **1'** and **2'**, respectively. The nuclearities of the self-assembly molecules and the detailed structures were confirmed to be imidazolate-bridged cyclic tetra- and hexa-nuclear structure for **1'** and **2'**, respectively, by the single-crystal X-ray analysis and the FABMS spectra. Variable-temperature magnetic susceptibility data are well reproduced using the Heisenberg model based on a cyclic tetranuclear structure for **1'** and a cyclic hexanuclear structure for **2'**, respectively. The reversible interconversion between the protonated monomeric and the deprotonated oligomeric species were confirmed by the pH-dependent potentiometric and electronic spectral titrations in the aqueous solutions.

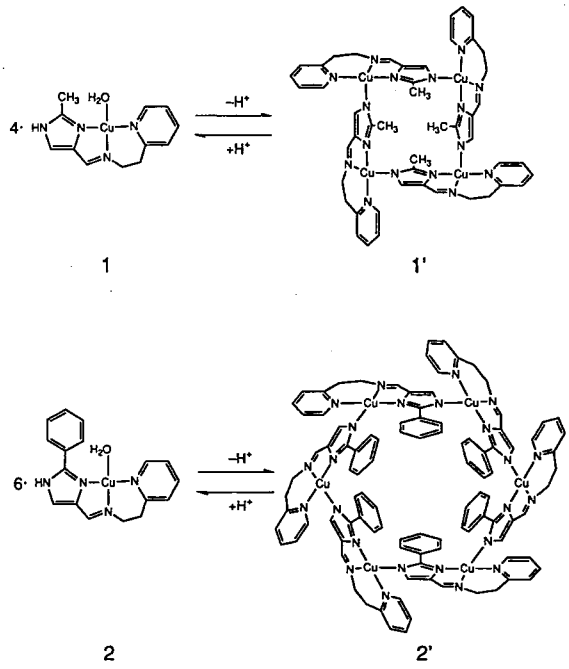

Scheme 1. pH-Dependent interconversion between protonated compound and self-assembled deprotonated compound. (top) monomer **1** ↔ tetramer **1'**, (bottom) monomer **2** ↔ hexamer **2'**.

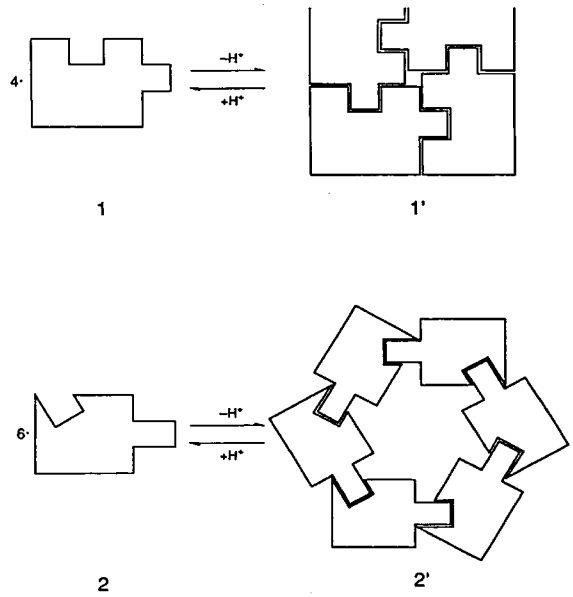

Scheme 2. Schematic illustration of self-assembly process for the formation of tetramer and hexamer from the modular building block.

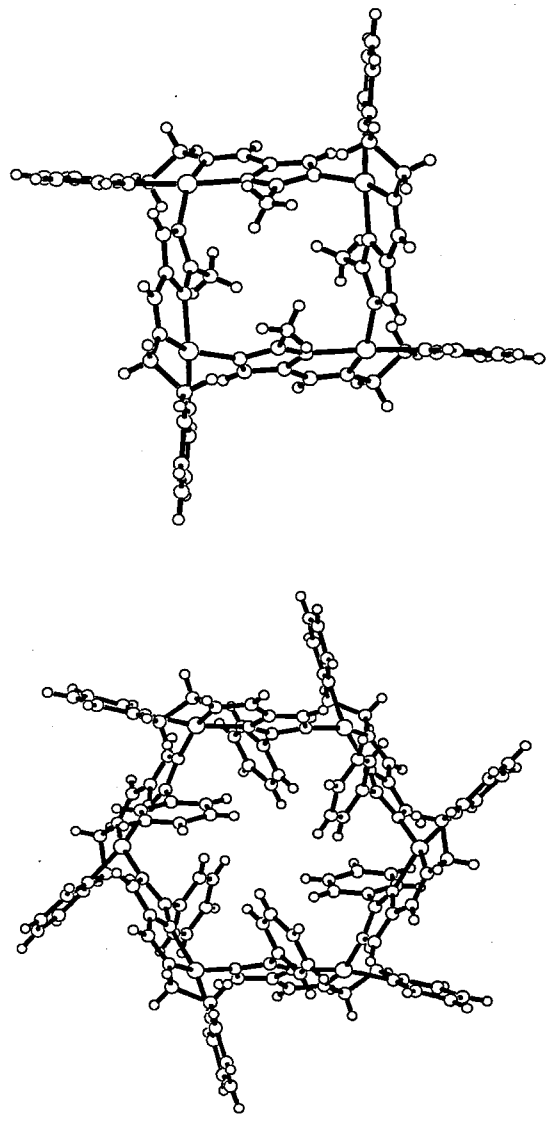

Figure 1. ORTEP drawings of a cyclic tetranuclear and hexanuclear copper(II) complexes

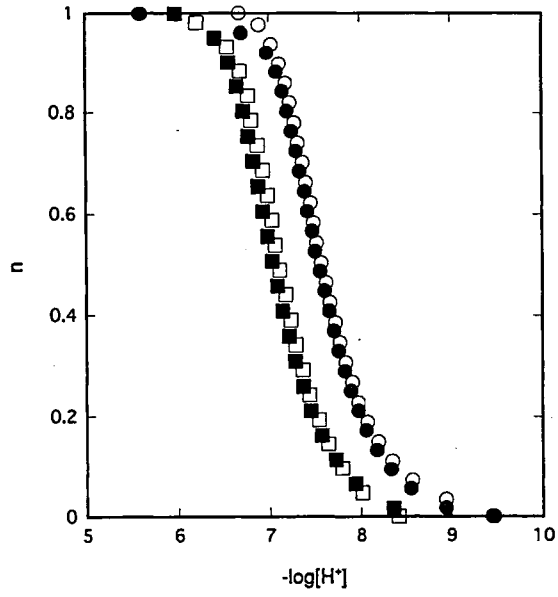

Figure 2. pH-Dependent potentiometric titration curves for the forward and reverse titrations of **1** and **2**, where a plot of the degree of proton association *n* vs. pH is given.

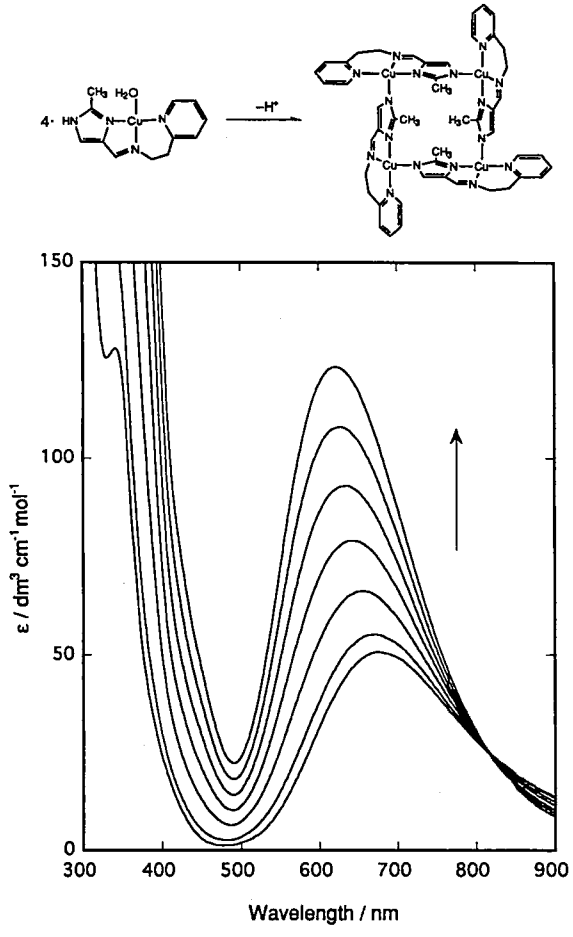

Figure 3. pH-Dependent electronic spectra of **1**. An aqueous solution of the protonated complex **1** (0.24 mmol in 80 ml water) was prepared. The spectrum was measured at every addition of 0.4 ml of 1 N NaOH solution to an aqueous solution of the protonated complex. The spectra were corrected by the volume due to the addition of 1 N NaOH solution.

VII-K-2 Steric-Hindrance Effect of a Substituent in the Self-Assembly Process of Copper(II) Complexes with Quadridentate Schiff-Base Ligands Involving a 2-Substituted-Imidazole Moiety

Naohide MATSUMOTO *(Kumamoto Univ. and IMS)*, **Masaaki MIMURA, Yukinari SUNATSUKI** *(Kumamoto Univ.)*, **Shingo EGUCHI, Yukiko MIZUGUCHI, Hitoshi MIYASAKA** *(Kyushu Univ.)* **and Toshio NAKASHIMA** *(Oita Univ.)*

Four copper(II) complexes with unsymmetrical quadridentate ligands involving an imidazole moiety, $[CuHL^n]ClO_4$ (**1-4**; n=1-4), have been prepared and characterized, where HL^1=*N*-salicylidene-*N'*-(2-methylimidazol-4-ylmethylidene)-1,3-propanediamine, HL^2=*N*-salicylidene-*N'*-(2-phenylimidazol-4-yl-methylidene)-1,3-propanediamine, HL^3=*N*-acetylacetonylidene-*N'*-(2-methylimidazol-4-ylmethylidene)ethylenediamine, HL^4=*N*-acetylacetonylidene-*N'*-(2-phenylimidazol-4-ylmethylidene)ethylenediamine, respectively. The corresponding deprotonated complexes **1'-4'** were obtained when **1-4** were treated under an alkaline condition. Deprotonation of the imidazole moiety of the copper(II) complex motivates a self-assembly process which is formed by an axial coordination of the imidazolate nitrogen atom of a molecular unit to the copper(II) ion of another unit. **1'-3'** assumes a self-assembled imidazolate-bridged infinite-chain structure $\{-Cu(II)-Im\}_n$ in the solid state, while the polymeric species dissociates to monomeric species in the solution state. **4'** consists of a discrete deprotonated monomeric species, even in the solid state. The physical measurements, including reflectance and absorption spectra, cryomagnetic measurements, and single-crystal X-ray analyses, revealed that the self-assembly behavior for the series of copper(II) complexes depends both on the steric effect of the substituent of 2-substituted-4-formylimidazole moiety and the ligand field strength of the equatorial quadridentate ligand.

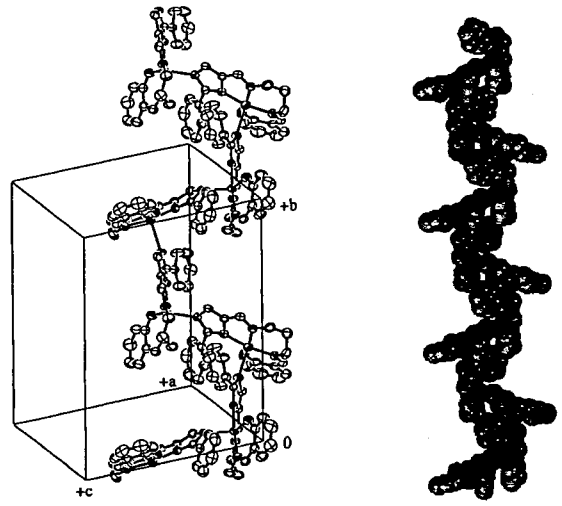

Figure 1. An one-dimensional helical structure of a deprotonated compound **2'** running along the b-axis. (a) ORTEP drawing, (b) space filling model

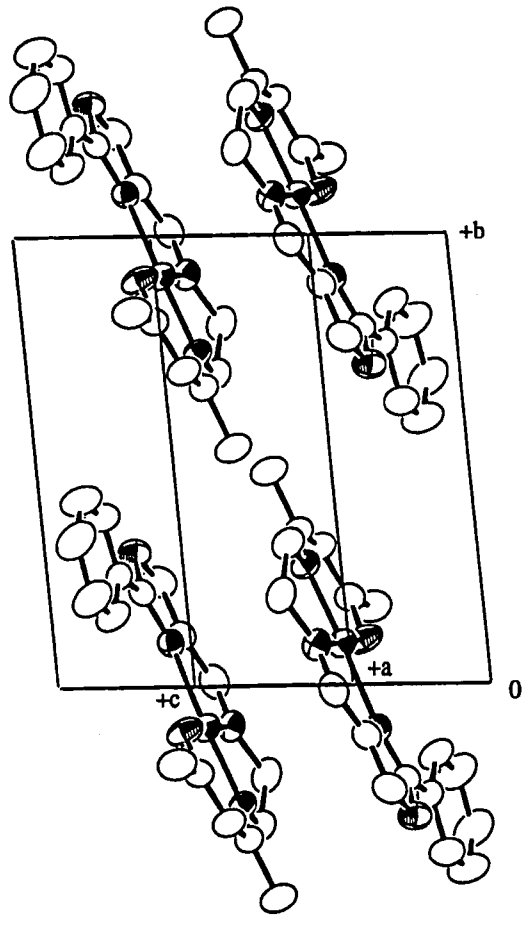

Figure 2. A packing diagram of a deprotonated compound **4'**, showing a parallel packing of the planar molecules and representing no intermolecular coordination bonding.

VII-K-3 Copper(II) Complexes of *N*, *N'*-Bis(2-substituted-imidazol-4-ylmethylene)-3, 3'-diaminodipropylamine (2-Substituent=H, Me): Δ and Λ Enantiomorphs of the Protonated Complex and Helical Structure of the Deprotonated Complex Formed by Hydrogen Bonds

Hitoshi MIYASAKA, Shingo OKAMURA *(Kyushu Univ.)*, **Toshio NAKASHIMA** *(Oita Univ.)* **and Naohide MATSUMOTO** *(Kumamoto Univ. and IMS)*

Copper(II) complexes with the quinquedentate ligands H_2L^n (n = 1, 2) of the 1:2 condensation products of 3, 3'-diaminodipropylamine and each of 4-formylimidazole and 4-formyl-2-methylimidazole have been synthesized and characterized, where the complexes have the general formula of $[Cu(H_2L^n)]X_2$ and are abbreviated as $\mathbf{1}\cdot X_2$, and $\mathbf{2}\cdot X_2$ (n = 1, 2 for 2-substituent = H, Me; X = ClO_4, NO_3, Cl). X-ray crystal structures of $\mathbf{1}\cdot(NO_3)_2$, and $\mathbf{2}\cdot(Cl)_2$ were determined: The complex assumes Δ or Λ enantiomorphs due to the spiral arrangement of the quinquedentate ligand around the copper(II) ion, and these Δ and Λ enantiomorphs of the cation for $\mathbf{1}\cdot(NO_3)_2$ and $\mathbf{2}\cdot(Cl)_2$ coexist as the racemic form in the crystals. When the protonated complexes were treated with NaOH, the deprotonated complexes with the formula $[CuHL^n]ClO_4$, $\mathbf{1'}\cdot ClO_4$ (n = 1) and $\mathbf{2'}\cdot ClO_4$ (n = 2), were obtained. The structures consist of an electronically monopositive copper(II) complex involving a deprotonated imidazolate moiety and a protonated imidazole moiety per molecular unit and a mononegative anion ClO_4^-, where an imidazolate nitrogen atom N(2) of the copper(II) complex is hydrogen bonded to the imidazole nitrogen atom N(6)* (* denotes the symmetry operation of 1/2+x, 1/2-y, -z) of the adjacent unit with the hydrogen bond distance of N(2)···N(6)* of 2.842(6) for $\mathbf{1'}\cdot ClO_4$ and 2.815(4) Å for $\mathbf{2'}\cdot ClO_4$ to give a one-dimensional helical structure running along the a-axis. Through the hydrogen bonds, the Δ isomer only aggregates with the Δ isomer and the Λ isomer only aggregates with the Λ isomer to give an extended helical chain structure described as ΔΔΔΔΔ... or ΛΛΛΛΛ..., respectively.

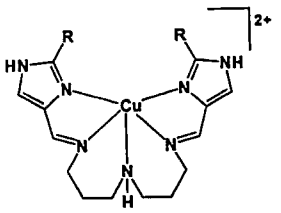

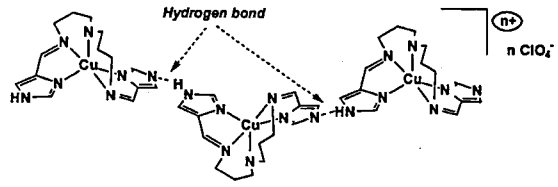

Scheme 1. Molecular structure of protonated compound and hydrogen-bonded structure of deprotonated compound.

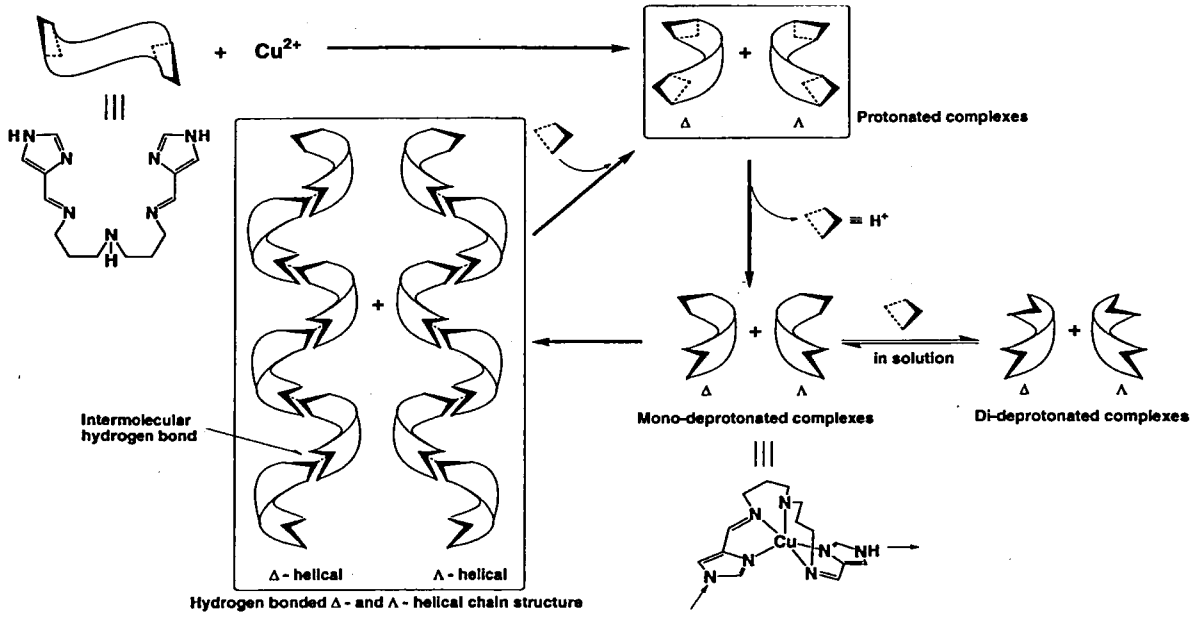

Scheme 2. Schematic representation of the formation of hydrogen-bonded helical chain structure.

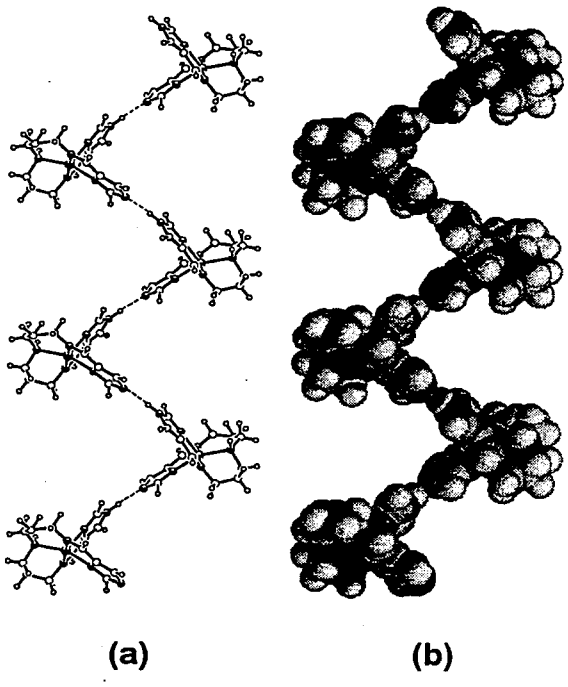

Figure 1. Hydrogen bonded helical chain structure of **1'**·ClO_4 (Λ-helical chain), which is made from Λ enantiomorph molecules, (a) the arrangement of spiral complexes where the dashed line exhibits the hydrogen bond, (b) space-filling representation.

VII-L Synthesis and Reactivity of Complexes Containing Peculiar Bonds between Transition Elements and Main Group Elements of Group 14

The bonds between transition elements and main group elements in the third and higher periods are attracting increasing attention in recent years. This is attributable not only to the great variety of the combination of elements but also to the peculiarity of their physical and chemical properties. We focused on transition metal complexes containing novel and peculiar bonds between transition elements and main group elements of group 14, particularly a multiple bond to a silicon atom. Some new silyl and silylene complexes were prepared and the reactivity of these complexes was investigated to gain a better understanding on the unsaturated bond systems involving silicon atoms.

VII-L-1 Iridium-Catalyzed Redistribution of Hydrodisilanes *via* a Silyl(silylene)iridium(III) Complex: Synthesis of a Donor-Stabilized Silyl(silylene)iridium(III) Complex

Masaaki OKAZAKI *(Tohoku Univ.)*, **Hiromi TOBITA** *(Tohoku Univ. and IMS)* **and Hiroshi OGINO** *(Tohoku Univ.)*

[*Chem. Lett.* 437 (1997)]

Reactions of an Ir(I) complex Ir{η^2-$Me_2Si(CH_2)_2PPh_2$}$(PMe_3)_3$ (**1**) with several hydrodisilanes have been investigated. Treatment of **1** with 1 equiv of $HSiMe_2SiMe_3$ at room temperature gave a hydrido(disilanyl)iridium(III) complex **2**. Complex **2** was then cleanly converted to **3** on heating in MeOH at 45 °C. A plausible mechanism involves the formation of silyl(silylene) complex **A** followed by the addition of MeOH to the Si=Ir double bond. The formation of silyl(silylene) complex was confirmed by the reaction of **1** with $HSiMe_2SiMe_2OMe$ at 45 °C. By this reaction, the silyl(silylene) intermediate was stabilized by the coordination of an internal donor, and bis(silylene) complex **4** was formed cleanly. Complex **4** is the first isolated bis(silylene) complex of a group 9 metal. Complex **1** can catalyze redistribution of substituents in hydrodisilanes. Thus, thermolysis of $HMePhSiSiMe_3$ in the presence of a catalytic amount of **1** resulted in the isomerization to give a mixture of $HMePhSiSiMe_3$ and $HMe_2SiSiMe_2Ph$ in the ratio of 2 : 3. The converse isomerization was also observed by the reaction of **1** with $HMe_2SiSiMe_2Ph$. This isomerization reaction can be explained by the mechanism involving silyl(silylene) complexes **B** and **C**, on which the 1,3-Me-shift occurs efficiently. In the reaction of **1** with $HMe(MeO)SiSiMe_3$, a similar 1,3-Me-shift occurs in the course of the reaction to give **4** cleanly.

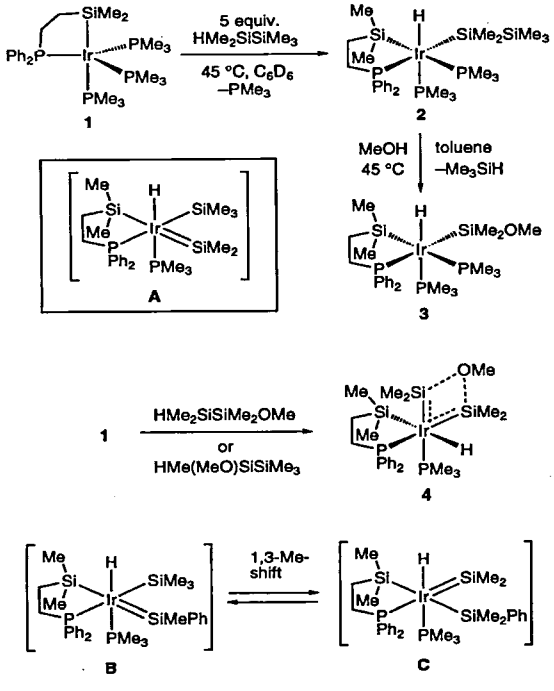

VII-L-2 Reactivity of a Donor-Stabilized Bis(silylene)ruthenium Complex toward Nucleophiles ROH (R = Me, H)

Hiroaki WADA *(Tohoku Univ.)*, **Hiromi TOBITA** *(Tohoku Univ. and IMS)* **and Hiroshi OGINO** *(Tohoku Univ.)*

[*Organometallics* **16**, 2200 (1997)]

The reactivity of a donor-stabilized bis(silylene)ruthenium complex $Cp(Ph_3P)Ru\{SiMe_2\cdots O(Me)\cdots SiMe_2\}$ (**1**) toward methanol and water has been investigated. Reaction of **1** with MeOH afforded an addition product *trans*-$Cp(Ph_3P)RuH(SiMe_2OMe)_2$ (**2**) in high yield. Complex **2** reacted further slowly with an excess of MeOH to give *trans*-$Cp(Ph_3P)Ru(H)_2(SiMe_2OMe)$ (**3**) and $Me_2Si(OMe)_2$. The reaction of **1** with MeOH is considered to be initiated by nucleophilic attack of MeOH at the strongly electrophilic silylene ligand. Thus, the slower rate of the reaction of MeOH with **2** compared to that with **1** indicates that the electrophilicity of a silyl ligand in **2** is lower than that of a slilylene ligand in **1**. In contrast, the reaction of **1** with H_2O yielded first the metallacycle *cis*-$Cp(Ph_3P)Ru(H)(\eta^2\text{-}SiMe_2OSiMe_2)$ (**4**), probably through the intramolecular condensation of $SiMe_2OH$ with $SiMe_2OMe$. Complex **4** was then converted to the tetrasiloxane complex *trans,trans*-$[Cp(Ph_3P)Ru(H)_2SiMe_2OSiMe_2]_2O$ (**5**) by the action of an excess of H_2O in DME. In a possible mechanism of the last reaction, the chelate ring of **4** is opened at the Ru-Si bond by the nucleophilic attack of H_2O to form $Cp(Ph_3P)Ru(H)_2SiMe_2OSiMe_2OH$, which then undergoes condensation with dehydration to give **5**. These results indicate that the silylene ligands of **1** is extremely electrophilic and readily attacked even by a weak nucleophile such as methanol or water.

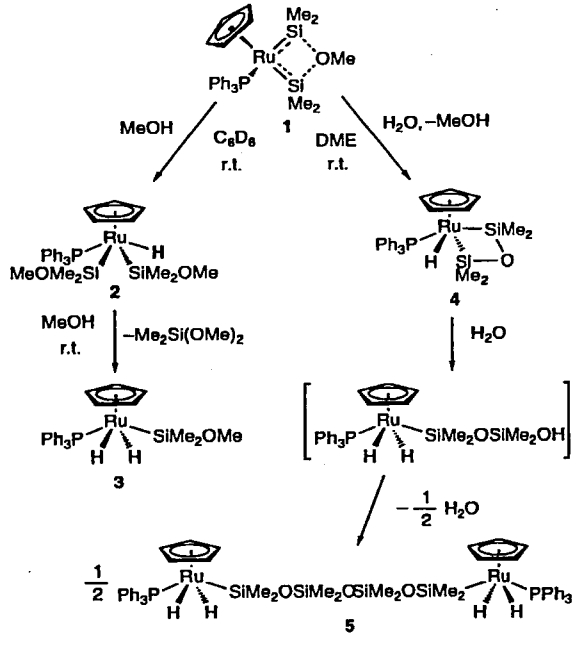

VII-L-3 Reaction of Silyl(carbonyl)iron Complexes with $LiAlH_4$ Giving Methylsilanes: Reduction of a Carbonyl Ligand and Coupling with a Silyl Group

Hiromi TOBITA *(Tohoku Univ. and IMS)*, **Rie SHIOZAWA and Hiroshi OGINO** *(Tohoku Univ.)*

[*Chem. Lett.* 805 (1997)]

We found that the reaction of $LiAlH_4$ with some silyl(carbonyl)iron complexes resulted in the formation of methylsilanes through the reduction of a carbonyl l igand followed by coupling with the silyl group. Thus, treatment of $FpSi(p\text{-Tol})_2H$ (Fp = $CpFe(CO)_2$) with $LiAlH_4$ in ether at room temperature afforded $CH_3Si(p\text{-Tol})_2H$ in 73% yield. Interestingly, the reaction of $FpSi(p\text{-Tol})_2H$ with $LiAlD_4$ exclusively produced $CHD_2Si(p\text{-Tol})_2D$, which was characterized by the ^1H NMR spectrum showing the Si-CHD_2 signal at 0.51 ppm as a quintet ($^2J_{HD}$ = 2.0 Hz) and the mass spectrum giving the molecular ion peak at *m/z* 229. The conversion of a carbonyl ligand in $FpSi(p\text{-Tol})_2H$ into a methyl group in $CH_3Si(p\text{-Tol})_2H$ was further confirmed by the ^{13}C labeling experiments: Reaction of $FpSi(p\text{-Tol})_2H$ enriched with ^{13}CO to 32% with $LiAlH_4$ afforded $*CH_3Si(p\text{-Tol})_2H$ in which the methyl carbon was enriched with ^{13}C. The reaction of silyl complexes without Si-H bonds, namely $FpSiR_3$ (R_3 = $(p\text{-Tol})_2Me$, MePh(1-naphthyl)), with $LiAlH_4$ gave CH_3SiR_3 as a major product, but, in these cases, the simple reduction product $HSiR_3$ was also formed. The NMR tube reaction of $FpSi(p\text{-Tol})_2H$ with $LiAlH_4$ in THF-d_8 showed the formation of an anionic species $[CpFe(CO)(CH_3)Si(p\text{-Tol})_2H]^-$ as a main product besides $CH_3Si(p\text{-Tol})_2H$. Interestingly, even on heating the reaction mixture to the boiling point of THF-d_8, the conversion of the anionic species to $CH_3Si(p\text{-Tol})_2H$ was not observed.

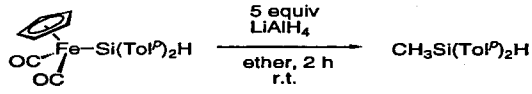

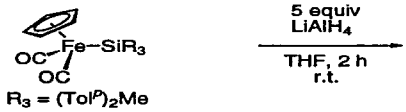

CH_3SiR_3		$HSiR_3$
64 %:	$R_3 = (Tol^p)_2Me$	32 %
26 %:	R_3 = MePh(1-Nap)	26 %

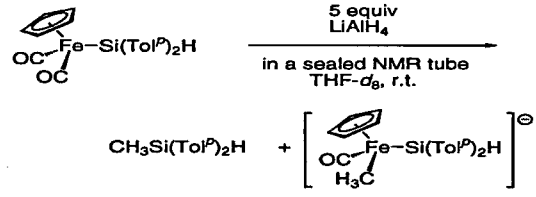

RESEARCH ACTIVITIES VIII
Computer Center

VIII-A Theoretical Studies of Highly Excited Vibrational States in Polyatomic Molecules

VIII-A-1 Theoretical Study of the Photodissociation Dynamics of OCS

Shinkoh NANBU, Hideki KATAYANAGI Toshinori SUZUKI and Mutsumi AOYAGI

Carbonyl sulfide (OCS) has the broad absorption band at wavelengths in the range 250~200nm (4.95 eV~6.1 eV). Due to the photoabsorption, OCS dissociates into CO + S. Houston et al. measured the internal energy distributions of the CO product, and reported as follows; the CO product was rotationally excited up to the rotational quantum number J_{co}=75, while the vibration was not excited by the photodissociation. Suzuki's group in IMS has measured the velocity and angular distribution of the fragment Sulfur atom by the ion imaging method. The results show that the dissociation occurs via two major channels, and both of these processes produce the asymptotic states in A' and A" symmetry. In the present work, the potential energy surfaces of the low-lying electronically excited states are calculated using the *ab initio* molecular orbital (MO) configuration interaction (CI) method. The photodissociation dynamics for OCS + hν→ CO + S are investigated by performing time-dependent quantum dynamical calculations on these surfaces. Our results show that the non-adiabatic transition between 1^1A' and 2^1A' states takes an important role in determining the rotational distribution of the CO product.

VIII-A-2 Semiclassical Study of Avoided Crossing

Toshiya TAKAMI

We study nonadiabatic process in classically nonintegrable systems such as 2D billiards and kicked rotators to reveal essence of the dynamical characters in the highly excited states of molecules. One of the typical character in the nonintegrable systems is avoided crossings between adiabatic levels. Nonadiabatic transition between adjacent states, which was described first by Landau and Zener, etc., is one of the well-known quantum processes in molecular systems. In the highly excited states of nonintegrable systems, however, it is difficult to predict the final state semilcassically, because each eigenlevels around the initial state can be a final state of the transition.

Our approach to this problem is twofold: (1) to study statistical properties of the transition by quantum mechanical calculations; (2) to analyze the interaction between adiabatic states by classical information such as periodic-orbit scars.

VIII-A-3 Theoretical Study of the Potential Energy Surfaces and Dynamics of CaNC/CaCN

Shinkoh NANBU, Satoshi MINAMINO and Mutsumi AOYAGI

[*J. Chem. Phys.* **106**, 8073 (1997)]

Potential energy surfaces for electronic ground and two low-lying excited states of CaNC/CaCN, were obtained by the ab initio molecular orbital (MO) configuration interaction (CI) calculations. On the obtained potential energy surfaces the wave packet dynamics for the nuclear motion were carried out to estimate the theoretical absorption and emission spectra.

We found that the stational structures of the $1^2\Sigma^+$ and $1^2\Pi$ states are linear conformation of calcium isocyanide (CaNC). And also these two states are characterized by ionic bonding and especially the potential energy along the bending coordinate are isotropic. In this study by using the wave packet propagation, we demonstrate the possibility of the large amplitude motion related to pseudorotational motion which could be seen as Ca^+ rotating around CN^- in the bending vibration. The estimated theoretical spectra reproduce the feature of experimental ones.

VIII-A-4 Theoretical Study of Elementary Reactions Relevant to Low-Temperature Silane Oxidation

Shigeo KONDO *(Nat. Inst. Materials and Chemical Research)*, **Satoshi MINAMINO and Mutsumi AOYAGI**

[*J. Phy.Chem. A* **101**, 6015 (1997)]

Ab initio G-2 calculations have been carried out for a number of elementary reactions relevant to low-temperature silane oxidation. The calculations have been made to identify the chain-branching process which enables the spontaneous ignition of silane at room temperature. Extensive calculations have also been performed for the reactions of major intermediates with hydrogen atoms and water vapor.

VIII-A-5 Theoretical Study of Reaction Rate Constant of Hydrofluorocarbon

Satoshi MINAMINO and Mutsumi AOYAGI

Hydrofluorocarbon(HFC) is recently the focus of the attention of the world as one of the alternatives for Chlorofluorocarbon(CFC). The study of the reaction of HFC with OH radical is also very important in

atmospheric chemistry. The reaction path and the rate constant of the H-abstraction reactions of fluoromethane and fluoroethane by OH radical are determined by using ab initio methods and variational transition state theory. Structures and harmonic frequencies of these reactions were determined by MP2 method with 6-311++G** basis sets. The activation energies were calculated by MP4(SDTQ)/6-311++G**. Zero curvature(ZC) and small curvature(SC) approximations together with a simple Wigner treatment were employed in order to understand the effect of a quantum mechanical tunneling and the effect of reaction path curvature through the H-abstraction.

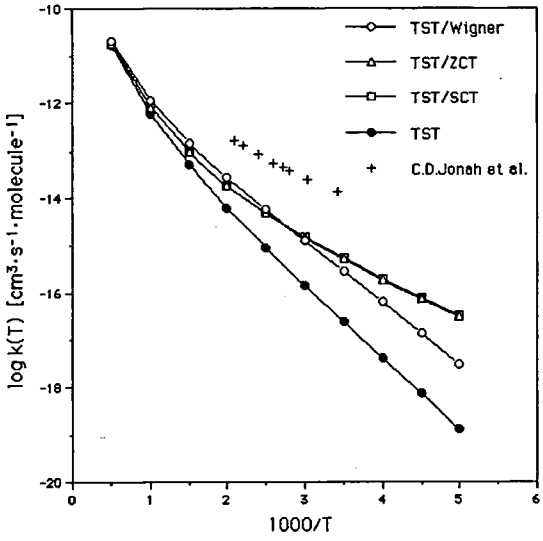

Figure 1. Calculated rate constants of CH_3F + OH reaction

Laser Research Center for Molecular Science

VIII-B Developments and Researches of New Laser Materials

Although development of lasers is remarkable, there are no lasers which lase in ultraviolet and far infrared regions. However, it is expected that these kinds of lasers break out a great revolution in not only the molecular science but also in the industrial world.

In this project we research characters of new materials for ultraviolet and far infrared lasers, and develop new lasers by using these laser materials.

VIII-B-1 Nanosecond Pump-and-Probe Study of Wurtzite GaN

Takashi AZUHATA, Hideyuki OHTAKE, Nobuhiko SARUKURA, Takahiro DEGUCHI *(Waseda Univ.)*, **Takayuki SOTA** *(Waseda Univ.)*, **Shigefusa CHICHIBU** *(Science Univ. of Tokyo)* **and Shuji NAKAMURA** *(Nichia Chemical Industries Ltd.)*

GaN is one of wide-bandgap semiconductors. Blue and green superbright light emitting diodes and purplish-blue continuous wave laser diodes are based on this material. We have performed a nanosecond pump-and-probe optical study of wurtzite GaN under the excitation condition that the carrier-longitudinal optical phonon scattering does not contribute to the energy relaxation process. Figure 1 shows transmission spectra for various delay time, τ_D. The delay time after which the isothermal condition is achieved is found to be about 50 ns. This comes from both the phonon structure in GaN and the fact that the carrier cooling depends on excess kinetic energies of carriers.

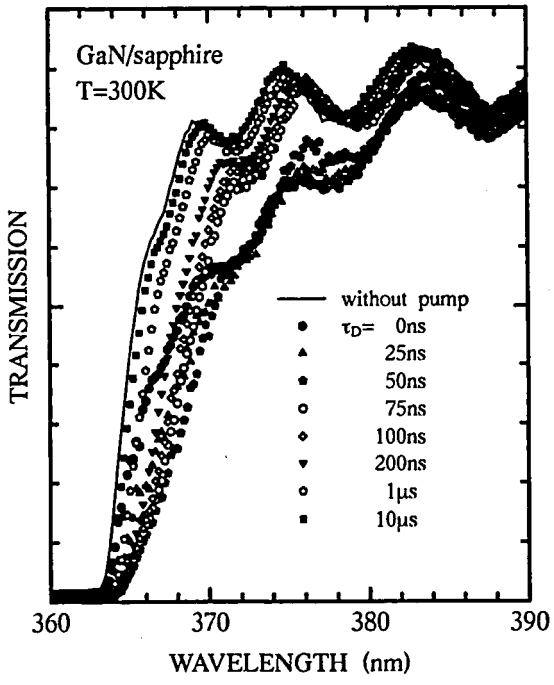

Figure 1. Transmission spectra of wurtzite GaN for various delay time, τ_D.

VIII-B-2 14-mJ Ultraviolet Short Pulses from an All-Solid-State Ce:LiCaF Master Oscillator and Power Amplifier System

Zhenlin LIU, Hideyuki OHTAKE, Nobuhiko SARUKURA, Mark A. DUBINSKII *(Wright lab., USA)*, **Vadim V. SEMASHKO** *(Kazan State Univ., Russia)*, **A. K. NAUMOV** *(Kazan State Univ., Russia)*, **Stella L. KORABLEVA** *(Kazan State Univ., Russia)* **and Ravil Yu. ABDULSABIROV** *(Kazan State Univ., Russia)*

There have been a few short-pulse works done with solid-state tunable UV-laser materials such as Ce^{3+} ion activated $LuLiF_4$ (LLF), $LiCaAlF_6$ (LiCAF), and $LiSrAlF_6$ (LiSAF) crystals. The fluorescence lifetime of Ce:LiCAF was reported to be 30 nsec, which is too short for constructing regenerative amplifiers, however, it is long enough for designing multi-pass amplifiers. The experimental setup of the Ce:LiCAF master oscillator and power amplifier (MOPA) is shown in Figure 1. A single 1-mJ, 1.0-nsec pulse at 289-nm was obtained from the low-Q, short cavity Ce:LiCAF master oscillator with pumping energy of 15 mJ. The amplifier consisted of a gain medium located at the beam waist of a confocal lens pair and a roof-reflector with dielectric coating for a small vertical displacement of each pass. The pumping source of the amplifier was another 10-nsec, Q-switched Nd:YAG laser operated synchronously to the Nd:YAG laser for pumping the oscillator. 266-nm pulses with 46-mJ and 34-mJ energies from each side were weakly focused. The 1-mJ input pulse was amplified up to 14-mJ, and the pulse duration of the amplified pulse was still 1.0 nsec.

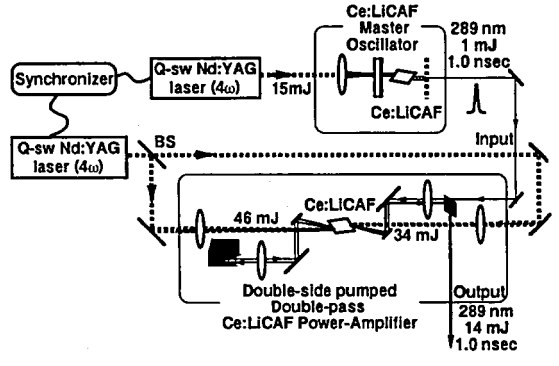

Figure 1. Experimental setup of Ce:LiCAF MOPA system.

VIII-B-3 High Average Power THz-Radiation from Femtosecond-Laser Irradiated InAs in a

Magnetic Field and Its Elliptical Polarization Characteristics

Hideyuki OHTAKE, Shinji IZUMIDA, Zhenlin LIU and Nobuhiko SARUKURA

The THz-radiation power from bulk InAs irradiated with femtosecond optical pulses is significantly enhanced and reaches 650 μW in a 1.7-T magnetic field with 1.5-W excitation power. This is the highest average power ever achieved in THz radiation at around a 100-MHz repetition rate. A 200-μW average power was obtained even using a compact 1-T permanent magnet. The THz-radiation power is related almost quadratically both to the magnetic field and excitation laser power. We have also found that the power of the THz radiation from an InAs sample in a magnetic field is over one order of magnitude higher than that from non-doped GaAs with a (100) surface in the same conditions. Figure 1 shows Magnetic field dependence of THz-radiation power. THz radiation from InAs (squares) increases dramatically as magnetic field increses. Additionally, we found a dramatic change of ellipticity, and the spectra of the horizontal and vertical polarization components are different.

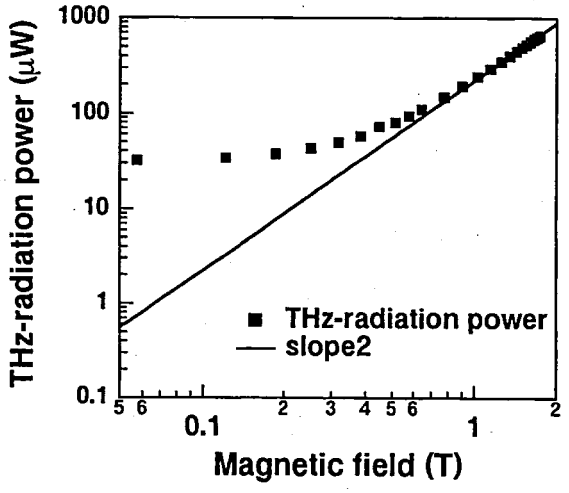

Figure 1. Magnetic field dependence of THz-radiation power. THz radiation from InAs (squares) increases dramatically as magnetic field increases. The solid line indicates slope 2.

Research Center for Molecular Materials

VIII-C Preparation and Properties of Novel Heterocyclic Compounds for Advanced Materials

Heterocycles containing chalcogen atoms are useful as components of organic conductors since heteroatoms in their rings are helpful to stabilize ions or ion-radical species, and extended π-conjugation decreases Coulombic repulsion. In addition intermolecular interactions caused by heteroatom contacts can be expected to form unique molecular assemblies. In this project novel electron acceptors, donors, and donor-acceptor compounds based on heterocycles such as 1,2,5-thiadiazole and 1,3-dithiole were synthesized and their properties including those of the charge-transfer complexes or ion-radical salts were investigated. Thiophene derivatives with fused heterocycles were also synthesized and led to new types of oligomers and polymers having narrow bandgaps.

VIII-C-1 Unusual Cation Radical Salts of Non-Planar Bis(1,3-dithiole) Donors Incorporating Solvent Molecules

Yoshiro YAMASHITA, Masaaki TOMURA and Kenichi IMAEDA

[*Chem. Commun.* 2021 (1996)]

Organic conductors are usually obtained from planar molecules showing multi-redox properties. For the non-planar molecules, ion radical states are in general unstable due to the limited conjugation, and two-electron redox is often observed. We recently prepared non-planar bis(1,3-dithiole) donor **1d** which gave metallic cation radical salts. In an extension of that work, we have now found that donors **1a-c** showing two-electron oxidation at one stage afforded cation radical salts incorporating solvent molecules. The cation radical salts of **1a-c** were isolated as single crystals when they were electrochemically oxidized in the presence of Bu_4NBF_4 in tetrahydrofuran (THF). The composition of the salts of **1b** and **1c** was 2:1:1 (donor:PF_6:THF), while **1a** gave a salt with a ratio of 1:1:1. The salt of **1c** showed a metallic temperature dependence of conductivity down to 180 K. Next the included THF molecule was replaced by 2,5-dihydrofuran (DHF) or 1,3-dioxolane (DO) to examine the effect of the included molecules. The room temperature conductivities of the DHF and DO included salts were the same as that of the THF one. However, they showed semiconducting behaviour with the different activation energies (0.19 eV for the DHF salt and 0.03 for the DO one). Therefore, the stability of the metallic state decreases in the included solvent order: THF < DO < DHF.

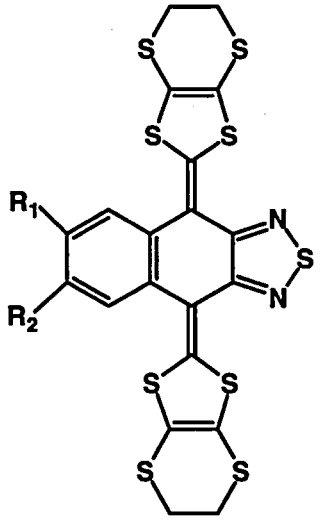

a $R_1 = R_2 = H$
b $R_1 = Me$, $R_2 = H$
c $R_1 = R_2 = Me$
d R_1, R_2 = benzo

1

VIII-C-2 Crystal Structure of Cation Radical Salts of Non-Planar Bis(1,3-dithiole) Donors

Masaaki TOMURA, Shoji TANAKA and Yoshiro YAMASHITA

Crystal structures of the PF_6 salts of non-planar bis(1,3-dithiole) donor **1**, which contain one solvent molecule [tetrahydrofuran (THF), 2,5-dihydrofuran (DHF) or 1,3-dioxolane (DO)], were investigated at room temperature and 150 K by an X-ray crystallographic analysis. The structures of $(\mathbf{1})_2(PF_6)$(THF), $(\mathbf{1})_2(PF_6)$(DHF) and $(\mathbf{1})_2(PF_6)$(DO) were isomorphous, and the cell parameters are very similar to each other. The calculation of overlap integral indicates that these salts have a two-dimensional property, as shown in Figure 1. In the crystal structures, no distinctive difference except for the part of the incorporated solvent was observed. The incorporated solvent molecules were located on the inversion center of the crystal, so that they were crystallographically disordered. Moreover, the conformational disordering of the THF molecule was observed at room temperature. Below the temperature of the metal-semiconductor transition (180 K), the cell volume of $(\mathbf{1})_2(PF_6)$(THF) was decreased by 4%. The values of overlap integrals ($\times 10^{-3}$) were changed to A = 3.64, p = 0.84 and q = -2.33. The disorder of the THF molecule

except for crystallographical one was extremely decreased at 150 K. These facts suggest that the solvent effect for the conducting property of $(\mathbf{1})_2(PF_6)$(solv) salt may be related to the ordering of the incorporated solvent molecules.

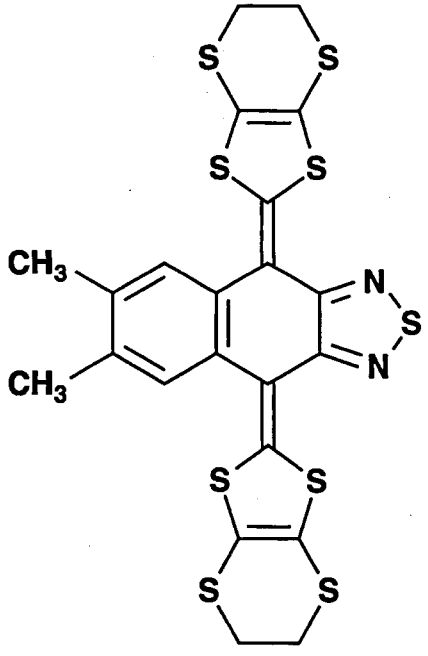

1

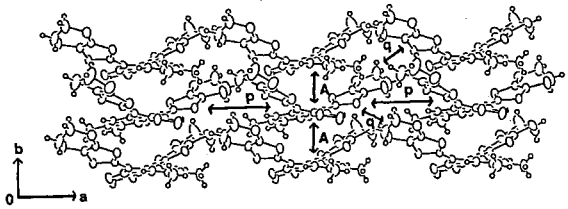

	THF	DHF	DOL
A	4.11	3.65	3.43
p	0.73	0.72	0.77
q	-2.45	-2.14	-2.12

Figure 1. Overlap integrals ($\times 10^{-3}$) for $(\mathbf{1})_2(PF_6)$(solv).

VIII-C-3 Novel Bis(1,3-dithiole) Electron Donors by Oxidative Intramolecular Cyclization of 2,2'-Bis(1,4-dithiafulven-6-yl)-3,3'-bithienyls

Akira OHTA and Yoshiro YAMASHITA

[*Mol. Cryst. Liq. Cryst.* **296**, 1 (1997)]

2,2'-Bis(1,4-dithiafulven-6-yl)-3,3'-bithienyls **1** were prepared by using either a Wittig or a Wittig-Horner reaction. The cyclic voltammograms of **1** revealed that they undergo an intramolecular cyclization by electrochemical oxidation. Chemical oxidation of **1** with tris(4-bromophenyl)aminium hexachloroantimonate gave intramolecular cyclization products **2** as dication salts. The hexachloroantimonate ion was found to act as an oxidizing agent in the reaction. Chemical reduction of the dication salts with zinc afforded the corresponding neutral bis(1,3-dithiole) donors **3** in high yields. The cyclic voltammograms of **3** showed reversible one-stage two-electron oxidation waves, and the potentials are fairly low. A conductive TCNQ complex was formed from one of them. X-ray analyses of the neutral and dication states of the donor show that there is a large conformational change between them. In contrast to the neutral molecule, in the dication the two 1,3-dithiole rings are almost orthogonal to the completely planar tricyclic system.

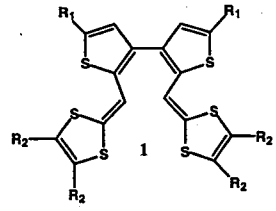

a; R_1 = H, R_2 = SMe
b; R_1 = H, R_2 = benzo
c; R_1 = Me, R_2 = H
d; R_1 = Me, R_2 = SMe
e; R_1 = Me, R_2 = benzo

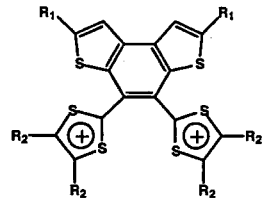

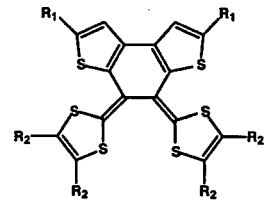

VIII-C-4 Preparation, Properties, and Oxidation of Novel Bis(1,3-dithiole) Compounds Containing a Di(2-thienyl)methane Unit

Akira OHTA and Yoshiro YAMASHITA

[*Heterocycles* **44**, 263 (1997)]

Novel bis(1,3-dithiole) compounds **1** and **2** containing a di(2-thienyl)methane unit have been prepared by either a Wittig or a Wittig-Horner reaction. These compounds showed irreversible cyclic voltammetric behavior. Oxidation products of **1** and **2** were strongly dependent on the substituents (R_1) on the C6-carbon atoms of the 1,4-dithiafulvenyl groups. In the case of R_1 = H (**1**), intermolecular coupling giving a redox-active oligomer took place. On the other hand, compounds **2** containing methyl substituents underwent deprotonation by oxidation to give the corresponding dithienylmethyl cations **4** which were also obtained by hydride abstruction of **2** with trityl tetrafluoroborate in dichloromethane. The cations show intense absorptions in the near-infrared region (> 900 nm in MeCN). The alkylthio groups on the 1,3-dithiole rings make the absorptions much red-shifted. The cation **3b** was prepared by the hydride abstruction method. The single crystal was obtained by recrystallization from acetonitrile. X-ray structure analysis revealed that the thienyldithiafulvenyl skeleton is almost planar and the bond alternation is decreased, indicating the polymethine cyanine-like structure of the cation. The cations form a dimer which is connected by the

counteranion BF_4^- with short F···H contacts to construct a ladder-like network.

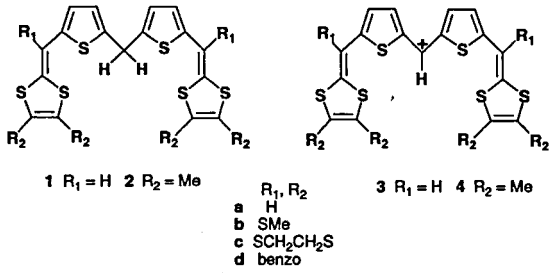

VIII-C-5 Synthesis and Reactions of 3,3'-Dibromodihydrodipyrrins

Chitoshi KITAMURA and Yoshiro YAMASHITA

[*J. Chem. Soc. Perkin Trans.* **1**, 1443 (1997)]

Most of the porphyrins prepared so far are meso-substituted compounds and β-substituted meso-non-substituted porphyrins have been rarely reported. We have now attempted to synthesize β-bromoporphyrin **1** using the reaction of dihydrodipyrrins **2** and **3**. The dibromodihydrodipyrrin diester **4** was first prepared by reaction of the corresponding pyrrole **5** with dimethoxymethane and BF_3·Et_2O. Subsequently **4** was converted to **2** in moderate yield. The diformyldihydrodipyrrin **3** was readily prepared by methylation of the pyrrole **6** with BF_3·Et_2O, followed by deprotection. Attempted synthesis of the porphyrin **1** from **2** and **3** has been unsuccessful because of the low reactivity of **2**. The reaction of **4** with hexabutylditin in the presence of a Pd catalyst produced a new type of tin complex **7** in low yield. This complex was also obtained by an alternative procedure in high yield and found to revert to **4** upon reaction with TFA.

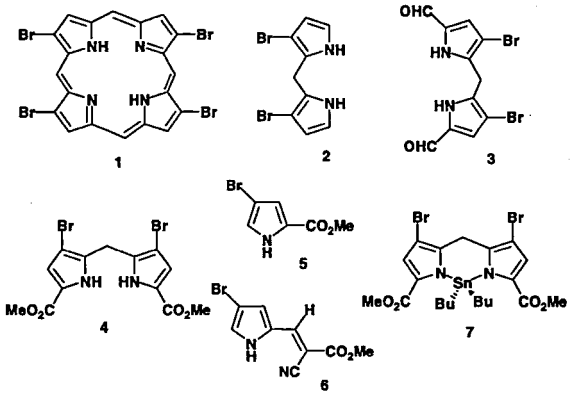

VIII-C-6 Synthesis and Properties of Benzobis(thiadiazole)s with Nonclassical π-Electron Ring Systems

Yoshiro YAMASHITA, Katsuhiko ONO, Masaaki TOMURA and Shoji TANAKA

[*Tetrahedron* **53**, 10169 (1997)]

Benzo[1,2-c:4,5-c']bis([1,2,5]thiadiazole) (**1a**) containing a hypervalent sulfur atom has a low LUMO level. The several derivatives **1b-g** were prepared here. The synthesis of the aryl derivatives were accomplished by using a Stille coupling reaction. The selenadiazole analogues were also synthesized. The electron accepting properties of these nonclassical heterocycles were shown by their high reduction potentials. The reduction potential of the dibromo derivative **1b** is comparable to that of *p*-benzoquinone. Introduction of electron-donating groups into the electron-withdrawing heterocycle afforded novel donor-acceptor compounds. Their cyclic voltammograms show that they are easily both oxidized and reduced. The amino derivatives **1d** and **1f** have the absorption maxima above 700 nm due to the small HOMO-LUMO separation. X-ray structure analysis of the diphenyl derivative **1c** revealed the formation of a tape-like network through short S···N contacts as shown in Figure 1.

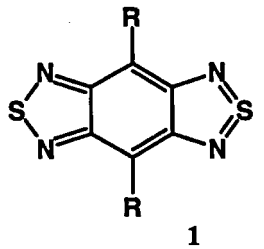

1

a: R = H
b: R = Br
c: R = Ph
d: R = *p*-$Me_2NC_6H_4$
e: R = 2,4-$(MeO)_2C_6H_3$
f: R = 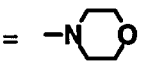
g: R = SPh

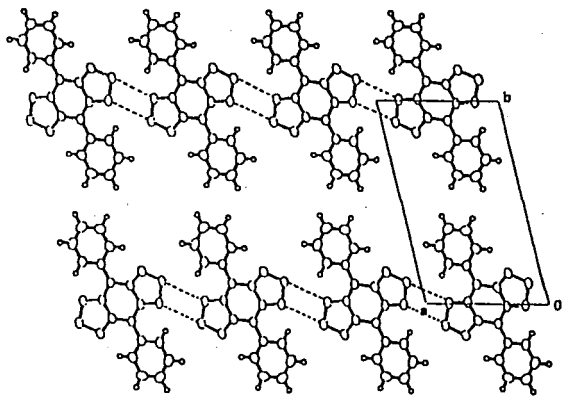

Figure 1. Crystal structure of **1c**, broken line S···N contacts (3.26Å).

VIII-C-7 A Novel Building Unit for Single Molecular Wires Based on *N*-Silylated Diaminothiophene

Shoji TANAKA and Yoshiro YAMASHITA

Single molecular wires (**SMWs**) will be the key components to construct electronic devices operating at the molecular level. The molecular-scale electronic wires can be viewed as one-dimensional conjugated systems with precisely defined backbone consisting of various type of functional units (donor/acceptor sites, multi-stage redox centers, and photoactive sites). In addition, **SMWs** should be surrounded by an insulating mantle to prevent unfavorable inter-chain hopping of the charge carriers. Here we describe a *N*-silyl-

protected 3',4',3",4"-tetraamino-2,2':5',5":2",2"'-quaterthiophene **1** as a promising building block for SMWs.

The result of X-ray structure analysis and the spectral data reveal that compound **1** has a high degree of coplanarity of the main chain both in solid state and in solution, in spite of the head-to-head orientation of the inner thiophene units possessing very bulky substituents. To get insights into this unique substituent effect, we carried out the conformation analyses using the AM1 method on the model system **1'** (Figure 1). The results elucidate that the main steric effect of the *N*-silyl substituents on the chain conformations is the selective stabilization of the *s-trans* coplanar structure. The space-filling model of **1** shows that the 'electrically-inert' alkyl groups of the substituents surround the main chain. These findings suggest a new strategy to design 'rigid and coplanar' oligo-aromatic π-systems with an insulating mantle of bulky substituents.

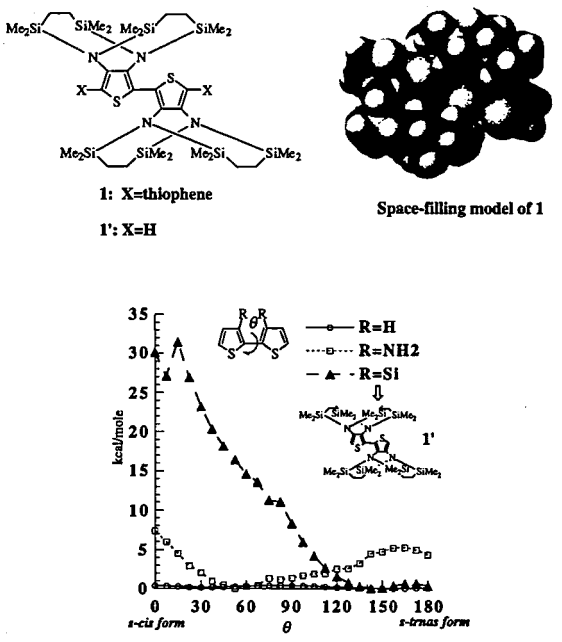

Figure 1. Variation of the torsional potential for 2,2'-bithiophenes as a function of the dihedral angles calculated by the AM1 method.

VIII-D Studies of Nanoscale Carbons

Nanotube has a unique structural feature visualized by rolling up a graphene sheet to form seamless tubule. Although the diameter of the single wall tubule is in the range between ~1 and 5 nm or so, the length of tubule is in the range of 1-10 micrometers or longer. Therefore, its diameter (or peripheral length) is recognizable as a molecule size while its length is a bulk one. Recently, it was found that such tubules formed a triangular packed crystalline bundles. Doping of electron-donor and electron-acceptor to intertubular spacing are studied in terms of modifying the electronic state of tubules, which will be either metallic or semiconducting depending on the cyclic boundary condition of circumference. The vibrational and electronic properties of pristine purified single- and multi-wall nanotubes are studied by the Raman scattering and electron spin resonance measurements.

VIII-D-1 Apparatus for High Yield Production of Single Wall Carbon Nanotube using Pulsed Laser Vaporization Method

Shunji BANDOW and Shuji ASAKA

In 1993, single wall carbon nanotube (SWNT) was found in the arc generated cabon soot prepared with a few atomic % of Fe,[1] Ni,[2] or Co[3] as catalyst. However, the content of SWNT was very low with a few %. In 1996, a high yield synthesis method of SWNT was developed at Rice university,[4] which uses two pluses of Nd: YAG laser (532 nm followed by 50 ns late 1064 nm) to vaporize both carbon and transition metal catalyst in a high temperature (1200 °C) Ar gas stream (500 Torr, 50 sccm). More recently, Journet *et al.*[5] found a good catalyst (Ni/Y) to produce SWNT with high yield by conventional arc burning method.

To study solid state properties of carbon nanotubes, we first aimed to synthesize large quantity of SWNTs with high yield. For the reason of easily controlling the experimental conditions, the laser vaporization method was selected to make SWNTs. Figure 1 is an illustration of laser vaporization apparatus. A two pulse sequence (532 nm followed by 37 ns late 1064 nm at 20 Hz, ~100 and ~85 mJ/pulse) from a Nd: YAG laser were focused onto a carbon target containing either Fe/Ni (0.6/0.6 atom%) or Co/Ni (2.6/2.6 atom%). The target was placed in a quartz tube at a high temperature tube furnace. Ar gas was introduced at the front of the furnace with a pressure of 500 Torr and a flow rate of 100 sccm that carried the SWNTs and other carbon products produced in the carbon plasma to out side of the furnace where the products were collected on a water-cooled Cu cold finger. The production rate is 10-20 mg/hour.

References

1) S. Iijima and T. Ichihashi, *Nature* 363, 603 (1993).
2) D. Bethune, *et al.*, *Nature* 363, 605 (1993).
3) Y. Saito, *et al.*, *J. Phys. Chem. Solids* 54, 1849 (1993).
4) A. Thess, *et al.*, *Science* 273, 483 (1996).
5) C. Journet, *et al.*, *Nature* 388, 756 (1997).

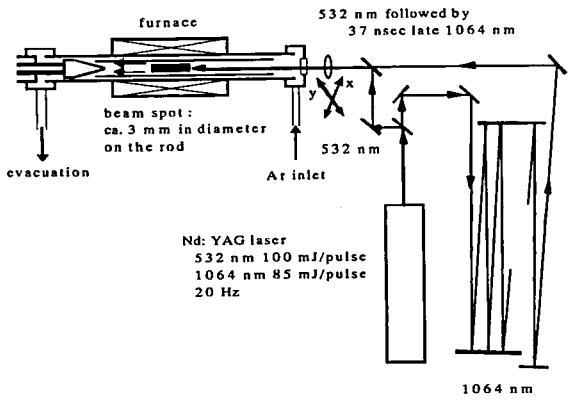

Figure 1. Illustration of laser vaporization apparatus for single wall carbon nanotubes.

VIII-D-2 Effect of Target Temperature for Yielding of Single Wall Carbon Nanotubes

Shunji BANDOW and Shuji ASAKA

Single wall carbon nanotubes (SWNTs) can be synthesized with high yield (> 70 %) by a two pulse sequence of laser vaporization of carbon rod containing a few atomic% of either Co/Ni or Fe/Ni as catalyst at high temperature. Temperature for synthesis of SWNTs was changed from 780 to 1050 °C under the conditions at a 500 Torr and a 100 sccm of Ar stream. At the highest temperature, numerous number of SWNT bundles could be seen in the electron micrograph. However, at 780 °C, only a few SWNTs bundles could be seen and the diameters of bundles decreased as compared with those of high temperature synthesized SWNT bundles. To quantify SWNT yield with respect to temperature, we simply counted the number of bundles per area. Results are shown in Figure 1. Although the number of bundles does not linearly proportion to SWNT content in each sample, the number of single wall tubules for higher temperature synthesized sample drastically increases due to the increase of the bundle diameter. Therefore, the slope in the range of T_t > 900 °C becomes much bigger. In Figure 1, the threshold temperature for significant SWNT production can be found to be in the range 850 - 900 °C. For room temperature (RT) synthesized sample, there was no SWNT bundle observed by electron microscopy. This fact suggests that the high temperature condition is important for synthesizing the SWNT. Furthermore, we have found that the tube diameter can be controlled by changing the target temperature.

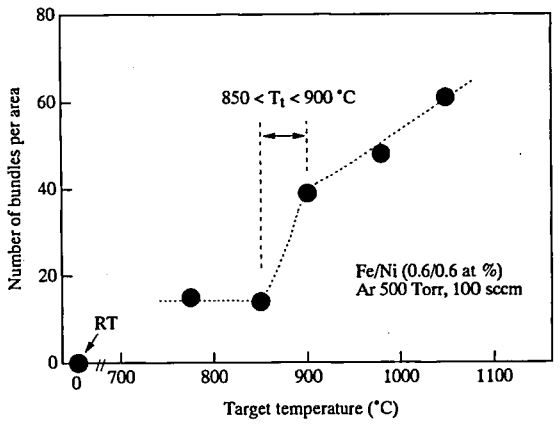

Figure 1. Temperature dependence of target temperature for single wall nanotube production. RT means room temperature. Threshold temperature for the production can be seen in the range 850 < T_t < 900 °C.

VIII-D-3 Diameter-Selective Raman Scattering from Vibrational Modes in Carbon Nanotubes

A. M. RAO,[a,b] E. RICHTER,[a] Shunji BANDOW, Bruce CHASE,[c] P. C. EKLUND,[a,b] K. A. WILLIAMS,[a] S. FANG,[a] K. R. SUBBASWAMY,[a] M. MENON,[a] A. THESS,[d] R. E. SMALLEY,[d] G. DRESSELHAUS[e] and M. S. DRESSELHAUS[e]
([a]Univ. Kentucky, [b]Center for Appl. Energy Res., [c]Dupont, [d]Rice Univ. and [e]MIT)

[*Science* **275**, 187 (1997)]

Single wall carbon nanotubes (SWNTs) that are found as close-packed arrays in crystalline ropes have been studied by using Raman scattering techniques with laser excitation wavelengths in the range from 514.5 to 1320 nanometers. Numerous Raman peaks were observed and identified with vibrational modes of armchair symmetry (*n*,*n*) SWNTs. The Raman spectra are in good agreement with lattice dynamic calculations based on C-C force constants used to fit the two-dimensional, experimental phonon dispersion of a single graphene sheet. Calculated intensities from a nonresonant, bond polarizability model optimized for sp^2 carbons are also in qualitative agreement with the Raman data (see Figure 1), although a resonant Raman scattering process is also taking place. This resonance results from the one-dimensional quantum confinement of the electrons in the nanotube.

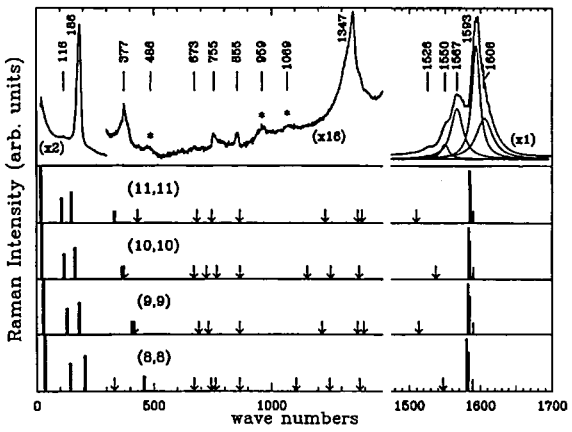

Figure 1. Raman spectrum (top) of SWNT samples taken with 514.5 nm excitation at ~2 W/cm^2. The * in the spectrum indicates features that are tentatively assigned to second-order Raman scattering. The four bottom panels are the calculated Raman spectra for armchair (n,n) nanotubes, $n = 8$ to 11. The downward pointing arrows in the lower panels indicate the positions of the remaining weak, Raman-active modes.

VIII-D-4 Evidence for Charge Transfer in Doped Carbon Nanotube Bundles from Raman Scattering

A. M. RAO,[a,b] P. C. EKLUND,[a,b] Shunji BANDOW, A. THESS[c] and R. E. SMALLEY[c] (*[a]Univ. Kentucky, [b]Center for Appl. Energy Res., and [c]Rice Univ.*)

[*Nature* **388**, 257 (1997)]

Single-walled carbon nanotubes[1] (SWNTs) are predicted to be metallic for certain diameters and pitches of the twisted graphene ribbons that make up their walls.[2] Chemical doping is expected to substantially increase the density of free charge carriers and thereby enhance the electrical (and thermal) conductivity. Here we use Raman spectroscopy to study the effects of exposing SWNT bundles to typical electron-donor (potassium, rubidium) and electron-acceptor (iodine, bromine) dopants. We find that the high-frequency tangential vibrational modes of the carbon atoms in the SWNTs shift substantially to lower (for K, Rb) or higher (for Br_2) frequencies. Little change is seen for I_2 doping. These shifts provide evidence for charge transfer between the dopants and the nanotubes, indicating an ionic character of the doped samples. This, together with conductivity measurements,[3] suggests that doping does increase the carrier concentration of the SWNT bundles.

References

1) A. Thess, *et al.*, *Science* 273, 483 (1996).
2) M. S. Dresselhaus, G. Dresselhaus, P. C. Eklund, *Science of Fullerenes and Carbon Nanotubes*, Chap. 19 (Academic Press, San Diego, 1996).
3) R. S. Lee, et al., *Nature* **388**, 255 (1997).

VIII-D-5 Purification of Single Wall Carbon Nanotubes by Microfiltration

Shunji BANDOW, A. M. RAO,[a,b] K. A. WILLIAMS,[b] A. THESS,[c] R. E. SMALLEY[c] and P. C. EKLUND[a,b] (*[a]Univ. Kentucky, [b]Center for Appl. Energy Res. and [c]Rice Univ.*)

[*J. Phys. Chem.* in press]

A purification procedure for single wall carbon nanotubes (SWNTs) prepared by laser ablation is discussed which separates coexisting carbon nanospheres (CNS), metal nanoparticles, poly-aromatic carbons and fullerenes from the SWNT fraction. The process involves the suspension of CNS, metal nanoparticles and SWNTs in aqueous solution using a cationic surfactant, and the subsequent trapping of SWNTs on a membrane filter. No oxidative treatment is required. Scanning/transmission electron microscopy and Raman scattering were used to evaluate the purification process and the vibrational features of SWNTs. Purity of SWNTs at the final stage sample is in excess of 90 % by weight and no evidence of impurity carbon phases was revealed in the Raman spectrum of the SWNT fraction.

VIII-D-6 Magnetic Properties of Purified Multi- and Single-Wall Carbon Nanotubes

Shunji BANDOW

The multi- and single-wall carbon nanotubes (MWNTs and SWNTs) can be separated from the coexisting carbon nanospheres (CNS) and micron graphite flakes by centrifugalization or microfiltration using a cationic surfactant of benzalkonium chloride. Details of the separation procedures are in the references 1 and 2. Briefly, MWNT and SWNT were dispersed in an aqueous solution of cationic surfactant (benzalkonium chloride) by ultrasonic agitation. The suspension was spun at 5000 rpm to settle the CNS and micron graphite flakes down for MWNTs sample, or filtrated the CNS using a membrane filter for SWNTs sample. The nanotubes thus separated were examined by electron spin resonance (ESR), magnetic susceptibility measurement and transmission electron microscopy, etc.

ESR spectrum for MWNTs indicated a rather broad linewidth $\Delta H \sim 55$ G and a g-value of 2.0096 ± 0.0004 at 300 K. While the g-value of graphite shows large temperature dependence due to a zero-gap semiconducting feature (degenerate band-edge structure),[3] the g-value of MWNTs showed smaller temperature dependence, by an order of magnitude, than that of graphite in the temperature range from 20 to 300 K. This difference is attributable to the difference in the band-edge structures between nanotube and graphite: as well known by the theoretical calculation,[4] the carbon nanotube can be either semiconductor or metal, allowing a finite ΔE for semiconducting tubule or a finite density of state at the Fermi level for metallic tubule unlike 2D-graphite. Such a difference in electronic structure would suppress the thermal excitation effect for nanotube, resulting in a small temperature dependence of g-value.

The SWNTs were prepared by the laser ablation[5] of an Fe/Ni (0.6/0.6 atom%) or a Co/Ni (2.6/2.6

atom%) composite carbon rod at 1050 °C, and were purified by the method based on the microfiltration[2] and acid treatment. ESR of purified SWNTs dispersed in hexane was measured in the temperature range from 7 to 300 K. However, there was no ESR signal detected originating in the conduction electrons. When we drove off hexane and thus the sample agglomerated, the Q-factor of a microwave resonator became worse and the microwave frequency (9.5 GHz) could not be locked. This is an evidence for the existence of itinerant electrons spread widely over the tube to tube (or the bundle to bundle) for dried agglomerated SWNTs. The reason of why the conduction-ESR could not be detected for isolated SWNT-bundles is not clear but is possibly due to the dimensionality of the system or the curved nature of the tube wall.

References

1) S. Bandow, *J. Appl. Phys.* 80, 1020 (1996).
2) S. Bandow, *et al.*, *J. Phys. Chem.* in press.
3) The thermal excitation of electrons to the upper energy level can easily occur due to the zero-gap feature and modifies the ground state of electrons. This modification of ground statec properties may cause the large temperature dependence of g-value.
4) M. S. Dresselhaus, G. Dresselhaus and P. C. Eklund, *Science of Fullerenes and Carbon Nanotubes* (Academic Press, San Diego, 1996).
5) A. Thess, *et al.*, *Science* 273, 483 (1996).

VIII-E The Applications of a Magic-Angle Turning Technique for Half-Integer Quadrupolar Nuclei

VIII-E-1 Spinning-Sideband Suppression in DOR NMR Spectra Using a Magic-Angle-Turning Technique

Daisuke KUWAHARA and Toshihito NAKAI

[*Chem. Phys. Lett.* **260**, 249 (1996)]

Spinning sidebands (SSBs) in double rotation (DOR) NMR spectra for quadrupolar nuclei having half-odd-integer spins were suppressed using a two-dimensional (2D) NMR method based on a magic-angle-turning technique. The resultant 2D spectrum showed substantially no SSBs along one frequency axis whereas, along the other axis, conventional SSBs exhibited themselves.

Equipment Development Center

VIII-F Activities of Division of "IMS Machines"

A group of the staff in the Equipment Development Center works on planning, researching, designing and constructing "IMS machines". This machine, crowned with the acronym of the Institute for Molecular Science, is a high-tech experimental instrument, with emphasis on new technical idea and co-operative work with staff inside and outside the Institute including those in industries. We collect suggestions of instruments once every year.

In this fiscal year, 1996, two project themes (1 and 2 in the list below) were adopted as IMS machines. IMS machine projects 2 and 3 (IMS machine 1994) below were completed.

1. Programmable Current Source
   (Proposed by Tomonori TOYODA)
2. Ultra-Thin-Window Optical Cell
   (Keisuke TOMINAGA, Masaaki NAGATA, Nobuaki MIZUTANI and Michio WATANABE)
3. High Precision Slit Driver for Ultra-High-Vacuum Monochromator
   (Masao KAMADA and Nobuaki MIZUTANI)

Brief reports on the projects 2 and 3 are presented in the following.

VIII-F-1 Ultra-Thin-Window Optical Cell

Keisuke TOMINAGA, Masaaki NAGATA, Nobuaki MIZUTANI and Michio WATANABE

We have developed new types of ultra-thin-window optical cells for containing liquids in ultra-fast spectroscopic experiments.

Usual thin-window optical cells are made entirely of glass, and their windows are polished to desired thickness after assembly. These types of cells have drawbacks such as mechanical weakness, high costs, and difficulty in window cleaning and replacement.

Two types of optical cells we have produced are shown in Figure 1 and 2, respectively. The cell in Figure 1 is for optical lengths of 5mm and 10mm, and the one in Figure 2 is for 1mm and 2 mm. The cell windows are commercial fused silica, 10mm in diameter and 0.1mm in thickness. The holders are made of metal, which enables mechanical strength and easy replacement of the window.

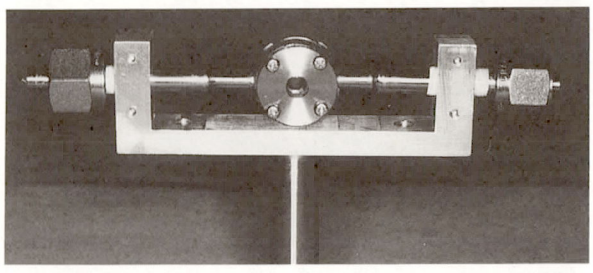

Figure 1. Ultra-thin-window optical cell for optical length of 5mm and 10mm.

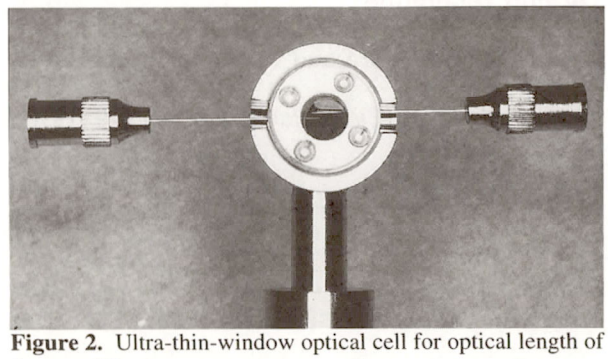

Figure 2. Ultra-thin-window optical cell for optical length of 1mm and 2mm.

VIII-F-2 High Precision Slit Driver for Ultra-High-Vacuum Monochromator

Masao KAMADA and Nobuaki MIZUTANI

We have developed an optical slit for a high resolution monochromator SGM-TRAIN which is set at BL5A in UVSOR facility.

The most important point in designing the present slit is how to secure the stability of the slit opening under remote operation (the distance between the slit and the operation point is about 300mm). We adopted a lever mechanism for the slit.

Mechanical slits generally have advantages in stability, but also have disadvantages in downsizing due to its complexity, and limitations in installation location.

The mechanical slit we produced is shown in Figure 3. Slit opening is controllable by using a lever mechanism with precision of 0.01μm and repeatability of 1μm. The whole slit chamber can be linearly translated up to ±30mm with precision of 2μm with use of a stepping motor. The slit we made has already been installed at the exit of SGM-TRAIN monochromator, and it is operated with satisfactory performance.

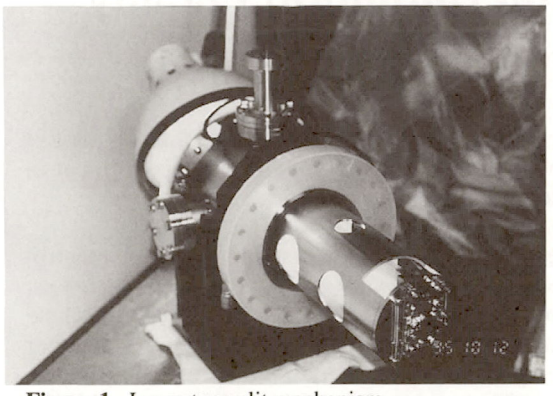

Figure 1. Lever type slit mechanism.

VIII-G Development of Experimental Devices

VIII-G-1 New Apparatus for the Precise Temperature Control of ^{3}He Refrigerator

Hisashi YOSHIDA and Kiyonori KATO

A new, simple, and low-cost apparatus was developed to control the temperature in the very low temperature region (0.3-3.3K) using a ^{3}He refrigerator. A low temperature was obtained by controlling the ^{3}He vapor pressure. The apparatus consists of a set of valves, an automated micro valve, a manually operated auxiliary valve, a controller including a one-board microcomputer using a Z80 CPU, which includes a 12 bit A/D and D/A converter, and parallel I/O ports on the CPU board. The flow rate of the micro valve is 0-25 cm^3/sec, which can be controlled by the external voltage source (0-15V). The microcomputer has following function: (1) to accept a set pressure input using a keyboard, (2) to get a pressure value from the pressure transducer by using the A/D converter, (3) to calculate an operation voltage to the valve, (4) to output the operation voltage through the D/A converter. The microcomputer repeats the functions (2)-(4) to keep the set pressure constant. The apparatus maintains the desired pressure for over 30 minutes, which is sufficient time for scanning high magnetic field (12 Tesla). The temperature drift was typically 0.002K at 0.85K.

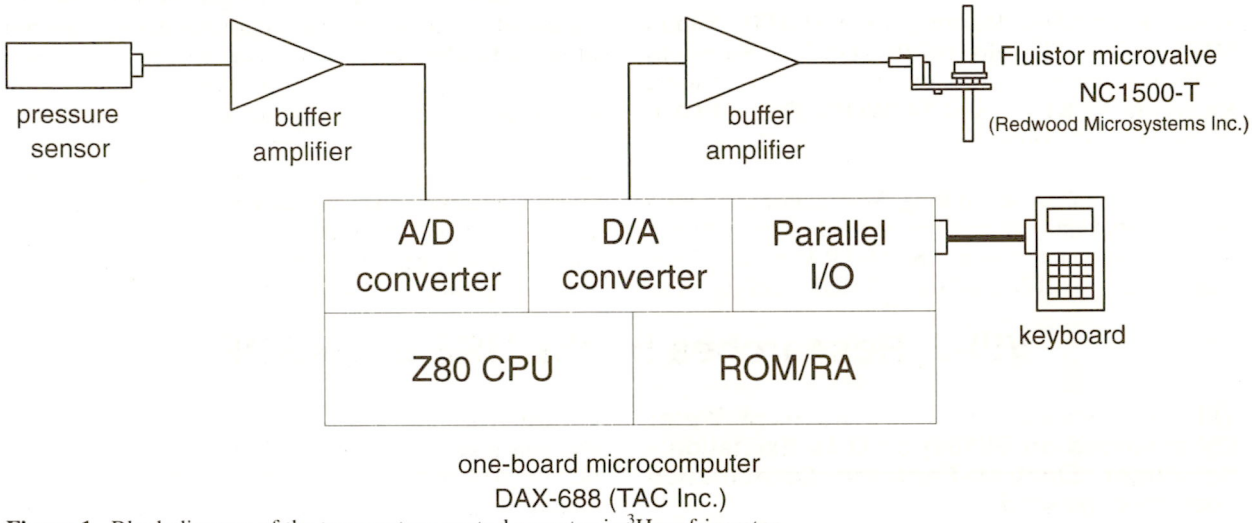

Figure 1. Block diagram of the temperature control appratus in ^{3}He refrigerator

Ultraviolet Synchrotron Orbital Radiation Facility

VIII-H Development of the UVSOR Light Source

Continuous development of the synchrotron radiation source is very important work to keep the competitive performance for research activities in various fields. Achievements are not only brought by improvement of equipment but also resulted from an aspect of the beam physics and/or the accelerator science.

VIII-H-1 Development of the Transverse Resonance Kicker

Toshio KINOSHITA, Shiro TAKANO *(SPring-8)*, **Jun-ichiro YAMAZAKI, Masahito HOSAKA and Hiroyuki HAMA**

To improve the beam handling on the storage ring, a transverse resonance kicker (TRK) system has been developed. On the UVSOR ring, a partial filling method is used to reduce an effect of the ion-trapping in multi-bunch mode. Electron bunch filling was controlled by selecting the RF bucket using a timing control system for the fast kicker extraction of the booster synchrotron so far. However it was difficult to erase specific bunches so that the transverse beam instability due to ion-trapping has been not completely damped and the purity of single-bunch mode has been not very well. The TRK system generates electromagnetic field with a very short duration less than 3 ps. To avoid distortion of the pulse due to reflection, whole system including electrodes and a vacuum chamber was designed to be matched to the intrinsic impedance of 50 Ω. The short pulse is synchronized with the revolution of a specific bunch, which is, moreover, modulated by the betatron oscillation frequency. Because the electron momentum on the ring is high (750 MeV/c), a huge power is required to kick out the bunch at once. Meanwhile, using the TRK system the electron bunch is transversely kicked at each turn, and the amplitude of betatron oscillation grows rapidly even with a relatively low kick power. The electrons finally may touch the wall of vacuum chambers or go out of the dynamic aperture. As a result, for example, the impurity ratio of the single bunch became less than $10^{-4\text{-}5}$ by sweeping the satellite bunches using the TRK.

VIII-I Development of Beam Lines and Equipment for UVSOR

VIII-I-1 Construction and Performance Test of SGM-TRAIN at UVSOR

Masao KAMADA, Masami HASUMOTO, Nobuo MIZUTANI,* Toshio HORIGOME,* Shin-ichi KIMURA, Shin-ichiro TANAKA, Kusuo SAKAI, Kazutoshi FUKUI and 5A-WORKING GROUP**
*(*Equipment Development Center, **Fukui Univ.)*

A new Spherical Grating Monochromator with Translational and Rotational Assembly Including a Normal incidence mount (SGM-TRAIN) has been constructed at BL5A of the UVSOR facility. The SGM-TRAIN is an improved version of a constant-length SGM to aim the following points; (1) wide energy range of 5-250 eV, (2) high resolving power, (3) use of linear and circular polarization, (4) reduction of second-order light, and (5) two driving modes by a computer control. The observed spectra were comparable with the ray-tracing calculation. The second-order light was well suppressed by using laminar-profile gratings and combinations of mirrors and gratings. Observed ionization spectrum of helium with slits of 0.01 mm and the pressure of 50 mTorr. showed Rydberg lines up to n=11, indicating the resolving power of about 4,000 at 60 eV.

VIII-J Researches by the USE of UVSOR

VIII-J-1 Desorption of H Ions from Water Chemisorbed on Si(100) by O-1s Excitation - An Auger Electron-Photoion Coincidence Spectroscopy study

Shin-ichiro, TANAKA, Kazuhiko MASE, Mitsuru NAGASONO and Masao KAMADA

Auger Electron-PhotoIon COincidence (AEPICO) spectroscopy, which has been recently developed and proved to be a very powerful technique for investigating the dynamics of desorption induced by the core-level excitation, is applied to the investigation of Auger stimulated ion desorption from the chemisorbed-water on the Si(100) surface induced by O-1s excitation. It is shown that the fast relaxation of the excited state with a core-hole and an excited electron takes place before the core-hole decay, and that the desorption yield is enhanced by the shake-up (and/or shake-off) excitation. The relative cross section for Auger stimulated ion desorption is estimated, and is shown to increases as holes are created at deeper level of the valence bands as the final state of the Auger decay. A comparison is also made with condensed H_2O.

VIII-J-2 Photoelectron Spectroscopic Study of Coadsorbed States of Cs and O on GaAs(100)

Naoshi TAKAHASHI, Shin-ichiro TANAKA, Masatake ICHIKAWA,* Yong. Q. CAI and**

Masao KAMADA *(*Fukui University, **Fritz-Haber-Institut der Max-Planck-Gesellschaft, Germany)*

[*J. Phys. Soc. Jpn.* **66**, 2798 (1997)]

]The electronic states of O/Cs/GaAs(100) have been investigated by using ultraviolet photoelectron spectroscopy in order to understand the initial coadsorption kinetics on the way to the negative electron affinity formation. It was found that the energy positions of the Ga-3d and As-3d peaks shift to the lower binding energy side by the first Cs deposition, while they shift to the higher binding energy side during the n-th Cs deposition (n $\geqq$ 3). It was also found that besides the appearance of oxidized As, the width of the Ga-3d peak becomes larger by the first oxygen exposure. In the case of the n-th Cs deposition and oxygen exposure, all photoelectron peaks and the work function made parallel shifts in energy, which can be well interpreted in terms of the change in band bending. These results indicate that the coadsorption kinetics can be classified into two stages: At first Cs deposition and oxygen exposure, both of Ga and As react with Cs and O, resulting in the rearrangement in the surface layers, while at n-th Cs deposition and oxygen exposure, surface layers or clusters consisting of Cs, O, As and Ga atoms are produced.

VIII-J-3 Combined Systems of SR and Laser for Solid-State Researches

Masao KAMADA, Sayumi HIROSE,* Shuji ASAKA, Toru TSUJIBAYASHI,[1] Masayuki WATANABE,[2] Osamu ARIMOTO,[3] Shigeki FUJIWARA,[3] Hiroshi ITOH,[4] Shunsuke NAKANISHI[4] and Minoru ITOH[5] *(*Sumitomo Heavy Industries,,[1] Osaka Dental Univ.,[2] Kyoto Univ.,[3] Okayama Univ.,[4] Kagawa Univ., [5] Shinshu Univ.)*

Synchrotron radiation and laser are very useful light sources having different characters. The combinational use of these two light sources is very interesting and promising for solid-state researches, but only a few pioneering works have been reported yet. The present authors have conducted two kinds of combined experiments in recent years. One is the laser-induced-fluorescence system to observe SR-induced desorption of alkali atoms from ionic crystals, which consists of a laser diode with high-repetition rate and SR under a single bunch operation. The other is the system of two-photon spectroscopy, which is based on the combination of SR pulses with low-intensity and high-repetition rate and Nd:YAG laser pulses with high-intensity and low-repetition rate.

VIII-J-4 Resonant Photoemission Studies of Thulium Monochalcogenides around the Tm 4*d* Threshold

Yüksel UFUKTEPE, Sinichi KIMURA, Toyohiko KINOSHITA, Krishna G. NATH, Hiroshi KUMIGASHIRA,* Takashi TAKAHASHI,* Takeshi MATSUMURA,* Takashi SUZUKI,* Haruhiko OGASAWARA and Akio KOTANI**** *(*Tohoku Univ., **Univ. Tokyo)*

Electronic structures of thulium monochalcogenides (TmS, TmSe, TmTe) were studied both experimentally and theoretically using a resonant photoemission technique in the photon energy range around Tm 4*d* edge (100-190 eV). The experiments were performed at the beamline BL2B1 of the UVSOR facility. The representative results of TmSe are shown in Figs. 1 and 2. The experimental results show a large resonant enhancement of 4*f* photoelectron emission around the 4*d* threshold with sharper multiplet structures than those reported before. The calculated results are in good agreement with the experimental ones both for divalent (0-5.6 eV binding energy) and trivalent (5.6-14eV binding energy) features of Tm ions. We observed different types of valence structures for TmS, TmSe and TmTe compounds, due to change in mean valence.

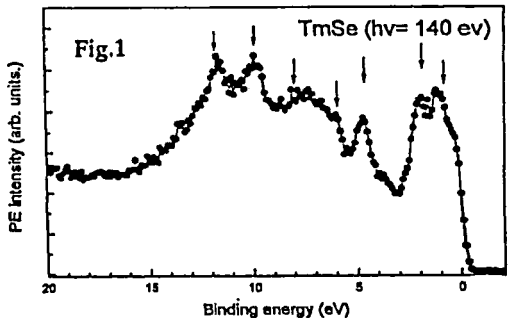

Figure 1. Off-resonant valence band photoemission spectrum of TmSe at $h\nu$=140 eV.

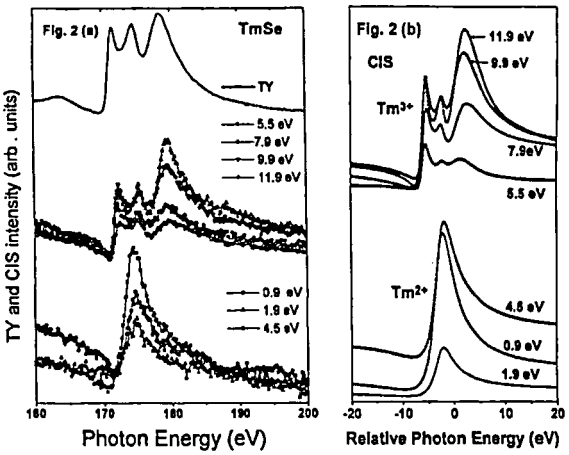

Figure 2(a). Experimental CIS (constant initial state) spectra of TmSe with TY (total photoelectron yield) spectrum. The selected binding energies are indicated by arrows in Fig. 1.
Figure 2(b). Calculated CIS spectra of corresponding binding energies as shown in Fig. 2(a).

VIII-J-5 Resonant Photoemission Studies of Thulium Monochalcogenides around the Tm 3*d* Threshold

Toyohiko KINOSHITA, Yüksel UFUKTEPE, Shinichi KIMURA, Krishna G. NATH, Hiroshi KUMIGASHIRA,* Takashi TAKAHASHI,* Takeshi MATSUMURA,* Takashi SUZUKI,*

Haruhiko OGASAWARA and Akio KOTANI****
*(*Tohoku Univ., **Univ. Tokyo)*

We have studied 3*d*-4*f* resonant photoemission for mixed valent materials, thulium monochalcogenides, in which the excitation energy of $h\nu$=1450-1520 eV was used. So far the resonant photoemission study in this energy region has been very difficult. We could perform the experiments by using the YB_{66} double crystal monochromator (the wiggler beamline BL7A of the UVSOR facility) and VG ESCALAB-220i XL with good energy resolution of less than 1eV. Figure 1 shows the representative results of 3*d*-4*f* resonant photoemission for TmSe. The experimental results are compared with the calculation. It is noticed that the contribution from the 4*f* divalent part (0-5.6 eV binding energy) and the trivalent part (5.6-14 eV binding energy) are more clearly distinguished and resolved than the results of 4*d*-4*f* resonant photoemission. The calculated results are in good agreement with the experimental ones both for divalent and trivalent features of Tm ions. We have estimated the mean valence of each samples from 3*d* absorption spectra and from off-resonant photoemission spectra (the result is not shown here). The latter should reflect more bulk sensitive information than that reported for 4*d*-4*f* photoexcitation region.

It is concluded that the 3*d*-4*f* resonant photoemission is more useful technique to investigate 4*f* electronic structures than 4*d*-4*f* photoemission, when we perform the experiments with relatively higher energy resolution.

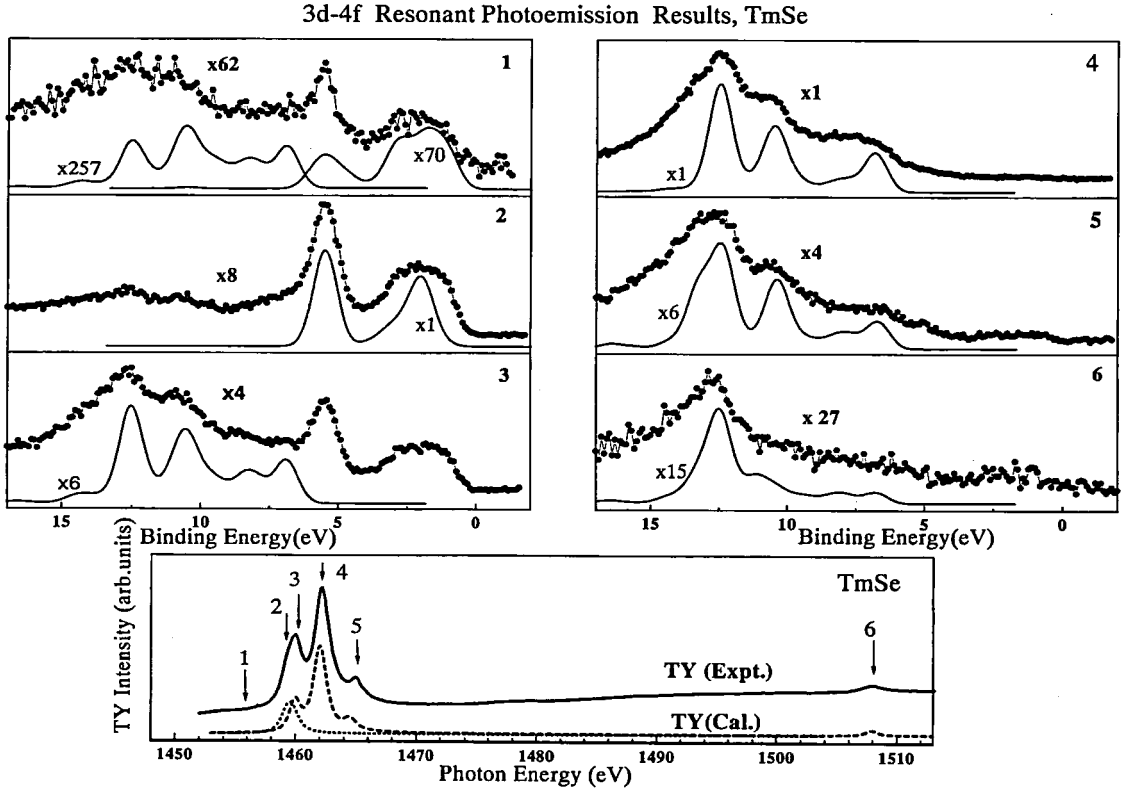

Figure 1. 3*d*-4*f* resonant photoemission spectra of TmSe. The spectra are taken at the representative photon energy positions indicated by numbers in the absorption (TY; total photoelectron yield) spectrum (bottom). The results of theoretical calculation for divalent and trivalent Tm ions are also shown for comparison.

VIII-J-6 Core Level Photoemission Spectroscopy and the Resonance Behavior of Mixed-Valence Tm Monochalcogenides

Krishna G. NATH, Yüksel UFUKTEPE, Shin-ichi KIMURA, Toyohiko KINOSHITA, Takeshi MATSUMURA,* Takashi SUZUKI,* Haruhiko OGASAWARA and Akio KOTANI**** *(*Tohoku Univ., **Univ. Tokyo)*

We have studied the photoemission spectra of 4*d* core level for thulium monochalcogenides, TmX (X = S, Se, Te) around the excitation energy of Tm 3*d*-4*f* resonance region both experimentally and theoretically. The experiments have been performed in the same way as above study (Resonant Photoemission Studies of Thulium Monochalcogenides around the Tm 3*d* Threshold) at the BL7A of the UVSOR facility. Figure 1(a) shows the absorption (TY; total photoelectron yield) spectrum for TmS which is known to be mostly trivalent sample. The agreement between the experimental result and the calculation is quite well. Figure 1(b) shows some of the resonant photoemission spectra of the Tm 4*d* core level. The calculated spectra are also shown. The spectrum taken by Mg*K*α line corresponds to off-resonant spectrum. The resonance effect for Tm 4*d* emission occurs through the partial decay channels of core 3*d* followed by the 3*d*-4*f* absorption. The lifetime broadening phenomenon that strongly depends on the binding energy is also employed for 4*d* level herewith. Moreover, the behavior of particular decay channel refereed as 3*d*4*d*4*f* followed by preferential

excited states was extensively studied throughout this experiment. In Fig. 1(b), the agreement between the experimental results and calculated ones is not so good. Further study may be necessary to understand the phenomena well.

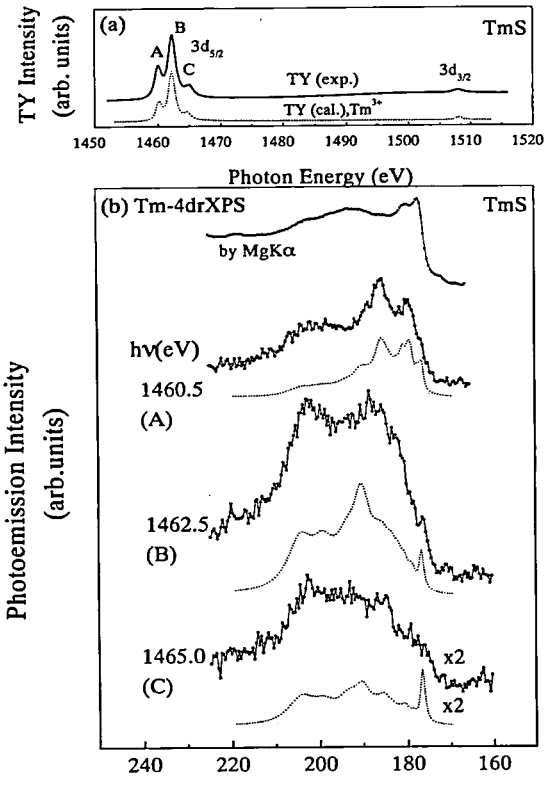

Figure 1. 3*d*-4*f* resonant photoemission spectra of TmSe. The spectra are taken at the representative photon energy positions indicated by numbers in the absorption (TY; total photoelectron yield) spectrum (bottom). The results of theoretical calculation for divalent and trivalent Tm ions are also shown for comparison.

VIII-J-7 Optical Study on Heavy Fermion and Mixed Valence in Yb_4As_3

Shin-ichi KIMURA, Mikihiko IKEZAWA,* Akira OCHIAI* and Takashi SUZUKI* *(*Tohoku Univ.)*

[*J. Phys. Soc. Japan* **65**, 3591 (1996)]

Temperature dependence of the electronic structure of Yb_4As_3 was investigated by the observation of the reflectivity spectra in the energy range from 2 meV to 50 eV at several temperatures from 39 to 320 K. In the photon energy range below 10 meV, the temperature dependence of the spectrum can be qualitatively explained by two-band model previously proposed. An absorption band with strong temperature dependence was observed at 0.4 eV. The origin is considered to be the mixing state between unoccupied Yb^{3+}-4*f* and 5*d*. The state is considered to be important to understand the anomalous temperature dependence of the physical properties. In the energy range above 1 eV, the spectrum does not change with the temperature. The structure of the occupied and unoccupied states near the Fermi level is clarified.

VIII-J-8 Photoabsorption Spectrum of Ozone in the K-Edge Region

Tatsuo GEJO, Kazumasa OKADA and Toshio IBUKI

[*Chem. Phys. Letters* in press]

Ozone is one of the most important molecules in chemistry since ozone in the stratosphere absorbs UV light emitted from the sun and prohibits humanity from the exposure by the UV light. In view of this, many experimental and theoretical exertions have been devoted to the spectroscopic studies of ozone. However, highly electronically excited states of ozone have not been fully understood yet, nor have the spectroscopic data exceeding 20 eV been reported so far as we know. In order to explore the electronic states of ozone, we have constructed an ozone supply apparatus on the beamline BL8B1 at UVSOR facility. The photoabsorption and total electron yield spectra of ozone have been successfully measured for the first time in the K-edge region, 520-555 eV.

In order to assign the peaks observed, we have performed the MO calculations based on the SCF approximation. The calculations predict there exist six excited states below the K edge: two π^* and four σ^* states. By comparing the term values obtained experimentally and theoretically, the proposed assignments in table 1 are obtained.

Reference

1) M. S. Banna, D. C. Frost, C. A. McDowell, L. Noodleman and B. Wallbank, *Chem. Phys. Letters* **49**, 213 (1977).

Table 1. Peak positions, term values and the proposed assignments.

Experiment		*ab initio* SCF calc.	Proposed assignments
Peak position (eV)	Term value (eV)	Term value (eV)	
529.1	12.4(O_T)	12.0(O_T)	$\pi^*(2b_1) \leftarrow 2a_1$
535.4	10.8(O_C)	13.4(O_C)	$\pi^*(2b_1) \leftarrow 1a_1$
536.3	5.2(O_T)	3.9(O_T)	$\sigma^*(7a_1) \leftarrow (2a_1/1b_2)$
-		0.7(O_T)	$\sigma^*(5b_2) \leftarrow 2a_1$
541.5[1](O_T)			$(2a_1)^{-1}$ or $(1b_2)^{-1}$
542.3	3.9(O_C)	3.4(O_C)	$\sigma^*(7a_1) \leftarrow 1a_1$
544.0	2.2(O_C)	1.6(O_C)	$\sigma^*(5b_2) \leftarrow 1a_1$
546.2[1](O_C)			$(1a_1)^{-1}$

VIII-J-9 Mixed Valence of Yb_3S_4

Shin-ichi KIMURA,* Yong Seung KWON* and Takashi SUZUKI** *(*Sung Kyun Kwan Univ. Korea, **Tohoku Univ.)*

[*Physica B* **301**, 230 (1997)]

Reflectivity and photoemission spectra of a mixed valence semiconductor, Yb_3S_4, were measured for the investigation of the electronic structure and the mean valence. The mean valence was determined to be 2.67 by the 4*f* and 5*p* photoemission spectra. The energy gap was recognized to be 0.4 eV by the optical conductivity spectrum but the absorption coefficient is small. The energy gap is considered to consists of the occupied S-3*p* and the unoccupied Yb^{3+}-4*f* states.

RESEARCH FACILITIES

In April 1997, two centers were newly established by reorganization of Instrument Center, Chemical Materials Center, and Low-Temperature Center. This section describes the latest equipment and activities of all research facilities including these new centers. For further information please refer to older IMS Annual Review issues (1978 - 1996).

Computer Center

The main computers at the Center are a supercomputer NEC SX-3/34R, NEC HSP (High Speed Scalar Processor) and IBM SP2. The computers are linked to international networks through Science Information Network (SINET). About 30% of the computer time is used by the research staff at IMS, and the remaining 70% is given out as research grants to scientists outside the institute in molecular science and related field. As of March 1996, the number of project group was 201, consisting of 712 users. In September, 1996, the NEC High Performance Computing (HPC) Server was installed. The library programs of the Center amount to 805. Among them, more than 200 programs can be executed immediately. Recent additions include GAUSSIAN 94-Linda and MOLPRO96 electronic structure codes for IBM SP2. The Quantum Chemistry Literature Database (QCLDB) has been developed by the Center in collaboration with the QCLDB group.

Laser Research Center for Molecular Science

This center was established by reorganization of a part of Instrument Center. Catching to the world trends in the laser spectroscopy, the Laser Research Center have newly equipped profitable all solid state light sources in various temporal and spectral regions, including femtosecond and nanosecond Optical Parametric Oscillators (OPO). The synchronously femtosecond OPO (OPAL; SPECTRA PHYSICS) is tunable from 1.1 mm up to 1.6 mm. The nanosecond OPO has extraordinary tuning range form 420 nm down to 2.2 mm. The Laser Research Center also replaced fluorescence analyzer (FLUOROLOG2; SPEX) which is composed of a xenon lamp house, a double monochromator which makes lamp beam monochromatic, and a single monochromator for spectroscopy. The detector is changeable by rotating a mirror (CCD and PM). Using these instrument, one can carry out various experiments in not only the ultrafast temporal region but also steady state photon counting region.

Research Center for Molecular Materials

This center was established by reorganization of Chemical Materials Center, Low-Temperature Center, and a part of Instrument Center. This center plays an important role in the synthesis and purification of chemical substances. Upon request, technicians carry out elemental and mass spectrometric analyses. Laboratory waste matters are also managed here. This center continues the task of Low-Temperature Center which supplies liquid helium and liquid nitrogen to the users in IMS. The total amount of liquid helium and nitrogen supplied from June, 1996 to May, 1997 were 47,233 and 79,004.2 L, respectively. The helium liquefier broke down in November, 1995. The cause was elucidated mainly in a Technical Division project. After the repair in December, 1996, the machine is working well. Automatic four-cycle X-ray diffractometer (Rigaku AFC-7R) and Imaging-Plate X-ray diffractometer (Rigaku R-Axis IV) equipped in 1996 are now available for general users.

Equipment Development Center

A number of research instruments have been designed and constructed at the mechanical, electronic and glass work sections in this Facility. Some examples of our works in this fiscal year of 1996 are listed below.

Sample rotator for liquid helium cryostat
Flow cell for infra-red spectroscopy
Sample mount for STM
Test furnace for sample preparation by arc discharge heating under high temperature
Double square pulse generator for infra-red spectroscopy
Data processing program for thermoelectric power measurement
Pulse driver for Piezo device
Bake-out temperature controller for vacuum chambers

Division of IMS Machines

Equipment Development Center has the division of IMS Machines. Activity of this division is described in detail in section "RESEARCH ACTIVITIES."

Ultraviolet Synchrotron Orbital Radiation Facility

The UVSOR accelerator complex consists of a 15 MeV injector linac, a 600 MeV booster synchrotron, and a 750 MeV storage ring. As additional devices, a higher harmonic cavity, a superconducting wiggler, and undulators are installed. A harmonic cavity was commissioned in Spring 1993 to suppress longitudinal coupled-bunch instability by Landau damping. The double rf system is routinely operated for user beam time, and the lifetime of

the beam has been improved to about 5 hours at 200 mA. The superconducting wiggler is a wavelength shifter type and the maximum magnetic field is 4T to supply intense soft x-rays. Since trouble in helium leakage from the refrigirator was fixed in 1994, the wiggler became operational. It is used for about one half of the user beam time in 1996. The storage ring was devided into four sections by gate valves in Spring 1995 in order to make a scheduled shutdown easier. The baking system was also replaced by new one including a controllable indirect heating. The rf power amplifier systems of the booster synchrotron and the storage ring were renewed to solid-state systems in 1996 in order to have more stable operation and easier maintenance. A helical undulator was installed to one of the four straight sections of the storage ring in 1996 to provide circularly polarized lights in the energy range of 5-250 eV. An optional version of the helical undulator is a helical optical kryostron, which is powerful for a free electron laser (FEL) experiment.

Nineteen experimental stations are now operational. They are two soft-x-ray stations equipped with a double-crystal monochromator, five extreme ultraviolet stations with a glancing incidence or a plane-grating monochromator, five vacuum-ultraviolet stations with a Seya-Namioka-type or a normal incidence-type monochromator, two (far) infrared stations equipped with a FT interferometer, and four white-light stations without monochromator. About one third of beamlines are upgraded in a couple of years. A Seya-Namioka monochromator at beamline 7B is being replaced by a normal-incidence monochromator to improve a resolving power and spectral range for solid state spectroscopy. Another one at beamline 2B2 is under replacement by a Dragon-type monochromator for gaseous experiments in VUV and EUV ranges. A multi-layer monochromator is also under installation to beamline 4A for photo-chemical reaction experiments. A glancing-incidence monochromator at BL8B1 has been replaced by a 15 m SGM monochromator. This new monochromator having a resolving power of 4,000 at 400 eV is used for solid and gaseous experiments in EUV region. A Bruker FT-IR interferometer has been installed to beamline 6A1 besides the old FT-FIR of a Martin-Puplett type, and then the improved system can cover the wide wavelength range from 1 mm to 3 mm. A new monochromator (SGM-TRAIN) has been constructed at beamline 5A for the use of cirlularly polarized lights from the helical undulator.

The UVSOR was shutdown from March to April in 1997 to fix the water leakage of the building. Since all the machines are located under ground, and also the UVSOR is fifteen years old, the maintenance of the building and utilities is very important.

SPECIAL RESEARCH PROJECTS

IMS has special research projects supported by national funds. Three projects in progress are:
(1) Development of microscopic environments with functionality and quantum steering for reactions(1995-)
(2) Study of molecular solid toward molecular electronics(1995-)
(3) Material control in multi-reaction centers(1993-)

These three projects are being carried out with close collaboration between research divisions and facilities. Collaborations from outside also make important contributions. Research fellows join these projects.

(1) Development of Microscopic Environments with Functionality and Quantum Steering for Reactions

Structures, Reactions and Spectroscopies of Molecules and Molecular Clusters

Suehiro IWATA, Seiichiro TEN-NO, Tsutomu IKEGAMI, Takeshi TSURUSAWA, Hidekazu WATANABE *(GUAS and IMS)*, **Yumin LI, Andreas FIEDLER, Pradipta BANDYOPADHYAY** *(GUAS and IMS)*, **So HIRATA** *(GUAS and IMS)*, **Tadayoshi SUZUKI** *(GUAS and IMS)*, **Kazutoshi OKADA** *(GUAS and IMS)*, **Feiwu CHEN, Fernando R. ORNELLAS** *(Sao Paulo Univ. and IMS)*, **Jan HRUSAK** *(J. Heyrovsky Institute of Physical Chemistry and IMS)*, **Wen-Ning WANG** *(Fudan Univ. and IMS)*, **Sourav PAL** *(National Chem. Lab., India and IMS)*

Ab initio molecular orbital methods were applied to various chemical and physical problems. The density functional method was also used in some of the studies. The works were carried out under close collaboration with several experimental groups. Besides, new theoretical techniques in molecular electronic calculation were developed. The followings are the titles of the topics we have been working in last few years.

1. Development of theoretical and numerical techniques in the study of molecular structures.
2. Hybrid procedures of ab initio MO calculations and Monte Carlo samplings.
3. Structures and reactions of atomic and molecular Clusters.
4. Structures and vibrational frequencies of infinite polymer chains.
5. Accurate studies of low-lying states of diatomic and triatomic molecules.
6. Application of ab initio MO and density functional methods to experimentally relevant molecules.

In particular, we have been studying on the water clusters and their complexes with atoms and molecules. Structural and spectroscopic properties of both cations and anions of the clusters are theoretically examined and compared with the experimental data, if available.

Prediction of Protein Tertiary Structures by Generalized-Ensemble Algorithms

Yuko OKAMOTO, Ulrich H.E. HANSMANN, Masato MASUYA, Ayori MITSUTAKE *(Graduate Univ. for Advanced Studies)* **and Hiroshi OHTSUKA** *(Graduate Univ. for Advanced Studies)*

Proteins are the most complicated molecules that exist in nature. Since protein structures are closely related to their biological functions, the prediction of their three-dimensional stuructures from the first principles (by minimizing their energy functions) is not only very challenging but also very important a problem in theoretical molecular science. To be more specific, it is widely believed that three-dimensional structure of proteins is determined by their amino-acid sequences. However, nobody has succeeded in predicting it solely from the amino-acid-sequence information (prediction from the first principles). There are two reasons for the difficulty. One reason is that the inclusion of accurate solvent effects is non-trivial because the number of solvent molecules that have to be considered is very large. The other reason for the difficulty is that there exist huge number of local minima in the energy function, and conventional simulation techniques necessarily get trapped in one of the local minima without ever finding the energy global minimum. Generalized-ensemble algorithms are new Monte Carlo algorithms that can alleviate this difficulty. We proposed to apply one of such methods, multicanonical algorithm, to the protein folding problem.[1] We have also developed a new generalized-ensemble algorithm that is effective for protein folding problem.[2] The goal of the present project is to further test the effectiveness of generalized-ensemble algorithms in the protein folding problem and to succeed eventually in the prediction of tertiary structures of proteins from the first principles.

References
1) U.H.E. Hansmann and Y. Okamoto, *J. Comp. Chem.* 14, 1333 (1993).
2) U.H.E. Hansmann and Y. Okamoto, *Phys. Rev. E* 56, 2228 (1997).

Quantum Mechanical and Semiclassical Studies of Chemical Dynamics

Hiroki NAKAMURA, Chaoyuan ZHU, Katsuyuki NOBUSADA, Oleg I. TOLSTIKHIN, Yoshiaki TERANISHI *(Graduate University for Advanced Studies)*, **Valentin N. OSTROVSKY** *(St. Petersburg Univ.)* **and Vladimir I. OSHEROV** *(Inst. of Chem. Phys.)*

By introducing the new hyperspherical coordinate system called hyperspherical elliptic coordinates, quantum dynamics of hydrogen transfer reactions can

now be efficiently investigated. In addition to this numerical efficiency, reaction mechanisms can be clarified qualitatively with use of the idea of vibrationally adiabatic potential ridge and nonadiabatic transitions at avoided potential curve crossings. These new methodologies have been applied to the $O(^3P)$ + HCl reaction. Further applications to other reaction systems are now in progress.

A new theory has been developed for the cumulative reaction probability. This is free from the ambiguities from which the previous theory suffers. In particular, no absorbing potentials are required for its implementations. The theory has been proved to work well in the $d + t\mu \rightarrow d\mu + t$ reaction.

Our new theory of nonadiabatic transition in the two-state curve crossing problems has been extended to the nonadiabatic tunneling type multi-channel problems. In comparison with quantum mechanically exact numerical calculations, the theory has been proved to work perfectly. Even detailed features of dense overlapping resonances are nicely reproduced. This suggests that we could apply the theory even to multi-dimensional processes such as hydrogen transfer 3D chemical reactions.

Theoretical studies of nonadiabatic transitions have also been extended in the following various directions: (i) time-dependent Landau-Zener type bow-tie model has been solved analytically exactly, (ii) semiclassical solutions have been derived for the nonadiabatic transition matrix in a generalized two-state exponential model, (iii) crossing of time-dependent two bands of potential curves has been analyzed, and (iv) compact fitting formulas have been derived for the Stokes constants for a general cubic potential.

Fifth-Order Two-Dimensional Vibrational Spectroscopy of a Morse Potential System in Condensed Phases

Yoshitaka TANIMURA

The nonlinear optical response of a molecular system in the condensed phase subjected to a series of five off-resonant femtosecond laser pulses has been studied using a quantum Fokker-Planck equation. This equation can treat a molecular system with any shape of potential coupled to a Gaussian-white noise-bath. We have presented the procedure to calculate the third- and fifth- order response functions, which are equivalent to the second- and third-order correlation functions of the molecular coordinate, by way of the equation of motion approach. Assuming the potential surface of a Cesium dimer [Cs2], which is modeled by the Morse potential, and the linear and nonlinear coordinate dependence of the polarizability, we calculated the third- and fifth-order response functions for various temperatures and heat-bath couplings. By plotting two time- evolution period involved in the fifth-order spectroscopy, we obtained the two-dimensional profiles of the signals. These 2D profiles are sensitive for a shape of potential and polarizability, even for a strong damping case, and depend on the temperature. This indicates that fifth-order two-dimensional spectroscopy carried out for a different temperature allows us to access information of the potential and the polarizability.

Constructing Molecular Theory of Chemical Processes in Solution

Fumio HIRATA, Andriy KOVALENKO, Hirofumi SATO, Ryo AKIYAMA, Takashi IMAI, Masahiro KINOSHITA *(Kyoto Univ.)*, **Song-Ho CHONG** *(Kyoto Univ.)*, **Kazunari NAKA** *(Kyoto Univ.)*, **Tateki ISHIDA** *(Kyoto Univ.)* **and Shigeki KATO** *(Kyoto Univ.)*

Our current research interests and activities are concentrated upon three important chemical processes in solution, in each of which solvent plays essential role:

A. the electronic structure of a molecule in solution,
B. solvation thermodynamics of protein and related molecules,
C. characterization of spatial and temporal density fluctuation in molecular liquids.

The RISM theory, an integral equation theory of molecular liquids, is our main machinery to attack the problem, which is coupled with other theoretical methodologies including the ab initio molecular orbital method, molecular simulations, and the generalized Langevin equation. Problems on which we have been working along the three lines are as follows:

1. Temperature dependence of autoionization of water or pKw.
2. Self-consistent determination of electronic structure and liquid state properties of water.
3. Solvatochlomism of triiodide ion in solutions.
4. Solvent effect on keto-enol tautomers of form-amide in aprotic solvents.
5. Type II SN2 reaction (Menshutkin reaction).
6. Salt effect on solubility of nonpolar solute in water.
7. Solvation dynamics and thermodynamics of ions.
8. Stability of peptide and protein conformations in aqueous solution.
9. Non-equilibrium free energy surface related to electron transfer reactions
10. Dynamical coupling between intra- and inter molecular motions in liquids.
11. Description of collective excitation in liquids by interaction site model.
12. Microscopic characterization of metal-liquid interface.

Development of High-Sensitivity Submillimeter-Wave to Far Infrared Spectrometer Systems for the Study of Transient Molecules

Hiroyuki OZEKI and Shuji SAITO

Spectroscopy in the submillimeter-wave to far infrared region has been less exploited when compared with that in other regions, because high spectral purity and tunable radiation sources have not been available. We developed a frequency-tunable far-infrared side-band spectrometer suitable for the study of transient molecules. We installed a stable high-power CO_2 laser and an optically pumped far-infrared laser and

constructed a mixer mounting with a non-linear element of Ga-As Schottky diode, which is mounted in a Martin-Puplett diplexer separating a tunable sideband radiation from the fundamental laser radiation as given in previous Annual Reviews.[1] The sideband can be generated within the range of +/- 40 GHz around far infrared laser radiation, with a typical power of several hundred nano-watts, and the minimum fraction of absorption of 10^{-4} can be detected with the 1 sec. detection time constant.

In the actual spectroscopic measurement however, we found that a large amplitude baseline distortion sometimes caused the system sensitivity to be lower, which is mainly due to mismatching of the microwave source and the diode mixer. In order to avoid this problem, we employed a double modulation technique, i.e. combination of frequency modulation with Zeeman or discharge or velocity modulation. These molecular modulation techniques will work effectively for transient molecule such as paramagnetic or ionic species. We checked the performance of the method by measuring the OH radical. The technique was then applied to a far infrared spectroscopic investigation of the NH_2 radical as reported in II-A-3.

References

1) H. Ozeki and S. Saito, *Ann. Rev.*, 200 (1996).

(1) Studies on Laser Cooling and Trapping of Neutral Atoms
(2) Laser Spectroscopic Studies of Ions in Liquid Helium

Norio MORITA, Mitsutaka KUMAKURA and Yoshiki MORIWAKI

For studies on laser cooling and trapping of neutral atoms, we have continued the work on a magneto-optical trap of helium atoms. Especially, ultracold collision processes in the laser trap has been studied. With the time-of-flight method, cross sections for Penning and associative ionization processes have separately been obtained for both $^3He^*$-$^3He^*$ and $^4He^*$-$^4He^*$ collisions(see II-D-1). In addition, a remarkable difference experimentally observed between the ionization cross sections with and without laser irradiation has successfully been explained through a result of our theoretical calculation(see II-D-2).

On the other hand, in laser spectroscopic studies of ions in liquid helium, we have clearly observed spectra of ions confined in bubbles of liquid helium (see II-E-1). Furthermore, we have also observed bubble-like spectra of magnesium atoms, and the spectra have reasonably been explained by a result of theoretical calculation based on a possible model of the $Mg\text{-}He_{10}$ system (see II-E-2).

Mechanism of Oxygen Activation by Heme-Copper Terminal Oxidase Superfamily

Teizo KITAGAWA, Takashi OGURA, Jörg MATYSIK, Michihiko AKI *(Graduate Univ. for Advanced Studies)*, **Shinya YOSHIKAWA***(Himeji Inst. Tech.)* **and Tatsushi MOGI***(Univ. of Tokyo)*

The terminal oxidase in respiratory chains is cytochrome *c* oxidase for aerobic organisms and quinol oxidase for *E. Coli*. Both have two heme groups; one works for electron transfers and the other provides the catalytic site for dioxygen reduction. The heme iron at the catalytic site is antiferromagnetically coupled with a copper ion in the oxidized state. The dioxygen reduction is coupled with proton translocation through membrane, generating electrochemical potential which could be used for ATP synthesis. The final goal of this study is to elucidate the coupling mechanism between the electron- and proton transfers, but currently a mechanism of dioxygen reduction at the catalytic site is of spectroscopic concern. For bovine cytochrome *c* oxidase, we investigated reaction intermediates present in the time range between 0.1 and 11 ms following initiation of the reaction by using time-resolved resonance Raman spectroscopy combined with our original "artificial cardiovascular system for pursuit of enzymic reaction". The first intermediate gave the oxygen isotope sensitive band at 571 cm^{-1} for $^{16}O_2$. Since the corresponding band for $^{16}O^{18}O$ split into two bands, it became confident that the binding of O_2 is of an end-on type. In subsequent steps, we observed three oxygen isotope sensitive bands at 804/764, 785/750 and 356/342 cm^{-1} for $^{16}O_2/^{18}O_2$ derivatives. Experiments at lower temperatures clarified that the 804 cm^{-1} species appears prior to the 785 cm^{-1} species, while the 356 cm^{-1} band was seen together with the 804 cm^{-1} band. Raman excitation of these intermediates between 570 and 617 nm provided both the 804/764 and 785/750 cm^{-1} bands for $^{16}O_2/^{18}O_2$ derivatives with similar relative intensites. However, excitation at 441.6 nm gave rise to only the 804/764 cm^{-1} band at the delay times of 0.27 and 1.1 ms, indicating distinct difference of the heme electronic states between the 804 and 785 cm^{-1} species. The 804 cm^{-1} species was not detected with cytochrome *bo* while others were observed. The 804 cm^{-1} band appeared with a similar rate in H_2O and D_2O, but the appearance of the 785 cm^{-1} band was significantly delayed in D_2O, suggesting that the generation of 785 cm^{-1} species from the 804 cm^{-1} species is coupled with the proton translocation. The experiments with $^{16}O^{18}O$ demonstrated that both bands should arise from the Fe=O stretching but not from the O-O stretching mode. The reaction of oxidized enzyme with hydrogen peroxide also gave the three sets of the oxygen-isotope-sensitive bands at the same frequencies as those of dioxygen reduction. It is likely that the 804 and 785 cm^{-1} bands arise from the Fe^{V}=O and Fe^{IV}=O stretching modes, respectively, while the 356 cm^{-1} band is associated with the His-Fe=O bending mode. Two Fe-CO stretching band was observed for a bovine enzyme at pH 7.3 and it was demonstrated that a residue with $pK_a = 7.6$ is located near CO in the heme pocket, affecting the Fe-CO frequency.

Laser Raman Beat Detection of Magnetic Resonance

Tatsuhisa KATO and Michio MATSUSHITA

Laser Raman beat detection is a coherent optical-RF double resonance technique where the optical and RF field induce coherence within a three level system and a resultant Raman beat signal is detected using heterodyne detection. This technique can be applied to the study of electron paramagnetic resonance and nuclear magnetic resonance not only in the ground state of a molecule but also in the electronic excited state.

There are some causes to hide the Raman beat signal, that is, the inhomogeneity of the circumstance of the molecule, the fluctuation of the applied field, and the interference by the crystal phonon. It is the key to success in the Raman beat detection to eliminate these cause of the incoherence. Then it is needed to prepare the sophisticated single crystal sample, the highly stabilized magnetic field, and a cryostat of liquid helium. It has been completed to set up the apparatus, and the Raman beat detection was applied to the study on the quadrupole transitions of ^{139}La nuclei around Pr^{3+} doped in LaF_3, as reported in Section II-I-1.

Liquid Dynamics Studied by New Ultrafast Nonlinear Spectroscopy

Keitaro YOSHIHARA, Keisuke TOMINAGA, Shaul MUKAMEL *(Univ. of Rochester)*, **Yuuichi FUJIMURA** *(Tohoku Univ.)*, **Tai Jong KANG** *(Taegu Univ. and IMS)* **and Stephen R. MEECH** *(Univ. of East Anglia and IMS)*

Vibrational spectra get broadened extensively and sometimes shifted in liquids compared to those in gas phase. This is because the solute molecule interacts with solvent molecules in a complex manner, and consequently molecular spectra can, in principle, serve as probes to obtain information about structure and dynamics of molecular liquids. One traditional approach to investigate microscopic details in liquids from molecular spectra is the lineshape analysis; one can analyze experimentally obtained spectra with some model function assumed for the spectral lineshape. However, the lineshape analysis sometimes requires certain amount of fitting parameters, especially in cases of complex microscopic models, and due to a large number of fitting parameters, the lineshape analysis always carries some ambiguity. In recent five years, however, new ultrafast spectroscopies based on higher-order nonlinearity have been developed to make more rigorous approach to the vibrational dynamics than the lineshape analysis. Raman echo is the seventh order experiment, which corresponds to photon echo of the electronic spectroscopy. One of the advantages of the higher-order experiment is that a wide variety of the nonlinear technique can be designed by choosing proper experimental conditions such as phase-matching. Two-dimensional impulsive stimulated Raman scattering (fifth order) and overtone vibrational dephasing (fifth order) fall into this category. In this project we develop two new higher order nonlinear spectroscopies experimentally and theoretically; 1) Two-Dimensional Overtone Vibrational Spectroscopy, which allows us to study correlation between fluctuations of two different vibrational states. 2) New nonlinear spectroscopies to study inhomogeneity of extremely broadened band such as the OH stretching of water.

Studies of Laser-Induced Photochemistry on Solid Surfaces

Yoshiyasu MATSUMOTO, Kazuya WATANABE, Kazuo WATANABE, Hiroyuki KATO *(Graduate Univ. for Advanced Studies)*, **Ikuo KINOSHITA** *(Yokohama City Univ.)* **and Toshihisa ANAZAWA**

Light sources such as lasers and synchrotron radiation can be useful for the various processes in the fabrication of microelectronics, including etching, chemical vapor deposition, atomic layer epitaxy. On the other hand, it has also been well recognized that there is an important class of catalytic reactions with the aid of photon irradiation. Although those applications of light are practically useful and important, fundamental understanding of these processes is still lacking. Therefore, this project is mainly aimed for investigating how the interaction of light and adsorbates and /or substrates promotes chemical reactions from the fundamental point of view.

We have continuously performed the studies on surface photochemistry particularly of nitrous oxide adsorbed on semiconductor surfaces and methane on Pt(111) and Pd(111) in this year. A UHV apparatus used is equipped with a retractable LEED/Auger electron spectrometer, a differentially pumped quadrupole mass spectrometer, a X-ray source, a photoelectron analyzer, an ion gun, a high precision sample manipulator, a closed cycle He refrigerator, and a gas doser. The main chamber was evacuated to a base pressure of 1×10^{-10} Torr by cascaded turbo-molecular pumps. With this apparatus, we can perform not only conventional analytical measurements in surface science including LEED, AES, temperature-programmed desorption, XPS, and work function measurements, but also measurements providing information on nuclei dynamics including angular-resolved time-of-flight spectroscopy of neutral species desorbed from the surface with sub-monolayer coverage.

In additon, we have newly developed an apparatus for multiphoton photoelectron spectroscopy that enables us to obtain electronically excited states of surface states of clean surfaces and those of adsorbates. The information of energetic positions and widths of the excited states is vital to understanding of excitation mechanisms in surface photochemistry. The apparatus is composed of light sources and a magnetically shielded UHV chamber. We have used two kinds of light sources: a tunable dye laser pumped by a Nd:YAG laser at a repetition rate of 10 Hz and a mode-locked Ti:Sapphire-seeded regenerative amplifier system (Spectra Physics, Spitfire) at a repetition rate of 50 kHz. Using this apparatus, we have investigated surface states at a clean Pt(111) surface and the electronic structure of CO chemisorbed on Pt(111).

Higher Vibrational States of Molecules and Clusters as Studied by Nonresonant Ionization Detected IR Spectroscopy

Masaaki FUJII

This special research project, started in April 1997 is planning to study spectroscopy and dynamics of molecules and clusters in higher vibrational state by the nonresonant ionization detected IR spectroscopy. The nonresonant ionization detected IR spectroscopy (shortly NID-IR) is a newly developed IR-UV double resonance spectroscopy which detects IR absorption by the selective ionization of a vibrationally excited molecule. Briefly, a jet-cooled molecule is excited to a vibrational level in the ground state by the IR laser. The vibrationally excited molecule is selectively ionized by the nonresonant two-photon process due to the UV laser. The simplest way of the selective ionization can be achieved by fixing the frequency of the UV laser to energy slightly less than a half of the ionization potential. Under this frequency condition, only the vibrationally excited molecule can be ionized by the two-photon process due to the UV laser. Therefore, the ion current is detected only when the IR laser is resonant to the vibrational level. This spectroscopy has an advantage in the sensitivity because of the weak background signal and the ionization detection.

The experimental setup for the measurement of the nonresonant ionization detected IR spectroscopy has been constructed in this six months. The tunable pulsed IR laser is generated by three ways. The IR laser in 2.5 - 4 mm region is generated by the differential mixing between the second harmonics of a Nd^{3+}:YAG laser and a dye laser pumped by a YAG laser. The IR laser in 1.2 - 2.5 mm region is also obtained by the differential mixing between the fundamental of the YAG laser and the dye laser light. The typical power of the IR laser is 0.3 to 1 mJ in the 3 mm region, 2 mJ in the 1.5 mm region, and 3 mJ in the 1 mm region. The UV laser is obtained by the frequency doubling of another dye laser pumped by the third harmonics of a YAG laser. Both the IR laser and the UV laser are introduced into a vacuum chamber and crossed a supersonic jet. Cations generated by lasers are pushed into a detector chamber and are detected by a channel multiplier through a quadrapole mass-filter.

The nonresonant ionization detected IR spectroscopy has been applied to several organic molecules such as phenol. The spectra shows clear vibrational structure of the jet cooled molecules. The detailed results will be reported in next review.

Laser Investigation of Elementary Reactions in the Gas Phase

Toshinori SUZUKI, Hideki KATAYANAGI, Hiroshi KOHGUCHI, Christian GEBAUER, Yuxiang MO and Haiyang LI

Detailed knowledge of elementary reactions in the gas phase is indispensable to understand combustion, plasma, and atmospheric chemistry. Knowledge on reaction dynamics is also important in seeking the possibility to steer the reactions by state-selective excitation. As demonstrated by Rutherford, scattering experiment is the most powerful means to study microscopic interaction potential. Since typical chemical reaction is low-energy event (<10 eV), internal excitations of atoms and molecules cannot be neglected in the dynamics, so that the internal degrees of freedom of particles must be resolved in scattering experiment. Such requirement in chemical dynamics experiment can only be fulfilled by the use of laser spectroscopic means that provides ultimate state resolution. We have constructed a new crossed molecular beam machine equipped with the ion imaging apparatus to measure state-resolved differential cross sections for inelastic and reactive scattering.

Light Induced Intermolecular Charge Transport in Organic Insulator Systems

Nobuyuki NISHI, Yoshiya INOKUCHI *(Kyusyu Univ. and Graduate Univ. for Advanced Studies)* **and Kazuhiko OHASHI**

Cationic holes in condensed aromatic molecular systems, such as clusters and pure liquids are now proved to exist in a dimeric unit of molecules with charge resonation between the two molecules. The most effective resonance is expected for the pair with completely identical (or interchangeable) molecules in a parallel configuration. The degree of the resonance is observable through the charge resonance electronic transition from the bound ground state to the bound-free excited state. In liquid benzene, we observed transient signals of the holes in near IR region by a femto-second pump and probe technique in collaboration with Prof. Yoshihara's group. Just after the generation of the hole the dimeric species show a spectrum similar to the gas phase dimer but in several picoseconds the hole becomes to be dressed by surrounding benzene molecules shifting the absorption maximum to further red. The result suggests that near IR light can transport the holes effectively through dissociation-collision induced hopping processes along the polarization vector of the IR beam. On the other hand, the excitation of in-plane C-H stretching vibration of dimer cation unit in benzene trimer cation proved the presence of charge hopping, probably in resonant with an asymmetric intermolecular vibrational motion. This experiment was done with various combination of isotopic mixtures with the aid of mass separated photodissociation spectroscopy. We are now trying to develop a new method of isolating charged portion of the associates using Coulomb explosion technique.

Photoabsorption and Photofragmentation of Triiodide Anion: Gas-Phase Analogue to I_3^- in Solution

Lei ZHU, Tatsuya TSUKUDA *(Univ. Tokyo)*, **Kazutaka TAKAHASHI** *(Univ. Tokyo)*, **Morihisa SAEKI** *(Univ. Tokyo and IMS)* **and Takashi NAGATA**

Photoabsorption of gas-phase triiodide anion, I_3^-, was studied by photofragmentation spectroscopy in the UV and visible regions. Two distinct dissociation channels, $I_3^- + h\nu \rightarrow I^- + 2I$ and $I_3^- + h\nu \rightarrow I_2^- + I$, were

observed in contrast to the fact that only the latter channel is accessible in the photodissociation of I_3^- in the condensed phase. The absorption spectrum obtained in the present study almost mimics that of I_3^- in ethanol, which shows strong absorption bands in the UV region as well as weak bands in the visible region. The angular distributions of the product anions are characteristic of parallel-type transitions in the entire spectral range. The kinetic energy release of the fragments was also estimated from the TOF spectral profiles, indicating that photodissociation initiates along the symmetric stretch coordinate of I_3^-. Addition of one C_2H_5OH molecule to I_3^- results in a drastic increase in the I_2^- yield as photoproduct, which opens up a possibility of studying "solvent effect" on the elementary photodissociation process of triiodide anion, not in the condensed phase but in the gas phase with a restricted number of solvent molecules.

Time-Resolved Spectroscopic Studies on Chemical Reactions Using Ultrafast Laser and Synchrotron Radiation

Tahei TAHARA, Satoshi TAKEUCHI, Atsuhiko SHIMOJIMA and Misa KAYAMA

Time-resolved spectroscopy is one of the most powerful tools for the studies of chemical reactions. It enables us to directly observe the temporal changes occurring in the course of chemical reactions. Recent progress of time-resolved spectroscopy relies on the drastic advances of the laser technology, and we are now able to examine the dynamics of the primary processes of chemical reactions with pico/femtosecond time-resolution. Time-resolved spectroscopy based on ultrafast lasers is, and will continue, playing a crucial role in physicochemical studies on chemical reactions. Synchrotron radiation, on the other hand, has unique potentiality to be alternative light source in time-resolved spectroscopy since it is intrinsically produced in the form of a picosecond pulse train. The potential of synchrotron radiation in time-resolved spectroscopy lies on the fact that it affords optical pulses in a very wide energy range from X-ray to far-infrared. Thus, synchrotron radiation may open up new possibility of time-resolved spectroscopy in the energy region which is not accessible with the existing lasers. The aims of this project are the development of new time-resolved spectroscopic methods and their application to the studies on chemical reactions, taking advantage of these two light sources which are complementary to each other. We already constructed two experimental setups in the last year; a femtosecond time-resolved fluorescence up-conversion spectrometer and a femtosecond optical heterodyne detected impulsive stimulated Raman scattering (OHD-ISRS) spectrometer. In this year, while continuing research with these setups, we have also constructed the following two setups; a femtosecond time-resolved uv-vis-nir absorption spectrometer and a picosecond time-resolved spontaneous Raman spectrometer. In addition, in order to examine potentiality of synchrotron radiation for time-resolved far-infrared measurements, we constructed a setup at beamline BL6B in our synchrotron radiation facility (UVSOR).

Development of UHV-STM System for Study of Surface Photochemical Reactions Induced by Synchrotron Radiation

Takayuki MIYAMAE, Shinya HIRANO, Hironaga UCHIDA *(Toyohashi Univ. Tech.)* **and Tsuneo URISU**

We have newly developed a scanning tunneling microscopy (STM) system for the study of surface photochemical reactions. The design of our UHV-STM system is schematically shown in Figure 1. The STM is located in the left-hand side of the main chamber. A back-view LEED, an atomic hydrogen doser, and a heating device are located on the right-hand side of the chamber. The pumping of the system is carried out by 300 *l*/s ion pump, 400 *l*/s Ti sublimation pump, and a non-evapolable getter pump (SAES GETTERS) for the main chamber and a turbomolecular pump for the sample preparation chamber which is stopped during the STM experiments. A pressure better than 1×10^{-10} Torr can be maintained in the main chamber. The STM body is suspended by three stainless steel springs for vibration isolation. The entire UHV system is mounted on an air-suspended vibration isolation table. Now experiments using STM for the geometrical topography and electronic structure of atomic hydrogen-chemisorbed Si(100) surface and its change by the synchrotron radiation stimulated surface reaction is underway.

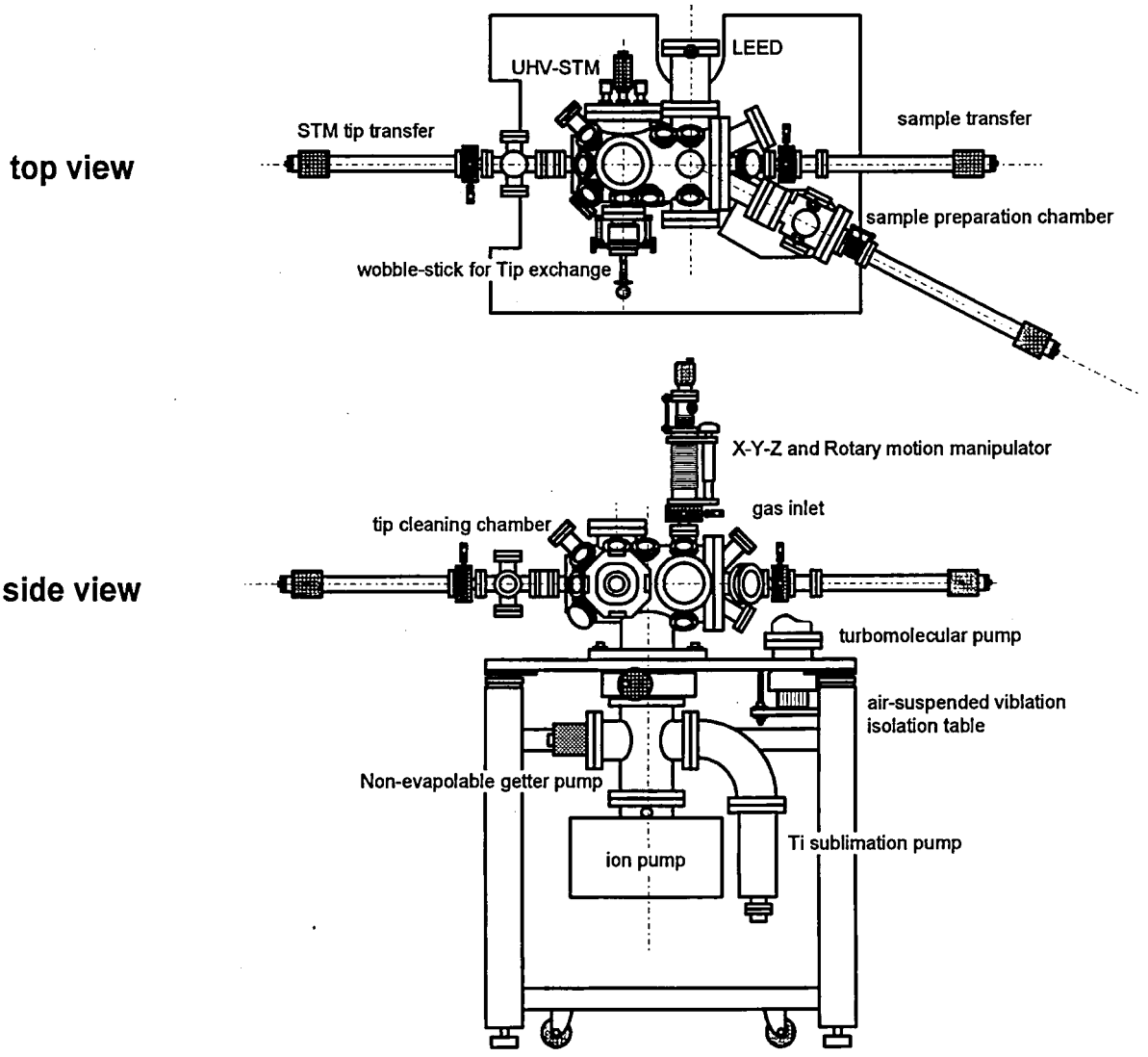

Figure 1. Schematic of the STM system operated in the UHV condition.

Pump-Probe Spectroscopy of Atoms and Molecules with the Combination of an Ultraviolet Laser and Synchrotron Radiation

Koichiro MITSUKE, Masakazu MIZUTANI, and Hiromichi NIIKURA *(Graduate Univ. for Advanced Studies)*

A mode-locked Ti:sapphire laser is made to oscillate at the frequency of the UVSOR storage ring in a multibunch operation mode. The second and third harmonics of the laser are generated in the wavelength ranges of 360 - 425 nm and 243 - 280 nm, respectively. Monochromatized synchrotron radiation (SR) from an undulator is introduced coaxially with the laser. The delay timing between SR and the laser can be changed from 0 to 11 ns with a precision of ±100 ps. The reliability and feasibility of this SR-laser combination technique are demonstrated by applying pump-probe experiments to the following two physical systems: (1) Two-photon ionization of helium atoms by way of the resonant state, He*($1s2p\ ^1P$), studied as the prototype of a time-resolved experiment, and (2) fluorescence excitation spectroscopy of $N_2^+(X\ ^2\Sigma_g^+)$ ions produced by SR photoionization of N_2 or N_2O. Laser induced fluorescence excitation spectra of the $(B\ ^2\Sigma_u^+, v' = 0) \leftarrow (X\ ^2\Sigma_g^+, v'' = 0)$ transition have been obtained as a function of the laser wavelength. This type of pump-probe technique will soon be widely available in the study of photodissociation and photoionization dynamics of gaseous molecules in the VUV and soft X-ray regions.

Vibrational Spectroscopy on Cryogenic Surfaces using Synchrotron Radiation

Makoto SAKURAI and Masuaki MATSUMOTO

Vibrational Spectroscopy makes it possible to analyze dynamical aspects of molecules adsorbed on surfaces. Molecular layers on cryogenic surfaces show specific structures which depend on the interaction between molecules and substrate, and the vibrational spectra reveal the details of the interaction. Infrared reflection absorption spectroscopy (IRAS) and high-resolution electron energy loss spectroscopy (HREELS) are useful tools for vibrational spectroscopy on surfaces, and they have complemental characteris-

tics, that is, IRAS is superior in resolution and stability whereas HREELS has higher sensitivity. Utilization of IRAS with HREELS in an identical vacuum system brings advantageous apparatus for researches of dynamical aspects of adsorbed molecules.

Under this project, we develop an apparatus for vibrational spectroscopy of molecules on cryogenic surfaces. The apparatus will comprise both measurement systems (IRAS and HREELS), a cryogenic sample holder and tools for preparation and characterization of surface cleanliness. The IRAS system will have optical system for inlet and outlet of synchrotron radiation in far-infrared (FIR) and infrared (IR) regions, since synchrotron radiation is brighter light source than conventional ones in this regions taking into account that the light source necessary for IRAS should have low emittance.

Rotation Induced Vibrational Mixing in Highly Excited Vibrational States of Formaldehyde

Mutsumi AOYAGI

The effects of both anharmonic and Coriolis interactions on the intramolecular dynamics in Formaldehyde are investigated quantum mechanically. Variational calculations including all of the vibrational modes, and the rotational modes are performed using the ab initio SDCI potential energy surface. Both time-dependent and time-independent analyses are made on the calculated eigenstates(up to 12000 cm^{-1}) to elucidate the role of Coriolis interaction in highly excited vibrational states. We also carried out the analyses of curvature distribution with respect to Hamiltonian parameters both on H_2CO and model Hamiltonian systems; the stadium billiard and the kicked rotator systems. We found that the anharmonic couplings assisted by b- and c-type Coriolis interactions and extensive K-mixings play a crucial role in the intramolecular dynamics at high energy region ($E>7500$ cm^{-1}). We also found that curvature distribution obtained from the H_2CO results shows similar characteristics with one from the stadium billiard system. Based on these results, we developed effective Hamiltonian of H_2CO system with a reduced dimensionality approximation.

Developments and Researches of New Laser Materials

Nobuhiko SARUKURA, Zhenlin LIU, Hideyuki OHTAKE and Shinji IZUMIDA

Although development of lasers is remarkable, there are no lasers which lase in ultraviolet and far infrared regions. However, it is expected that these kinds of lasers break out a great revolution in not only the molecular science but also in the industrial world.

In this project we research characters of new materials for ultraviolet and far infrared lasers, and develop new lasers by using these laser materials.

Ultra-High-Vacuum Friction Test Apparatus

Tatsuharu TORII, Takuhiko KONDOH, Shuji ASAKA and Michio WATANABE

Actuators that can operate in ultra-high vacuum are useful for experimental apparatus in many fields of molecular science. Such actuators consist of many moving parts which require no seizing and no degassing. In order to develop such actuators, we have newly designed an apparatus to test friction under UHV shown in Figure 1. The apparatus consists of an analyzing system of the degassing, a specimen temperature measuring system, and a friction force measuring system. At present friction test is possible in vacuum at pressure of 1.8×10^{-10}Torr. By using this apparatus, as the first step we will evaluate some coatings that reduce seizing and degassing on metal surfaces.

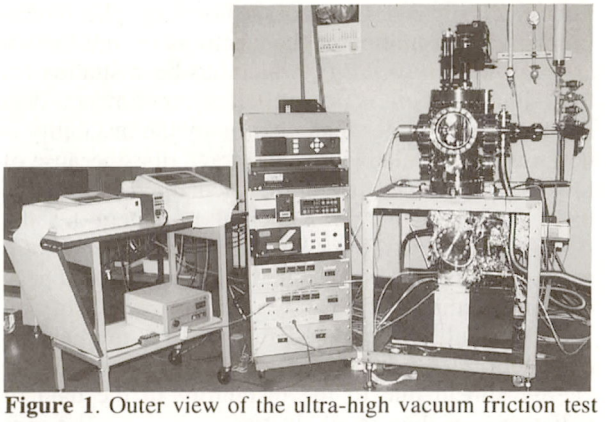

Figure 1. Outer view of the ultra-high vacuum friction test apparatus.

Investigation of Electronic Structures of Solid/Surface by Using Synchrotron Radiation

Masao KAMADA and Shin-ichiro TANAKA

Insulator surface is one of the interesting targets for surface science, but usual techniques such as UPS, Auger, and LEED are not available because of the charging of the samples. Therefore, we have grown thin insulator films on semiconductor surfaces and investigated their electronic structures, using photoelectron and optical spectroscopy with synchrotron radiation from the UVSOR storage ring. For examples, we found clear peaks due to the surface core-excitons in NaCl/Si(100). We have also investigated the co-adsorbed states of alkali atoms and oxygen atoms on GaAs(100), which is useful to achieve photo-sensitive surfaces with negative electron affinity.

Moreover, we are investigating the desorption dynamics on alkali halide surfaces and H_2O adsorbed on Si, using laser-induced fluorescence method or electron-ion coincidence techniques. The fast desorption of the ground-state neutral atoms was discovered on potassium halides.

It is important subject to develop new experimental systems and methods with synchrotron radiation. New beamline consisting of the helical undulator, monochromator covering the energy range of 5-250 eV with high resolving power, and a spin- and angle-resolved photoelectron spectrometer has been

constructed. By using this beamline we will carry out the complete experiment of the electronic structures of non-magnetic materials and also investigate the dynamics of the spin memory in the excited-states in insulators/semiconductor surfaces. In recent years, we have successfully developed the combined experiment of synchrotron radiation with laser to reach different excited states by means of two-photon excitation. (see UVSOR ACTIVITY REPORT 1997)

Study for High Brilliant Radiation Using the UVSOR Electron Storage Ring

Hiroyuki HAMA, Hitoshi TANAKA(*SPring-8*) and Masahito HOSAKA

Nonlinear phenomena on the accelerators are now in new field of physics for high energy accelerators and mathematical physics. One of the nonlinear phenomena in longitudinal motion of the electrons is well-known as *microwave instability*, which has been studied for long time but there is not sufficient experimental data and analysis to understand. Normally the instability is not occurred in relatively new storage rings because of low coupling impedance of the vacuum chambers. We have observed the phenomenon by operating the UVSOR storage ring with negative momentum compaction factor. It was found that the threshold peak current for the instability was much lower than that with ordinal operation with positive momentum compaction. We have also measured increase of the energy spread due to the instability in the data of radiation from the optical klystron.

Bunch deformation and the increase of the energy spread have been simulated by using a simple model for the interaction between the bunch of electrons and the inductive and resistive impedance of the vacuum chamber. At present the nonlinear bunch lengthening and an instability in phase space of the bunch have been able to be reproduced. Accordingly the combination of the inductive and the resistive impedance seems to play an important role. Further investigation of the experiments and the calculation is in progress.

Studies of Solid Surfaces by Photoelectron Spectroscopy

Toyohiko KINOSHITA

We are studying the electronic structures of solid surfaces, interfaces and adsorbates by using photo-electron spectroscopy, especially with synchrotron radiation from the UVSOR storage ring. Since 1995, we have constructed the new equipment for photo-electron spectro-microscopy measurements (see, annual review of IMS, 1995, p.158). The apparatus has been connected to the 2 beamlines (BL5B and BL7A) and we have obtained the preliminary data for the ferro-magnetic iron crystal in 1996. In 1997, a sample preparation chamber which is equipped with a LEED optics, evaporation guns, a quartz thickness monitor and so on has been connected with the photoelectron spectro-microscopy system. Figure 1 shows the picture of the whole apparatus. The use of the new sample preparation chamber enables us to perform the photo-electron spectro-microscopy studies for many kinds of samples.

We have also studied the resonant photoemission spectra for Tm monocharcogenides around the excitation threshold of $4d$-$4f$ and $3d$-$4f$ resonant regions. The details of these studies are appeared in this issue (Research activities at ultraviolet synchrotron orbital radiation facility; UVSOR).

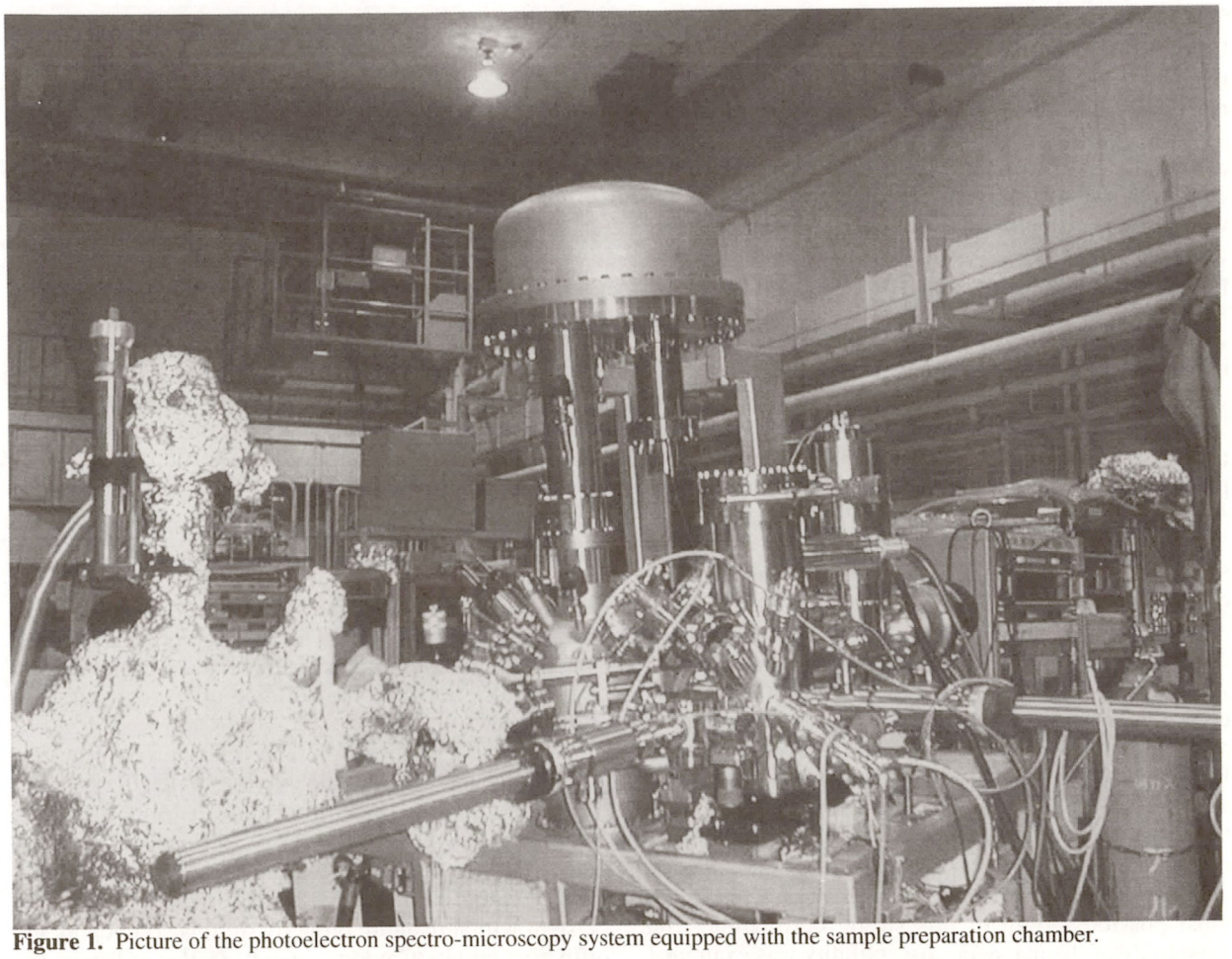

Figure 1. Picture of the photoelectron spectro-microscopy system equipped with the sample preparation chamber.

(2) Study of Molecular Solid toward Molecular Electronics

Theory of Electronic Phases in Molecular Conductors and Insulators: Electron Correlations in Quasi-One-Dimensional Systems

Kenji YONEMITSU, Jun-ichiro KISHINE, Takuhiro OGAWA and Michiyasu MORI

Electron correlations in quasi-one-dimensional electron systems have been studied with various techniques. (i) Mott transitions accompanied with Peierls distortion or $4k_F$ charge-density wave in $(DCNQI)_2M$ (M=Ag, Cu) are reproduced and their mechanisms are clarified by using a slave-boson mean-field plus $1/N$ corrections, and a perturbative renormalization-group approach based on the bosonization. (ii) Spin-density wave, superconductor, and metallic phases in $(TMTCF)_2X$ are interpreted in terms of decreasing dominance of the particle-hole channel which is equally singular to the particle-particle channel in pure one dimension by using a renormalization-group approach. (iii) d-wave superconductivity and one-particle vs. two-particle dimensional crossovers in $Sr_{14-x}Ca_xCu_{24}O_{41}$ are studied with a perturbative renormalization-group approach including the transverse single-particle hopping to the second order. The spin gap in even-leg ladder systems is shown to suppress the one-particle dimensional crossover inducing incoherent electron motion in the transverse direction. (iv) Fully saturated ferromagnetism in the ferromagnetic Kondo lattice model is shown, by the exact diagonalization technique, to be easily replaced by a paramagnetic state with the inclusion of the antiferromagnetic Heisenberg coupling, which is appropriate for $CoPc(AsF_6)_{0.5}$. Effect of the Kondo coupling on the metal-insulator transition and its interference with long-range Coulomb repulsion are currently under investigation. (v) Competition between spin-density wave and superconducting phases in $Pd(dmit)_2$ salts are studied by using the unconstrained Hartree-Fock approximation as a first step. The scaling behavior in two-dimensional systems with different degrees of the Fermi surface nesting will be investigated numerically.

Materials Science on Molecular Devices π-d Interaction in Molecular Metals

Kyuya YAKUSHI, Yukako YONEHARA and Iakov L. KOGAN

We have undertaken a systematic study on the solid molecular systems in which transition metals are embedded in a π-conjugated system from the viewpoint of the future design of the superconducting material.

The highly conductive phthalocyanine salts such as $CoPc(AsF_6)_{0.5}$ and $NiPc(AsF_6)_{0.5}$ are the prototype of the one-dimensional conductors in which the d- and π-orbitals form a double-chain and two-band system.

The finding of the pressure-induced metal-ligand charge transfer means that the charge-transfer continuously occurs from the narrow d-band to the wide π-band, which will change the ground state. We examined the electrical resistivity and thermoelectric power under high pressure. The electrical resistivity shows a metal-insulator transition, temperature of which increases upon increasing the pressure. The thermoelectric power indicated that this insulating phase was expanded upon increasing the pressure. This insulating phase is induced by the randomly generated positive charge on Ni chain which is produced by the pressure-induced metal-ligand charge transfer. (*See IV-A-1*)

Instead of high pressure, we made an attempt to shift the Fermi energy of the wide π-band by using electrochemical method. An electrode was built embedding solid phthalocyanine into poly-bisphenol-A-carbonate. PF_6^- ions were doped into and dedoped from the solid phthalocyanine in the polycarbonate controlling the electrochemical potential. This doping and dedoping was characterized by X-ray diffraction, ESR, optical absorption spectrum, electrical resistance and thermoelectric power. The examination of the controllability of the stoichiometry of $NiPc(AsF_6)_x$ is now in progress.(*see IV-A-2 and 3*)

The effect of the magnetic moment on CoPc is the most possible origin of this strong correlation. The anisotropy of the magnetic susceptibility was examined using oriented single crystals of $CoPc(AsF_6)_{0.5}$. The anisotropy of the susceptibility is much larger than the anisotropy of the g-factor of CoPc, which means that the exchange interaction has a strong anisotropy. Comparison with the XY model, which describes the system having anisotropic exchange interaction, put forward the quartet cluster $(CoPc)_2^+$ as the repeating unit of this magnetic conductor. (*see IV-A-4*)

Search for Negative-*U* Materials in Molecular Solid

Kyuya YAKUSHI, Mikio URUICHI, Jianyong Ouyang, Yoshiro YAMASHITA and Jingui QIN

The negative-*U* material comprises the molecule which has a negative on-site Coulomb energy or, in other words, an attractive force between two electrons within the molecule. We are looking for such compounds from the two directions: (1) a strong electron-molecular vibration coupling and (2) a strong nearest neighbor Coulomb repulsion. (1) A strong electron-molecular vibration interaction may overcome the repulsive force within the molecule and stabilize an on-site bipolaron state. The similar state has been found in the insulating compound, Cs_2SbCl_6, superconducting compound, $BaPb_{1-x}Bi_xO_3$, and conducting polymer, polypyrrole, but never been in an organic charge-transfer compound. (2) The molecular distance between the neighboring molecules is about 3.4Å, whereas recently synthesized long conjugated molecule has more than 15Å If we use the long conjugated molecule which is stacked in an eclipsed overlapping mode, the on-site Coulomb repulsion energy happens to be smaller than the nearest neighbor Coulomb repulsion occasionally.

To look for such molecules, multi-step-oxidation properties of electron donors are one of the key parameters. Generally, the difference (ΔE) between the first and second oxidation potentials is thought to be a measure of the on-site Coulomb energy in the organic conductor. BDNT shows an unusual property that the first and second oxidation potentials are not resolved. From the analysis of the width of the oxidation wave, ΔE is estimated to be 0.024 eV. Subsequently to the characterization of the charge-transfer compounds $(BDNT)_n[M(mnt)_2]_m$ (M=Co, Ni, Cu, Au, Pd, and Pt), it was elucidate by ESR that $Ni(mnt)_2$ takes the role of ferromagnetic interaction and BDNT is responsible to the conducting property in $(BDNT)_2$-$[Ni(mnt)_2]$. They are not interacting with each other. This ferromagnetic interaction seems to come from the McConell's spin polarization mechanism. The research program for the magnetic susceptibility experiment under high pressure is going on including the building up of high-pressure cell. (*IV-B-3*)

Nearest neighbor Coulomb repulsion is largest in the molecular conductor having half-filled band. Generally such a system becomes a Mott insulator. However, DMTSA-BF_4 shows a metallic behavior above 100 K. Through the polarized reflection spectroscopy, this compound is characterized as the Peierls system with a metallic property. In this compound, the effective on-site Coulomb energy U-V is still positive but overcome by the large transfer integral t=0.33 eV, which makes this compound metallic. Since the high pressure increases V, high-pressure experiment is planned in near future. (*See IV-B-1*) We are now examining new organic metals based on a long conjugated molecule BDT-TTP as well.

Toward Comprehensive Understanding of Various Electronic Phases in Molecular Conductors; Role of Long-Range Coulomb Repulsion

Kazushi KANODA, Yasuhiro NAKAZAWA, Kazuya MIYAGAWA, Hiromi TANIGUCHI, Koichi HIRAKI and Atsushi KAWAMOTO
(Ochanomizu Univ.)

In these years, we focused our attention to the family of dimeric $(BEDT\text{-}TTF)_2X$ quasi-two-dimensional systems, where metallic, superconducting and insulating states appear, depending on the molecular arrangement within the conducting layer or the kind of anion. After systematic NMR and specific heat studies, we concluded that the superconductor-insulator transition in this family is the Mott transition, where the on-site Coulomb interaction plays a crucial role. On the other hand, the ground states of the quasi-one-dimensional systems, $(R_1,R_2\text{-}DCNQI)_2M$ (M=Li, Ag), are insulators. However, the manner of the charge and spin ordering depends on R_1 and R_2. In this year's program, we aimed at clarifying the origin of the

paramagnetic and insulating state in $(DI\text{-}DCNQI)_2Ag$. The susceptibility and ^{13}C NMR studies have revealed that the origin is the Wigner Crystallization of electrons, which is different from the Mott insulator. This fact shows that the long-range Coulomb repulsion is responsible for the insulating state of this system. There are several candidates of Wigner Crystallization of holes in $(BEDT\text{-}TTF)_2X$. The experimental study in this line is now going on.

Development of New Organic Metals and Superconductors

Hayao KOBAYASHI, Hiroki AKUTSU, Emiko ARAI, Akane SATO, Hideki FUJIWARA, Hisashi TANAKA *(Univ. Tokyo)* **and Akiko KOBAYASHI** *(Univ. Tokyo)*

We have studied a series of λ-type BETS (=bis(ethyleneditio)tetraselenafulvalene) conductors λ-$BETS_2M_xM'_{1-x}X_yY_{4-y}$ (M, M'=Ga, Fe; X, Y=F, Cl, Br) and new organic conducting systems based on multi-chalcogen π donor molecules. The main results are as follows.

(1) λ-$BETS_2GaBr_{1.5}Cl_{2.5}$ is a semiconductor at ambient pressure but it transforms to a superconductor above 1 kbar. At 3 kbar, the onset of the superconducting transition was observed at 10.7 K. The midpoint temperature was 9.7 K, which is almost equal to that of so-called "10 K-class organic superconductor", κ-$ET_2Cu(NCS)_2$ ($T_c(^{12}C)$=9.6 K, ET= BEDT-TTF). λ-Type BETS system is the first example of 10 K class non-ET organic superconductor.

(2) The molecular superconductors ever studied seem to share a common phase diagram. That is, the antiferromagnetic insulating phase borders on the superconducting phase. However, the susceptibility measurement on the insulating phase of the above-mentioned system, λ-$BETS_2GaBr_{1.5}Cl_{2.5}$ suggested the nonmagnetic nature down to 10 K. This observation is consistent with the theoretical prediction by Seo and Fukuyama suggesting this compound is located near the border between spin gap phase and antiferromagnetic phase.

(3) By the systematic examination of the alloy systems λ-$BETS_2Ga_xFe_{1-x}Cl_4$, an unprecedented superconductor-to-antiferromagnetic insulating phase transition was discovered. This finding will open a new possibility of the design of the magnetic organic superconductors.

(4) Since the first report on (TTF)(TCNQ), a large number of organic metals have been synthesized. But almost all the systems can be classified into the same group, that is the organic metals based on TTF-like donor molecules. Therefore the development of non-TTF organic metals is one of the urgent problems. We have discovered the first organic metal based on peri-chalcogen bridged polyacene molecules with high conducting state (~10^3 Scm^{-1} at 4.2K).

High Pressure Structures of Molecular Conductors

Hayao KOBAYASHI, Takafumi ADACHI and Akiko KOBAYASHI *(Univ. Tokyo)*

As the first step of the high-pressure X-ray studies on the molecular crystals, we have made the structure determinations on the molecular conductors, α-BEDT-TTF_2I_3 and $[(CH_3)_2(C_2H_5)_2N][Pd(dmit)_2]_2$ by using beryllium cylinder cell at about 5 kbar. The pressure dependence of the lattice constants showed that the compressibility of organic conductor α-BEDT-TTF_2I_3 is much larger than that of the conductors composed of transition metal complex $[(CH_3)_2(C_2H_5)_2N][Pd(dmit)_2]_2$. X-Ray diffraction intensities were collected by Weissenberg type X-ray imaging plate system. The structures were refined by the procedure adopted in the usual ambient-pressure crystal structure analysis. The R-values were about 10 %. Through these studies, many information necessary for the X-ray crystal structure studies at higher pressure by diamond anvil cell was obtained.

NMR Study of Liquid Crystals

Osamu OISHI, Hiroki FUJIMORI, Daisuke KUWAHARA, Jean-Pierre BAYLE, Hironori OGATA, Toshihito NAKAI* and Seiichi MIYAJIMA *(*Univ. Tsukuba)*

Extensive NMR investigations were conducted on the dynamical properties of liquid crystal. (i) Pulsed-field gradient spin-echo spectrometer was improved for slower diffusion measurement in solids and liquid crystals. Versatile pule programmer was designed and constructed. (ii) Theoretical framework was established for the analysis of the field-aligned NMR spectrum. (iii) Microscopic origin of antiferroelectricity is being studied with ^{13}C NMR. (iv) Natural abundance ^2H NMR was applied to detect the mass effect on the dynamics and phase transitions. (v) Transient dipolar oscillation of the ^{13}C magnetization was detected for the newly synthesized liquid crystal, and was proved useful for the analysis of the dynamics and segmental orders. (vi) New probehead was designed and constructed for the NMR of liquid crystal under hydrostatic pressure.

Solid State NMR Studies of Hydrogen-Bonded Dielectrics and C_{60}-Based Superconductors

Tomoyuki MOCHIDA, Daisuke KUWAHARA, Hironori OGATA and Seiichi MIYAJIMA

Single crystal ^2H NMR was conducted at low temperature to analyze the microscopic origin and mechanism of the deuterium-induced antiferroelectric ordering and the deuterium-induced incommensurate phase. Newly synthesized superconductors with the formulae of $A_xH_yC_{60}$ (A are alkali metals) were studied with ^{13}C, ^1H, and ^{23}Na NMR. Structural and electronic properties were analyzed.

Pressure Effect on Molecule-Based Magnetic Materials

Yuko HOSOKOSHI, Masaki MITO*, Kazuyoshi TAKEDA* and Katsuya INOUE *(*Kyushu Univ.)*

We have developed a pressure clamp cell for magnetic measurements with high accuracy and have already observed a unique pressure effect of the suppression of the structural change on galvinoxyl and F_5PNN. In this year, we performed more detailed study on these two compounds by means of the heat capacity measurements under pressure.

For galvinoxyl, we extended the study down to 0.5 K. Both magnetic and heat capacity were measured under 6.4 kbar. Quasi one-dimensional nature of this material is confirmed and a three-dimensional phase transition is observed at 0.72 K.(see V-G-1)

F_5PNN (F_5PNN = pentafluorophenyl nitronyl nitroxide) is described by an alternating linear chain, where the Hamiltonian is $H = -2J \Sigma_i \{S_{2i-1} \cdot S_{2i} + \alpha S_{2i} \cdot S_{2i+1}\}$. Change of the alternating factor (α) from 0.4 to 1 with applied pressure was observed in our previous susceptibility measurements. We examined the heat capacity under several pressure. The results are consistent with that of the susceptibilities. Moreover, gradual increase of α with applying pressure is observed. Enhancement of the value of J is rather small than α. The detailed study for the mechanism of the pressure effect on this material is now underway.

Quantitative Analysis of Organic Thin Films Using Angle-Resolved UPS

Nobuo UENO, Masaru AOKI, Shinji HASEGAWA, Koji Kamiya OKUDAIRA*, Yoshiya HARADA*, Hisao ISHII and Kazuhiko SEKI**** *(*Chiba Univ., **Nagoya Univ.)*

Angle-resolved photoelectron spectroscopy (ARUPS) is a well-known technique to investigate the electronic structure of surfaces. One can in principle determine the orientation and electronic states of molecules adsorbed on crystal surfaces by the quantitative analysis of the photoelectron angular distribution. For thin films of functional organic molecules, which are promising candidates to realize new electronic devices, the determination of molecular orientation and the electronic structure in the ultrathin films is of fundamental importance, since the molecular orientation is different from that in a bulk crystal, and thus new electronic states appear owing to the molecule/substrate, molecule/overlayer and molecule/molecule interactions which depend on the molecular orientation. Although ARUPS experiments have been widely performed on such thin films, the quantitative analysis of the ARUPS intensity and the determination of molecular orientation have little been realized due to the difficulty of quantitative analysis of the photoelectron angular distribution. We have recently succeeded to analyze the photoelectron angular distributions from thin films of large functional organic molecules.

The goal of our project is to obtain quantitative information on the full geometrical structure of ultrathin films of functional organic molecules as well as the electronic structure typical of the films by the quantitative analysis of photoelectron angular distribution, and open a door to realize quantitative chemical analysis of organic ultrathin films using ARUPS with synchrotron radiation.

In order to perform the project, a new ARUPS spectrometer, which enable us to measure accurate photoelectron angular distributions from functional organic thin films, will be constructed at the BL8B2 of the UVSOR facility. The spectrometer consists of a 75 mm hemispherical sector analyzer with two-axes rotations, electrostatic lens of various operation offering various angles of acceptance, and a μ-metal UHV chamber.

Construction of UV-Inverse Photoemission Spectrometer and Measurements of Conduction Band DOS of Transparent Conducting Oxides

Hideo HOSONO,* Naoyuki UEDA * and Hiroshi KAWAZOE** *(*IMS, **Tokyo Inst. Tech.)*

In most oxides, high electrical conductivity is not compatible with high transparency to visible radiation. We have created transparent metallic conducting crystalline and amorphous oxides following a working hypothesis. Examples are $MgIn_2O_4$, $ZnGa_2O_4$ and Cd_2GeO_4. It is considered that these materials have a small DOS in the bottom part of the conduction band. The purpose of this project is to measure the conduction band DOS of these novel materials by inverse photoemission spectrometer constructed here. The progress in 1996 was as follows:

(1) UPS and XPS units were joined to a vacuum chamber system and their performance was examined.

(2) An electron gun and an ellipsoidal mirror were installed in the BIS-chamber and optical alignment was finished. Resolution of ~0.6 eV was obtained for the spectra of Au Fermi.

New Organic Materials Based on Novel Heterocyclic Compounds

Yoshiro YAMASHITA, Shoji TANAKA and Masaaki TOMURA

We have succeeded in preparing new electron donors with extended π-conjugation. For example, novel bis(1,3-dithiole) electron donors were prepared by oxidative intramolecular cyclization of 2,2'-bis(1,4-dithiafulven-6-yl)-3,3'-bithienyls. X-ray analyses of the neutral and dication states of the donor revealed that there is a large conformational change between them. Bis(1,3-dithiole) compounds containing a di(2-thienyl)methane unit underwent deprotonation by oxidation to give dithienylmethyl cations with intense absorptions in the near infrared region. X-ray analysis indicates the polymethine cyanine-like structure of the cation. Non-planar bis(1,3-dithiole) donors containing a fused xylene and a thiadiazole ring were also prepared. The properties of the cation radical salts were dependent on the incorporated solvent molecules, where a THF incorporated salt showed metallic behavior although the corresponding salts incorporating

2,5-dihydrofuran or 1,3-dioxolane were semiconductors. Furthermore, we have prepared several donor-acceptor compounds containing both electron-donating heterocycles and electron-accepting ones. They showed small HOMO-LUMO gaps which were characterized by redox potentials and absorption spectra. Details of these works are described in VIII-C section.

(3) Material Control in Multi-Reaction Centers

Conversion of Myoglobin into a Peroxygenase: A Catalytic Intermediate of Sulfoxidation and Epoxidation by the F43H/H64L Mutant

Shin-ichi OZAKI, Toshitaka MATSUI and Yoshihito WATANABE

[*J. Am. Chem. Soc.*, **118**, 6666 (1997)]

The superposition of the active site structures of Mb and other hemoproteins enables us to utilize Mb as heme enzyme models for the elucidation of structure-biological function relationship. We have engineered sperm whale Mb based on the comparison of crystal structures of oxymyoglobin and an oxy form of cytochrome *c* peroxidase (C*c*P). Although the Leu29 → His and His → Leu double replacement of Mb seems to create a peroxidase-like active site, the imidazole is located too far from the heme center to interact with hydroperoxide bound to the iron. Our previous results suggest that L29H/H64L Mb cannot efficiently cleave O-O bond to generate a ferryl π radical cation species, equivalent to compound I of peroxidase. Thus, we have mutated Phe43 to a histidine residue because the predicted distance between His43 and the heme iron is approximately equal to that of C*c*P. The novel F43H/H64L Mb mutant oxidizes sulfide and styrene more efficiently than peroxidase. More interestingly, we have identified a compound I like species of the Mb mutant as the catalytic intermediate for the first time; i.e., the mixing of F43H/H64L Mb and *m*CPBA causes the decrease in absorbance at 406 nm, followed by the shift to longer wavelength by 12 nm. The formation of the first intermediate proceeds at the rate of $k_{obs1} = 110\ s^{-1}$, and the Soret shifts to 418 nm at the rate of $k_{obs2} = 9.2\ s^{-1}$. Decrease in the absorbance of the Soret and intense absorbance around 500 - 700 nm are characteristic for the conversion of ferric to ferryl porphyrin radical cation, and the following Soret shift is due to the decay of compound I to compound II as observed for other heme containing peroxidases. Upon the addition of styrene or thioanisole to the compound I intermediate, absorbance of the Soret band for the intermediate is recovered back to the level of ferric state. Thus, it is now convincing that the observed species bears two-electron oxidation equivalents. These results clearly indicate that the alignment of the distal histidine is important for the reactivity as well as the direct observation of the transient catalytic species for Mb.

Molecular Assembly on Surface through Coordination Bonds Towards Solution-Phase Molecular Epitaxy

Masa-aki HAGA, Hideaki MONJUSHIRO, Yasushi KAWATA, Md. Delower HOSSAIN and Kezhi WANG

The assembling of polynuclear metal complexes at the interface is one of the potential synthetic routes to realize the solution-phase molecular epitaxy towards molecular electronic devices. In order to control the molecular ordering in two dimensions, the incorporation with coordination bond has advantage compared to the other molecular interactions such as hydrogen bonding and electrostatic interaction from the viewpoint of strength of interaction and molecular geometry around mental ion. However, the incorporation with coordination bond at the interface has not extensively studied so far. Our final goal of this 'surface coordination chemistry" project is to construct the supra- or supermolecular assembly in the controlled manner through the coordination bond at the interface, and to find a molecular function as a switch by external stimuli.

We have started to prepare self-assembled solid state multilayer films based on the metal complexes. The stepwise layer-by-layer formation on surface can be achieved by anchoring the ligand on the surface at first and then coordination of the metal ion, and again incorporation of the bifunctional ligand to the first metal ion and so on. Since these processes in solution are almost identical to the gas-phase molecular beam epitaxy, this process can be regarded as solution-phase molecular epitaxy, which will be more versatile than the gas-phase one. For making the self-assembled multilayer films on gold, we used new anchoring ligand, 2,6-bis(N-(1-mercaptooctyl)-benzimidazolyl)-pyridine(merbzim). Incorporation of Fe^{2+}, Co^{2+}-merbzim complexes with tetracarboxybipyridine layer is under way.

The multilayer films can also be produced by the Langmuir-Blodgett(LB) techniques. Bis(benzimidazolyl)-pyridine with long alkyl chain(L) was used as a ligand for LB method. We found that the complex, $[Ru(L)(tppz)]^{2+}$, formed a stable monolayer film on the Langmuir trough air-water interface and transferred to solid surface. The incorporation of Cu^{2+} ion to the amphiphilic Ru complex from the subphase was confirmed by the XPS and XRD measurements.

Assembled Metal Centers in Enzymes

Takeshi SAKURAI and Hidemi NAGAO

Metal centers as the active site in metalloproteins and metalloenzymes do not exist as isolated centers but as functionally related centers or as metal clusters to exert integrated functions such as electron-transfer, activation of small molecules like dioxygen, NOx,

SOx, etc. Laccase, ascorbate oxidase, ceruloplasmin, and bilirubin oxidase, which belong to a super family of multicopper oxidase are such the enzymes. The active site of these enzymes is composed of the three types of coppers, the type 1 Cu(blue Cu) the type 2 Cu(non-blue Cu), and a pair of the type 3 Cu's (EPR non-detectable Cu at the resting state). The latter two types of copper form the unique trinucelar site, at which electrons transferred from the type 1 Cu site by the intramolecular long range process are pooled and a dioxygen is reduced to two water molecules. Such the four-electron reduction of dioxygen is performed only by multicopper oxidases and the Cu-Fe center in terminal oxidases in the respiration process. Our goal of the study is to reveal the unique steric structure and magnetic property of the Cu trinuclear center and the reaction mechanism by using absorption, CD, MCD, EPR, SQUID, electrochemistry, etc. Another target of our study is NO reductase from a denitrifying bacterium, *Paracoccus halodenitrificans*. Although special attention has been paid for NO for these years, many studies have been focused on to forming and detecting this inorganic hormone. We have finished to establish the purification method of this membrane protein and started the biophysical characterization of it. NO reductase is apparently a complex of *b* type and *c* type cytochromes. We also determined amino acid sequences of both subunits and studied their higher order structure from molecular evolutional point of view. The aim is not only to reveal the structure of each active site but also to reveal the integrated function of them.

Metal Assisted Control and Functionalization of Biomolecules

Mitsuhiko SHIONOYA, Kentaro TANAKA, Motoyuki TASAKA *(Graduate Univ. for Advanced Studies)*, **Kazuki SHIGEMORI** *(Graduate Univ. for Advanced Studies)*, **Akihiko HATANO** *(Graduate Univ. for Advanced Studies)*, **Hiromasa MORISHITA** *(Graduate Univ. for Advanced Studies)*, **Jik CHIN** *(McGill Univ. and IMS)*, **Luigi G. MARZILLI** *(Emory Univ. and IMS)* **and Patricia A. MARZILLI** *(Emory Univ. and IMS)*

In the control of gene regulation, DNA functions are carried out through interactions with other molecules such as gene regulatory proteins and smaller molecules associated by characteristic conformational changes (curvature, unwinding, melting, etc). Therefore, molecules that induce structural changes of specific sites of DNA would effect gene expression and could possibly be applicable in the treatment of genetic disorders. In addition, the understanding of molecular basis of noncovalent complexes cooperatively formed with DNA can aid in the design of artificial DNA or peptides with tailored functions. Based on these concepts, we have been working on the following projects.

(1) Metal Complexes targeting AT-rich TATA-box in the Transcriptional Regulatory Domains of DNA
(2) Artificial DNA: Metal Alignment at the Axis of ds-DNA with Chelating Nucleobases
(3) Artificial Peptide: Alignment of Functionalized Metal Complexes tethered to Amino-acid Residues
(4) Modeling of DNA Polymerases by Newly Designed Binuclear Metal Complexes
(5) Molecular Recognition of DNA by Metal Assisted Self-Assembly: Anti-sense and Macro-ring
(6) Metal Assisted Self-Replication of Small Molecules and DNA

Activation of Carbon Dioxide on Metal Complexes Directed Toward Carbon-Carbon Bond Formation

Koji TANAKA, Kiyoshi TSUGE, Hideki SUGIMOTO and Tetsunori MIZUKAWA

Direct electrochemical reduction of CO_2 is not thermodynamically favorable process because of the large negative redox potential of $E°(CO_2/CO_2^-)$ at -2.21 V (*vs.* SCE). On the other hand, carbon dioxide bonded to metals is subject to a C-O bond cleavage reaction to form metal-CO complex since the electron density of the CO_2 moiety is highly enhanced by π-back donation from occupied d orbital to empty π^* orbital of CO_2. Along this line, a variety of metal complexes have been used as catalysts precursors for the reduction of CO_2, though the active species have hardly been confirmed in those reactions. Highly reduced products such as HCHO, CH_2OH, HOOCCHO and $HOOCCH_2OH$ have been obtained in electrochemical CO_2 reduction catalyzed by Ru-polypyridyl complexes at low temperature, and the reaction mechanism is established by successive reduction of CO_2 to CH_2OH on Ru. To construct more efficient catalytic system that can reduce CO_2 at ambient temperature, site opening and closing would be preferable for stabilization of the reaction centers, inhibition of side reactions, and promotion of eliminating the products from a reaction center. An equilibrium of chelation and dechelation of ligands with a little configuration barrier may be utilized as the construction of homogeneous catalysts. The purpose of this project is to develop new catalytic systems directed toward the activation of not only CO_2 but also small molecules.

Self-Assembling Molecular Systems

Makoto FUJITA, Takahiro KUSUKAWA, Shu-Yan YU, Fumiaki IBUKURO and Masaru AOYAGI

We have been studying the self-assembly of finite and infinite structures based on coordination chemistry, where coordinate bonds induce the generation of defined structures. Our studies are focused on the self-assembly of such finite structures as macrocycles, catenanes (interlocked molecules), and cages, as well as infinite network structures. In the construction of the discrete structures, our strategy may be characterized by the use of palladium's 90 degree coordination. Thus, the structure of a molecular square assembling from (en)Pd(NO3)2 and 4,4'-bipyridine was confirmed by X-ray crystallography. We also found that rationally designed molecular boxes composed of transition

metals and organic ligands are quantitatively catenated if the boxes involve parallelly arranged aromatic sides with the interplane separation of ca 3.5 Å. On the other hand, a hollow, roughly spherical nanocage framework (ca 2 nm in diameter) was constructed by self-assembly from ten species, four organic ligands held together by six metal ions. It was shown that the self-assembled cage can hold as many as four adamantane molecules inside its nanosized cavity. Construction of infinite systems involving molecular ladders, bricks, rods, grids, and nets was achieved through transition metal coordination.

OKAZAKI CONFERENCES

The Fifty-Sixth Okazaki Conference

Condensed Phase Quantum Dynamics: Application to Chemical Systems

Organizers: Y. TANIMURA *(IMS)*, **R. COALSON** *(Univ. Pittsburgh)* **and K. TOMINAGA** *(IMS)*
Invited Overseas Speakers: Rob. D. COALSON *(Univ. Pittsburgh)*, **Jose ONUCHIC** *(UCSD)*, **J. HUPP** *(Northwestern Univ.)*, **Majed CHERGI** *(Univ. Lausanne)*, **David KLUG** *(Imperial College)*, **Norbert SCHERER** *(Univ. Penn.)*, **Vladimir CHERNYAK** *(Univ. Rochester)* **and Y.-J. YANG** *(Hong Kong Univ.)*

Over the past two decades experimental and theoretical tools have reached an unsurpassed level of sophistication in describing the dynamics of simple molecular systems. Crucial to this have been the breathtaking developments in laser spectroscopic techniques, in particular since the advent of ultrashort pulse lasers, and in the development of new theoretical concepts combined with the impressive increase in computational capacity. More recently, the effort has passed from diagnosing reactions to controlling them, opening very promising prospects for a large class of applications in Chemistry, Physics and Material Science. The emphasis is now shifting to systems of ever greater complexity such as condensed phases and biological systems. Indeed, most biological functions and chemical reactions in Nature take place in the condensed phases or in heterogeneous media. The same holds for preparative chemistry in Industry. The study of condensed phase dynamics has witnessed a tremendous development over the past few years due to the variety of situations encountered and problems to be solved. These call for expertise in the fields of Physics, Chemistry and Biology.

The purpose of this conference is to foster development of an international network of young (and not so young!) experimentalists and theoreticians working in the exciting area of condensed phase quantum dynamics. The program of this meeting emphasized various aspects of quantum dynamics in many body systems, as probed by conventional and ultrafast laser techniques. The topics that will be covered during the meeting include photoinduced dynamics in:

- solids
- liquids
- biological systems

Thirteen invited talks were presented to an audience about 50 persons. We hoped that this format would allow intense discussions and a fruitful exchange of ideas. A poster session was also held to discuss the topics more closely and to exchange information.

The Fifty-Seventh Okazaki Conference

Reaction Field and Mechanics of Respiratory Terminal Oxidases *(October 28 - 30, 1996)*

Organizers: T. MOGI *(Univ. Tokyo)* **and T. OGURA** *(IMS)*
Invited Overseas Speakers: R. B. GENNIS *(Univ. Illinois, Urbana, U.S.A.)*, **M. SARASTE** *(European Molec. Biol. Lab., Germany)*, **M. WIKSTROM** *(Univ. Helsinki, Finland)*, **O. EINARSDOTTIR** *(Univ. California, Santa Cruz, U.S.A.)*, **W. B. TOLMAN** *(Univ. Minnesota, U.S.A.)*, **F. MILLET** *(Univ. Arkansas, U.S.A.)* **and B. LUDWIG** *(Univ. Johan-Wolfgang-Goethe, Germany)*

From bacteria to human, life of all aerobic organisms is supported mainly by energy derived from oxidation of foods. For example, over 90 % of dioxygen taken up through the human lungs is consumed in aerobic respiration. Electrons liberated from respiratory substrates are used to reduce dioxygen, the ultimate electron acceptor, to water. Simultaneously, protons are pumped out by a mechanism coupled with intramolecular electron transfer, thus establishing a transmembrane electrochemical gradient of protons. The heme-copper binuclear center that offers an efficient reaction field for dioxygen reduction, has been found in a superfamily of respiratory terminal oxidases and is characterized by its unique coordination structure. In 1995 the X-ray crystallographic structures of cytochrome *c* oxidases from bovine and P. denitrificans have been determined with an atomic resolution. They provide us a molecular basis to elucidate the electron-transfer-coupled proton pump, one of the main themes in biological energy transduction. Taking this special occasion, this conference was held.

The conference began with a plenary lecture by Dr. M. Saraste followed by 4 oral and a poster sessions. Seventeen invited talks and eleven posters were presented. The oral sessions were divided into four topics: (1) Structure, (2) Molecular Biology, (3) Dynamics and Mechanics, and (4) Reaction Field, of Terminal Oxidases. At the beginning of each session, the chair briefly explained the state of the art and the problems to be solved of each topic. The poster session began with two minutes briefing by individual presenter.

Productive and stimulating discussions about the topics were made. The poster session, started at 7:30 pm, continued till as late as 11:00 pm. Several new plans for international joint research were proposed. As a whole, this conference was scientifically fruitful and in this sense it was successful thanks to the distinguished participants and the supports from IMS.

The Fifty-Eighth Okazaki Conference

Recent Development and Future Prospects of Molecule-Based Conductors *(March 7-9, 1997)*

Organizer: H. Kobayashi *(IMS)* **and K. Yakushi** *(IMS)*
Invited Speakers: Prof. D. Schweitzer *(Univ. Stuttgart, Germany)*, **Dr. U. Geiser** *(Argonne National Laboratory, U.S.A.)*, **Prof. Daoben Zhu** *(Institute of Chemistry, Beijing, China)*, **Prof. M. Kurmoo** *(IPCMS-GMI, Strasbourg University, France)*, **Prof. A. E. Underhill** *(Univ. Wales, UK)*, **Dr. P. Cassoux** *(CNRS, Toulouse, France)*, **Dr. V. N. Laukhin** *(Chernogolovka, Russia)*, **Prof. E. Coronado** *(Univ. Valencia, Spain)*, **Prof. R. T. Henriques** *(Instituto Superior Tecnico, Portugal)* **and Prof. E. B. Yagubskii** *(Institute of Chemical Physics, Chernogolovka, Russia)*

The first clear evidence of the existence of the metal electrons in the molecular crystals was obtained by the X-ray observation of the giant Kohn anomaly about 25 years ago. Since then extremely large progress has been achieved in the physics and chemistry of molecular conducting systems. Especially, the discovery of the organic superconductor in 1979-1980 encouraged greatly the development of new molecular metal systems. The structure-chemical concept of the molecular design of the two-dimensional systems with stable metallic states was developed in the middle of 1980s. The appearance of various two-dimensional π metals and superconductors enabled the sophisticated experimental studies on the low-temperature magneto-transport properties of the organic conducting systems, which revealed the molecular metals to be "clean systems" with well-defined Fermi surfaces.

The main aim of this Okazaki Conference was to review the important conducting systems developed in the last decade and to find new clue for future progress. The main topics of the conference are (1) the development of new BEDT-TTF conductors and superconductors and the new physics of the two-dimensional organic conducting systems, (2) new conducting metal dithiolene complexes with extended π electron systems, (3) organic metals with magnetic anions and molecular metals with π-d mixing bands, (4) trials toward the development of organic ferromagnetic conductors, (5) syntheses and characterization of new organic conductors.

The conference consisted of 40 oral and 63 poster presentations, and was attended by 153 scientists. The scale of the 58th Okazaki Conference was exceptionally large. The very fruitful discussions were made to get the future prospects of molecule-based conductors.

The Fifty-Ninth Okazaki Conference

Molecular Architecture and Function of Inorganic Self-Assembled Multilayers (*August 7-9, 1997*)

Organizers: A. YAMAGISHI *(Hokkaido Univ.)*, **M. HAGA** *(IMS)*, **M. FUJITA** *(IMS)*, **T. ENDO** *(Tohoku Univ.)*, **K. KURODA** *(Waseda Univ.)* **and K. TANAKA** *(IMS)*
Invited Overseas Speakers: R. ROBSON *(Univ. Melbourne, Australia)*, **T. E. MALLOUK** *(Penn State Univ.,USA)*, **H. D. ABRUNA** *(Cornell Univ., USA)*, **G. DECHER** *(Univ. Louis Pasteur, France)*, **H. YANG** *(Univ. Toronto, Canada)*, **C. P. KUBIAK** *(Purdue Univ., USA)* **and K. R. DUNBAR** *(Michigan State Univ., USA)*

Self-assembled multilayer structures on surfaces based on inorganic compounds comprise one of the up-surging fields in materials chemistry. Comprehension of 2D or 3D molecular assemblies on surfaces and of controlled self-organization of multilayers will provide us with a new paradigm for future advances in material science. The aim of this conference is to discuss the synthesis and structural control of multilayer materials based on the inorganic compounds, molecular assembled solids linked by molecular building blocks, and characterization and electrochemical/photochemical functions of new structures. The conference consists of four major topics: (1) syntheses and characterization of multilayer materials on surfaces, (2) structural control of self-assembled multilayer materials based on inorganic layered solids, or molecular building blocks, (3) molecular architecture of supramolecular inorganic-organic co-assemblies, (4) electrochemical/photochemical functions of multilayer materials. The conference involves twenty-six oral presentations and also fifty-four posters, and was attended by 120 scientists. The conference offered the opportunity for a full and informal discussion of recent achievements and problems, and exchanges of ideas among the scientists in different fields such as solid-state chemistry, surface chemistry, electrochemistry, and inorganic chemistry, organic chemistry. The molecular design through self assembly, fundamental surface characterization, and properties and function of inorganic monolayer and multilayers were extensively discussed.

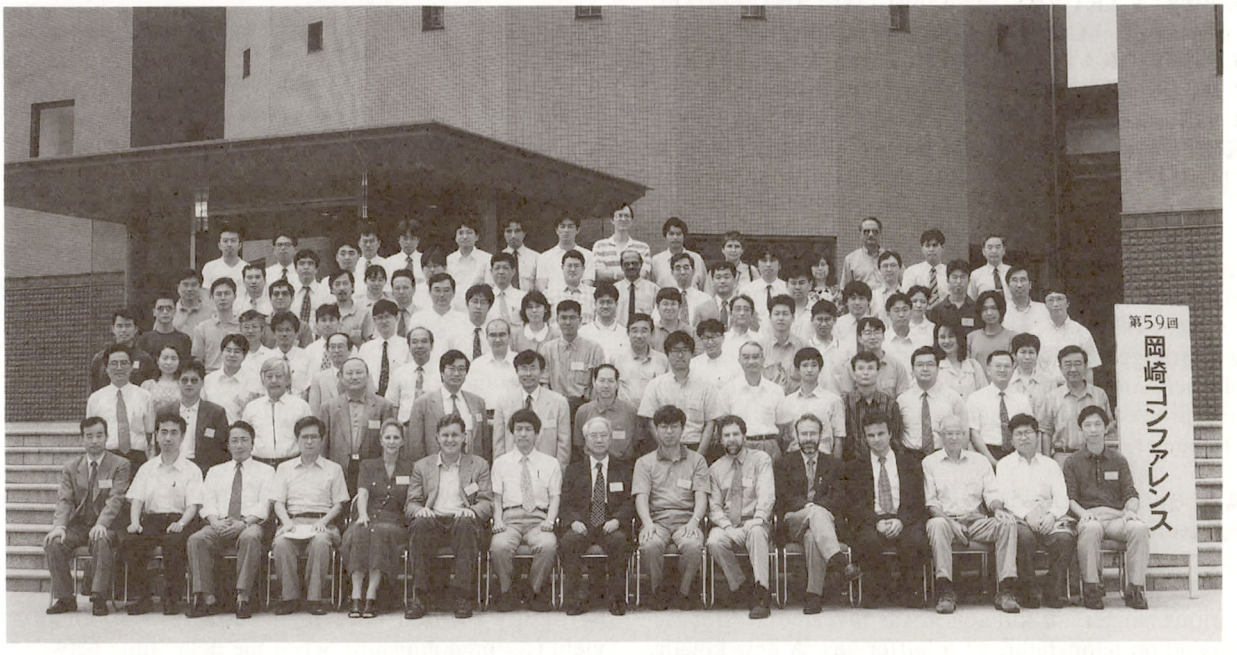

59th Okazaki Conference (1997. 8. 7 8. 9)

JOINT STUDIES PROGRAMS

As one of the important functions of an inter-university research institution, IMS undertakes joint studies programs for which funds are available to cover research expenses as well as travel and living expenses of individuals. The proposals from domestic scientists are reviewed and controlled by an inter-university committee. The programs are carried out under one of five categories:

(1) Joint Studies on Special Projects (a special project of significant relevance to the advancement of molecular science can be carried out by a team of several groups of scientists).
(2) Research Symposia (on timely topics, organized by collaboration between outside and IMS scientists).
(3) Cooperative Research (carried out by outside sientists with collaboration from an IMS scientist).
(4) Use of Facility (the Computer Center, Laser Research Center for Molecular Science and other research facilities at IMS are open to all researchers throughout the country).
(5) Joint Studies Programs Using UVSOR Facilities.
A. Special Projects, B. Cooperative Research Projects, C. Invited Research Projects,
D. Use-of-UVSOR Projects.

In the fiscal year 1996, the numbers of joint studies programs accepted for categories (1) - (4) were 2, 10, 92 and 252, respectively, and those accepted for subcategories (5)A - (5)D were 3, 24, 1 and 147, respectively.

(1) Special Projects

A Advanced Research of Carbon Clusters

Contributors: **Yusei MARUYAMA** *(Hosei Univ.)*, **Kyuya YAKUSHI, Tadaoki MITANI** *(JAIST)*, **Hirotsugu ACHIBA** *(Tokyo Metropolitan Univ.)*, **Tatsuhisa KATO, Hidetoshi FUKUYAMA** *(Univ. Tokyo)*, **Hiroyoshi SUEMATSU** *(Univ. Tokyo)*, **Toshiyasu SUZUKI** *(NEC)*, **Seiichi MIYAJIMA, Keiichirou NASU** *(KEK)* **and Yoshihiro IWASA** *(JAIST)*

The aim of this research is to search for new families of fullerene materials and to obtain a comprehensive understanding of various unique features of fullerene materials. The research was carried out over a wide range covering physical chemistry, solid state physics, surface sciences. To accelerate our collaborative project we have held a workshop on 21 and 22 December, 1996.

A-1 Selective formation of specific isomers of fullerenes

Systematic fractional change in the yield of various isomers of fullerenes was revealed to strongly depend on temperature of a buffer gas. A new kinetic consideration is proposed for understanding the observed temperature- and pressure-dependence of yield of fullerenes. The model consists of three competitive reactions in consideration of plausible behaviors of a precursor, (1) decomposition into smaller fragments, (2) isomerization leading to formation of a stable fullerene cage, and (3) growth into a large carbon cluster. Arrhenius activation energy of formation of stable fullerenes was determined to be 0.8eV for both C_{60} and C_{70}, while a higher energy of 2.0-3.3eV for seven different isomers of higher fullerenes raging from C_{76} to C_{84}. Correlation in the activation energy is noted for a series of higher fullerenes with different sizes, suggesting the existence of a specific precursors in their formation process.

A-2 Photoionization/fragmentation of endohedral fullerenes

Photoionization/fragmentation of endohedral-fullerenes was investigated by use of laser-desorption time-of flight (LD-TOF) mass spectroscopy. The variety distribution of the parent ion (LaC_{82}^+) was found to be bimodal, as has previously shown for laser desorbed C_{60}^+. The fragment ions have velocity distribution corresponding predominantly to the fast parent ion distribution. The LD-TOF mass spectra taken with a relatively low laser fluence were independent of the decay time of the extraction pulses, showing only a monotonically decreasing patterns of LaC_{2n}^+ (as n decreased). However, with higher laser fluence, it was shown that the mass distributions drastically changed from the monotonically decreasing pattern to that of C_{2n}^+, and LaC_{2n}^+ with magic numbers. Based on these findings, a plausible photoionization/fragmentation mechanism is presented and discussed.

A-3 Preferential formation of C_{10}^- upon tandem irradiation of graphite with IR and UV laser pulses

Infrared pulse laser ablation of graphite followed by tightly focused ultraviolet pulse laser irradiation yield C_{10}^- predominantly when the delay time between the two laser pulses is set at about 50-200 microseconds. The mechanism of the formation of C_{10}^- is deduced to be the attachment of slow photoelectrons to neutral C_{10} produced by fragmentation of hot neutral clusters of larger sizes. There is an indication that C_{10} and its anion have cyclic structure in contrast to the other chainlike clusters.

A-4 Metal-insulator transition of ammoniated K_3C_{60}

Magnetic susceptibility, electron spin resonance and ^{13}C-NMR data on $NH_3K_3C_{60}$ reveal that $NH_3K_3C_{60}$ is a narrow-band metal with a transition to an insulating ground state at 40K. This transition suppresses the superconductivity that is expected to

occur around 30K according to a simple empirical relation between Tc and the cell volume in alkali-metal-doped C_{60} superconductors.This is a first indication of the proximity of superconductivity and insulator in fullerene materials.

A-5 Superconductivity in $K_3Ba_3C_{60}$

A new ternary superconducting fulleride was synthesized by intercalation of potassium into Ba_3C_{60}. Bulk superconductivity with the onset temperature was 5.6K was observed in $K_3Ba_3C_{60}$, which forms a body-centered-cubic (bcc) lattice parameter of a=11.24Å. A nave electron counting predicts that the Fermi level of $K_3Ba_3C_{60}$ is at the center of the t_{1g}-derived band, in sharp contrast with also superconducting Ba_6C_{60}. This result indicates that the superconductivity of fullerides occurs at the half-filled states both of the t_{1u}- and t_{1g}-derived bands.

A-6 Formation of C_{60} aggregates in solution

Formation of C_{60} aggregates has been found in toluene solution by using photoluminescence spectroscopy. From the detailed investigation of the temperature dependence of luminescence, it has been confirmed that the formation of C_{60} aggregates occurs simultaneously with the liquid-solid transition of the solution and that the aggregates remain in liquid-solution at temperatures (170-210K) slightly higher than the melting point of the solution in the warming process. the 0-0 transition energy in their luminescence spectrum has been found to be blue-shifted in comparison with that of the C_{60} crystal.

A-7 Pressure-induced C_{70} polymers

We found evidence for polymerization of C_{70} induced by high pressure. X-ray diffraction, infrared spectra, ultraviolet-visible absorption spectra unambiguously confirmed the occurrence of cross linking of C_{70} molecules. As was observed in C_{60} polymers, C_{70} polymer is not soluble in toluene, and revert to conventional monomer crystals by heating to 300°C at ambient pressure.

A-8 Electronic transport and magnetic properties of carbon nanotubes

Electric conductance of a multi-wall carbon nanotube shows a decreasing temperature dependence with decreasing temperature, but with a kink about 15 K. Temperature dependence of conductance both above and below 15 K which can be explained in terms of two-dimensional weak localization with different parameters in each region. Magnetoconductance reveals oscillation with magnetic field at low temperatures, which can be explained by universal conductance fluctuations.

We have succeeded to align multi-wall carbon nanotubes under magnetic field. Carbon nanotubes align along magnetic field owing to anisotropy in magnetic susceptibility. With use of aligned carbon nanotubes the diamagnetic susceptibility for magnetic field parallel and perpendicular to the tube axis are determined to be -8.0 and -9.5 emu/g at 300 K, respectively.

B Oxygen Molecular Conversion with Chemical Models of Metalloenzymes

Contributors: **Yoshinori NARUTA** *(Kyushu Univ.)*, **Yoshito WATANABE, Fumito TANI** *(Kyushu Univ.)*, **Alain KOSSANYI** *(Kyushu Univ.)*, **Kanako ICHIHARA** *(Kyushu Univ.)* **and Takao SASAKI** *(Kyushu Univ.)*

This research project aims at the molecular-level understanding of the reaction mechanism of metalloenzymes participating the molecular conversion of oxygen, i. e., cytochrome P-450, cytochrome *c* oxidase, and oxygen-evolving complex in plant PSII by use of artificial chemical models and the developing new reaction systems with these catalysts.

B-1 Stabilization O_2 Complex by Strong Hydrogen Bonding in Fe 'Single-coronet' porphyrin

Formation of hydrogen bonding between a oxygen atom and proximal polar group is important in the stabilization of heme-O2 complexes. We prepared the Fe complex of 'single coronet' porphyrin (**SC**) bearing phenolic OH groups inside the cavity as a new heme protein model (Figure 1). This complex showed almost irreversible binding of O_2 [$P_{1/2}(O_2) < 10^{-5}$ Torr], which was the lowest value ever recorded. The O_2 complexes stabilized by nearby OH groups. On the other hand, the corresponding CO complex was rather unstable [$P_{1/2}(CO)$ = 0.054 Torr]. from flash photolysis, rate constants of formation and dissociation of the CO complex were determined to be $k_B^{+CO} = 2.5 ¥ 10^6\ M^{-1}\ s^{-1}$ and $k_B^{-CO} = 1.31\ s^{-1}$. Thus, the CO complex of this model was destabilized than Mb and the related model complexes. The FT-IR and resonance Raman spectra also support this destabilization (Figure 2). The stretching frequencies of C-O and Fe-C were appeared at lower frequency region and they are explained by polar interaction between the OH groups and the binding CO.

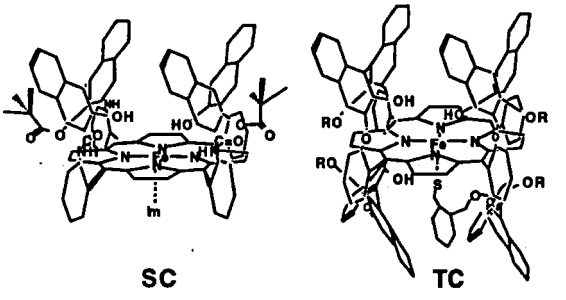

Figure 1. Structure of the Fe derivatives of 'single-coronet' porphyrin (**SC**) and 'twin-coronet' porphyrin bearing thiolate ligand (**TC**). Double bonds are omitted for clarity.

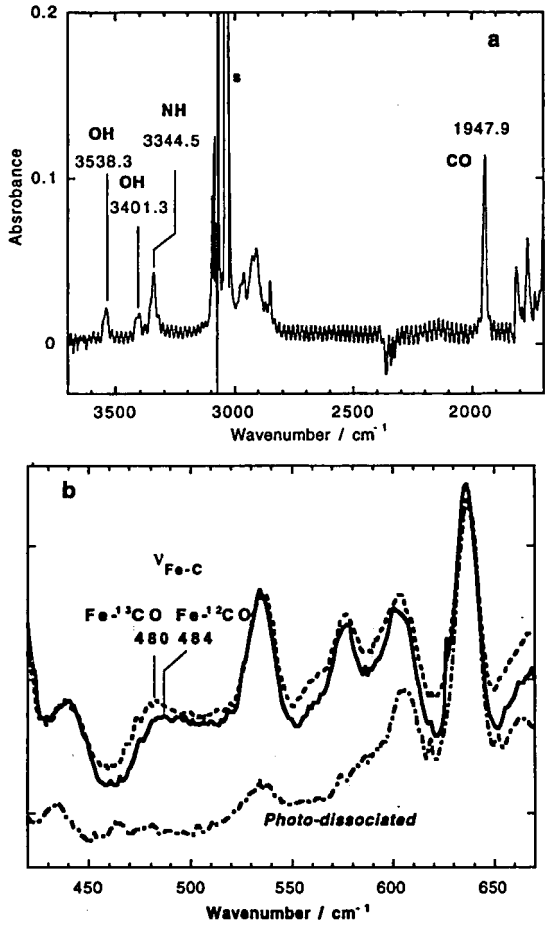

Figure 2. FT-IR (**a**) and resonance Raman spectra (**b**) of the SC-FeCO.

B-2 Modeling of Cytochrome P-450 Active Center with New Chiral Porphyrins bearing Hydroxyl Groups at the O_2-binding Site

Cytochrome P-450 has an array of polar peptide residues around its O_2-binding/activation site. These groups are assumed to play a key role in proton relay and the acceleration of O-O bond cleavage. As a model compound, we prepared the Fe complex of 'twin-coronet' porphyrin (**TC**) which have hydroxyl groups at the proximal position of the Fe ion inside one cavity and a thiolate ligand in other cavity (Figure 1). The CO complex showed characteristic visible absorption spectra l_{max} = 447 nm. Spectroscopic characterization of the corresponding O_2 complex and its application to catalytic oxidation is in the way.

B-3 New Modeling System of Cu_B-heme a_3 Center in Cytochrome *c* Oxidase

In cytochrome *c* oxidase (CcO), the Cu_B-heme a_3 center performs four-electron reduction of O_2 and promotes the resulting proton flow through membrane. Tris(pyridylmethyl)amino group (TPA)-linked porphyrin derivatives were prepared as its active-center model compounds. At lower temperature (-20°C). it formed the corresponding intermediary O_2 complex (l_{max} = 420 nm), which was confirmed by ESI-MS [*m/z* = 1094 ($^{16}O_2$), 1098 ($^{18}O_2$)]. Upon warming this complex to 0°C, it changed to a new complex (l_{max} = 441 nm), which showed oxygen-active resonance Raman spectra at n = 822 cm^{-1} ($D(^{16}O_2/^{18}O_2)$ = 39 cm^{-1}). This band is not $n_{O\text{-}O}$ from the spectra with $^{16}O^{18}O$. It is most likely Fe^{III}-O-Cu^{II} or Fe^{IV}(=O).

B-4 Formation and Characterization of Convergent High-Valent Mn Oxo Porphyrins as the Model Reaction of Oxygen-Evolution in PSII

Manganese porphyrin dimers having appropriate Mn-Mn separation showed catalytic activity toward O_2 evolution by water oxidation under anodic oxidation conditions. In order to determine the active intermediate and the reaction mechanism of this reaction, oxidation of the dimanganese complex with peracid oxidation with mCPBA. Detailed analysis of the course of the oxidation revealed the stepwise formation of Mn^{V}(=O) intermediate through the corresponding manganese(III) perbenzoate complex. The compound is easily transferred to $Mn^{IV}(OR)_2$ dimer in the presence of water or alcohol, which was assigned by ESI-MS, ESR, and elemental analysis. Thus, the transiently formed Mn^{V}(=O) rapidly transferred to the Mn^{IV} species, which is a good precursor to the corresponding Mn^{V}(=O) dimer.

C Multi-Functional Molecular Solids with p-d Electronic Structures

Contributors: **Susumu KITAGAWA** *(Tokyo Metropolitan Univ.)*, **Hayao KOBAYASHI, Masahiro YATASHITA** *(Nagoya Univ.)*, **Norimichi KOJIMA** *(Univ. Tokyo)*, **Toshiaki ENOKI** *(Tokyo Inst. Tech.)* **and Hiroshi KITAGAWA** *(JAIST)*

Recently electric, magnetic and optical properties of molecular solids have attracted the increasing interest. Up to now, these three properties of the molecular solids have been studied separately. The aim of this research project is the design, development and characterization of new molecular solids exhibiting multi-functional properties. Since the nontrivial electronic properties of molecular solid are always originated from the incompletely occupied molecular (or atomic) orbitals, the systems with two types of incompletely occupied orbitals will be examined systematically.

C-1 Organic Conductors with Magnetic Anions

By virtue of the progress in the molecular design of the two-dimensional p metals in 1980s, it becomes easy to prepare the organic conducting systems which retain metallic state down to low temperatures. In order to cultivate new field in the organic metal systems, we are now trying to obtain the electrically and magnetically active molecular systems. The simplest way to vest the magnetic properties to organic conductors is to use magnetic ions such as $FeCl_4^-$ and $CuCl_4^{2-}$ as counter anions. In these systems, the highest

occupied molecular orbital of organic molecule and *d* orbitals of anion are the incompletely occupied. Needless to say, the π electrons convey the electrical current and the 3d electrons are mainly responsible for the magnetic properties.

We have recently examined several molecular magnets based on organic charge transfer complexes. Organic charge transfer complexes form a large variety of electric structures, which are governed by the transfer integrals and the on-site Coulomb interaction. The localized magnetic moments of *d* electrons embedded in insulating complexes are expected to interact with each other through superexchange interaction mediated by the organic π electron system, while localized *d* spins in metallic complexes are coupled to each other *via* π-d interaction.

$[Ni(dddt)_2]_3(FeBr_4)_2$ is a typical semiconducting molecular magnets exhibiting the antiferromagnetic transition at 6 K. The susceptibility behavior indicates the three-dimensional nature of the spin system. Therefore the superexchange interlayer interaction through Fe-Br···[Ni(dddt)$_2$]···Br-Fe should play an essential role in this system (Figure 1).

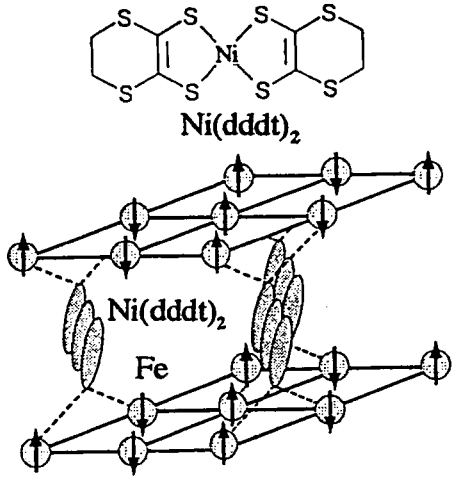

Figure 1. Schematic drawing of the magnetic structure of $[Ni(dddt)_2]_3(FeBr_4)_2$.

C-2 Transition Metal Complexes with Chloranilate Ligands

Owing to the unique redox nature of the chloranilate (CA), the one-dimensional transition metal complexes with CA as the bridging ligands (M-CA-M-) are expected to be interesting magnetic materials. We have recently synthesized linear complex with paramagnetic Cu^{2+} ions, $[Cu(CA)(pyz)]_n$ (pyz=pyrazine). The magnetic susceptibility indicated the weak antiferromagnetic interaction between Cu^{2+} ions (J=-3 cm^{-1}). $[M(CA)(H_2O)_2](phz)_n$ (M=Mn, Fe: phz=phenazine) with high-spin metal atoms [S=5/2 (Mn), S=2 (Fe)] were also prepared. Considering the fairly high energy level of *d* orbitals of these metal atoms, it might be possible that the $(CA^{3-})^{\bullet}$ radical could be produced by the electrochemical oxidation. Then the system will become one-dimensional ferrimagnet with strong Fe(S=5/2)···CA$^{\bullet}$ (S=1/2) antiferromagnetic interaction.

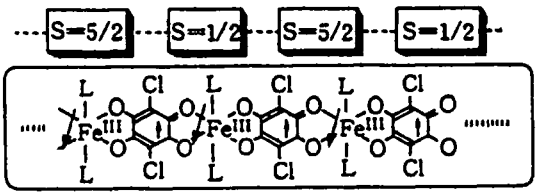

Figure 1. Schematic drawing of ferrimagnetic chain of $[M(CA)(H_2O)_2](phz)_n$ system.

(2) Research Symposia

(from September '96 to August '97)

1. Recent Development and Future Prospects of Molecular Science Using Laser-Synchrotron Radiation Combination
   (October 28th-29th, 1996)
   Chair: Koichiro Mitsuke
2. Nonlinear Reactions and Cooperative Phenomena
   (November 16th-17th, 1996)
   Chair: Ichiro Hanazaki
3. Solvent and Salt Effects on Stability of Biopolymer in Aqueous Solutions
   (November 27th-29th, 1996)
   Chair: Fumio Hirata
4. The 7th Japan-Korea Joint Symposium on Molecular Spectroscopy of Clusters and Related Compounds
   (January 6th-8th, 1997)
   Chair: Suehiro Iwata
5. IMS International Conference on "Electronic Structure and Reactin Dynamics"
   (March 17th-20th, 1997)
   Chair: Yoshiyasu Matsumoto
6. Symposium or Physical Chemistry for Young Researchers of Molecular Science
   (June 7th, 1997)
   Chair: Atsushi Nakajima (Keio Univ.)
7. International Workshop to Study the Future Functions of Small Storage Rings and Free Electron Lasers
   (August 8th-10th, 1997)
   Chair: Hiroyuki Hama
8. Structures and Functions of Coordination Compounds with a Nanometerscale
   (August 19th-21st, 1997)
   Chair: Satoru Onaka (Nagoya Inst. of Tech)

(3) Cooperative Research

This is the most important programs IMS undertakes for conducting its own research of the common interest to IMS. During the first half of the fiscal year of 1996 ending on September 30, 36 outside scientists joined this program and during the second half, 56 outside scientists did. The names and affiliations of those collaborators are found in Research Activities.

(4) Use of Facilities

The number of projects accepted for the Use-of-Facility Program of the Computer center during the fiscal year 1996 amounted to 201 (719 users) and computer time spent for these projects is 51551 hours (converted to the HITAC M-680H time), and amounted to 70% of the total annual CPU time used. The number of projects accepted for the Use-of-Facility Program of the Instrument Center during the fiscal year 1996 amounted to 51 (154 users).

(5) UVSOR

In the UVSOR Facility with the 750 MeV electron storage ring, there are nineteen beam lines available for synchrotron radiation research. The Experimental Facility of each beam line is discribed in the UVSOR ACTIVITY REPORT 1997. Under the following programs, a number of SR studies have been carried out by many users outside and inside IMS: A the UVSOR Special Projects, B the UVSOR Cooperative Research Projects, C the UVSOR Invited Research Projects, and D the Use-of-UVSOR Projects.

A UVSOR Special Project

In the fiscal year of 1996, the following UVSOR special projects were carried out.

1. Title: Construction of multilayer monochromator system for photochemical reactions
   Beam Line: 4A
   Representative: **Tsuneo URISU** *(IMS)*
2. Title: Construction of glancing incident monochromator at BL2B2
   Beam Line: 2B2
   Representative : **Koichiro MITSUKE** *(IMS)*
3. Title: Upgrade of VUV beam line with installation of new monochromator
   Beam Line: 7B
   Representative: **Hideyuki NAKAGAWA** *(Fukui Univ.)*

B UVSOR Cooperative Research Projects

Under this joint-study program, many synchrotron radiation experiments have been carried out with the beam lines of in-house staff in cooperation with scientists who were invited from other institutions. The total number of the projects in this category was 24 in the fiscal year of 1996.

C UVSOR Invited Research Projects

Under this joint-study program, several scientists were invited from other institutions of help for construction of new beam lines and improvement of the UVSOR storage ring and others. The total number of the projects in this category was 1 in the fiscal year of 1996.

D Use-of-UVSOR Projects

Ten out of the total of nineteen UVSOR beam lines are available for general users outside and inside IMS for their synchrotron radiation studies in the field of molecular science. The total number of the projects in this category was 146 in the fiscal year of 1996.

FOREIGN SCHOLARS

Visitors from abroad are always welcome at IMS and they have always played an important role in the research activities of the Institute. The foreign scientists who visited IMS during the past year (Aug. 1996 - July 1997) are listed below.

*1 indicates attendance at an Okazaki Conference; *2 a MONBUSHO (the Ministry of Education, Science, Sports and Culture, Japan) or JSPS (the Japan Society for the Promotion of Science) Invited Fellow; *3 an IMS councillor; *4 an IMS visiting professor or associate professor from abroad (period of stay from 6 to 12 months); *5 a JSPS Post-Doctoral or Ronpaku Fellow; *6 an IMS visiting scientist and *7 a visitor to IMS.

Scientists who would like to visit IMS under programs *2 and *4 are invited to make contact with IMS staff in their relevant field.

Dr. Li Yumin*5*6		(China)	Jun. '95-
Mr. P. Severino*6		(Italy)	May '96-
Dr. A. Fiedler*5		(Germany)	May '96-
Prof. Ann Kwang-Hyun*2	Kyung Hee Univ.	(Korea)	-Aug. '96
Ms. S. Maw*7	Manchester Univ.	(U.K.)	-Aug. '96
Prof. W. C. Lineberger*7	Univ. of Colorado	(U.S.A.)	-Aug. '96
Prof. T. C. Steimle*7	Arizona State Univ.	(U.S.A.)	Aug. '96, Jan. '97
Prof. M. D. E. Forbes*7	Univ. of North Carolina at Chapel Hill	(U.S.A.)	Aug. '96
Dr. Z. Jakubek*7	RIKEN	(Japan)	Aug. '96
Ms. P. I. Sansom*7	Univ. of Texas at Austin	(U.S.A.)	Aug. '96
Prof. W. Jarzeba*7	Jagiellonian Univ.	(Porland)	Aug. '96
Ms. N. Gayathri*2	Indian Inst. of Sci.	(India)	Aug.-Sep. '96
Dr. M. V. Simonyan*2	Armenian Natl. Acad. of Sci.	(Armenia)	-Sep. '96
Prof. H. Szichman*4	Soveq Nuclear Res. Inst.	(Israel)	-Sep. '96
Prof. Chang-Guo Zhan*5	Central China Normal Univ.	(China)	-Sep. '96
Prof. Qingshi Zhu*7	Univ. of Sci. and Tech. of China	(China)	Sep. '96
Prof. Minbo Chen*7	Shanghai Inst. of Organic Chem.	(China)	Sep. '96
Prof. Chengbu Liu*7	Shangdong Univ.	(China)	Sep. '96
Dr. Yuanhe Huang*7	Beijing Normal Univ.	(China)	Sep. '96
Prof. Xin Xu*7	Xiamen Univ.	(China)	Sep. '96
Prof. Luyuan Hao*7	Univ. of Sci. and Tech. of China	(China)	Sep. '96
Prof. Yang Cao*7	Suzhou Univ.	(China)	Sep. '96
Prof. Yuansheng Jiang*7	Nanjing Univ.	(China)	Sep. '96
Prof. Hualiang Jiang*7	Chinese Acad. of Sci.	(China)	Sep. '96
Prof. Lemin Li*7	Peking Univ.	(China)	Sep. '96
Prof. Song Ye*7	Yunnan Univ.	(China)	Sep. '96
Prof. Daiqian Xie*7	Sichuan Univ.	(China)	Sep. '96
Prof. Huixin Zhang*7	Natl. Normal Sci. Foundation of China	(China)	Sep. '96
Prof. Zhida Chen*7	Peking Univ.	(China)	Sep. '96
Prof. Xiaoyuan Fu*7	Beijing Normal Univ.	(China)	Sep. '96
Prof. Qianer Zhang*7	Xiamen Univ.	(China)	Sep. '96
Prof. Zhenyi Wen*7	Northwest Univ.	(China)	Sep. '96
Prof. Kangnian Fan*7	Fudan Univ., Shanghai	(China)	Sep. '96
Prof. Chengda Zhao*7	North-East Normal Univ.	(China)	Sep. '96
Prof. Shuhua Li*7	Nanjing Univ.	(China)	Sep. '96
Prof. Tiejin Li*7	Jilin Univ.	(China)	Sep. '96
Prof. P. G. Mezey*7	Univ. of Saskatchewan	(Canada)	Sep. '96
Prof. M. Chergui*1	Univ. de Lausanne	(France)	Sep. '96
Prof. J. N. Onuchic*1	Univ. of California at San Diego	(U.S.A.)	Sep. '96
Prof. R. D. Coalson*1*2	Univ. of Pittsburgh	(U.S.A.)	Sep., Dec. '96
Prof. N. Scherer*1	Univ. of Pennsylvania	(U.S.A.)	Sep. '96
Prof. J. T. Hupp*1	Northwestern Univ.	(U.S.A.)	Sep. '96
Prof. D. R. Klug*1	Imperial College of Sci. Tech. and Medicine	(U.K.)	Sep. '96
Prof. YiJing Yan*1	Hong Kong Univ. of Sci. and Tech.	(Hong Kong)	Sep. '96
Prof. V. Cherniyak*1	Univ. of Rochester	(U.S.A.)	Sep. '96
Prof. T. Oka*2	Univ. of Chicago	(U.S.A.)	Sep. '96
Prof. V. M. Yartsev*7	Venezuelan Inst. for Scientific Res.	(Venezuela)	Sep. '96
Prof. E. M. Kosower*7	Tel-Aviv Univ.	(Israel)	Sep. '96
Prof. N. S. Kosower*7	Tel-Aviv Univ.	(Israel)	Sep. '96
Prof. Wang Zhiwen*7	Jilin Univ.	(China)	Sep. '96
Ms. A. K. Lees*7	Imperial College	(U.K.)	Sep. '96

Prof. A. A. Zakhidov*7	Uzbekistan Acad. of Sci.	(Uzbek)	Sep.-Oct. '96
Dr. I. L. Kogan*2	Inst. of Chem. Phys. in Chernogolovka	(Russia)	Sep. '96-
Dr. I. Nenner*6	SPAM, Centre d'Etudes de Saclay	(France)	Oct. '96
Prof. E. R. Bernstein*7	Colorado State Univ.	(U.S.A.)	Oct. '96
Prof. A. Bino*7	The Hebrew Univ. of Jerusalem	(Israel)	Oct. '96
Mr. B. L. V. Prasad*7	Hyderabad Univ.	(India)	Oct. '96
Prof. P. J. Sarre*7	Univ. of Nottingham	(U.K.)	Oct. '96
Prof. G. W. Winnewisser*7	Univ. of Köln	(Germany)	Oct. '96
Prof. N. Sathyamurthy*2	Chem. Dept. Indian Inst. of Tech. Kanpur	(India)	Oct. '96
Prof. J. Horacek*4	Chales Univ.	(Czech)	Oct.-Dec. '96
Ms. Yang Hui-Jun*7	Beijing Health School	(China)	Oct. '96-Mar. '97
Dr. I. Yourova*6	The Univ. St. Petersburg	(Russia)	Oct. '96-Jul. '97
Prof. V. N. Ostrovsky*4	The Univ. St. Petersburg	(Russia)	Oct. '96-Jul. '97
Dr. J. Hrusak*2	J. Heyrousky Inst. of Phys. Chem.	(Czech)	-Nov. '96
Prof. G. Rábai*2	Kossuth Lajos Univ.	(Hungary)	-Nov. '96
Prof. M. C. Heaven*4	Emory Univ.	(U.S.A.)	-Nov. '96
Dr. Yang Shi*2	Inst. of Chem., Chinese Acad. of Sci.	(China)	-Nov. '96
Prof. V. A. Ivanov*2	Russian Acad. of Sci.	(Russia)	-Nov. '96
Prof. P. Cassoux*7	Centre Natl. Recherche Sci. (CNRS)	(France)	Nov. '96
Dr. K. Pokhodnya*7	Inst. Semiconductors, Ukrainian Natl. Acad. Sci.	(Ukraine)	Nov. '96
Dr. C. Alba-Simionesco*7	Univ. de Paris-Sud	(France)	Nov. '96
Prof. K. M. Kadish*7	Univ. of Houston	(U.S.A.)	Nov. '96
Prof. R. H. Fish*7	Univ. of California	(U.S.A.)	Nov. '96-Jul. '97
Prof. A. L. Verma*7	North-Eastern Hill Univ.	(India)	Nov. '96
Prof. T. A. Keidering*7	Univ. of Illinois	(U.S.A.)	Nov. '96
Prof. Zu-Xun Gong*7	Shanghai Inst. of Biochemistry	(China)	Nov. '96
Prof. Shi-Zhou Ao*7	Shanghai Inst. of Biochemistry	(China)	Nov. '96
Dr. M. M. Rohmer*7	Lab. de Chim. Quantique	(France)	Nov. '96
Prof. I. Rips*7	The Weizmann Inst. of Sci.	(Israel)	Nov. '96
Prof. J. M. Lisy*2	Univ. of Illinois	(U.S.A.)	Dec. '96
Prof. W. H. Miller*3	Univ. of California, Berkeley	(U.S.A.)	Dec. '96
Prof. P. G. Wolynes*3	Univ. of Illinois	(U.S.A.)	Dec. '96
Dr. E. V. Savchenko*7	Verkin Inst. for Low Temp. Phys. and Engin.	(Ukraine)	Dec. '96
Prof. S. Jéan-Pascal*4	Inst. chem. de la Matiere Condencee de Bordeaux	(France)	Dec. '96-Mar. '97
Dr. Md. B. Zaman*6	Dhaka Univ.	(Bangladesh)	Dec. '96-Mar. '97
Dr. A. Wagner*2	Argonne National Lab.	(U.S.A.)	Dec. '96-Apr. '97
Prof. M. V. Basilevsky*7	Karpov Inst.	(Russia)	Jan. '97
Prof. J.-P. Sauvage*7	Louis Pastew Univ.	(France)	Jan. '97
Prof. Kee Joo Chang*7	Korea Advanced Inst. of Sci. and Tech.	(Korea)	Jan. '97
Director Mu Shik Jhon*7	Korea Advanced Inst. of Sci. and Tech.	(Korea)	Jan. '97
Prof. Taiha Joo*7	Pohang Univ. of Sci. and Tech.	(Korea)	Jan. '97
Prof. Kyung-Hoon Jung*7	Korea Advanced Inst. of Scie. and Tech.	(Korea)	Jan. '97
Dr. Dongho Kim*7	Korea Research Inst. of Standards and Sci.	(Korea)	Jan. '97
Prof. Hackjin Kim*7	Chungnam Natl. Univ.	(Korea)	Jan. '97
Prof. Hong Lae Kim*7	Kangwon Natl. Univ.	(Korea)	Jan. '97
Dr. Jang-Joo Kim*7	Electronics and Telecommunications Res. Inst.	(Korea)	Jan. '97
Prof. Kwang Soo Kim*7	Pohang Univ.of Sci. and Tech.	(Korea)	Jan. '97
Prof. Sang Kyu Kim*7	Inha Univ.	(Korea)	Jan. '97
Prof. Ja Kang Ku*7	Pohang Univ. of Sci. and Tech.	(Korea)	Jan. '97
Prof. Young Dong Park*7	Ajou Univ.	(Korea)	Jan. '97
Prof. Seokmin Shin*7	Seoul Natl. Univ.	(Korea)	Jan. '97
Dr. Sae Chae Jeong*2*7	Korea Res. Inst. of Stand. and Sci. (KRISS)	(Korea)	Jan., Jul. '97-
Prof. Minhaeng Cho*4*7	Korean Univ.	(Korea)	Jan., Jul. '97-
Dr. C. Gebauer*6		(Germany)	Jan. '97-
Prof. K.-P. Dinse*7	Tech. Univ. of Darmstadt	(Germany)	Jan. '97
Mr. N. Smith*7	Univ. of East Anglia	(U.K.)	Jan.-Mar. '97
Prof. Y. Band*2	Ben-Gurion Univ.	(Israel)	Jan.-Feb. '97
Prof. G. Y. Korenman*7	Inst. of Nucl. Phys, Moscow State Univ.	(Russia)	Feb. '97
Dr. I. Rittaporn*7	Suranaree Univ. of Tech.	(Thailand)	Feb. '97
Mr. Viwat P.*7	Suranaree Univ. of Tech.	(Thailand)	Feb. '97
Mr. Anucha P.*7	Suranaree Univ. of Tech.	(Thailand)	Feb. '97
Mr. Prasit K.*7	Suranaree Univ. of Tech.	(Thailand)	Feb. '97
Mr. Somboon Li*7	Suranaree Univ. of Tech.	(Thailand)	Feb. '97
Mr. Udomvit M.*7	Suranaree Univ. of Tech.	(Thailand)	Feb. '97
Mr. Pongpairee M.*7	Suranaree Univ. of Tech.	(Thailand)	Feb. '97

Dr. F. Barigelletti*7	Instituto-FRAE-CNR	(Italy)	Feb. '97
Prof. L. G. Marzilli*2	Emory Univ.	(U.S.A.)	Feb. '97-
Dr. I. K. Ahmad*2	Univ. of London	(U.K.)	Feb. '97-
Prof. K. J. Brewer*7	Virginia Polytechnic Inst. and State Univ.	(U.S.A.)	Feb. '97
Dr. I. V. Rubtsov*6	Russian Academy of Sciences	(Russia)	-Mar. '97
Prof. J. S. Miller*7	Univ. of Utah	(U.S.A.)	Mar. '97
Prof. L. Ouahab*1*7	Univ. of Rennes	(France)	Mar. '97
Dr. A. Currao*7	Kyushu Natl. Industrial Res. Inst.	(Japan)	Mar. '97
Dr. Y. Schumacher*7	Kyushu Natl. Industrial Res. Inst.	(Japan)	Mar. '97
Dr. J. A. Harrison*7	Massey Univ.	(New Zealand)	Mar. '97
Dr. M.-A. Thelen*7	Massey Univ.	(New Zealand)	Mar. '97
Dr. Chaejoon Cheong*7	Korea Basic Sci. Inst.	(Korea)	Mar. '97
Prof. J. T. Groves*7	Princeton Univ.	(U.S.A.)	Mar. '97
Prof. M. Kurmoo*1	Inst. de Phys. Chem. des Matériaux de Strassbourg	(France)	Mar. '97
Prof. E. B. Yagubskii*1	Inst. of Chem. Phys., Russian Acad. of Sci.	(Russia)	Mar. '97
Prof. E. Coronado*1	Univ. de Valencia	(Spain)	Mar. '97
Prof. R. T. Henriques*1	Inst. Superior Tecnico	(Portugal)	Mar. '97
Prof. Daoben Zhu*1	Acad. Sinica Inst. of Chem.	(China)	Mar. '97
Prof. D. Schweitzer*1	Univ. Stuttgart	(Germany)	Mar. '97
Dr. V. Geiser*1	Argonne Natl. Lab.	(U.S.A.)	Mar. '97
Dr. P. Cassoux*1	LCC/CNN, Centre Natl. Recherche Sci. (CNRS)	(France)	Mar. '97
Prof. A. E. Underhill*1	Univ. of Wales	(U.K.)	Mar. '97
Prof. V. N. Laukhin*1	Inst. of Chem. Phys., Russian Acad. of Sci.	(Russia)	Mar. '97
Dr. E. Lavkhina*1	Inst. of Chem. Phys., Russian Acad. of Sci.	(Russia)	Mar. '97
Prof. F. Siebert*7	Univ. of Freiburg	(Germany)	Mar. '97
Prof. C. A. Floudas*7	Princeton Univ.	(U.S.A.)	Mar. '97
Dr. Chin-Kun Hu*7	Inst. of Phys., Acad. Sinica	(Taiwan)	Mar. '97
Dr. W. Wang*7	Fudan Univ.	(China)	Mar. '97
Prof. G. Gangopadhyay*5	Inst. of Atom. and Mol. Sci. Acad. Sinica	(India)	Mar. '97
Prof. G. Walker*7	Univ. of Pittsburgh	(U.S.A.)	Mar. '97
Prof. E. W. Schlag*3	Tech. Univ. of München	(Germany)	Mar. '97
Prof. F. F. Crim*7	Univ. of Wisconsin-Madison	(U.S.A.)	Mar. '97
Prof. P. Casavecchia*7	Univ. Perugia	(Italy)	Mar. '97
Dr. U. Buck*7	Max-Planck-Inst.	(Germany)	Mar. '97
Prof. G. Scoles*7	Princeton Univ.	(U.S.A.)	Mar. '97
Dr. D. J. Auerbach*7	IBM Almaden	(U.S.A.)	Mar. '97
Prof. S. T. Ceyer*7	Massachusetts Inst. of Tech.	(U.S.A.)	Mar. '97
Prof. G. R. Fleming*7	Univ. of Chicago	(U.S.A.)	Mar. '97
Prof. J.-L. Martin*7	ENSTA-Ecole Polytechnique	(France)	Mar. '97
Prof. P. A. Anfinrud*7	Harvard Univ.	(U.S.A.)	Mar. '97
Prof. Yen-Chu Hsu*7	Inst. of Atomic and Molec. Sci. (IAMS)	(Taiwan)	Mar. '97
Prof. Yuan-Pern Lee*7	Natl. Tsin Hua Univ.	(Taiwan)	Mar. '97
Prof. I-Chia Cheu*7	Natl. Tsin Hua Univ.	(Taiwan)	Mar. '97
Prof. King-Chueu Lin*7	Inst. of Atomic and Molec. Sci. (IAMS)	(Taiwan)	Mar. '97
Dr. Xue-Ming Yaug*7	Inst. of Atomic and Molec. Sci. (IAMS)	(Taiwan)	Mar. '97
Dr. Kopin Liu*7	Inst. of Atomic and Molec. Sci. (IAMS)	(Taiwan)	Mar. '97
Prof. S. R. Meech*7	Univ. of East Anglia	(U.K.)	Mar. '97
Dr. S. Pal*4	Natl. Chem. Lab. (NCL)	(India)	Mar. '97-
Prof. A. S. Markosyan*2	Moscow State Univ. Lab. of Problems for Magnetism	(Russia)	Mar. '97-
Prof. V. Ivanov*7	The Univ. of St. Petersburg	(Russia)	Mar.-Apr. '97
Prof. M. Y. Amusia*7	Ioffe Phys. Tech. Inst.	(Russia)	Apr. '97
Prof. G. Kaupp*7	Univ. of Oldenburg	(Germany)	Apr. '97
Prof. I. H. Munro*7	CCLRC, Daresbury Lab.	(U.K.)	Apr. '97
Dr. S. R. Gandhi*6		(U.S.A.)	Apr.-Jul. '97
Prof. B. Bagchi*7	Indian Acad. of Sci.	(India)	May '97
Prof. A. W. Castleman, Jr.*2	Pennsylvania State Univ.	(U.S.A.)	May '97
Prof. J. McGarvey*7	Queen's Univ. of Belfast	(U.K.)	May '97
Dr. Tian Fuli*6	Inner Mongolia Univ.	(China)	May-Jul. '97
Prof. C. Y. Ng*2	Iowa State Univ.	(U.S.A.)	Jun. '97
Dr. S. I. Gheyas*2	Bangladesh Agricultural Univ.	(Bangladesh)	Jun. '97-
Dr. Haiyang Li*6	Dalian Inst. of Phys.	(China)	Jun. '97-
Prof. Jik Chin*6*7	McGill Univ.	(Canada)	Jun. '97-
Dr. P. A. Marzill*6	Emory Univ.	(U.S.A.)	Jun. '97-
Prof. Hungi Hong*2	Sejong Univ.	(Korea)	Jun. '97-

Prof. J. W. Park*7	Ewha Womans Univ.	(Korea)	Jun. '97
Prof. C. S. Chin*7	Sogang Univ.	(Korea)	Jun. '97
Prof. R. Glaser*2	Univ. of Missouri-Columbia	(U.S.A.)	Jul. '97
Prof. S. Speiser*2	Technion Israel Inst. of Tech.	(Israel)	Jul. '97
Prof. E. A. Agustinelli*7	Rome Univ.	(Italy)	Jul. '97
Prof. A. X. Trautwein*7	Medizinische Universitat zu Lübeck, Inst. of Phys.	(Germany)	Jul. '97
Prof. B. Lippert*7	Univ. of Dortmund	(Germany)	Jul. '97
Prof. B. Dunford*7	Univ. of Alberta	(Canada)	Jul. '97
Prof. C. P. Rao*7	Indian Inst. of Tech.	(India)	Jul. '97
Prof. C. T. Migita*7	The School of Allied Health Sciences, Yamaguchi Univ.	(Japan)	Jul. '97
Prof. C. Dismukes*7	Princeton Univ.	(U.S.A.)	Jul. '97
Prof. E. I. Solomon*7	Stanford Univ.	(U.S.A.)	Jul. '97
Prof. G. Smulevich*7	Univ. di Firenze	(Italy)	Jul. '97
Prof. I. Bertini*7	Univ. di Firenze	(Italy)	Jul. '97
Prof. J. O. Alben*7	Ohio State Univ.	(U.S.A.)	Jul. '97
Prof. J. Terner*7	Virginia Commonwealth Univ.	(U.S.A.)	Jul. '97
Prof. J. A. Shelnutt*7	Sandia Natl. Lab.	(U.S.A.)	Jul. '97
Prof. J. Lipscomb*7	Univ. of Minnesota	(U.S.A.)	Jul. '97
Prof. J. A. "Bill" Peterson*7	The Univ.of Texas Southwestern Medical Center	(U.S.A.)	Jul. '97
Prof. K. D. Karlin*7	Johns Hopkins Univ.	(U.S.A.)	Jul. '97
Prof. L. Que, Jr.*7	Univ. of Minnesota	(U.S.A.)	Jul. '97
Dr. M. Dahan*7	The Hebrew Univ.	(Israel)	Jul. '97
Prof. N. M. Kostic'*7	Iowa State Univ.	(U.S.A)	Jul. '97
Prof. N. P Farrell*7	Virginia Commonwealth Univ.	(U.S.A)	Jul. '97
Prof. P. M. H. Kroneck*7	Univ. Konstanz	(Germany)	Jul. '97
Prof. R. S. Armstrong*7	The Univ. of Sydney	(Australia)	Jul. '97
Prof. R. S. Czernuszewicz*7	Univ. of Houston	(U.S.A)	Jul. '97
Prof. R. Hille*7	Ohio State Univ.	(U.S.A)	Jul. '97
Prof. S. Mitra*7	TATA Inst. of Fundamental Res.	(India)	Jul. '97
Mr. Sang-Kyu Lee*7	Univ. of Minnesota	(U.S.A)	Jul. '97
Prof. T. G. Spiro*7	Princeton Univ.	(U.S.A)	Jul. '97
Prof. W. B. Tolman*7	Univ. of Minnesota	(U.S.A)	Jul. '97
Prof. W. E. Smith*7	Univ. of Strathclyde	(Scotland)	Jul. '97
Prof. Wolf-D. Woggon*7	Univ. Basel	(Switzerland)	Jul. '97
Prof. W. Nam*7	Ewha Womans Univ.	(Korea)	Jul. '97
Dr. Yun Qu*7	Virginia Commonwealth Univ.	(U.S.A.)	Jul. '97
Prof. Zhong-Xian Huang*7	Fudan Univ.	(China)	Jul. '97
Ms. G. Yeong Mee*7	Ewha Womans Univ.	(Korea)	Jul. '97
Ms. L. Yoon Jung*7	Ewha Womans Univ.	(Korea)	Jul. '97
Prof. K. Hodgson*7	Stanford Univ.	(U.S.A.)	Jul. '97
Prof. B. Hedman*7	Stanford Univ.	(U.S.A.)	Jul. '97
Prof. J. H. Dawson*7	Univ. of South Carolina	(U.S.A.)	Jul. '97
Prof. E. Agostinelli*7	Rome Univ.	(Italy)	Jul. '97
Prof. T. Yonetani*7	Univ. of Pennsylvania	(U.S.A.)	Jul. '97
Prof. M. Ikeda-Saito*7	Case Western Reserve Univ.	(U.S.A.)	Jul. '97
Dr. S.-Y. Yu*6	Fujian Inst. of Res. on the Structure of Matter	(China)	Jul. '97-
Dr. A. Tadjeddine*7	LURE, Centre Natl. Recherche Sci. (CNRS)	(France)	Jul. '97-
Dr. F. Fabre*7	LURE, Commissariat à l'Energie Atomique (CEA)	(France)	Jul. '97-
Prof. O.Vansyutinskii*4	Russian Acad. of Sci.	(Russia)	Jul. '97-
Prof. Xin Sun*4	Fudan Univ.	(China)	Jul. '97-

AWARDS

Professor Kobayashi's Scientific Achievements

Professor Hayao Kobayashi of Department of Molecular Assemblies received the Divisional (Physical Chemistry) Award of the Chemical Society of Japan in 1997 for his contributions on "Design and Development of Molecular Metals and Superconductors".

He has clarified the nature of several molecular conductors with a view of "molecular design and analysis on structural chemistry" based on the tight-binding band structure and produced many two-dimensional π-metal system and superconductors. He has also clarified the existence of the molecular metal with the π-d hybridized metal band and developed the stable π-molecular metals involving the magnetic moment. He has always led the research of molecular conductors which expands its activities to the discovery of organic and transition metal complex superconductors, the design and development of stable two-dimensional systems, the molecular conductors based on the p-d electron system and molecular magnetic metals.

Professor Nishi's Scientific Achievements

Professor Nobuyuki Nishi of Department of Applied Molecular Science received the Divisional (Physical Chemistry) Award of the Chemical Society of Japan in 1997 for his contribution to "Studies of Characteristics of Molecular Clusters Directly Isolated from Liquid Droplets with a Newly Developed Adiabatic Expansion Technique".

His scientific achievements relevant to the award are summarized in the following.

1. Development of a method of isolating clusters directly from liquid through adiabatic expansion of liquid droplets into a vacuum. With mass spectrometric analysis of the isolated clusters, he has studied association of solutes and solvents in liquids at a molecular level.
2. Studies of hydrophobic hydrations and hydrophobic interactions of carboxylic acids. He has proved that dimerization or polymerization of aliphatic carboxylic acids in aqueous solutions is mainly due to hydrophobic interactions between the alkyl groups.
3. Investigations of hydrogen-bonding cluster formation and hydrophobic solute association in aqueous solution of ethanol. He has demonstrated that the addition of a small amount of ethanol in water causes drastic destruction of the network structure of the water molecules.
4. Studies of structure of clusters in ethanol–water binary solutions through X-ray diffraction measurements of the intact solutions in addition to the mass spectrometric analysis of the isolated clusters.

Professor Obi's Scientific Achievements

Prof. Kinichi Obi (Visiting Professor from Tokyo Institute of Technology) of Department of Electronic Structure received the Chemical Society of Japan Award in 1997 for his contributions to "Studies on Photochemical Reaction Dynamics Initiated by Laser Excitation".

His main scientific contributions are summarized in the following.

1. Electronic structure and dynamical behavior in excited states. He succeeded to combine the pump-probe technique with thermal lensing spectroscopy. This method opened a new route for the quantitative study of photochemical processes via highly excited triplet states. He developed a new technique generating supersonic beams of molecular radicals with a beam source coupled with mercury photosensitization, laser photolysis, and pulse discharge. With this method, he performed excellent spectroscopic studies on SiH_2 and GeH_2.
2. Photochemical processes studied by probing spin polarization. He demonstrated that the spin quantum numbers of the molecular pairs in excited triplet states are conserved during triplet-triplet energy transfer processes and triplet de-excitation by radical species. He also found the generation of radicals with anomalously large spin polarization in the process of enhanced intersystem crossings of counterpart excited molecules.

Mr. Kato's Technological Achievements

Mr. Kiyonori Kato, the chief of the technical section of Molecular Materials Development Center, received the Award of the Technological Development in Chemistry for 1996.

This Award is made every year by the Chemical Society of Japan to a person who has contributed to the development or improvement of the experimental technique in chemistry or chemical engineering. Mr. Kiyonori Kato is recognized for his contribution to "Development and Popularization of Low-Temperature Technique". Mr. Kato developed the following system and devices for the non-expert liquid helium users: (1) the computer-controlled liquid helium transfer system, (2) the dynamic seal for the transfer tube, (3) the liquid helium level meter. All of these devices made the handling of liquid helium quite easy and safe. These system and devices has been exported not only to the institutions within Japan but also to abroad. Mr. Kato developed a system to regulate the temperature between 3 K and 0.5 K by controlling the vapor pressure of helium as well. This low-temperature regulation system was applied for the instrument to detect the quantum oscillation of the resistivity.

Dr. Nagasawa's Scientific Achievements

The 13th Inoue Research Award for Young Scientists in 1996 was given to Dr. Yutaka Nagasawa, who was a graduate student studying in the Department of the Electronic Structure.

This award is given to young scientists (under 35 years old) who obtained remarkable results during their Ph.D. work in the fields of basic science, engineering, medicine, pharmacy, and agriculture. Dr. Nagasawa was awarded this prize for his Ph.D. thesis, "Studies on a New Type of Electron Transfer Faster than Solvation Process".

LIST OF PUBLICATIONS

S. TEN-NO and S. IWATA, "Multi-configuration self-consitent field procedure employing linear combination of atomic-electron distributions," *J. Chem. Phys.* **105**, 3604 (1996).

H. WATANABE and S. IWATA, "Does the proton transfer reaction take place in the ground state of phenol-$(H_2O)_4$cluster," *Int. J. Quant. Chem.* **60, S30**, 1607 (1996).

S. TEN-NO and S. IWATA, "On approximating electron repulsion integrals with linear combination of atomic-electron distribution," *Int. J. Quant. Chem.* **60, S30**, 1319 (1996).

F. R. ORNELLAS and S. IWATA, "Ab initio studies of silicon and nitrogen clusters: Cyclic or linear Si_2N?, " *J. Phys. Chem.* **100**. 10919 (1996).

H. KAWAMATA, Y. NEGISHI, R. KISHI, S. IWATA, A. NAKAJIMA and K. KAYA, "Photoelectron spectroscopy of silicon-fluorine binary cluster anions (Si_nF_m)," *J. Chem. Phys.* **105**, 5369 (1996).

T. ASADA and S. IWATA, "Hybrid procedure of ab initio molecular orbital calculation and Monte Carlo simulation for studying the intracluster reactions: Applications to $M_g^+(H_2O)_n$ (n=1 - 4)," *Chem. Phys. Letters,* **260**, 1 (1996).

F. R. ORNELLAS and S. IWATA, "Structures and energetics of new nitrogen and silicon molecules: an ab initio studies of Si_2N_2," *J. Phys. Chem.* **100**, 16155 (1996).

T. IKEGAMI and S. IWATA, "Size dependence of the photoabsorption spectra of Ar_n^+, n = 4-25: a solvation effect on the Ar_3^+ chromophore," *J. Chem. Phys.* **105**, 10734 (1996).

C. -G. ZHAN and S. IWATA, "Theoretical prediction of the ^{31}P NMR chemical shift of the hexa-coordinate phosphorus intermediate for the phosphoryl ester exchange and N $\rightarrow$ O migration reactions of dimethyloxy-phosphoryl-threonin," *Chem. Letters* , 3 (1997).

H. WATANABE and S. IWATA, "Molecular orbital studies of the structures and reactions of a singly charged calcium ion with water clusters, $Ca^+(H_2O)_n$,"*J. Phys. Chem.* **A101**, 487 (1997).

C. -G. ZHAN and S. IWATA, "Ab initio studies on the structures, vertical electron detachment energies and fragmentation energies of C_nB^- clusters," *J. Phys .Chem.* **A101**, 591 (1997).

X. ZHAO, H. IMAHORI, C. -G. ZHAN, Y. SAKATA, S. IWATA and T. KITAGAWA, "Resonance Raman and FTIR spectra of isotope-labeled reduced 1,4-benzoquinone and its protonated forms in solution," *J. Phys. Chem.* **A101**, 591 (1997).

Y. M. LI and S. IWATA, "Theoretical studies of cyclic isomers of HNO_x (x= 2 - 6)," *Bull. Chem. Soc. Jpn.* **70**, 79 (1997).

F. R. ORNLLAS,L.T.UENO and S. IWATA, "Diazasilene (SiNN): Is there a conflict between experiment and theory?," *J. Chem. Phys.* **106**, 151 (1997).

J. HRUSAK and S. IWATA, "The vibrational spectrum of $H_2O_2^+$ radical cation: An illustration of symmetry breaking," *J. Chem. Phys.* **106**, 4877 (1997).

J. HRUSAK, S. TEN-NO and S. IWATA, "Quadratic Configuration Interaction versus Coupled Cluster Theory: Importance of Orbital Relaxation Phenomena in CuH and CuF," *J. Chem. Phys.* **106**, 7185 (1997).

J. HRUSAK, D. SCHRODER, H. SCHWARZ and S. IWATA, "Comparative ab initio and hybrid DFT studies relevant to an experimental investigation of neutral and cationic [Si, P, H_2] isomers," *Bull. Chem. Soc. Jpn.* **70**, 777 (1997).

J. HRUSAK, D. SCHRODER and S. IWATA, "The ground state ($^1A_1$) and the lowest ($^3B_2$) of the phenyl $C_6H_5^+$," *J. Chem. Phys.* **106**, 7541 (1997).

J. K. PARK and S. IWATA, "Ab initio study of photchemical reactions of ammonia dimer systems," *J. Phys. Chem.* **A101**, 3613 (1997).

A. FIEDLER and S. IWATA, "Portrait of diatomic FeN.A theoretical study," *Chem. Phys. Letters* **271**, 143 (1997).

Y. M. LI and S. IWATA, "Theoretical study of cyclic radicals NO_x (x=2 -6)," *Chem. Phys.* **219**, 209 (1997).

Y. M. LI and S. IWATA, "Potential energy surfaces of the ground and low-lying states of HCCS and NCS: CASSCF, MRCI and CCSD(T) studies," *Chem. Phys. Letters* **273**, 91 (1997).

W. N. WANG, K. N. FAN and S. IWATA, "Ab initio MO studies of Si_4NO^+ cluster," *Chem. Phys. Letters* **273**, 337 (1997).

T. TSUKUDA, M. SAEKI, S. IWATA and T. NAGATA, "Reaction of negatively-charged clusters of carbon dioxide with CH_3I: Formation of novel molecular anion $CH_3CO_2I^-$," *J. Phys. Chem.* **A101**, 5103 (1997).

U. H. E. HANSMANN and Y. OKAMOTO, "Monte Carlo Simulations in Generalized Ensemble: Multicanonical Algorithm versus Simulated Tempering," *Phys. Rev. E* **54**, 5863 (1996).

U. H. E. HANSMANN and Y. OKAMOTO, "Numerical Comparisons of Three Recently Proposed Algorithms in the Protein Folding Problem," *J. Comp. Chem.* **18**, 920 (1997).

M. KINOSHITA, Y. OKAMOTO and F. HIRATA, "Calculation of Hydration Free Energy for a Solute with Many Atomic Sites Using the RISM Theory: Robust and Efficient Algorithm," *J. Comp. Chem.* **18**, 1320 (1997).

M. KINOSHITA, Y. OKAMOTO and F. HIRATA, "Solvation Structure and Stability of Peptides in Aqueous Solutions Analyzed by the Reference Interaction Site Model Theory," *J. Chem. Phys.* **107**, 1586 (1997).

U. H. E. HANSMANN and Y. OKAMOTO, "Generalized-Ensemble Monte Carlo Method for Systems with Rough Energy Landscape," *Phys. Rev. E* **56**, 2228 (1997).
U. H. E. HANSMANN, "Simulated Annealing with Tsallis Weights - A Numerical Comparison," *Physica A* **242**, 250 (1997).
K. STEFANSKI, K. SOMEDA and H. NAKAMURA, "Divergences of the Semiclassical S-matrix Formula in Irregular Scattering," *Reports on Mathematical Physics* **38**, No.3, 398 (1996).
C. ZHU and H. NAKAMURA, "Semiclassical Theory of Multi-Channel Curve Crossing Problems: Landau-Zener Case," *J. Chem. Phys.* **106**, 2599 (1997).
K. NOBUSADA, K. MORIBAYASHI and H. NAKAMURA, "Quantum Dynamics of $O(^3P)$+HCl → OH+Cl: Effects of Reagent Rotational Excitation," *J. Chem. Soc. Faraday Transactions*, **93**, 721 (1997).
M. HIYAMA and H. NAKAMURA, "Two-Center Coulomb Functions," *Comp. Phys. Comm.* **103**, 209 (1997).
M. HIYAMA and H. NAKAMURA, "Gaussian Expansions of the Two-Center Coulomb Functions," *Comp. Phys. Comm.* **103**, 197 (1997).
Y. TERANISHI and H. NAKAMURA, "Semiclassical Theory of Time-Dependent Curve Crossing Problems," *J. Chem. Phys.* **107**, 1904 (1997).
C. ZHU and H. NAKAMURA, "Usefulness of the Newly Completed Semiclassical Theory of Curve Crossing: Multi-Channel Resonant Scattering," *Chem. Phys. Lett.* **274**, 205 (1997).
A. K. KAZANSKY, H. NAKAMURA, and V. N. OSTROVSKY, "Rydberg Atom in Time-Periodic Fields: Intrashell Dressed States and Quasienergy Spectrum," *Laser Physics* **7**, 1 (1997).
K. OKUMURA and Y. TANIMURA, "Unified time-path approach to the effect of anharmonicity on the molecular vibational spectroscopy in solution," *J. Chem. Phys.* **105**, 7294 (1996).
K. OKUMURA and Y. TANIMURA, "Femtosecond two-dimensional spectroscopy from anharmonicvibrational modes of molecules in the condensed phase," *J. Chem. Phys.* **107**, 2267 (1997).
K. OKUMURA and Y. TANIMURA, "The (2n+1)th-order off-resonant spectroscopy from the(n+1)th-order anharmonicites for molecular vibrational modes in the condensed phase," *J. Chem. Phys.* **106**, 1687 (1997).
N. TOMITA, S. TEN-NO and Y. TANIMURA, "Resonating Hartree-Fock approach to electron correlation problems in ab initio molecular orbital calculations: Superposition of non-orthogonal Slater determinants," *Chem. Phys. Lett.* **263**, 687 (1996).
Y. TANIMURA and K. OKUMURA, "First-, third-, and fifth-order resonant spectroscopy of anharmonic displaced oscillators system in the condensed phase," *J. Chem. Phys.* **106**, 2078 (1997).
K. OKUMURA and Y. TANIMURA, "Two-time correlation functions of a harmonic system non-bilinearly coupled to a heat bath: the spontaneous Raman spectroscopy," *Phys. Rev. E.* **56**, 2747 (1997).
Y. TANIMURA and Y. MARUYAMA, "Gaussian-Markovian quantum Fokker-Planck approach to nonlinear spectroscopy of a displaced Morse potentials system: dissociation, predissociation and optical Stark effects," *J. Chem. Phys.* **107**, 1779 (1997).
M. KINOSHITA and F. HIRATA, "Analysis on Salt Effects on Solubility of Noble Gases in Water Using the Reference Interaction Site Model Theory," *J. Chem. Phys.* **106**, 5202 (1997).
M. KINOSHITA, Y. OKAMOTO and F. HIRATA, "Calculation of Hydration Free Energy for a Solute with Many Atomic Sites Using the RISM Theory: Robust and Efficient Algorithm," *J. Comp. Chem.* **18**, 1320 (1997).
S. -H. CHONG, and F. HIRATA, "Ion Hydration: Thermodynamic and Structural Analysis with an Integral Equation Theory of Liquids," *J. Phys. Chem. B* **101**, 3209 (1997).
M. KINOSHITA, Y. OKAMOTO and F. HIRATA, "Solvation Structure and stability of peptides in aqueous solutions analyzed by the reference interaction site model theory," *J. Chem. Phys.* **107**, 1586 (1997).
S. YOSHIDA, F. HIRATA and T. MUNAKATA, "Shear-Induced Distortion of Intramolecular and Intermolecular Correlations in Liquids: Time-Dependent Density-Functional Theory," *Phys. Rev. E* **54**, 1763 (1996).
T. MUNAKATA, S. YOSHIDA and F. HIRATA, "Statistical mechanics of deformable molecular liquids: Thermal expansion and isomerization of diatomic molecules," *Phys. Rev. E* **54**, 3687 (1996).
S. -H. CHONG, and F. HIRATA, "Nonlinear Electrical Potential Fluctuations of Solvent around Solutes: an Integral Equation Study," *J. Chem. Phys.* **106**, 5225 (1997).
M. TAKEZAKI, N. HIROTA, M. TERAZIMA, H.SATO, T. NAKAJIMA and S. KATO, "Geometries and Energies of Nitrobenzene Studied by CAS-SCF Calculations," *J. Phys. Chem. A* **101**, 5190 (1997).
R. AKIYAMA, A. YOSHIMORI, T. KAKITANI, Y. IMAMOTO, Y. SHICHIDA and Y. HATANO, "Analysis of Excited State Dynamics of 13 - trans - Locked - Bacteriorhodopsin," *J. Phys. Chem. A* **101**, 412 (1997).
K. YONEMITSU and M. IMADA, "Spin Gap in One-Dimensional Electron-Phonon Systems," *Mol. Cryst. Liq. Cryst.* **285**, 223 (1996).
K. YONEMITSU, "Mott Transition in Quasi-One-Dimensional Electron Systems at Quarter Filling," *Synth. Met.* **85**, 1635 (1997).
T. NISHIO, K. YONEMITSU and H. EBISAWA, "Quasi-Particle Band Structure and Gapless Superconductivity in the Vortex-Lattice State," *J. Phys. Soc. Jpn.* **66**, 953 (1997).
K. YONEMITSU, J. KISHINE and T. OGAWA, "Various Transitions in Quasi-One-Dimensional Systems under High Pressure," *Special Issue of Rev. High Press. Sci. Tech.* **6**, 360 (1997).
J. KISHINE and H. FUKUYAMA, "Spin Gap of S=1/2 Heisenberg Ladder: Field Theoretical Study of Magnetic Susceptibility and NMR Relaxation Rate," *J. Phys. Soc. Jpn.* **66**, 26 (1997).

J. KISHINE, "Nuclear Gaussian Spin Echo Decay in S=1/2 Heisenberg Ladder," *J. Phys. Soc. Jpn.* **66**, 1229 (1997).

M. TONOOKA, S. YAMAMOTO and S. SAITO, "The Microwave Spectrum of the NH_2 Radical: The Hyperfine Structure of the $^2B_1$ Ground Electronic State," *J. Chem. Phys.* **106**, 2563 (1997).

H. FUJIWARA, K. KOBAYASHI, H. OZEKI, S. SAITO and A. I. JAMAN, "Submillimeter-wave Spectra of AsH and AsD Radicals in the X $^3\Sigma^-$ Electronic State," *J. Chem. Soc. Faraday Trans.* **93**, 1045 (1997).

K. KOBAYASHI and S. SAITO, "Microwave Spectrum of NCl in the Second Electronically Excited State (b $^1\Sigma^+$)," *J. Phys. Chem. A* **101**, 1068 (1997).

M. GUELIN, J. CERNICHARO, M. J. TRAVERS, M. C. McCARTHY, C. A. GOTTLIEB, P. THADDEUS, M. OHISHI, S. SAITO and S. YAMAMOTO, "Detection of a New Linear Carbon Chain Radical: C_7H," *Astron. Astrophys.* **317**, L1 (1997).

I. K. AHMAD, H. OZEKI and S. SAITO, "Microwave Spectroscopic Detection of HCCP in the X $^3\Sigma^-$ Electronic State: Phospho-carbene, Phospho-allene, or Phosphorene?," *J. Chem. Phys.* **107**, 1301 (1997).

S. SAITO and S. YAMAMOTO, "The Microwave Spectrum of Cyanomethyl Radical $CH_2CN(^2B_1)$," *J. Chem. Phys.* **107**, 1732 (1997).

R. S. HAYANO, T. ISHIKAWA, H. TAMURA, H. A. TORII, M. HORI, F. E. MAAS, N. MORITA, M. KUMAKURA, I. SUGAI, F. J. HARTMANN, H. DANIEL, T. von EGIDY, B. KETZER, R. POHL, D. HORVATH, J. EADES, E. WIDMANN and T. YAMAZAKI, "Observation of Double-Resonant Laser-Induced Transitions in the $v = n$-l-1 = 2 Metastable Cascade of Antiprotonic ^{4}He Atoms," *Phys. Rev. A* **55**, R1 (1997).

T. YAMAZAKI, B. KETZER, E. WIDMANN, J. EADES, H. DANIEL, F. J. HARTMANN, M. HASINOFF, R. POHL, R. SCHMIDT, T. von EGIDY, D. HORVATH, M. KUMAKURA, N. MORITA, I. SUGAI, Y. FUJITA, H. A. TORII, M. HORI, T. ISHIKAWA, F. E. MAAS, H. TAMURA and R. S. HAYANO, "Laser Resonance Studies of the Interactions of Metastable Antiprotonic Helium Atomcules $\bar{p}^4He^+$ with Surrounding H_2 Molecules," *Chem. Phys. Lett.* **265**, 137 (1997).

B. KETZER, F. J. HARTMANN, T. von EGIDY, C. MAIERL, R. POHL, J. EADES, E. WIDMANN, T. YAMAZAKI, M. KUMAKURA, N. MORITA, R. S. HAYANO, M. HORI, T. ISHIKAWA, H. A. TORII, I. SUGAI and D. HORVATH, "Hydrogen-Assisted Laser-Induced Resonant Transitions between Metastable States of Antiprotonic Helium Atoms," *Phys. Rev. Lett.* **78**, 1671 (1997).

T. YAMAZAKI, E. WIDMANN, J. EADES, M. KUMAKURA, N. MORITA, H.A. TORII, M. HORI, T. ISHIKAWA, F. E. MAAS, H. TAMURA, R. S. HAYANO, I. SUGAI, Y. FUJITA, B. KETZER, H. DANIEL, F. J. HARTMANN, M. HASINOFF, R. POHL, R. SCHMIDT, T. von EGIDY and D. HORVATH, "High-Precision Structural Studies of the Antiprotonic Helium Atom $\bar{p}^4He^+$ by Observing Laser Resonances with $\Delta v = \Delta\,(n$-l-1) = 2," *Phys. Rev. A* **55**, R3295 (1997).

T. KITAGAWA, T. OGURA, S. HIROTA, D. A. PROSHLYAKOV, K. SHINZAWA-ITOH, S. YOSHIKAWA and E. H. APPELMAN, "Time-Resolved Resonance Raman Study on Mechanism of Dioxygen reduction by Cytochrome c Oxidase," *VIIth Intrn. Conf. Time-resolved Vib. Spectrosc.* W. H. Woodruff, Ed. Los Alamos 39 (1995).

S. HIROTA, T. OGUARA, S. SHINZAWA-ITOH, S. YOSHIKAWA and T. KITAGAWA, "Observation of Multiple CN-isotope-sensitive Raman Bands for CN-adducts of Hemoglobin, Myoglobin, and Cytochrome *c* Oxidase; Evidence for Vibrational Coupling between the Fe-C-N Bending and Porphyrin In-Plane Modes," *J. Phys. Chem.* **100**, 15274 (1996).

S. HIROTA, T. LI, G. N. PHILLIPS Jr., J. S. OLSON, M. MUKAI and T. KITAGAWA, "Perturbation of the Fe-O_2 Bond by Near-by Residues in Heme Pocket: Observation of $\nu_{Fe\text{-}O_2}$ Raman Bands for Oxymyoglobin Mutants," *J. Am. Chem. Soc.* **118**, 7845 (1996).

M. ASANO-SOMEDA, K. AOYAGI and T. KITAGAWA, "Time-Resolved Resonance Raman Spectra of Octaethyl-Porphinato Copper(II) in the Lowest Excited Triplet State," *Chem. Phys. Lett.* **257**, 492 (1996).

T. KITAGAWA, S. NAKASHIMA, Y. MIZUTANI, M. MUKAI and J. S. OLSON, "Resonance Raman Spectrosocpy of Protein Dynamics," *ICORS XV* (S. A. Asher and P. B. Stein Eds.) John-Wiley & Sons Inc. 426 (1996).

S. KAMINAKA, A. TSUNESHIGE, T. YONETANI and T. KITAGAWA, "Ultraviolet Resonance Raman Study of Fe-Zn Metal-Hybrid Hemoglobins as a T-State Model," *ICORS XV* (S. A. Asher and P. B. Stein Eds.) John-Wiley & Sons Inc. 432 (1996).

S. G. KRUGLIK, Y. MIZUTANI, V. A. ORLOVICH and T. KITAGAWA, "Time-Resolved Stokes/Anti-Stokes Resonance Raman Study of Primary Photoprocesses in the Solutions of Nickel-Porphyrins," *ICORS XV* (S. A. Asher and P. B. Stein Eds.) John-Wiley & Sons Inc. 122 (1996).

V. A. ORLOVICH, Y. UESUGI, Y. MIZUTANI, S. G. KRUGLIK, A. G. SHVEDKO and T. KITAGAWA, "SRS-Based Source of 3ps, 1 kHz Pulses in Near-UV-Visible Spectral Range for TR^3 Applications," *ICORS XV* (S. A. Asher and P. B. Stein Eds.) John-Wiley & Sons Inc. 1242 (1996).

T. KITAGAWA, Y. MIZUTANI, Y. UESUGI and S. G. KRUGLIK, "Vibrational Cooling of Electronically Excited Metallo-Porphyrins Revealed by ps Time-Resolved Resonance Raman Spectroscopy," *Annu. Meet. Korian Chem. Soc.* **SB12**, 561 (1996).

D. A. PROSHLYAKOV, I. R. PAENG, K.-J. PAENG and T. KITAGAWA, "Resonance Raman Studies of Compounds I and II of *Arthromyces Ramosus* Peroxidase: Close Similarities in Their Raman Spectra but Distinct Oxygen Exchangeability of the Fe=O Heme," *Biospectroscopy* **2**, 317 (1996).

X. ZHAO, H. IMAHORI, C.-G. ZHAN, Y. MIZUTANI, Y. SAKATA and T. KITAGAWA, "Ultraviolet Resonance Raman Spectra and *Ab Initio* Vibrational Analysis of 1,4-Benzoquinone; Reassignments of the ν_2 and ν_3 Bands," *Chem. Phys. Lett* **262**, 643 (1996).

S. HIKICHI, H. KOMATSUZAKI, N. KITAJIMA, M. AKITA, M. MUKAI, T. KITAGAWA and Y. MORO-OKA, "Characterization of a μ-η^2: η^2-Peroxo Dinuclear Cobalt(II) Complex," *Inorg. Chem.* **36**, 266 (1997).

M. MUKAI, S. NAGANO, M. TANAKA, K. ISHIMORI, I. MORISHIMA, T. OGURA, Y. WATANABE and T. KITAGAWA, "Effects of Concerted Hydrogen Bonding of Distal Histidine on Active site Structures of Horseradish Peroxidase; Resonance Raman Studies with Asn-70 Mutants," *J. Am. Chem. Soc.* **119**, 1758 (1997).

X. ZHAO, H. IMAHORI, C.-G. ZHAN, Y. SAKATA, S. IWATA and T. KITAGAWA, "Resonance Raman and FTIR Spectra of Isotope-Labeled Reduced 1,4-Benzoquinone and Their Protonated Forms in Solutions," *J. Phys. Chem.* **101**, 622 (1997).

S. G. KRUGLIK, Y. MIZUTANI and T. KITAGAWA, "Time-Resolved Resonance Raman Study of the Primary Photo-Processes of Nickel(II) Octaethylporphyrin in Solutions," *Chem. Phys. Lett.* **266**, 283 (1997).

X. ZHAO, T. OGURA, M. OKAMURA and T. KITAGAWA, "Observation of the Resonance Raman Spectra of the Semiquinones. $Q_A^{\cdot-}$ and $Q_B^{\cdot-}$ in Photosynthetic Reaction Centers from *Rb, Sphaeroides* R26," *J. Am. Chem. Soc.* **119**, 5263 (1997).

T. KITAGAWA, T. OGURA, S. HIROTA, D. A. PROSHLYAKOV, J. MATYSIK, E. H. APPELMAN, K. SHINZAWA-ITOH and S. YOSHIKAWA, "Time-Resolved Resonance Raman Study of Dioxygen Reduction by Cytochrome *c* Oxidase," *J. Inorg. Biochem.* **67**, 6 (1997).

T. KOUZUMA, N. HORIKOSHI, S. SUZUKI, S. NAGATOMO and T. KITAGAWA, "Electron-Transfer Reactions and Resonance Raman Spectroscopic Studies of Two Distinct Azurins from Alcaligenes Xylosoxidans NCIB 11015," *J. Inorg. Biochem.* **67**, 45 (1997).

N. HORIKOSHI, S. NAGATOMO, T. KITAGAWA and T. KOUZUMA, "Resonance Raman Spectroscopic Studies of a Copper-Containing Nitrite Reductase from the Alcaligenes Xylosoxidans NCIB 11015," *J. Inorg. Biochem.* **67**, 46 (1997).

H. TSUKUI, E. SUZUKI, S. NAGATOMO, T. KITAGAWA, Y. SUGIMURA, F. YOSHIZAKI and T. KOUZUMA, "Gene Expression and Characterization of a Novel Plastocyanin from the Cyanobacterium *Synechococcus Sp.* PCC7942," *J. Inorg. Biochem.* **67**, 48 (1997).

T. OGURA, Y. KOBAYASHI, K. SHINZAWA-ITOH, S. YOSHIKAWA and T. KITAGAWA, "A pH Dependent Polarity Change at the Heme a_3-Cu_B Site of Bovine Cytochrome *c* Oxidase Probed Through the Fe-CO Stretching Raman Band," *J. Inorg. Biochem.* **67**, 107 (1997).

T. OGURA, M. AKI and T. KITAGAWA, "A Third-Generation UV Resonance Raman Spectrophotometer Using Solar-Blind ICCD and a Quasi-CW UV Light Source for Biological Applications," *J. Inorg. Biochem.* **67**, 428 (1997).

T. TOMITA, T. OGURA, S. TSUYAMA, Y. IMAI and T. KITAGAWA, "Effects of GTP on Bound Nitric Oxide of Soluble Guanylate Cyclase Revealed by Resonance Raman Spectroscopy," *Biochemistry* **36**, 10155 (1997).

T. TOMITA, S. TSUYAMA, Y. IMAI and T. KITAGAWA, "Purification of Bovine Soluble Guanylate Cyclase and ADP-Ribosylation on Its Small Subunit by Bacterial Toxins," *J. Biochem.* (Tokyo) **122**, 531 (1997).

T. KATO, T. AKASAKA, K. KOBAYASHI, S. NAGASE, K. YAMAMOTO, H. FUNASAKA and T. TAKAHASHI, "ESR Study on the Reactivity of Two Isomers of LaC_{82} with the Disilirane," *Appl. Mag. Res.* **11**, 293 (1996).

M. MATSUSHITA and T. KATO, "Nuclear quadrupole resonance of ^{139}La around Pr^{3+} doped in LaF_3. Raman heterodyne detection using optical transition of Pr^{3+} ions," *Chem. Phys. Lett.* **273**, 291 (1997).

H. SHIROTA, H. PAL, K. TOMINAGA and K. YOSHIHARA, "Deuterium Isotope Effect on the Solvation Dynamics of Methanol: CH_3OH, CH_3OD, CD_3OH, and CD_3OD," *J. Phys. Chem.* **100**, 1457 (1996).

S. KUMAZAKI, I. IKEGAMI and K. YOSHIHARA, "Excitation and Electron Transfer from Selectively Excited Primary Donor Chlorophyll (P700) in a Photosystem I Reaction Center," *J. Chem. Phys. A* **101**, 597 (1997).

N. A. SMITH, S. LIN, S. R. MEECH and K. YOSHIHARA, "Ultrafast Optical Kerr Effect and Solvation Dynamics of Liquid Aniline, " *J. Phys. Chem.* A **101**, 3641 (1997).

K. TOMINAGA and K. YOSHIHARA, "Temporally Two-Dimensional Overtone Vibrational Dephasing in Liquids," *Phys. Rev. A* **55**, 831 (1997).

S. LEE, B. KIM and K. YOSHIHARA, "Predissociating Resonances of Cs_2 - Theory and Experiment," *Ber. Bunsen. Geselschaft.* **101**, 407 (1997).

H. KATO, J. LEE, K. SAWABE and Y. MATSUMOTO, "Adsorption-State Specific Photodissociation Dynamics of N2O on Si(100)," *Surf. Sci.* **386**, 93 (1997).

N. TANAKA, U. NAGASHIMA, M. TAKAYANAGI, H. L. KIM and I. HANAZAKI, "Photochemical Reaction Dynamics of the $N_2O{\cdot}H_2{}^{18}O$ van der Waals Complex," *J. Phys. Chem. A* **101**, 507 (1997).

V. VANAG and I. HANAZAKI, "Effect of Light on the Belousov-Zhabotinsky Reaction in Water-in-Oil Microemulsions of Aerosol OT in Octane," *J. Phys. Chem. A* **101**, 2147 (1997).

G. RÁBAI and I. HANAZAKI, "Light-Induced Route to Chaos in the H_2O_2-HSO_3^--HCO_3^--$Fe(CN)_6^{4-}$ Flow System," *J. Am. Chem. Soc.* **119**, 1458 (1997).

A. KAMINAGA and I. HANAZAKI, "Photo-induced Excitability in the *Tris*-(bipyridyl)ruthenium(II)-catalyzed Minimal Bromate Oscillator," *Chem. Phys. Lett.* **278**, 16 (1997).

T. OMI, H. SHITOMI, N. SEKIYA, K. TAKAZAWA and M FUJII, "Nonresonant Ionization Detected IR Spectroscopy for the Vibrational Study in a Supersonic Jet," *Chem. Phys. Lett.* **252**, 287 (1996).

H. IKOMA, K. TAKAZAWA, Y. EMURA, S. IKEDA, H. ABE, H. HAYASHI and M. FUJII, "Internal Rotation of Methyl Group in o- and m-Toluidine Cations as Studied by Pulsed Field Ionization - Zero Kinetic Energy Spectroscopy," *J. Chem. Phys.* **105**, 10201 (1996).

N. HASHIMOTO and T. SUZUKI, "Pump-Probe Measurements of Predissociation Reaction Time of C_2H_2 from $A(^1A_u)$ State," *Chem. Phys. Lett.* **264**, 545 (1997).

T. SUZUKI, Y. SHI and H. KOHGUCHI, "Detection of Metastable Triplet Acetylene Produced by Intersystem Crossing from the Excited $A(^1A_u)$ State," *J. Chem. Phys.* **106**, 5292 (1997).

Y. MATSUSHITA, S. NOGUCHI, N. OHIWA and K. OBI, "Photochemical Reaction in the Molecular Culasters of Benzophenone with Hydrogen Donors Formed in a Supersonic Free Jet Expansion," *J. Photochem. Photobiol. A: Chem.* **102**, 93 (1996).

M. MITSUI, K. TAKEDA, Y. KOBORI, A. KAWAI and K. OBI, "The First Observation of CIDEP Generated through the Interaction between an Excited Singlet Oxygen Molecule and a Free Radical," *Chem. Phys. Lett.* **262**, 125 (1996).

T. ISHIWATA, Y. KASAI and K. OBI, "Observation of the $0_u^-(^3P_1)$ Ion-Pair State of Cl_2 by Pertubation-Facilitated Optical-Optical Double Resonance," *Chem. Phys. Lett.* **261**, 175 (1996).

S. WADA, Y. MATSUSHITA and K. OBI, "Laser Induced Fluorescence Spectroscopy of Jet Cooled Benzophenone Ketyl Radical," *J. Phys. Chem.* **101**, 2423 (1997).

M. TAKAYANAGI, M. NAKATA, Y. OZAKI, K. IRIYAMA and M. TASUMI, "Conformational Analysis and Photoisomerization of Merocyanine Dyes Studied by Visible Absorption, Resonance Raman and IR Spectroscopies," *J. Mol. Struct.* **405**, 239 (1997).

M. TAKAYANAGI, M. NAKATA, Y. OZAKI, K. IRIYAMA and M. TASUMI, "Intermolecular Interaction of Merocyanine Dyes Studied by Visible Absorption, Resonance Raman and Infrared Spectroscopies," *J. Mol. Struct.* **407**, 85 (1997).

J. QIN, C. YANG, K. YAKUSHI, Y. NAKAZAWA and K. ICHIMURA, "Synthesis and Properties of a New Ferromagnetic 2,2'-Bipyridine-$MnPS_3$ Intercalation Compound," *Solid State Commun.*, **100**, 427 (1996).

A. OTSUKA, G. SAITO, A. ZAKHIDOV, K. YAKUSHI, M. KUSUNOKI and K. SAKAGUCHI, "Alkali Metal Doping to C_{60} CT Complexes," *Mol. Cryst. Liq. Cryst.* **285**, 187 (1996).

M. E. KOZLOV, A. A. ZAKHIDOV and K. YAKUSHI, "ESR Study of High-Pressure Phases of C60 Fullerene," *phys. stat. sol. (b)* **197**, 187 (1996).

J. DONG, K. YAKUSHI, K. TAKIMIYA and T. OTSUBO, "Characterization of the half-filled DMTSA-BF_4 by optical and magnetic measurements," *Synthetic Metals* **84**, 633 (1997).

A. OTSUKA, G. SAITO, A. A. ZAKHIDOV and K. YAKUSHI, "Superconductivity in charge transfer complexes of C_{60}" *Synthetic Metals* **85**, 1459 (1997).

J. QIN, C. YANG, K. YAKUSHI, Y. NAKAZAWA, K. ICHIMURA and D. LIU, "Synthesis and Ferromagnetism of a New Intercalation Compound: $Mn_{0.86}PS_3(bipy)_{0.56}$," *Synthetic Metals* **85**, 1673 (1997).

V. A. IVANOV, K. YAKUSHI and J. DONG, "Electron-electron correlation with particular attention to *m*-BDNT-PF_6: spin susceptibility," *Synthetic Metals* **86**, 2107 (1997).

K. YAKUSHI and T. HIEJIMA, "Pressure-Induced Charge Transfer in Phthalocyanine Conductors," *Synthetic Metals* **86**, 2137 (1997).

T. HIEJIMA, K. YAKUSHI, T. ADACHI, O. SHIMOMURA and I. SHIROTANI, "Compressibility of One Dimensional Phthalocyanine Conductors, $NiPc(AsF_6)_{0.5}$ and $CoPc(AsF_6)_{0.5}$," *Synthetic Metals* **86**, 2167 (1997).

T. HIEJIMA and K. YAKUSHI, "Pressure and Temperature Dependence of the Electrical Resistivity of One-dimensional Phthalocyanine Conductor, $NiPc(AsF_6)_{0.5}$," *Synthetic Metals* **86**, 2185 (1997).

M. E. KOZLOV, V.A. IVANOV, K. YAKUSHI, and M. TOKUMOTO, "Electron-molecular vibration coupling in organic charge-transfer salts: application of spectroscopic and Hubbard models," *Synthetic Metals* **86**, 2177 (1977).

T. MANABE, T. KAWASHIMA, M. YAMASHITA, H. OKAMOTO, H. KITAGAWA, T. MITANI, M. INOKUCHI and K. YAKUSHI, " Competition between Electron-Correlation in Ni(III) and Electron-Lattice Interaction in Pd(II)-Pd(IV) in Mixed-Metal MX-Chain, $Ni_{1-x}Pd_x(chxn)_2Br_3$," *Synthetic Metals* **86**, 2233 (1997).

M. E. KOZLOV, M. TOKUMOTO and K. YAKUSHI, " Preparation and study of high-pressure phases of C_{60} fullerene," *Synthetic Metals* **86**, 2349 (1997).

H. KAJII, H. ARAKI, A. A. ZAKHIDOV, K. YAKUSHI and K. YOSHINO," Low-field microwave absroption and ESR in "conducting polymer-fullerene-alkali metal" superconductors: comparative study of various host matrices," *Synthetic Metals* **86**, 2351 (1997).

T. HIEJIMA, K. YAKUSHI, T. ADACHI, O. SHIMOMURA, K. TAKEDA, I. SHIROTANI, K. IMAEDA and H. INOKUCHI, "Compressibility and high-pressure electrical resistivity of one-dimensional phthalocyanine conductors: the relationship with d-π charge transfer," *Mol. Cryst. Liq. Cryst.* **296**, 255 (1997).
T. YAMASHITA, T. ENOKI, M. URUICHI, K. YAKUSHI, T. MIYAMAE and T. MIYAZAKI, "Galvanomagnetic, Optical Properties and Ultraviolet Photoelectron Spectra of Potassium-Oxygen-Graphite Intercalation Compounds," *J. Phys. Soc. Jpn.* **66**, 158 (1997).
M. E. KOZLOV, M. TOKUMOTO and K. YAKUSHI, "Spectroscopic characterization of pressure modified C_{60},"*Appl. Phys. A* **64**, 241 (1997).
V. IVANOV, K. YAKUSHI and E. UGOLKOVA, "Electronic structure of κ-ET_2X salts, where "ET" is bis(ethylenedithio)tetrathio) tetrathiafulvalene (BEDT-TTF) molecue," *Physica C* **275**, 26 (1997).
K. UEDA, M. YAMANOHA, T. SUGIMOTO, H. FUJITA, A. UGAWA, K. YAKUSHI and K. KANO, "New Spiro Donor Molecules: Bis(tetrathiafulvalenyldithio)-methane and -germane,"*Chem. Lett.* 461 (1997).
H. KAJII, H. ARAKI, A. A. ZAKHIDOV, K. TADA, K. YAKUSHI and K. YOSHINO, "Microwave heating effect on two Josephson-junction systems in granular PAT12-C_{60}-Rb composites: low-field microwave absorption study," *Physca C* **227**, 277 (1997).
V. A. IVANOV and K. KANODA, "Strong Electron Correlation in κ-$(BEDT\text{-}TTF)_2X$ Salts," *Physica C* **268**, 205 (1996).
V. A. IVANOV and K. KANODA, "κ-BEDT-TTF Salts as Layered Correlated Electron Systems," *Mol. Cryst. Liq. Cryst.* **285**, 211 (1996).
K. HIRAKI and K. KANODA, "Ground States of DCNQI-Metal Complexes, $(R_1,R_2\text{-}DCNQI)_2M$; ($R_1$, R_2=CH_3, I, M=Ag, Cu, $Li_{1-x}Cu_x$," *Mol. Cryst. Liq. Cryst.* **285**, 157 (1996).
K. HIRAKI and K. KANODA, "Electronic State of the Organic Salt, $(DI\text{-}DCNQI)_2Ag$, where DI-DCNQI is 2,5-diiodo-N, N-dicyanoquinonediimine," *Phys. Rev. B* **54**, 17276 (1996).
K. KANODA, "Recent Progress in NMR Studies on Organic Conductors (invited)," *Hyperfine Interactions* **104**, 235 (1997).
Y. NAKAZAWA and K. KANODA, "Low-Temperature Specific Heat of κ-$(BEDT\text{-}TTF)_2Cu[N(CN)_2]Br$ in the Superconducting State," *Phys. Rev. B* **55**, R8670 (1997).
A. KAWAMOTO, K. MIYAGAWA and K. KANODA, "Deuterated κ-$(BEDT\text{-}TTF)_2Cu[N(CN)_2]Br$: a System on the Border of the Superconductor/Magnetic-Insulator Transition," *Phys. Rev. B* **55**, 14140 (1997).
Y. NAKAZAWA and K. KANODA, "Reply to the 'Comment on Electronic structure of insulating salts of the κ-$(BEDT\text{-}TTF)_2X$ family studied by low-temperature specific heat measurements'," *Phys. Rev. B* **56**, 951 (1997).
H. TANIGUCHI, Y. NAKAZAWA and K. KANODA, "Vortex State in the Highly Anisotropic Superconductor, α-$(BEDT\text{-}TTF)_2NH_4Hg(SCN)_4$," *Synth. Met.* **85**, 1553 (1997).
Y. NAKAZAWA and K. KANODA, "Low-Temperature Specific Heat Studies of Superconductors and Mott Insulators of κ-$(BEDT\text{-}TTF)_2X$ system," *Synth. Met.* **85**, 1563 (1997).
K. MIYAGAWA, A. KAWAMOTO and K. KANODA, "^{13}C-NMR Study of β-$(BEDT\text{-}TTF)_2I_3$," *Synth. Met.* **85**, 1537 (1997).
A. KAWAMOTO, K. MIYAGAWA, H. TANIGUCHI and K. KANODA, "^{13}C NMR Study of Mott Insulating Phases in κ-$(BEDT\text{-}TTF)_2X$ Family," *Synth. Met.* **85**, 1547 (1997).
K. MIYAGAWA, A. KAWAMOTO and K. KANODA, "NMR Study of Superconductivity in κ-$(BEDT\text{-}TTF)_2X$," *Synth. Met.* **85**, 1545 (1997).
A. KAWAMOTO, K. MIYAGAWA and K. KANODA, "NMR Study of (BEDT-TTF)(TCNQ) at Selective Nuclear Sites," *Synth. Met.* **85**, 1601 (1997).
K. HIRAKI and K. KANODA, "Comparative Study of Magnetism and Conductivity of $(DI\text{-}DCNQI)_2M$ [M=Li, Cu and Ag]," *Synth. Met.* **86**, 2103 (1997).
K. HIRAKI and K. KANODA, "Carrier Doping to $(DCNQI)_2Li$," *Synth. Met.* **86**, 2111 (1997).
A. KAWAMOTO, K. MIYAGAWA and K. KANODA, "^{15}N and ^{13}C NMR Study of $(DMe\text{-}DCNQI)_2Cu$," *Synth. Met.* **86**, 2083 (1997).
K. MIYAGAWA, A. KAWAMOTO and K. KANODA, "Nesting Instability in a Family of α-$(BEDT\text{-}TTF)_2MHg(SCN)_4$ [M=K, Rb, NH_4] Studied by ^{13}C NMR," *Synth. Met.* **86**, 1987 (1997).
H. OHTA, S. KIMURA, Y. YAMAMOTO, J. AZUMA, K. AKIOKA, M. MOTOKAWA and K. KANODA, "Submillimwter wave AFMR of Mott Insulator κ-$(BEDT\text{-}TTF)_2Cu[N(CN)_2]Cl$," *Synth. Met.* **86**, 2079 (1997).
H. OHTA, Y. YAMAMOTO, K. AKIOKA, M. MOTOKAWA and K. KANODA, "Cyclotron Resonance of α-$(BEDT\text{-}TTF)_2RbHg(SCN)_4$ Observed at above and below the Transition Temperature," *Synth. Met.* **86**, 1913 (1997).
K. AKIOKA, H. OHTA, Y. YAMAMOTO, M. MOTOKAWA and K. KANODA, "Submillimeter Wave ESR and Cyclotron Resonance Measurements of α-$(BEDT\text{-}TTF)_2NH_4Hg(SCN)_4$," *Synth. Met.* **86**, 2051 (1997).
H. TANAKA, A. KOBAYASHI, T. SAITO, K. KAWANO, T. NAITO and H. KOBAYASHI, "1-Type BETS salts containing Mixed Halide Gallium Anion, GaX_xY_{4-x} (X, Y= F, Cl. Br; BETS=Bis(ethylenedithio)tetra-selenafulvalene)," *Adv. Mater.* **8**, 811 (1996).

M. INOKUCHI, H. TAJIMA, T. OHTA, A. KOBAYASHI, H. KURODA, T. NAITO and H. KOBAYASHI, "Electrical Conductivity and Upper Critical Magnetic Field of the Molecular Superconductor, a-(EDT-TTF)[Ni(dmit)$_2$]$_2$," *Adv. Mater. for Optics and Electronics* **6**, 367 (1996).

M. NAKATA, A. KOBAYASHI, T. SAITO, H. KOBAYASHI, K. TAKIMIYA, T. OTSUBO and F. OGURA, "Crystal Structures and Electrical Conductivities of Cation-radical Salys of a Tellurium-containing Donor:3,4-Dimrthylanthra[1,9-cd:4,10-c'd']bis[1,2]Ditellurolr, "*J. C. S. Chem. Commun.* 593 (1997).

T. NAITO, H. KOBAYASHI and A. KOBAYASHI, "The Electrical Behavior of Charge -transfer Salts Based on an Unsymmetrical Donor Bis(ethylenedithio)diselenadithiafulvalene (STF): Disorder Effect on the Transport Properties," *Bull. Chem. soc. Jpn.* **70**, 107 (1997).

H. KOBAYASHI, E. ARAI, T. NAITO, H. TANAKA, A. KOBAYASHI and T. SAITO, "Structural and Electrical Properties of a Series of Organic Superconductors l-BETS$_2$GaX$_z$Y$_{4-z}$ (X=Br,Cl,F; 0<z<4)," *Synth. Metals* **85**, 1463 (1997).

H. TAJIMA, A. KOBAYASHI, T. NAITO and H. KOBAYASHI, "Shubnikov-de Haas effect and Angular-dependent Magnetoresistance Oscillation of κ-(BETS)$_2$GaCl$_4$," *Synth. Metals* **86**, 1911 (1997).

I. OLEJNICZAK, A. GRAJA, N. D. KUSH, P. CASSOUX and H. KOBAYASHI, "Microreflectance Infrared Study of the Organic Conductor κ-(BETS)$_2$FeCl$_4$," *Synth. Metals.* **86**, 2155 (1997).

M. TOKUMOTO, T. NAITO, H. KOBAYASHI, A. KOBAYASHI, V. N. LAUKHIN, L. BROSSAED and P. CASSOUX, "Magnetic Anisotropy of Organic Conductors λ-(BETS)$_2$FeCl$_4$," *Synth. Metals* **86**, 2161 (1997).

A. KOBAYASHI, A. SATO, E. ARAI, H. KOBAYASHI, C. FAULMANN, N. KUSH and P. CASSOUX, "A Stable Molecular Metal with a Binuclear Magnetic Anion,θ- (BETS)$_4$Cu$_2$Cl$_6$," *Solid State Commun.* **103**, 371 (1997).

O. A. BOGDANOVA, V. V. GRITSENKO, O. D. DYACHENKO, E. I. ZHILYAEVA, A. KOBAYASHI and H. KOBAYASHI, R. N. LYUBOVSKAYA, R. B. LYUBOVSKII and G. V. SHILOV, "New BETS Salt with Iodomercurate Anion: (BETS)$_4$Hg$_3$I$_8$," *Chem. Lett.* 675 (1997).

A. KOBAYASHI and H. KOBAYASHI, "κ- and Modified κ-Type Molecular Arrangements and Electrical Resistivities of (BETS)$_2$InCl$_4$, (BETS)$_2$ClO$_4$(TCE)$_{0.5}$, (BETS)$_2$BF$_4$(TCE)$_{0.5}$ and (BETS)$_2$[(C$_2$H$_5$)$_4$N]$_{0.7}$InCl$_5$," *Mol. Cryst. Liq. Cryst.* **296**, 181 (1997).

H. FUJIWARA, E. ARAI and H. KOBAYASHI, "Synthesis, Structure and Physical Properties of the New Selenium Containing Metal Complex NBu$_4$[Ni(ddds)$_2$]," *J. Chem. Soc. Chem. Commun.* 837 (1997).

H. TAJIMA, M. INOKUCHI, A. KOBAYASHI, A. SATO, T. NAITO, H. KOBAYASHI and H. KURODA, "Magnetic and Transport Properties of an Ambient-pressure Superconductor α-EDT-TTF[Ni(dmit)$_2$]," *Synth. Metals* **85**, 1585 (1997).

H. KOBAYASHI, E. ARAI, A. SATO, T. NAITO, H. TANAKA, A. KOBAYASHI and P. CASSOUX, "Structural and Electrical Properties of BETS Compounds with Transition Metal Complex Anions," *Synth. Metals* **85**, 1595 (1997).

L. BROSSARD, P. CASSOUX, O. DYACHENKO, C. FOULMANN, A. GRAJA, H. KOBAYASHI, A. KOBAYASHI, K. POKHODNYA and M. TOKUMOTO, "Interplay of Conductivity, Magnetism (and Nonlinear Optics) in Organic-inorganic Compounds," *Synth. Metals* **86**, 1785 (1997).

T. NAITO, T. INABE, E. ARAI, M. TAMURA, Y. NISHIO, K. KAJITA, A. KOBAYASHI and H. KOBAYASDHI, "Electrical and Magnetic Properties of DED Salts," *Synth. Metals* **86**, 1815 (1997).

A. KOBAYASHI, T. NAITO, A. SATO and H. KOBAYASHI, "Development and Low-temperature Crystal Structures of M(dmiX)$_2$ (X=S,Se) Conductors," *Synth. Metals* **86**, 1841 (1997).

H. TAJIMA, A. KOBAYASHI and T. NAITO and H. KOBAYASHI, "Shubnikov-de Haas effect and Angular-dependent Magneto-resistance Oscillation of κ-(BETS)$_2$GaCl$_4$," *Synth. Metals* **86**, 1911 (1997).

Y. NISHIO, M. TAMURA, K. KAJITA, S. AOMUMA, R. KATO and H. KOBAYASHI, "Thermal Study of antiferromagnetic Ordering in Deuterated (DMe-DCNQI)$_2$Cu," *Synth. Metals* **85**, 1739 (1997).

N. TAJIMA, K. MATUO, M. TAMURA, Y. NISHIO, K. KAJITA, T. NAITO and H. KOBAYASHI, "Magnetotransport Phenomena of α-(BEDT-TSeF)$_2$I$_3$," *Synth. Metals* **86**, 1981 (1997).

N. SOMEYA, Y. NISHIO, M. TAMURA, K. KAJITA, S. AOMUMA, H. SAWA, R. KATO and H. KOBAYASHI, "Thermal Study od Reentrant Metal-Insulator Transition in Deuterated (DMe-DCNQI)$_2$Cu," *Synth. Metals* **86**, 2077 (1997).

O. OISHI and S. MIYAJIMA, "New PFG NMR Spectrometer with a Rotatable Quadrupole Coil for the Measurement of an Anisotropic Self-Diffusion Coefficient Tensor," *J. Magn. Reson.* **123 A**, 64 (1996).

T. TOYODA, H. YOSHIDA, O. OISHI and S. MIYAJIMA, "Personal Computer-Controlled 16 Channel Versatile Pulse Generator for Nuclear Magnetic Resonance," *Rev. Sci. Instrum.* **68**, 3140 (1997).

H. OGATA, H. FUJIMORI, S. MIYAJIMA, K. KOBASHI, T. CHIBA, R. E. TAYLOR and K. ENDO, "Modification of Electronic Structure by Charge Transfer and Molecular Motion in Titanium Disulfide-Ethylenediamine Intercalation Compound," *J. Phys. Chem. Solids* **58**, 701 (1997).

J. H. KO, B. G. KIM, J. J. KIM, H. FUJIMORI and S. MIYAJIMA, "Anisotropic Glass Freezing in Rubidium/Ammonium Dihydrogen Phosphate Mixed Crystal and its Deuterated Analogue," *J. Phys. Condens. Matter* **9**, 4403 (1997).

I. TAKASU, T. MOCHIDA, A. IZUOKA and T. SUGAWARA, "Dielectric Property of Hydrogen-bonded Squaric Acid Derivatives,"*Mol. Cryst. Liq. Cryst.* **285**, 275 (1996).

T. MOCHIDA, T. HASEGAWA, S. KAGOSHIMA, S. SUGIURA and Y. IWASA, "Synthesis, Structure, and Electronic Properties of (BEDT-TTF)(R1R2TCNQ); (R1=R2=H, F, Cl, Br, CH3)," *Synth. Met.* **86**, 1797 (1997).
T. HASEGAWA, S. KAGOSHIMA, T. MOCHIDA, S. SUGIURA and Y. IWASA, "Synthesis, Structure, and Electronic Properties of (BEDT-TTF)(F*n*TCNQ)," *Synth. Met.* **86**, 1801 (1997).
T. HASEGAWA, K. INUKAI, S. KAGOSHIMA, T. SUGIURA, T. MOCHIDA, S. SUGIURA and Y. IWASA, "(BEDT-TTF)(F1TCNQ) and (BEDT-TTF)(F2TCNQ)0.5(TCNQ)0.5; All-Organic Metals Down to 2 K," *J. Chem. Soc. Chem. Commun.* 1377 (1997).
T. HASEGAWA, S. KAGOSHIMA, T. MOCHIDA, S. SUGIURA and Y. IWASA, "Electronic States and Anti-ferromagnetic Order in Mixed-Stack Charge Transfer Compound (BEDT-TTF)(F2TCNQ)," *Solid State Commun.* **103**, 489 (1997).
H. OKAMOTO, Y. SHIMADA, Y. OKA, A. CHAINANI, T. TAKAHASHI, H. KITAGAWA, T. MITANI, K. TORIUMI, K. IOUE, T. MAMABE and M. YAMASHITA, "Electronic Structure of the Quasi-One-Dimensional Halogen-Bridged Ni Complexes," *Phys. Rev.* **B54**, 8438 (1997).
H. OKAMOTO, Y. OKA, T. MITANI and M. YAMASHITA, "Dynamics of Solitons and Polarons in the Quasi-0ne-Dimensional MX Chain Compound [Pt(en)2][Pt(en)2I2](ClO4)4," *Phys. Rev.* **B55**, 6330 (1997).
T. MANABE, T.OHISHI, M. YAMASHITA, T. TAKEUCHI, T.YOSHIDA, Y. YU, Z. HONADA and K. KATSUMATA, "S=1 New Haldane Gap Systems and Spin Glass Behaviors: Syntheses, Structures and Magnetic Properties of Linear-Chain Ni(II) Complexes," *Synth. Met.*, **85**, 1717 (1997).
Z. HONDA, K. KATSUMATA, T. OHISHI, T. MANABE and M. YAMASHITA, " Inducing a Magnetic Ordering in the Haldane Material Ni(C5H14N2)2N3(ClO4) by Magnetic Field," *J. Phys.: Condens. Matter* **9**, L83 (1997).
Y. KAGAMI, F. IWAHORI, T. OHISHI, T. HAMA, T. MANABE, M. YAMASHITA, H. KITAGAWA, K. SAKAI and T. MITANI, "Physical Properties of Quasi-One-Dimensional Charge-Transfer Metal Complexes; [M(HBQD)2]TCNQ(M=Ni, Pd; H2BQD=1, 2-Benzoquinoedioxime)," *Synth. Met.*, **86**, 1803 (1997).
T. SEKIKAWA, K. MIYAKUBO, S. TAKEDA, and T. KOBAYASHI, "Charge-transfer Effects in a Strongly Hydrogen-bonded System: Potassium Salt of Acetylenedicarboxylic Acid," *J. Phys. Chem.* **100**, 5844 (1996).
S. TAKEDA, H. KATAOKA, S. IKEDA and K. YAMAGUCHI, "Rotational Tunneling of Methyl Groups of Sc(CH3COO)3 and Sc(CD3COO)3," *Physica B* **226**, 174 (1996).
S. TAKEDA, F. KONDOH, N. NAKAMURA and K. YAMAGUCHI, "Proton Tunneling and Local Symmetry of the Hydrogen Bond in Rb3H(SO4)2," *Physica B* **226**, 157 (1996).
M. NISHINO, M. TANAKA, S. TAKEDA, K. MASHIMA, W. MORI, K. TANI, A. NAKAMURA and K. YANAGUCHI, "Theoretical Studies of Direct Exchange Couplings between Transition Metal Ions I. Naked Binuclear Chromium(II) and Molybdenum(II) Systems," *Mol. Cryst. Liq. Cryst.* **286**, 193 (1996).
M. NISHINO, M. TANAKA, S. TAKEDA, K. MASHIMA, W. MORI, K. TANI, A. NAKAMURA and K. YAMAGUCHI, "Theoretical Studies of Direct Exchange Couplings between Transition Metal Ions II. Tetranuclear Transition Metal Systems, " *Mol. Cryst. Liq. Cryst.* **286**, 201 (1996).
T. KAWAKAMI, S. TAKEDA, W. MORI and K. YAMAGUCHI, "Theoretical Studies of Effective Exchange interactions between nitroxides via Hydrogen Atoms," *Chem. Phys. Lett.* **261**, 129 (1996).
S. TAKEDA, H. FUKUMOTO, K. MASHIMA, G. MARUTA, K. YAMAGUCHI and A. NAKAMURA, "Thermochromism and Dynamics of Organometallic Conjugated Systems: Zirconocene Complex of 1,4-Diphenyl-1,3-butadiene," *J. Phys. Chem.* **101**, 278 (1997).
M. NISHINO, S. TAKEDA, W. MORI, A. NAKAMURA and K. YAMAGUCHI, "Theoretical Studies of Organometallic Conjugated Systems: Prussian Blue Analogs," *Synth. Metals* **85**, 1763 (1997).
K. MASHIMA, M. TANAKA, K. TANI, A. NAKAMURA, S. TAKEDA, W. MORI and K. YAMAGUCHI, "Elongation of the Quadruple Cr^{II}-Cr^{II} Bond Induced by Two $PtMe_2$ Moieties in the Linearly Aligned Tetrametal System, $PtMe_2\cdots Cr\text{-}Cr\cdots PtMe_2$," *J. Am. Chem. Soc.* **119**, 4307 (1997).
K. KAMIYA, T. MIYAMAE, M. OKU, K. SEKI, H. INOKUCHI, C. TANAKA and J. TANAKA, "Ultraviolet Photoemission Spectra of Perchlorate-Doped cis-and trans-Polyacetylene," *J. Phys. Chem.* **100**, 16213 (1996).
A. IZUOKA, T. MURASE, M. TSUKADA, Y. ITO, T. SUGAWARA, A. UCHIDA, N. SATO and H. INOKUCHI, "Crystal Structure and Thermodynamical Behavior of Tetrabenzo[*de,hi,op,st*]pentacene Endoperoxide," *Tetrahedron Lett.* **38**, 245 (1997).
T. TANAKA, T. ATAKE, Z. SHI, C. NAKANO, T. ENOKI, G. SAITO and H. INOKUCHI, "Calorimetric Studies of Tetrakis(alkylthio)tetrathiafulvalene, TTCn-TTF (n = 3,8)," *J. Phys. Chem. Solids* **58**, 295 (1997).
K. IMAEDA, J. KRÖBER, H. INOKUCHI, Y. YONEHARA and K. ICHIMURA, "Superconductivity in Sodium-Hydrogen-C_{60} Ternary Compound," *Synth. Met.* **85**, 1575 (1997).
C. NAKANO, K. IMAEDA, J. KRÖBER and H. INOKUCHI, "Rietveld Analysis of the Superconducting $Na_xH_yC_{60}$," *Chem. Lett.* 343 (1997).
T. MATSUI, S. NAGANO, K. ISHIMORI, Y. WATANABE and I. MORISHIMA, "Preparation and Reactions of Myoglobin Mutants Bearing both Proximal Cysteine Ligand and Hydrophobic Distal Cavity: Protein Models for the Active Site of P-450," *Biochemistry* **35**, 13118 (1996).
S. OZAKI, T. MATSUI and Y. WATANABE, "Conversion of Myoglobin into a Highly Stereospecific Peroxygenase by the L29H/H64L Mutation,"*J. Am. Chem. Soc.* **118**, 9784 (1996).

S. NAGANO, M. TANAKA, K. ISHIMORI, Y. WATANABE and I. Morishima, "Catalytic Roles of Distal Site Aspargine-Histidine Couple in Peroxidases," *Biochemistry* **35**, 14251 (1996).

S. OZAKI, Y. INADA and Y. WATANABE, "Catalytic Intermediates of Polyethylene Glycolated Horseradish Peroxidase in Benzene," *Keio J. Med.* **45**, S68 (1996).

Y. WATANABE, S. OZAKI and T. MATSUI, "Mechanism Based Molecular Design of Peroxygenases," *Keio J. Med.* **45**, S24 (1996).

M. MUKAI, S. NAGANO, M. TANAKA, K. ISHIMORI, I. MORISHIMA, T. OGURA, Y. WATANABE and T. KITAGAWA, "Effects of Concerted Hydrogen Bonding of Distal Histidine on Active Site Structures of Horseradish Peroxidase; Resonance Raman Studies with Asn-70 Mutants," *J. Am. Chem. Soc.* **119**, 1758 (1997).

S. OZAKI, T. MATSUI and Y. WATANABE, "Conversion of Myoglobin into a Peroxygenase: A Catalytic Intermediate of Sulfoxidation and Epoxidation by the F43H/H64L Mutant," *J. Am. Chem. Soc.* **119**, 6666 (1997).

T. MATSUI, S. OZAKI and Y. WATANABE, "Roles of the Location of Distal Histidine in the Oxidation Activities of Myoglobin," *J. Inorg. Biochem.* **67**, 86 (1997).

S. OZAKI, Y. INADA and Y. WATANABE, "Catalytic Intermediates of Polyethylene Glycolated Horseradish Peroxidase in Organic Media," *J. Inorg. Biochem.* **67**, 87 (1997).

Y. GOTO, S. WADA, Y. WATANABE and I. MORISHIMA, "Oxidation of Aldehydes by Ferric Peroxo Porphyrin Complexes," *J. Inorg. Biochem.* **67**, 96 (1997).

T. MURAKAMI, Y. WATANABE and I. MORISHIMA, "New Oxidation Reaction of an Iron Porphyrin Complex Related to Heme Catabolism," *J. Inorg. Biochem.* **67**, 97 (1997).

S. OGO, S. NAKAMURA, H. CHEN, K. ISOBE, Y. WATANABE and R. H. FISH, "A New Water Soluble NMR Shift Reagent Based on Molecular Recognition Principles: Non-Covalent p-p Interactions of Water Soluble Aromatic Guest Substrates with A Bioorganometallic Host, $[Cp^*Rh(2'\text{-deoxyadenosine})]_3(OTf)_3$," *J. Inorg. Biochem.* **67**, 296 (1997).

S. WADA, M. IWASE, Y. WATANABE, K. JITSUKAWA, H. MASUDA and H. EINAGA, "Ligand Oxidation by Activation of Hydrogen Peroxide with Non-Heme Iron(III) Complex," *J. Inorg. Biochem.* **67**, 324 (1997).

K. INOUE and H. IWAMURA, "Spontaneous Magnetization in a 2 : 3 Complex Formed by 3,4',5-Tris(N-oxy-tert-butylamino)biphenyl and Manganese(II) bis(hexafluoroacetylacetonate)," *Adv. Mater.* **8**, 73 (1996).

H. IWAMURA, K. INOUE and T. HAYAMIZU, "High-spin polynitroxide radicals as versatile bridging ligands for transition metal complexes with high ferri/ferromagnetic T_C," *Pure Appl. Chem.* **68**, 243 (1996).

K. INOUE and H. IWAMURA, "Magnetic Characterization of One-dimensional Molecule-based Metamagnet made of Mn(II)(hfac)2 and 1,3-Bis(*N*-oxy-*tert*-butylamino)benzene," *Mol. Clyst. Liq. Cryst.* **286**, 133 (1996).

K. INOUE and H. IWAMURA, "Ferrimagnets Made by Assembling High-Spin Organic Polyradicals by Mean of Complexation with Magnetic Metal Ions. VII. One-Dimensional Chains Made by an Alternating Array of $Mn(II)(hfac)_2$ and 1,3-Bis(*N*-oxy-*tert*-Butylamino)Benzenes," *Proc., Mater. Res. Soc.* **413**, 313 (1996).

KAWAKAMI, A. ODA, W. MORI, K. YAMAGUCHI, K. INOUE and H. IWAMURA, "Theoretical Studies of the Ferromagnetic Intermolecular Interaction of *p*-Carboxylate Phenyl Nitronyl Nitroxide," *Mol. Cryst. Liq. Cryst.* **279**, 29 (1996).

J. -L. STANGER, J. -L. ANDRE, P. TUREK, Y. HOSOKOSHI, M. TAMURA, M. KINOSHITA, P. REY, J. CIRUJEDA and J. VECIANA, "Role of the Demagnetizing Field Effects in the Epr of Organic Radical Magnets," *Phys.Rev.* **B55**, 8398 (1997).

K. UEDA, T. SUGIMOTO, S. ENDO, N. TOYOTA, M. KOHAMA, K. YAMAMOTO, Y. SUENAGA, H. MORIMOTO, T. YAMAGUCHI, M. MUNAKATA, N. HOSOITO, N. KANEHISA, Y. SHIBAMOTO and Y. KAI, "1:2 TCNQ/$TCNQ^-$ Mixed Salts Exhbiting Ferromagnetic Behavior at Room Temperature," *Chem. Phys. Lett.* **261**, 295 (1996).

K. UEDA, T. SUGIMOTO, T. TADA, K.-I. NISHIMURA, S. ENDO, N. TOYOTA, M. KOHAMA, K. YAMAMOTO, T. YAMAGUCHI, Y. SUENAGA, M. MUNAKATA, N. KANEHISA, Y. SHIBAMOTO, Y. KAI and N. HOSOITO, "Temperature Dependence of Crystal Structures, and Electrical Conducting and Magnetic Properties in Plate Crystals of 1:2 Tetrafluorotetracyanoquinodimethane/Tetrafluorotetracyanoquinodimethanide Mixed Tetramethyl-ammonium and -phosphonium Salts," *Mol. Cryst. Liq. Cryst.* **296**, 323 (1997).

K. UEDA, M. GOTO, T. SUGIMOTO, S. ENDO, N. TOYOTA, K. YAMAMOTO and H. FUJITA, "Synthesis, and Electrical Conducting and Magnetic Properties of a Neutral Bis(dimethylthiotetrathiafulvalenyldithiolate)copper Complex," *Synth. Metals* **85**, 1679 (1997).

K. UEDA, M. YAMANOHA, T. SUGIMOTO, H. FUJITA, A. UGAWA, K. YAKUSHI and K. KANO, "New Spiro Donor Molecules: Bis(tetrathiafulvalenyldithio)-methane and -germane," *Chem. Lett.* 461 (1997).

H. KITAGAWA, N. ONODERA, J.-S. AHN, T. MITANI, M. KIM, Y. OZAWA, K. TORIUMI, K. YASUI, T. MANABE and M. YAMASHITA, "Mixed-Valence States in MMX-Chains Complex, $Pt_2(dta)_4I$, " *Mol. Cryst. Liq. Cryst.* **285**, 311 (1996).

K. OHASHI, Y. INOKUCHI and N. NISHI, "Photodissociation spectroscopy of phenol dimer ion: Lack of resonance interaction between the aromatic rings," *Chem. Phys. Lett.* **257**, 137 (1996).

K. OHASHI and N. NISHI, "Spectroscopy and excited-state dynamics of benzene-trimer ion," *Surface Review Letters* **3**, 601 (1996).

K. OHASHI, Y. INOKUCHI and N. NISHI, "Pump-probe photodepletion spectroscopy of $(C_6H_6)_2^+$: Identification of spectrum in the charge resonance band region," *Chem. Phys. Lett.* **263**, 167 (1996).

Y. INOKUCHI, M. MATSUMOTO, K. OHASHI, and N. NISHI, "Charge Resonance and Charge Transfer Interactions in Naphthalene Homo- and Hetero-Dimers," *Resonance Ionization Spectroscopy* **1996**, 231 (1997).
Y. NAKAI, K. OHASHI and N.NISHI, "Electronic structures and photoevaporation dynamics of benzene cluster ions," *J. Phys. Chem.* **101**, 472 (1997).
Y. INOKUCHI, Y. NAITOH, K. OHASHI, K. SAITOW, K. YOSHIHARA and N. NISHI, "Formation of benzene dimer cations in neat liquid benzene studied by femtosecond transient absorption spectroscopy," *Chem. Phys. Lett.* **269**, 298 (1997).
M. MATSUMOTO, Y. INOKUCHI, K. OHASHI and N. NISHI, "Charge Delocalization in Benzene-Naphthalene Hetero-Dimer Cation," *J. Phys. Chem.* **101**, 4574 (1997).
T. ICHIMURA, Y. MORI, H. SHINOHARA, and N. NISHI, "Photofragmentation of Chlorotoluenes and Dichlorobenzenes: Substituent effects on the dissociation mechanism, and angular distribution of Cl fragment," *J. Chem. Phys.* **107**, 835 (1997).
T. TSUKUDA, M. A. JOHNSON and T. NAGATA, "Photoelectron Spectroscopy of $(CO_2)_n^-$ Revisited: Core Switching in the $2 \leqq n \leqq 16$ range," *Chem. Phys. Letters*, **268**, 429 (1997).
K. KANDA, S. KATSUMATA, T. NAGATA, T. KONDOW, A. HIRAYA, K. TABAYASHI and K.SHOBATAKE, "Photodissociation Spectroscopy of ICN in the Vacuum Ultraviolet Region," *Chem. Phys.*, **218**, 199 (1997).
T. TSUKUDA, M. SAEKI, S. IWATA and T. NAGATA, "Reaction of Negatively-Charged Clusters of Carbon Dioxide with CH_3I: Formation of Novel Molecular Anion $CH_3CO_2Iυ$, " *J. Phys. Chem.*, **101**, 5103 (1997).
J. ADACHI, N. KOSUGI, E. SHIGEMASA and A. YAGISHITA, "Vibronic Couplings in the C $1s \rightarrow ns\sigma_g$ Rydberg Excited States of CO_2," *J. Phys. Chem.* **100**, 19783 (1996).
N. WATANABE, J. ADACHI, K. SOEJIMA, E. SHIGEMASA, A. YAGISHITA, N. G. FOMINYKH and A. A. PAVLYCHEV, "Fixed-Molecule $1s\sigma_{g,u}$ Photoelectron Angular Distributions as a Probe of σ_g* and σ_u* Shape Resonances of CO_2," *Phys. Rev. Lett.* **78**, 4910 (1997).
E. ITO, H. OJI, T. ARAKI, K. OICHI, H. ISHII, Y. OUCHI, T. OHTA, N. KOSUGI, Y. MARUYAMA, T. NAITO, T. INABE and K. SEKI, "Soft X-ray Absorption and X-ray Photoelectron Spectroscopic Study of Tautomerism in Intramolecular Hydrogen Bonds of N-Salicylideneaniline Derivatives," *J. Am. Chem. Soc.* **119**, 6336 (1997).
A. P. HITCHCOCK, S. G. URQUHART, A. T. WEN, A. L. D. KILCOYNE, T. TYLISZCZAK, E. RÜHL, N. KOSUGI, J. D. BOZEK, J. T. SPENCER, D. N. MCILROY and P. A. DOWBEN, "Inner-Shell Excitation Spectroscopy of *closo*-Carboranes," *J. Phys. Chem. B* **101**, 3483 (1997).
N. KOSUGI, R. G. CAVELL and A. P. HITCHCOCK, "(LS) versus (jj) Coupling in P 2p Inner-Shell Excited States of PF_3," *Chem. Phys. Lett.* **265**, 490 (1997).
S. MATSUO and T. TAHARA, "Phase-stabilized Optical Heterodyne Detection of Impulsive Stimulated Raman Scattering," *Chem. Phys. Lett.* **264**, 636 (1997).
S. TAKEUCHI and T. TAHARA, "Ultrafast Fluorescence Study on the Excited Singlet State Dynamics of *all-trans* Retinal," *J. Phys. Chem.* **101A**, 3052 (1997).
Y. PARK, S. RHEE, Y. IMAIZUMI and T. URISU, "Structual Changes of Silicon Dioxide Films Caused by Synchrotron Irradiation," *J. Appl. Phys.* **80**, 1236 (1996).
Y. IMAIZUMI, Y. TSUSAKA, T. URISU and T. IBUKI, "Carbon Contamination in Synchrotron-Radiation-Stimulated Al Deposition Using a Low Temperature Condensed Layer of Dimethyl Aluminum Hydride," *Jpn. J. Appl. Phys.* **35**, 6588 (1996).
A. YOSHIGOE, S. HIRANO, K. MASE and T. URISU, "*In situ* Observation of Surface Reactions with Synchrotron Radiation Induced Semiconductor Processes by Infrared Reflection Absorption Spectroscopy Using Buried Metal Layer Substrate," *Trans. IEE of Japan.* **116-C**, 1348 (1996).
S. GHEYAS, M. NISHIO, T. URISU and H. OGAWA, "Adsorption and Thermal Decomposition of Diethyltellurium on GaAs(100)," *Appl. Surf. Sci.* **100/101**, 211 (1996).
T. URISU, T. IBUKI, Y. IMAIZUMI and M. KAWASAKI, "Potential of Site Specific Photochemical Processing Using Synchrotron Radiation," *Nucl. Instrum. Methods Phys. Res.* **B122**, 364 (1997).
K. MASE, M. NAGASONO, S. TANAKA, M. KAMADA, T. URISU and Y. MURATA, "Development of Electron-Ion Coincidence Spectroscopy for the Study of Surface Dynamics Combined with Synchrotron Radiation," *Rev. Sci. Inst.* **68**, 1703 (1997).
K. MASE, M. NAGASONO, S. TANAKA and T. URISU, "Study of Ion Desorption Induced by Core Level Excitations of Condensed $Si(CH_3)_4$ by Using Photoelectron-Photoion Coincidence Spectroscopy (PEPICO) Combined with Synchrotron Radiation," *Surf. Sci.* **377-379**, 376 (1997).
M. NAGASONO, K. MASE, S. TANAKA and T. URISU, "Auger-Final-State Selected Ion Desorption Study of Condensed NH_3 and ND_3 by Using Auger Electron-Photoion Coincidence Spectroscopy," *Surf. Sci.* **377-379**, 380 (1997).
Y. HIKOSAKA, H. HATTORI, T. HIKIDA and K. MITSUKE, "Formation of Autoionizing Atomic Nitrogen from Superexcited States of Nitric Oxide," *J. Chem. Phys.* **105**, 6367 (1996).
M. MIZUTANI, M. TOKESHI, A. HIRAYA and K. MITSUKE, "Development of a Tunable UV Laser System Synchronizing Precisely with Synchrotron Radiation Pulses from UVSOR," *J. Synchrotron Rad.* **4**, 6 (1997).

H. HATTORI, Y. HIKOSAKA, T. HIKIDA and K. MITSUKE, "Two-Dimensional Photoelectron Spectroscopy of Acetylene: Rydberg-Valence Interaction between the $(3\sigma_g)^{-1}(3p\sigma_u)^1$ and$(3\sigma_g)^{-1}(3\sigma_u)^1$ Status," *J. Chem. Phys.* **106**, 4902 (1997).

Y. HIKOSAKA, H. HATTORI, T. HIKIDA and K. MITSUKE, "Superexcited States of OCS Probed by Using Photoelectron Spectroscopy for Autoionizing Atomic Sulfur," *J. Chem. Phys.* **107**, 2950 (1997).

T. IBUKI, M. KONO, Y. ASARI, A. HIRAYA and K. SHOBATAKE, "Photoabsorption and Fluorescence Cross Sections of $SiCl_4$ in the Region of 6.2-31 eV," *J. Chem. Phys.* **106**, 4853 (1997).

N. UENO, "Angle-Resolved UPS of Ultrathin Films of Functional Organic Molecules with Synchrotron Radiation: Determination of Molecular Orientation by Quantitative Analysis of Photoelectron Angular Distribution," *J. Electron Spectr. Relat. Phenom.* **78**, 345 (1996).

N. UENO, A. KITAMURA, K. K. OKUDAIRA, T. MIYAMAE, Y. HARADA, S. HASEGAWA, H. ISHII, H. INOKUCHI, T. MIYAZAKI and K. SEKI, "Angle-resolved ultraviolet photoelectron spectroscopy of thin films of bis(1,2,5 thiadiazolo)-p-quinobis (1,3-dithiole) on the MoS_2 surface," *J. Chem. Phys.* **107**, 2079 (1997).

T. MIYAMAE, D. YOSHIMURA, H. ISHII, Y. OUCHI, T. MIYAZAKI, T. KOIKE, T. YAMAMOTO, Y. MURAMATSU, H. ETORI, T. MARUYAMA AND K. SEKI, "Ultraviolet Photoelectron Spectroscopy of N-Type Conducting Polymers," *Synth. Met.* **84**, 939 (1997).

N. UEDA, H. HOSONO and H. KAWAZOE, "Novel Transparent Semiconductor $MgIn_2O_4$," *Solid State Phenomena* **51/52**, 317 (1996).

H. HOSONO, Y. YAMASHITA, N. UEDA, H. KAWAZOE and K. SHIMIZU, "New Amorphous Semiconductor : $2CdO{\cdot}PbO_x$," *Appl. Phys. Lett.* **68**, [5] 661 (1996).

H. MIZOGUCHI, H. KAWAZOE, T. UEDA, S. HAYASHI, H. HOSONO and N. UEDA, "Formation and Optical Absorption Spectra of Mixed Valence State of Tl in $Tl_2Nb_2O_{6+x}$ with Pyrochlore Structure," *Bull. Chem. Soc. Jpn.* **69**, [1] 111 (1996).

H. HOSONO, N. KIKUCHI, N. UEDA and H. KAWAZOE, "Working Hypothesis to Explore Novel Wide Band Gap Electrically Conducting Amolphous Oxides and Examples," *J. Non-Cryst. Solids* **198/200**, 165 (1996).

H. MIZOGUCHI, T. OMATA, H. KAWAZOE, S. FUJITSU, H. HOSONO and N. UEDA, "Features of Valence Band Structure of $TlAlF_4$," *J. Phys. Condens. Matter* **8**, 303 (1996).

T. OMATA, H. IKAWA, S. FUJITSU, N. UEDA, H. HOSONO and H. KAWAZOE, "Optical Absorption Spectra and the Nature of Conduction Carriers of Helo-Doped $Sr_{1+x}La_{1-x}FeO_4$," *Solid State Commun.* **97**, [5] 411 (1996).

H. HOSONO, H. KAWAZOE and J. NISHII, "Defect Formation in SiO_2 : GeO_2 Glasses Studied by Irradiation with Excimer Laser Light," *Phys. Rev.* **B53**, [18] 11921 (1996).

H. HOSONO, K. KAWAMURA, H. KAWAZOE and J. NISHII, "Nanometer -Scale Geterogeneity in SiO_2-GeO_2 Glass Preforms and Fibers Prepared by Vapor Phase Axial Deposition Methods," *J. Appl. Phys.* **80**, [5] 3115 (1996).

K. KAWAMURA, H. HOSONO and H. KAWAZOE, "Proton-Implantation-Induced Nanosized Ge Crystal Formation in SiO_2: GeO_2 Glasses," *J. Appl. Phys.* **80**, [3] 1357 (1996).

K. KAWAMURA, H. HOSONO, H. KAWZOE, N. MATSUNAMI and Y. ABE, "Large Enhancement of Electical Conductivity in Magnesium Phosphate Glasses by Ion Implantation of Proton," *J. Ceram. Soc. Jpn.* **104**, [7] 688 (1996).

J. NISHII, H. YAMANAKA, H. HOSONO and H. KAWAZOE, "Preparation of Bragg Gratings in Sputter-Deposited GeO_2-SiO_2 Glasses by Excimer-Laser Irradiatin," *Opt. Lett.* **21**, [17] 1360 (1996).

J. NISHII, A. CHYAHARA, K. FUKUMI, K. FUJII, H. YAMANAKA, H. HOSONO and H. KAWAZOE, "Comparison of Formation Process of Ultraviolet Induced Color Centers in GeO_2-SiO_2 Glass Fiber Prefoorm and Ge-Implanted SiO_2," *Nucl. Instr. Meth. Phys. Res.* **B116**, 150 (1996).

H. HOSONO, M. YASUKAWA and H. KAWAZOE, "Novel Oxide Amorphous Semiconductors : Transparent conducting amorphous oxides," *J. Non-Cryst. Solids* **203**, 334 (1996).

H. HOSONO, M. MIZUGUCHI, H. KAWAZOE and J. NISHII, "Correlation between Ge E' Centers and Optical Absorption Bands in SiO_2: GeO_2 Glasses," *Jpn. J. Appl. Phy.* **35**, [2B] L234 (1996).

H. MIZOGUCHI, H. KAWAZOE and H. HOSONO, "Enhancement of Electrical Conductivity of Polycrystalline β-PbO by Exposure to Ozone Gas at Room Temperature," *Chem. Mater.* **8**, 2769 (1996).

H. HOSONO and H. KAWAZOE, "Approach to Novel Crystalline and Amorphous Oxide Materials for Optoelectronics by Ion Implantation," *Mater. Sci. & En.*, **B41**, 39 (1996).

R. F. HAGLAND, R. H. MAGRUDER, C. W. WHITE, R. A. ZUHR and H. HOSONO, "Probing Interface Properties of Nanocomposites by Third-Order Nonlinear Optics," *Appl. Phys.* **A62**, 403 (1996).

H. HOSONO, H. TANOUE, S. HISHITA and A. NAKAMURA, "Formation and Optical Properties of Nanometer-Sized Amorphous Arsenic Clusters Embedded in Amorphous SiO_2 by Ion Implantation," *Nucl. Instr. Meth.* **B116**, 178 (1996).

D. E. WEIBEL, T. NAGAI, T. HIRAYAMA, I.ARAKAWA and M.SAKURAI, "Electronic Energy Transfer in Rare-Gas Solid Alloys Studied by Photon Stimulated Desorption," *Langmuir* **12**, 193 (1996).

T. HIRAYAMA, T. NAGAI, M. ABO, I. ARAKAWA, K. MITSUKE and M. SAKURAI, "Excitonic Energy Transfer Process in Ne-Kr Alloy Studied by Photon Stimulated Desorption of Metastable Atoms," *J. Electron Spectrosc.* **80**, 101 (1996).

F. J. CURRELL, J. ASADA, K. ISHII, A. MINOH, K. MOTOHASHI, K. NISHIZAWA, S. OHTANI, K. OKAZAKI, M. SAKURAI, H. SHIRAISHI, S. TSURUBUCHI and H. WATANABE, "A New Versatile Electron-Beam Ion Trap," *J. Phys. Soc. Jpn.* **10**, 3186 (1996).

M. MATSUMOTO, T. KAWAUCHI, M. KIM and T.OKANO, "Renovation of Water Damaged Books with Vacuum Freeze-Drying," *J. Vac. Soc. Jpn.* **40**, 163 (1997).

H. ISHII, S. NARIOKA, K. EDAMATSU, K. KAMIYA, S. HASEGAWA, T. OHTA, N. UENO and K. SEKI, "Angle-Resolved Ultraviolet Photoelectron Spectroscopy of Oriented Film of a Model Compound of Poly(*p*-phenylene): Wave Number(k)-conservation and k-blurring in a System with Small Number of Repeating Units," *J. Electron Spectrosc. Relat. Phenom.* **78**, 395 (1996).

H. ISHII, A. YUYAMA, S. HASEGAWA, M. FUJINO, H. ISAKA, M. FUJIKI, K. FURUKAWA, N. MATSUMOTO and K. SEKI, "Electronic Structures of Silicon-Based Organic Compounds Studied by UV Photoemission," *Mol. Cryst. Liq. Cryst.* **285**, 205 (1996).

K. SEKI, T. TANI and H. ISHII, "Electronic Structures of Organic-Inorganic Interfaces Studied by UV Photoemission," *Thin Solid Films* **273**, 20 (1996).

D. YOSHIMURA, H. ISHII, S. NARIOKA, M. SEI, T. MIYAZAKI, Y. OUCHI, S.HASEGAWA, Y. HARIMA, K. YAMASHITA and K. SEKI, "The Electronic Structure of Porphyrin/metal Interfaces Studied by Ultraviolet Photoelectron Spectroscopy," *J. Electron Spectrosc. Relat. Phenom.* **78**, 359 (1996).

I. MORI, T. ARAKI, H. ISHII, Y. OUCHI, K. SEKI and K. KONDO, "NEXAFS Studies on the Rubbing Effec of the Surface Structure of Polyimide BPDA-C8," *J. Electron Spectrosc. Relat. Phenom.* **78**, 371 (1996).

K. NAGAYAMA, M. SEI, R. MITSUMOTO, E. ITO, T. ARAKI, H. ISHII, Y. OUCHI, K. SEKI and K. KONDO, "Polarized NEXAFS Studies on the Mechanical Rubbing Effec of Poly(tetrafluoroethylene) Oligomer and its Model Compound," *J. Electron Spectrosc. Relat. Phenom.* **78**, 375 (1996).

K. SEKI, H. ISHII, A. YUYAMA, M. WATANABE, K. FUKUI, E. ISHIGURO, J. YAMAZAKI, S. HASEGAWA, K. HORIUCHI, T. OHTA, H. ISAKA, M. FUJINO, M.FUJIKI, K. FURUKAWA and N. MATSUMOTO, "Electronic Structures of Polysilanes and Related Compounds," *J. Electron Spectrosc. Relat. Phenom.* **78**, 403 (1996).

K. NAGAYAMA, T. MIYAMAE, R. MITSUMOTO, H. ISHII, Y. OUCHI and K. SEKI, "Polarized VUV Absorption and Reflection Spectra of Oriented Films of Poly(tetrafluoroethylene)$(CF_2)_n$ and its Model Compound," *J. Electron Spectrosc. Relat. Phenom.* **78**, 407 (1996).

Y. OUCHI, Y. YOSHIOKA, H. ISHII, K. SEKI, M. KITAMURA, R. NOYORI, Y.TAKANISHI and I. NISHIYAMA, "Effect of Configuration of the Branching Terminal Group on the Stability of Antiferroelectric Liquid Crystals," *Ferroelectrics* **178**, 287 (1996).

T. OKAJIMA, S. NARIOKA, S. TANIMURA, K. HAMANO, T. KURATA, Y. UEHARA, T. ARAKI, H. ISHII, Y. OUCHI, K. SEKI, H. NAKAHARA, T. OGAWA and H. KOEZUKA, "Study of a-Sexithienyl Thin Film by Polarized Near Edge X-ray Absorption Fine Structure," *Jpn. J. Appl. Phys.* **35**, 2822 (1996).

K. SUGIYAMA, D. YOSHIMURA, E.ITO, T.MIYAZAKI, Y.HAMATANI, I. KAWAMOTO, Y. OUCHI, K. SEKI and H. ISHII, "UV photoemission Study of 8-Hydroxyquinoline Aluminum (Alq3) / metal Interfaces," *Mol. Cryst. Liq. Cryst.* **286**, 239 (1996).

D. YOSHIMURA, H. ISHII, S. NARIOKA, M. SEI, T. MIYAMAE, Y. OUCHI, S. HASEGAWA, Y. HARIMA, K. YAMASHITA and K. SEKI, "The Electronic Structure of Porphyriin/metal Interfaces Studied by UV Photoemission Spectroscopy," *Syn. Metals* **86**, 2399 (1997).

T. MIYAMAE, D. YOSHIMURA, H. ISHII, Y. OUCHI, T, MIYAZAKI, T. KOIKE, T. YAMAMOTO, Y. MURAMATSU, H. ETORI, T. MARUYAMA and K. SEKI, "Ultraviolet Photoelectron Spectroscopy of n-Type Conducting Polymer," *Syn. Metals* **84**, 939 (1997).

H. ISHII, S. HASEGAWA, D. YOSHIMURA, K. SUGIYAMA, S. NARIOKA, M. SEI, Y. OUCHI, K. SEKI, Y. HARIMA and K. YAMASHITA, "Electronic Structures of Porphyrins and Their Interfaces with Metals Studied by UV Photoemission," *Mol. Cryst. Liq. Cryst.* **296**, 427 (1997).

E. ITO, H. OJI, T. ARAKI, K. OICHI, H. ISHII, Y. OUCHI, T. OHTA, N. KOSUGI, Y. MARUYAMA, T. NAITO, T. INABE and K. SEKI, "Soft X-ray Absorption and X-ray Photoelectron Spectroscopic Study of Tautomerism in Intramolecular Hydrogen Bonds of N-Salicylideneaniline Derivatives," *J. Am. Chem. Soc.* **119**, 6336 (1997).

Y. NONOGAKI, T. IGUCHI, Y. FUJIWARA and Y. TAKEDA, "Formation of InAs Islands on InP (001) by Droplet Hetero-epitaxy," *Appl. Surf. Sci.* **117/118**, 665 (1997).

K. TANAKA, A. ICHIMURA, I. KINOSHITA, M. HAGA, W. MORI, M. KATO and S. YANO, "Comparison with Several Oxidation States of Ruthenium Binuclear Complexes; Ruthenium Analogue for Iron-Protein Active Site Model," *Mol. Cryst. Liq. Cryst.* **286**, 127 (1996).

T. TANASE, Y. YAMADA, K. TANAKA, T. MIYAZU, M. KATO, K. LEE, Y. SUGIHARA, W. MORI, A. ICHIMURA, I. KINOSHITA, Y. YAMAMOTO, M. HAGA, Y. SASAKI and S. YANO, "Synthesis, Structures, and Spectroscopic, Magnetic, and Electrochemical Properties of (μ-Alkoxo)bis(μ-carboxylato)-diruthenium Complexes, $M[Ru_2(dhpta)(\mu\text{-}O_2CR)_2]$(M = Na and K, $dhptaH_2$ = 1,3-Diamino-2-hydroxypropane-tetracetic Acid)," *Inorg. Chem.* **35**, 6230 (1996).

A. HIRAI, H. MONJUSHIRO and H. WATARAI, "Laser-Photophoresis of a Single Droplet in o/w Emulsions," *Langmuir* **12**, 5570 (1996).

K. MASHIMA, N. KOMURA, T. YAMAGATA, K. TANI and M HAGA, "Synthesis and Crystal Structure of A Cationic Trinuclear Ruthenium(II) Complex $[Ru_3(\mu^2\text{-}Cl)_3(\mu^3\text{-}Cl)_2\{1,2\text{-bis(diphenylphosphino)benzene}\}_3]PF_6$," *Inorg. Chem.* **36**, 2908 (1997).

K MIZUSIMA, M. NAKAURA, S-B. PARK, H. NISHIYAMA, H. MONJUSHIRO, K. HARADA and M. HAGA, "Ruthenium(II) Complexes with Tetradentate 6,6'-Bis(oxazolinyl or benzimidazolyl)-2,2'-bipyridine Ligand: Synthesis, Electrochemical Properties, and Catalytic Reactivities," *Inorg. Chim. Acta* **261**, 175 (1997).

H. MONJUSHIRO, K. HARADA, M. NAKAURA, N. KATO, M. HAGA, M. RYAN and A. B. P. LEVER, "Preparation of Surfactant Ruthenium Complexes Containing (Benzimidazolyl)pyridine Derivatives with Long Alkyl Chains," *Mol. Crys. Liq. Crys.* **294**, 15 (1997).

A. INAGAKI, Y. TAKAYA, T. TAKAMORI, H. SUZUKI, M. TANAKA and M. HAGA, "Trinuclear Ruthenium Complex with a Face-Capping Benzene Ligand. Hapticity Change Induced by Two-Electron Redox Reaction," *J. Am. Chem. Soc.* **119**, 625 (1997).

M. D. HOSSAIN, M. HAGA, H. MONJUSHIRO, B. GHOLAMKHASS, K. NOZAKI and T. OHNO, "Synthesis and Photoinduced Electron Transfer Processes in $Ru(II)(bpy)_2/Os(III)_2$-Based Triad Complexes Containing Functionalized Diimide Ligands," *Chem. Lett.* 573 (1997).

M. HIRATA, H. MONJUSHIRO, R. SAEKI, J. ONOE, H. NAKAMATSU, T. MUKOYAMA, H. ADACHI and K. TAKEUCHI, "Valence Electronic Structure of Uranyl Nitrate $UO_2(NO_3)_2 \cdot 2H_2O$," *J. Electron Spectrosc.* **83**, 59 (1997).

T. SAKURAI, F. NOSE, T. FUJIKI and S. SUZUKI, "Reduction and Oxidation Processes of Blue Copper Proteins, Azurin, Pseudoazurin, Umecyanin, Stellacyanin, Plantacyanin and Plastocyanin Approached by Cyclic and Potential Step Voltammetries," *Bull. Chem. Soc. Jpn.* **69**, 2855 (1996).

K. TSUKAHARA, C. KIMURA and T. SAKURAI, "Intracomplex Quenching by Copper(II) Ion of Excited Singlet and Triplet States of Zinc Myoglobin Modified with Diethylenetriaminepentaacetic Acid," *Chem. Lett.* 601 (1996).

A. SHIMIZU, T. SAKURAI, S. YAMAGUCHI and T. SAMAJIMA, "Mutation of Bilirubin Oxidase by Protein Engineering for Elucidating Electron Pathway," *J. Inorg. Biochem.* **67**, 56 (1997).

T. SAKURAI, H. HUANG, H. MONJUSHIRO and S. TAKEDA, "SQUID and EPR of the Trinuclear Center in Laccase and Ascorbate Oxidase," *J. Inorg. Biochem.* **67**, 57 (1997).

N. SAKURAI and T. SAKURAI, "Isolation and Characterization of Nitric Oxide (NO) Reductase from a Denitrifying Bacterium, *Paracoccus halodenitrificans*," *J. Inorg. Biochem.* **67**, 105 (1997).

K. TSUKAHARA, M. MATSUI and T. SAKURAI, "Preparation and Characterization of Myoglobin Modified with Diethylenetriaminepentaacetato-Cobaltate(III)," *J. Inorg. Biochem.* **67**, 409 (1997).

M. NAKANO, Y. MATSUZAKI, H. NAGAO, S. YAMADA, I. SHIGEMOTO and K. YAMAGUCHI, "Damping wave packet approach: a calculation method of nonpertubative nonlinear optical susceptibilities including effects of nuclear motion at finite temperatures," *Chem. Phys. Lett.* **258**, 307 (1996).

H. NAGAO, H. KAWABE, T. KAWAKAMI, M. OKUMURA, W. MORI, K. NISHIKAWA and K. YAMAGUCHI, "Calculation of Magnetization by Path Integral Method I," *Mol. Cry. Liq. Cry.* **286**, 171 1996).

T. KAWAKAMI, H. NAGAO, K. UEDA, W. MORI and K. YAMAGUCHI, "Calculation of Magnetization by Path Integral Method II," *Mol. Cry. Liq. Cry.* **286**, 177 (1996).

H. KAWABE, H. NAGAO and K. NISHIKAWA, "Path integral formulation for many-electron system," *Intern. J. Quantum. Chem.* **59**, 457 (1996).

H. NAGAO, M. NAKANO, S. YAMANAKA, Y. SHIGETA, S. YAMADA, D. YAMAKI, I. SHIGEMOTO, S. KIRIBAYASHI and K. YAMAGUCHI, " Many-electron-wavepackets method," *Int. J. Quantum Chem.* **60**, 1291 (1997).

H. NAGAO, H. KAWABE, K. KODAMA, Y. SHIGETA, K. NISHIKAWA, M. NAKANO and K. YAMAGUCHI, "Nonadiabatic treatment of molecular system by the wavepackets method," *Int. J. Quantum Chemistry* **60**, 1261 (1997).

H. KAWABE, H. NAGAO and K. NISHIKAWA, "Path integral monte carlo method for ab initio calculation," *Int. J. Quantum Chem.* **60**, 1223 (1997).

M. NAKANO, H. NAGAO and K. YAMAGUCHI, "Many-electron hyperpolarizability density analysis: application to dissociation process of one-dimensional H_2," *Phys. Rev. A* **55**, 1503 (1997).

H. NAGAO, M. NAKANO, S. YAMADA, K. OHTA and K. YAMAGUCHI, "Theoretical study on the second hyperpolarizability of H_3^+ system by path integral method," *Synthetic Metals*, **85**,1159(1997)

S. KIRIBAYASHI, M. NAKANO, S. YAMADA, I. SHIGEMOTO, H. NAGAO and K. YAMAGUCHI, "Theoretical studies for second hyperpolarizabilities of alternant and condensed-ring conjugated systems II," *Synthetic Metals* **85**, 1163 (1997).

T. KAWAKAMI, H. NAGAO, W. MORI and K. YAMAGUCHI, "Calculation of magnetization by path integral method," *Synthetic Metals* **85**, 1753 (1997).

X. H. BU, D. L. AN, Y. T. CHEN, M. SHIONOYA and E. KIMURA, "Synthesis, Crystal Structure and Properties of the Copper(II) Complex of New Dioxocyclam Appended with Two 8-Methylquinoline as Additional Donor Pendants," *Inorg. Chim. Acta* **249**, 125 (1996).

X. H. BU, D. L. AN, Z. A. ZHU, Y. T. CHEN, M. SHIONOYA and E. KIMURA, "Crystal Structure and Properties of the Nickel(II) Complex of a New Dioxo[13]aneN4 bearing Quinoline Pendants. Striking Differences with Its Copper Analogue," *Polyhedron* **16**, 179 (1997).

X. H. BU, D. L. AN, Y. T. CHEN, M. SHIONOYA and E. KIMURA, "Crystal Structure and Properties of the Copper(II) Complex of a New Dioxocyclam Appended with 8-Methylquinoline as Donor Pendant (Dioxocyclam = 1,4,8,11-tetraazacyclotetradecane-2,4-dione)," *J. Inclusion Phenom.* **27**, 245 (1997).
E. KIMURA, M. SASADA, M. SHIONOYA, T. KOIKE, H. KUROSAKI and M. SHIRO, "Structure and O_2–Uptake Properties of a Novel Nickel(II) Complex of Pyridyl–Pendant Dioxocyclam (1-(2-Pyridyl)methyl-5,7-dioxo-1,4,8,11-tetraazacyclotetradecane)," *J. Bioinorg. Chem.* **2**, 74 (1997).
M. HIROTSU, M. KOJIMA, K. NAKAJIMA, S. KASHINO and Y. YOSHIKAWA, "Stereochemistry and Electrochemistry of Cobalt(II) and Cobalt(III) Complexes Containing Optically Active Tetradentate Schiff Base Ligands," *Bull. Chem. Soc. Jpn.* **69**, 4925 (1996).
M. MURATA, M. KOJIMA, M. KITA, S. KASHINO and Y. YOSHIKAWA, "Preparation of a Stable Sulfonato-Cobalt(III) Complex by Oxidation of a Sulfinato-*O* Complex," *Chem. Lett.* 675 (1996).
M. KOJIMA, F. MD. AKHTER, K. NAKAJIMA, and Y. YOSHIKAWA, "Photolysis of Cobalt(III) Complexes Containing Sulfinate-*S* Ligands. Formation of Organic Peroxide Complexes through Desulfurization," *Bull. Chem. Soc. Jpn.* **69**, 2889 (1996).
K. NAKAJIMA, M. KOJIMA, S. AZUMA, R. KASAHARA, M. TSUCHIMOTO, Y. KUBOZONO, H. MAEDA, S. KASHINO, S. OHBA, Y. YOSHIKAWA and J. FUJITA, "Interconversion between Polymeric Orange and Monomeric Green Forms of a Schiff Base-Oxovanadium(IV) Complex," *Bull. Chem. Soc. Jpn.* **69**, 3207 (1996).
M. TASAKA, M. HIROTSU, M. KOJIMA, S. UTSUNO and Y. YOSHIKAWA, "Syntheses, Characterization, and Molecular Mechanics Calculations of Optically Active Silatrane Derivatives," *Inorg. Chem.* **35**, 69816 (1996).
Y. OHMORI, M. KOJIMA, S. KASHINO and Y. YOSHIKAWA, "Chromatographic Resolution Mechanism of a Tris(1,10-phenanthroline)silicon(IV) Complex," *J. Coord. Chem.* **39**, 219 (1996).
K. YUTOH, M. KOJIMA and Y. YOSHIKAWA, "New Triamine-type Platinum(II) Complexes of Phenyl-substituted Ethylenediamine: Reactivity with 5'-GMP," *J. Coord. Chem.* **40**, 265 (1996).
M. HIROTSU, M. KOJIMA and Y. YOSHIKAWA, "Mononuclear and Mixed-Valence Trinuclear Manganese Complexes Containing Tripodal Tetradentate Ligands. Phenolato, Carboxylato, and Alkoxo Bridges," *Bull. Chem. Soc. Jpn.* **70**, 649 (1997).
Y. KURODA, S. KONNO, Y. YOSHIKAWA, H. MAEDA, Y. KUBOZONO, H. HAMANO, R. KUMASHIRO and M. NAGAO, "Stabilization of Copper Metal Cluster in Mordenite Nanopores: Water Treatment of Evacuated Copper Ion-Exchanged Mordenite at 300 K," *J. Chem. Soc. Faraday Trans.* **93**, 2125 (1997).
Y. KURODA, H. MAEDA, Y. YOSHIKAWA, R. KUMASHIRO and M. NAGAO, "Characterization of Active Sites on Copper Ion-Exchanged Mordenite for Dinitrogen Adsorption by Using CO as a Probe Molecule," *J. Phys.Chem.* **B101**, 1312 (1997).
Y. KURODA, T. WATANABE, Y. YOSHIKAWA, R. KUMASHIRO, H. HAMANO and M. NAGAO, "Specific Feature of Dielectric Behavior of Water Adsorbed on Ag_2O Surface," *Langmuir* **13**, 3823 (1997).
Y. YAMAGUCHI, H. NAKAZAWA, M. KISHISHITA and K. MIYOSHI, "Reactivity of Cationic Phosphenium Complexes of Molybdenum: Migration of OR, SR, and NR_2 on a Tertiary Phosphorus Compound to a Phosphenium Ligand," *Organometallics* **15**, 4383 (1996).
H. NAKAZAWA, Y. YAMAGUCHI and K. MIYOSHI, "Formation of a Six Membered Metallacycle Consisting of Iron, Carbon, Phosphorus, Boron, and Two Oxygens: The First Example of Precedence of Migratory Insertion of CO into an M-C Bond over OR Abstraction from Coordinating Phosphite by BF_3," *Organometallics* **15**, 4661 (1996).
T. MIZUTA, A. OKANO, T. SASAKI, H. NAKAZAWA and K. MIYOSHI, "Palladium(II) and Platinum(II) Complexes of a Tetraphosphamacrocycle. X-ray Crystal Structures of Phosphorus Analogs of a (Tetramethylcyclam)metal Complex," *Inorg. Chem.* **36**, 200 (1997).
H. NAKAZAWA, M. KISHISHITA, S. YOSHINAGA, Y. YAMAGUCHI, T. MIZUTA and K. MIYOSHI, "Migratory Insertion Reaction of a Phosphenium Ligand into Mo- and W-alkyl Bonds," *J. Organomet. Chem.* **529**, 423 (1997).
H. NAKAZAWA, Y. UEDA, K. NAKAMURA and K. MIYOSHI, "Reaction of Cationic Piano Stool Iron Complexes Containing Phosphorus Ligands with Phosphorus Ylide," *Organometallics* **16**, 1562 (1997).
T. DANIEL, H. NAGAO, H. NAKAJIMA, K. TANAKA and A. NAKAMURA, "Seven-coordinated 2,2':6'2"-terpyridinemolybdenum(II) complexes: synthesis, Structure and reactivity of [Mo(CO)(C7H8)(4.,4',4"-R3terpy)X]X' (R= H or tBu)," *J. Organometallic Chem.* **509**, 225 (1996).
K. TOYOHARA, H. NAGAO, T. ADACHI, T. YOSHIDA and K. TANAKA, "Crystal Structure of [Ru(bpy)2(CO)(h1-C(O)OH)]+ (bpy =2,2'-bipyridine) as a Key Intermediate in CO2/CO Conversion," *Chem. Lett.* 27 (1996).
H. NAKAJIMA, H. NAGAO and K. TANAKA, "Control of the Co-ordination Mode of 1,5-Naphthylidine Ligated to Ruthenium(II) Bipyridine Complexes," *J. Chem. Soc. Dalton Trans.* 1405 (1996).
T. OOKUBO, H. SUGIMOTO, T. NAGAYAMA, H. MASUDA, T. SATO, K. TANAKA, Y. MAEDA, H. OKAWA, Y. HAYASHI, A. UEHARA and M. SUZUKI, "*cis-m*-1,2-Peroxo Diiron Complex: Structure and Reversible Oxygenation," *J. Am. Chem. Soc.* **118**, 701 (1996).
H. NAKAJIMA, T. TSUGE and K. TANAKA, "Oxide Transfer Reaction from Carbonate to Metal-CO Complex, Affording Metal-h1-CO2 Complex and Carbon Dioxide," *Chem. Lett.* 485 (1997).

K. TANAKA and K. Tsuge, "Activation of CO2 on metal complexes directed toward multi-electron reduction and carbon-carbon bond formation," *Trends in Chem* **4**, 145 (1996).
K. TANAKA and K. Tsuge, "Model of Reductive Catalysts", in "Photchemical Energy Conversion," M. KANEKO Ed., IPC, 225 (1997).
M. FUJITA, F. IBUKURO, H. SEKI, O. KAMO, M. IMANARI and K. OGURA, "Catenane Formation from Two Molecular Rings through Very Rapid Slippage. A Mobius Strip Mechanism," *J. Am. Chem. Soc.* **118**, 899 (1996).
M. FUJITA and K. OGURA, "Supramolecular Self-Assembly of Macrocycles, Catenanes, and Cages through Coordination of Pyridine-Based Ligands to Transition Metals," *Bull. Chem. Soc. Jpn.* **69**, 1471 (1996).
M. FUJITA, O. SASAKI, T. MITSUHASHI, T. FUJITA, J. YAZAKI, K. YAMAGUCHI and K. OGURA, "On the Structure of Transition Metal-Linked Molecular Squares," *J. Chem. Soc. Chem. Commun.* 1535 (1996).
M. FUJITA and K. OGURA, "Transition-Metal-Directed Assembly of Well-Defined Organic Architectures Possessing Large Voids: From Macrocycles to [2]Catenanes," *Coord. Chem. Rev.* **148**, 249 (1996).
M. FUJITA, M. AOYAGI and K. OGURA, "Self-Assembly of Macrocyclic Dinuclear Complexes from (en)Pd(NO3)2 and Pyridine-based Bidentate Ligands," *Inorg. Chim. Acta* **246**, 53 (1996).
M. FUJITA and K. OGURA, "Self-assembling [2]catenanes: molecular magic rings," *Supramolecular Sci.* **3**, 37 (1996).
M. FUJITA, "Supramolecular Self-assembly of Finite and Infinite Frameworks through Coordination," *J. Synth. Org. Chem. Jpn.* **54**, 953 (1996).
N. RE, E. GALLO, C. FLORIANI, H. MIYASAKA and N. MATSUMOTO, "Anomalous Magnetic Properties of K[Mn(3-MeOsalen)]$_2$[Mn(CN)$_6$]. A Metamagnet Exhibiting a Strong Negative Magnetization (3-MeOsalen= N,N'-Ethylenebis(3-methoxysalicylideneaminato)," *Inorg. Chem.* **35**, 5964 (1996).
N. RE, E. GALLO, C. FLORIANI, H. MIYASAKA and N. MATSUMOTO, "Magnetic Properties of a One-Dimensional Ferromagnet Containing a Mn(III)-NC- Fe(III) Linkage: Synthesis and Crystal Structure of a Chain-like [Mn(acacen)Fe(CN)$_6$]$_n^{2-}$ Polyanion," *Inorg. Chem.* **35**, 6004 (1996).
G. MAGO, M. HINAGO, H. MIYASAKA, N. MATSUMOTO and H. OKAWA, "One-dimensional structures of manganese(II) complexes [Mn(hfac)2L] (hfac=hexafuloroacetylacetonato anion and L=N-(4-pyridylmethyl)-imidazole, trans-1,2-bis(4-pyridyl)ethylene, and imidazole)," *Inorg. Chim. Acta* **254**, 145 (1997).
H. MIYASAKA, N. MATSUMOTO, N. RE, E. GALLO and C. FLORIANI, "Synthesis, Crystal Structure, and Magnetic Property of a Ferrimagnetic Layer Compound, [NEt4][Mn(5-Clsalen)]2[Fe(CN)6] (NEt$_4$=Tetraethyl-ammonium, 5- Clsalen=N,N'-Ethylenebis(5-chlorosalicylideneiminato))," *Inorg. Chem.* **36**, 670 (1997).
S. NANBU, S. MINAMINO and M. AOYAGI, "Theoretical study of the potential energy surfaces and dynamics of CaNC/CaCN," *J. Chem. Phys.* **106**, 8073 (1997).
S. KONDO, K. TOKUHASHI, M. AOYAGI, K. MOGI and S. MINAMINO, "Ab initio energetic calculations of elementary reactions relevant to low-temperature Silane oxidation by Gaussian-2 theory," *J. Phys. Chem. A* **101**, 6015 (1997).
N. SARUKURA, Z. LIU, H. OHTAKE, Y. SEGAWA, M. DUBINSKII, V. V. SEMASHKO, A. K. NAUMOV, S. L. KORABLEVA and R. Y. ABDULSABIROV, "Ultraviolet short pulses from an all-solid-state Ce:LiCAF master-oscillator-power-amplifier system," *Opt. Lett.* **22**, 994 (1997).
N. SARUKURA, Z. LIU, H. OHTAKE, S. IZUMIDA, T. YAMANAKA, Y. SEGAWA, T. ITATANI, T. SUGAYA and T. NAKAGAWA, "All-solid-state, THz radiation source using a saturable Bragg reflector in a femtosecond mode-locked laser," *Jpn. J. Appl. Phys.* **36**, 560 (1997).
R. KOMATSU, T. SUGAWARA, K. SASSA, N. SARUKURA, Z. LIU, S. IZUMIDA, Y. SEGAWA, S. UEDA, T. FUKUDA and K. YAMANOUCHI, "Growth and ultraviolet application of $Li_2B_4O_7$ crystals: Generation of the fourth and fifth harmonics of Nd:$Y_3Al_5O_{12}$ lasers," *Appl. Phys. Lett.* **70**, 3492 (1997).
N. SARUKURA, Z. LIU, H. OHTAKE, S. IZUMIDA, T. YAMANAKA, Y. SEGAWA, T. ITATANI, T. SUGAYA and T. NAKAGAWA, "All-solid-state, THz radiation source using a saturable Bragg reflector in a femtosecond mode-locked laser," *OSA Trends in optics and photonics* **10**, 347 (1997).
N. SARUKURA, Z. LIU, H. OHTAKE, Y. SEGAWA, M. DUBINSKII, V. V. SEMASHKO, A. K. NAUMOV, S. L. KORABLEVA and R. Y. ABDULSABIROV, "14-mJ, 1-nsec, 289-nm pulses from an all-solid-state Ce:LiCAF master oscillator and power amplifier system," *OSA Trends in optics and photonics* **10**, 25 (1997).
Y. YAMASHITA, M. TOMURA and K. IMAEDA, "Unusual Cation Radical Salts of Non-planar Bis(1,3-dithiole) Donors Incorporating Solvent Molecules," *Chem. Commun.* 2021 (1996).
A. OHTA and Y. YAMASHITA, "Preparation, Properties, and Oxidation of Novel Bis(1,3-dithiole) Compounds Containing a Di(2-thienyl)methane Unit,"*Heterocycles* **44**, 263 (1997).
C. KITAMURA and Y. YAMASHITA, "Synthesis and Reactions of 3,3'-Dibromodihydrodipyrrins," *J. Chem. Soc., Perkin Trans. 1* 1443 (1997).
S. TANAKA and Y. YAMASHITA, "A Novel Monomer Candidate for Intrinsically Conductive Organic Polymers Based on Nonclassical Thiophene," *Synth. Met.* **84**, 229 (1997).
Y. YAMASHITA, M, TOMURA, S. TANAKA and K. IMAEDA, "Novel Organic Metals Based on Nonplanar Bis(1,3-Dithiole) Donors," *Synth. Met.* **84**, 1795 (1997).
M. TOMURA and Y. YAMASHITA, "Synthesis, Structure, and Physical Properties of Novel Component Molecules with Fused Heterocycles for Organic Conductor," *Synth. Met.* **84**, 1871 (1997).

Y. YAMASHITA, K. ONO, M. TOMURA and S. TANAKA, "Synthesis and Properties of Benzobis-(thiadiazole)s with Nonclassical π-Electron Ring Systems," *Tetrahedron* **53**, 10169 (1997).
A. OHTA and Y. YAMASHITA, "Novel Bis(1,3-dithiole) Electron Donors by Oxidative Intramolecular Cyclization of 2,2'-Bis(1,4-dithiafulven-6-yl)-3,3'-bithienyls," *Mol. Cryst. Liq. Cryst.* **296**, 1 (1997).
T. SUZUKI, Y. YAMASHITA, T. FUKUSHIMA and T. MIYASHI, "Tetracyanoquinodimethanes Fused with a 1,2,5-Chalcogenadiazole Ring," *Mol. Cryst. Liq. Cryst.* **296**, 165 (1997).
A. M. RAO, E. RICHTER, S. BANDOW, B. CHASE, P. C. EKLUND, K. A. WILLIAMS, S. FANG, K. R. SUBBASWAMY, M. MENON, A. THESS, R. E. SMALLEY, G. DRESSELHAUS and M. S. DRESSELHAUS, "Diameter-Selective Raman Scattering from Vibrational Modes in Carbon Nanotubes," *Science* **275**, 187 (1997).
A. M. RAO, P. C. EKLUND, S. BANDOW, A. THESS and R. E. SMALLEY, "Evidence for charge transfer in doped carbon nanotube bundles from Raman scattering," *Nature* **388**, 257 (1997).
D. KUWAHARA and T. Nakai, "Spinning-sideband suppression in DOR NMR spectra using a magic-angle-turning technique," *Chem.Phys.Lett.* **260**, 249 (1996).
T. TOYODA, H. YOSHIDA, O. OISHI and S. MIYAJIMA, "Personal computer-controlled 16 channel versatile pulse generator for nuclear magnetic resonance," *Rev. Sci. Instrum.* **68**, 3140 (1997).
M. ITOH, K. SAWADA, H. HARA, N. OHNO and M. KAMADA, "Phonon broadening of line widths of Auger-free luminescence in wide-gap ionic crystals," *J. Luminescence* **72**, 762 (1997).
N. TAKAHASHI, S. TANAKA, M. ICHIKAWA, Y. Q. CAI and M. KAMADA, "Photoelectron spectroscopic study of coadsorbed states of Cs and O on GaAs(100)," *J. Phys. Soc. Jpn.* **66**, 2798 (1997).
J. W. KIM, S. KIM, J. M. SEO, S. TANAKA and M. KAMADA, "Surface core-level shift of InSb(111)-2x2," *Phys. Rev. B* **54**, 4476 (1996).
J. W. KIM, S. KIM, J. M. SEO, S. TANAKA and M. KAMADA, "Angle-resolved photoemission of InSb(111)-2x2," *J. Phys. Condensed Matter* **8**, 4189 (1996).
N. TAKAHASHI, S. TANAKA, M. ICHIKAWA, S. OHARA, Y. FUJII, K. NAKANISHI and M. KAMADA, "Construction of a Compact Spin- and Angle-Resolved Photoelectron Spectrometer," *Jpn. J. Appl. Phys.* **35**, 6314 (1996).
M. ASHIDA, O. OHTA, M.KAMADA, M. WATANABE and R. KATO, "VUV reflection spectra of ferroelectric NaNO2," *J. Electron Spectroscopy and Related Phenomena* **79**, 55 (1996).
M. A. TEREKHIN, N. YU. SVECHNIKV, V. G. STANKEVITCH, A. A. KOLMAKOV, V. A. STEPANOV, N. BEZMELNITSIN, M. KAMADA, K. KAN'NO and I. AKIMOTO, "Radiative transitions in C60 thin films under SR excitation," *J. Electron Spectroscopy and Related Phenomena* **78**, 445 (1996).
K. MASE, M. NAGASONO, S. TANAKA, M. KAMADA, T. URISU and Y. MURATA, "Development of electron-ion coincidence spectroscopy for the study of surface dynamics combined with synchrotron radiation," *Rev. Sci. Instrum.* **68**, 1703 (1997).
K. MASE, M. NAGASONO, S. TANAKA, T. URISU and S. NAGAOKA, "Study of ion desorption induced by core-level excitations of condensed $Si(CH_3)_4$ by using photoelectron-photoion coincidence spectroscopy (PEPICO) combined with synchrotron radiation," *Surf. Sci.* **377**, 376 (1997).
M. NAGASONO, K. MASE, S. TANAKA and T. URISU, "Auger-final-state selected ion desorption study of condensed NH_3 and ND_3 by using Auger electron-photoion coincidence spectroscopy," *Surf. Sci.* **377**, 380 (1997).
Jr. J. COLE, S. TANAKA, P. GERBER, J. R. POWER and T. FARRELL, "Temperature-dependent optical anisotropy of the vicinal Si(100)(2x1) surface," *Phys. Rev. B* **54**, 13444 (1997).
T. OUCHI, I. NAKAI, M. KAMADA, S. TANAKA and T. HAGIWARA, "On the Assignment of Core Electron Absorption Spectra of the Films of Polyethylene Terephthalate and Polyethylene Naphthalate by Means of Total Electron Yield Method," *Progress in Polymer Physics in Japan* **39**, 505 (1997).
T. ABE, Y. MIZUTANI, M. ASANO, T. HARADA, M. KAWASE, S. TANAKA and M. KAMADA, "Carbon K edge XANES spectra of stage 2 $FeCl_3$-graphite intercalation compound,"*Carbon* **34**, 1160 (1996).
S. KIMURA, "Optical Study of Low Carrier Concentration Systems, "*J. Phys. Soc. Jpn.* **65** Suppl. B, 109 (1996).
S. KIMURA, A. OCHIAI, T. SUZUKI and M. IKEZAWA, "Optical Study on Heavy Fermion and Mixed Valence State of Yb_4As_3," *J. Phys. Soc. Jpn.* **65**, 3591 (1996).
S. KIMURA, A. OCHIAI and T. SUZUKI, "Low Energy Excitation of Yb_4As_3"*Physica B* **230-232**, 705 (1997).
S. KIMURA, Y. S. KWON and T. SUZUKI, "Mixed Valence of Yb_3S_4, "*Physica B* **230-232**, 301 (1997).
M. H. JUNG, Y. S. KWON, T. KINOSHITA and S. KIMURA, "Optical Properties of $CeTe_2$ and $LaTe_2$,"*Physica B* **230-232**, 151 (1997).

REVIEW ARTICLES AND TEXTBOOKS

Y. OKAMOTO, "Optimization and Protein Tertiary Structure Predictions," *Suri Kagaku* (in Japanese) **401**, November, 66 (1996).
M. MASUYA, "ABC Graphics Suite Guide," (in Japanese) Softbank Books (1997).
M. MASUYA, "Windows Draw Official Guide," (in Japanese) Computer Age (1997).
M. HIYAMA and H. NAKAMURA, "Characteristic and Dynamics of Superexcited States of CO," in "Dissociative Recombination: Theory, Experiment and Application," edited by D. Zaifman, B. Mitchell, B. Rowe and D.Schwalm, World Scientific, pp.212-215 (1996).
H. NAKAMURA, "New Developments of the Theory of Nonadiabatic Transitions," *Butsuri* (in Japanese), **51**, 829-834 (1996).
H. NAKAMURA, "Theoretical Studies of Chemical Dynamics --Overview of Some Fundamental Mechanisms," *Ann. Rev. of Phys. Chem.* **48**, 293 (1997).
F. HIRATA, "Recent Progress in Liquid State Theory in Chemistry", (in japanese) *Bussei Kenkyu* (Kyoto), **68**, 367 (1997).
H. SATO, "Electronic Structure Theory of Chemical Process in Solution",(in japanese) *Bussei Kenkyu* (Kyoto), **68**, 434 (1997).
T. KITAGAWA and T. OGURA, "Oxygen activation mechanism at binuclear site of heme-copper oxidase superfamily as revealed by time-resolved resonance Raman spectroscopy," *Prog. Inorg. Chem.* **45**, pp.431-479 (1997).
T. KITAGAWA, T. OGURA, S. HIROTA, D. A. PROSHLYAKOV, J. MATYSIK, E. H. APPELMAN, K. SHINZAWA-ITOH and S. YOSHIKAWA, "Time-resolved resonance Raman study of dioxygen reduction by cytochrome c oxidase," in "Oxygen Homeostasis and Its Dynamics," Y. Ishimura, ed., Springer-Verlag, Tokyo (1997).
T. KITAGAWA, "Vibrational Spectroscopy–Principles for Measurements and Examples of Their Applications. (in Japanese)," in *"Structural Biology and Its Analysis,"* (Y. Kyogoku & T. Tsukihara, Eds.) pp. 156-174, Kyoritsu Shuppan (1997).
T. OGURA, D. A. PROSHLYAKOV, J. MATYSIK, E. H. APPELMAN, K. SHINZAWA-ITOH, S. YOSHIKAWA and T. KITAGAWA, "Mechanism of Dioxygen Reduction Catalyzed by Cytochrome *c* Oxidase as Studied by Time-Resolved Resonance Raman Spectroscopy," in "Oxygen Homeostasis and Its Dynamics," Y. Ishimura, ed., Springer-Verlag, Tokyo (1997).
T. OGURA, "Time-Resolved Resonance Raman Study on Reaction Intermediates of Heme Enzymes with Oxygen," Shokubai ("Catalyst" in Japanese) **38**, pp.542-549 (1996).
S. KUMAZAKI and K. YOSHIHARA, "Primary Processes in Photosynthesis: Recent Progress Made by Femto- and Picosecond Spectroscopies," *J. Spectrosc. Soc. Jpn* (in Japanese) **46**, 3 (1997).
K. TOMINAGA, "Recent Developments of Off-Resonant Nonlinear Spectroscopy in Liquids," *Surface* (in Japanese) **35**, 425 (1997).
K. TOMINAGA, G.P. KEOGH, J. MA and K. YOSHIHARA, "Time-Resolved Higher Order Nonlinear Spectroscopy in Liquids, Overtone Vibrational Dephasing," in "Proceedings of the 7th International Conference on Time-Resolved Vibrational Spectroscopy," W. Woodruff Ed. 305 (1996).
K. YOSHIHARA, H. PAL, H. SHIROTA, Y. NAGASAWA and K. TOMINAGA, "Effects of Vibrations in Chemical Dynamics: High-Frequency Vibrational and Low-Frequency Solvent Dynamical Effects on Intermolecular Electron Transfer," in "Proceedings of the 7th International Conference on Time-Resolved Vibrational Spectroscopy," W. Woodruff Ed. 69 (1996).
K. TOMINAGA and K. YOSHIHARA, "Fifth and Seventh Order Nonlinear Spectroscopy with Femtosecond Pulses," in "Proceedings of Frontiers in Laser Physics and Spectroscopy", S. Watanaba Ed., Pergamon 371 (1996).
K. YOSHIHARA, K.A. McLAUCHLAN and M.A. EL-SAYED, "Biography of Prof. Saburo Nagakura," *J. Phys. Chem. A* **101**, 325 (1997).
K. SAWABE, and Y. MATSUMOTO, "Photoinduced Reaction of Surface Adsorbates," Review and Topics on Surface Science & Technology Avant-garde (Hyomen) (in Japanese), **34**, 273 (1996).
A. KOBAYASHI and H. KOBAYASHI, "Molecular Metals and Superconductors Based on Transition Metal Complexes" Handbook of Organic Conductive Molecules and Polymers," Vol. *1* , H. S. Nalwa Ed., Wiley (Chichester, New York), p249-292 1997
H. KOBAYASHI, "Organic Superconductors/semiconductors /CT salt," *Current Opinion in Solid State & Matrials Science*, 2,440 (1997)
S. MIYAJIMA and O. OISHI, "Spatial Dynamics and the Structure of Complex Systems-Progress in Pulsed Field Gradient NMR Spectroscopy-," *Kotaibutsuri* (in Japanese), **31**, 947 (1996).
H. INOKUCHI and K. IMAEDA, "Three Component Organic Semiconductors, Conductors and Superconductors," in *Electrical and Related Properties of Organic Solids*, R. W. Munn and A. M. B. Kuchta Eds., Kluwer Academic Publishers, pp. 227-239 (1997).
Y. WATANABE and T. MATSUI, "Molecular Mechanism of Oxygen Activation by Heme Enzymes," *J. Syn. Org. Chem.* (in Japanese), **54**, 1045 (1996).
Y. WATANABE, "Model Studies on Heme Monooxygenases," in "Oxygenases and Model Systems," T. Funabiki Ed., Kluwer Academic Publishers, 223-282 (1997).

K. MATSUDA, N. NAKAMURA, K. TAKAHASHI, K. INOUE, N. KOGA and H. IWAMURA, "Design, Synthesis, and Characerization of *p*-Cross-Conjugated Polycarbenes with High-Spin Ground States," Mark M. Turnbull, Toyonari Sugimoto, Laurence K. Thompson (Ed.): *Molecule-based Magnetic Materials.*, (ACS Symposium Series), **644**, 142-156 (1996).
H. IWAMURA, K. INOUE and N. KOGA, "How to Assemble Free Radicals into a Magnet," *Jounal of Synthetic Organic Chemistry* (in Japanease), **55**, 417-426 (1997).
H. IWAMURA, K. INOUE, N. KOGA and T. HAYAMIZU, "Assemblage of Organic Polyradicals With the Aid of Magnetic Metal Ions and Ordering of Their Spins in Macroscopic Scales ," Olivier Kahn Ed. Magnetism: A Supermolecular Function, *NATO ASI Series,* **C484**, 157-179 (1996).
T. SUGIMOTO and K. UEDA, "Synthesis of Organic Ferromagnets by use of Charge-Transfer Complexes" (in Japanese) in "Molecular Magnetism -New Magnets and Reaction Control-" K. Itoh Ed., Gakkai Shuppan Center (Tokyo), pp. 180-205 (1996).
T. SUGIMOTO, K. UEDA, N. KANEHISA, Y. KAI, M. SHIRO, N. HOSOITO, N. TAKEDA and M. ISHIKAWA, "Weak-Ferromagnetism and Ferromagnetism in Tetrafluorotetracyanoquinodimethanide Salts," in "Molecule-Based Magnetic Materials" M. M. Turnbull, T. Sugimoto, L. K. Thompson Eds., ACS Symposium Series, No. 644, pp. 276-295 (1996).
T. NAGATA, "Molecular Reaction Dynamics," in "Introduction to Chemistry," (in Japanese), H. Hamaguchi, R. Kuroda and T. Nagata Ed., Chikuma, Tokyo, p92, 1997.
J. ADACHI and N. KOSUGI, "Molecular Vibrational Spectroscopy Using High-Resolution Soft X-Rays," *Butsuri* (in Japanese) **52**, 96 (1997).
H. ISHII, and K. SEKI, "UV photoemission spectroscopy of organic/metal interfaces", *Hyomen* (in Japanese) **34**, 57 (1996).
T. SAKURAI and S. SUZUKI, "Spectroscopy of Cucumber Ascorbate Oxidase and Fungal Laccase ", in "Multi-Copper Oxidases," A. Messerschmidt Ed., World Scientific, pp. 225-250 (1997).
K. TANAKA and K. TSUGE, "Activation of CO2 on metal complexes directed toward multi-electron reduction and carbon-carbon bond formation," *Trends in Chem.*, **4**, 145 (1996).
K. TANAKA and K. TSUGE, "Model of Reductive Catalysts," in "Photochemical Energy Conversion," M. KANEKO Ed., IPC, 225 (1997).
M. FUJITA, "Self-assembled Macrocycles, Cages, and Catenanes Containing Transition Metals in Their Backbones," Comprehensive Supramolecular Chemistry (Ed by J.-M. Lehn), Pergamon Press Vol.9; Chap 7 (1996).
M. FUJITA, Supramolecular Chemsitry and Structurally New Polymers – Self-accumlatiing Polymers Linked by Hydrogen or Coordinate Bonds," Koubunnshi (in Japanese), **45**, 255 (1996).
M. FUJITA, "New Supramolecules" in "Chemistry Aiming at Supramolecules (in Japanese)," Ed. by Chemical Society of Japan, Gakkai Shuppan Center pp. 144-148 (1997).
M. FUJITA and K. OGURA, "Supramolecular Self-assembly" in "Molecular Recognition Chemistry (in Japanese)," Ed. by H. Tsukube, Sankyo Shuppan pp. 197-218 (1997).

AUTHOR INDEX TO RESEARCH ACTIVITIES AND SPECIAL RESEARCH PROJECTS

A

Abdulsabirov, Ravil Yu. 199
Abe, Haruo 72
Abo, Munehide 156
Achiba, Yohji 154
Adachi, Jun-ichi 134, 135
Adachi, Osao 52
Adachi, Takafumi 95, 227
Ahmad, Imtiaz K. 45
Akaki, Osamu 155
Aki, Michihiko 53, 218
Akiyama, Mamoru 190
Akiyama, Ryo 39, 217
Akutsu, Hiroki 90, 91, 227
Ali, Md. Meser 166
Alves, Nelson A. 28
Amaya, Kiichi 78
Anazawa, Toshihisa 68, 219
Ando, Kenjiro 78
Ann, Jeung-sun 112
Aoki, Masaru 228
Aoyagi, Masaru 185, 186, 230
Aoyagi, Mutsumi 55, 73, 143, 197, 223
Arai, Emiko 90, 91, 96, 97, 98, 227
Arakawa, Ichiro 156
Araki, Mitsunori 47
Araki, Tohru 135, 158
Arimoto, Osamu 211
Asada, Toshio 18
Asaka, Shuji 204, 205, 211, 223
Asari, Yukiko 151
Asato, Masaki 129
Atake, Tooru 107
Azuhata, Takashi 199
Azuma, Shunryo 177

B

Bandow, Shunji 204, 205, 206
Bandyopadhyay, Pradipta 18, 23, 216
Bayle, Jean-pierre 101, 102, 227
Benedict, C. 111
Berdague, Philippe 101
Brossard, Luc 91

C

Cai, Yong. Q. 210
Cassoux, P. 90, 91
Chainani, Ashish 112, 155
Chase, Bruce 205
Chen, Feiwu 17, 216
Chichibu, Shigefusa 199
Chin, Jik 175, 176, 230
Cho, Minhaeng 33
Chong, Song-ho 36, 38, 39, 217

D

Dahan, Francoise 190
Dai, Jie 187
Daniel, H. 48, 49
Daniel, Thomas 181
Daniele, Stephane 183
Daniels, Lizla B. 73
De Felicio, J. R. Drugowich 28
De Forcrand, Philippe 26
Deguchi, Takahiro 199
Dinnocenzo, Joseph P. 116
Doi, Takao 155
Dong, Jian 82
Dresselhaus, G. 205
Dresselhaus, M. S. 205
Dubinskii, Mark A. 199

E

Eades, J. 48, 49
Ebisawa, Hiromichi 42
Egashira, Kazuhiro 128
Eguchi, Shingo 192
Einaga, Hisahiko 117
Eklund, P. C. 205, 206
Emura, Yuji 72
Endo, Satoshi 122, 123
Enoki, Toshiaki 107
Etori, Hideki 154

F

Fan, Knag-nian 19
Fang, S. 205
Fiedler, Andreas 22, 216
Fish, Richard H. 117
Fominykh, N. G. 135
Fuchi, Shingo 159
Fujii, Masaaki 24, 71, 72, 220
Fujiki, M. 158
Fujiki, Takayuki 167
Fujimori, Hiroki 100, 101, 227
Fujimura, Yuuichi 219
Fujino, M. 158
Fujita, Hideo 83, 123, 124
Fujita, Junnosuke 177
Fujita, Makoto 184, 185, 186, 230
Fujita, Toshiyasu 184
Fujita, Y. 48
Fujiwara, Hideki 95, 96, 97, 98, 227
Fujiwara, Hideo 45, 47
Fujiwara, Shigeki 211
Fujiwara, Yasufumi 159
Fukaishi, Kenji 184
Fukuda, Ryuji 52
Fukui, Kazutoshi 158, 210
Fukumoto, Hiroki 110, 164
Fukushima, Masaru 76
Fukutani, Katsuyuki 157
Fukuyama, Hidetoshi 40, 41
Fukuzumi, Shun-ichi 116
Funaki, Hidenori 185
Furihata, Masatoshi 110
Furukawa, K. 158

G

Gan, Xinmin 188
Gangopadhyay, Gautam 34
Gebauer, Christian 75, 220
Gejo, Tatsuo 213
Gheyas, Syed Irfan 143
Gholamkhass, B. 165
Ghosall, Sharmisthia 34
Gomei, Motoki 20
Goodman, Frank O. 31
Goto, Makoto 123
Goto, Tsuneaki 120
Goto, Yoshio 116

H

Haga, Masa-aki 160, 161, 162, 163, 164, 165, 166, 229
Hama, Hiroyuki 210, 224
Hama, Tetsuo 113
Hamano, Hideaki 178
Hanazaki, Ichiro 69, 70
Hansmann, Ulrich H. E. 25, 26, 27, 28, 216
Hara, Isao 168
Harada, Kazumasa 161, 162, 164, 165
Harada, Yoshiya 153, 228
Hartmann, F. J. 48, 49
Hasegawa, Shinji 153, 158, 228
Hasegawa, Tatsuo 106
Hashimoto, Nobuhisa 74
Hasinoff, M. 48, 49
Hasumoto, Masami 210
Hata, Yuko 175
Hatano, Akihiko 174, 230
Hatsui, Takaki 136
Hattori, Hideo 147
Hayama, Akira 156
Hayamizu, Takashi 119
Hayano, R. S. 48, 49
Hayashi, Hisaharu 72
Hayashi, Hisashi 17
Hayashi, Naoki 57
Hayashi, Yoshihito 181
Heaven, Michael C. 75
Higai, Shin'ichi 105
Hikida, Takumi 147, 151
Hikosaka, Yasumasa 147
Hino, Kazuhiko 128
Hino, Shojun 154
Hino, Takashi 152
Hiraki, Ko-ichi 88, 226
Hirano, Shinya 142, 143, 221
Hirata, Fumio 25, 26, 27, 34, 35, 36, 37, 38, 39, 217
Hirata, So 21, 22, 216
Hiraya, Atsunari 134, 148, 149, 151
Hirayama, Takato 156
Hirose, Sayumi 211
Hirose, Takayuki 131
Hirota, Noboru 64, 65
Hirota, Shun 52, 168
Hirotsu, Masakazu 176, 177
Hiyama, Miyabi 31

Honada, Zentaro 113
Hori, Hiroshi 52
Hori, M. 48, 49
Horigome, Toshio 47, 102, 210
Horiuchi, K. 158
Horvath, D. 48, 49
Hosaka, Masahito 210, 224
Hosoito, Nobuyoshi 122
Hosokoshi, Yuko 120, 121, 228
Hosono, Hideo 152, 153, 228
Hossain, Md. Delower 160, 165, 229
Hrusak, Jan 23, 216
Huang, Hong-wei 168

I

Ibuki, Toshio 141, 151, 152, 213
Ibukuro, Fumiaki 185, 230
Ichikawa, Masatake 210
Ichimura, Kenji 108
Iguchi, Tadashi 159
Ikeda, Shigeru 72
Ikeda, Takuya 172
Ikegami, Tsutomu 19, 216
Ikenaga, Eiji 145, 146
Ikezawa, Mikihiko 213
Ikoma, Hideyuki 72
Imachi, Ron 109, 110
Imaeda, Kenichi 105, 108, 201
Imai, Takashi 217
Imai, Yoshio 51
Imaizumi, Y. 142
Imaizumi, Yoshiaki 141, 142
Imanari, Mamoru 185
Inabe, Tamotsu 111, 135, 158
Inada, Yuji 116
Inagaki, Akiko 163
Inatani, Junji 47
Inokuchi, Hiroo 105, 106, 107, 108, 153
Inokuchi, Makoto 112
Inokuchi, Yoshiya 65, 125, 126, 127, 220
Inoue, Katsuya 118, 119, 120, 121, 228
Ioue, Kazuo 112
Irisa, Masayuki 27
Iriyama, Keiji 79
Isaka, H. 158
Ishida, Takayuki 109, 110
Ishida, Tateki 35, 217
Ishiguro, E. 158
Ishii, Hisao 135, 153, 154, 157, 158, 228
Ishikawa, T. 48, 49
Ishimori, Koichiro 115
Ishiuchi, Shun-ichi 71
Isobe, Kiyoshi 117, 182
Ito, Eisuke 135, 158
Ito, Yuko 107
Itoh, Hiroshi 211
Itoh, Koichi 78
Itoh, Minoru 211
Ivanov, Valery A. 82
Iwahori, Fumiyasu 113
Iwamatsu, Masaki 123, 124
Iwamura, Hiizu 118, 119, 120
Iwasa, Yoshihiro 106
Iwasaki, Kentaro 154
Iwase, Masakazu 117
Iwata, Suehiro 17, 18, 19, 20, 22, 23, 24, 132, 133, 143, 216
Izumida, Shinji 200, 223
Izuoka, Akira 107, 111

J

Jitsukawa, Koichiro 117
Johnson, Mark A. 130
Jones, Jeffrey P. 116
Judeinstein, Patrick 102

K

Kaga, Yoshio 112
Kagami, Yuka 113
Kagoshima, Seiichi 106
Kai, Yasushi 122
Kaifu, Norio 47
Kamada, Masao 157, 208, 210, 211, 223
Kambayashi, Hide 184
Kamikawa, Tadao 189
Kaminaga, Akiko 70
Kamiya, Koji 106
Kamo, Osamu 185
Kanamori, Hideto 21, 57, 58
Kanda, Kazuhiro 151
Kanehisa, Nobuko 122
Kang, Tai Jong 65, 219
Kano, Kenji 83, 123, 166
Kanoda, Kazushi 83, 84, 85, 86, 87, 88, 89, 226
Kasahara, Ryuichi 177
Kasai, Kayoko 186
Kashino, Setsuo 176, 177
Katayanagi, Hideki 73, 74, 75, 197, 220
Kato, Hiroyuki 67, 219
Kato, Kiyonori 91, 209
Kato, Noriaki 161, 162
Kato, Shigeki 35, 217
Kato, Tatsuhisa 55, 56, 57, 58, 218
Katsumata, Koichi 113
Kawabe, Hiroyuki 168, 169, 170, 171, 172
Kawai, Akio 77
Kawakami, Takashi 109, 168, 169, 170
Kawamoto, Atsushi 83, 84, 85, 89, 226
Kawamura, Kazumori 180
Kawasaki, Masahiro 141
Kawashima, Takuya 112
Kawata, Yasushi 161, 229
Kawazoe, Hiroshi 152, 153, 228
Kaya, Koji 20
Kayama, Misa 138, 139, 221
Kazansky, Andrey K. 31
Ketzer, B. 48, 49
Kikuchi, Koichi 154
Kikuchi, Naoto 153
Kimura, Chieko 167
Kimura, Shin-ichi 157, 210, 211, 212, 213
Kinoshita, Ikuo 68, 219
Kinoshita, Masahiro 25, 26, 27, 35, 36, 37, 217
Kinoshita, Minoru 121
Kinoshita, Toshio 210
Kinoshita, Toyohiko 144, 211, 212, 224
Kiribayashi, Shinji 169, 170
Kishi, Reiko 20
Kishine, Jun-ichiro 39, 40, 225
Kishishita, Mitsuru 179
Kitagawa, Hiroshi 112, 124
Kitagawa, Susumu 188, 190
Kitagawa, Teizo 51, 52, 53, 54, 115, 168, 218
Kitajima, Yoshinori 134
Kitamura, Akinori 153
Kitamura, Chitoshi 203
Klafter, Joseph 34
Klisch, Egbert 43
Kobayashi, Akiko 90, 91, 92, 93, 94, 95, 96, 97, 227
Kobayashi, Hayao 90, 91, 92, 93, 94, 95, 96, 97, 98, 227
Kobayashi, Kaori 43, 44, 45, 46
Kobayashi, Kimiko 175
Kobayashi, Tatsuo 78
Kobori, Yasuhiro 77
Kodama, Koichi 169, 171, 172
Kodama, Takeshi 55
Kogan, Iakov L. 80, 225
Kohama, Masakado 122
Kohguchi, Hiroshi 74, 75, 220
Koike, Tohru 175, 176
Koike, Toshihiro 156
Koike, Tsuneaki 154
Kojima, Masaaki 176, 177
Komeda, Nobutoshi 183
Komura, Naoki 163
Kondo, Shigeo 197
Kondo, Tomonori 185
Kondoh, Takuhiko 223
Konno, Shin-ichi 178
Kono, Mitsuhiko 151
Korableva, Stella L. 199
Kosugi, Kentaro 128, 129
Kosugi, Nobuhiro 134, 135, 136, 158
Kotani, Akio 211, 212
Kovalenko, Andriy 217
Kröber, Jonas 108
Krishnamurtya, Sailaja 24
Kruglik, Sergei G. 54
Kubo, Kazuyuki 180
Kubozono, Yoshihiro 177, 178
Kumagai, Motohiro 57, 58
Kumakura, Mitsutaka 48, 49, 50, 218
Kumasaki, Mieko 96
Kumashiro, Ryotaro 178
Kumigashira, Hiroshi 211
Kumita, Hideyuki 167
Kuninobu, Takafumi 156
Kurihara, Masato 183
Kuroda, Yasushige 178
Kuroda-sowa, Takayoshi 187, 188, 189
Kurokawa, Sinya 78
Kurosaki, Hiromasa 176
Kushi, Yoshinori 182
Kusukawa, Takahiro 185, 230
Kuwahara, Daisuke 100, 102, 103, 104, 207, 227
Kwon, Yong Seung 213
Kwon, Yoon-jung 186

L

Langer, U. 111
Lesot, Philippe 101
Lever, A. B. P. 161
Li, Haiyang 74, 75, 220

Li, Yumin 20, 216
Limbach, H. H. 111
Lin, Shujie 61, 62
Liu, Zhenlin 199, 200, 223

M

Ma, Yunsheng 41
Maas, F. E. 48, 49
Maeda, Hironobu 177, 178
Maeda, Yonezo 181
Maekawa, Hatsuko 160
Maekawa, Masahiko 187, 188, 189, 190
Magome, Tamotsu 157
Maierl, C. 48
Manabe, Toshio 112, 113
Maruta, Goro 109, 110, 111
Maruyama, Tukasa 154
Maruyama, Yusei 135, 158
Maruyama, Yutaka 32
Marzilli, Luigi G. 173, 230
Marzilli, Patricia A. 173, 230
Mase, Kazuhiko 143, 145, 146, 210
Mashima, Kazushi 110, 163, 164
Masuda, Hideki 117, 167, 181
Masui, Shin 143
Masuya, Masato 26, 27, 216
Matsui, Toshitaka 115, 116, 229
Matsumoto, Hiroki 168
Matsumoto, Masaki 126
Matsumoto, Masuaki 157, 222
Matsumoto, N. 158
Matsumoto, Naohide 190, 192
Matsumoto, Yoshiyasu 66, 67, 68, 219
Matsumura, Takeshi 211, 212
Matsuo, Hideki 146
Matsuoka, Norihiro 128
Matsushita, Kazunobu 52
Matsushita, Michio 56, 57, 58, 218
Matsushita, Michio M. 111
Matsushita, Yoshihisa 77
Matsuura, Ikuya 155
Matsuzaki, Yoichi 168
Matysik, Jörg 218
Maw, Sarah 34
Meech, Stephen R. 61, 62, 219
Mekaru, Harutaka 143, 144
Menon, M. 205
Mimura, Masaaki 190, 192
Minamino, Satoshi 197
Mitani, Masaki 171
Mitani, Tadaoki 112, 113, 124
Mito, Masaki 121, 228
Mitsuhashi, Takashi 184
Mitsui, Masaaki 77
Mitsuke, Koichiro 147, 148, 149, 150, 156, 222
Mitsumoto, Ryuichi 158
Mitsutake, Ayori 27, 216
Miura, Yozo 78
Miyagawa, Kazuya 83, 84, 85, 89, 226
Miyajima, Seiichi 98, 99, 100, 101, 102, 103, 104, 105, 227
Miyamae, Takayuki 106, 143, 144, 153, 154, 155, 158, 221
Miyasaka, Hitoshi 192, 193
Miyazaki, Takafumi 153, 154, 155
Miyazawa, Keisuke 47
Miyoshi, Katsuhiko 179, 180
Mizuguchi, Yukiko 192
Mizukawa, Tetsunori 230
Mizuno, Seiji 105
Mizushima, Kazuya 165
Mizuta, Tsutomu 180
Mizutani, Masakazu 148, 149, 222
Mizutani, Nobuaki 208
Mizutani, Nobuo 210
Mizutani, Yasuhisa 53, 54
Mo, Yuxiang 72, 73, 220
Mochida, Tomoyuki 103, 104, 106, 227
Mogi, Koichi 55
Mogi, Tatsushi 218
Monjushiro, Hideaki 161, 162, 164, 165, 166, 168, 229
Mori, Michiyasu 41, 225
Mori, Wasuke 109, 110, 169, 170
Moribayashi, Kengo 28
Morimoto, Hiroshi 122
Morishima, Isao 115, 116
Morishita, Hiromasa 175, 230
Morita, Norio 48, 49, 50, 51, 218
Moriwaki, Kazuma 187, 188
Moriwaki, Yoshiki 50, 51, 218
Motoda, Yuri 190
Mukai, Masahiro 54, 115
Mukaida, Masao 183
Mukamel, Shaul 219
Munakata, Megumu 122, 187, 188, 189, 190
Munakata, Toyonori 38
Murakami, Tatsuya 116
Muramatsu, Yukiko 154
Murase, Tomohide 107
Murata, Mariko 172
Muto, Akiko 57

N

Nagai, Masako 52
Nagai, Toshihiro 156
Nagai, Yukifumi 52
Nagano, Shingo 115
Nagao, Hidemi 168, 169, 170, 171, 172, 229
Nagao, Hirotaka 181, 182, 183
Nagao, Mahiko 178
Nagashima, Umpei 69
Nagasono, Mitsuru 145, 146, 210
Nagata, Masaaki 208
Nagata, Takashi 130, 131, 132, 133, 151, 220
Nagatomo, Shigenori 52
Nagayama, Kohei 158
Nagayama, Toshihiko 181
Naito, Toshio 135, 158
Naitoh, Yukito 60, 62, 63, 64, 65, 127
Naka, Kazunari 217
Nakai, Toshihito 100, 207, 227
Nakai, Yasuhiro 126
Nakajima, Atsushi 20
Nakajima, Hiroshi 181, 183
Nakajima, Kiyohiko 176, 177
Nakamoto, Masami 184
Nakamura, Akira 110, 164, 181
Nakamura, Eiken 144
Nakamura, Hiroki 28, 29, 30, 31, 32, 216
Nakamura, Keiichi 179
Nakamura, Shigeyuki 117
Nakamura, Shuji 199
Nakanishi, Shunsuke 211
Nakano, Chikako 107, 108
Nakano, Hiroki 120, 121
Nakano, Masayoshi 168, 169, 170, 171
Nakao, Kenji 105, 108
Nakashima, Satoru 54
Nakashima, Toshio 190, 192, 193
Nakata, Masahiro 97
Nakata, Munetaka 79
Nakaura, Miho 161, 165
Nakazawa, Hiroshi 179, 180
Nakazawa, Takashi 27
Nakazawa, Yasuhiro 86, 87, 88, 226
Namiki, Kei-ichi 46
Nanba, Takao 157
Nanbu, Shinkoh 31, 73, 197
Nath, Krishna G. 211, 212
Naumov, A. K. 199
Niikura, Hiromichi 148, 149, 222
Nishi, Kaori 128
Nishi, Nobuyuki 65, 125, 126, 127, 128, 129, 220
Nishiguchi, Masaharu 128
Nishii, Junji 152
Nishikawa, Kiyoshi 169, 170, 171, 172
Nishimura, Kei-ichiro 122
Nishino, Masamichi 171
Nishio, Mitsuhiro 143
Nishio, Takayuki 42
Nishioka, Takanori 182
Nishiyama, Hisao 165
Nobusada, Katsuyuki 28, 29, 216
Nogami, Takashi 109, 110
Noguchi, Shogo 77
Nonogaki, Youichi 159
Nose, Fumitaka 167
Nozaki, Koichi 165, 166

O

Obi, Kinichi 76, 77
Ochiai, Akira 213
Oda, Akifumi 111
Ogasawara, Haruhiko 211, 212
Ogata, Hironori 102, 105, 227
Ogata, Masao 41
Ogawa, Hiroshi 143
Ogawa, Takuhiro 39, 225
Ogino, Hiroshi 195, 196
Ogo, Seiji 117
Ogura, Fumio 97
Ogura, Katsuyuki 184, 185, 186
Ogura, Takashi 53, 115, 218
Ohashi, Kazuhiko 65, 125, 126, 127, 128, 220
Ohba, Shigeru 177
Ohishi, Masatoshi 47
Ohishi, Tachi 113
Ohiwa, Naotaka 77
Ohmori, Yasuharu 177
Ohno, Takeshi 165
Ohno, Yasuhiro 187
Ohta, Akira 202
Ohta, Kaoru 64, 65

Ohta, Koji 170, 171
Ohta, Toshiaki 135, 136, 158
Ohtake, Hideyuki 199, 200, 223
Ohtsuka, Hiroshi 216
Oichi, Kazuyoshi 135, 158
Oishi, Osamu 98, 227
Oji, Hiroshi 135, 158
Ojida, Akio 173, 174
Oka, Yasuo 112, 113
Okada, Atsuhiko 78
Okada, Kazumasa 151, 152, 213
Okada, Kazutoshi 216
Okamoto, Hiroshi 112, 113
Okamoto, Yuko 25, 26, 27, 29, 36, 37, 216
Okamura, Hidekazu 157
Okamura, Shingo 193
Okano, Tatsuo 157
Okawa, Hisashi 181
Okazaki, Masaaki 195
Okishio, Nobuyuki 52
Oku, Makoto 106
Okudaira, Koji Kamiya 153, 228
Okumura, Ko 33
Okumura, Mitutaka 168
Olson, John S. 54
Omi, Takuichiro 71
Ono, Katsuhiko 203
Onodera, Noriaki 112, 124
Ookubo, Takaharu 181
Ornellas, Fernando R. 22, 23, 216
Osherov, Vladimir I. 30, 216
Ostrovsky, Valentine N. 29, 30, 31, 32, 216
Otsubo, Tetsuo 82, 97
Ouchi, Yukio 135, 154, 158
Ouyang, Jianyong 226
Ozaki, Shin-ichi 115, 116, 229
Ozaki, Yukihiro 79
Ozawa, Y. 124
Ozeki, Hiroyuki 43, 44, 45, 47, 217

P

Pal, Haridas 59
Pal, Sourav 17, 24, 216
Park, Jong K. 20
Park, Soon-bong 165
Park, Y. 142
Pavlychev, A. A. 135
Pohl, R. 48, 49

Q

Qin, Jingui 82, 226

R

Rao, A. M. 205, 206
Rayssac, Vincent 101, 102
Rhee, S. 142
Richter, E. 205
Roy, Ram Kinkar 24
Rubstov, Igor V. 60
Ryan, Matthew 161

S

Saeki, Morihisa 132, 133, 220
Saito, Gunzi 107
Saito, Kazuhito 76
Saito, Koh 152
Saito, Shuji 43, 44, 45, 46, 47, 217
Saito, Taro 96
Saitow, Ken-ichi 63, 65, 127
Sakai, Ken-ichi 113
Sakai, Kusuo 210
Sakurai, Makoto 156, 157, 222
Sakurai, Nobuhiko 167
Sakurai, Takeshi 167, 168, 229
Sarukura, Nobuhiko 199, 200, 223
Sasada, Masatoshi 176
Sasaki, Osamu 184, 186
Sato, Akane 90, 92, 93, 94, 98, 227
Sato, Hirofumi 34, 35, 217
Sato, Hiroyasu 166
Sato, Naoki 107
Sato, Takahisa 181
Savchenko, E. V. 156
Schmidt, R. 48, 49
Schröder, Detlef 23
Schwarz, Helmut 23
Seki, Hiroko 185
Seki, Kazuhiko 106, 135, 153, 154, 157, 158, 228
Sekimoto, Yutaro 47
Sekitani, Tetsuji 145, 146
Sekiya, Hiroshi 128
Sekiya, Nobutake 71
Semashko, Vadim V. 199
Severino, Patrizio 25
Shi, Yang 74
Shi, Zurong 107
Shibamoto, Yoshiyuki 122
Shibata, Takeshi 74
Shigemasa, Eiji 134, 135
Shigemori, Kazuki 174, 230
Shigemoto, Isamu 168, 169, 170
Shigeta, Yasuteru 169, 170, 172
Shimada, Yuji 112
Shimojima, Atsuhiko 139, 140, 221
Shionoya, Mitsuhiko 172, 173, 174, 175, 176, 230
Shiotsuka, Michito 173, 174
Shiozawa, Rie 196
Shiro, Motoo 176
Shirota, Hideaki 59, 60, 62
Shitomi, Hiroshi 71
Shobatake, Kosuke 151
Simonyan, Mkhital 81
Smalley, R. E. 205, 206
Smith, Neil A. 61, 62
Soejima, Koichi 135
Sota, Takayuki 199
Steimle, Timothy C. 46
Subbaswamy, K. R. 205
Suenaga, Yusaku 122, 187, 188, 189
Sugai, I. 48, 49
Sugawara, Tadashi 103, 104, 107, 111
Sugimoto, Hideki 181, 230
Sugimoto, Kunihisa 189
Sugimoto, Toyonari 83, 122, 123, 124
Sugiura, S. 106
Sugiyama, Kiyoshi 157
Sun, Xin 41
Sunatsuki, Yukinari 192
Suzuki, Hiroharu 163
Suzuki, Masatatsu 181, 183
Suzuki, Schinnichiro 167
Suzuki, Shugo 105, 108
Suzuki, Tadayoshi 24, 216
Suzuki, Takashi 211, 212, 213
Suzuki, Toshinori 72, 73, 74, 75, 197, 220
Suzuki, Yoko 33

T

Tabayashi, Kiyohiko 152
Tada, Toshiharu 122
Tagata, Tsuyoshi 184
Tahara, Tahei 137, 138, 139, 140, 141, 221
Takahashi, Kazutaka 220
Takahashi, Minoru 120, 121
Takahashi, Mitsue 120
Takahashi, Naoshi 210
Takahashi, Takashi 112, 155, 211
Takami, Toshiya 197
Takamizawa, Satoshi 110
Takano, Hiroshi 34
Takano, Shiro 210
Takata, K. 124
Takata, Yasutaka 134, 136
Takaya, Yoshiaki 163
Takayanagi, Masao 69, 79
Takazawa, Ken 71, 72
Takeda, Kazuyoshi 121, 228
Takeda, Keizo 77
Takeda, Sadamu 109, 110, 111, 168
Takeda, Yoshikazu 159
Takemori, Toshifumi 163
Takenaka, Hisataka 143
Takeuchi, Satoshi 137, 138, 139, 221
Takeuchi, Tetsuya 113
Takimiya, Kazuo 82, 97
Takizawa, Kohichi 120
Tamura, H. 48, 49
Tamura, Masafumi 121
Tanaka, Chizuko 106
Tanaka, Hisashi 90, 91, 92, 96, 227
Tanaka, Hitoshi 224
Tanaka, Jiro 106
Tanaka, Ken-ichiro 145, 146
Tanaka, Kentaro 173, 174, 175, 176, 230
Tanaka, Koji 181, 182, 183, 184, 230
Tanaka, Masako 163
Tanaka, Motomasa 115
Tanaka, Shin-ichiro 145, 146, 210, 223
Tanaka, Shoji 201, 203, 228
Tanaka, Toshiaki 107
Tani, Kazuhide 163, 164
Taniguchi, Hiromi 86, 226
Tanimoto, Mitsutoshi 46
Tanimura, Yoshitaka 32, 33, 34, 217
Tasaka, Motoyuki 173, 175, 230
Tasumi, Mitsuo 79
Tatsumi, Natsuo 157
Teki, Yoshio 78
Ten-no, Seiichiro 17, 18, 23, 34, 216
Teranishi, Yoshiaki 30, 216
Thess, A. 205, 206
Tobita, Hiromi 195, 196

Tokeshi, Manabu 148
Tokumoto, Madoka 91
Tolstikhin, Oleg I. 29, 32, 216
Tominaga, Keisuke 59, 60, 61, 63, 64, 65, 208, 219
Tomita, Takeshi 51
Tomura, Masaaki 201, 203, 228
Tonokura, Kenichi 73
Tonooka, Mizuho 43, 44
Torii, H. A. 48, 49
Torii, Tatsuharu 102, 223
Toriumi, Koshiro 112, 124
Toyoda, Tomonori 99
Toyohara, Kiyotsuna 182, 183
Toyota, Eijiro 143
Toyota, Naoki 122, 123
Tsubaki, Motonari 52
Tsuboyama, Sei 175
Tsuchimoto, Motonobu 177
Tsuge, Kiyoshi 182, 183, 230
Tsujibayashi, Toru 211
Tsukada, Mitsuyoshi 107
Tsukahara, Keiichi 167
Tsukuda, Tatsuya 130, 131, 132, 133, 220
Tsuneshige, Antonio 52
Tsurusawa, Takeshi 17, 19, 216
Tsusaka, Yoshiyuki 143, 144
Tsuyama, Shingo 51
Tuchagues, Jean-pierre 191

U

Uchida, Akira 107
Uchida, Hironaga 221
Udagawa, Yasuo 17
Ueda, Kazumasa 83, 122, 123, 124
Ueda, Kenji 169
Ueda, Naoyuki 153, 228
Ueda, Yoshiko 179
Uehara, Akira 181
Ueno, Nobuo 153, 228
Ueno, Sadaharu 78
Uesugi, Yuki 53
Ufuktepe, Yüksel 211, 212
Ugawa, Akito 83, 123, 141
Ugolkova, Elena 82
Umishita, Kazunori 154
Urisu, Tsuneo 141, 142, 143, 144, 145, 146, 221
Uruichi, Mikio 82, 226
Ushakov, Vladimir G. 30

V

Vetrivel, Rajappan 24
Von Egidy, T. 48, 49

W

Wada, Akira 21
Wada, Hiroaki 195
Wada, Senji 117
Wada, Shin-ichi 77
Wang, Kezhi 162, 229
Wang, Wen-ning 19, 216
Watanabe, Hidekazu 18, 143, 216
Watanabe, Katsumi 157
Watanabe, Kazuo 66, 67, 219
Watanabe, Kazuya 67, 219
Watanabe, Kenya 186
Watanabe, Makoto 158
Watanabe, Masayuki 211
Watanabe, Michio 102, 208, 223
Watanabe, Naoki 135
Watanabe, Noboru 17
Watanabe, Yoshihito 115, 116, 117, 229
Widmann, E. 48, 49
Williams, K. A. 205, 206
Winnewisser, Gisbert 43
Wu, Liang Ping 187, 188, 189

X

Xu, Xiaohua 41

Y

Yagishita, Akira 134, 135
Yakushi, Kyuya 80, 81, 82, 83, 112, 123, 141, 225, 226
Yamada, Satoru 168, 169, 170
Yamagata, Tsuneaki 163
Yamagiwa, Yoshiro 189
Yamaguchi, Kentaro 184, 185, 186
Yamaguchi, Kizashi 109, 110, 111, 168, 169, 170, 171, 172
Yamaguchi, Toshiyuki 122
Yamaguchi, Yoshitaka 179, 180
Yamakage, Hirokazu 78
Yamaki, Daisuke 169
Yamamoto, Kaoru 136
Yamamoto, Koji 122, 123
Yamamoto, Mikiko 187, 188
Yamamoto, Satoshi 43, 44, 47
Yamamoto, Takakazu 154
Yamanaka, Syuusuke 169
Yamanoha, Masaru 83, 123
Yamashita, Koichi 73
Yamashita, Masahiro 112, 113, 125
Yamashita, Yoshiro 82, 201, 202, 203, 226, 228
Yamauchi, Osamu 168
Yamazaki, Jun-ichiro 158, 210
Yamazaki, T. 48, 49
Yan, Sheng-gang 190
Yasukawa, Masahiro 153
Yazaki, Jun 184
Yokoyama, Toshihiko 136
Yonehara, Yukako 80, 108, 225
Yonekura, Nobuaki 74
Yonemitsu, Kenji 39, 40, 41, 42, 225
Yonetani, Takashi 53
Yoshida, Hiroaki 150
Yoshida, Hisashi 47, 99, 209
Yoshida, Shuhei 38
Yoshida, Taturu 113
Yoshigoe, Akitaka 142, 143
Yoshihara, Keitaro 59, 60, 61, 62, 63, 64, 65, 127, 219
Yoshikawa, Shinya 218
Yoshikawa, Yuzo 176, 177, 178
Yoshimura, Daisuke 154, 157
Yoshioka, Yasuhiro 171
Yu, Shu-yan 230
Yu, Yan 113
Yuyama, Akira 158

Z

Zhan, Chang-guo 21, 24
Zhao, Hua 41
Zhao, Xiaojie 52
Zhu, Chaoyuan 29, 30, 216
Zhu, Lei 132, 133, 220

Institute for Molecular Science, Myodaiji, Okazaki 444-8585, Japan